Hadronic Contributions to Light-by-Light Scattering and Muon $(g-2)$

Volodymyr BILOSHYTSKYI

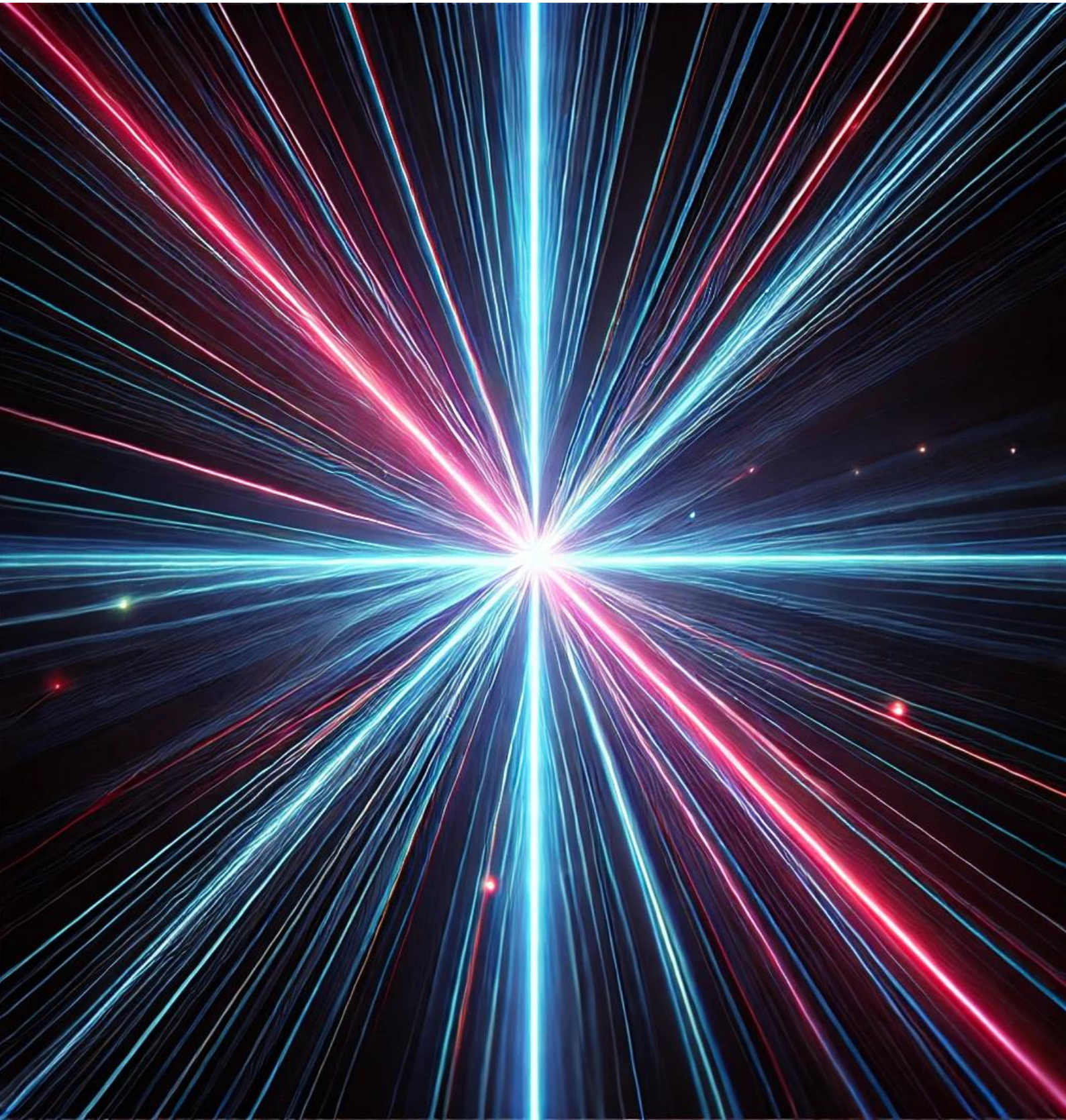

Hadronic Contributions to Light-by-Light Scattering and Muon $(g-2)$

Dissertation
zur Erlangung des Grades
"Doktor der Naturwissenschaften"

am Fachbereich Physik, Mathematik und Informatik
der Johannes Gutenberg-Universität Mainz

vorgelegt von
Volodymyr Biloshytskyi
geboren in Cherson (Ukraine)

Mainz, November 2024

Abgabe der Dissertation (submission of the dissertation): 25.11.2024
Datum der Promotionsprüfung (date of the doctoral examination): 06.02.2025

Betreuer (Advisor):
Dr. Vladimir Pascalutsa
Institut für Kernphysik & PRISMA Cluster of Excellence
Johannes Gutenberg-Universität Mainz
55128 Mainz
pascalut@uni-mainz.de

Zweitbetreuer (Co-advisor):
Prof. Dr. Marc Vanderhaeghen
Institut für Kernphysik & PRISMA Cluster of Excellence
Johannes Gutenberg-Universität Mainz
55128 Mainz
vandma00@uni-mainz.de

To Anastasiia, Mariia and Elisabeth

Abstract

Low-energy observables, such as the anomalous magnetic moment (AMM) of the muon and the energy spectra of light muonic atoms, provide a unique avenue for testing the Standard Model (SM) at the precision frontier of physics. However, the accuracy of SM predictions for these quantities is constrained by uncertainties in hadronic contributions. Understanding these contributions, particularly those related to light-by-light (LbL) scattering and Compton scattering processes, is therefore crucial for precise theoretical predictions. This thesis primarily focuses on these hadronic contributions while incidentally exploring exotic resonances, hadron polarizabilities, and briefly addressing parity and time-reversal violation effects in Compton scattering.

The hadronic corrections to the muonic AMM are analyzed from two perspectives. To refine the hadronic vacuum polarization (HVP) contribution using lattice QCD, a novel approach to compute electromagnetic corrections via a Cottingham-like formula is introduced. Verified within quantum electrodynamics (QED) and scalar QED, this approach demonstrates potential for lattice QCD calculations by circumventing the power-law finite-volume effects associated with photons on the lattice. Additionally, the Schwinger sum rule method–a dispersive, data-driven approach based on doubly-virtual Compton scattering–is investigated. This method offers alternative calculations for both the HVP and hadronic light-by-light (HLbL) contributions to the muon AMM. Tested within effective field theories and the SM, it is applied to the calculation of the leading-order HLbL contribution arising from neutral pion exchange.

Regarding exotic resonances, the recently observed fully charmed states in the di-J/ψ spectrum are examined within the context of real LbL scattering to study their possible contribution in LbL cross sections at the Large Hadron Collider (LHC). To facilitate future LHC measurements, a phenomenological model based on LbL scattering sum rules is proposed to simulate the hadronic background at low energies or small scattering angles. An improved parametrization of scattering amplitudes for resonances in the elastic scattering of spinless particles is also proposed, developing a dispersive inverse amplitude method which will be helpful for analyzing lattice QCD data.

Within the Compton scattering framework, the Bernabéu-Tarrach sum rule for static electric dipole polarizability is investigated. This sum rule is perturbatively verified within covariant baryon chiral perturbation theory, yielding a dispersive formula for the subtraction contribution in the data-driven approach to the Lamb shift in hydrogen-like atoms. Additionally, the puzzling negative electric polarizability of the neutral pion, predicted by meson chiral perturbation theory (χPT), is revisited. For the first time, it is evaluated using a light-front quark model.

Forward Compton scattering analysis is also extended to cases involving parity and time-reversal violation. New sum rules for the anapole and electric dipole moments are derived and perturbatively verified.

Zusammenfassung

Niederenergie-Observablen, wie das anomale magnetische Moment (AMM) des Myons und die Energiespektren leichter myonischer Atome, bieten eine einzigartige Möglichkeit, das Standardmodell der Teilchenphysik (SM) durch Präzisionsmessungen und -vorhersagen zu testen. Die Genauigkeit der SM-Vorhersagen für diese Größen wird jedoch durch Unsicherheiten in den hadronischen Beiträgen eingeschränkt. Das Verständnis dieser Beiträge, insbesondere jener in Licht-Licht (LbL) und Compton-Streuprozessen, ist daher entscheidend für präzise theoretische Vorhersagen. Diese Dissertation befasst sich primär auf diese hadronischen Beiträge. Außerdem werden exotische Resonanzen, Polarisierbarkeiten von Hadronen sowie Paritäts- und Zeitumkehrverletzungseffekte in der Compton-Streuung untersucht.

Die hadronischen Korrekturen zum myonischen AMM werden aus zwei Perspektiven analysiert. Um die Gitter-QCD-Vorhersage der hadronischen Vakuumpolarisation (HVP) zu verfeinern, wird ein neuer Ansatz vorgestellt, der elektromagnetische Korrekturen über eine Formel ähnlich der Cottingham Summenregel berechnet. Dieser Ansatz, der innerhalb der Quantenelektrodynamik (QED) und der skalaren QED überprüft wurde, zeigt Potenzial für Gitter-QCD-Berechnungen, da er die mit Photonen auf dem Gitter verbundenen Volumeneffekte nach dem Potenzgesetz umgeht.. Zusätzlich wird die Schwinger-Summenregel-Methode, ein dispersiver, datenbasierter Ansatz auf der Grundlage doppelt-virtueller Compton-Streuung, untersucht. Diese Methode bietet alternative Berechnungen sowohl für die (HVP) als auch für den Beitrag der hadronischen Licht-Licht-Streuung (HLbL) zum myonischen AMM. Innerhalb effektiver Feldtheorien und des SM getestet, wird sie auf die Berechnung des führenden HLbL-Beitrags angewendet, der aus dem Austausch neutraler Pionen resultiert.

Im Hinblick auf exotische Resonanzen werden die kürzlich beobachteten vollständig charmhaltigen Zustände im di-J/ψ-Spektrum im Kontext der realen LbL-Streuung untersucht, um ihren möglichen Beitrag zu LbL-Wirkungsquerschnitten am Large Hadron Collider (LHC) zu analysieren. Um zukünftige LHC-Messungen zu erleichtern, wird ein phänomenologisches Modell basierend auf LbL-Streuungs-Summenregeln vorgeschlagen, das den hadronischen Untergrund bei niedrigen Energien oder kleinen Streuwinkeln simuliert. Eine verbesserte Parametrisierung der Streuamplituden für Resonanzen in der elastischen Streuung spinloser Teilchen wird ebenfalls vorgeschlagen, indem eine dispersive Methode der inversen Amplitude entwickelt wird, die bei der Analyse von Gitter-QCD-Daten hilfreich sein wird.

Im Rahmen der Compton-Streuung wird die Bernabéu-Tarrach-Summenregel für die statische elektrische Dipolpolarisierbarkeit untersucht. Diese Summenregel wird innerhalb der kovarianten baryonischen chiralen Störungstheorie perturbativ überprüft, was eine dispersive Formel für den Subtraktionsbeitrag im datenbasierten Ansatz zur Lamb-Verschiebung in wasserstoffähnlichen Atomen ergibt. Darüber hinaus wird die rätselhafte negative elektrische Polarisierbarkeit des neutralen Pions, die durch die mesonische chirale Störungstheorie (χPT) vorhergesagt wird, erneut untersucht. Zum ersten Mal wird sie mithilfe eines lichtfrontbasierten Quarkmodells bewertet.

Die Analyse der Vorwärts-Compton-Streuung wird auch auf Fälle ausgeweitet, die Paritäts- und Zeitumkehrverletzungen beinhalten. Neue Summenregeln für die Anapol- und elektrischen Dipolmomente werden hergeleitet und perturbativ überprüft.

List of publications

Articles in refereed journals

1. Volodymyr Biloshytskyi, Iulian Ciobotaru-Hriscu,Franziska Hagelstein, Vadim Lensky, Vladimir Pascalutsa, *The QED of Bernabéu-Tarrach sum rule for electric polarizability and its implication for the Lamb shift*,
   Phys.Rev.D 109 (2024) 1, 016026 [hep-ph/2305.08814]

   The Bernabéu-Tarrach sum rule, which connects a particle's static dipole polarizability to its total photoabsorption cross section, is revisited. Arguments supporting the sum rule's convergence and validity are presented through its perturbative verification within covariant baryon chiral perturbation theory and an empirical estimate of the πN-channel contribution to the proton's electric polarizability. Building on this, a related sum rule for the subtraction function, relevant to data-driven calculations of polarizability effects in the Lamb shift, is proposed, perturbatively validated, and empirically tested on the πN-channel.

   The author conducted all the analytic calculations related to the Bernabéu-Tarrach sum rule, making the corresponding figures.

2. Volodymyr Biloshytskyi, En-Hung Chao, Antoine Gérardin, Jeremy R. Green, Franziska Hagelstein, Harvey B. Meyer, Julian Parrino and Vladimir Pascalutsa, *Forward light-by-light scattering and electromagnetic correction to hadronic vacuum polarization*,
   JHEP 03 (2023) 194[hep-lat/2209.02149]
   The method to handle the electromagnetic corrections to the hadronic vacuum polarization contribution to the anomalous magnetic moment of the muon by using the Cottingham-like formula is proposed. This method is particularly suitable for the lattice quantum chromodynamics calculations, since it allows one to avoid power-law finite-size effects connected to the internal photon propagator. Introducing the separation scale $\Lambda \sim 400$ MeV into this propagator allows one to split the calculation into a short-distance part, regulated in the ultraviolet limit by the lattice and in the infrared limit by the scale Λ, and an ultraviolet-finite long-distance part to be treated with coordinate-space lattice quantum chromodynamics methods. The long-distance part can be predicted by expressing the ultraviolet-regulated electromagnetic correction to the

hadronic vacuum polarization via the forward hadronic light-by-light scattering amplitude and related the latter via a dispersive sum rule to $\gamma^*\gamma^*$ fusion cross-sections.

The author verified the approach by continuum calculation in quantum electrodynamics and scalar quantum electrodynamics, providing various benchmark points for the further lattice QCD evaluations.

3. Volodymyr Biloshytskyi, Vladimir Pascalutsa, Lucian Harland-Lang, Bogdan Malaescu, Kristof Schmieden and Matthias Schott, *Two-photon decay of X(6900) from light-by-light scattering at the LHC*,
Phys.Rev.D 106 (2022) 11, L111902 [hep-ph/2207.13623]

   Possibly a first fully charmed tetraquark state $X(6900)$, observed in di-J/ψ mass spectrum at the LHC, is investigated for its decay into two photons. The corresponding branching ratio is estimated using the vector-meson dominance model and also extracted from the recorded LHC data for the light-by-light scattering in ultraperipheral Pb-Pb collisions by fitting $X(6900)$ into this process.

   All calculations, figures and the initial paper draft were completed by the author.

4. Igor Danilkin, Volodymyr Biloshytskyi, Xiu-Lei Ren, Marc Vanderhaeghen, *Analytical dispersive parameterization for elastic scattering of spinless particles*,
Phys.Rev.D 107 (2023) 7, 074021 [hep-ph/2206.15223]

   This paper introduces an improved parametrization of elastic spinless particle scattering based on a dispersive representation for the inverse scattering amplitude. Incorporating the dispersion relation significantly constrains the form of the inverse amplitude, addressing limitations in existing approaches by properly including the left-hand cut through a conformal variable expansion. The resulting compact analytic expressions ensure correct Adler zero and threshold behavior for $J > 0$, offering a robust tool for analyzing lattice quantum chromodynamics data in the elastic region.

   The author carried out the calculations, accompanied by uncertainty estimates using the bootstrap technique. The analysis included extraction of the resonance pole parameters and the chiral extrapolation of the Adler zero position, which is illustrated by corresponding figures in the text.

Conference proceedings

1. Volodymyr Biloshytskyi, Igor Danilkin, Xiu-Lei Ren, Marc Vanderhaeghen, *Analytical dispersive parameterization for S-wave $\pi\pi$ and πK scattering*,
   [hep-ph/2302.08443]

2. Volodymyr Biloshytskyi, Vladimir Pascalutsa, Lucian Harland-Lang, Bogdan Malaescu, Kristof Schmieden and Matthias Schott, *Two-photon decay of fully-charmed tetraquarks from light-by-light scattering at the LHC*,
   EPJ Web Conf. 274 (2022) 06007 [hep-ph/2211.10266]

Unless otherwise noted, figures in this thesis were created by the author. Feynman diagrams were generated using JaxoDraw [1], while other figures were created with Mathematica [2], ROOT [3] or Adobe Illustrator [4]. Analytic calculations were primarily performed using Mathematica, utilizing Package-X [5, 6] or LoopTools [7] for one-loop calculations. The complicated tensor calculations were executed using FORM [8]. The text corrections and the hardcover picture were made using ChatGPT [9].

Table of contents

Chapter 1

Introduction

1.1 Theory of strong interactions

The strong force is one of the four fundamental forces in nature, alongside gravity, electromagnetism, and the weak force. It is responsible for forming protons, neutrons, and other hadrons, as well as holding these nucleons together within atomic nuclei. Being the most powerful of the interactions at the subatomic scale, the strong force presents significant complexities in theoretical analysis due to its unique properties.

The journey toward the theory of strong interactions began in 1930's, prominently with H. Yukawa's theory of mesons as carriers of the strong force between nucleons [10]. The Yukawa potential $V(r)$,

$$V(r) = -\frac{g^2}{4\pi}\frac{e^{-m_\pi r}}{r}, \tag{1.1}$$

where m_π is a Yukawa meson (pion) mass, r is the distance between nucleons and g is the coupling constant, correctly captured the short-range behavior of the nuclear force, rapidly decreasing beyond the scale of ~ 1 fm. The mesons were discovered in 1947, which earned Yukawa the Nobel Prize in 1949. By the 1950s and 1960s, cosmic ray studies and particle accelerators had uncovered a plethora of hadrons, leading to the so-called "particle zoo". The observed variety of hadronic states suggested an underlying structure to these particles. In 1953, to explain the behavior of these new particles, M. Gell-Mann introduced the concept of "strangeness" [11] – the quantum number that is conserved in strong, but not weak interactions. The empirical relation of the strangeness S with electric charge Q, third component of isospin I_3 and baryon number B was reflected by the Gell-Mann-Nishijima formula [12, 13]:

$$Q = I_3 + \frac{B+S}{2}. \tag{1.2}$$

This finding subsequently resulted in the eightfold way – an organization scheme for hadrons according to representations of the $SU(3)$ symmetry group - discovered by M. Gell-Mann [14] and independently

by Y. Ne'eman [15]. Specifically, it was shown that the discovered particles follow an octet (mesons and baryons) and a decuplet (baryons) representations of $SU(3)$ group.

A major breakthrough came in 1964 when M. Gell-Mann [16] and G. Zweig [17] independently proposed the quark model, introducing quarks as elementary building blocks for hadrons. Further developments of this idea, supplemented with the idea of color charge to resolve issues with the Pauli exclusion principle [18, 19], lead to successful categorization of all known hadrons and predicted the existence of new particles.

During the same period, quantum field theory (QFT) faced significant challenges. Prominent physicists such as L. Landau pointed out inconsistencies in the theory, particularly the problem of the "Landau pole" or "zero-charge problem". Landau and his colleagues showed that in quantum electrodynamics (QED), the effective charge of the electron increases with energy, potentially becoming infinite at a finite energy scale – a phenomenon suggesting the breakdown of the theory [20–22]. The issue was particularly severe for strong interactions, where the coupling constant was large. This led to a widespread belief in the 1950s and early 1960s that QFT might be fundamentally flawed, a sentiment sometimes referred to as the "death of QFT".

In response to these challenges, some physicists turned to alternative approaches. The S-matrix theory, proposed by W. Heisenberg in the late 1940s and further developed in the 1960s by G. Chew, S. Mandelstam, S. Frautschi, V. Gribov and others. It was focused on the observable quantities in particle interactions without relying on unobservable intermediate states, thus avoiding the problematic concepts of QFT. The S-matrix theory emphasized principles such as analyticity, relativity, unitarity, and crossing symmetry to constrain the scattering amplitudes. While it provided valuable insights and tools, e.g. giving the birth to the string theory, it lacked predictive power without additional inputs and could not fully explain the underlying dynamics of strong interactions.

Parallel to these developments the deep inelastic scattering experiments were carried out at SLAC [23], and were successfully explained by R. Feynman with a parton model [24]. In this model, protons and neutrons are composed of point-like partons. The parton model laid the ground for understanding the internal structure of hadrons and has later been reconciled with the quark model. The identification of partons with quarks and gluons became clear with the development of Quantum Chromodynamics (QCD), integrating the parton model into the QCD framework. H. Fritzsch, M. Gell-Mann, and H. Leutwyler were instrumental in developing QCD as the theory of strong interactions [25].

The classical QCD Lagrangian is based on $SU(3)_c$ color group and is given by:

$$\mathcal{L}_{\text{QCD}} = \sum_{f=1}^{N_f} \bar{\psi}_{j,f} \left(i\gamma^\mu \left[D_\mu \right]_{jk} - m_f \delta_{jk} \right) \psi_{k,f} - \frac{1}{4} \sum_{a=1}^{N_c^2-1} G^a_{\mu\nu} G^{a,\mu\nu}, \tag{1.3}$$

where $\psi_{j,f}$ represents the quark field of color j, flavor f, mass m_f and belongs to the fundamental representation of the $SU(3)$ group. The color index runs over three colors ($N_c = 3$): red, green, blue. The mass term is diagonal in colors, being proportional to the Kronecker symbol δ_{jk}. The sum over f runs over six quark flavors ($N_f = 6$), which are up, down, strange, charm, bottom and top. The

covariant derivative $\left[D_\mu\right]_{jk}$ is defined as:

$$\left[D_\mu\right]_{jk} = \delta_{jk}\partial_\mu - ig_s\left[T^a\right]_{jk}A^a_\mu, \tag{1.4}$$

with g_s being the strong coupling constant, T^a are the $a = 8$ generators of the $SU(3)$ color group satisfying the commutation relations:

$$[T^a, T^b] = if^{abc}T^c, \tag{1.5}$$

and A^a_μ are the gluon fields, which belong to the adjoint representation of $SU(3)$ group. The gluon field strength tensor $G^a_{\mu\nu}$ is given by:

$$G^a_{\mu\nu} = \partial_\mu A^a_\nu - \partial_\nu A^a_\mu + g_s f^{abc}A^b_\mu A^c_\nu, \tag{1.6}$$

where f^{abc} are the structure constants of the $SU(3)$ group.

One of the most important properties of QCD as a field theory is its *renormalizability*, which was proven by G. 't Hooft and M. Veltman [26, 27]. This became possible after Faddeev and Popov formulated the proper quantization procedure for Yang-Mills theories [28], introducing ghost fields through the functional integral. According to their procedure, the following Lagrangian terms should supplement Eq. (1.3): the gauge-fixing term, $\mathcal{L}_{\text{gauge}}$, and ghost term, $\mathcal{L}_{\text{ghost}}$, which are given by

$$\mathcal{L}_{\text{gauge}} = \frac{1}{2\xi}(\partial^\mu A^a_\mu)^2, \tag{1.7}$$

$$\mathcal{L}_{\text{ghost}} = \partial_\mu\eta^\dagger_a\left([D^\mu]_{ab}\eta_b\right). \tag{1.8}$$

Here ξ is a gauge-fixing parameter for the class of covariant gauges, and η_a is a complex scalar anticommutative field.

Another remarkable property of QCD is *asymptotic freedom*, which means the interaction between quarks becomes weaker at higher energies or shorter distances. This phenomenon was independently discovered by D. Gross and F. Wilczek [29], and H. D. Politzer [30] in 1973, resolving the "zero-charge problem" highlighted by L. Landau and others. The running of the strong coupling constant $g_s(\mu) \equiv \sqrt{4\pi\alpha_s(\mu)}$ with the energy scale μ is governed by the renormalization group equation:

$$\mu^2\frac{d\alpha_s}{d\mu^2} = \beta(\alpha_s), \tag{1.9}$$

where the beta function $\beta(\alpha_s)$ at one-loop level is:

$$\beta(\alpha_s) = -\frac{\alpha_s^2}{12\pi}\left(11C_A - 2n_f\right). \tag{1.10}$$

Here C_A is the Casimir invariant of the adjoint representation of the gauge group (for $SU(3)$ in QCD, $C_A = 3$) and n_f is the number of active quark flavors. Since $11 - \frac{2}{3}n_f > 0$ for $n_f < 16.5$, the beta

function is negative, leading to a decrease of g_s with increasing μ. Integrating the renormalization group equation yields:

$$\alpha_s(\mu) = \frac{1}{b_0 \log(\mu^2/\Lambda^2_{\text{QCD}})}, \tag{1.11}$$

where $b_0 = (11 - 2n_f/3)/(4\pi)$ and Λ_{QCD} is the QCD scale parameter, which is of order 200 MeV. This parameter appears due to the violation of the scale invariance induced by quantum correction, known as "dimensional transmutation". The asymptotic freedom explains the success of the parton model in deep inelastic scattering experiments, where quarks behave as free particles at high energies.

Despite the success of perturbative QCD at high energies, where the coupling constant is small and perturbation theory is applicable, understanding QCD in the non-perturbative regime remains a significant challenge. At low energies, the coupling constant becomes large, rendering perturbative methods ineffective. This non-perturbative regime of Quantum Chromodynamics (QCD) is crucial for explaining phenomena such as quark confinement—the fact that quarks have never been observed in isolation—and the generation of hadron masses. For the proton, for instance, only about 1% of its mass is explained by the Higgs mechanism, while the remaining 99% arises primarily from the binding energy of the strong nuclear force, mediated by gluons, which confines quarks within hadrons.

To address these challenges, non-perturbative methods have been developed. One such approach is *Lattice QCD*, proposed by K. Wilson in 1974 [31]. Lattice QCD discretizes Euclidean spacetime into a finite grid or lattice, allowing numerical simulations of QCD processes using Monte Carlo methods. The gauge fields are represented by link variables $U_\mu(x) = e^{iag_s A_\mu(x)}$, where a is the lattice spacing. The Wilson action for pure gauge fields is given by:

$$S_{\text{G}} = \beta \sum_{\text{plaquettes}} \left(1 - \frac{1}{N_c} \text{Re Tr}\, U_{\mu\nu}(x)\right), \tag{1.12}$$

where $\beta = 2N_c/g_s^2$, N_c is the number of colors, and $U_{\mu\nu}(x)$ is the plaquette operator defined as:

$$U_{\mu\nu}(x) = U_\mu(x) U_\nu(x + \hat{\mu}a) U^\dagger_\mu(x + \hat{\nu}a) U^\dagger_\nu(x). \tag{1.13}$$

For fermions, discretization introduces challenges such as fermion doubling and chiral symmetry breaking. Various formulations, such as Wilson fermions, Kogut-Susskind staggered fermions, and domain wall fermions, have been developed to address these issues. Expectation values of observables are computed using Monte Carlo methods:

$$\langle O \rangle = \frac{1}{Z} \int \mathcal{D}U \mathcal{D}\psi \mathcal{D}\bar{\psi}\, O\, e^{-S_{\text{lat}}}, \tag{1.14}$$

with Z being the partition function. Gauge field configurations are generated according to the probability distribution $e^{-S_{\text{lat}}}$. Lattice QCD has become an indispensable tool for studying non-perturbative aspects of QCD from first principles. It has been instrumental in calculating hadron masses, decay constants and form factors, providing results that are in remarkable agreement with

experimental data. For instance, the hadron spectrum computed in lattice QCD closely matches the observed masses of low-lying mesons and baryons [32].

Another remarkable approach to tackling the non-perturbative regime of QCD at low energy is *Chiral Perturbation Theory* (χPT). This effective field theory works at the level of hadrons, the actual degrees of freedom at low energies, rather than quarks and gluons. Its development is grounded on S. Weinberg's idea, which he provided in the seminal paper "Phenomenological lagrangians" [33]:

> *"If one writes down the most general possible Lagrangian, including all terms consistent with assumed symmetry principles, and then calculates matrix elements with this Lagrangian to any given order of perturbation theory, the result will simply be the most general possible S-matrix consistent with analyticity, perturbative unitarity, cluster decomposition and the assumed symmetry principles."*

The χPT systematically describes the interactions of the pseudo-Goldstone bosons resulting from the spontaneous breaking of chiral symmetry in QCD [33–36]. It exploits the approximate chiral symmetry of QCD for light quarks (up, down, and strange) and provides a systematic expansion in powers of momenta and quark masses over the chiral symmetry breaking scale $\Lambda_\chi \sim 1$ GeV. This scale is usually associated either with the ρ-meson mass, $m_\rho \approx 770$ MeV or with the χPT scale of spontaneous chiral symmetry breaking $4\pi f_\pi \approx 1160$ MeV. The χPT has been extremely successful in describing low-energy hadronic processes such as pion-pion scattering [37], meson-nucleon interactions [38], also including the electromagnetic interactions [39], and even applied to few-nucleon systems and nuclear physics, bridging the gap between QCD and nuclear phenomenology.

Although χPT and lattice QCD have significantly advanced our understanding of low-energy strong interactions, they do not cover the entire non-perturbative domain of QCD. χPT, as an effective field theory, is primarily applicable at energies well below the chiral symmetry breaking scale, and its perturbative expansion may converge slowly, requiring higher-order terms and introducing numerous low-energy constants that must be determined experimentally or through lattice QCD. The latter, while offering a first-principles approach, faces computational limitations such as finite lattice spacing, finite volume effects, and challenges in simulating real-time dynamics. In these cases, traditional S-matrix methods become invaluable. Specifically, dispersion relations offer model-independent connections between different observables by exploiting the analytic properties of scattering amplitudes. These relations lead to integral equations known as sum rules.

Sum rules are particularly powerful tools because they provide a data-driven determination of physical quantities without relying on specific theoretical models. Typically, they connect certain physical observables with the integrals of another measurable quantities, e.g. scattering cross-sections. This allows one to extract fundamental parameters directly from experimental data and serves as a crucial test for theoretical models, which must satisfy these sum rules to be consistent with basic physical principles. A classic example is the Gerasimov-Drell-Hearn (GDH) sum rule, which connects the anomalous magnetic moment (AMM) of a particle to an integral over its spin-dependent photoabsorption cross-sections. This sum rule offers a stringent test for models of nucleon structure

and provides deep insights into the spin dynamics of the nucleon. Another important example is the Cottingham sum rule, which estimates the electromagnetic contribution to the proton-neutron mass difference by relating it to the nucleon's forward virtual Compton scattering amplitude.

The present work employs all listed non-perturbative methods to evaluate certain hadronic contributions. In particular, the dispersive methods are applied, sometimes in combination with χPT, to make either standalone prediction or provide a support to the lattice QCD evaluations. The apparent diversity of covered topics, such as exotic hadrons, light-by-light scattering, muon AMM, hadron polarizabilities and atomic spectroscopy, demonstrates the power and flexibility of the used framework.

In what follows, brief introductory remarks on each of the covered topics are given.

1.2 Exotic hadrons

Over the past few decades, our understanding of strong interactions has been significantly deepened by remarkable advancements in the field of hadron spectroscopy. Traditionally, hadrons—particles composed of quarks and gluons bound together by the strong force—have been classified within the quark model as either mesons, consisting of a quark and an antiquark, or baryons, comprising three quarks. However, experimental observations, e.g. [40–43], suggest the existence of "exotic" hadrons that do not fit neatly into this conventional classification, prompting a re-examination of the fundamental principles governing hadronic matter.

Exotic states are hadronic particles whose quark configurations extend beyond the traditional quark-antiquark or three-quark models. These states include tetraquarks, which consist of two quarks and two antiquarks; pentaquarks, comprising four quarks and one antiquark or vice versa; hybrid mesons, containing a quark-antiquark pair with an excited gluonic field; and glueballs, which are bound states of gluons without valence quarks.

The lightest examples of exotic states are the $f_0(500)$ (or σ) resonance observed in pion-pion scattering and the $K_0^*(700)$ (or κ) resonance observed in pion-kaon scattering. The existence of these resonances was a subject of debate for many years due to their broad widths and the complexities involved in disentangling them from background processes. However, a precise dispersive analysis of $\pi\pi$ [44–49, 37] and πK [50–53] scattering data applying Roy (or Roy-Steiner) equations [54] complemented by recent lattice QCD studies [55–65] have confirmed the existence of these resonances, strongly supporting the idea of their tetraquark nature.

A proper determination of resonance parameters requires the search for poles in the complex plane of the scattering amplitude. This is particularly important when there is an interplay between several inelastic channels or when the pole lies very deep in the complex plane. For this purpose, various complicated dispersive techniques have been developed, notably the aforementioned Roy equations and the N/D approach [66]. They are designed to provide the correct analytic continuation of the amplitude, driven by the fundamental constraints of the S-matrix. However, in practical applications, the rigorous implementation of these methods is almost impossible, since it requires either experimental knowledge of all partial waves with different isospin in the direct and crossed

channels (Roy equations) or knowing the scattering amplitude in unphysical region (left-hand cut in N/D method). Moreover, these methods require solving (a system of) integral equations. However, since some of the resonances are connected almost exclusively to the elastic channels (especially in the lattice calculations with unphysically-large masses for light quarks), it is not always necessary to solve the dispersive integral equation for the direct amplitude. Therefore one often uses very simplistic parametrizations of the scattering amplitude, which usually ignoring crossing and even analyticity constraints. This brings a significant systematic uncertainty to the extracted resonance parameters (see, e.g. [58]). In Chapter 3, we propose an improved, but still simple parametrization of the single-channel scattering amplitude for spinless particles, while satisfying as much of the S-matrix constraints as possible. This parametrization may be particularly useful for the analysis of lattice data.

Another way to investigate the properties of exotic states is to search for them in specific reactions. One such reaction is the light-by-light (LbL) scattering of quasi-real photons, which was recently observed at the Large Hadron Collider (LHC). The experimental results and theoretical status of this reaction are briefly reviewed in the following section.

1.3 LbL scattering at LHC

The scattering of light by light is essentially a quantum process, which cannot be deduced from classical electrodynamics. Given that the cross section of this process is suppressed by a factor $\alpha_{\text{em}}^4 \approx 2.8 \times 10^{-9}$, the direct observation of such a scattering process is an extremely challenging task. Indeed, even the most powerful modern lasers still cannot provide the intensity required for the observation of LbL scattering. Nevertheless, there are several ways to measure this process indirectly. Currently, the most accessible one is based on ultraperipheral heavy-ion collisions. It involves the collision of two charged ions at a sufficiently large impact parameter, which should be greater than the ion diameter. At such a large impact parameter, the ions do not interact strongly, but mostly through the electromagnetic field, which in this case can be represented as a flux of quasireal photons emitted by the ions. The virtuality Q^2 of such photons is smaller than the inverse charge radius of the ion R, i.e., $Q^2 < R^{-1}$. Typically, $Q^2 < 10^{-3}$ GeV^2, hence the flux of these photons can be safely considered in the equivalent-photon approximation (see, e.g., [67–69]). The quasireal photons, emitted by the colliding ions, do scatter, so one can detect the two-photon pair in the final state. The process of $\gamma\gamma \to \gamma\gamma$ scattering is then described by the exclusive LbL cross section $\sigma_{\text{LbL}}^{\text{excl.}}$, which corresponds to the scattering process depicted in Fig. 1.1. This cross section can be expressed via the elementary LbL cross section convoluted with the spectra of equivalent photons [70]:

$$\sigma_{\text{LbL}}^{\text{excl.}} = \sigma\left(AB \xrightarrow{\gamma\gamma} A\gamma\gamma B\right) = \int \frac{d\omega_A}{\omega_A}\frac{d\omega_B}{\omega_B} f_{\gamma/A}(\omega_A) f_{\gamma/B}(\omega_B) \sigma_{\gamma\gamma\to\gamma\gamma}\left(\sqrt{s_{\gamma\gamma}}\right). \tag{1.15}$$

Here $f_{\gamma/A}$ and $f_{\gamma/B}$ are the fluxes of equivalent photons with energies ω_A and ω_B emitted by the ions A and B. The key idea of this method is manifested in the heavy-ion collisions, where the two-photon

flux obtains an extremely large enhancement factor proportional to Z^4, where Z is a charge number of the interacting ion. Indeed, for the fully ionized Pb-Pb collisions this factor reads $82^4 \approx 4.5 \times 10^7$.

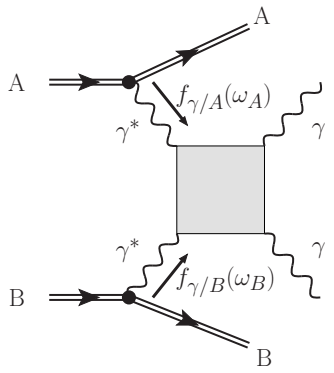

Fig. 1.1 The ultraperipheral heavy-ion collision with initiated LbL scattering.

The idea of measuring LbL scattering at the LHC was first proposed by d'Enterria and Silveira [70] in 2013, who also provided theoretical estimates of the exclusive LbL cross sections for several colliding nuclei: proton-proton, proton-lead, and lead-lead. By virtue of the Z^4 enhancement and controllable background, only the latter reaction was argued to allow for an unambiguous observation of LbL scattering.

Since 2017, experimental evidence for light-by-light (LbL) scattering at the LHC has been reported by both the ATLAS [71–73] and CMS [74] Collaborations using data from Pb-Pb collisions. In 2020, ATLAS performed a combined analysis of the previously collected data, increasing the integrated luminosity. The remarkable feature of this analysis is that the unfolding procedure was performed, and the differential fiducial cross sections of LbL scattering were obtained for the first time. The corresponding distributions with respect to the diphoton mass $m_{\gamma\gamma}$, absolute diphoton rapidity $|y_{\gamma\gamma}|$, averaged photon transverse momentum $(p_{\mathrm{T}}^{\gamma_1} + p_{\mathrm{T}}^{\gamma_2})/2$, and the absolute cosine of the diphoton scattering angle in the c.o.m. frame $|\cos(\theta^\star)|$ are shown in Fig. 1.2. The integrated fiducial cross section, $\sigma_{\mathrm{fid.}}^{\mathrm{LbL}}(\mathrm{Exp})$, compared to the various theoretical predictions, $\sigma_{\mathrm{fid.}}^{\mathrm{LbL}}(\mathrm{Theo})$, amounts to

$$\sigma_{\mathrm{fid.}}^{\mathrm{LbL}}(\mathrm{ATLAS}) = 120 \pm 17\,(\mathrm{stat.}) \pm 13\,(\mathrm{syst.}) \pm 4\,(\mathrm{luminosity})\ \mathrm{nb}, \quad [73] \tag{1.16a}$$

$$\sigma_{\mathrm{fid.}}^{\mathrm{LbL}}(\mathrm{Theo}) = \begin{cases} 80 \pm 8\ \mathrm{nb}, & [75] \\ 78 \pm 8\ \mathrm{nb}, & [76,\ 77] \end{cases} \tag{1.16b}$$

Thus, the agreement between measured and predicted values was established only within two standard deviations of the experimental result.

Given that the electromagnetic and weak contributions to real LbL are described by perturbative diagrams with sufficiently high precision, the discrepancy may stem from the hadronic contributions. Moreover, the discrepancy appears to be well beyond the leading-order (LO) pQCD contribution from quark loops, used for theoretical predictions in Refs. [75] and [76, 77], which cannot be explained by

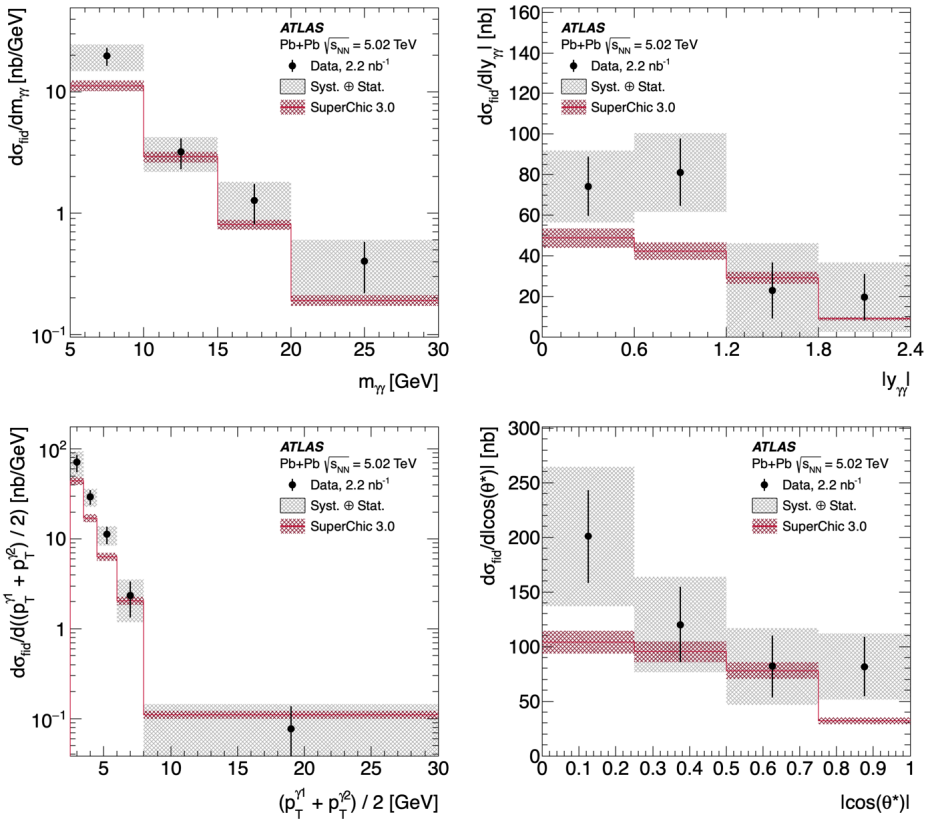

Fig. 1.2 Differential fiducial cross sections of the exclusive LbL scattering measured by ATLAS [73] at the LHC. Figures are taken from HepData [78].

the next-to-leading-order (NLO) pQCD corrections [79]. This fact hints towards the strong effect of non-perturbative QCD, which is of high interest and may be useful for hadronic spectroscopy in context of the recently observed resonance structures in di-J/ψ mass spectrum [80–82]. Indeed, since the production of vector states is forbidden in photon-photon fusion due to the Landau-Yang theorem, the real LbL scattering may serve as a filter for exotic resonances with certain quantum numbers, provided that the hadronic background is known with sufficient precision. Moreover, since the real LbL scattering serves as an important reference point for the calculation of hadronic effects in the muon AMM, having a correct model of the hadronic contributions at low and intermediate two-photon energies will be of great interest.

1.4 Anomalous magnetic moment of the muon

The AMM of the muon is one of the most precisely measured physical observables, already at the parts per million (ppm) level, which provides a stringent test of the SM. A discrepancy between measured and theoretically predicted values could be an indication of physics beyond the SM, such

as supersymmetry, dark photons, or leptoquarks [83]. Reducing the theoretical uncertainties of the hadronic contribution to the SM predictions is essential for interpreting this anomaly.

The AMM is a fundamental parameter that quantifies the deviation of a spin-1/2 particle's magnetic dipole moment, $\vec{\mu}$, from the value predicted by Dirac's theory for a point-like particle. In Dirac theory, the gyromagnetic ratio g is exactly 2, leading to a magnetic moment

$$\vec{\mu} = g\frac{q}{2m}\vec{\jmath}, \tag{1.17}$$

where q is the particle's charge, m is its mass, and $\vec{\jmath}$ is the spin vector of the particle. Quantum loop effects introduce corrections, causing g to differ slightly from 2. Thus, it is convenient to define the AMM as:

$$\varkappa = \frac{g-2}{2}. \tag{1.18}$$

A contribution to the AMM originating from a heavy particle with mass M, scales as [84]

$$\varkappa \sim \frac{m^2}{M^2}. \tag{1.19}$$

Therefore, the AMM of the muon is $m_\mu^2/m_e^2 \approx 43\times10^3$ times more sensitive to heavy-particle contributions than the AMM of electron. Hence, the precise measurement of the muon AMM provides a unique opportunity to examine the SM. Any significant deviation from the SM prediction, if detected, is a signal for new physics.

From the 1950's, a number of measuremets of the muon AMM have been carried out with progressively enhanced accuracy. Currently, the most precise measurement is by the E989 experiment at the Fermilab National Accelerator Laboratory (FNAL), which aims to reach the final precision of 140 ppb. This would be a factor of four improvement compared to the previous result, which has been achieved at the Brookhaven National Laboratory (BNL) during the E821 experiment [85]. Recently, the Fermilab reported their results having processed the data collected in runs 1-3 [86] and averaged them with the BNL value:

$$\varkappa_\mu(\text{BNL}) = 116592080(63)\times10^{-11}\,(0.54\,\text{ppm}), \tag{1.20a}$$

$$\varkappa_\mu(\text{FNAL run1/2/3}) = 116592055(24)\times10^{-11}\,(0.20\,\text{ppm}), \tag{1.20b}$$

$$\varkappa_\mu(\text{Exp, averaged}) = 116592059(22)\times10^{-11}\,(0.19\,\text{ppm}). \tag{1.20c}$$

As one can see, the FNAL measurement agrees with BNL within the uncertainty, and the averaging with BNL provides us with experimental knowledge of the muon AMM with the 0.19 ppm precision. To achieve the same level of precision on the theory side, the Muon $(g-2)$ Theory Initiative was established to comprehensively assess all aspects of the SM and provide a unified reference value for comparing with experimental results. In 2020, the Theory Initiative published the first White Paper (WP) [87], reflecting the contributions of numerous authors. The provided consensus for the

theoretical value of the muon AMM was

$$\varkappa_\mu(\mathrm{WP}) = 116591810(43)\times 10^{-11}\,(0.37\,\mathrm{ppm}). \tag{1.21}$$

As one can immediately see, this value is still more uncertain than the experimental FNAL result. Thus, reducing the theoretical uncertainty is a primary goal, which the Muon $(g-2)$ Theory Initiative community is intensively working on for the last five years.

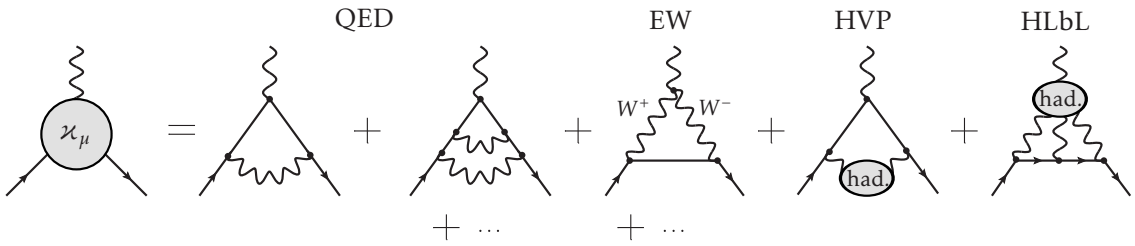

Fig. 1.3 The leading term and various contributions to the muon AMM: QED, electroweak (EW) and hadronic corrections (HVP and HLbL). The hadronic blobs represent the contribution from QCD alone.

For theoretical evaluations of the muon AMM, it is convenient to consider separately the contributions from QED, electroweak and hadronic physics, as schematically shown in Fig. 1.3. Let us briefly review the status of each of them.

QED The QED corrections to $\varkappa_\mu$ can be conveniently expressed as a series in α_{em}:

$$\varkappa_\mu(\mathrm{QED}) = \sum_{\ell=1}^{\infty}\left(\frac{\alpha_{\mathrm{em}}}{\pi}\right)^{\ell} a_\mu^{(2\ell)}, \tag{1.22}$$

where each of the coefficients $a_\mu^{(2\ell)}$ can be splitted according to the muon, electron and tau mass dependence as

$$a_\mu^{(2\ell)} = A_1^{(2\ell)} + A_2^{(2\ell)}\left(m_e/m_\mu\right) + A_2^{(2\ell)}\left(m_e/m_\tau\right) + A_3^{(2\ell)}\left(m_e/m_\mu, m_e/m_\tau\right). \tag{1.23}$$

The index ℓ thus indicates the number of loops in the diagrams, which are needed to evaluate for each term. The first term, $\ell = 1$, gives the LO contribution to $\varkappa_\mu$, which comes from the one-loop vertex graph (the first one on the r.h.s. of Fig 1.3) yielding the celebrated "Schwinger term" $\alpha_{\mathrm{em}}/2\pi$. However, to reach the sub-ppm accuracy, one needs to know all contributions up to $\ell = 5$. This was done numerically by Aoyama, Hayakawa, Kinoshita and Nio [88]. The total result depends on the value of α_{em}, extracted either from atomic spectroscopy measurement in Rb atoms or from the measurement of the electron AMM $\varkappa_e$:

$$\varkappa_\mu(\mathrm{QED}) = 10^{-11}\times\begin{cases} 116584718.951(80) & \alpha_{\mathrm{em}}\,\text{from Rb}, \\ 116584718.846(37) & \alpha_{\mathrm{em}}\,\text{from}\,\varkappa_e. \end{cases} \tag{1.24}$$

The term $A_1^{(10)}$ was subsequently cross-checked by Volkov [89, 90], who found a small mistake. The corresponding inaccuracy, however, is far below the leading uncertainty of the total SM result for $\varkappa_\mu$.

Electroweak The LO contributions, discussed in Section 6.4 of Chapter 6, originate from the one-loop graphs with Z^0, $W^\pm$ and Higgs bosons. They were obtained already in the 1970's. The full two-loop NLO contribution was obtained in [91, 92] and more recently it was cross-checked numerically by [93]. The final result, quoted in the WP, is

$$\varkappa_\mu(\mathrm{EW}) = 153.6(1.0)\times 10^{-11}. \tag{1.25}$$

Hadronic Due to the non-perturbative nature of the strong interactions, this contribution is the main source of theoretical uncertainty. For the sake of conveniece, it is divided into the hadronic vacuum polarization (HVP) and the hadronic light-by-light (HLbL) contributions. Despite the latter being around two orders of magnitude smaller than the HVP contribution, it is much more involved for theoretical calculations. In order to resolve non-perturbative QCD effects in these contributions, dispersive and/or lattice QCD techniques are widely invoked. As of 2020, the hadronic contributions, quoted in the WP, were

$$\varkappa_\mu(\mathrm{HVP}) = 6845(40)\times 10^{-11}, \tag{1.26a}$$
$$\varkappa_\mu(\mathrm{HLbL}) = 92(18)\times 10^{-11}. \tag{1.26b}$$

Although the relative uncertainty of the HLbL contribution is larger than that of the HVP contribution, the latter has larger absolute uncertainty. Therefore reducing the HVP uncertainty is nowadays the most important task for the theoretical community.

As a significant part of the present work is dedicated to both HVP and HLbL contributions to the muon AMM, let us provide more details in what follows.

1.4.1 Hadronic contributions to muon AMM

A precise phenomenological evaluation of LO HVP [94–101] mainly relies on the dispersive data-driven approach that can be concisely expressed via the well-known formula [102, 84]:

$$a_\mu^{\mathrm{HVP\,LO}} = \left(\frac{\alpha_{\mathrm{em}} m_\mu^2}{3\pi}\right)^2 \int_{s_{\mathrm{th}}}^{\infty} \frac{ds}{s^2} R_{\mathrm{had}}(s) K(s). \tag{1.27}$$

Here $R(s)$ is the ratio of the experimentally measured cross-section $\sigma(e^+e^- \to \text{hadrons})$ to $\sigma(e^+e^- \to \mu^+\mu^-)$,

$$R_{\mathrm{had}}(s) = \frac{3s}{4\pi\alpha_{\mathrm{em}}^2}\sigma(e^+e^- \to \text{hadrons}), \tag{1.28}$$

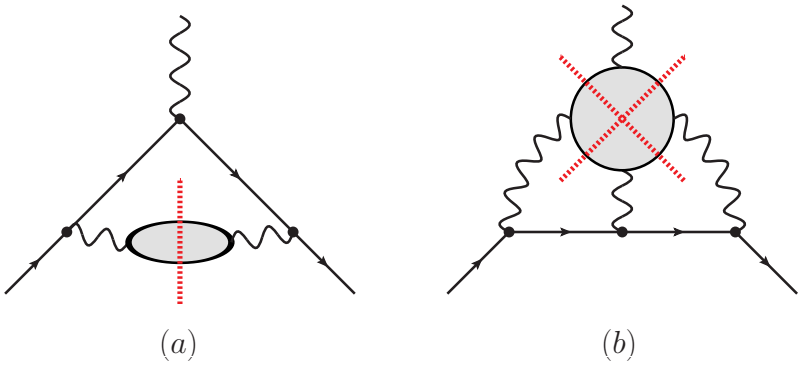

Fig. 1.4 Hadronic contributions to the muon AMM with dispersive cuts through hadronic blobs: HVP (a) and HLbL (b).

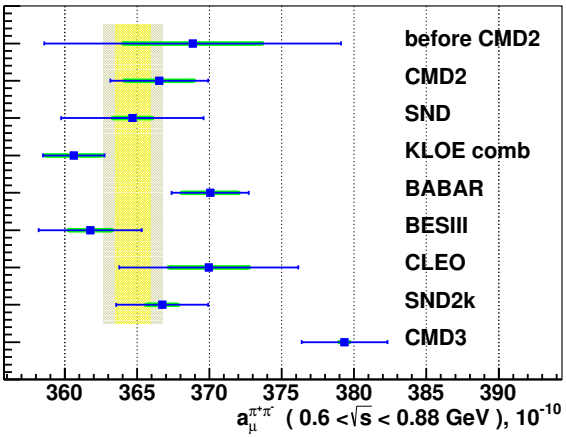

Fig. 1.5 The $\pi^+\pi^-$ contribution to the κ_μ (denoted as $a_\mu^{\pi^+\pi^-}$ from the energy range $0.6 < \sqrt{s} < 0.88$ GeV obtained from the CMD-3 data and other experiments. Figure is taken from [113].

and $K(s)$ is a known kernel function

$$K(s) = \frac{3s}{m_\mu^4} \int_0^1 dx \frac{x^2(1-x)}{x^2 + \frac{s}{m_\mu^2}(1-x)}. \tag{1.29}$$

The formula (1.27) corresponds to the cut through the HVP blob shown in Fig. 1.4 (a). While the lowest hadroproduction threshold s_{th} in Eq. (1.27) corresponds to $\pi^0\gamma$ production, $s_{\text{th}} = m_{\pi^0}^2$, the main contribuiton originates from $\pi^+\pi^-$ channel. During the past two decades, this particular contribution has been measured by several collaborations: CMD-2 [103–105], SND [106], KLOE [107, 108], BaBar [109], BESIII [110], CLEO [111] and very recently CMD-3 [112, 113]. The corresponding contributions to the muon AMM are shown in Fig. 1.5 [113]. It is clearly seen that the CMD-3 result significantly deviates from all the previous results, whose average is depicted by the yellow band (the gray band includes additional uncertainty inflation due to the KLOE/BaBar tension). The difference

amounts to around 5σ. Taken alone, the CMD-3 result reduces the discrepancy between the theoretical (1.21) and experimental (1.20) results for the AMM from approximately 4σ to 1.5σ. Unfortunately, the reason why the CMD-3 result differs so much from the results of previous measurements, is still unclear. Nevertheless, intensive work on the refinement of the contributions stemming from other channels is ongoing. Thus, once the tension between CMD-3 and the other measurements is resolved, a sub-percent uncertainty of the phenomenological HVP evaluation is expected to be achieved.

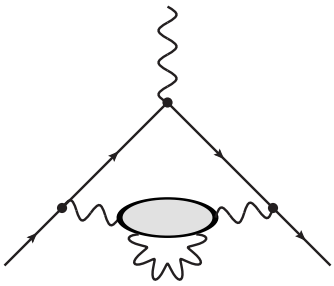

Fig. 1.6 Electromagnetic corrections to leading-order HVP.

Complementary to the dispersive data-driven approach, the HVP contribution has recently been determined in several precise lattice QCD calculations from intermediate hadronic distance scales [114–118, 101]. One of the lattice-QCD based calculations, done by the BMW Collaboration [115], has already reached a subpercent-level of precision for the full LO HVP contribution, thus becoming competitive with the data-driven dispersive approach. At this level of precision, care must also be taken of the leading isospin-breaking corrections, both the strong isospin-breaking effect stemming from the unequal u and d quark masses, and the e.m. effect arising from the quarks carrying electric charges, as shown in Fig. 1.6. These effects are taken into account by lattice collaborations (e.g., Ref. [114, 115, 119]); however, few stringent cross-checks are possible at present. First of all, these effects depend on the precise point in the parameter space of isospin-symmetric QCD, which is not exactly the same in different calculations. Furthermore, it has not been possible to rigorously compare the size of these effects to phenomenological predictions, partly because the (QED) radiative correction to the HVP is divergent if one does not account for the counterterms associated with the quark masses and the strong-coupling, whose finite parts depend on the conventional choice of the "physical point" in isospin-symmetric QCD [120]. A new method, leveraging a Cottingham-like formula and potentially addressing the listed issues, is proposed in Chapter 5.

The HLbL contribution is much more challenging than the HVP contribution due to the involved full four-point LbL hadronic tensor $\mathcal{M}^{\mu\nu\rho\lambda}$ with off-shell photons. A conventional phenomenological approach relies on the dispersive representation of the hadronic blob shown in Fig. 1.4 (b), embedded into the two-loop QED diagram. Thus, the contribution to the AMM can be expressed in terms of the hadronic tensor components $\mathcal{M}_i$ in some basis, which is free from kinematic singularities, integrated

with known QED kernels K_i [121–123]:

$$\varkappa_\mu^{\mathrm{HLbL}} = \frac{2\alpha_{\mathrm{em}}^3}{3\pi^2}\int_0^\infty dQ_1\int_0^\infty dQ_2\int_{-1}^1 d\tau\sqrt{1-\tau^2}Q_1^3Q_2^3\sum_i K_i(Q_1,Q_2,\tau)\mathcal{M}_i(Q_1,Q_2,\tau). \quad (1.30)$$

In this formula, Q_i denote space-like virtualities of internal photons, provided that $Q_3^2 = Q_1^2 + 2Q_1Q_2\tau + Q_2^2$. The components $\mathcal{M}_i$ can then be obtained applying, if possible, the data-driven dispersive analysis of the hadronic intermediate states or, if not possible, use phenomenological models and constraints from pQCD. Similar to the formula for HVP (1.27), the QED kernels in Eq. (1.30) suppress the high-energy contributions. Consequently, the leading contribution comes from the long-range π^0 exchange, i.e. π^0-pole contribution[1]. In order to describe the π^0-pole contribution, a sufficient experimental input would be the pion transition form factor for space-like photons, $F_{\pi^0\gamma^*\gamma^*}$. This form factor can be modelled [124], measured, e.g. at BESIII [125], or obtained from lattice QCD [126]. Besides the pion-pole, the further contributions come from η- and η'- poles and from $\pi^+\pi^-$ rescattering. These and other channels were extensively investigated in Refs. [127–137]. Along with the long-range contributions, driven by the resonance exchanges, important estimations of the short-distance constraints were carried out in Refs. [138–144].

The full HLbL contribution has already been evaluated on the lattice [145–147]. In particular, the recent evaluation by the Mainz group, where u, d and s quarks have been taken into account, amounts to [147]

$$\varkappa_\mu^{\mathrm{HLbL}}(\mathrm{Mainz}) = (109.6 \pm 15.9)\times 10^{-11}. \quad (1.31)$$

The obtained value agrees with phenomenological WP value (1.26b) within its uncertainty.

In view of the intensive development of the electron-muon scattering experiments, such as the forthcoming MUonE experiment [148], which aims for an independent determination of the HVP contribution, the Schwinger sum rule was proposed as an alternative approach suited for the evaluation of both: HVP and HLbL [149]. The idea relies on the precise measurement of the hadronic channels in polarized electron-muon scattering, which can be connected to $\varkappa_\mu$ via the Schwinger sum rule in a model-independent way. Several aspects of this approach are considered in Chapter 6.

1.5 Electromagnetic polarizabilities of hadrons and atomic spectroscopy

Another avenue of the precision frontier in hadron physics is atomic spectroscopy. The well-developed theory of the lightest hydrogen-like atoms allows for testing hadronic contributions with extremely high precision. A particularly important role is played by muonic hydrogen, where, due to the comparatively large muon mass, and, consequently, the distinctly small Bohr radius, hadronic effects are more pronounced than in ordinary hydrogen. One of the key fine-structure characteristics of the energy spectrum of hydrogen-like atom is the Lamb shift - the energy difference between the $2S_{1/2}$ and $2P_{1/2}$ states. This shift arises from quantum electrodynamic effects and is sensitive to the

[1]Due to the dispersive cut, the exchange particle goes on-shell in this framework, yielding just a pole contribution

proton's internal structure, making it a valuable probe for hadronic physics. In 2013, the CREMA Collaboration reported on the Lamb shift measurement in muonic hydrogen, which amounts [150]:

$$E^{\text{exp}}_{2\text{P}-2\text{S}}(\mu\text{H}) = 202.3706(23)_{\text{total}}\,\text{meV}. \tag{1.32}$$

To achieve the same precision in theoretical description of this quantity, one needs assess the hadronic contributions at the order $(Z\alpha_{\text{em}})^5$, where Z is the charge number of the atom (here $Z = 1$ for the proton). At this order, the nuclear polarizability effects start to play import role. The latter, in turn, are responsible for the leading uncertainty in the theoretical prediction. At the given order, the polarizability contribution can be conveniently described in terms of the forward two-photon exchange. However, it has been argued that the latter cannot be expressed in a fully data-driven fashion due to the necessity of a subtraction in the dispersion relations for the forward Compton amplitude. This subtraction introduces significant model dependence, which leads to a large uncertainty in the full contribution. Various estimates of the subtraction contribution in different models, which are then combined with the data-driven parts, are provided in Tab. 1 of [151] (see also [152] for the rôle of $\Delta(1232)$-resonance in the polarizability contribution). Among these, the most precise evaluation of two-photon exchange contribution is [153]:

$$E^{(2\gamma)}_{2\text{P}-2\text{S}} = (33 \pm 2)\,\mu\text{eV}. \tag{1.33}$$

Thus, in view of the forthcoming measurements of the Lamb shift in muonic hydrogen at PSI, which will increase the precision by a factor of five, a significant refinement of the theoretical description is highly needed.

In this work, we propose a method to construct a fully data-driven approach for the two-photon exchange contribution to the Lamb shift. This approach became feasible after revisiting a dispersion relation for the Compton scattering amplitude of longitudinally-polarized photons. If convergent, this dispersion relation will define the subtraction contribution in terms of the measurable longitudinal structure function, which is explained in detail in Chapter 7.

The convergence of this dispersion relation implies the convergence of the sum rule for the static electric dipole polarizability, known as the Bernabéu-Tarrach sum rule [154, 155]. When combined with the well-established Baldin sum rule for the sum of electric and magnetic dipole polarizabilities, the Bernabéu-Tarrach sum rule shows great potential for model-independent, data-driven determination of each nucleon polarizability independently. This is especially interesting in the context of a tension between recent measurements of the proton polarizabilities made by HIGS [156] and A2 [157] Collaborations. Given that a convergent Bernabéu-Tarrach sum rule constrains the static electric dipole polarizability to be positive, one encounters a contradiction with the meson χPT prediction for the neutral pion. In Chapter 7, we attempt to revisit the χPT calculation and provide a novel alternative estimation of this quantity using a light-front quark model.

1.6 Structure of the thesis

In Chapter 2, we present the details of the framework used throughout this work. Along with a brief explanation of the general roadmap for dispersion relations and sum rules, we explicitly provide those utilized across the study. In Chapter 3, we develop a simple parametrization for the elastic scattering of spinless particles, incorporating as many S-matrix constraints as possible. This parametrization proves particularly useful for analyzing lattice QCD data on exotic resonances. We compare this parametrization to other existing parametrizations and test it on various examples, interpreting both real scattering data and lattice QCD results. Chapter 4 focuses on the hadronic contributions to the real LbL scattering process, with an emphasis on investigating exotic states. Specifically, we fit the existing LbL scattering data provided by ATLAS to the recently observed, potentially fully-heavy tetraquark state X(6900). Chapters 5 and 6 address the muon AMM. In Chapter 5, we test and validate a Cottingham-like formula for the electromagnetic corrections to the HVP on a lattice in both QED and scalar QED (sQED). Chapter 6 discusses the Schwinger sum rule method, focusing on the Hadronic Light-by-Light (HLbL) contribution. Also, the problem of asymptotic constant appearing in the sum rule is analysed on examples of effective field theories and the electroweak contribution from the SM. Chapter 6 utilizes the framework of Compton scattering, which is also employed in the subsequent two Chapters. In Chapter 7, we investigate the convergence of the Bernabéu-Tarrach sum rule for the static electric dipole polarizability in χPT and available low-energy experimental data on nucleon photoabsorption. We particularly examine the dispersive formula for the subtraction contribution in the data-driven approach to the Lamb shift. Additionally, we discuss the electric polarizability of the neutral pion and provide a novel evaluation using a light-front quark model (albeit with scalar quarks). The final Chapter, 8, is dedicated to extending Compton scattering to include parity and time-reversal invariance violation. Here, we develop new sum rules for the anapole moment and electric dipole moment. The thesis conclusions and outlook are provided in the Chapter 9.

Chapter 2

General framework

Most methods used in the present work rely on the dispersive framework of field theory. In general, it is based on the S-matrix concept, which is mainly centered on measurable quantities in particle interactions, avoiding dependence on unobservable intermediate states. The S-matrix, or scattering matrix, S_{fi} relates the initial state $|i\rangle$ of a physical system before an interaction to its final state $|f\rangle$ after an interaction, encapsulating all possible scattering processes:

$$S_{fi} = \langle f|\hat{S}|i\rangle, \tag{2.1}$$

where $\hat{S}$ is the S-matrix operator. It is decomposed into a trivial part, $\hat{S} = \mathbb{1}$ when the scattering does not occur, and the part given by a transition matrix $T_{fi} = \langle f|\hat{T}|i\rangle$ as

$$S_{fi} = \delta_{fi} + iT_{fi}. \tag{2.2}$$

Since the probability to find the system in all possible final states should be unit,

$$\sum_f \left|\langle f|\hat{S}|i\rangle\right|^2 = \langle i|\hat{S}^\dagger\hat{S}|i\rangle = 1, \tag{2.3}$$

the S-matrix should be unitary, $S^\dagger S = SS^\dagger = 1$. This requirement, hereafter referred as unitarity, translates into the relation for the transition matrix:

$$T - T^\dagger = iTT^\dagger. \tag{2.4}$$

If the transition matrix T is symmetric with respect to the interchange of initial and final states, $T_{fi} = T_{if}$, then the relation (2.4) results in the so-called optical theorem:

$$2\,\mathrm{Im}\,T_{fi} = \sum_n \int d\Phi_n T_{fn} T^*_{in}, \tag{2.5}$$

where n denotes the allowed intermediate state, which can be observed as a final state, and Φ_n is the n-particle phase space. The transition (or scattering) amplitude f is related to the transition matrix element by a four momentum-conserving δ-function:

$$T_{fi} = (2\pi)^4 \delta^{(4)} \left(\sum p_i - \sum p_f \right) f(p_i, p_f), \tag{2.6}$$

where p_i and p_f are the four momenta of initial and final particles, respectively.

2.1 A roadmap for dispersion relations and sum rules

The basic constraints on a physical scattering amplitude $f(s)$ rely on the following fundamental principles, usually referred as the scattering-matrix constaints:

- unitarity (a reflection of the conservation of probability, cf. Eq. (2.4))
- analyticity (due to causality)
- crossing (caused by particle-antiparticle duality)

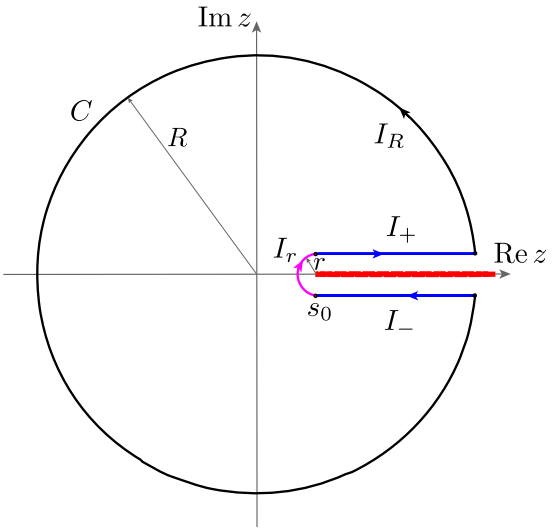

Fig. 2.1 Analytic structure of a scattering amplitude $f(z)$ with a branch cut that starts from $z = s_0$. The contour C encloses the analyticity domain of $f(z)$.

These fundamental principles are reflected in dispersion relations, which the scattering amplitudes should obey. Here we briefly consider the basics of dispersion relations and see how they become sum rules.

2.1.1 Analyticity and unitarity

Let us consider a simple case of forward particle scattering, when the scattering amplitude $f(s)$ depends on only one real kinematic variable s. Being an analytic function, the forward scattering amplitude of this process satisfies the Cauchy theorem in a complex plane of variable z:

$$f(z) = \frac{1}{2\pi i}\oint_C dz' \frac{f(z')}{z'-z} = I_C(z), \tag{2.7}$$

where C is any closed contour in an analyticity domain of the amplitude $f(z)$. Let us assume that the scattering amplitude contains no singularities except only one branch cut (or right-hand cut) along the real axis due to unitarity, which starts from the inelastic particle-production threshold at $z = s_0$. Then C can be chosen as shown in Fig. 2.1, and can be divided into four integrals:

$$I_C(z) = I_r(z) + I_+(z) + I_R(z) + I_-(z), \tag{2.8}$$

where

$$I_r(z) = \frac{r}{2\pi}\int_{\frac{3\pi}{2}}^{\frac{\pi}{2}} d\phi e^{i\phi}\frac{f(s_0 + re^{i\phi})}{s_0 + re^{i\phi} - z}, \tag{2.9}$$

$$I_\pm(z) = \pm\frac{1}{2\pi i}\int_{s_0}^{R} ds' \frac{f(s_0 \pm ir)}{s' - z \pm ir}, \tag{2.10}$$

$$I_R(z) = \frac{1}{2\pi}\int_{\arctan r/s_0}^{2\pi - \arctan r/s_0} d\phi \frac{e^{i\phi} f(Re^{i\phi})}{e^{i\phi} - z/R}. \tag{2.11}$$

In the limit $r \to 0$, the integral I_r vanishes. Next the sum of the integrals $I_\pm$ can be expressed via an integral over a discontinuity of $f(z)$ across the branch cut:

$$I_{\rm DR}(z) = I_+(z) + I_-(z) = \frac{1}{2\pi i}\int_{s_0}^{R} ds' \left[\frac{f(s'+ir)}{s'+ir-z} - \frac{f(s'-ir)}{s'-ir-z}\right] \overset{r\to 0}{=} \frac{1}{2\pi}\int_{s_0}^{R} ds' \frac{{\rm Disc}_s f(s')}{s'-z}. \tag{2.12}$$

Due to the Schwarz reflection principle for analytic functions, i.e. $f^*(z) = f(z^*)$, the discontinuity in this case is simply given by the imaginary part of $f(z)$:

$${\rm Disc}_s \equiv \lim_{\epsilon\to 0}\left[f(s+i\epsilon) - f(s-i\epsilon)\right] = 2i\,{\rm Im}\, f(s). \tag{2.13}$$

Thus, if the integral I_R vanishes at large radius $R \to \infty$, then the whole amplitude can be expressed through its imaginary part without any further inputs.

What is the possible behavior of the integral I_R? It obviously depends on the asymptotic behavior of $f(z)$ at $z \to \infty$. Since we have no theory valid at arbitrary high energies so far, we must consider all possible scenarios. The best one realizes if the scattering amplitude vanishes at high energies, i.e.

$$\lim_{|z|\to\infty} f(z) = 0. \tag{2.14}$$

This condition ensures not only that the integral I_R approaches zero as $R \to \infty$, but also guarantees the convergence of the integral $I_{\rm DR}$ at its upper limit. Thus, for the entire function $f(z)$ one obtains

$$f(z) = \lim_{R\to\infty} I_{\rm DR} = \frac{1}{\pi}\int_{s_0}^{\infty} ds' \frac{\mathrm{Im}\, f(s')}{s'-z}, \tag{2.15}$$

which is the simplest dispersive representation of the amplitude $f(z)$.

The worst scenario realizes when the scattering amplitude behaves asymptotically as

$$f(z) \overset{|z|\to\infty}{=} O(|z|^{\alpha}), \quad \alpha > 0. \tag{2.16}$$

In this case the integral $I_{\rm DR}$ diverges at the upper limit, which is compensated by the nonvanishing integral I_R. However, there is still a way to write a dispersive representation of such an amplitude, by making a subtraction in Eq. (2.15). This procedure relies in moving the I_R-contribution together with the divergence in $I_{\rm DR}$ into an additive constant parameter. A single subtraction at the point z_1 works as follows:

$$\begin{aligned} f(z) &= I_R(z)|_{R\to\infty} + \frac{1}{\pi}\int_{s_0}^{\infty} ds' \frac{\mathrm{Im}\, f(s')}{s'-z} \\ &= \underbrace{I_R(z))|_{R\to\infty} + \frac{1}{\pi}\int_{s_0}^{\infty} ds' \frac{\mathrm{Im}\, f(s')}{s'-z_1}}_{f(z_1)} - \frac{1}{\pi}\int_{s_0}^{\infty} ds' \frac{\mathrm{Im}\, f(s')}{s'-z_1} + \frac{1}{\pi}\int_{s_0}^{\infty} ds' \frac{\mathrm{Im}\, f(s')}{s'-z} \\ &= f(z_1) + \frac{(z-z_1)}{\pi}\int_{s_0}^{\infty} ds' \frac{\mathrm{Im}\, f(s')}{(s'-z_1)(s'-z)}. \end{aligned} \tag{2.17}$$

This way we also end up with expression for the amplitude in terms of the convergent integral over its imaginary part with the only additional information on the value of $f(z)$ at some particular point z_1. If a single subtraction is insufficient to obtain the convergent dispersive integral, the subtraction procedure can be iterated as many times as needed. If during this iteration the subtraction is always performed at the same point, e.g., z_1, then the entire procedure is analogous to the Taylor series.

$$f(z) = \sum_{n=0}^{N} \frac{f^{(n)}(z_1)}{n!}(z-z_1)^n + \frac{(z-z_1)^N}{\pi}\int_{s_0}^{\infty} ds' \frac{\mathrm{Im}\, f(s')}{(s'-z_1)^N(s'-z)}. \tag{2.18}$$

In general, it is feasible to implement subtractions at various points during each iterative step. Then one obtains the following expression

$$f(z) = P_N(z) + \frac{S(z)}{\pi}\int_{s_0}^{\infty} ds' \frac{\mathrm{Im}\, f(s')}{S(s')(s'-z)}, \quad S(z) = \Pi_{i=1}^{N}(z-z_i), \tag{2.19}$$

which contains a subtraction polynomial of order $N-1$ in variable z denoted by P_N. Hence, in order to establish a convergent dispersion relation for $f(z)$, which has sufficiently "bad" asymptotic behavior, one needs to know up to N values of $f(z)$ at N different points or up to N-th order derivatives of $f(z)$

at one point. A common physical interpretation of the subtraction procedure is a renormalization program of QFT. Usually, one can establish exact correspondence between subtraction terms in dispersion relations and counterterms in QFT amplitudes.

The interesting situation happens when the scattering amplitude at infinite energy tends to a constant. In this case the dispersive integral in (2.15) is convergent, but the contribution from I_R is finite and not vanishing. Its value can be determined using the Sugawara-Kanazawa theorem [158]:
Sugawara-Kanazawa theorem (simplified): *If one has a function $f(z)$, which is*

1. *analytic everywhere in the complex z-plane except for the unitarity cut on the real axis,*
2. *assumed to have a divergence at $|z| = \infty$ along some direction in a complex plane, not stronger than a large but finite power of $|z|$,*
3. *has a finite limit $f(\infty \pm i\epsilon)$ along the cut,*

then the limits of $f(z)$ when z approaches infinity in any other direction are

$$\begin{aligned} \lim_{|z|\to\infty} f(z) &= f(\infty + i\epsilon) \quad \textit{in the upper half-plane}, \\ &= f(\infty - i\epsilon) \quad \textit{in the lower half-plane}. \end{aligned} \tag{2.20}$$

Hence the dispersion relation for $f(z)$ becomes

$$f(z) = \frac{1}{\pi}\int_{s_0}^{\infty} ds' \frac{\operatorname{Im} f(s')}{s'-z} + \frac{1}{2}\lim_{s\to\infty}[f(s+i\epsilon) + f(s-i\epsilon)], \tag{2.21}$$

where the limit is taken along the unitarity cut.
In other words, if the amplitude tends to a constant at infinite energy, then the dispersion relation (2.15) should be modified by this constant, having

$$f(z) = f(\infty) + \frac{1}{\pi}\int_{s_0}^{\infty} ds' \frac{\operatorname{Im} f(s')}{s'-z}. \tag{2.22}$$

Despite the right-hand cut structure, the other important consequence of unitarity is the optical theorem, which, for a $2 \to 2$ particle scattering, relates imaginary part of the forward elastic scattering amplitude with the total inclusive cross section σ_{tot} of $2 \to X$ scattering,

$$\operatorname{Im} f(s) = \frac{\Phi_2(s)}{2}\sigma_{\text{tot}}(s), \quad \Phi_2(s) = 2\sqrt{\lambda(s, m_1^2, m_2^2)}, \tag{2.23}$$

where Φ_2 is a relativistic flux factor of two incident particles with masses m_1 and m_2, and $\lambda(x,y,z) = x^2 + y^2 + z^2 - 2xy - 2xz - 2yz$ is the Källén function. Therefore, having a convergent dispersion relation (2.15), one can fully reconstruct the whole forward amplitude $f(z)$ via the observable cross section σ_{tot}.

2.1.2 Crossing

Crossing relations for a scattering process usually implies a certain symmetry of the scattering amplitude. Consider the cases of $f(z)$ being even or odd,

$$f^{\text{even}}(-z) = f^{\text{even}}(z), \quad f^{\text{odd}}(-z) = -f^{\text{odd}}(z). \tag{2.24}$$

In this case, in addition to the unitarity cut, the amplitude will have a cut in a crossed channel, say crossing cut, which starts from $z = -\infty$ and ends at $z = -s_0$. Therefore the contour should be deformed to avoid this cut. The dispersion relation will then be modified as follows:

$$\begin{aligned} f^{\text{even}}(z) &= \frac{2}{\pi}\int_{s_0}^{\infty} ds' \frac{s' \operatorname{Im} f^{\text{even}}(s')}{s'^2 - z^2}, \\ f^{\text{odd}}(z) &= \frac{2z}{\pi}\int_{s_0}^{\infty} ds' \frac{\operatorname{Im} f^{\text{odd}}(s')}{s'^2 - z^2}. \end{aligned} \tag{2.25}$$

When a dispersion relation works with subtractions, the subtraction polynomials will also obey certain crossing properties. Specifically, it is impossible for odd amplitudes to approach a constant value at infinite energy.

2.1.3 Low-energy theorems and sum rules

While the imaginary part of the $2 \to 2$ forward scattering amplitude is given by the observable total cross section via the optical theorem (2.23), there exist several constraints that fix the low-energy behavior of the amplitude. These constraints are called "low-energy theorems". They can be derived by associating terms in the low-energy expansion with certain terms of the corresponding effective low-energy Hamiltonian. In other words, the low-energy theorems define the coefficients a_i in the low-energy expansion of the scattering amplitude f,

$$f(s) = \sum_{i=0}^{N} a_i s^i + O(s^{N+1}), \tag{2.26}$$

in terms of certain physical observables. For instance, in the case of Compton scattering, a celebrated example is the Thomson term, which represents the low-energy limit of the spin-independent forward Compton scattering on a particle with mass M:

$$f_{\text{Compton}}(\nu = 0) = -\frac{e^2}{4\pi M}. \tag{2.27}$$

Finally, the dispersive representation of a scattering amplitude (2.15) in combination with the optical theorem (2.23) and the low-energy theorem (2.26) can provide an essentially new relation between two different observables: the low-energy observable a_i and the total scattering cross section

σ_{tot}. This relation, typically having a form of an integral relation

$$a_i = \frac{1}{2\pi}\int_{s_{\text{inel}}}^{\infty} ds' \frac{\Phi_2(s')\sigma_{\text{tot}}(s')}{s'^{i+1}}, \tag{2.28}$$

where the integration starts from the first inelastic threshold, are called "sum rules". As is usually stated, the remarkable power of these relations lies in their model independence, i.e. the derivation relies only on fundamental S-matrix constraints and requires no further assumptions on the particular theoretical model behind the given scattering process. Practically, it depends on the theory, whether the integral in Eq. (2.28) converges as it is, without requiring additional subtractions. Therefore it is important to make perturbative verification of the sum rule in "reasonable" theories, i.e. theories that exhibit tree-level unitarity or have the stronger constraint of renormalizability, as well as test them on available data.

2.2 Elastic scattering of scalar particles

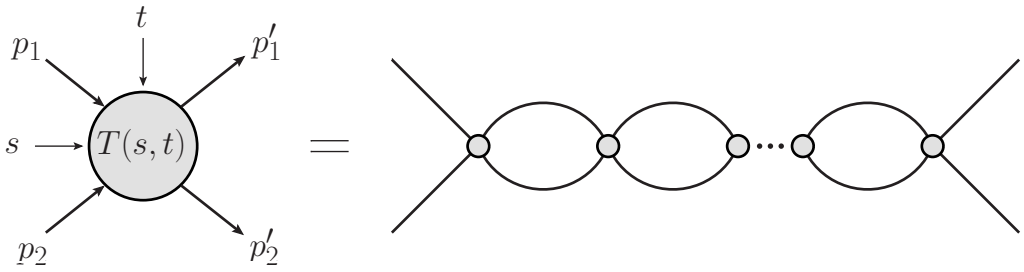

Fig. 2.2 Elastic $2 \to 2$ scattering of particles of types 1 and 2 with initial four-momenta p_1 and p_2 and final four-momenta p_1' and p_2' as a single-channel rescattering in s-channel.

In this section, we provide the basics of partial-wave single-channel analysis of elastic $2 \to 2$ scattering of spinless particles, which is schematically shown in Fig. 2.2. Here the formalism of dispersion relations, discussed in the previous section, is already widely applied to make a proper analytical continuation of the partial-wave amplitudes onto the whole complex plane. The latter is an essential step for subsequent pole analysis in the complex plane of S-matrix and precise determination of the resonance parameters. The content provided serves as a general introductive part to Chapter 3.

2.2.1 Partial-wave expansion and unitarity

The kinematics $2 \to 2$ elastic scattering, schematically depicted in Fig. 2.2, can be conveniently described in terms of the Mandelstam invariants s, t and u, which are related to the particle momenta as

$$s = (p_1+p_2)^2 = (p_1'+p_2')^2, \quad t = (p_1-p_1')^2 = (p_2-p_2')^2, \quad u = (p_1-p_2')^2 = (p_2-p_1')^2. \tag{2.29}$$

Given that these invariants are linearly related, $s+t+u=2(m_1^2+m_2^2)$, the scattering amplitude depends only on two of them. It is also convenient to consider this process in c.o.m. frame, where it characterized by the c.o.m. scattering energy $\sqrt{s}$ and the scattering angle θ between the initial and final directions of two-particle motion. In this case, the three-momentum of the system reads

$$p(s)=\frac{\lambda^{1/2}(s,m_1^2,m_2^2)}{2\sqrt{s}}\equiv\sqrt{\frac{(s-m_-^2)(s-m_+^2)}{4s}}\,, \tag{2.30}$$

with λ being the Källén function and $m_\pm=m_1\pm m_2$.

Then the s-channel partial-wave decomposition for the amplitude for $2\to 2$ scattering process is then given by

$$T(s,t)=16\pi\mathcal{N}\sum_{J=0}^{\infty}(2J+1)\,t_J(s)\,P_J(\cos\theta)\,, \tag{2.31}$$

where $P_J(x)$ are Legendre polynomials of degree J, which corresponds to the total angular momentum. For the scattering of identical particles, $\mathcal{N}=2$, while $\mathcal{N}=1$ for non-identical particles. This factor is useful in ensuring the same unitarity condition for both identical and non-identical two-particle scattering, which in the elastic approximation is given by

$$\mathrm{Im}\,t_J(s)=\rho(s)\,|t_J(s)|^2\,\theta(s-s_{\rm th})\,, \tag{2.32a}$$

$$\mathrm{Im}\,[t_J(s)]^{-1}=-\rho(s)\,\theta(s-s_{\rm th})\,, \tag{2.32b}$$

where $s_{\rm th}=(m_1+m_2)^2$ is the two-particle production threshold. The phase space factor $\rho(s)$ for partial-wave amplitudes is given by

$$\begin{aligned}\rho(s)&\equiv 16\pi\int\frac{d^3\vec{p}_1'}{(2\pi)^3 2E_1'}\int\frac{d^3\vec{p}_2'}{(2\pi)^3 2E_2'}\frac{(P_J(\cos\theta))^2}{2(2J+1)}\delta^{(4)}(p_1+p_2-p_1'-p_2')(2\pi)^4\\&=\frac{2\,p(s)}{\sqrt{s}}\,.\end{aligned} \tag{2.33}$$

At low energy, the effective range expansion for partial waves is conventionally defined as

$$\frac{2}{\sqrt{s_{th}}}\mathrm{Re}\,t_J(s)\simeq p^{2J}(s)\left(a_J+b_J\,p^2(s)+...\right), \tag{2.34}$$

where a_J and b_J denote the scattering length and the slope parameter, respectively. At high energy, the unitarity condition (2.32) guarantees that the partial-wave amplitudes at infinity approach at most constants

$$-\frac{1}{2\rho(s)}\le\mathrm{Re}\,t_J(s)\le\frac{1}{2\rho(s)},\quad 0\le\mathrm{Im}\,t_J(s)\le\frac{1}{\rho(s)} \tag{2.35}$$

and in accordance with that, we assume throughout this section that

$$t_J \overset{s\to\pm\infty}{\to} \text{const}\,. \tag{2.36}$$

2.2.2 Dispersion relations and their solutions

Here, for the sake of simplicity, let us consider the S-wave ($J = 0$) scattering of spinless particles, since in this case we do not need to worry about angular momentum barrier factors. In view of the maximal analyticity assumption [159, 160], the partial-wave amplitude t_J has two cuts along the real axis: right-hand cut due to unitarity, $s \in [s_{\rm th}, \infty)$, and left-hand cut due to crossing, $s \in (-\infty, s_L]$.The amplitude thus satisfies, according to Eq. (2.36), the once-subtracted dispersion relation,

$$\begin{aligned} t_0(s) &= t_0(s_M) + \frac{s-s_M}{s_B-s_M}\frac{g_B^2}{s_B-s} \\ &\quad + \frac{s-s_M}{\pi}\left[\int_{-\infty}^{s_L}\frac{ds'}{s'-s_M}\frac{\mathrm{Im}\,t_0(s')}{s'-s} + \int_{s_{\rm th}}^{\infty}\frac{ds'}{s'-s_M}\frac{\mathrm{Im}\,t_0(s')}{s'-s}\right] \\ &\equiv t_0(s_M) + \frac{s-s_M}{s_B-s_M}\frac{g_B^2}{s_B-s} + \frac{s-s_M}{\pi}\int_{L,R}\frac{ds'}{s'-s_M}\frac{\mathrm{Im}\,t_0(s')}{s'-s}\,. \end{aligned} \tag{2.37}$$

The symbols L and R denote integrals over left- and right-hand cuts, respectively. The choice of the subtraction point at $s = s_M$ in general is irrelevant and will be discussed later. For completeness, we admitted in Eq. (2.37) a possible bound state at $s = s_B$ with the coupling g_B, which we will drop later on for simplicity. Using the unitarity relation (2.32) on the right-hand cut, Eq. (2.37) simplifies to

$$t_0(s) = U(s) + \frac{s-s_M}{\pi}\int_{s_{\rm th}}^{\infty}\frac{ds'}{s'-s_M}\frac{\rho(s')\,|t_0(s')|^2}{s'-s}\,, \tag{2.38}$$

where we combined the subtraction constant together with the left-hand cut contributions into the function $U(s)$,

$$U(s) \equiv t_0(s_M) + \frac{s-s_M}{\pi}\int_{L}\frac{ds'}{s'-s_M}\frac{\mathrm{Im}\,t_0(s')}{s'-s}\,. \tag{2.39}$$

The solution to (2.38) can be written using the N/D ansatz [66]

$$t_0(s) = \frac{N(s)}{D(s)}\,, \tag{2.40}$$

where the contributions of left- and right-hand cuts are separated into $N(s)$ and $D(s)$ functions, respectively.

An interesting feature of the N/D ansatz lies in the ambiguity of having poles in both N and D functions simultaneously, provided that the pole positions coincide. This is the celebrated Castillejo-Dalitz-Dyson (CDD) ambiguity [161], which can be used as a trick for explicit parametrization of

poles or zeros in the N/D ansatz. The D-function with CDD pole at $s = s_{CDD}$ reads

$$D(s) = 1 - \frac{s - s_M}{s - s_{CDD}} R_D - \frac{1}{\pi} \int ds' \frac{s - s_M}{s' - s_M} \frac{\rho(s') N(s')}{s' - s}, \tag{2.41}$$

where R_D is a free parameter.The N-function then becomes

$$N(s) = U(s) D(s) + \frac{s - s_M}{s - s_{CDD}} R_N + \frac{s - s_M}{\pi} \int \frac{ds'}{s' - s_M} \frac{\rho(s') N(s') U(s')}{s' - s}, \tag{2.42}$$

where R_N is the second parameter introduced by the CDD ambiguity. The ratio N/D, provided by Eqs. (2.41) and (2.42), is then fully independent on the CDD pole position s_A, which is manifested by the CDD ambiguity.

The N/D ansatz implies a set of linear integral equations [162, 163], which can be solved by, e.g., the matrix inversion method. However, before solving them, one needs to model the left-hand-cut contributions, i.e. $U(s)$. This process typically involves expressing the function as a series in terms of an appropriately constructed conformal variable $\omega(s)$ (see Appendix 2.B for details), which encapsulates the analytic structure of the amplitude,

$$U(s) = \sum_{n=0}^{\infty} C_n \omega^n(s). \tag{2.43}$$

The unknown coefficients C_n of this series are then either treated as fit parameters to experimental data or fixed using predictions from χPT.

Due to the technical complexity of solving integral equations of N/D method, simplified parametrizations (or ansatzes) are widely used. They are especially important in interpretation of the hadronic spectrum obtained by lattice QCD evaluations. The simplest one is the Breit-Wigner parametrization:

$$t_0(s) = -\frac{1}{\rho(s)} \frac{\sqrt{s}\Gamma(s)}{s - M_0^2 + i\sqrt{s}\Gamma(s)}, \tag{2.44}$$

where $\Gamma(s)$ is the energy-dependent width, given by

$$\Gamma(s) = \Gamma_0 \frac{p(s)}{p(M_0^2)} \frac{M_0}{\sqrt{s}}. \tag{2.45}$$

For narrow resonances, Γ_0 and M_0 correspond to the resonance width and mass, which is clearly visible on the cross section data. However, if the resonance lies deep in the complex plane, the Breit-Wigner parametrization produces various artifacts. Despite this parametrization satisfies unitarity, it immediately violates crossing, since it has no left-hand cut contribution. Consequently, due to the missing physics, the dispersion relation for t_0 can be spoiled by unphysical (spurious) poles, thus violating even analyticity.

A slightly improved, but still quite simple parametrization, the K-matrix approach, exploits the unitarity relation for the inverse amplitude (2.32b). The partial-wave amplitude in this approach can

be written in a general form as

$$[t_0(s)]^{-1} = K^{-1}(s) - i\rho(s)\,. \tag{2.46}$$

Due to unitarity, the function $K(s)$ is real, and usually parametrized by a pole term and some polynomial. While preserving unitarity, this parametrization, when applied, usually neglects the left-hand cut at all and does not satisfy the dispersion relation (2.38), thus violating analyticity constraint. Various forms of this kind of parametrizations will be discussed in details in Chapter 3.

2.2.3 Poles in the complex plane

Once the partial-wave amplitude is properly continued in the complex plane using any method discussed above, we can start looking for poles of the S-matrix. For elastic scattering, the amplitude possesses two Riemann sheets, which are continuously connected along the unitarity branch cut. The first (physical) Riemann sheet is associated with physical scattering processes and is characterized by the behavior of the partial-wave amplitude along the upper edge of the unitarity cut, say t_J^{I}. This sheet corresponds to the observable domain where real scattering events occur, with energy values above the physical threshold. On this sheet, any pole, which lies on the real axis below the threshold, correspond to a bound state.

The partial-wave amplitude t_J^{II} on the second (unphysical) Riemann sheet can be found from t_J^{I} by crossing the unitarity cut. Using unitarity relation for the physical amplitude t_J^{I},

$$t_J^{\mathrm{I}}(s+i\epsilon) - t_J^{\mathrm{I}}(s-i\epsilon) = 2i\rho(s)t_J^{\mathrm{I}}(s+i\epsilon)t_J^{\mathrm{I}}(s-i\epsilon), \tag{2.47}$$

we can relate the values of the amplitude above and below unitarity cut, hence defining this amplitude on the second Riemann sheet:

$$t_J^{\mathrm{II}}(s-i\epsilon) = t_J^{\mathrm{I}}(s+i\epsilon) = \frac{t_J^{\mathrm{I}}(s-i\epsilon)}{1-2i\rho(s)t_J^{\mathrm{I}}(s-i\epsilon)} \overset{\epsilon\to 0}{\to} t_J^{\mathrm{II}}(s) = \frac{t_J^{\mathrm{I}}(s)}{1-2i\rho(s)t_J^{\mathrm{I}}(s)}. \tag{2.48}$$

Thus, the solution to the equation

$$1 - 2i\rho(s)t_J^{\mathrm{I}}(s) = 0 \tag{2.49}$$

will define a pole on the second Riemann sheet, which can be interpreted as either resonance (complex-valued, lies above unitarity threshold) or virtual bound state (real-valued, lies below unitarity threshold).

Since Eq. (2.49) usually cannot be solved analytically and has nontrivial dependence on the parameters entering the amplitude t_J^{I}, uncertainty propagation with respect to these parameters could be a nontrivial task. Moreover, there could be cases when the pole moves from a resonance to a (virtual) bound state within the parameter uncertainties. The most suitable approach in these cases is the bootstrap technique. According to this technique, the mean value and the uncertainty are calculated from a statistical pool of solutions to Eq. (2.49). Each solution entering the pool is obtained for amplitude parameters that are randomly picked around their mean values according to their distribution

functions. This approach allows one to handle skewed distributions and easily obtain the correct shapes for a given confidence level.

2.3 Light-by-light scattering

This section provides the general formalism for the real and virtual LbL scattering. In general, the structure of the fully off-shell LbL tensor is quite complicated [123]. It involves 138 Lorentz structures, which reduce to 41 due to Ward identities. However, for this work it is enough to consider the special cases of the forward doubly-virtual LbL scattering and the real LbL scattering. The dispersion relations and sum rules, provided in this section, will be extensively used in Chapters 4 and 5.

2.3.1 Forward doubly-virtual LbL scattering

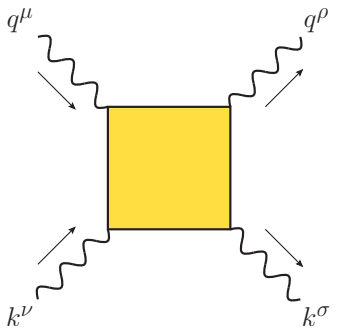

Fig. 2.3 Forward doubly-virtual light-by-light scattering.

A convenient Lorentz-invariant basis for the forward doubly-virtual LbL scattering has been worked out a long time ago by Budnev et al. [164, 165]. Following their prescriptions, the LbL tensor can be written as follows [166]

$$\begin{aligned}\mathcal{M}^{\mu\nu\rho\sigma} = \sum_{i=1}^{8} T_i^{\mu\nu\rho\sigma}\,\mathcal{M}_i &= R^{\mu\rho}R^{\nu\sigma}\,\mathcal{M}_{TT} + \left[R^{\mu\nu}R^{\rho\sigma} - R^{\mu\sigma}R^{\rho\nu}\right]\mathcal{M}_{TT}^{a} \\ &+ R^{\mu\rho}l_k^\nu l_k^\sigma\,\mathcal{M}_{TL} + R^{\nu\sigma}l_q^\mu l_q^\rho\,\mathcal{M}_{LT} \\ &+ \frac{1}{2}\left[R^{\mu\nu}R^{\rho\sigma} + R^{\mu\sigma}R^{\rho\nu} - R^{\mu\rho}R^{\nu\sigma}\right]\mathcal{M}_{TT}^{\tau} + l_q^\rho l_q^\mu l_k^\sigma l_k^\nu\,\mathcal{M}_{LL} \\ &- \left[R^{\mu\nu}l_q^\rho l_k^\sigma - R^{\mu\sigma}l_q^\rho l_k^\nu + (\mu\nu\leftrightarrow\rho\sigma)\right]\mathcal{M}_{TL}^{\tau} \\ &- \left[R^{\mu\nu}l_q^\rho l_k^\sigma + R^{\mu\sigma}l_q^\rho l_k^\nu + (\mu\nu\leftrightarrow\rho\sigma)\right]\mathcal{M}_{TL}^{\tau a},\end{aligned} \tag{2.50}$$

where

$$l_q^\mu = \sqrt{\frac{-q^2}{X}}\left(k^\mu - \frac{\nu}{q^2}q^\mu\right), \quad l_k^\mu = \sqrt{\frac{-k^2}{X}}\left(q^\mu - \frac{\nu}{k^2}k^\mu\right), \quad k\cdot l_k = q\cdot l_q = 0,$$

$$R^{\mu\nu} = -g^{\mu\nu} + \frac{1}{X}\left[\nu\,(q^\mu k^\nu + q^\nu k^\mu) - q^2 k^\mu k^\nu - k^2 q^\mu q^\nu\right] = R^{\nu\mu}, \quad R^{\mu\nu} q_\nu = R^{\mu\nu} k_\nu = 0,$$
$$X = \nu^2 - q^2 k^2, \quad \nu = q \cdot k. \tag{2.51}$$

and T_i are eight independent invariant amplitudes that are free of kinematical zeros and singularities. The polarization vectors ε^μ are normalized by the following convention

$$g_{\mu\nu}\varepsilon_a^\mu(p_i)\varepsilon_b^{*\nu}(p_i) = (-1)^a \delta_{ab}, \tag{2.52a}$$
$$\sum_{a=0,\pm1} (-1)^a \varepsilon_a^\mu(p_i)\varepsilon_b^{*\nu}(p_i) = g^{\mu\nu} - \frac{p_i^\mu p_i^\nu}{p_i^2}, \tag{2.52b}$$
$$\varepsilon_a(p_i) \cdot p_i = 0. \tag{2.52c}$$

Here $a, b = 0, \pm1$ denote the photon polarizations, p_i stand for the photon momenta, $p_1 = q$, $p_2 = k$. In c.o.m. frame, i.e. $\vec{q} = -\vec{k}$, one can choose the polarization vectors such that

$$\varepsilon_a^*(p_i) = \varepsilon_{-a}(p_i), \quad \varepsilon_{\pm1}(k) = \varepsilon_{\mp1}(q), \quad \varepsilon_0(q) = i l_q, \quad \varepsilon_0(k) = i l_k. \tag{2.53}$$

The remarkable feature of the chosen basis is that all the tensor structures are orthogonal to each other, hence they immediately can be used as the projectors to certain combinations of helicity amplitudes. In the aformentioned notations the helicity amplitudes are defined by

$$\begin{aligned} M_{aba'b'} &= \varepsilon_a^\mu(q)\varepsilon_b^\nu(k)\mathcal{M}_{\mu\nu\rho\sigma}\varepsilon_{a'}^{*\rho}(q)\varepsilon_{b'}^{*\sigma}(k)(-1)^{b+b'} \\ &= M_{-a-b-a'-b'} = M_{a'b'ab}. \end{aligned} \tag{2.54}$$

There are eight independent amplitudes, which absorptive parts $W_{a'b'ab} \equiv \mathrm{Im}\, M_{a'b'ab}$ correspond to certain cross sections via the optical theorem, namely

$$W_{TT} = 2\sqrt{X}\sigma_{TT} = \frac{1}{2}\left[W_{++++} + W_{+-+-}\right], \tag{2.55a}$$
$$W_{LT} = 2\sqrt{X}\sigma_{LT} = W_{0+0+}, \tag{2.55b}$$
$$W_{TL} = 2\sqrt{X}\sigma_{TL} = W_{+0+0}, \tag{2.55c}$$
$$W_{LL} = 2\sqrt{X}\sigma_{LL} = W_{0000}, \tag{2.55d}$$
$$W_{TT}^a = 2\sqrt{X}\tau_{TT}^a = \frac{1}{2}\left[W_{++++} - W_{+-+-}\right], \tag{2.55e}$$
$$W_{TT}^\tau = 2\sqrt{X}\tau_{TT} = W_{++--}, \tag{2.55f}$$
$$W_{TL}^\tau = 2\sqrt{X}\tau_{TL} = \frac{1}{2}\left[W_{++00} - W_{0+-0}\right], \tag{2.55g}$$
$$W_{TL}^{\tau a} = 2\sqrt{X}\tau_{TL}^a = \frac{1}{2}\left[W_{++00} + W_{0+-0}\right], \tag{2.55h}$$

with the correspondence $W_{LT}(\nu, q^2, k^2) = W_{TL}(\nu, k^2, q^2)$. The polarized cross sections σ_{ab} are associated with the fusion of two photons with polarizations a and b. Only σ_{TT}, σ_{TL}, σ_{LT} and σ_{LL} are positive-definite. Only the amplitudes $\mathcal{M}^{a}_{TT}$ and $\mathcal{M}^{\tau a}_{TL}$ are odd in ν; the rest are even.

2.3.1.1 Dispersion relations and sum rules

The analyticity of the forward doubly-virtual scattering amplitudes in the entire ν-plane except for the branch cuts on the real axis, allows one to express these amplitudes through dispersion relations. Thus, for any fixed values $Q^2, K^2 > 0$, depending on whether the amplitude is even/odd in ν, it is defined by its nonanalytic part as follows [167]

$$M_{\text{even}}(\nu) = \frac{2}{\pi}\int_{\nu_0}^{\infty} d\nu' \frac{\nu'}{\nu'^2 - \nu^2 - i0^+}\,\text{Im}\, M_{\text{even}}(\nu'), \tag{2.56}$$

$$M_{\text{odd}}(\nu) = \frac{2\nu}{\pi}\int_{\nu_0}^{\infty} d\nu' \frac{1}{\nu'^2 - \nu^2 - i0^+}\,\text{Im}\, M_{\text{odd}}(\nu'), \tag{2.57}$$

where $\nu_0 > 0$ is the lowest particle production threshold. These dispersion relations are derived under the assumption that the amplitudes decay sufficiently rapidly, so that only the integral along the branch cut contributes. If this is not the case, then subtracted dispersion relations are needed. For our purposes it is enough to consider once-subtracted relations,

$$M_{\text{even}}(\nu) = M_{\text{even}}(\bar{\nu}) + \frac{2(\bar{\nu}^2 - \nu^2)}{\pi}\int_{\nu_0}^{\infty} d\nu' \frac{\nu'\,\text{Im}\, M_{\text{even}}(\nu')}{(\bar{\nu}^2 - \nu'^2)(\nu'^2 - \nu^2 - i0^+)}, \tag{2.58}$$

$$M_{\text{odd}}(\nu) = M_{\text{odd}}(\bar{\nu}) + \frac{2(\bar{\nu} - \nu)}{\pi}\int_{\nu_0}^{\infty} d\nu' \frac{(\nu'^2 + \nu\bar{\nu})\,\text{Im}\, M_{\text{odd}}(\nu')}{(\bar{\nu}^2 - \nu'^2)(\nu'^2 - \nu^2 - i0^+)}. \tag{2.59}$$

Here $\bar{\nu}$ is the subtraction point, which could be chosen arbitrarily. For simplicity, it is usually chosen at zero energy of the two-photon pair, i.e. taking $\bar{\nu} = 0$, given that the LbL amplitudes will vanish at this point if one of the photons is real.

The asymptotic behaviour of the helicity amplitude can be qualitatively estimated by means of a Regge pole model, giving that [164]

$$\begin{aligned} &W_{TT}, W_{LL} \sim \nu^{\alpha_P(0)}, \quad W_{TL}, W_{LT} \lesssim \nu^{\alpha_P(0)}, \\ &W^{\tau}_{TT}, W^{a}_{TT} \sim \nu^{\alpha_\pi(0)}, \quad W^{\tau}_{TL}, W^{\tau a}_{TL} \sim \nu^{\alpha_\pi(0)-1}, \end{aligned} \tag{2.60}$$

where $\alpha_P(0) \simeq 1.08$ and $\alpha_\pi(0) \simeq -0.014$ are the intercepts of the Pomeron and pion trajectories, respectively. Taking into account this behaviour of the amplitudes at high energies, one can immediately decide for each amplitude, whether or not it requires a subtraction, obtaining the following set of

dispersion relations for the even helicity amplitudes,

$$M_{++++}(\nu,Q^2,K^2)+M_{+-+-}(\nu,Q^2,K^2)=M_{TT}(0,Q^2,K^2)+\frac{4\nu^2}{\pi}\int_{\nu_0}^{\infty}d\nu'\frac{\sqrt{X'}\sigma_{TT}(\nu',Q^2,K^2)}{\nu'(\nu'^2-\nu^2-i0^+)}, \tag{2.61a}$$

$$M_{0+0+}(\nu,Q^2,K^2)=M_{LT}(0,Q^2,K^2)+\frac{4\nu^2}{\pi}\int_{\nu_0}^{\infty}d\nu'\frac{\sqrt{X'}\sigma_{LT}(\nu',Q^2,K^2)}{\nu'(\nu'^2-\nu^2-i0^+)} \tag{2.61b}$$

$$M_{+0+0}(\nu,Q^2,K^2)=M_{TL}(0,Q^2,K^2)+\frac{4\nu^2}{\pi}\int_{\nu_0}^{\infty}d\nu'\frac{\sqrt{X'}\sigma_{TL}(\nu',Q^2,K^2)}{\nu'(\nu'^2-\nu^2-i0^+)} \tag{2.61c}$$

$$M_{0000}(\nu,Q^2,K^2)=M_{LL}(0,Q^2,K^2)+\frac{4\nu^2}{\pi}\int_{\nu_0}^{\infty}d\nu'\frac{\sqrt{X'}\sigma_{LL}(\nu',Q^2,K^2)}{\nu'(\nu'^2-\nu^2-i0^+)} \tag{2.61d}$$

$$M_{++--}(\nu,Q^2,K^2)=M^{\tau}_{TT}(0,Q^2,K^2)+\frac{4\nu^2}{\pi}\int_{\nu_0}^{\infty}d\nu'\frac{\sqrt{X'}\tau_{TT}(\nu',Q^2,K^2)}{\nu'(\nu'^2-\nu^2-i0^+)} \tag{2.61e}$$

$$M_{++00}(\nu,Q^2,K^2)-M_{0+-0}(\nu,Q^2,K^2)=\frac{8}{\pi}\int_{\nu_0}^{\infty}d\nu'\frac{\nu'\sqrt{X'}\tau_{TL}(\nu',Q^2,K^2)}{\nu'^2-\nu^2-i0^+}, \tag{2.61f}$$

and for the odd ones

$$M_{++++}(\nu,Q^2,K^2)-M_{+-+-}(\nu,Q^2,K^2)=\frac{4\nu}{\pi}\int_{\nu_0}^{\infty}d\nu'\frac{\sqrt{X'}\tau^a_{TT}(\nu',Q^2,K^2)}{\nu'^2-\nu^2-i0^+}, \tag{2.62a}$$

$$M_{++00}(\nu,Q^2,K^2)+M_{0+-0}(\nu,Q^2,K^2)=\frac{8\nu}{\pi}\int_{\nu_0}^{\infty}d\nu'\frac{\sqrt{X'}\tau^a_{TL}(\nu',Q^2,K^2)}{\nu'^2-\nu^2-i0^+}, \tag{2.62b}$$

where $M_{ab}(0,Q^2,K^2)$ denote the subtraction functions at $\bar{\nu}=0$ subtraction point, and the following relations between the cross sections were used

$$\sigma_{TT}\equiv\sigma_{\parallel}+\sigma_{\perp}\equiv\sigma_0+\sigma_2, \tag{2.63a}$$

$$\tau^a_{TT}\equiv\sigma_0-\sigma_2, \tag{2.63b}$$

$$\tau_{TT}\equiv\sigma_{\parallel}-\sigma_{\perp}. \tag{2.63c}$$

Here the subscripts 0(2) stand for the total helicitiy of the photon pair, and $\parallel$ ($\perp$) indicate the linear polarizations of the incoming photons, with both photon polarization directions parallel (perpendicular) to each other, respectively.

2.3.2 Real LbL scattering

2.3.2.1 Off-forward real LbL scattering

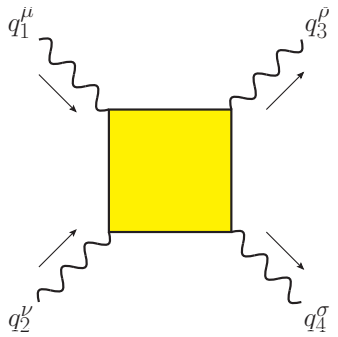

Fig. 2.4 Light-by-light scattering with real photons.

For LbL scattering of real photons with all different four-momenta $q_1, ..., q_4$ (cf. Fig. 2.4), $q_i^2 = 0$, there are in general sixteen different helicity amplitudes, which depend on the Mandelstam variables

$$s = (q_1+q_2)^2 = 2q_1\cdot q_2, \quad t = (q_1-q_3)^2 = -2q_1\cdot q_3, \quad u = (q_1-q_4)^2 = -2q_1\cdot q_4, \tag{2.64}$$

which satisfy $s+t+u = 0$. It is convenient to work in c.o.m frame, setting

$$q_1 = \omega\begin{pmatrix}1\\0\\0\\1\end{pmatrix}, \qquad q_2 = \omega\begin{pmatrix}1\\0\\0\\-1\end{pmatrix} \qquad q_3 = \omega\begin{pmatrix}1\\\sin\theta\\0\\\cos\theta\end{pmatrix}, \qquad q_4 = \omega\begin{pmatrix}1\\-\sin\theta\\0\\-\cos\theta\end{pmatrix}, \tag{2.65}$$

where the photon energy ω and functions of the scattering angle θ are related to the Mandelstam invariants

$$\omega = \frac{\sqrt{s}}{2}, \quad \cos\theta = \frac{t-u}{s}, \quad \sin\theta = \frac{2\sqrt{tu}}{s}. \tag{2.66}$$

Bose and crossing symmetries, parity conservation and time-reversal invariance impose the following relations between the helicity amplitudes:

$$\begin{aligned} M_{\pm\pm\mp\pm}(s,t,u) &= M_{\pm\mp\pm\pm}(s,t,u) = M_{\pm\mp\mp\mp}(s,t,u) \\ &= M_{---+}(s,t,u) = M_{+++-}(s,t,u), \end{aligned} \tag{2.67a}$$

$$\begin{aligned} M_{\pm\mp\mp\pm}(s,t,u) &= M_{\pm\mp\pm\mp}(s,u,t) \\ &= M_{++++}(t,s,u) = M_{++++}(t,u,s), \end{aligned} \tag{2.67b}$$

$$M_{\pm\mp\pm\mp}(s,t,u) = M_{----}(u,t,s) = M_{++++}(u,t,s), \tag{2.67c}$$

$$M_{--++}(s,t,u) = M_{++--}(s,t,u). \tag{2.67d}$$

From these relations, it follows that there are only five independent helicity amplitudes, namely

$$M_{++++}(s,t,u), \quad M_{+--+}(s,t,u), \quad M_{+-+-}(s,t,u),$$
$$M_{+++-}(s,t,u), \quad M_{++--}(s,t,u) \tag{2.68}$$

out of sixteen. It also follows that all LbL amplitudes are invariant under permutations of the last two arguments, and the amplitudes $M_{+++-}(s,t,u)$ and $M_{++--}(s,t,u)$ are totally crossing invariant (invariant under permutations $s \leftrightarrow t \leftrightarrow u$). Hence, the first three helicity amplitudes from the set (2.68) are described by the same function by permuting the variables. Thus, one can construct the following crossing invariant combinations form the remaining amplitudes:

$$\begin{aligned} M^{CI}(s,t,u) &= M_{++++}(s,t,u) + M_{+--+}(s,t,u) + M_{+-+-}(s,t,u) \\ &= M_{++++}(s,t,u) + M_{++++}(t,s,u) + M_{++++}(u,t,s). \end{aligned} \tag{2.69}$$

Thus, according to Refs. [168, 169], it is convenient to choose three independent helicity amplitudes as $M_{++++}(s,t,u)$, $M_{+++-}(s,t,u)$ and $M_{++--}(s,t,u)$. Then the other amplitudes can be expressed via the latter ones as follows

$$\begin{aligned} M_{+---}(s,t,u) &= M_{-+--}(s,t,u) = M_{--+-}(s,t,u) = M_{---+}(s,t,u) \\ &= M_{-+++}(s,t,u) = M_{+-++}(s,t,u) = M_{++-+}(s,t,u) = M_{+++-}(s,t,u), \end{aligned} \tag{2.70}$$

$$M_{-+-+}(s,t,u) = M_{+-+-}(s,t,u) = M_{++++}(u,t,s), \tag{2.71}$$

$$M_{-++-}(s,t,u) = M_{+--+}(s,t,u) = M_{++++}(t,s,u), \tag{2.72}$$

$$M_{----}(s,t,u) = M_{++++}(s,t,u), \tag{2.73}$$

$$M_{++--}(s,t,u) = M_{--++}(s,t,u). \tag{2.74}$$

In terms of these amplitudes, the squared amplitude, averaged over initial and summed over final polarizations, reads:

$$\begin{aligned} |M(s,t,u)|^2 = \sum_{\lambda_1\lambda_2\lambda_3\lambda_4} \left|M_{\lambda_1\lambda_2\lambda_3\lambda_4}(s,t,u)\right|^2 &= 8\,|M_{+++-}(s,t,u)|^2 + 2\,|M_{++--}(s,t,u)|^2 + \\ &+ 2\,|M_{++++}(s,t,u)|^2 + 2\,|M_{++++}(u,t,s)|^2 + 2\,|M_{++++}(t,s,u)|^2 . \end{aligned} \tag{2.75}$$

Then the total unpolarized LbL cross section can be calculated in c.o.m. frame as follows

$$\sigma(s) = \frac{1}{256\pi s}\int_{-1}^{1} d\cos\theta \left|M\left(s, -\frac{s}{2}(1-\cos\theta), -\frac{s}{2}(1+\cos\theta)\right)\right|^2, \tag{2.76}$$

where θ is the angle between incoming and outgoing photons.

2.3.2.2 Forward limit and sum rules

In the limit of the forward scattering, i.e. $t = 0$, the number of independent amplitudes reduces to three: M_{++++}, M_{+-+-} and M_{++--}. Following Eqs. (2.61a), (2.62a) and (2.61e), they should obey the sum rules

$$M_{++++}(s) + M_{+-+-}(s) = \frac{2s^2}{\pi} \int\limits_0^\infty ds' \frac{\sigma_{TT}(s')}{s'^2 - s^2 - i0^+} = \mathcal{S}_1^{\rm LbL}(s), \tag{2.77a}$$

$$M_{++++}(s) - M_{+-+-}(s) = \frac{2s}{\pi} \int\limits_0^\infty ds' \frac{s'\tau_{TT}^a(s')}{s'^2 - s^2 - i0^+} = \mathcal{S}_2^{\rm LbL}(s), \tag{2.77b}$$

$$M_{++--}(s) = \frac{2s^2}{\pi} \int\limits_0^\infty ds' \frac{\tau_{TT}(s')}{s'^2 - s^2 - i0^+} = \mathcal{S}_3^{\rm LbL}(s). \tag{2.77c}$$

Note that due to the low-energy theorem, the LbL scattering amplitudes for the real photons should vanish at low energy of the two-photon pair, thus the subtraction constants in the dispersion relations are equal to zero.

2.4 Forward doubly-virtual Compton scattering on spin-1/2 particles

This Section is mainly based on the comprehensive reviews by Drechsel, Pasquini and Vanderhaeghen [170], Hagelstein, Miskimen and Pascalutsa [171] as well as the manuscript by V. Pascalutsa "Causality rule" [172] (see [173] for the second edition). In what follows, we specify the conventions on Compton amplitudes, low-energy theorems, photoabsorption cross sections and sum rules that will be used in Chapters 6, 7 and 8.

2.4.1 Invariant amplitudes and dispersion relations

In the forward scattering regime, the amplitude of the doubly-virtual Compton scattering on spin-1/2 target (say nucleon N with electric charge e) $\gamma^*(q,\lambda) + N(p) \to \gamma^*(q,\lambda) + N(p)$ can be conveniently described in terms of the Lorentz and gauge invariant Compton tensor $T^{\mu\nu}$. Beind defined as the matrix element of the two-current correlator,

$$T^{\mu\nu}(p,q) \equiv ie^2 \int d^4y\, e^{-iqy} \,\langle p|T\left[J^\nu_{\rm em}(0) J^\mu_{\rm em}(y)\right]|p\rangle, \tag{2.78}$$

the Compton tensor consists of four independent gauge-invariant tensor structures,

$$\begin{aligned} T^{\mu\nu}(p,q) = &\left(-g^{\mu\nu} + \frac{q^\mu q^\nu}{q^2}\right) T_1(\nu, Q^2) + \frac{1}{M^2}\left(p^\mu - \frac{p\cdot q}{q^2} q^\mu\right)\left(p^\nu - \frac{p\cdot q}{q^2} q^\nu\right) T_2(\nu, Q^2) \\ &+ \frac{i\epsilon^{\mu\nu\alpha\beta} q_\alpha}{M}\left[\mathcal{s}_\beta S_1(\nu, Q^2) + \left(\mathcal{s}_\beta (p\cdot q) - (\mathcal{s}\cdot q) p_\beta\right)\frac{1}{M^2} S_2(\nu, Q^2)\right], \end{aligned} \tag{2.79}$$

having the spin-independent amplitudes T_1 and T_2 as well as the spin-dependent ones S_1 and S_2. These amplitudes are functions of the photon energy $\nu = (s-u)/4M$ and virtuality $Q^2 = -q^2$; M is a target mass. The spin-dependent part is linear in the target spin four-vector $\mathfrak{s}^\mu$, which satisfies $p \cdot \mathfrak{s} = 0$ and $\mathfrak{s}^2 = -1$. The invariant amplitudes T_1, T_2, S_1 and S_2 have certain symmetry properties under the photon crossing, $\nu \to -\nu$,

$$\begin{aligned} T_1(-\nu, Q^2) &= T_1(\nu, Q^2), & T_2(-\nu, Q^2) &= T_2(\nu, Q^2), \\ S_1(-\nu, Q^2) &= S_1(\nu, Q^2), & S_2(-\nu, Q^2) &= -S_2(\nu, Q^2), \end{aligned} \tag{2.80}$$

which can be easily read out from Eq. (2.79).

Given that the Compton amplitude satisfies general principles of unitarity, causality and crossing, one can write down the following dispersion relations for the invariant Compton amplitudes T_1, T_2 and S_1 as

$$\{T_1, T_2, S_1\}(\nu, Q^2) = \frac{2}{\pi} \int_{\nu_{\rm el}}^{\infty} \frac{d\nu' \nu'}{\nu'^2 - \nu^2 - i0^+} \operatorname{Im} \{T_1, T_2, S_1\}(\nu', Q^2), \tag{2.81}$$

where $\nu_{\rm el} = Q^2/2M$ is the threshold energy for elastic scattering. The dispersive representation for the amplitude S_2, however, needs a remark. This amplitude has a pole in the subsequent limits of $Q^2 \to 0$ and then $\nu \to 0$. As will be explained further, such a pole can only emerge in the pole part of the Born contribution. Indeed, from Eqs. (2.93) it follows that the amplitudes T_1, T_2 and S_1 do not have a pole in the aforementioned limit, whereas S_2 does. Therefore the dispersion relation that involves this amplitude should be written for $\nu S_2(\nu, Q^2)$, which is pole-free for real photons, as follows

$$\nu S_2(\nu, Q^2) = \frac{2}{\pi} \int_{\nu_{\rm el}}^{\infty} d\nu' \frac{\nu'^2 \operatorname{Im} S_2(\nu', Q^2)}{\nu'^2 - \nu^2 - i0^+}. \tag{2.82}$$

The imaginary parts of the amplitudes that enter the dispersion relations (2.81) and (2.82) are related via the optical theorem to the nucleon structure functions, f_1, f_2, g_1 and g_2, or equivalently, to the cross sections of virtual-photon absorption $\gamma^* N \to X$ [1]:

$$\operatorname{Im} T_1(\nu, Q^2) = e^2 \frac{\pi}{M} f_1(x, Q^2) = \sqrt{\nu^2 + Q^2} \sigma_T(\nu, Q^2), \tag{2.83a}$$

$$\operatorname{Im} T_2(\nu, Q^2) = e^2 \frac{\pi}{\nu} f_2(x, Q^2) = \frac{Q^2}{\sqrt{\nu^2 + Q^2}} [\sigma_T + \sigma_L](\nu, Q^2), \tag{2.83b}$$

$$\operatorname{Im} S_1(\nu, Q^2) = e^2 \frac{\pi}{\nu} g_1(x, Q^2) = \frac{M\nu}{\sqrt{\nu^2 + Q^2}} \left[\sigma_{TT} + \frac{Q}{\nu} \sigma_{LT}\right](\nu, Q^2), \tag{2.83c}$$

$$\operatorname{Im} S_2(\nu, Q^2) = e^2 \frac{\pi M}{\nu^2} g_2(x, Q^2) = \frac{M^2}{\sqrt{\nu^2 + Q^2}} \left[\frac{\nu}{Q} \sigma_{LT} - \sigma_{TT}\right](\nu, Q^2), \tag{2.83d}$$

[1] Hereafter we will mostly follow the conventions from the review [171], implying, however, the Gilman's notation [174, 170] for the normalization of the virtual photon flux.

where the Bjorken variable $x = Q^2/2M\nu$ is introduced. The cross sections σ_T, σ_{TT} and σ_L can be defined in terms of the cross sections $\sigma_{\lambda+h}$ for definite photon (λ) and target (h) helicities as

$$\sigma_T = \frac{1}{2}\left(\sigma_{1/2}+\sigma_{3/2}\right), \quad \sigma_{TT} = \frac{1}{2}\left(\sigma_{1/2}-\sigma_{3/2}\right), \quad \sigma_L = \frac{1}{2}\left(\sigma_{1/2}+\sigma_{-1/2}\right). \tag{2.84}$$

Here the subscript L stands for longitudinally polarized photons while the subscript T stands for the transversely polarized photons. The cross section σ_{LT} corresponds to the simultaneous helicity flip of the photon and the spin flip of the target. While being a physical observable, it is not a cross section in the usual sense, but a response function (it is not positive-definite).

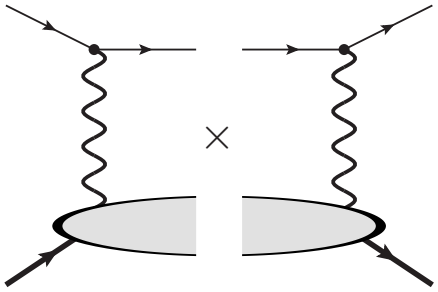

Fig. 2.5 The inclusive cross section of electron scattering on a spin-1/2 target, schematically shown as a two-photon exchange box.

These cross sections can be obtained by measuring inclusive inelastic cross section σ of the process of electron - spin-1/2 target scattering depicted in Fig. 2.5. The directly-measured quantity then can be written as

$$\frac{d\sigma}{d\Omega dE'} = \Gamma_V \left[\sigma_T + \epsilon\sigma_L - hP_x\sqrt{2\epsilon(1-\epsilon)}\sigma_{LT} - hP_z\sqrt{1-\epsilon^2}\sigma_{TT}\right]. \tag{2.85}$$

Here Γ_V is the virtual photon flux factor,

$$\Gamma_V = \frac{\alpha_{\text{em}}}{2\pi^2}\frac{E'}{E}\frac{\sqrt{Q^2+\nu^2}}{Q^2}\frac{1}{1-\epsilon}, \tag{2.86}$$

with the photon polarization

$$\epsilon = \frac{1}{1+2\left(1+\frac{\nu^2}{Q^2}\right)\tan^2\frac{\theta}{2}}. \tag{2.87}$$

The virtual photon, in its turn, is emitted by the relativistic electron, which changes its energy from E to E' being scattered on the angle θ. Since the electron is relativistic, its initial and final states are characterized by the same helicity $h = \pm 1/2$. The components of the target polarization with respect to the direction of the virtual photon three-momentum are pointed as P_x (perpendicular alignment in scattering plane) and P_z (parallel alignment).

Imposing the unitarity relations, given by Eqs. (2.83), into the dispersion relations (2.81) and (2.82) yields

$$T_1(\nu,Q^2)=\frac{2e^2}{M}\int_0^1\frac{dx}{x}\frac{f_1(x,Q^2)}{1-x^2(\nu/\nu_{\rm el})^2-i0^+}=\frac{2}{\pi}\int_{\nu_{\rm el}}^\infty d\nu'\frac{\nu'\sqrt{\nu'^2+Q^2}\sigma_T(\nu',Q^2)}{\nu'^2-\nu^2-i0^+}, \tag{2.88a}$$

$$T_2(\nu,Q^2)=\frac{4e^2M}{Q^2}\int_0^1 dx\frac{f_2(x,Q^2)}{1-x^2(\nu/\nu_{\rm el})^2-i0^+}=\frac{2Q^2}{\pi}\int_{\nu_{\rm el}}^\infty d\nu'\frac{\nu'\left[\sigma_T+\sigma_L\right](\nu',Q^2)}{\sqrt{\nu'^2+Q^2}(\nu'^2-\nu^2-i0^+)}, \tag{2.88b}$$

$$S_1(\nu,Q^2)=\frac{4e^2M}{Q^2}\int_0^1 dx\frac{g_1(x,Q^2)}{1-x^2(\nu/\nu_{\rm el})^2-i0^+}=\frac{2M}{\pi}\int_{\nu_{\rm el}}^\infty d\nu'\frac{\nu'^2\left[\sigma_{TT}+\frac{Q}{\nu'}\sigma_{LT}\right](\nu',Q^2)}{\sqrt{\nu'^2+Q^2}(\nu'^2-\nu^2-i0^+)}, \tag{2.88c}$$

$$\nu S_2(\nu,Q^2)=\frac{4e^2M^2}{Q^2}\int_0^1 dx\frac{g_2(x,Q^2)}{1-x^2(\nu/\nu_{\rm el})^2-i0^+}=\frac{2M^2}{\pi}\int_{\nu_{\rm el}}^\infty d\nu'\frac{\nu'^2\left[\frac{\nu'}{Q}\sigma_{LT}-\sigma_{TT}\right](\nu',Q^2)}{\sqrt{\nu'^2+Q^2}(\nu'^2-\nu^2-i0^+)}. \tag{2.88d}$$

It was established experimentally, that due to the convergence properties of T_1 the unsubtracted dispersion relation in the form (2.88a) does not hold. The easiest way to see the issue is to consider this amplitude at zero energy and virtuality, where it should yield the (negative) Thomson term,

$$T_1(0,0)=-\frac{e^2}{M}<0, \tag{2.89}$$

while the r.h.s is positively-defined:

$$\frac{2}{\pi}\int_{\nu_{\rm el}}^\infty d\nu'\sigma_T(\nu',Q^2=0)>0. \tag{2.90}$$

Therefore the dispersion relation (2.88a) requires one subtraction. Choosing the subtraction point at $\nu=0$, we obtain:

$$T_1(\nu,Q^2)=T_1(0,Q^2)+\frac{2\nu^2}{\pi^2}\int_{\nu_{\rm el}}^\infty d\nu'\frac{\sqrt{\nu'^2+Q^2}\sigma_T(\nu',Q^2)}{\nu'(\nu'^2-\nu^2-i0^+)}. \tag{2.91}$$

2.4.2 Born and pole contributions

The Born contribution to the Compton amplitudes, which corresponds to the target particle exchange in the intermediate state, can be found by calculation of the Born diagram (see Fig. 2.6) with electromagnetic vertex of the form

$$\Gamma^\mu(Q^2)=e\mathcal{F}_1(Q^2)\gamma^\mu+e\mathcal{F}_2(Q^2)\frac{i\sigma^{\mu\nu}q_\nu}{2M}, \tag{2.92}$$

where $\mathcal{F}_1$ and $\mathcal{F}_2$ are the Dirac and Pauli form factors, respectively. They are normalized to $\mathcal{F}_1(0)=1$ and $\mathcal{F}_2(0)=\varkappa$, whith $\varkappa$ being the anomalous magnetic moment. Then the corresponding Born parts of

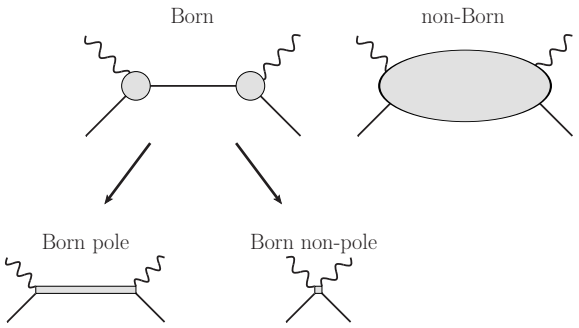

Fig. 2.6 Schematic splitting of the Compton amplitude into the Born and non-Born parts.

the Compton amplitude read

$$T_1^{\rm Born}(\nu,Q^2) = \frac{e^2}{M}\left\{\frac{\nu_{\rm el}^2}{\nu_{\rm el}^2-\nu^2}G_M^2(Q^2) - \mathcal{F}_1^2(Q^2)\right\} \tag{2.93a}$$

$$T_2^{\rm Born}(\nu,Q^2) = e^2\frac{2\nu_{\rm el}}{\nu_{\rm el}^2-\nu^2}\frac{G_E^2(Q^2)+\tau G_M^2(Q^2)}{1+\tau} \tag{2.93b}$$

$$S_1^{\rm Born}(\nu,Q^2) = \frac{e^2}{2M}\left\{\frac{Q^2}{\nu_{\rm el}^2-\nu^2}G_M(Q^2)\mathcal{F}_1(Q^2) - \mathcal{F}_2^2(Q^2)\right\} \tag{2.93c}$$

$$S_2^{\rm Born}(\nu,Q^2) = -\frac{e^2}{2}\frac{\nu}{\nu_{\rm el}^2-\nu^2}G_M(Q^2)\mathcal{F}_2(Q^2), \tag{2.93d}$$

where the electric (G_E) and magnetic (G_M) Sachs form factors were introduced. They are related to the Dirac and Pauli form factors as follows

$$G_E(Q^2) = \mathcal{F}_1(Q^2) - \tau\mathcal{F}_2(Q^2), \quad G_M(Q^2) = \mathcal{F}_1(Q^2) + \mathcal{F}_2(Q^2), \quad \tau = \frac{Q^2}{4M^2}. \tag{2.94}$$

The Born contributions, given by Eqs. (2.93), are already divided into pole (proportional to $[\nu_{\rm el}^2-\nu^2]^{-1}$) and non-pole parts.

The elastic parts of the structure functions are given as follows

$$f_1^{\rm el}(x,Q^2) = \frac{1}{2}G_M^2(Q^2)\delta(1-x), \tag{2.95}$$

$$f_2^{\rm el}(x,Q^2) = \frac{1}{1+\tau}\left[G_E^2(Q^2)+\tau G_M^2(Q^2)\right]\delta(1-x), \tag{2.96}$$

$$g_1^{\rm el}(x,Q^2) = \frac{1}{2}\mathcal{F}_1(Q^2)G_M(Q^2)\delta(1-x), \tag{2.97}$$

$$g_2^{\rm el}(x,Q^2) = -\frac{\tau}{2}\mathcal{F}_2(Q^2)G_M(Q^2)\delta(1-x). \tag{2.98}$$

Substituting these expressions to the dispersion relations (2.88), one obtains the pole contributions for the corresponding invariant Compton amplitudes:

$$T_1^{\text{pole}}(\nu, Q^2) = \frac{e^2}{M} \frac{\nu_{\text{el}}^2 G_M^2(Q^2)}{\nu_{\text{el}}^2 - \nu^2} = T_1^{\text{Born}}(\nu, Q^2) + \frac{e^2 \mathcal{F}_1^2(Q^2)}{M}, \tag{2.99a}$$

$$T_2^{\text{pole}}(\nu, Q^2) = \frac{2e^2 \nu_{\text{el}}}{\nu_{\text{el}}^2 - \nu^2} \frac{G_E^2(Q^2) + \tau G_M^2(Q^2)}{1+\tau} = T_2^{\text{Born}}(\nu, Q^2), \tag{2.99b}$$

$$S_1^{\text{pole}}(\nu, Q^2) = \frac{e^2 \nu_{\text{el}}}{\nu_{\text{el}}^2 - \nu^2} \mathcal{F}_1(Q^2) G_M(Q^2) = S_1^{\text{Born}}(\nu, Q^2) + \frac{e^2 \mathcal{F}_2^2(Q^2)}{2M}, \tag{2.99c}$$

$$\begin{aligned} [\nu S_2]^{\text{pole}}(\nu, Q^2) &= -\frac{e^2}{2} \frac{\nu_{\text{el}}^2}{\nu_{\text{el}}^2 - \nu^2} \mathcal{F}_2(Q^2) G_M(Q^2) \\ &= [\nu S_2]^{\text{Born}}(\nu, Q^2) - \frac{e^2}{2} G_M(Q^2) \mathcal{F}_2(Q^2), \end{aligned} \tag{2.99d}$$

with the Born part for $[\nu S_2]$ given by

$$[\nu S_2]^{\text{Born}}(\nu, Q^2) = \frac{e^2}{2} \left[1 - \frac{\nu_{\text{el}}^2}{\nu_{\text{el}}^2 - \nu^2} \right] G_M(Q^2) \mathcal{F}_2(Q^2). \tag{2.100}$$

Therefore it is useful to write the dispersion relations for the non-Born contributions, $\overline{T} \equiv T - T^{\text{Born}}$, as

$$\overline{T}_1(\nu, Q^2) = \frac{e^2}{M} \mathcal{F}_1^2(Q^2) + T_1(0, Q^2) + \frac{2\nu^2}{\pi} \int_{\nu_{\text{inel}}}^{\infty} d\nu' \frac{\sqrt{\nu'^2 + Q^2} \sigma_T(\nu', Q^2)}{\nu' (\nu'^2 - \nu^2 - i0^+)}, \tag{2.101a}$$

$$\overline{T}_2(\nu, Q^2) = \frac{2Q^2}{\pi} \int_{\nu_{\text{inel}}}^{\infty} d\nu' \frac{\nu' \left[\sigma_T + \sigma_L\right](\nu', Q^2)}{\sqrt{\nu'^2 + Q^2} (\nu'^2 - \nu^2 - i0^+)}, \tag{2.101b}$$

$$\overline{S}_1(\nu, Q^2) = \frac{e^2}{2M} \mathcal{F}_2^2(Q^2) + \frac{2M}{\pi} \int_{\nu_{\text{inel}}}^{\infty} d\nu' \frac{\nu'^2 \left[\sigma_{TT} + \frac{Q}{\nu'} \sigma_{LT}\right](\nu', Q^2)}{\sqrt{\nu'^2 + Q^2} (\nu'^2 - \nu^2 - i0^+)}, \tag{2.101c}$$

$$\overline{\nu S_2}(\nu, Q^2) = \frac{2M^2}{\pi} \int_{\nu_{\text{inel}}}^{\infty} d\nu' \frac{\nu'^2 \left[\frac{\nu'}{Q} \sigma_{LT} - \sigma_{TT}\right](\nu', Q^2)}{\sqrt{\nu'^2 + Q^2} (\nu'^2 - \nu^2 - i0^+)}. \tag{2.101d}$$

where the energy ν_{inel} corresponds to the lowest inelastic particle production threshold.

2.4.3 Low-energy theorems

The low-energy behavior of Compton amplitudes is driven by the low-energy theorems, which relate the expansion terms with particular electromagnetic quantities of the nucleon, such as polarizabilities. For instance, the expansion in ν and Q^2 of the non-pole parts of spin-independent ampliudes T_1 and T_2 reads

$$T_1^{\text{n/pole}}(\nu, Q^2) \equiv T_1(\nu, Q^2) - T_1^{\text{pole}}(\nu, Q^2) = -\frac{e^2}{M} + \left(\frac{e^2}{3M} \langle r^2 \rangle_1 + 4\pi \beta_{M1} \right) Q^2 + 4\pi (\alpha_{E1} + \beta_{M1}) \nu^2$$

$$+4\pi\left[\alpha_{E1\nu}+\beta_{M1\nu}+\frac{1}{12}(\alpha_{E2}+\beta_{M2})\right]\nu^4+\mathcal{O}(\mathcal{E}^6), \tag{2.102}$$

$$T_2^{\text{n/pole}}(\nu,Q^2)\equiv T_2(\nu,Q^2)-T_2^{\text{pole}}(\nu,Q^2)=4\pi\,(\alpha_{E1}+\beta_{M1})\,Q^2$$
$$+4\pi\left[\alpha_{E1\nu}+\beta_{M1\nu}+\frac{1}{12}(\alpha_{E2}+\beta_{M2})\right]Q^2\nu^2+\mathcal{O}(\mathcal{E}^6), \tag{2.103}$$

where $\langle r^2\rangle_1 = -6{}^d\!/_{dQ^2}\mathcal{F}_1(Q^2)|_{Q^2=0}$ is the Dirac radius, and the energy variable $\mathcal{E}$ refers to either Q or ν. The parameters α_{E1} and β_{M1} are the electric and magnetic static dipole polarizabilities, while $\alpha_{E1\nu}$ and $\beta_{M1\nu}$ represent their dispersive corrections. They describe a linear response of the system to electric ($\boldsymbol{E}$) and magnetic ($\boldsymbol{H}$) fields, which depend on the photon frequency ω, as [175]

$$\boldsymbol{d}(\omega)=4\pi(\alpha_{E1}+\alpha_{E1\nu}\omega^2+...)\boldsymbol{E}(\omega), \tag{2.104}$$
$$\boldsymbol{\mu}(\omega)=4\pi(\beta_{M1}+\beta_{M1\nu}\omega^2+...)\boldsymbol{H}(\omega), \tag{2.105}$$

with $\boldsymbol{d}$ and $\boldsymbol{\mu}$ being the electric and magnetic dipole moments, correspondingly. At the same time, the coefficients α_{E2} and β_{M2} are quadrupole polarizabilities, quantifying the electric (Q_{ij}) and magnetic (M_{ij}) quadrupole moments induced in a system when subjected to an external field gradients $E_{ij}={}^1\!/_2\left(\nabla_i E_j+\nabla_j E_i\right)$ and $H_{ij}={}^1\!/_2\left(\nabla_i H_j+\nabla_j H_i\right)$ [175]:

$$Q_{ij}=\frac{2\pi}{3}\alpha_{E2}E_{ij}, \tag{2.106a}$$
$$M_{ij}=\frac{2\pi}{3}\beta_{M2}H_{ij}. \tag{2.106b}$$

Similarly, the spin-dependent amplitudes S_1 and S_2 can be expanded at low energies in terms of the so-called spin polarizabilities [176]:

$$S_1^{\text{n/pole}}(\nu,Q^2)=-\frac{e^2\varkappa^2}{2M}+4\pi M\gamma_0\nu^2+MQ^2\left\{\frac{e^2\varkappa^2}{6M^2}\langle r^2\rangle_2+4\pi\gamma_{E1M2}\right.$$
$$\left.-3Me^2\left[P'^{(M1,M1)1}(0)+P'^{(L1,L1)1}(0)\right]\right\}+\mathcal{O}(\mathcal{E}^4) \tag{2.107a}$$

$$\nu S_2^{\text{n/pole}}(\nu,Q^2=0)=-M^2\nu^2\left\{4\pi(\gamma_0+\gamma_{E1E1})\right.$$
$$\left.-3Me^2\left[P'^{(M1,M1)1}(0)-P'^{(L1,L1)1}(0)\right]\right\}+\mathcal{O}(\nu^4) \tag{2.107b}$$

where $\varkappa\equiv\mathcal{F}_2(0)$ is the anomalous magnetic moment of the nucleon, $\langle r^2\rangle_2 = -6/\varkappa\,{}^d\!/_{dQ^2}F_2(Q^2)|_{Q^2=0}$ is the mean-square Pauli radius; γ_0 is the forward spin polarizability and γ_{E1M2} and γ_{E1E1} are the spin polarizabilities that correspond to the effective interaction of the spin with the electromagnetic fields via [177]

$$\mathcal{H}_{\text{eff}}=-4\pi\left[\frac{1}{2}\gamma_{E1E1}\boldsymbol{\sigma}\cdot\left(\boldsymbol{E}\times\dot{\boldsymbol{E}}\right)+\frac{1}{2}\gamma_{M1M1}\boldsymbol{\sigma}\cdot\left(\boldsymbol{H}\times\dot{\boldsymbol{H}}\right)\right.$$

$$-\gamma_{M1E2}E_{ij}\sigma_i H_j+\gamma_{E1M2}H_{ij}\sigma_i E_j\Big], \tag{2.108}$$

where $\boldsymbol{\sigma}$ is a vector of Pauli matrices. The derivatives of the generalized polarizabilities $P'^{(M1,M1)1}(0)$ and $P'^{(L1,L1)1}(0)$ come from the virtual Compton scattering [170, 171], provided that

$$P'^{(M1,M1)1}(0)\pm P'^{(L1,L1)1}(0)\equiv\frac{d}{d\boldsymbol{q}^2}\left[P^{(M1,M1)1}(\boldsymbol{q}^2)\pm P^{(L1,L1)1}(\boldsymbol{q}^2)\right]_{\boldsymbol{q}^2=0}. \tag{2.109}$$

In contrast to the spin-independent polarizabilities, the spin-dependent ones have no simple analogue in classical electrodynamics. We will not delve further into details about them, as they are beyond the scope of the present study.

2.4.4 Sum rules

2.4.4.1 Sum rules for AMM

In the soft-photon limit, i.e. both ν and Q^2 tend to 0, the non-Born part of spin-dependent amplitude S_1 must vanish. Hence, in this limit, making use of the dispersive representation (2.101c), one obtains a sum rule for the Born non-pole part of the amplitude,

$$-\frac{e^2\varkappa^2}{2M}=\frac{2M}{\pi}\int_{\nu_{\text{inel}}}^{\infty}d\nu'\frac{\sigma_{TT}(\nu',0)}{\nu'}, \tag{2.110}$$

which is the celebrated Gerasimov-Drell-Hearn-Hosoda-Yamamoto (GDH) sum rule [178–180]. Usually this sum rule is derived starting from the real forward Compton scattering. For this case the Compton tensor reduces to (see, e.g. [181])

$$T^{\mu\nu}(p,q)=-g^{\mu\nu}f(\nu)+i\sigma^{\mu\nu}g(\nu), \tag{2.111}$$

where $f(\nu)$ ($g(\nu)$) are the invariant amplitudes, symmetric (antisymmetric) in ν. The helicity amplitudes then have the0 form

$$T_{\lambda,h\to\lambda',h'}=\chi^{\dagger}_{h'}\left\{f(\nu)\vec{\varepsilon}^{\,*}_{\lambda'}\cdot\vec{\varepsilon}_{\lambda}+g(\nu)i\left(\vec{\varepsilon}^{\,*}_{\lambda'}\times\vec{\varepsilon}_{\lambda}\right)\cdot\vec{\sigma}\right\}\chi_h, \tag{2.112}$$

where $\varepsilon_\lambda=(0,\vec{\varepsilon}_\lambda)$ ($\varepsilon^*_{\lambda'}=(0,\vec{\varepsilon}^{\,*}_{\lambda'})$) is the polarization vector of the incoming (outgoing) photon with helicitiy λ (λ'); χ_h ($\chi^{\dagger}_{h'}$) is the Dirac spinor with helicity h (h') for the incoming (outgoing) spin-1/2 target. The helicity combination responsible for the GDH sum rule is

$$\frac{1}{2}\left[T_{1,\frac{1}{2}\to1,\frac{1}{2}}-T_{1,-\frac{1}{2}\to1,-\frac{1}{2}}\right]=S_1(\nu,0)\frac{\nu}{M}=4\pi g(\nu), \tag{2.113}$$

where the 4π normalization factor was added to follow the common convention for $f(\nu)$ and $g(\nu)$ amplitudes. Then the optical theorem for the amplitude $g(\nu)$ reads

$$\mathrm{Im}\, g(\nu) = \frac{\nu \sigma_{TT}(\nu)}{4\pi}. \tag{2.114}$$

Given that the amplitude $g(\nu)$ is antisymmetric in ν, it should satisfy the following dispersion relation

$$g(\nu) = \frac{\nu}{2\pi^2} \int_{\nu_{\rm el}}^{\infty} d\nu' \frac{\nu' \sigma_{TT}(\nu')}{\nu'^2 - \nu^2}, \tag{2.115}$$

which is similar to Eq. (2.88c). Implying the low-energy theorem for $g(\nu)$ in the l.h.s. of Eq. (2.115), one immediately obtains the GDH sum rule.

Owing to the fact that the amplitude νS_2 should vanish in the limit $\nu \to 0$, while keeping $Q^2 \geq 0$, the same steps lead to the well-known Burkhardt-Cottingham (BC) sum rule [182]:

$$\frac{e^2}{2}(1+\varkappa)\varkappa = \frac{2M^2}{Q^2} \int_{\nu_{\rm inel}}^{\infty} \frac{d\nu'}{\sqrt{\nu'^2+Q^2}} \left[\frac{\nu'}{Q} \sigma_{LT} - \sigma_{TT} \right] (\nu', Q^2). \tag{2.116}$$

Adding the elastic part to both sides of Eq. (2.116) yields the BC sum rule in the following form

$$0 = \int_0^1 g_2(x, Q^2) dx. \tag{2.117}$$

Furthermore, the linear combination S_{LT} of the amplitudes S_1 and νS_2,

$$S_{LT}(\nu, Q^2) = M S_1(\nu, Q^2) + \nu S_2(\nu, Q^2), \tag{2.118}$$

whose imaginary part is proportional to just σ_{LT},

$$\mathrm{Im}\, S_{LT}(\nu, Q^2) = \frac{M^2 \sqrt{\nu^2+Q^2}}{Q} \sigma_{LT}(\nu, Q^2) \tag{2.119}$$

allows one to write one more interesting sum rule. Given that this combination is even in ν, the non-pole part should obey the following dispersion relation

$$S_{LT}(\nu, Q^2) = \frac{2M^2}{\pi} \int_{\nu_{\rm inel}}^{\infty} d\nu' \frac{\nu' \sqrt{\nu'^2+Q^2}}{\nu'^2 - \nu^2 - i0^+} \frac{\sigma_{LT}(\nu', Q^2)}{Q}. \tag{2.120}$$

The Born non-pole part of S_{LT} is given by

$$S_{LT}^{\text{Born, n/pole}}(\nu, Q^2) = \frac{e^2}{2} \mathcal{F}_1(Q^2) \mathcal{F}_2(Q^2). \tag{2.121}$$

Thus, in the limit $\nu, Q^2 \to 0$ the dispersion relation (2.120) reduces to

$$\mathcal{F}_1(0)\mathcal{F}_2(0) = \frac{4M^2}{e^2\pi}\int_{\nu_{\text{inel}}}^{\infty} d\nu' \frac{\sigma_{LT}(\nu', Q^2)}{Q}\bigg|_{Q^2\to 0}, \tag{2.122}$$

which is the Schwinger sum rule [183–185]. For charged particles it linearly relates the integrated polarized photoabsorption observable σ_{LT} with the AMM of the particle

$$\varkappa = \frac{4M^2}{e^2\pi}\int_{\nu_{\text{inel}}}^{\infty} d\nu' \frac{\sigma_{LT}(\nu', Q^2)}{Q}\bigg|_{Q^2\to 0}. \tag{2.123}$$

Since the AMM appears linearly, determining its value to a given order in α_{em}, e.g., $O(\alpha_{\text{em}})$, requires knowledge of the observable σ_{LT} up to α_{em}^2. In contrast, achieving the same precision using the GDH or BC sum rules, where $\varkappa$ enters quadratically, necessitates knowledge of the corresponding cross sections up to α_{em}^3. This means that the Schwinger sum rule can be checked against the nontrivial result for $\varkappa$ already at the one-loop level in perturbative calculations. It was firstly done in QED by J. Schwinger and his group (W. Tsai, L. DeRaad and K. Milton) [183, 185], who reproduced the famous $\alpha_{\text{em}}/2\pi$ correction. The leading-order verification of this sum rule also was made for the contribution of a neutral massive vector field [149].

2.4.4.2 Sum rules for polarizabilities

The most prominent sum rule for spin-independent polarizabilities, namely for α_{E1} and β_{M1} is the Baldin sum rule [186]:

$$\alpha_{E1} + \beta_{M1} = \frac{1}{2\pi^2}\int_{\nu_{\text{inel}}}^{\infty} d\nu' \frac{\sigma_T(\nu', Q^2 = 0)}{\nu'^2}. \tag{2.124}$$

It can be immediately obtained by equalling ν^2-terms in the low-energy expansion of the dispersion relation (2.101a) for $\overline{T}_1$ with the corresponding low-energy theorem (2.102). Alternatively, it can be also derived from the amplitude T_2. This sum rule has been instrumental for the data-driven evaluations of the nucleon polarizabilities, and since long [187] provides the most stringent empirical constraint on the sum of proton polarizabilties, see [181] for the state of the art. Even in the recent experimental determinations of the proton electromagnetic polarizabilities by the A2 [157] and HIGS [156] Collaborations, the Baldin sum rule was used to constrain the fits to the experimental data, serving as an additional experimental point (A2) or a strict constraint (HIGS).

Due to the squared energy factor in the denominator under the integral of Eq. (2.124), the Baldin sum rule converges rather fast. The high-energy asymptotics, given by Regge phenomenology, either does not spoil its convergence. Indeed, as was shown in [188] for the photoabsorption data on the proton, the high-energy behavior of σ_T could be parametrized by the Reggeon (R), soft (P_s) and hard (P_h) Pomerons:

$$\sigma_T(\nu, Q^2 = 0) \propto A_R \nu^{\alpha_R - 1} + A_{P_s}\nu^{\alpha_{P_s}-1} + A_{P_h}\nu^{\alpha_{P_h}-1}, \tag{2.125}$$

with the intercept parameters $\alpha_R = 0.524$, $\alpha_{P_s} = 1.0667$, $\alpha_{P_h} = 1.452$. Thus, the integrand in Eq. (2.124) behaves at worst as[2]

$$\frac{\sigma_T(\nu \to \infty, Q^2 = 0)}{\nu^2} \propto \nu^{-1.548}, \tag{2.126}$$

providing the rapid convergence even at high energies.

While the Baldin sum rule for the sum of the polarizabilities is well-established, it is of great interest to have similar relations for each individual polarizabilitiy. Unfortunately, one cannot write down a sum rule for β_{M1} from the Q^2-term of T_1 amplitude given that it will be expressed through the unknown subtraction function $T_1(0, Q^2)$:

$$\beta_{M1} = -\frac{e^2}{12\pi M}\langle r^2\rangle_1 + \left.\frac{\partial T_1(0,Q^2)}{\partial Q^2}\right|_{Q^2\to 0}. \tag{2.127}$$

However, one can consider the invariant Compton amplitude T_L, which corresponds to the scattering of longitudinally-polarized photons:

$$T_L(\nu, Q^2) = \left(1 + \frac{\nu^2}{Q^2}\right) T_2(\nu, Q^2) - T_1(\nu, Q^2). \tag{2.128}$$

The low-energy behavior of its non-pole part is given by

$$\begin{aligned} T_L^{\text{n/pole}}(\nu, Q^2) = &\left(-\frac{e^2\varkappa}{4M} + 4\pi\alpha_{E1}\right) Q^2 \\ &+ 4\pi\left[\alpha_{E1\nu} + \beta_{M1\nu} + \frac{1}{12}(\alpha_{E2} + \beta_{M2})\right] Q^2\nu^2 + O(\mathcal{E}^6), \end{aligned} \tag{2.129}$$

where the term with anomalous magnetic moment $\varkappa$ comes from the Born non-pole part [170]. It can be derived by substituting the Born parts for T_1 and T_2 amplitudes into Eq. (2.128), which yields

$$\begin{aligned} T_L^{\text{Born}}(\nu, Q^2) &= \left(\frac{\nu_{\text{el}}(\nu_{\text{el}} + 2M)}{2M\nu_{\text{el}}^2} - \frac{\nu_{\text{el}}^2 - \nu^2}{2M\nu_{\text{el}}^2}\right) T_2^{\text{Born}}(\nu, Q^2) - T_1^{\text{Born}}(\nu, Q^2) \\ &= -\frac{e^2 Q^2 \mathcal{F}_2^2(Q^2)}{4M^3} + e^2 \frac{2\nu_{\text{el}}}{\nu_{\text{el}}^2 - \nu^2} G_E^2(Q^2). \end{aligned} \tag{2.130}$$

The unsubtracted dispersion relation for T_L reads

$$T_L(\nu, Q^2) = \frac{2}{\pi}\int_{\nu_{\text{el}}}^{\infty} d\nu' \frac{\nu'\sqrt{\nu'^2 + Q^2}\,\sigma_L(\nu', Q^2)}{\nu'^2 - \nu^2 - i0^+}, \tag{2.131}$$

[2] In reality, hard Pomeron decouples for $Q^2 \to 0$, thus $\sigma_T(\nu \to \infty, Q^2 = 0)$ behaves approximately as $\nu^{0.07}$ modulo logarithmic terms.

were the optical theorem has been used to relate the imaginary part of T_L with the polarized photoabsorption cross section σ_L,

$$\mathrm{Im}\, T_L(\nu, Q^2) = \sqrt{\nu^2 + Q^2}\,\sigma_L(\nu, Q^2). \tag{2.132}$$

Now, relating the low-energy behavior of T_L, given by Eq. (2.129), with the dispersion relation (2.131), we arrive at the sum rule for electric polarizability, a "virtual sibling" of the Baldin sum rule:

$$\alpha_{E1} - \frac{\alpha_{\mathrm{em}}\varkappa^2}{4M^3} = \frac{1}{2\pi^2}\int_{\nu_{\mathrm{inel}}}^{\infty} d\nu'\, \frac{\sigma_L(\nu, Q^2)}{Q^2}\bigg|_{Q^2\to 0}. \tag{2.133}$$

The smooth limit $Q^2 \to 0$ of the integrand is guaranteed by gauge invariance, i.e. the longitudinal photon brings a factor of Q in the photoabsorption amplitude. The sum rule (2.133), while mentioned in 1972 by Sucher [154], has been explicitely written down by Bernabéu and Tarrach [155] in 1975. The detailed discussion of its convergence and possible further useful outcomes will be discussed in details in Chapter 7.

Appendices

2.A Conventions

We perform the calculations in the natural units, $\hbar = c = 1$ and rely on the following convention of the Minkowski metric:

$$g_{\mu\nu} = \begin{pmatrix} 1 & 0 & 0 & 0 \\ 0 & -1 & 0 & 0 \\ 0 & 0 & -1 & 0 \\ 0 & 0 & 0 & -1 \end{pmatrix}, \tag{2.134}$$

defining the scalar product of four-vectors $a^\mu = (a^0, \boldsymbol{a})$ and $b^\mu = (b^0, \boldsymbol{b})$ as

$$a \cdot b = g_{\mu\nu} a^\mu b^\nu = a_0 b^0 - \boldsymbol{a} \cdot \boldsymbol{b}. \tag{2.135}$$

For calculations at light cone, we use the metric

$$g^{LC}_{\mu\nu} = \begin{pmatrix} 0 & 1 & 0 & 0 \\ 1 & 0 & 0 & 0 \\ 0 & 0 & -1 & 0 \\ 0 & 0 & 0 & -1 \end{pmatrix}, \tag{2.136}$$

where the scalar product of light-cone four vectors $a^\mu = (a^+, a^-, \boldsymbol{a}_\perp)$ and $b^\mu = (b^+, b^-, \boldsymbol{b}_\perp)$, with $(a^\pm, b^\pm) \equiv 1/2 \left\{ (a^0, b^0) \pm (a^3, b^3) \right\}$, as

$$a \cdot b = g^{LC}_{\mu\nu} a^\mu b^\nu = (a^+ b^- + a^- b^+) - \boldsymbol{a}_\perp \cdot \boldsymbol{b}_\perp. \tag{2.137}$$

The Pauli matrices are defined as usual

$$\sigma_x = \begin{pmatrix} 0 & 1 \\ 1 & 0 \end{pmatrix}, \quad \sigma_y = \begin{pmatrix} 0 & -i \\ i & 0 \end{pmatrix}, \quad \sigma_z = \begin{pmatrix} 1 & 0 \\ 0 & -1 \end{pmatrix}. \tag{2.138}$$

We use the gamma matrices in Dirac representation, defined as

$$\gamma^0 = \begin{pmatrix} \mathbb{1} & 0 \\ 0 & -\mathbb{1} \end{pmatrix}, \quad \gamma^k = \begin{pmatrix} 0 & \sigma_k \\ -\sigma_k & 0 \end{pmatrix}, \quad \gamma_5 = i\gamma^0\gamma^1\gamma^2\gamma^3 = \begin{pmatrix} 0 & \mathbb{1} \\ \mathbb{1} & 0 \end{pmatrix}. \tag{2.139}$$

The one-loop results are usually expressed in terms of the scalar Passarino-Veltman integrals [189] in `LoopTools` [7] or `Package-X` [5, 6] notations. In particular, the scalar integral C_0 of the triangle

loop is defined as

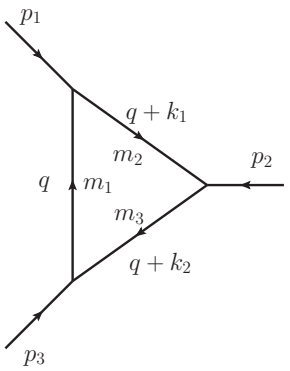

$$= \begin{cases} C_0(p_1^2, p_2^2, (p_1+p_2)^2; m_1^2, m_2^2, m_3^2) & \texttt{LoopTools notations} \\ C_0(p_1^2, p_2^2, (p_1+p_2)^2; m_1, m_2, m_3) & \texttt{Package-X notations} \end{cases}$$

$$= \frac{\mu^{4-\mathrm{d}}}{i\pi^{\mathrm{d}/2}} \frac{\Gamma(1-2\epsilon)}{\Gamma^2(1-\epsilon)\Gamma(1+\epsilon)} \int d^{\mathrm{d}}q \frac{1}{(q^2-m_1^2)\left[(q+k_1)^2-m_2^2\right]\left[(q+k_2)^2-m_3^2\right]}, \tag{2.140}$$

where $\mathrm{d} = 4-2\epsilon$, $k_1 = p_1$ and $k_2 = p_1+p_2$. The loop calculations in this work were performed mostly employing `Package-X` and partially `LoopTools`.

Also, the Källén (or triangular) function λ is widely used,

$$\lambda(x,y,z) = x^2+y^2+z^2-2xy-2xz-2yz. \tag{2.141}$$

2.B Conformal mapping variable $\omega(s)$

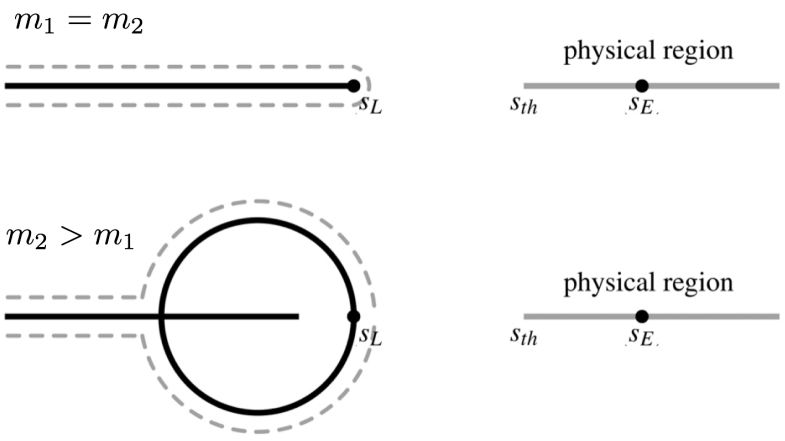

Fig. 2.7 Left-hand cut singularities (solid black curves) in the complex s-plane for the case when $m_1 = m_2$ (upper plane) and $m_2 > m_1$ (lower plane). In the plot, we schematically show the position of the closest left-hand cut singularity (s_L), threshold (s_{th}), and the expansion point (s_E). Dashed lines determine the specific form of the conformal map and subsequently the domain of convergence of the conformal expansion. Figure is taken from [190].

The form of $\omega(s)$ depends on the cut structure of the reaction. Since it is impossible to write a dispersive representation for the inverse amplitude in the coupled-channel case, we do not consider an inclusion into $\omega(s)$ possible inelastic cuts[3], as it was proposed in [193–195]. Therefore $\omega(s)$ is solely specified by the position of the closest left-hand cut branching point (s_L) and an expansion point (s_E), around which the series is expanded, $\omega(s_E) = 0$. The latter typically is chosen in the middle between the threshold and the energy of the last data point that is fitted to the data,

$$\sqrt{s_E} = \frac{1}{2}\left(\sqrt{s_{th}} + \sqrt{s_{max}}\right) . \tag{2.142}$$

This particular choice guarantees a fast convergence of the conformal expansion in that region. To access some of the systematic uncertainties, the value of s_E can be varied around its central value (2.142).

Since for the scattering of the particles with $m_1 = m_2 = m$ the left-hand cut lies on the real axis, $-\infty < s < s_L$, one can use a simple function

$$\begin{aligned} \omega(s) &= \frac{\sqrt{s - s_L} - \sqrt{s_E - s_L}}{\sqrt{s - s_L} + \sqrt{s_E - s_L}}, \\ s_L &= 4m^2 - t_x , \end{aligned} \tag{2.143}$$

where t_x is the lowest threshold in the crossed t or u channels. For instance for $\pi\pi \to \pi\pi$ or $D\bar{D} \to D\bar{D}$ scattering $t_x = 4m_\pi^2$.

For the case when $m_2 > m_1$ (e.g. $\pi K \to \pi K$ or $\pi D \to \pi D$ scattering), the left-hand cut structure is a bit more complicated (see Fig. 2.7). In addition to the left-hand cut lying on the real axis $-\infty < s < (m_2 - m_1)^2$, there is a circular cut at $|s| = m_2^2 - m_1^2$. The conformal map that meets these requirements is defined as

$$\begin{aligned} \omega(s) &= -\frac{\left(\sqrt{s} - \sqrt{s_E}\right)\left(\sqrt{s}\sqrt{s_E} + s_L\right)}{\left(\sqrt{s} + \sqrt{s_E}\right)\left(\sqrt{s}\sqrt{s_E} - s_L\right)}, \\ s_L &= m_2^2 - m_1^2 . \end{aligned} \tag{2.144}$$

We note that for the forms of $\omega(s)$, given in Eqs. (2.143) and (2.144), the conformal series, being truncated at any finite order, is bounded asymptotically. This is consistent with the assigned asymptotic behavior.

[3]The correct way of implementing inelastic cuts is through the coupled-channel dispersion relation for the direct amplitude [191, 192] or by considering Roy-like equations [44–49, 37, 50–53].

Chapter 3

Dispersive inverse amplitude method for elastic scattering of spinless particles

This Chapter introduces an improved approach to parameterizing elastic scattering amplitudes for spinless particles that adheres to fundamental S-matrix constraints while offering practical applicability. The method centers on writing a dispersion relation for the inverse amplitude. The left-hand cut contribution in the physical region are parametrized using a conformal mapping expansion, respecting its analytical structure. Possible Adler zeros are incorporated as additive pole terms in the inverse amplitude and implements angular momentum barrier factors for higher partial waves. This dispersive parameterization offers several advantages over conventional techniques. Unlike common Breit-Wigner or K-matrix parameterizations, our method rigorously accounts for the left-hand cut and avoids introducing spurious poles. It also allows for a more systematic implementation of the Adler zero constraint, which is often overlooked or treated phenomenologically in other approaches. Furthermore, our framework extends beyond existing methods like the K-matrix with Chew-Mandelstam phase space or previous conformal map parameterizations. By requiring the inverse amplitude to satisfy the dispersion relation, we significantly constrain the possible forms of the parametrization, leading to more reliable results. We also demonstrate the equivalence of partial-wave dispersion relations for direct and inverse amplitudes in elastic scattering and show how our approach encompasses the modified Inverse Amplitude Method (mIAM) as a special case. This chapter will detail the formalism of our dispersive parameterization, compare it conceptually with existing methods, and present numerical test cases, with a particular focus on recent lattice data for S-wave isoscalar $\pi\pi$ and πK scattering. Through this exploration, we aim to provide a more rigorous and versatile tool for extracting resonance properties from both experimental and lattice QCD data.

The work presented in this Chapter is based on the publication [190], for which the author conducted all the numerical calculations, and the proceeding [196].

3.1 Dispersive parametrization of inverse amplitude

3.1.1 S-wave scattering

We start explaining the method with the simplest case – the S-wave ($J = 0$) scattering. The possible zero of the amplitude, $t_0(s_A) = 0$ (which in the case of the $\pi\pi$ and πK scattering corresponds to the Adler zero), can be incorporated either as a zero of $N(s)$ or as a pole in $D(s)$. In the former case, the easiest is to choose $s_M = s_A$, leading to

$$\begin{aligned} D(s) &= 1 - \frac{s - s_A}{\pi} \int_{s_{th}}^{\infty} \frac{ds'}{s' - s_A} \frac{N(s')\,\rho(s')}{s' - s}, \\ N(s) &= U(s) + \frac{s - s_A}{\pi} \int_{s_{th}}^{\infty} \frac{ds'}{s' - s_A} \frac{N(s')\,\rho(s')\,(U(s') - U(s))}{s' - s}. \end{aligned} \tag{3.1}$$

where $U(s_A) = 0$ from (2.39). On another side, the set of integral equations with the so-called Castillejo-Dalitz-Dyson (CDD) pole [161] at s_A has the following form (for any $s_M \neq s_A$)

$$\begin{aligned} D(s) &= 1 - \frac{s - s_M}{\pi} \int_{s_{th}}^{\infty} \frac{ds'}{s' - s_M} \frac{N(s')\,\rho(s')}{s' - s} + (s - s_M) \frac{g_1}{s - s_A}, \\ N(s) &= U(s) + \frac{s - s_M}{\pi} \int_{s_{th}}^{\infty} \frac{ds'}{s' - s_M} \frac{N(s')\,\rho(s')\,(U(s') - U(s))}{s' - s} + (s - s_M) \frac{g_1\,(U(s) - U(s_A))}{s - s_A}. \end{aligned} \tag{3.2}$$

Using a toy model, both (3.1) and (3.2) have been checked numerically to give the same solution that satisfies the initial p.w. dispersion relation (2.38) with the constraint $t_0(s_A) = 0$. Even though the realization through the CDD pole looks more complicated, it allows us to obtain a simple analytical formula under the assumption that $U(s) \approx U_0 = const$. In this case Eq.(3.2) reduces to

$$[t_0(s)]^{-1} \approx \frac{1}{U_0} + \frac{s - s_M}{\pi} \int_{s_{th}}^{\infty} \frac{ds'}{s' - s_M} \frac{-\rho(s')}{s' - s} + (s - s_M) \frac{g_1/U_0}{s - s_A}. \tag{3.3}$$

For the more complicated form of the left-hand cut, one needs to solve an integral equation numerically using the matrix inversion method, which requires significant computation time in the case of bootstrap fits.

Alternative to the conventional p.w. dispersion relation, for the elastic scattering one can write a partial wave dispersion relation for the inverse amplitude

$$[t_0(s)]^{-1} = [t_0(\tilde{s}_M)]^{-1} + \frac{s - \tilde{s}_M}{\pi} \int_{L,R} \frac{ds'}{s' - \tilde{s}_M} \frac{\mathrm{Im}\,[t_0(s')]^{-1}}{s' - s} + \frac{s - \tilde{s}_M}{s_A - \tilde{s}_M} \frac{g_A}{s - s_A}, \tag{3.4}$$

where we allowed for the pole contribution at $s = s_A$, which corresponds to the Adler zero in $\pi\pi$ and πK scattering. The integral over the right-hand cut can be fixed again from unitarity in Eq. (2.32),

leading to the following integral equation

$$[t_0(s)]^{-1} = [t_0(\tilde{s}_M)]^{-1} + \frac{s-\tilde{s}_M}{\pi}\int_L \frac{ds'}{s'-\tilde{s}_M}\frac{\text{Im}\,[t_0(s')]^{-1}}{s'-s} + \frac{s-\tilde{s}_M}{\pi}\int_{s_{th}}^{\infty}\frac{ds'}{s'-\tilde{s}_M}\frac{-\rho(s')}{s'-s} + \frac{s-\tilde{s}_M}{s_A-\tilde{s}_M}\frac{g_A}{s-s_A}\,. \tag{3.5}$$

We emphasize that Eqs. (3.5) and (2.37) are equivalent: $t_0(s)$ and $[t_0(s)]^{-1}$ have the same analytic structure, except for the possible presence of the poles (or zeros) in $t_0(s)$ and $[t_0(s)]^{-1}$. It could be a pole in $t_0(s)$ that correspond to the bound state and therefore $[t_0(s_B)]^{-1} = 0$. Another possibility is a pole in $[t_0(s)]^{-1}$, that correspond to the Adler zero, $t_0(s_A) = 0$. The constraints of $t_0(s_A) = 0$ and $[t_0(s_B)]^{-1} = 0$ can be easily incorporated in Eqs. (2.37) and (3.5) by choosing $s_M = s_A$ and $\tilde{s}_M = s_B$, respectively. We checked numerically for the elastic isoscalar $\pi\pi$ S-wave scattering that Eqs. (2.37) and (3.5) are consistent with each other using a toy model for the left-hand cut discontinuity in Eq. (2.37).

In a general scattering problem, little is known about the left-hand cuts, except their analytic structure in the complex plane. The progress has been made in [197–200]. It relies on the consideration of an analytic continuation of the left-hand cut contributions to the physical region, employing a series expansion in terms of a suitably constructed conformal mapping variable $\omega(s)$. The latter is chosen such that it maps the left-hand cut plane onto the unit circle [201]. For the most typical cases the exact forms of $\omega(s)$ was given in Appendix 2.B. In [191, 192] the function $U(s)$ of Eq. (2.38) was expanded in the conformal mapping series. Here we suggest to apply the conformal mapping expansion to the first two terms of Eq. (3.5), which leads to the following parametrization of the inverse of $t_0(s)$,

$$[t_0(s)]^{-1} \simeq \sum_{n=0}^{\infty} C_n\,\omega^n(s) + R(s,\tilde{s}_M) + \frac{s-\tilde{s}_M}{s_A-\tilde{s}_M}\frac{g_A}{s-s_A}\,, \tag{3.6}$$

$$R(s,\tilde{s}_M) \equiv \frac{s-\tilde{s}_M}{\pi}\int_{s_{th}}^{\infty}\frac{ds'}{s'-\tilde{s}_M}\frac{-\rho(s')}{s'-s}\,. \tag{3.7}$$

The unknown coefficients C_n, g_A and s_A can be adjusted to reproduce the experimental or lattice data or fixed from the effective field theory by imposing some matching condition. Note that when the conformal series is truncated to a single dominant term, Eq.(3.6) coincides with Eq.(3.3), which was derived from the N/D ansatz.

The advantage of (3.5) compared to (2.38) in the elastic approximation is twofold. First of all, when in both dispersion representations the left-hand cut is approximated by the conformal expansion, Eq. (3.5) becomes much simpler than Eq. (2.38), because one does not need to solve numerically the integral equation. Secondly, as it will be shown below, it is easy to extend the formalism to $J \neq 0$. However, the dispersion relation for the inverse amplitude has a clear limitation: it cannot be extended to the coupled-channel case [202, 203]. Due to the matrix inversion, there would be a mixture of the left-hand cuts of all involved channels, which can also affect the physical region where one has an

overlapping cut structure. The typical example is the coupled-channel $\{\pi\pi, K\bar{K}\}$ scattering [204], in which the left-hand cut of $K\bar{K} \to K\bar{K}$ starts at $4\,(m_K^2 - m_\pi^2)$ and the matrix inversion will therefore produce a spurious contribution to the $\pi\pi \to \pi\pi$ unitarity cut. In contrast, the overlapping of the left and right-hand cuts in $K\bar{K} \to K\bar{K}$ does not jeopardize the N/D framework, since it happens in the non-physical region (see Ref. [191, 192] for more details and its application to $f_0(980)$).

3.1.2 $J \neq 0$, $m_1 = m_2$ scattering

For the case of scattering with $J \neq 0$ one needs to take into account the angular momentum barrier factor which implies that around the threshold the amplitude should behave as

$$t_J(s) \sim p(s)^{2J} \overset{m_1=m_2}{\sim} (s - s_{th})^J \,. \tag{3.8}$$

This is implemented by writing a $J+1$ subtracted dispersion relation for the ratio

$$f_J(s) \equiv \frac{(s - s_{th})^J}{t_J(s)}\,, \tag{3.9}$$

which is free from kinematic constraints. It leads to

$$\begin{aligned} f_J(s) = &\sum_{i=0}^{J} \frac{1}{i!} f_J^{(i)}(s_{th})\,(s - s_{th})^i \\ &+ \frac{(s - s_{th})^{J+1}}{\pi} \int_{L,R} \frac{ds'}{(s' - s_{th})^{J+1}} \frac{\text{Im}\, f_J(s')}{s' - s}, \end{aligned} \tag{3.10}$$

where no Adler-related pole was added since there is no known reaction where the amplitude has an extra zero in addition to the one at $s = s_{th}$ given in Eq. (3.8). Note, that here we subtracted the dispersion relation at the threshold. It allows us to bring the integral over the right-hand cut into the form of Eq. (3.7). Indeed, re-expressing $f_J(s)$ in terms of $t_J(s)$ and applying the unitarity relation (2.32), we obtain

$$\begin{aligned} [t_J(s)]^{-1} = &\frac{1}{(s - s_{th})^J} \sum_{i=0}^{J} \frac{1}{i!} f_J^{(i)}(s_{th})\,(s - s_{th})^i \\ &+ \frac{s - s_{th}}{\pi} \int_L \frac{ds'}{s' - s_{th}} \frac{\text{Im}\,[t_J(s')]^{-1}}{s' - s} \\ &+ \frac{s - s_{th}}{\pi} \int_{s_{th}}^{\infty} \frac{ds'}{s' - s_{th}} \frac{-\rho(s')}{s' - s}. \end{aligned} \tag{3.11}$$

Since $f_J^{(i)}(s_{th})$ are in general unknown constants, one can write a general parametrization

$$[t_J(s)]^{-1} \simeq \frac{1}{(s - s_{th})^J} \sum_{i=0}^{J-1} \frac{1}{i!} f_J^{(i)}(s_{th})\,(s - s_{th})^i + \sum_{n=0}^{\infty} C_n\, \omega^n(s) + R(s, s_{th})\,,$$

where as before, the contribution from the left-hand cut together with the constant term was expanded in a suitably constructed conformal mapping series. For instance, for $J = 1$ it corresponds to

$$[t_1(s)]^{-1} \simeq \frac{a}{s - s_{th}} + \sum_{n=0}^{\infty} C_n \omega^n(s) + R(s, s_{th}), \tag{3.12}$$

and similar for $J = 2$

$$[t_2(s)]^{-1} \simeq \frac{a}{(s - s_{th})^2} + \frac{b}{s - s_{th}} + \sum_{n=0}^{\infty} C_n \omega^n(s) + R(s, s_{th}). \tag{3.13}$$

The parameters a, b and C_n will be fitted to the data in Sec. 3.4.

3.1.3 $J \neq 0$, $m_1 \neq m_2$ scattering

In case of non-equal masses, we propose to write a dispersive representation for the amplitude

$$g_J(s) \equiv \frac{p(s)^{2J}}{t_J(s)}, \tag{3.14}$$

which is free from any kinematic constraints. The corresponding $J+1$-times subtracted dispersion relation reads

$$g_J(s) = P_J(s) + \frac{Q_{J+1}(s)}{\pi} \int_{L,R} \frac{ds'}{Q_{J+1}(s')} \frac{\text{Im}\, g_J(s')}{s' - s}, \tag{3.15}$$

where $P_J(s)$ is a polynomial of degree J and $Q_{J+1}(s)$ is defined as

$$Q_{J+1}(s) \equiv (s - s_{M_1})(s - s_{M_2}) \dots (s - s_{M_{J+1}}). \tag{3.16}$$

The choice of the subtraction points s_{M_i} is in general arbitrary. However, it is useful to choose s_{M_i} in such a way, that the integral over the right-hand cut can be written in terms of $R(s, \tilde{s}_M)$ given in Eq. (3.7) (which is known analytically). Therefore, for the case of $m_1 = m_2$ it is useful to put all subtraction points at the threshold $s_{M_i} = s_{th}$, thus reproducing Eq. (3.11). On another side, for $J = 1$ and $m_1 \neq m_2$, it is useful to choose $s_{M_1} = m_-^2$ and $s_{M_2} = m_+^2$, which leads to Eq. (3.19). For $J > 1$ and $m_1 \neq m_2$ it is unfortunately impossible to express the answer in terms of $R(s, \tilde{s}_M)$. For simplicity, let us choose s_{M_i} at the same point s_M

$$[t_J(s)]^{-1} = \frac{1}{p^{2J}(s)} \left(\sum_{i=0}^{J} \frac{1}{i!} g_J^{(i)}(s_M) (s - s_M)^i \right.$$
$$\left. + \frac{(s - s_M)^{J+1}}{\pi} \int_{L,R} \frac{ds'}{s' - s_M} \frac{\text{Im}\ [t_J(s)]^{-1}}{s' - s} \frac{p^{2J}(s')}{(s' - s_M)^J} \right) \tag{3.17}$$

and approximate (as described before) the contribution from the left-hand cut together with the constant term in a suitably constructed conformal mapping series. It holds

$$[t_J(s)]^{-1} = \frac{1}{p^{2J}(s)} \left(\sum_{i=0}^{J-1} a_i \, (s - s_M)^i + (s - s_M)^J \left\{ \sum_{n=0}^{\infty} C_n \, \omega^n(s) + R_J(s, s_M) \right\} \right),$$

where

$$R_J(s, s_M) \equiv \frac{s - s_M}{\pi} \int_{s_{th}}^{\infty} \frac{ds'}{s' - s_M} \frac{-\rho(s')}{s' - s} \frac{p^{2J}(s')}{(s' - s_M)^J} \,. \tag{3.18}$$

In Eq. (3.18), the constants a_i and C_n are unknown.

To illustrate an application of the general formulas to a simple example, let us consider the $J = 1$ case (with an example in mind of πK or πD scattering). In this case, we write a twice-subtracted dispersion relation for $g_1(s)$ in the following form

$$g_1(s) = a + b\,s + \frac{(s - m_-^2)(s - m_+^2)}{\pi} \int_{L,R} \frac{ds'}{(s' - m_-^2)(s' - m_+^2)} \frac{\mathrm{Im}\, g_1(s')}{s' - s},$$

where $m_\pm = m_1 \pm m_2$. Re-expressing $g_1(s)$ in terms of $t_1(s)$ we obtain

$$\begin{aligned} [t_1(s)]^{-1} &= \frac{a + b\,s}{p^2(s)} + \frac{s}{\pi} \int_L \frac{ds'}{s'} \frac{\mathrm{Im}\, [t_1(s')]^{-1}}{s' - s} + \frac{s}{\pi} \int_{s_{th}}^{\infty} \frac{ds'}{s'} \frac{-\rho(s')}{s' - s} \\ &\simeq \frac{a + b\,s}{p^2(s)} + \sum_{n=1}^{\infty} C_n \, (\omega^n(s) - \omega^n(0)) + R(s, 0) \,. \end{aligned} \tag{3.19}$$

Note that for $m_1 = m_2$, Eq. (3.19) reduces to Eq. (3.12) with the proper redefinition of the unknown parameters.

3.2 Comparison to other parametrizations

Before applying dispersively justified representations to the physical cases, it is instructive to compare Eqs. (3.6, 3.12, 3.13, 3.19) with the commonly used parametrizations.

3.2.1 K-matrix approach

For general J, the K-matrix approach can be written as

$$[t_J(s)]^{-1} = \frac{1}{p(s)^{2J}} K^{-1}(s) + I(s) \,, \tag{3.20}$$

where $\mathrm{Im}\, I(s) = -\rho(s)$. The standard K-matrix implementations correspond to [205]

$$K(s) = \frac{g^2}{m^2 - s} + \sum_n \gamma_n s^n , \tag{3.21}$$

with $I(s)$ being the conventional phase-space $I(s) = -i\,\rho(s)$ or its Chew-Mandelstam [66] version, $I(s) = I(s_M) + R(s, s_M)$. The possible Adler zero is typically added by weighting $K(s)$ by a factor $(s - s_A)$ [58],

$$K(s) = (s - s_A)\left(\frac{g^2}{m^2 - s} + \sum_n \gamma_n s^n\right). \tag{3.22}$$

The attempt of adding the left-hand cut contribution was made in [206], using the conformal mapping expansion. The suggested parameterization for the case with Adler zero was written as

$$K^{-1}(s) = \frac{m_\pi^2}{s - s_A}\left(\frac{2 s_A}{m_\pi \sqrt{s}} + \sum_{n=0}^{\infty} C_n\, \omega^n(s)\right) \tag{3.23}$$

or in an alternative form as [194, 195]

$$K^{-1}(s) = \frac{m_\pi^2}{s - s_A}\left(\sum_{n=0}^{\infty} C_n\, \omega^n(s)\right). \tag{3.24}$$

First of all, we emphasize that all the parametrizations with conventional phase-space are at best limited to the physical region only. Below threshold, they have unphysical left-hand singularities and cannot be connected to the dispersion relation. The non-analytic behaviour of $\rho(s)$ below the two-particle threshold also often causes spurious poles in the complex plane. The attempt of fixing this problem by adding an additional $\sqrt{s}$ term in Eq.(3.23) only place this parameterization further away from the dispersive construction. In the parametrizations with Chew-Mandelstam phase-space, the subtraction point s_M and the constant $I(s_M)$ are typically freely chosen. However, in some cases it can essentially affect the structure of the left-hand cut contribution. For instance, for $J = 1$ and $m_1 \neq m_2$ the particular form of Chew-Mandelstam phase space with $s_M = 0$ is connected to the particular form of the left-hand cut contribution (see Eq.(3.19)).

The commonly used K-matrix implementations given by Eqs. (3.21, 3.22) at best assume that the left-hand cut contribution can be approximated by a constant. The inclusion of the left-hand cuts in Eqs. (3.23, 3.24) is a step forward, however its implementation is non-dispersive for two main reasons. First, the left-hand cut contribution in Eqs. (3.23, 3.24) is multiplied by the pole contribution from the Adler zero. The correct implementation of the analytic properties, in turn, requires additive contribution from the left-hand cut and the pole due to Adler zero as derived in Eqs. (3.5,3.11,3.19). Second, the proposed form of $\omega(s)$ in [206, 194, 195] accounts not only for the left-hand cut, but also for the inelastic cuts. This more general form of $\omega(s)$ can only help with an effective description around the inelastic threshold. It does not improve the validity of the parameterization in the complex plane, since both on the left-hand and inelastic cuts the conformal mapping expansion does not

converge by construction, i.e. $\omega(s) = 1$. As emphasized before, it is not possible to write a dispersion relation for the inverse amplitude in the coupled-channel case and therefore the inclusion of the contribution from the inelastic cuts into $\omega(s)$ does not have a firm dispersive ground.

3.2.2 mIAM and IAM

Finally, let's compare Eqs. (3.5) and (3.11) with the IAM (mIAM) [207–211]. The latter is a widely used way of unitarizing χPT (see e.g. Refs.[212–214, 203, 215]). For the elastic S-wave scattering it has the following form

$$t_0^{\rm mIAM}(s) = \frac{\left[t_0^{\rm LO}(s)\right]^2}{t_0^{\rm LO}(s) - \left[t_0^{\rm NLO}(s) - t_0^{\rm LO}(s)\right] + A^{\rm mIAM}(s)}\,, \tag{3.25}$$

where $t_0^{\rm LO}$ and $t_0^{\rm NLO}$ are leading order (LO) and next-to-leading order (NLO) S-wave scattering amplitudes in χPT, respectively. Note, that Eq. (3.25) can be naively derived in the physical region by performing NLO expansion of $\mathrm{Re}[t(s)]^{-1}$ and plugging it into $[t(s)]^{-1} = \mathrm{Re}[t(s)]^{-1} - i\,\rho(s)$ relation. On the other hand, it has been shown in Ref. [211] that Eq. (3.25) can be justified by writing the p.w. dispersion relation for the inverse amplitude and approximating the subtraction constants and the left-hand cut discontinuity by its chiral expansion. The $A^{\rm mIAM}(s)$ term in needed to remove a spurious pole on the real axis below threshold and at the same time incorporate correctly the Adler zero.

By taking LO and NLO SU(2) χPT amplitudes from [216] with low energy constants from [217] for the isoscalar S-wave $\pi\pi$ scattering we have checked that mIAM given in Eq. (3.25) indeed satisfies the dispersion relation for the inverse amplitude (3.5)

$$\left[t_0^{\rm mIAM}(s)\right]^{-1} = \left[t_0^{\rm mIAM}(\tilde{s}_M)\right]^{-1} + \frac{s-\tilde{s}_M}{s_A-\tilde{s}_M}\frac{g_A}{s-s_A} + \frac{s-\tilde{s}_M}{\pi}\int_{L,R}\frac{ds'}{s'-\tilde{s}_M}\frac{\mathrm{Im}\left[t_0^{\rm mIAM}(s')\right]^{-1}}{s'-s},$$
$$g_A = \left(\left.\frac{\mathrm{d}t_0^{\rm mIAM}(s)}{\mathrm{d}s}\right|_{s=s_A}\right)^{-1}. \tag{3.26}$$

This implies that mIAM is a specific case of the proposed parameterization given in Eq.(3.6). We have checked that for fixed s_A, g_A to the mIAM and by adjusting just one leading term in the conformal expansion $C_0 = t_0^{\rm mIAM}(\tilde{s}_M = s_{th})$ we can reproduce the results of the mIAM in the physical region and in the complex plane around $\sigma/f_0(500)$ resonance with $\sim 5\%$ accuracy.

Note that it is not guaranteed by the dispersion construction (see e.g. Eq.(3.5) or Eq.(3.26)) that the inverse amplitude would not turn zero somewhere in the complex plane leading to unphysical poles of the amplitude itself. That is exactly what happens with mIAM, which does not satisfy the dispersion relation for the direct amplitude (2.38) due to two spurious poles on the 1st Riemann sheet at $s = -0.87 \pm 0.49\,i$ GeV^2. These spurious poles are an artifact of a specific model for the left-hand cuts. In general, the mIAM, or the more general parameterization given in Eq.(3.6), is not meant to be

	Fit parameters						Pole position	
	g_A	a	b	C_0	C_1	χ^2/d.o.f	$\sqrt{s_p}$, MeV	$\sqrt{s_p^{\text{Roy-like}}}$, MeV
$\pi\pi \to \pi\pi$								
$(J=0, I=0)$, Exp	0.44	-	-	4.86	-	0.4	$468 - i\,239$	$457^{+14}_{-13} - i\,279^{+11}_{-7}$
$(J=0, I=0)$, Lattice $m_\pi = 239$ MeV	0.56	-	-	1.37	-	0.8	$560 - i\,169$	-
$(J=0, I=2)$, Exp	-0.84	-	-	-23.98	-	0.0	-	-
$(J=1, I=1)$, Exp	-	2.30	-	-5.42	-	3.0	$758 - i\,73$	$763.7^{+1.7}_{-1.5} - i\,73.2^{+1.0}_{-1.1}$
	-	1.92	-	-4.26	-4.44	0.9	$762 - i\,71$	
$(J=2, I=0)$, Exp	-	0.04	10.01	-7.87	-	1.1	$1261 - i\,94$	$1267.3^{+0.9}_{-0.9} - i\,87(9)$
$\pi K \to \pi K$								
$(J=0, I=1/2)$, Exp	0.44	-	-	2.30	-	2.1	$707 - i\,246$	$648(7) - i\,280(16)$
	0.22	-	-	1.48	1.54	0.0	$684 - i\,312$	
$(J=0, I=1/2)$, Lattice $m_\pi = 239$ MeV	0.63	-	-	1.53	-	0.4	$764 - i\,278$	-
$(J=0, I=3/2)$, Exp	-0.86	-	-	-7.86	-	0.5	-	-
$(J=1, I=1/2)$, Exp	-	0.86	-1.05	-	-	0.7	$889 - i\,27$	$890(2) - i\,25.6(1.2)$

Table 3.1 Fit parameters entering Eqs. (3.6, 3.12, 3.13, 3.19) which were adjusted to reproduce available pseudo-data from the Roy-like analyses [44–46, 52, 53] or lattice data [58, 60]. In Eq. (3.6), the Adler position s_A is fixed from the LO χPT (given in Eq. (3.29)), while the subtraction constant is chosen to be at threshold, $\tilde{s}_M = s_{th}$. In the right columns we collect pole positions found on the 2nd Riemann sheet and compare them with the Roy-like extractions [218, 44–46, 52, 53]. See text for more details.

applied in the unphysical region of the 1st Riemann sheet. What is more important, is that there are no spurious poles on the 2nd Riemann sheet, where the $\sigma/f_0(500)$ pole resides.

For the P-wave $\pi\pi$ scattering, we checked that $t_1^{\text{IAM}}(s)$ given by [207–210]

$$t_1^{\text{IAM}}(s) = \frac{\left[t_1^{\text{LO}}(s)\right]^2}{t_1^{\text{LO}}(s) - \left[t_1^{\text{NLO}}(s) - t_1^{\text{LO}}(s)\right]}, \tag{3.27}$$

satisfies the p.w. dispersion relations for the inverse amplitude given by Eq. (3.11), i.e.

$$\left[t_1^{\text{IAM}}(s)\right]^{-1} = \frac{f_1^{\text{IAM}}(s_{th})}{s - s_{th}} + \left[f_1^{\text{IAM}}(s_{th})\right]' + \frac{s - s_{th}}{\pi}\int_{L,R}\frac{ds'}{s' - s_{th}}\frac{\text{Im}\left[t_1^{\text{IAM}}(s')\right]^{-1}}{s' - s}, \tag{3.28}$$
$$f_1^{\text{IAM}}(s) \equiv \frac{s - s_{th}}{t_1^{\text{IAM}}(s)}.$$

Here, similarly to the S-wave, one can adjust the parameters of the conformal expansion in Eq.(3.12) such that Eq.(3.12) reproduces IAM almost exactly. We have also checked that in P-wave IAM does not have any spurious poles.

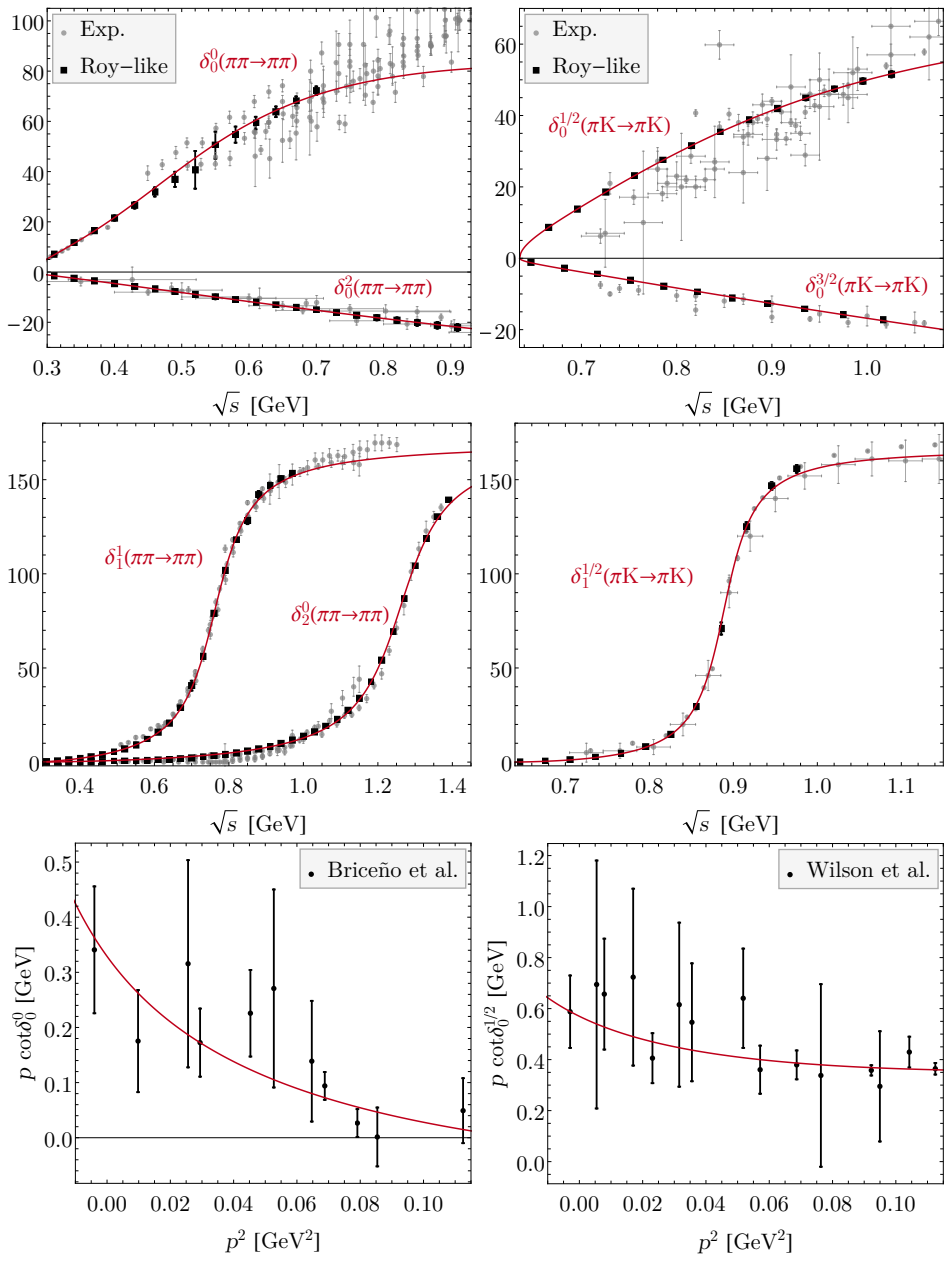

Fig. 3.1 Results of the fits (δ_J^I) to the pseudo-data from the Roy-like analyses (top and central panels) [44–46, 52, 53] and lattice data (bottom panels) [58, 60]. In all cases (except δ_0^0 and δ_0^2 and fits to lattice data) the last fitted data point is around ~ 1 GeV, which corresponds to the validity of Roy-like solution. In the case of δ_0^0, however, we limited the fit till 700 MeV, since above the effect of the $f_0(980)$ becomes important. For δ_0^2 we took $s_{max}^{1/2} = 1.42$ GeV, which correspond to the highest point where the set of forward dispersion relations was applied [44–46, 52, 53].

The main difference between the proposed dispersive inverse amplitudes given in Eqs. (3.6, 3.12, 3.13, 3.19) and mIAM (IAM) is that the former can be applied to any elastic scattering, and it is not limited to the Lagrangian based resummation scheme [219]. The unknown parameters in Eqs. (3.6, 3.12, 3.13, 3.19)

can be fixed directly from the experimental or lattice data (some numerical examples will be shown below). The only required input for the $\pi\pi$ and πK scattering is the Adler zero position, since it lies in the unphysical region and typically can not be constrained well by the data. On another side, the unknown parameters in Eqs. (3.6, 3.12, 3.13, 3.19) can be estimated from χPT (an example is shown at the end of Section 3.4), which allows to connect continuously the results with different quark masses, similar to mIAM.

3.3 Adler zero

For the S-wave $\pi\pi$ and πK scattering one has to account for an Adler zero of the amplitude required by chiral symmetry. Its position typically lies very close to the left-hand cut and cannot be determined precisely from the fit to data in the physical region. Around the Adler zero the chiral perturbation theory (χPT) converges relatively fast. For the physical pion mass the higher-order corrections shifts the LO results

$$s_A^{I=0} = \frac{m_\pi^2}{2}, \;\; s_A^{I=2} = 2m_\pi^2, \;\; s_A^{I=3/2} = m_\pi^2 + m_K^2,$$
$$s_A^{I=1/2} = \frac{1}{5}\left(m_\pi^2 + m_K^2 + 2\sqrt{4\,(m_K^2 - m_\pi^2)^2 + m_\pi^2\, m_K^2}\right). \tag{3.29}$$

only slightly. For larger than physical pion mass values the position of the Adler zero becomes more sensitive to the input from the LECs, which enter at higher orders. As an example, in Fig. 3.2 we

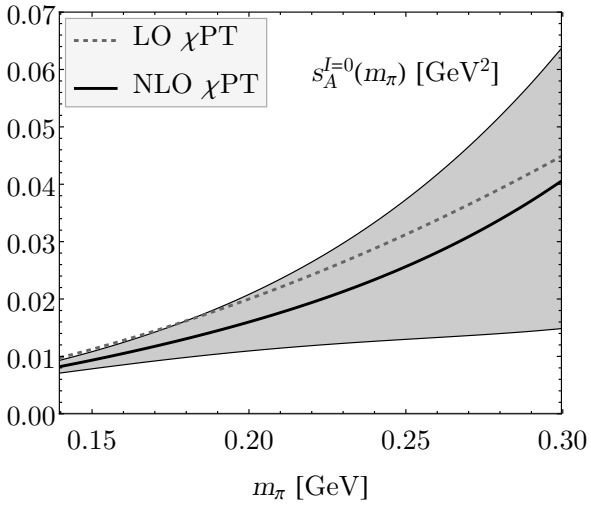

Fig. 3.2 Adler zero position s_A as a function of the pion mass for the S-wave isoscalar $\pi\pi$ scattering. In the plot we used SU(2) χPT p.w. amplitudes at leading order (LO) and next-to-leading order (NLO) from [216] (expressed in terms of the pion decay constant in the chiral limit) and low-energy constants (LECs) $l_1^r = -4.03(63)\times 10^{-3}$, $l_2^r = 1.87(21)\times 10^{-3}$, $l_3^r = 0.8(3.8)\times 10^{-3}$, $l_4^r = 6.2(1.3)\times 10^{-3}$ from [217].

show the isoscalar Adler zero position as a function of the pion mass up to NLO order using the expressions of the p.w. amplitudes [216] in terms of the pion decay constant in the chiral limit, f_0. The maximal m_π is considered to be ~ 300 MeV, which lies well within the χPT range of applicability. The LECs were taken from [217] and assumed to be uncorrelated. This assumption is rather strong and effectively includes an uncertainty related to the truncation error of the chiral expansion.

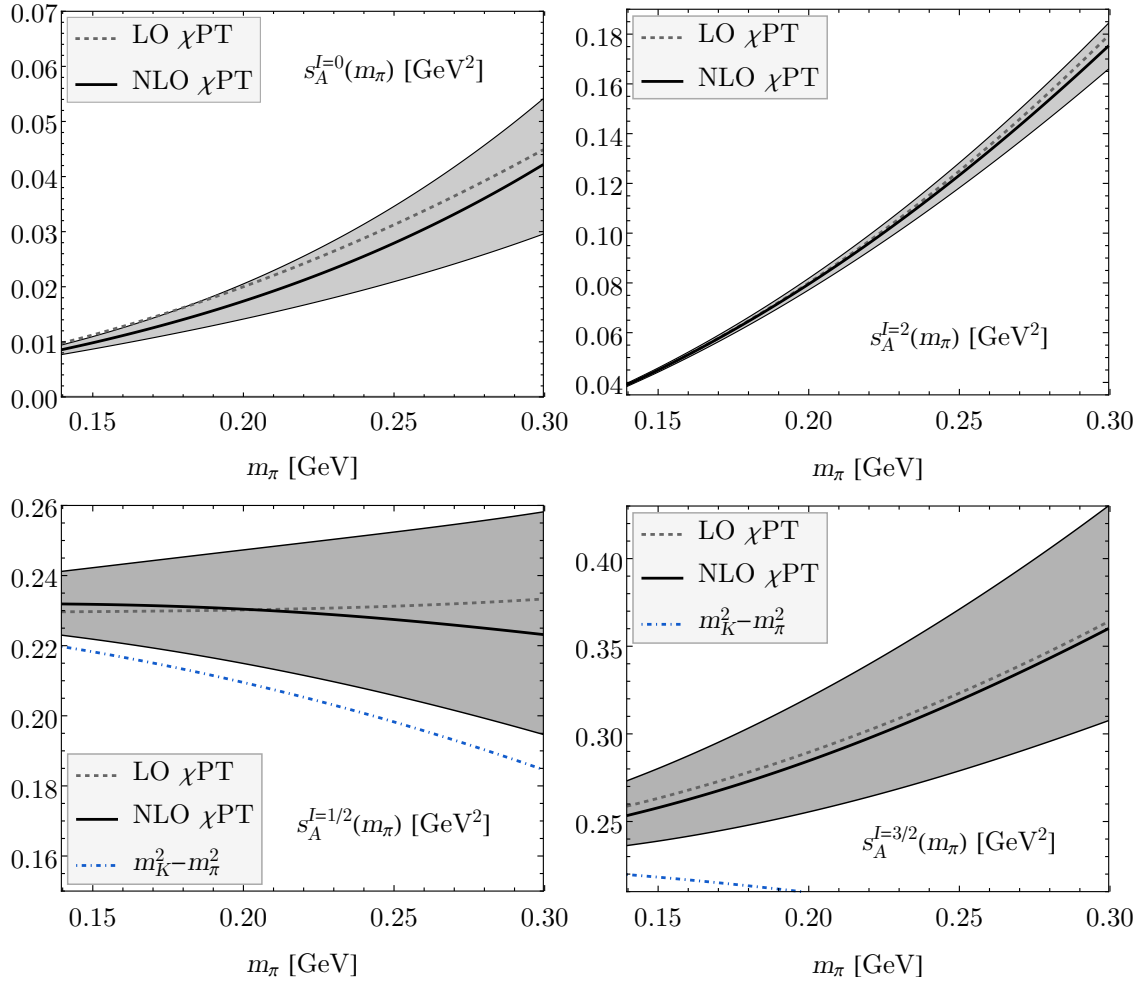

Fig. 3.3 The positions of the Adler zero, predicted by LO and NLO χPT, with respect to the pion mass. For $I = 1/2, 3/2$ we fixed the strange-quark mass effectively via the LO χPT meson mass relations with $m_\pi = 239$ MeV and $m_K = 508$ MeV taken from [60]. The gray bands illustrate the 1σ uncertainty propagated from the LECs using the bootstrap technique. The black curves correspond to the central values of LECs. *Top panel:* $I = 0, 2$ from SU(2) χPT with LECs from [217]. *Bottom panel:* $I = 1/2, 3/2$ from SU(3) χPT with LECs ("p^4"-fit) from [217]. The blue dot-dashed line shows the closest left-hand cut branch point.

For isospin $I = 3/2$, however, the p.w. amplitudes, being expanded in terms of f_0, have quite a bad convergence at high pion masses. This can be partially improved employing an alternative expansion of the χPT amplitudes in terms of the physical pion decay constant f_π. The pion mass dependence of

the latter is then fixed by its NLO perturbative expansion. This strategy effectively resumes some of the higher-order χPT corrections, enhancing the χPT convergence. The corresponding behavior of the Adler zero, given by SU(2) and SU(3) χPT at LO and NLO, is shown in Fig. 3.3. The SU(3) χPT amplitudes are taken from [203], while both the LECs for the SU(2) and SU(3) χPT theories are taken from [217] (for SU(3), the "p^4"-fit values are taken). The error bands on both Figs. 3.2 and 3.3 are estimated by propagating the uncertainties from the low-energy constants[1] (LECs) of the theory, assuming that they are uncorrelated.

Since the lattice data do not provide enough information to control the amplitude around the Adler zero, it is important to implement this chiral constraint in the fits. As it will be shown in the next section, for $m_\pi = 239$ MeV the error on the $f_0(500)$ pole parameters due the Adler zero position is suppressed compared to the statistical error from the lattice data [58]. For pion masses sufficiently larger than 300 MeV, the Adler zero constraint may be less accurate. In this case, a reasonable strategy is to perform the fit both with and without the Adler zero constraint.

3.4 Numerical examples

In this section, we present some test fits to the well-established $\pi\pi$ and πK scattering with $J = 0, 1, 2$ in the low energy region. Here we do not attempt to provide a detailed analysis of experimental data. Instead, we opt for fitting the result of the Roy (Roy-Steiner) analyses [44–46, 52, 53], as the best representation of the data. The goal is to show that the proposed dispersive parametrizations are suitable to the search for poles in the complex plane and can describe both: wide tetraquark states (like $\sigma/f_0(500)$) and relatively narrow quark-antiquark states (like the $\rho(770)$ or $f_2(1270)$ mesons). For simplicity, we present our numerical test results using the LO input (3.29)

As one can see in Table 3.1 and Fig. 3.1, an accurate description of the Roy (Roy-Steiner) pseudo-data is achieved with at most 3 parameters. We also observed, that adding more terms in the conformal expansion, one can systematically improve the fits. Note that by fitting the Roy (Roy-Steiner) results, which are smooth functions, the $\chi^2/d.o.f$ loses its statistical meaning and can be < 1.

As an example, we also perform a numerical comparison between Eq.(3.6) and the most advanced analytical $\sigma/f_0(500)$ parameterization given by Eqs. (7, 10, 12, 14) of Ref. [194]. That parameterization corresponds to Eqs.(3.20,3.24) with $I(s) = R(s, 0)$ and the conformal variable,

$$\omega(s) = \frac{\sqrt{s} - \alpha\sqrt{4m_K^2 - s}}{\sqrt{s} + \alpha\sqrt{4m_K^2 - s}}, \tag{3.30}$$

with the typical choice of $\alpha = 1.0$ [194]. The variation of α around 1.0 or replacing Eq. (3.30) by (2.143), leads to the very compatible results. The two parameter fit to Roy solution up to $s_{max}^{1/2} = 700$

[1] We use those LECs that do not depend on meson masses, but on the regularization scale. Hence they are treated as fixed parameters in chiral extrapolation.

MeV gives $\chi^2/\text{d.o.f} = 1.7$, [2] and the pole position at $\sqrt{s_p} = 448(7) - i\,205(4)$ MeV. In order to improve the obtained width of $\sigma/f_0(500)$, one needs to add a third parameter. This is clearly not as good as the fit given in Table 3.1, which produces a pole position at $\sqrt{s_p} = 468(8) - i\,239(4)$ MeV, i.e. much closer to the Roy solution with just two parameters. Another useful comparison of Eq.(3.6) and Eqs. (3.20,3.24,3.30) is the employment of them as the unitarization method of χPT. By constraining two unknown parameters in Eqs. (3.20,3.24,3.30) and Eq. (3.6) from the χPT threshold parameters $a_{0,\text{NNLO}} = 0.220(5)$ and $b_{0,\text{NNLO}} = 0.276(6)$ [37] one obtains $\sqrt{s_p} = 389(15) - i\,262(13)$ MeV and $\sqrt{s_p} = 426(29) - i\,263(22)$ MeV, respectively. Clearly, the dispersive parameterization (3.6) produces the results closer to the Roy-like analysis.

For the description of the lattice data of S-wave isoscalar $\pi\pi \to \pi\pi$ ($m_\pi = 239$ MeV) scattering [58] HadSpec collaboration used 8 different parameterizations, leading to the wide spread of the $\sigma/f_0(500)$ pole position, $\sqrt{s_p} = 550\ldots780 - i\,(115\ldots285)$ MeV. We would like to emphasize, that out of all applied parameterizations, only the "fit 3a" (which corresponds to Eqs.(3.20,3.22) with $\gamma_n = 0$ and $I(s) = -\text{Re}[R(m^2, s_{th})] + R(s, s_{th})$) can be cast into the dispersive form for the inverse amplitude with the conformal series truncated at $n_{max} = 0$. However, it translates one-to-one only under an assumption that g^2 and m^2 in Eq.(3.22) can also take on negative values. It can also be reinforced by the fact that in order to reproduce χPT threshold parameters for the physical pion mass $a_{0,\text{NNLO}} = 0.220$ and $b_{0,\text{NNLO}} = 0.276$, one needs to use $g^2 = -3.78$ and $m^2 = -1.47$. In turn, for $m_\pi = 239$ MeV the "fit 3a" from HadSpec and Eq.(3.6) truncated at $n_{max} = 0$ coincide, leading to a significant reduction of the spread of the $\sigma/f_0(500)$ pole position. When more precise data will be available, the extension of "fit 3a" dispersively goes with additional parameters related to the left-hand cuts C_n in Eqs.(3.6,2.143), rather than polynomial γ_n terms in Eq.(3.22). In Table 3.1 we reproduced the results of "fit 3a" close enough, given the fact that we performed a simple fit to $p\cot\delta$ instead of the energy levels. The former is sufficient for our following discussion related to the chiral extrapolation.

As a first step, we quantify the uncertainty due to the Adler zero position. Using NLO χPT amplitudes expanded in f_0, we obtain (see Fig. 3.2)

$$s^{I=0}_{A,\text{NLO}}(m_\pi = 239\,\text{MeV}) = 0.023(10)\,\text{GeV}^2\,, \tag{3.31}$$

which is a very conservative estimate, since the LECs were assumed to be uncorrelated. The propagation of Eq.(3.31) into the pole position gives $\sqrt{s_p} = 561(4) - i\,171(7)$ MeV. In case when both the uncertainties of lattice data and Adler zero input are taken into account, one gets

$$\sqrt{s_p} = 559^{+48}_{-53} - i\,168^{+20}_{-17}\,\text{MeV}\,, \tag{3.32}$$

[2] The fit of Eqs. (3.24,3.30) to Roy-like solution up to $s^{1/2}_{max} = 800$ MeV gives $\chi^2/\text{d.o.f} = 4.0$ compared to $\chi^2/\text{d.o.f} = 1.5$ using Eq. (3.6).

where the error corresponds to 1σ confidence level provided by the bootstrap analysis. We have also checked that exactly the same result is achieved when only the uncertainty of lattice data is accounted for, while the Adler zero is fixed to its central NLO position. This points out that the current lattice data completely dominate the uncertainty, and the final result is not very sensitive to the exact position of the Adler zero in Eq.(3.31).

Next, we compare the values of the fitted parameters to lattice data [58]

$$g_A = 0.58(10), \quad C_0 = 1.36(26)\,, \tag{3.33}$$

with the corresponding estimations from NLO χPT ($m_\pi = 239$ MeV)

$$\begin{aligned} g_{A,\mathrm{NLO}} &= \left(\left. \frac{\mathrm{d}t_0^{\mathrm{NLO}}(s)}{\mathrm{d}s} \right|_{s=s_A} \right)^{-1} = 0.45(3)\,, \\ C_{0,\mathrm{NLO}} &= \left[t_0^{\mathrm{NLO}}(s_{th}) \right]^{-1} = 1.42(6)\,. \end{aligned} \tag{3.34}$$

As one can see, the fitted parameters are consistent with χPT extrapolation. Similarly, expanding χPT amplitudes in physical pion decay constant, we obtain...

Pole	Adler zero bootstrap	Full bootstrap
$\sqrt{s_\sigma}$, MeV	$555(3) - i171(4)$	$553^{+46}_{-52} - i167^{+19}_{-16}$
$\sqrt{s_\kappa}$, MeV	$765(2) - i279(13)$	$765^{+61}_{-58} - i275^{+40}_{-31}$

Table 3.2 The parameters of σ and κ poles, which correspond to the left panel of Fig. 3.4.

Unfortunately, currently the error bars of the lattice data are too large to impose some constraints on the LECs. However, more data is expected in the near future with the improved precision. In addition, the existing lattice data for the P-wave [220–222] (calculated also at the physical pion mass [223, 224]) can help to constraint LECs even at the two loop level, as has been demonstrated in [216]. We emphasise that in the proposed dispersive parametrizations, we are free to choose where to do the matching to χPT. The natural choice is around the Adler zero and/or the threshold. Once the matching is done, the proposed parameterizaition can be used to predict the pion mass dependence and the obtained LECs will correspond exactly to the ones in perturbative χPT calculations, as opposed to mIAM (IAM). We have checked that Eq. (3.6), truncated to the leading term in the conformal expansion with parameters fixed from NLO χPT (see left hand side of Eq. (3.34)), produces the same qualitative behaviour of the $f_0(500)$ pole as in mIAM [212]. With increasing pion mass values the imaginary part of the pole decreases, and then $f_0(500)$ becomes a virtual bound state.

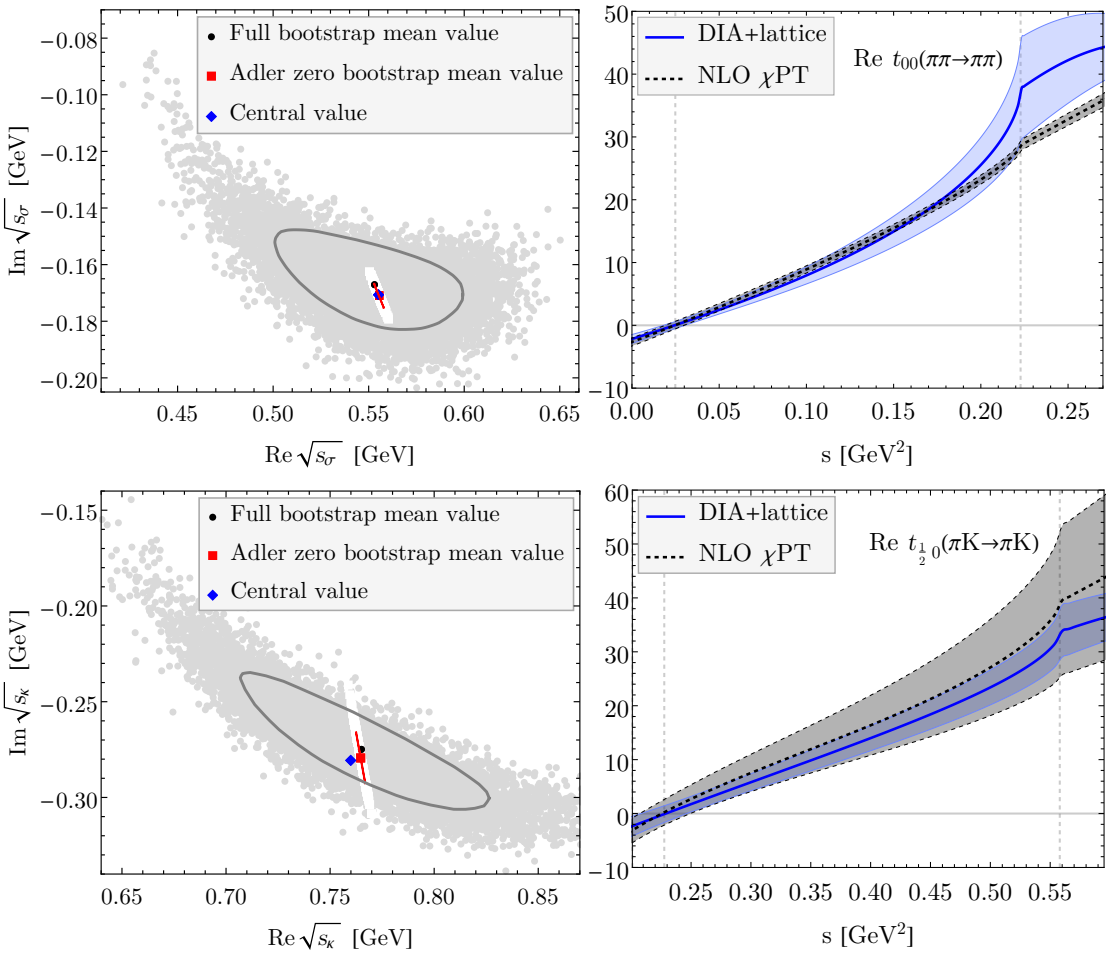

Fig. 3.4 *Left panel:* the σ and κ poles ($m_\pi \sim 240\,\text{MeV}$) are shown with their 1σ uncertainties. The full bootstrap mean value (black point), its uncertainty (black line) and bootstrap points (gray points) are given. The mean value of the Adler zero bootstrap (red point), the corresponding uncertainties (red line) and the bootstrap points (white points) are also shown. The central value (blue point) corresponds to the pure fit without an error analysis. *Right panel:* The dispersive inverse amplitudes (DIA) from the fit to the lattice data (blue bands) [58, 60] compared to the extrapolated NLO χPT results (gray bands).

3.5 Conclusion and outlook

In this Chapter, improved parametrizations for elastic p.w. amplitudes are proposed, see Eqs. (3.6, 3.12, 3.13, 3.19). They are based on dispersive representations for the inverse p.w. amplitudes. In this approach unitarity and analyticity constraints are implemented exactly. The contributions from the left-hand cuts were accounted for in a model-independent way using the expansion in a conformal variable, which maps the left-hand cut plane onto the unit circle. For the S-wave scattering special attention was paid to the possible Adler zero contribution. For the higher partial waves, the angular momentum barrier factors were carefully implemented. The approach was also compared with the

mIAM (IAM) and argued that both for the S and P-waves the constructed parametrizations can be understood as a more general method, where one is not assuming a particular Lagrangian-based form for the left-hand cuts and subtraction constants. The latter is useful for lattice calculation with the relatively large m_π or scattering of πK, πD, KD, etc.

The new parametrizations were applied to the well-studied test cases of $\pi\pi$ and πK scattering with $J = 0, 1, 2$, showing that at most 3 parameters are needed to reproduce very precise Roy/Roy-Steiner pseudo-data in the physical region. The obtained pole positions lie fairly close to the exact solutions.

The main motivation for developing these so-called dispersive inverse amplitudes (DIA), is their application to the upcoming lattice data in $\pi\pi$, πK, πD and KD channels. In addition, these parametrizations can be beneficial for the fits to data constrained by Roy-like equations or forward dispersion relations [218, 44–46, 195, 225]. However, the framework is general and not specific to the particular reactions, thus laying the groundwork for analyses of any lattice or experimental data in the elastic region.

Chapter 4

Real light-by-light scattering in ultraperipheral heavy-ion collisions at LHC

In this chapter, the real LbL scattering is considered in view of the recent measurements of this reaction in ultraperipheral heavy-ion collisions at LHC by ATLAS [71–73] and CMS [74] Collaborations. The first evidence of this reaction was reported by ATLAS in 2017 [71]. The analyzed data were from Pb-Pb collisions at a center-of-mass energy of 5.02 TeV with an integrated luminosity of 0.48 nb^{-1}, which were recorded in 2015 during Run 2 at LHC. Around seven $\gamma\gamma \to \gamma\gamma$ signal events out of thirteen observed were reported in the diphoton mass region 5-30 GeV. The significance of the observation was estimated at approximately 4σ. The obtained integrated fiducial cross section amounted to $\sigma_{\text{fid.}} = 70 \pm 24, (\text{stat.}), \pm 17 (\text{syst.})$ nb. This corresponded to the experimental cuts on the transverse energy of each photon, $E_{\text{T}}^{\gamma} > 3$ GeV, diphoton invariant mass $m_{\gamma\gamma} > 6$ GeV, photon pseudorapidity $|\eta| < 2.4$, and diphoton acoplanarity $A_{\phi} < 0.01$. The available theoretical predictions for the integrated cross section over this fiducial phase space were 45 ± 9 nb [70] and 49 ± 10 nb [75]. Hence, agreement between the observed and predicted values was declared within the (large) experimental uncertainty, albeit the theoretical central value lay at the edge of the experimental uncertainty.

Later, in 2018, the CMS Collaboration also established evidence of LbL scattering in Pb-Pb collisions [74] by analyzing the data collected in 2015. The measurement was performed at the same center-of-momentum (c.o.m.) energy of the Pb beam, however, with a smaller integrated luminosity of 0.39 nb^{-1}. The fiducial phase space was limited by cuts on the transverse photon energy, $E_{\text{T}}^{\gamma} > 2$ GeV, diphoton invariant mass $m_{\gamma\gamma} > 5$ GeV, photon pseudorapidity, and diphoton acoplanarity. The latter two were the same as in the case of the ATLAS 2017 observation. Fourteen event candidates were detected, nine of which were treated as a signal with around 3.5σ significance. The obtained

integrated fiducial cross section was $\sigma_{\text{fid}} = 120 \pm 46\,(\text{stat.}) \pm 28\,(\text{syst.}) \pm 12\,(\text{theo.})$ nb [1], compared to the theoretically estimated value 116 ± 12 nb from [70]. Thus, despite the very low statistics, a remarkably good agreement between theory and experiment was observed. In 2019, the ATLAS Collaboration analysed the dataset with higher luminosity of 1.73 nb^{-1}, collected in 2018, and observed the LbL scattering signal with 8.2σ significance [72]. For this analysis, relatively stringent cuts were used on the diphoton mass, $m_{\gamma\gamma} > 6$ GeV, and the single-photon transverse energy, $E_{\text{T}}^{\gamma} > 3$ GeV.

Finally, in 2020, ATLAS performed a combined analysis of the data recorded in 2015 and 2018, with a total luminosity of 2.2 nb^{-1} [73]. The improved trigger efficiency and purity in the proton identification allowed for the employment of wider kinematic cuts: in diphoton invariant mass, $m_{\gamma\gamma} > 5$ GeV, and single-photon transverse energy, $E_{\text{T}}^{\gamma} > 2.5$ GeV, which has increased the signal yield by about 50% compared to the previous more stringent cuts. The performed analysis resulted in 97 event candidates, where 45 signal events and 27 are background events were expected.

As was pointed out in section 1.3, Eqs. (1.16), the unfolded data show the discrepancy with theoretical prediction of around 2σ. The distributions, shown in Fig. 1.2 demonstrate that the discrepancy comes from the 5-10 GeV region in diphoton mass and wide $\gamma\gamma \to \gamma\gamma$ scattering angle (or, equivalently, small photon rapidity), whereas the remaining experimental points follow the theoretical predictions pretty well. Moreover, it is assumed that the phase space related to aforementioned discrepancy is still such that the pQCD can be safely applied. The latter fact is incorporated in all existing event generators for LbL scattering [70, 75, 226], where the process at wide angles is modeled just by the sum of one-loop contributions of leptons and quarks. Therefore, assuming the correct data analysis, several scenarios can be served as an explanation of the observed discrepancy:

1. the underlying theoretical model for the LbL scattering is incomplete or inadequate at diphoton energies below 10 GeV; the next-to-leading order SM corrections and/or nonperturbative QCD effects should be properly included;

2. there exist some unknown resonance structures with pronounced $\gamma\gamma$-decay width, which are pertinent to the energy region 5-10 GeV.

Furthermore, the intriguing aspect is that the specified energy regime has not been investigated previously. The available data, obtained on the hadroproduction via the two-photon fusion, consists of the production of the lowest-lying pseudoscalar mesons π^0, η and η'[227–229] and the total unpolarized cross section of $\gamma\gamma \to$hadrons [230–236]. While the data on the former are collected only at low energies ranging from 0.1 to 4 GeV, the total two-photon fusion hadronic cross section was measured up to 160 GeV, covering the region of interest. However, in this region the total unpolarized two-photon fusion cross section is fully dominated by QCD background, making impossible the observation of the narrow resonances with small $\gamma\gamma$ couplings.

[1] The 10% theo. uncertainty was derived from the spread of various approaches to implement the nonhadronic-overlap condition in the simulation.

Therefore, a brief review of the theoretical models of real LbL scattering at various energies is first provided. Subsequently, a simple update to the pQCD-based model, which is used in modern event generators, is presented. The proposed model, based on the forward LbL sum rules, is designed to cover the low-energy region and the soft diffractive regime of near-forward scattering. Finally, the observed discrepancy is addressed by fitting the fully charmed tetraquark state into the LbL scattering.

The content of this Chapter is partially based on the publication [237] and the proceeding [238]. It also contains a significant part of unpublished results concerning the hadronic model for LbL scattering and the two-photon width estimation in the diquark-antidiquark picture using the quark model.

4.1 Real LbL scattering at various energies

4.1.1 QED contribution

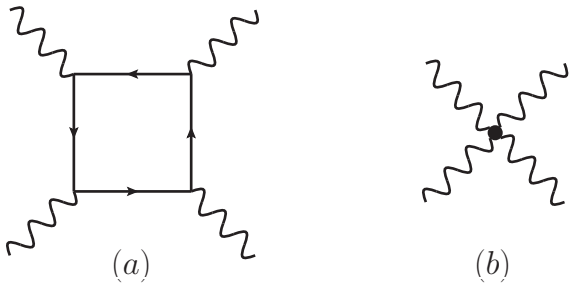

Fig. 4.1 Leading-order QED contribution to the LbL scattering (a) and its approximation by an effective low-energy theory (b).

According to QED, the leading contribution to the LbL scattering is of order α_{em}^2 and comes from the one-loop box diagram depicted in Fig. 4.1 (a) together with its crossed-channel versions. Electrons, muons and τ-leptons are running in the loop, but the leading contribution stems from the former. This contribution was firstly obtained directly by Karplus and Neuman in 1951 [239] and subsequently proven via dispersive evaluation by De Tollis et al. [240, 241]. The corresponding helicity amplitudes, compactly written in terms of Passarino-Veltman scalar integrals in, e.g., [169] and [242], are given in Appendix 4.A. The behavior of the helicity amplitudes at the limiting values of energies is given in Tab. 4.1. It can be seen that only the spin-conserving helicity amplitudes survive at high energies, whereas the double helicity-flip amplitude M_{+++-} is suppressed compared to the others at all energies.

The low-energy result can be also obtained invoking the low-energy effective field theory. When the photon energies are much smaller than electron mass, one can integrate out the heavy degrees of freedom from the generating functional and build the corresponding low-energy effective theory with constant photon-photon interaction, as shown in Fig. 4.1 (b). Quantitatively this constant can be read

helicity amplitude	$\omega \ll m_e$, $O(\omega^6/m_e^6)$	$\omega \gg m_e$, $O(m_e/\omega)$
$M_{++++}(s,t,u)$	$e^4 \frac{11s^2}{45m_e^4}$	$-16e^4 \log^2\left(\frac{\omega}{m_e}\right)$
$M_{+--+}(s,t,u)$	$e^4 \frac{11t^2}{45m_e^4}$	0
$M_{+-+-}(s,t,u)$	$e^4 \frac{11u^2}{45m_e^4}$	$-16e^4 \log^2\left(\frac{\omega}{m_e}\right)$
$M_{++--}(s,t,u)$	$-e^4 \frac{s^2+t^2+u^2}{15m_e^4}$	0
$M_{+++-}(s,t,u)$	0	0

Table 4.1 The leading behavior of the LbL helicity amplitudes in QED at low and high photon c.o.m. energy ω.

out from the Euler-Heisenberg Lagrangian [243],

$$\mathcal{L}_{\rm EH} = -\frac{1}{4}F_{\mu\nu}F^{\mu\nu} - \frac{\alpha_{\rm em}}{8\pi}\int_0^\infty \frac{ds}{s} e^{-i(s+i\varepsilon)m^2} \frac{{\rm Re}\cos(esX)}{{\rm Im}\cos(esX)} F_{\mu\nu}\widetilde{F}^{\mu\nu}, \tag{4.1}$$

where the function X depends on the electromagnetic fields as

$$X = \sqrt{\frac{1}{2}F_{\mu\nu}F^{\mu\nu} + \frac{i}{2}F_{\mu\nu}\widetilde{F}^{\mu\nu}}, \tag{4.2}$$

with the dual electromagnetic tensor $\widetilde{F}^{\mu\nu} = {}^1\!/_2\epsilon^{\mu\nu\alpha\beta}F_{\alpha\beta}$. This Lagrangian can be obtained by integrating out the electrons from the QED generating functional, and is essentially the low-energy approximation of the interaction of an arbitrary amount of photons at the one-loop level in QED (cf. Fig. 4.2). At low photon energies, the leading-order terms in effective Lagrangian for $\gamma\gamma \to \gamma\gamma$

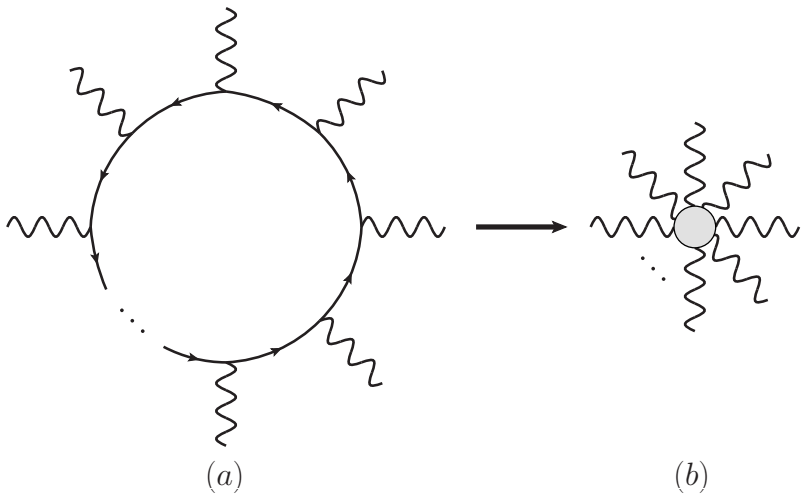

Fig. 4.2 The one-loop QED diagrams that are resummed by the Euler-Heisenberg Lagrangian.

scattering are given by

$$\mathcal{L}^{(8)} = c_1\left(F_{\mu\nu}F^{\mu\nu}\right)^2 + c_2\left(F_{\mu\nu}\widetilde{F}^{\mu\nu}\right)^2, \tag{4.3}$$

thus containing the operators of dimension eight. In QED the constants c_1 and c_2 are given by [244]

$$c_1 = \frac{\alpha_{\rm em}^2}{90m^4}, \quad c_2 = \frac{7\alpha_{\rm em}^2}{360m^4}. \tag{4.4}$$

The independent helicity amplitudes at this order read

$$M^{(8)}_{++++}(s,t,u) = 8s^2(c_1+c_2), \tag{4.5a}$$
$$M^{(8)}_{+++-}(s,t,u) = 0, \tag{4.5b}$$
$$M^{(8)}_{++--}(s,t,u) = 8(s^2+t^2+u^2)(c_1-c_2). \tag{4.5c}$$

Note that the same low-energy behavior of these amplitudes and the QED boxes that are given in Tab. 4.1 is a general consequence of gauge invariance. Since the LbL amplitude should satisfy Ward identities,

$$k_1^\mu M_{\mu\nu\alpha\beta} = 0, \quad k_2^\nu M_{\mu\nu\alpha\beta} = 0, \quad k_3^\alpha M_{\mu\nu\alpha\beta} = 0, \quad k_4^\beta M_{\mu\nu\alpha\beta} = 0, \tag{4.6}$$

it should be proportional to a quadruple product of the photon momenta $k_1, ..., k_4$. Hence its low-energy expansion should start at least from the energy to the power of four.

In general case, the low-energy constants c_1 and c_2 can be determined in a data-driven way via the polarized two-photon fusion cross sections [245, 167] as

$$c_1 = \frac{1}{8\pi}\int_{s_{\rm th}}^\infty \frac{ds}{s^2}\sigma_\parallel(s), \quad c_2 = \frac{1}{8\pi}\int_{s_{\rm th}}^\infty \frac{ds}{s^2}\sigma_\perp(s). \tag{4.7}$$

The next-to-leading order effective Lagrangian for the two-photon scattering with the operators of dimension ten, can be constructed using derivatives of the electromagnetic tensor [167].

Given that the Euler-Heisenberg Lagrangian was derived using one-particle Dirac equation neglecting the electron-positron pair, its prediction is not valid already at the pair-creation threshold. Moreover, as an effective low-energy theory, it violates unitarity such that the amplitudes grow with energy too fast, which is a consequence of the high power of the photon momenta in the numerator.

4.1.2 Hadronic contribution

A much more subtle contribution comes from the hadron physics. It could be nominally splitted into the different regions in energy ω and scattering angle θ of the two-photon pair:

1. *low-energy region*, where $\omega \lesssim$ 1-2 GeV, which roughly corresponds to the BχPT and resonance applicability region,
2. *high-energy near-forward (diffractive, Regge) region*, for which $\omega \gg 1$ GeV and $\cos\theta \sim 1$,
3. *high-energy off-forward (perturbative QCD) region* with $\omega \gg 1$ GeV and $\cos\theta \sim 0$,
4. *intermediate region*, where the above regions go one to another.

The low-energy region is represented by the contributions from low-energy hadron spectrum, say pions, kaons etc. and the corresponding scalar and tensor resonances that emerge in meson-meson rescattering[2]. While the pion and kaon contributions can be successfully described in the framework of the SU(2) or SU(3) meson χPT, a proper account for the η-mesons and resonances is more involved. For instance, the lowest-lying scalar resonance $f_0(500)$, or σ, has a quite large total decay width, $\Gamma_\sigma \approx 250$ MeV, which is essentially dominated by the decay channel into two pions. The decay of this state into two photons, however, has an estimated width of just a few keV. Thus, in order to correctly account for its effect on the LbL process, a couple-channel analysis is unavoidably required. A situation for η- and η'-mesons is even more subtle. For η-meson, there are three main decay channels, namely $\gamma\gamma$ (40%), $3\pi^0$ (33%) and $\pi^+\pi^-\pi^0$ (23%), while the η'-meson decays to the photon pair only in 2.3% cases. Its decay is mainly driven by $\pi^+\pi^-\eta$ (43%), $\rho^0\gamma$ (30%) and $\pi^0\pi^0\eta$ (22%). Moreover, one should not forget about the η-η' mixing.

4.1.2.1 Low-energy region: Lagrangian-based model for hadronic exchanges

Due to the aforementioned numerous complications, a precise and self-consistent treatment of all the known low-energy hadronic states is a highly-nontrivial task. However if we are not interested in a high precision, but just in an approximate model for the hadronic background, we can simplify the picture by relaxing certain physical criteria. Following [248], the most simple way is to consider the meson exchanges in the narrow-width approximation, choosing the Breit-Wigner parametrization with the energy-dependent total ($\Gamma_{\rm tot}(s)$) and two-photon decay ($\Gamma_{x\to\gamma\gamma}(s)$) widths. Then the propagator Δ_x for the meson exchange will read

$$\Delta_x^{\mu_1\mu_2\ldots\mu_{2N},\nu_1\nu_2\ldots\nu_{2N}}(k) = \frac{i\hat{\mathcal{P}}^{\mu_1\mu_2\ldots\mu_{2N},\nu_1\nu_2\ldots\nu_{2N}}(k)}{k^2 - m_x^2 + i m_x \Gamma_{\rm tot}(k^2)}. \tag{4.8}$$

Here $\hat{\mathcal{P}}^{\mu_1\mu_2\ldots\mu_{2N},\nu_1\nu_2\ldots\nu_{2N}}(k^2)$ is the projection operator, which is given by the nature of the resonance exchange. It couples to the $x\gamma\gamma$ vertex by $2N$ indices, $\mu_1\ldots\mu_{2N}$ or $\nu_1\ldots\nu_{2N}$. For instance, for (pseudo)scalar exchanges the projection operator is equal to unity, and for the tensor exchanges it is given by

$$\hat{\mathcal{P}}^{\mu_1\mu_2,\nu_1,\nu_2} = \frac{1}{2}(\tilde{g}^{\mu_1\nu_1}\tilde{g}^{\mu_2\nu_2} + \tilde{g}^{\mu_1\nu_2}\tilde{g}^{\mu_2\nu_1}) - \frac{1}{3}\tilde{g}^{\mu_1\mu_2}\tilde{g}^{\nu_1\nu_2}, \tag{4.9}$$

with $\tilde{g}^{\alpha\beta} = -g^{\alpha\beta} + k^\alpha k^\beta / k^2$.

The $x\gamma\gamma$ interaction vertices in turn are given by the corresponding interaction Lagrangian terms. In the present work, we are interested in the scalar, pseudoscalar and tensor interactions:

1. $\gamma\gamma$-scalar vertex, $\Delta\mathcal{L} = -g_{x\gamma\gamma}\phi F_{\mu\nu}F^{\mu\nu}$:

$$\Gamma^{\mu\nu}(q_1,q_2) = -2ig_{x\gamma\gamma}(q_1\cdot q_2 g^{\mu\nu} - q_1^\nu q_2^\mu). \tag{4.10}$$

[2]Exchange of the vector states are forbidden due to the Landau-Yang theorem [246, 247].

2. $\gamma\gamma$-pseudoscalar vertex, $\Delta\mathcal{L} = -\frac{g_{x\gamma\gamma}}{2}\phi\epsilon^{\mu\nu\alpha\beta}F_{\alpha\beta}F^{\mu\nu}$:

$$\Gamma^{\mu\nu}(q_1,q_2) = 2ig_{x\gamma\gamma}\epsilon^{\mu\nu\alpha\beta}q_{1\,\alpha}q_{2\beta}. \tag{4.11}$$

3. $\gamma\gamma$-tensor vertex, $\Delta\mathcal{L} = \left[a_{x\gamma\gamma}(\partial_\rho F_{\mu\nu})(\partial_\lambda F^{\mu\nu}) + b_{x\gamma\gamma}F_{\mu\rho}F^{\mu}_{\lambda}\right]\left(g^{\rho\rho'} - \frac{1}{4}g^{\rho\lambda}g^{\rho'\lambda'}\right)\phi_{\rho'\lambda'}$:

$$\Gamma_{\mu\nu\rho\lambda}(q_1,q_2) = 2a_{x\gamma\gamma}\Gamma^{(0)}_{\mu\nu\rho\lambda}(q_1,q_2) - b_{x\gamma\gamma}\Gamma^{(2)}_{\mu\nu\rho\lambda}(q_1,q_2), \tag{4.12}$$

where the helicity-0 and helicity-2 parts are defined, correspondingly, as

$$\Gamma^{(0)}_{\mu\nu\rho\lambda}(q_1,q_2) = \left(q_1\cdot q_2 g_{\mu\nu} - q_{2\mu}q_{1\nu}\right)\left(q_{1\rho}q_{2\lambda} + q_{2\rho}q_{1\lambda} - \frac{1}{2}q_1\cdot q_2 g_{\rho\lambda}\right) \tag{4.13}$$

$$\begin{aligned}\Gamma^{(2)}_{\mu\nu\rho\lambda}(q_1,q_2) =& q_1\cdot q_2\left(g_{\mu\nu}g_{\rho\lambda} + g_{\mu\lambda}g_{\rho\nu}\right) + g_{\mu\nu}\left(q_{1\rho}q_{2\lambda} + q_{2\rho}q_{1\lambda}\right)\\ &- q_{1\nu}q_{2\lambda}g_{\mu\rho} - q_{1\nu}q_{2\rho}g_{\mu\lambda} - q_{2\mu}q_{1\lambda}g_{\nu\rho} - q_{2\mu}q_{1\rho}g_{\nu\lambda}\\ &- \left(q_1\cdot q_2 g_{\mu\nu} - q_{2\mu}q_{1\nu}\right)g_{\rho\lambda}.\end{aligned} \tag{4.14}$$

Here the four-momenta of the two photons incoming into each vertex are q_1^μ and q_2^ν.

The corresponding sets of the helicity amplitudes read

- (pseudo)scalar exchanges

$$M^{\mathrm{S}}_{++++}(s,t,u) = -g^2_{x\gamma\gamma}\frac{s^2}{s - m_x^2 + im_x\Gamma_{\mathrm{tot}}(s)}, \tag{4.15a}$$

$$M^{\mathrm{S}}_{+++-}(s,t,u) = 0, \tag{4.15b}$$

$$\begin{aligned}M^{\mathrm{S}}_{++--}(s,t,u) =& -\mathrm{P}_x g^2_{x\gamma\gamma}\left[\frac{s^2}{s - m_x^2 + im_x\Gamma_{\mathrm{tot}}(s)}\right.\\ &\left. + \frac{t^2}{t - m_x^2 + im_x\Gamma_{\mathrm{tot}}(t)} + \frac{u^2}{u - m_x^2 + im_x\Gamma_{\mathrm{tot}}(u)}\right],\end{aligned} \tag{4.15c}$$

where $\mathrm{P}_x = \pm 1$ stands for the parity of the exchanged meson state x.

- tensor exchanges

$$\begin{aligned}M^{\mathrm{T}}_{++++}(s,t,u) =& s^2\left[\frac{a^2_{x\gamma\gamma}}{6}\frac{s^2 - 6tu}{s - m_x^2 + im_x\Gamma_{\mathrm{tot}}(s)}\right.\\ &\left. + b_{x\gamma\gamma}\left(\frac{1}{t - m_x^2 + im_x\Gamma_{\mathrm{tot}}(t)} + \frac{1}{u - m_x^2 + im_x\Gamma_{\mathrm{tot}}(u)}\right)\right],\end{aligned} \tag{4.16a}$$

$$\begin{aligned}M^{\mathrm{T}}_{+++-}(s,t,u) =& a_{x\gamma\gamma}b_{x\gamma\gamma}stu\left[\frac{1}{s - m_x^2 + im_x\Gamma_{\mathrm{tot}}(s)}\right.\\ &\left. + \frac{1}{t - m_x^2 + im_x\Gamma_{\mathrm{tot}}(t)} + \frac{1}{u - m_x^2 + im_x\Gamma_{\mathrm{tot}}(u)}\right],\end{aligned} \tag{4.16b}$$

$$M^{\mathrm{T}}_{++--}(s,t,u) = \frac{a^2_{x\gamma\gamma}}{6}\left[\frac{s^2(t^2+u^2-4tu)}{s-m_x^2+im_x\Gamma_{\mathrm{tot}}(s)} + \frac{t^2(s^2+u^2-4su)}{t-m_x^2+im_x\Gamma_{\mathrm{tot}}(t)} + \frac{u^2(t^2+s^2-4ts)}{u-m_x^2+im_x\Gamma_{\mathrm{tot}}(u)}\right]. \tag{4.16c}$$

It worth mentioning that the real part of the decay width $\Gamma_{\mathrm{tot}}(s)$, which enters the above expressions, has the natural step-like behavior generated by the square root,

$$\Gamma_{\mathrm{tot}}(s) \sim \sqrt{s-s_{\mathrm{thr.}}} \to \sqrt{s-s_{\mathrm{thr.}}}\,\theta(s-s_{\mathrm{thr.}}) + i\sqrt{s_{\mathrm{thr.}}-s}\,\theta(s_{\mathrm{thr.}}-s), \tag{4.17}$$

so in the physically allowed kinematic domain it does not produce any imaginary contribution to the t- and u-channel exchanges.

Neglecting the energy dependence in the decay width in Eqs. (4.15) and (4.16) , one obtains the amplitudes, which reproduce the correct behavior only in a small vicinity of the resonance, while strongly violate unitarity at high energies. This can be clearly seen from the high power of the momenta in the numerator than in the denominator, which is more severe for the tensor exchanges than for the scalar ones and causes dramatic asymptotic behavior. This problem is nothing but a manifestation of the non-renormalizability (ultraviolet-incompleteness) of the low-energy effective field theory.

A straightforward phenomenological way to overcome this issue is to introduce the form factors, which suppress the dramatic increase of the amplitudes at high energies. However, such an approach is usually implemented in purely *ad hoc* way having no systematic theory behind and ignoring fundamental physical constraints. The situation becomes especially complicated, when there is no experimental way to measure such a form factor. For instance, in case of the meson exchange in $\gamma\gamma \to \gamma\gamma$, currently there is no way for direct measure of the meson-γ-γ vertex for real photons and virtual meson. Therefore, in [248] authors use the phenomenological form factors of exponential form,

$$F^{x\gamma\gamma}(s) = \exp\left[-\frac{(s-m_x^2)^2}{\Lambda^4_{\mathrm{exp}}}\right], \quad F^{x\gamma\gamma}(\{t,u\}) = \exp\left[\frac{\{t,u\}-m_x^2}{\Lambda^2_{\mathrm{exp}}}\right], \tag{4.18}$$

for s- or t- and u-channel with a free phenomenological parameter $\Lambda_{\mathrm{exp}} = 2\mathrm{GeV}$. Clearly, among other fundamental S-matrix constraints, e.g. unitarity and analiticity, these form factors explicitly violate crossing symmetry. A possible improvement on the purely ad-hoc form factors like (4.18) is to consider the one-loop $\gamma\gamma$-meson vertex instead of the constant one, as shown in Fig. 4.3:

$$F^{x\gamma\gamma}(s) = 2M_\psi^2 \int_0^1 dx \int_0^{1-x} dy \frac{1}{M_\psi^2 - xy\,s} \equiv -2m_x^2\, C_0(0,0,s;M_\psi^2,M_\psi^2,M_\psi^2). \tag{4.19}$$

It is normalized such that

$$F^{x\gamma\gamma}(0) = 1. \tag{4.20}$$

A particle ψ that runs inside the loop could be thought as some fermion with sufficiently large mass M_ψ. This form factor has a straightforward physical meaning, giving, e.g., the leading correction to

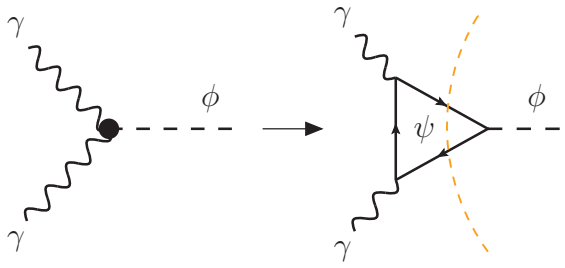

Fig. 4.3 ChPT-inspired $\gamma\gamma$-meson form factor with heavy fermion field ψ in the loop. The two-particle cut, which causes cusps in the cross section, is shown by orange dashed line.

the chiral anomaly in BχPT. In this case the heavy fermion in the loop is nothing but the nucleon, say proton, which is the lowest physical fermionic d.o.f. at energies below 1 GeV . Despite the simplicity of such a model (it has only one free parameter M_ψ), it does not contradict any basic physical principles, i.e. unitarity, analyticity, crossing-symmetry, gauge invariance etc. Effectively, the explicit inclusion of a heavy d.o.f. works as an ultraviolet completion of the considered low-energy model.

However, the price one needs to pay for such a simple solution is the cusp-like behavior of the cross section near $s = 4M_\psi^2$. This behavior originates from the s-channel amplitudes, when the energy of the two-photon pair is enough to put the two particles ψ on shell. Basically, it corresponds to the two-particle cut of the loop, shown in Fig. 4.3. If one assumes the loop particle to be a proton, then the cut starts well above the applicability of BχPT, and could be treated as unphysical. Thus, such a model should work well in the low-energy region, but fail for higher energies, where the perturbative QCD and/or diffractive effects come into play.

An alternative way to correct the Lagrangian-based model is to require it to satisfy the dispersion relations or sum rules pertinent to the process under consideration. In case of the real LbL scattering one has three sum rules for the forward scattering, given by Eqs. (2.77). Since the sum rules are formulated based on the general assumptions of S-matrix theory, their satisfaction implies that all fundamental S-matrix constraints are inherently incorporated into the model. In this way, the sum rules can be used as an essential physical constraints for the constructed model of hadronic exchanges in LbL scattering.

Now let us focus on the single-channel (pseudo)scalar meson exchanges and first test the helicity amplitudes (4.15) against the sum rules (2.77) in the narrow-width approximation, i.e. $\Gamma_{\text{tot}} \approx \Gamma_{\gamma\gamma} \ll m_x$. The polarized $\gamma\gamma \to$meson-fusion cross sections are given by [167, 237]:

$$\sigma_0(s) = 16\pi^2 \frac{\Gamma_{\gamma\gamma}}{m_x}\,\delta(s - m_x^2), \quad \sigma_2(s) = 0, \tag{4.21a}$$

$$\begin{cases} \sigma_\parallel(s) = \sigma_0(s), \quad \sigma_\perp(s) = 0, & \text{for scalar,} \\ \sigma_\perp(s) = \sigma_0(s), \quad \sigma_\parallel(s) = 0, & \text{for pseudoscalar.} \end{cases} \tag{4.21b}$$

Thus the dispersive integrals yield the following helicity amplitudes:

$$\frac{2s^2}{\pi}\int\limits_0^\infty ds'\,\frac{\sigma_0(s')}{s'^2-s^2-i0^+}=\frac{32\pi\Gamma_{\gamma\gamma}}{m_x}\frac{s^2}{m_x^4-s^2-i0^+} \tag{4.22a}$$

$$\frac{2s}{\pi}\int\limits_0^\infty ds'\,\frac{s'\sigma_0(s')}{s'^2-s^2-i0^+}=32\pi\Gamma_{\gamma\gamma}\frac{sm_x}{m_x^4-s^2-i0^+} \tag{4.22b}$$

$$\frac{2s^2}{\pi}\int\limits_0^\infty ds'\,\frac{\sigma_\parallel(s')-\sigma_\perp(s')}{s'^2-s^2-i0^+}=\mathrm{P}_x\frac{32\pi\Gamma_{\gamma\gamma}}{m_x}\frac{s^2}{m_x^4-s^2-i0^+}, \tag{4.22c}$$

where the overall sign $+(-)$ in the last expression corresponds to the scalar (pseudoscalar) exchange.

However, the model, given by Eqs. (4.15), in the forward limit leads to the following results for the l.h.s. of Eqs. (2.77)

$$M^{\mathrm{S}}_{++++}(s)+M^{\mathrm{S}}_{+-+-}(s)=\frac{32\pi\Gamma_{\gamma\gamma}}{m_x}\frac{s^2}{m_x^4-s^2-i0^+}, \tag{4.23a}$$

$$M^{\mathrm{S}}_{++++}(s)-M^{\mathrm{S}}_{+-+-}(s)=\frac{32\pi\Gamma_{\gamma\gamma}}{m_x^3}\frac{s^3}{m_x^4-s^2-i0^+}, \tag{4.23b}$$

$$M^{\mathrm{S}}_{++--}(s)=\mathrm{P}_x\frac{32\pi\Gamma_{\gamma\gamma}}{m_x}\frac{s^2}{m_x^4-s^2-i0^+}. \tag{4.23c}$$

Comparing Eqs. (4.22) and (4.23), namely, r.h.s. and l.h.s. of the sum rules (2.77), one can see that the considered model for the meson exchanges satisfy the sum rules (2.77a) and (2.77c), but does not satisfy the sum rule (2.77b). Indeed, comparing the model calculation, given by Eq. (4.23b), with the dispersive integral result (4.22b), one obtains inconsistency by a factor of s^2/m_x^4. This contradiction can be easily resolved by modifying the numerators of the model amplitudes (4.15) by removing one power of the Mandelstam variable, i.e. making the substitution $\{s^2,t^2,u^2\}\to\{s,t,u\}\times m_x$. The modified nonzero amplitudes then read

$$M^{\mathrm{S}\star}_{++++}(s,t,u)=-\frac{g^2_{x\gamma\gamma}}{m_x^2}\frac{s}{s-m_x^2+im_x\Gamma_{\mathrm{tot}}(s)}, \tag{4.24a}$$

$$\begin{aligned}M^{\mathrm{S}\star}_{++--}(s,t,u)=-\mathrm{P}_x\frac{g^2_{x\gamma\gamma}}{m_x^2}\Bigg[&\frac{s}{s-m_x^2+im_x\Gamma_{\mathrm{tot}}(s)}\\&+\frac{t}{t-m_x^2+im_x\Gamma_{\mathrm{tot}}(t)}+\frac{u}{u-m_x^2+im_x\Gamma_{\mathrm{tot}}(u)}\Bigg],\end{aligned} \tag{4.24b}$$

In the forward scattering limit, the expressions for $M^{\mathrm{S}}_{++++}+M^{\mathrm{S}\star}_{+-+-}$ and $M^{\mathrm{S}\star}_{++--}$ remain unchanged compared to Eqs. (4.23a) and (4.23c), whereas the problematic combination $M^{\mathrm{S}\star}_{++++}-M^{\mathrm{S}\star}_{+-+-}$ will read

$$M^{\mathrm{S}\star}_{++++}(s)-M^{\mathrm{S}\star}_{+-+-}(s)=32\pi\Gamma_{\gamma\gamma}\frac{s}{m_x^4-s^2-i0^+}, \tag{4.25}$$

which agrees with the dispersive integral result given by Eq. (4.22b).

The comparison of the total LbL cross section, calculated using different models, is shown in Fig. 4.4. Here one can explicitly see the problematic high-energy behavior of the "bare" amplitudes, which are obtained just from the effective low-energy Lagrangian, and how it can be corrected either including C_0 or exponential form factors or modifying the amplitudes according to the LbL sum rules. A questionable cusp, which originates from the C_0 form factor, moves the cross section even higher than the whole pQCD prediction in the vicinity of the two-proton production threshold.

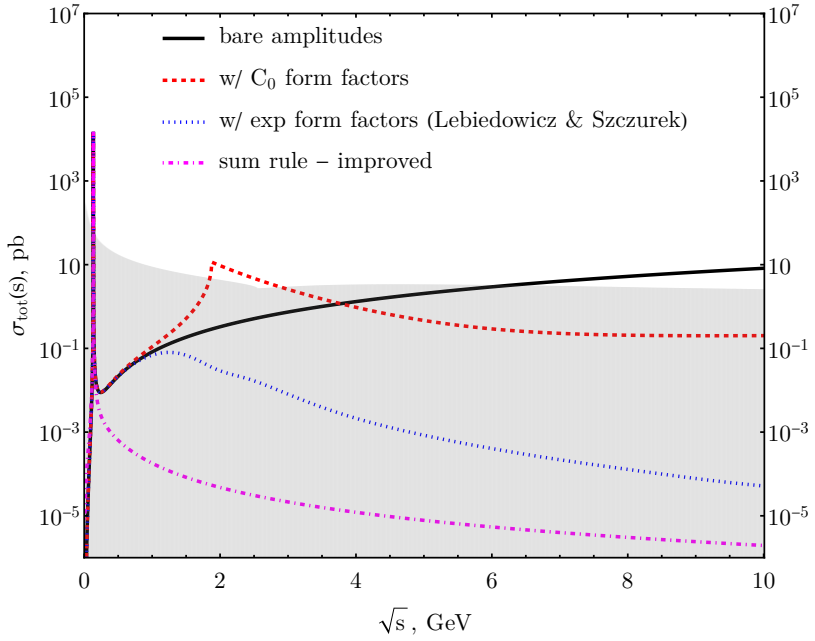

Fig. 4.4 The total LbL cross section for the π^0-exchange, calculated using various models for the helicity amplitudes is shown compared to the pQCD loops (gray band). "Bare" amplitudes are given by Eqs. (4.23).The C_0 form factor is given by Eq. (4.19). The exponential form factors are taken from Lebiedowicz & Szczurek [248] and given by Eq. (4.18). The sum rule - imroved amplitudes are written in Eqs. (4.24)

While the performed modification corrects the high-energy behavior of the LbL amplitudes, it spoils their threshold behavior (the behavior around $s = 0$). Indeed, as was mentioned before, the low-energy expansion of the amplitudes should start at least from the energy in fourth power, say s^2, meanwhile the modified expressions show linear dependence on s in this regime. In order to maintain both the correct $\gamma\gamma$-production threshold and high-energy behavior, a comprehensive analysis in (unitarized) field theory is needed. It must involve the introduction of the energy-dependent decay width, the realistic shape of the photoabsorption cross section etc. However, since at very low energies the LbL process is totally dominated by the QED contribution, the hadronic part below the π^0- production threshold is beyond the scope of the current work.

4.1.2.2 Perturbative QCD contribution

The leading-order perturbative QCD contribution to the LbL helicity amplitudes is given by the quark loops. The expressions for the amplitudes are the same as for the QED contribution, but now they shoud be summed over all six quark flavors, supplemented by the correct charges of each quark, and over three colors as well. Given that the free quarks have not been observed, it seems more correct to consider just a real part of the amplitudes instead of the whole expressions, removing in this way the part that corresponds to the on-shell quark pair creation. However, this has no pronounced effect on the total cross section, which is shown in Fig. 4.5

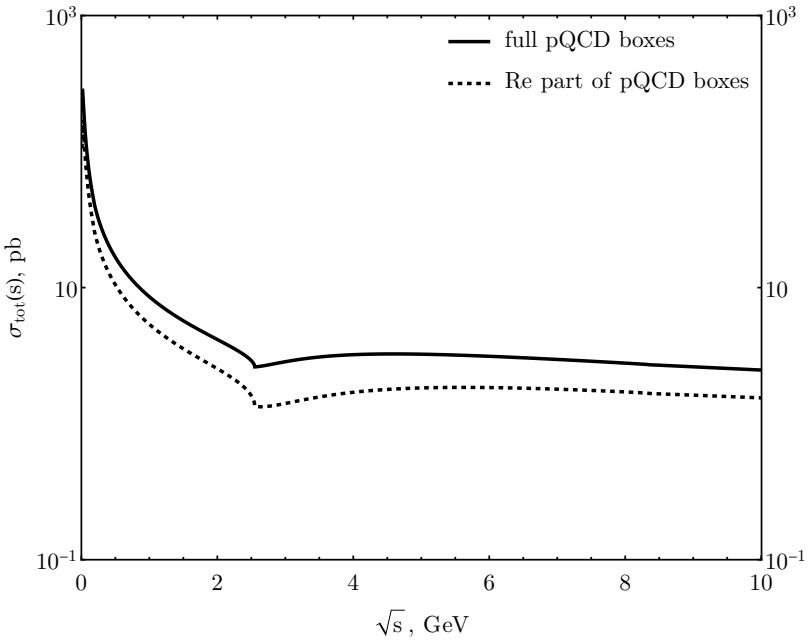

Fig. 4.5 The total LbL cross section obtained from the full pQCD amplitudes or from the real parts of these amplitudes.

Recently, the effect of NLO pQCD corrections was investigated in details in [79]. In this work, the two-loop LbL scattering amplitudes were calculated in pQCD (and QED) using two different numerical methods. Within the ATLAS fiducial phase space [72], the obtained LO+NLO pQCD+QED total fiducial cross section increases by $\approx 6.5^{+2.1}_{-1.2}\%$ with respect to the LO cross section, yielding $81.2^{+1.6}_{-0.9}$ nb vs. 76 nb. It was found that the influence of NLO correction is more pronounced for lower diphoton masses. In particular, the 13% effect in the diphoton-mass bin at 5-10 GeV reduces to 0.7% in the bin at 20-30 GeV. However, in view of the non-perturbative nature of QCD either at low energies or low scattering angles, the pQCD predictions should be used cautiously below 5 GeV in diphoton mass or for the near-forward LbL scattering regime.

4.1.2.3 Regge region

At high energies in the near-beam scattering regime, the hadronic part of LbL cross section should have a power-like, or Regge, behavior. Among the hadronic two-photon fusion cross sections, which are connected to the LbL scattering via sum rules (2.77), only the total unpolarized one, σ_{TT}, is known experimentally. It can be described empirically by a simple fit inspired by the Regge theory, which consists of a few power-like terms. The main assumption, which is usually made for the fit function for the $\gamma\gamma \to$had. cross section relies on the Gribov factorization, when the photon is treated like a proton. It implies that all the cross sections $\gamma\gamma \to$had., $pp \to$had. and $p\bar{p} \to$had. can be fitted with the same pomeron (X) plus reggeon (Y) ansatz as [249]

$$\sigma_{\text{tot}}^{AB}(s) = X^{AB} s^{\epsilon} + Y^{AB} s^{-\eta}, \tag{4.26}$$

with A and B being the photon or the proton. The powers ϵ and η are the same for all listed processes and are determined in, e.g., the combined fit by Donoghue et al. [250] . Assuming the factorization of pomeron and reggeon terms,

$$X^{AB} = \chi_P^A \chi_P^B, \quad Y^{AB} = \upsilon_R^A \upsilon_R^B, \tag{4.27}$$

one can connect the fit parameters for $\gamma\gamma \to$had. cross section with the ones for $\gamma p \to$had., $pp \to$had. and $p\bar{p} \to$had. cross sections:

$$X^{\gamma\gamma} = \frac{(X^{\gamma p})^2}{X^{pp}}, \quad Y^{\gamma\gamma} = \frac{2(Y^{\gamma p})^2}{Y^{pp} + Y^{p\bar{p}}}. \tag{4.28}$$

One can weaken the factorization assumption, assuming that it holds for the entire total cross sections, arriving to the following approximate formula

$$\sigma_{\text{tot}}^{\gamma\gamma} = \frac{2(\sigma_{\text{tot}}^{\gamma p})^2}{\sigma_{\text{tot}}^{pp} + \sigma_{\text{tot}}^{p\bar{p}}}. \tag{4.29}$$

Practically, this formula works with a good accuracy of around a percent [249].

A current fit of the existing data on $\sigma_{\text{tot}}^{\gamma\gamma}$ provided by Particle Data Group [251], also relies on the Gribov factorization and implies the simultanious fitting of $\sigma_{\text{tot}}^{\gamma\gamma}$, $\sigma_{\text{tot}}^{\gamma p}$, σ_{tot}^{pp} and $\sigma_{\text{tot}}^{p\bar{p}}$. The fit function reads (see p.583 in [252])

$$\sigma_{\gamma\gamma}(s) = \delta^2 \left[H \log^2 \left(\frac{s}{s_{\gamma\gamma}} \right) + P_{\gamma\gamma} \right] + R_{\gamma\gamma} \left(\frac{s}{s_{\gamma\gamma}} \right)^{-\eta}, \tag{4.30}$$

whith the parameters

$$\delta = (3.063 \pm 0.014) \times 10^{-3}, \tag{4.31a}$$

$$s_{\gamma\gamma} = M^2, \quad M = (2.1206 \pm 0.0094)\,\text{GeV} \tag{4.31b}$$

$$H = \pi \frac{(\hbar c)^2}{M^2} = (0.272 \pm 0.0024)\,\text{mb}, \tag{4.31c}$$

$$P_{\gamma\gamma} = (34.41 \pm 0.13)\,\text{mb}, \tag{4.31d}$$

$$R_{\gamma\gamma} = (-4 \pm 11) \times 10^{-6}\,\text{mb}, \tag{4.31e}$$

$$\eta = (0.4473 \pm 0.0077). \tag{4.31f}$$

Here, $P_{\gamma\gamma}$ is the Pomeranchuk's constant term, $R_{\gamma\gamma}$ is the effective Regge pole contribution. Furthermore, the Heisenberg's $\log^2(s)$ term [253] was included as well. However, the PDG fit has minimum theory behind it and can be thought as just an empirical one.

A qualitative theoretical explanation of the $\gamma\gamma \to$had. cross section behavior can be given by considering the wave function of realistic (not a point-like) virtual photon, splitting it into the following terms [249, 254]:

$$|\gamma\rangle = c_0|\gamma_0\rangle + \sum_{V=\rho^0,\omega,\phi,J/\psi,\Upsilon\ldots} c_V|V\rangle + \sum_{q=u,d,s,c,b,t} c_q|q\bar{q}\rangle + \sum_{l=e,\mu,\tau} c_l|l^+l^-\rangle + \sum_{W^\pm} c_W|W^+W^-\rangle. \tag{4.32}$$

Here $|\gamma_0\rangle$, $|V\rangle$, $|q\bar{q}\rangle$, $|l^+l^-\rangle$ and $|W^+W^-\rangle$ are wave functions of the point-like photon, a vector meson V, a pair of quarks $q^\pm$, leptons $l^\pm$ or weak bosons $W^\pm$. In this form of the photon wave function the low-energy and high-energy as well as low-virtuality and high-virtuality parts are separated. The vector meson part, which is responsible for low virtualities, can be described by the vector-meson-dominance (VMD) model. The vector meson coefficients c_V are defined in terms of the decay constant F_V,

$$c_V = \frac{\sqrt{4\pi\alpha_{\text{em}}}}{F_V}, \tag{4.33}$$

whereas f_V can be found from the experimental data on the decay $V \to l^+l^-$. Above some characteristic virtuality scale p_0 the perturbative QCD comes into play with the coefficients c_q, which now behave like

$$c_q^{\text{high-virtuality}} \approx \frac{\alpha_{\text{em}}}{2\pi} 2e_q^2 \log \frac{\mu_{\text{had}}^2}{p_0^2}, \tag{4.34}$$

where μ_{had} is the characteristic energy scale of the considered parton process. Note that the VMD part does not depend on the scale μ_{had}. Thus, the $\gamma\gamma \to$had. cross section consists of the VMD $\times$ pQCD terms as follows [255]

$$\sigma_{\gamma\gamma}(\nu, Q^2) = (\text{VMD})^2 + (\text{pQCD})^2 + 2(\text{VMD}) \times (\text{pQCD}). \tag{4.35}$$

For the real photons the first term with both photons being soft is the dominating one. Hence one can sum up all of the contributions from the known vector mesons, assuming that they lie on the same Regge trajectory. This approach was implemented in, e.g., Badełek et al. [256], obtaining the

following prediction on the $\sigma_{\gamma\gamma}$

$$\sigma_{\gamma\gamma}(s) = \alpha_{\rm em} \sum_{V=\rho^0,\omega,\phi} \frac{\sigma_{V\gamma}(s)}{C_V}, \tag{4.36}$$

with the Regge ansatz for the vector meson cross sections with one pomeron and one reggeon terms:

$$\sigma_{V\gamma}(s) = a_V^P \left(\frac{s}{s_0}\right)^{\lambda_P} + a_V^R \left(\frac{s}{s_0}\right)^{\lambda_R}. \tag{4.37}$$

The pomeron and reggeon powers, $\lambda_P = 0.0808$ and $\lambda_R = -0.4525$ were taken from the fit by Donnachie et al. [250], whereas the coefficients C_V were fixed from the vector meson decay constants:

$$C_V = \{1.98, 21.07, 13.83\}. \tag{4.38}$$

The pomeron an reggeon couplings were estimated assuming the additive quark model and duality (for reggeon), yielding

$$a_V^P = \{1,1,2\} \times \frac{2}{3} a_{\gamma p}^P, \quad a_{\gamma p}^P = 0.0677\,\text{mb}, \tag{4.39}$$

$$a_V^R = \{1,1,0\} \times \frac{5}{9} a_{\gamma p}^R, \quad a_{\gamma p}^R = 0.129\,\text{mb}. \tag{4.40}$$

This model describes the existing data for $\sigma_{\gamma\gamma}$ with $\chi^2 = 1.04$.

However, for our purposes of modelling just the real LbL scattering, the precise fit to the $\sigma_{\gamma\gamma}(s)$ data is needed. Therefore it is desirable to have a simple but precise fit to $\gamma\gamma \to$had. data individually. Such a fit has been done by O. Gryniuk [257]. It relies just on two power-like terms and has a reasonably better χ^2 compared to PDG fit, 0.91 versus 1.52, respectively[3]. It is seen from Fig. 4.6 that the fit by Gryniuk follows the data the best, especially at high energies. Therefore it was chosen to be used in our calculations of the dispersive integrals containing $\sigma_{TT}^{\gamma\gamma}$.

4.1.2.4 Sum-rule-inspired ansatz for off-forward real LbL

The LbL sum rules can be used not only to constrain Lagrangian-based models, but rather build the new ones on their own. Having in mind the full crossing invariance of the LbL helicity amplitude M_{++--} and the combination $M_{++++} + M_{+--+} + M_{+-+-}$, one can assume [237] that they should satisfy the following sum rules:

$$M_{++++}(s,t,u) + M_{+--+}(s,t,u) + M_{+-+-}(s,t,u) =$$

[3]The provided values of χ^2 have been obtained taking into account only the y-axis (cross section) uncertainties of the data.

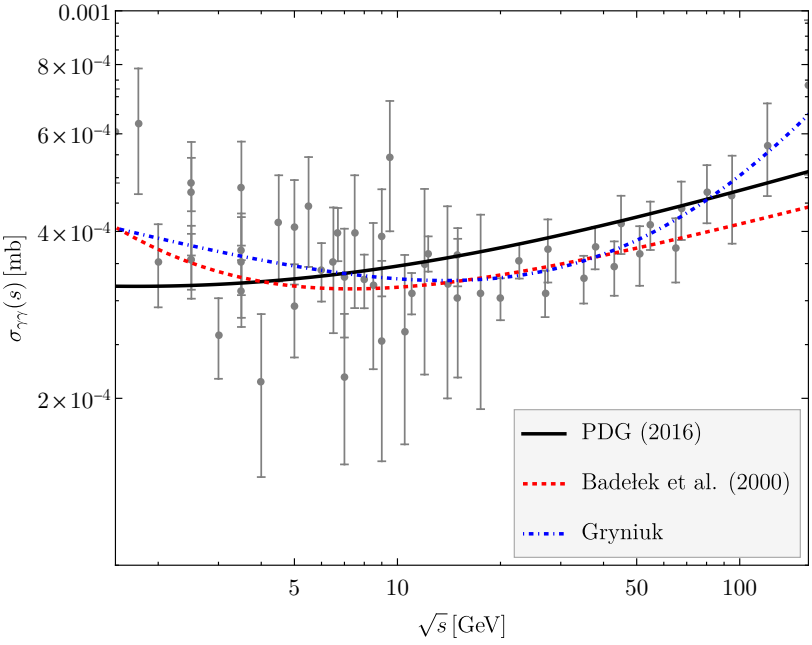

Fig. 4.6 The central curves of the fits by PDG [252] (black solid line), Badełek et al. [256] (red dashed line) and Gryniuk [257] (blue dashed line) to the data on the hadronic two-photon fusion cross section (grey points with vertical errorbars) are shown.

$$= \frac{1}{\pi}\int_0^\infty ds'\sigma_{TT}(s')\left(\frac{s}{s'-s}+\frac{t}{s'-t}+\frac{u}{s'-u}\right) = \mathcal{S}_{\rm sum}^{\rm LbL,\,a_1}(s,t,u), \tag{4.41a}$$

$$M_{++--}(s,t,u) = \frac{1}{\pi}\int_0^\infty ds'\tau_{TT}^{a}(s')\left(\frac{s}{s'-s}+\frac{t}{s'-t}+\frac{u}{s'-u}\right) = \mathcal{S}_{3}^{\rm LbL,\,a_1}(s,t,u). \tag{4.41b}$$

The r.h.s. of these relations are manifestly crossing-invariant, and in the forward limit they reduce to Eqs. (2.77a) and (2.77c). Note that for the real photons, the ansatz could be written in an equivalent form, using the identity

$$\left(\frac{s}{s'-s}+\frac{t}{s'-t}+\frac{u}{s'-u}\right) = \frac{1}{s'}\left(\frac{s^2}{s'-s}+\frac{t^2}{s'-t}+\frac{u^2}{s'-u}\right)+\frac{s+t+u}{s'}, \tag{4.42}$$

where the second term in r.h.s. is zero.

This ansatz could be obtained from the twice-subtracted fixed-t dispersion relation for the S-wave (scalar) crossing-invariant scattering amplitude $\mathcal{M}(s,t)$ (cf. Appendix E in [121]), which is given by

$$\mathcal{M}(s,t) = C(t)+\frac{1}{\pi}\int_0^\infty \frac{ds'}{s'^2}\left\{\frac{s^2}{s'-s}+\frac{u^2}{s'-u}\right\}\mathrm{Im}\,\mathcal{M}(s',t), \tag{4.43}$$

where $C(t)$ is the subtraction function that does not depend on s. Imposing $s \leftrightarrow t$ crossing symmetry, one obtains

$$\mathcal{M}(s,t) = C(0) + \frac{1}{\pi}\int_0^\infty \frac{ds'}{s'^2}\left\{\frac{s^2}{s'-s} + \frac{t^2}{s'-t} + \frac{u^2}{s'-u}\right\} \mathrm{Im}\,\mathcal{M}(s',t) + \frac{2t^2}{\pi}\int_0^\infty \frac{ds'}{s'(s'^2-t^2)}\Big[\mathrm{Im}\,\mathcal{M}(s',0) - \mathrm{Im}\,\mathcal{M}(s',t)\Big], \tag{4.44}$$

or, alternatively,

$$\mathcal{M}(s,t) = C(0) + \frac{1}{\pi}\int_0^\infty \frac{ds'}{s'^2}\left\{\frac{s^2}{s'-s} + \frac{u^2}{s'-u} - \frac{t^2}{s'+t}\right\} \mathrm{Im}\,\mathcal{M}(s',t) + \frac{2t^2}{\pi}\int_0^\infty \frac{ds'}{s'(s'^2-t^2)}\,\mathrm{Im}\,\mathcal{M}(s',0). \tag{4.45}$$

Neglecting the second integral term in Eq. (4.44) and observing the vanishing $C(0)$ for real photons, we exactly obtain the crossing-invariant ansatz discussed above. Hence one can conclude that the ansatz given by Eqs. (4.41a) and (4.41b) is just an S-wave approximation of the full angular dependence. Therefore we can expect that this ansatz should work exactly for the (pseudo)scalar exchanges, but could fail for the exchanges of higher angular momenta or LbL boxes. The latter will be considered in details in the following section.

4.1.3 Weak contribution

The leading contribution of the weak sector of SM comes from the one-loop LbL diagrams with $W^\pm$-bosons in the loop. The corresponding independent helicity amplitudes are obtained in Refs. [168, 169] and explicitely written in Appendix 4.A. The high energy scale of the weak force, compared to the other contributions stemming from SM, implies that this contribution becomes important at the phonon c.o.m. energies of order of two gauge boson masses, i.e. > 100 GeV.

4.2 Model for hadronic LbL scattering at low and moderate energies

4.2.1 Crossing-invariant sum rule

Written as a dispersive integral over the observable two-photon fusion hadronic cross section, the crossing-invariant ansatz (4.41), if it works, provides a very powerful and fully data-driven tool for the main contribution to the off-forward LbL scattering. This ansatz will be tested here on QED and sQED one-loop contributions and on the (pseudo)scalar hadronic exchanges in LbL. Firstly, let us note that except the considered ansatz, which implies the following substitution under the dispersive integral (we will refer to it as a_1),

$$\text{Ansatz } a_1: \quad \frac{s^2}{s'^2-s^2} \to \frac{s}{s'-s} + \frac{t}{s'-t} + \frac{u}{s'-u} \quad \text{or} \quad \frac{1}{s'}\left(\frac{s^2}{s'-s} + \frac{t^2}{s'-t} + \frac{u^2}{s'-u}\right), \tag{4.46}$$

another fully crossing-invariant ansatz can be written. It will correspond to the substitution

$$\text{Ansatz } a_2: \quad \frac{s^2}{s'^2 - s^2} \to -\left[\frac{st}{(s'-s)(s'-t)} + \frac{su}{(s'-s)(s'-u)} + \frac{tu}{(s'-t)(s'-u)}\right]. \tag{4.47}$$

However, it will be seen in the following, that the latter one does not reproduce the correct threshold behavior for the LbL one-loop contributions and cannot reproduce the (pseudo)scalar exchanges.

Newertheless, it is important to keep in mind that both ansatze a_1 and a_2 have the correct forward limit, i.e.

$$\text{Ansatze } a_1, a_2\big|_{t\to 0} = \frac{s^2}{s'^2 - s^2}. \tag{4.48}$$

4.2.1.1 (Pseudo)scalar exchanges

Inserting the two-photon fusion cross sections for the narrow (pseudo)scalar state given by Eqs. (4.21) into the dispersive integrals of Eqs. (4.41), we immediately obtain the corresponding set of modified helicity amplitudes of meson exchanges (4.24). Alternatively, the equivalent version of the ansatz a_1 with squared Mandelstam variables in numerators (cf. Eq. (4.42)) yields the unmodified helicity amplitudes (4.15). The crossing-invariant ansatz a_2, despite it reproduces the forward LbL sum rule in the limit $t \to 0$, results in completely wrong expressions for the helicity amlitudes. Thus, we can concude that both equivalent versions of the ansatz a_1 work with the (pseudo)scalar meson exchanges in the narrow width approximation, but not the ansatz a_2.

4.2.1.2 (S)QED one-loop boxes

Given that in forward scattering limit both ansatze a_1 and a_2 reduce to the LbL sum rules (4.22a) and (4.22c), which are exact relations between cross sections and amplitudes, the most pronounced difference between exact amplitudes and ansatz predictions should show up in wide-angle scattering regime. Let us compare the behavior of the LbL polarized amplitudes in this regime, say when the c.o.m. scattering angle is $\theta = \pi/2$ with the ansatz predictions.

A comparison of the exact one-loop LbL amplitudes with those given by the ansatz a_1 is shown on Fig. 4.7. The first important observation, which outcomes from these plots, is the relatively weak dependence of the amplitudes with the scattering angle. Indeed, the imaginary part, given by the ansatz, is totally independent on the scattering angle, while the real part changes with this angle very weakly. The second observation one can point out is that the ansatz reproduces the helicity amplitude M_{++--} significantly better than the crossing-invariant combination of the helicity amplitudes $M_{++++} + M_{+--+} + M_{+-+-}$. This also applies for the near-threshold behavior as well as the high-energy behavior. These facts provide a hint that the amplitude M_{++--} is mainly driven by the S-wave, while the amplitude M_{++++} has a significant D-wave admixture. Thus, while the considered ansatz a_1 can be served as a good data-driven model for the helicty amplitude M_{++--}, it should be improved by inclusion of the D-waves for the case of other helicity amplitudes.

The results for ansatz a_2, shown in Fig. 4.8, demonstrate that this ansatz works considerably worse in comparison to the ansatz a_1 for all helicity amplitudes. It incorrectly reproduces either the near-threshold region or the high-energy behavior. This fact may point to the dominance of S-wave contribution to all of the considered helicity amplitudes.

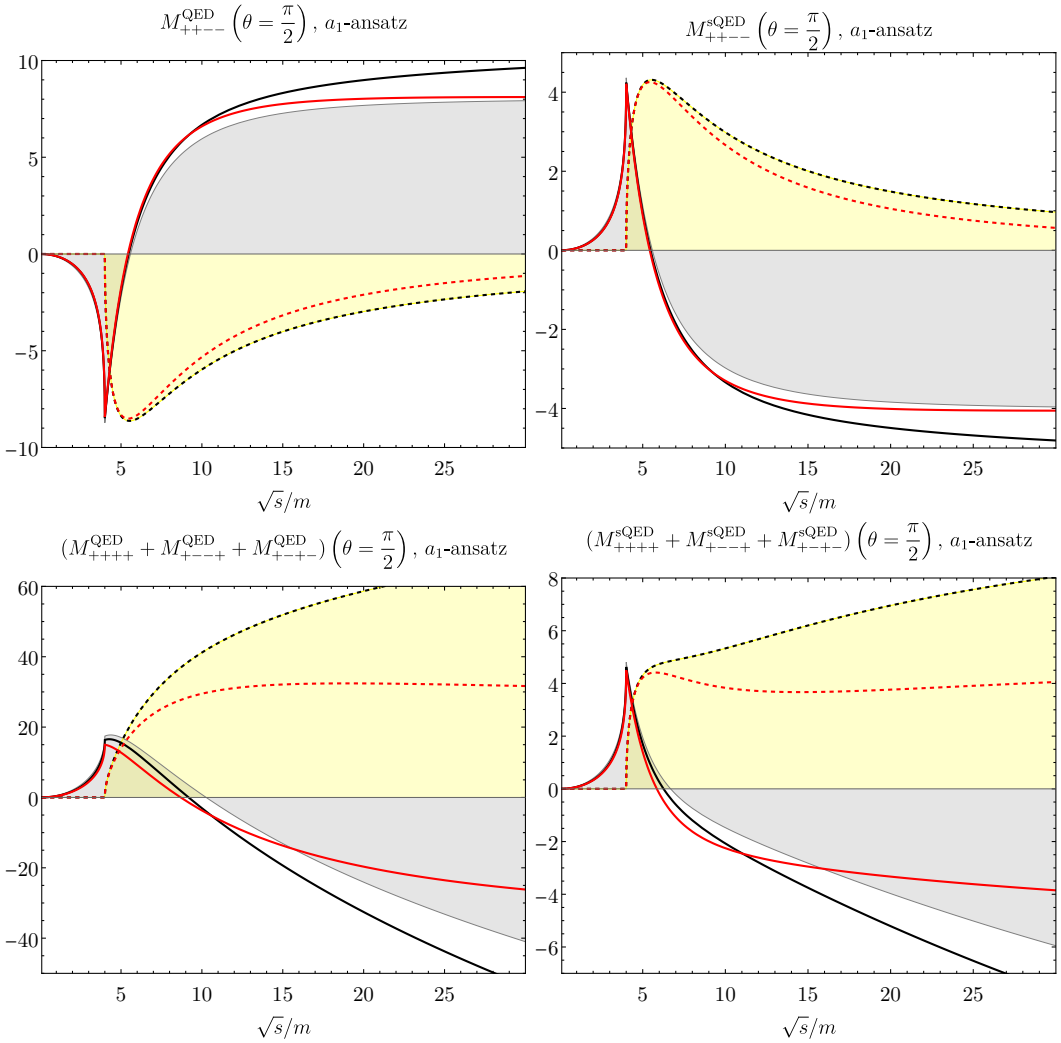

Fig. 4.7 The LbL helicity amplitudes in QED and sQED, given by the exact one-loop calculation (red) and the crossing-invariant ansatz a_1 (black) at the scattering angle $\theta = 90°$. The real (solid) and imaginary (dashed) parts are shown. The gray and yellow bands show the real and imaginary parts, respectively, of exact LbL amplitudes in forward limit.

4.2.2 Partial-wave expansion and formulation of the model

The scattering amplitude for the two particles with spin, which obeys the azimuthal symmetry, with the initial and final helicities λ_i and λ_f correspondingly, can be expanded in the following series of

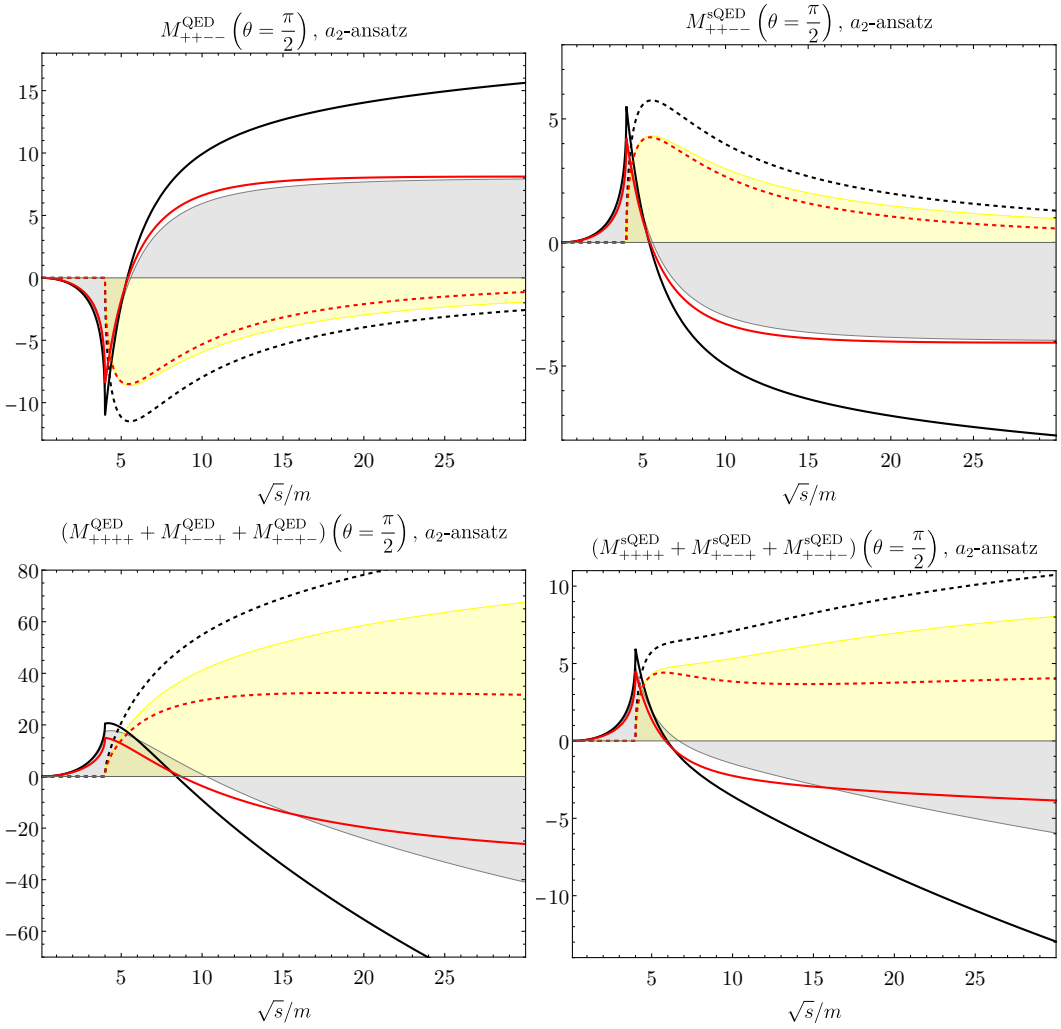

Fig. 4.8 The LbL helicity amplitudes in QED and sQED, given by the exact one-loop calculation (red) and the crossing-invariant ansatz a_2 (black) at the scattering angle $\theta = 90°$. The real (solid) and imaginary (dashed) parts are shown. The gray and yellow bands show the real and imaginary parts, respectively, of exact LbL amplitudes in forward limit.

partial waves

$$T_{\lambda_i,\lambda_f}(s,\theta) = \sum_{J=0}^{\infty}(2J+1)\mathcal{T}^J_{\lambda_i,\lambda_f}(s)d^J_{\lambda_i,\lambda_f}(\theta), \tag{4.49}$$

where, for LbL scattering, $J = 2k$, $k \in \mathbb{N}$, and $d^J_{\lambda_i,\lambda_f}(\theta)$ stands for the Wigner's function. We quote here explicitely the first few Wigner's functions, which will be needed in further calculations. They are given in terms of the c.o.m. scattering angle θ and, alternatively, in terms of the Mandelstam invariants s, t and u:

$$d^2_{0,0}(\theta) = \frac{1}{2}(3\cos^2\theta - 1) = 1 - 6\frac{tu}{s^2} \qquad d^2_{2,0}(\theta) = \frac{\sqrt{6}}{4}\sin^2\theta = \sqrt{6}\frac{tu}{s^2}$$

$$d^2_{2,2}(\theta) = \left(\frac{1+\cos\theta}{2}\right)^2 = \left(\frac{u}{s}\right)^2, \qquad d^2_{2,-2}(\theta) = \left(\frac{1-\cos\theta}{2}\right)^2 = \left(\frac{t}{s}\right)^2. \tag{4.50}$$

Expanding the LbL helicity amplitudes into the partial waves according to Eq. (4.49), we obtain:

$$M_{++++}(s,t,u) = a_0(s) + 5a_1(s) - 30a_1(s)\frac{tu}{s^2}, \tag{4.51a}$$

$$M_{+--+}(s,t,u) = 5b_1(s)\left(\frac{t}{s}\right)^2, \tag{4.51b}$$

$$M_{+-+-}(s,t,u) = 5c_1(s)\left(\frac{u}{s}\right)^2, \tag{4.51c}$$

$$M_{+++-}(s,t,u) = 5\sqrt{6}d_1(s)\frac{tu}{s^2}, \tag{4.51d}$$

$$M_{++--}(s,t,u) = e_0(s) + 5e_1(s) - 30e_1(s)\frac{tu}{s^2}, \tag{4.51e}$$

where $a_0(s)$, $e_0(s)$ and $a_1(s) - e_1(s)$ are some functions on the Mandelstam variable s. It is clear from (4.51) that the partial wave expansion conserves the $t \leftrightarrow u$ crossing symmetry, whereas the total crossing symmetry, $s \leftrightarrow t \leftrightarrow u$ is violated, e.g. for the amplitudes $M_{+++-}(s,t,u)$ and $M_{++--}(s,t,u)$.

In forward scattering regime ($t = 0$), from Eqs. (2.77) and (4.51), one has the following set of equations

$$a_0(s) + 5a_1(s) + c_1(s) = \mathcal{S}_1^{\mathrm{LbL}}(s), \tag{4.52}$$

$$a_0(s) + 5a_1(s) - c_1(s) = \mathcal{S}_2^{\mathrm{LbL}}(s), \tag{4.53}$$

$$e_0(s) + 5e_1(s) = \mathcal{S}_3^{\mathrm{LbL}}(s), \tag{4.54}$$

Combining Eqs. (4.52) and (4.53) one immediately obtains

$$a_0(s) + 5a_1(s) \equiv \tilde{a}_0(s) = \frac{1}{2}\left[\mathcal{S}_1^{\mathrm{LbL}}(s) + \mathcal{S}_2^{\mathrm{LbL}}(s)\right], \quad c_1(s) = \frac{1}{2}\left[\mathcal{S}_1^{\mathrm{LbL}}(s) - \mathcal{S}_2^{\mathrm{LbL}}(s)\right]. \tag{4.55}$$

Due to the unviolated $t \leftrightarrow u$ crossing symmetry, the functions b_1 and c_1 are given by

$$b_1(s) = c_1(s) = \frac{1}{2}\left[\mathcal{S}_1^{\mathrm{LbL}}(s) - \mathcal{S}_2^{\mathrm{LbL}}(s)\right]. \tag{4.56}$$

Unfortunately, at this level, it is not possible to separate the function $a_1(s)$ from the sum $\tilde{a}_0(s)$ nor to define the term, proportional to tu/s^2, since the essentially "off-forward" input is required. Hence, neglecting this term, the final expressions for the first three amplitudes become

$$M_{++++}(s,t,u) = \frac{1}{2}\left[\mathcal{S}_1^{\mathrm{LbL}}(s) + \mathcal{S}_2^{\mathrm{LbL}}(s)\right] \tag{4.57a}$$

$$M_{+--+}(s,t,u) = \frac{1}{2}\left[\mathcal{S}_1^{\mathrm{LbL}}(s) - \mathcal{S}_2^{\mathrm{LbL}}(s)\right]\left(\frac{t}{s}\right)^2 \tag{4.57b}$$

$$M_{+-+-}(s,t,u) = \frac{1}{2}\left[\mathcal{S}_1^{\mathrm{LbL}}(s) - \mathcal{S}_2^{\mathrm{LbL}}(s)\right]\left(\frac{u}{s}\right)^2 \tag{4.57c}$$

The results of the model (4.57) are shown in Figs. 4.9, 4.10 and 4.11 for both QED and sQED cases, with the comparison to the exact one-loop helicity amplitudes. It worth noting that due to the various crossing-invariance relations, the helicity amplitudes obey the following relations:

$$M_{++++}(s,\theta=0) = M_{++++}(s,\theta=\pi), \tag{4.58}$$

$$M_{+--+}(s,\theta=0) = 0, \tag{4.59}$$

$$M_{+-+-}(s,\theta=0) = M_{+--+}(s,\theta=\pi). \tag{4.60}$$

Therefore, the model (4.57) automatically reproduces exactly the amplitudes $M_{++++}(s,\theta=0,\pi)$, $M_{+--+}(s,\theta=0)$, $M_{+-+-}(s,\theta=0)$ and, subsequently, $M_{+--+}(s,\theta=\pi)$.

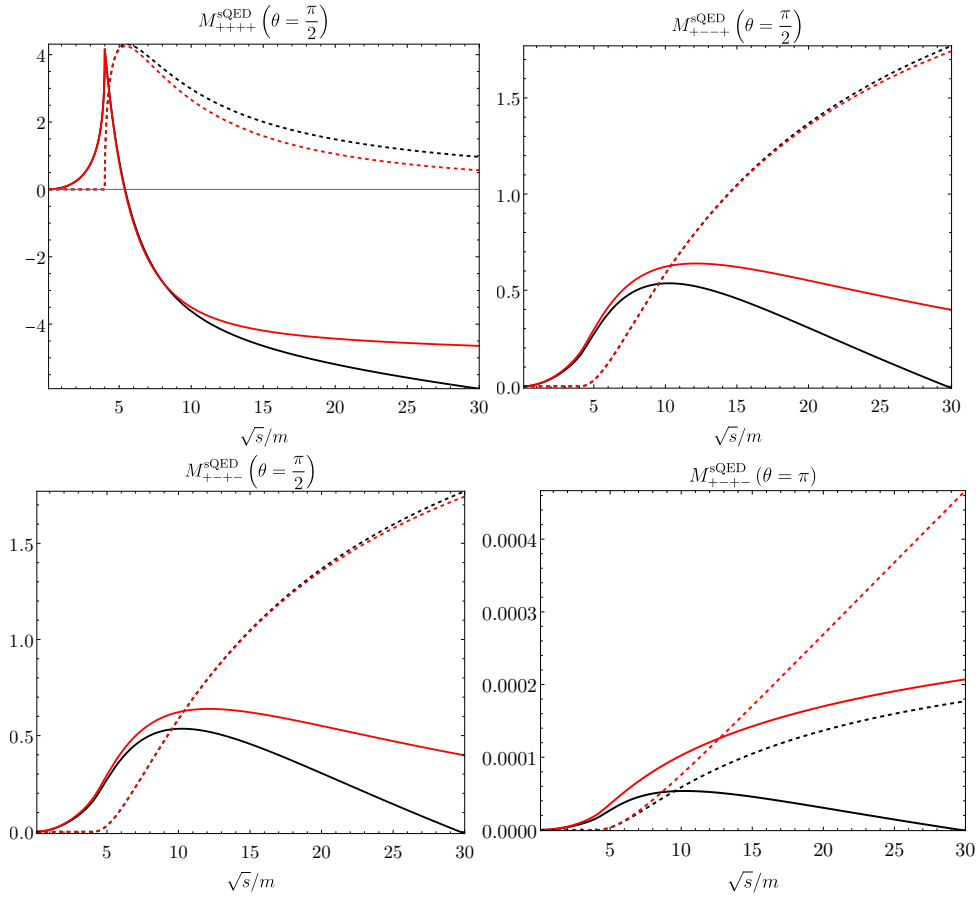

Fig. 4.9 The cases when the most pronounced difference between exact LbL helicity amplitudes in sQED and their approximation by the model (4.57) is observed.

Looking at the Figs. 4.9-4.11, one can conclude that the set of equations (4.57) successfully describes the scalar and fermion boxes up to (and near the) two-particle threshold, whereas at sufficiently high energy its prediction starts to deviate significantly from the correct result. Nevertheless, the sum of helicity amplitudes $M_{++++}+M_{+--+}+M_{+-+-}$, which is shown in Fig. 4.11, behaves better than the

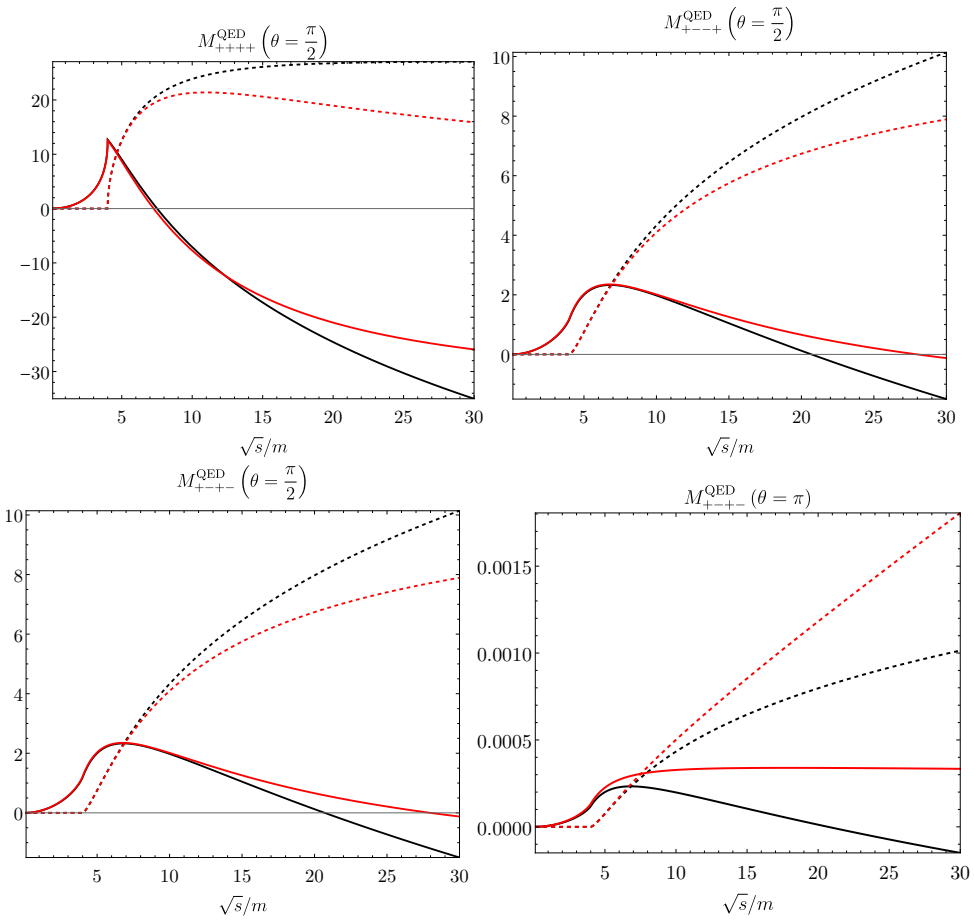

Fig. 4.10 Cases where the most pronounced difference between exact LbL helicity amplitudes in QED and their approximation by the model (4.57) is observed.

one predicted by the ansatz (4.41a). Moreover, in contrast to the ansatz a_1, the considered model describes the helicity amplitudes M_{++++}, M_{+--+} and M_{+-+-} separately, which is very important for, e.g., calculation of the total LbL cross section (2.76).

Let us now turn to the crossing invariant amplitude M_{++--}. Repeating the arguments above, one anticipates the following form for this amplitude:

$$M_{++--}(s,t,u) = \mathcal{S}_3^{\mathrm{LbL}}(s). \tag{4.61}$$

Since this amplitude is totally crossing-invariant, one can also try to approximate it by the aforementioned ansatz a_1,

$$M^{a_1}_{++--}(s,t,u) \equiv \mathcal{S}_3^{\mathrm{LbL},a_1}(s,t,u). \tag{4.62}$$

It turns out (cf. Fig. 4.12), that the partial-wave expansion model (4.61) gives better approximation for the high-energy behavior of $M_{++--}(s,t,u)$ than the a_1-ansatz (4.62), while the latter describes more precisely the region up to and near the two-particle threshold.

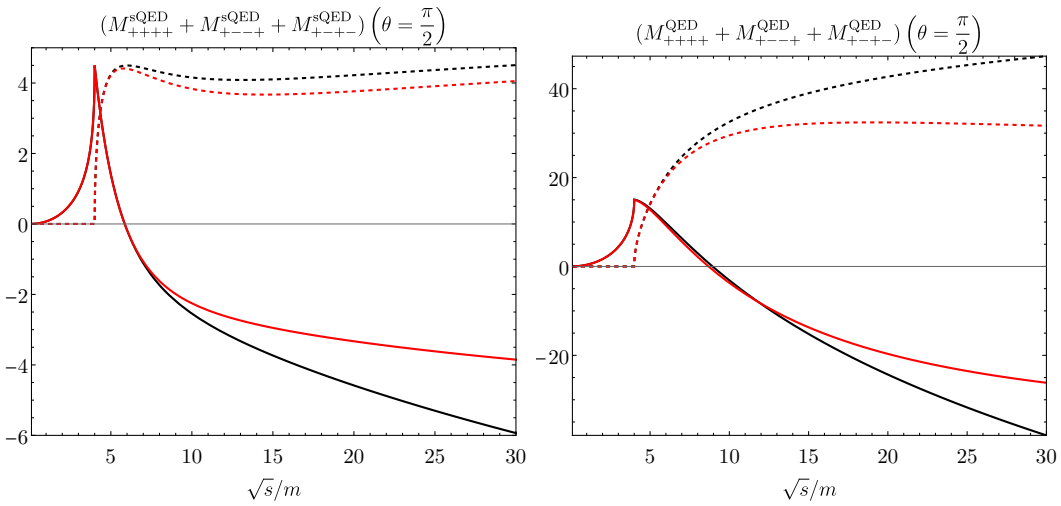

Fig. 4.11 A comparison of the model prediction, given by Eq. (4.57), with the exact result for the sum of helicity amplitudes $M_{++++} + M_{+--+} + M_{+-+-}$ in QED and sQED at wide scattering angle θ.

The numerical analysis of the remaining totally crossing-invariant helicity amplitude, M_{+++-}, which vanishes in the forward limit, shows, that it is small in comparison with the other amplitudes even at large scattering angles for all considered cases of particles in boxes. Thus, despite the fact that it cannot be obtained in considered framework from the forward sum rules, one can neglect its contribution to the total amplitude, especially at energies below the two-particle threshold.

4.2.3 Limits of applicability and matching to pQCD

Both the ansatz a_1 and the model based on the partial wave expansion correctly reproduce the LbL amplitudes in forward limit, i.e. when $t = 0$. Also, these models reproduce sufficiently well the low-energy behavior of the LbL amplitudes, namely up to the two-particle threshold. However, they fail to describe the high-energy regime with wide scattering angle. Given that this region can be correctly described by pQCD, a matching between the model and pQCD prediction is needed. Let us define the residue function as

$$\Delta_\sigma(s,\theta) \equiv \frac{d\sigma^{\mathrm{LbL}}_{\mathrm{model}}(s,\theta) - d\sigma^{\mathrm{LbL}}_{\mathrm{exact}}(s,\theta)}{d\sigma^{\mathrm{LbL}}_{\mathrm{exact}}(s,\theta)}, \tag{4.63}$$

where $d\sigma^{\mathrm{LbL}}_{\mathrm{model}}$ and $d\sigma^{\mathrm{LbL}}_{\text{1-loop}}$ are the modeled and exact one-loop LbL differential cross sections, respectively. Thus, the matching curve can be defined as a solution of the equation

$$\Delta_\sigma(s,\theta) = R_\sigma, \tag{4.64}$$

with respect to s and θ, where R_σ is a predefined characteristic scale representing the accuracy of matching procedure. The solution to the mentioned equation can be found numerically and then fitted

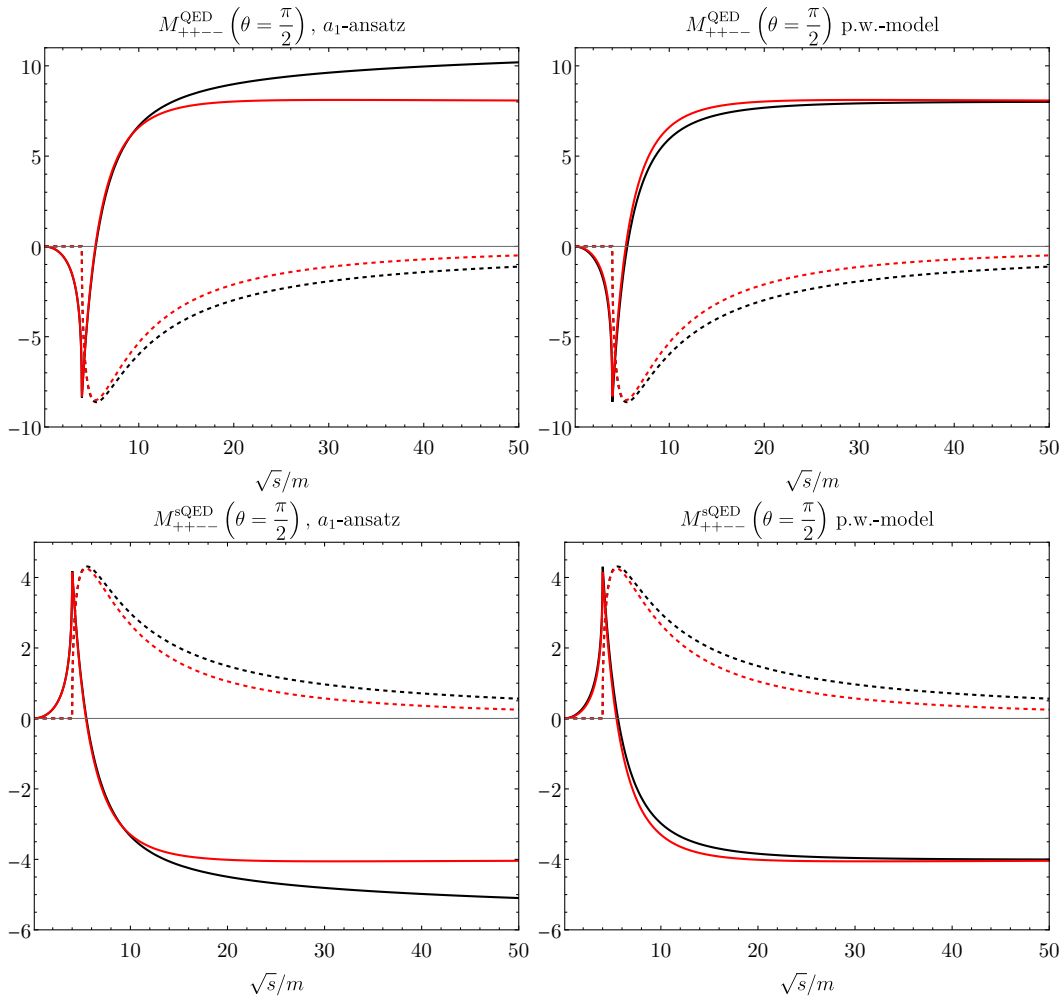

Fig. 4.12 A comparison of the a_1-ansatz (4.62) (left) and partial-wave expansion model (4.61) (right) results on estimation of M_{++--} LbL helicity amplitude in QED (top string) and sQED (bottom string).

with appropriate fit function. Given that Δ_σ is fully crossing-invariant, in order to construct the fit function it worth turning from s and θ to the fully crossing-invariant variables η and ξ as

$$\eta = stu = \frac{s^3}{4}\left(1-\cos^2\theta\right), \tag{4.65}$$

$$\xi = -(st+tu+su) = \frac{s^2}{4}\left(3+\cos^2\theta\right). \tag{4.66}$$

These variables are related via the Mandelstam variable s as follows

$$\xi = s^2 - \frac{1}{s}\eta, \tag{4.67}$$

Fit parameter	$\Delta_\sigma = 0.1$		$\Delta_\sigma = 1$	
	sQED	QED	sQED	QED
A	166	182	1.26	52.56
B	-	-	169	-
α	-2.51	-2.84	3.84	-0.543
β	-	-	-5.58	-
ρ	0.957	0.861	-5.11	0.960

Table 4.2 Fit parameters to the functions (4.69) and (4.70).

and have the following behavior in the forward limit

$$\eta(\theta = 0) = 0, \quad \xi(\theta = 0) = s^2. \tag{4.68}$$

Hence, one can anticipate the following simple parametric form for the fit function:

$$s(\theta) = A\frac{(3+\cos\theta)^\alpha}{(1-\cos^2\theta)^\rho}, \tag{4.69}$$

where A, α and ρ are free parameters. Choosing $R_\sigma = 0.1$, we obtain a good description of the exact numerical solution by the fit function (4.69) with the parameter values listed in Tab. 4.2. The corresponding curve is plotted in Fig. 4.14 on top of the exact numerical solution. For higher values of R_σ the behavior of the QED boxes does not change significantly, and can be successfully parametrized by the same function (4.69). The corresponding curve for $R_\sigma = 1$ is shown on the left side of Fig. 4.15. However, this is not valid for sQED boxes, provided that the fit function should be adjusted by inclusion of an extra term:

$$s(\theta) = \frac{A(3+\cos\theta)^\alpha + B(1-\cos\theta)^\beta}{(1-\cos^2\theta)^\rho}. \tag{4.70}$$

For $R_\sigma = 1$, this function parametrizes the numerical solution sufficiently well, which is demonstrated on the right side of Fig. 4.15. The corresponding parameters are listed in Tab. 4.2 as well.

The important observation, which one can immediately make looking at Figs. 4.13, 4.14 and 4.15 is that the sQED boxes are described by the model sufficiently well up to much higher energies, then the QED ones. In particular, the relative difference between the modeled unpolarized differential LbL cross sections does not excess 60% even at $s = 100m^2$ (cf. Fig. 4.13). Since the observed lowest charged hadronic degrees of freedom are scalar particles (pions and kaons), the model should work with appropriate accuracy up to ≈ 1 GeV. Moreover, since the observed hadronic charged spin-1/2 degrees of freedom start from protons, the reasonable limits of applicability could be defined via sQED box soving the equation

$$\Delta_\sigma^{\text{sQED}}(s/m_{\pi^\pm}^2, \theta) = R_\sigma, \tag{4.71}$$

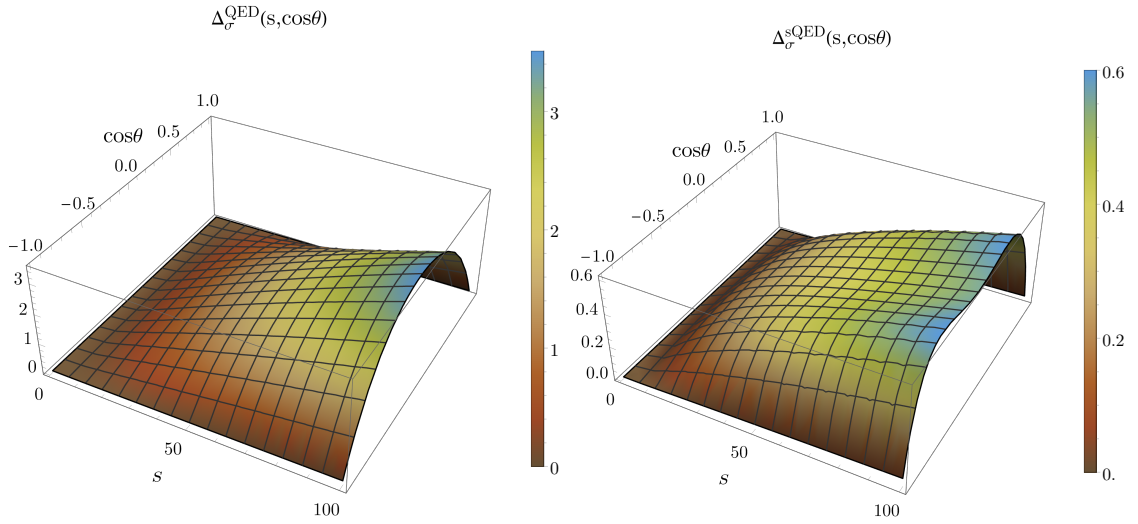

Fig. 4.13 The behavior of residue function $\Delta_\sigma(s,\cos\theta)$ for QED (left) and sQED (right) boxes.

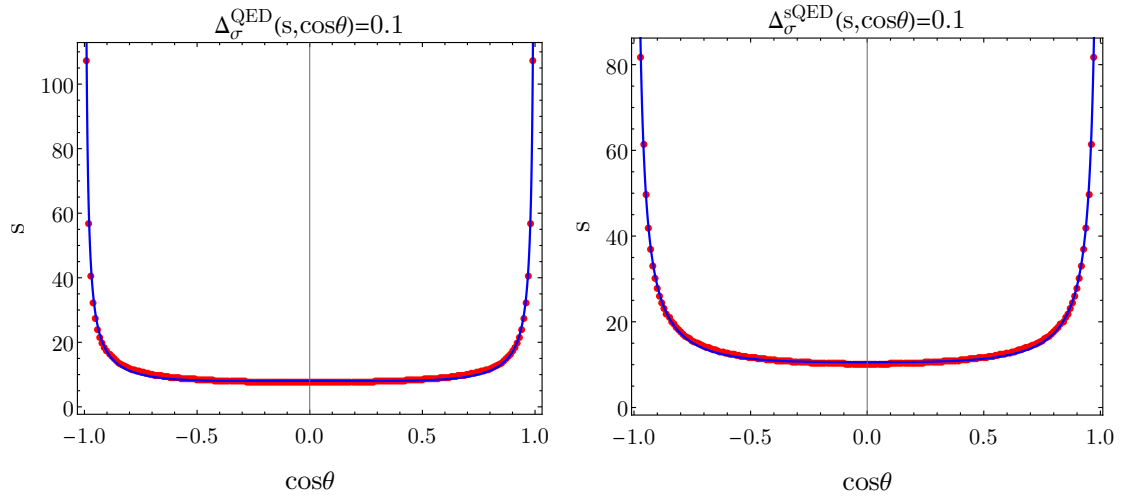

Fig. 4.14 The exact numerical solution of the equation $\Delta_\sigma(s,\theta)=0.1$ (red points) together with its fit given by Eq. (4.69) (blue solid line) is shown for QED (left) and sQED (right) boxes.

with R_σ in a range limited by 0.9. The latter corresponds to the two-proton threshold. Thus, we can conclude that the considered model can cover the hadronic LbL scattering at wide angles with reasonable accuracy only up to the c.o.m. two-photon energies of $\sqrt{s}\approx 2$ GeV.

A matching function, which connects the partial wave-expansion model and pQCD predictions along the matching curve, should be chosen as, e.g. a Fermi function

$$f(x;x_0,w)=\frac{1}{1+e^{\frac{x-x_0}{w}}},\quad f(\infty,w)=0,\quad f(-\infty,w)=1,\quad f(x_0,w)=\frac{1}{2}, \tag{4.72}$$

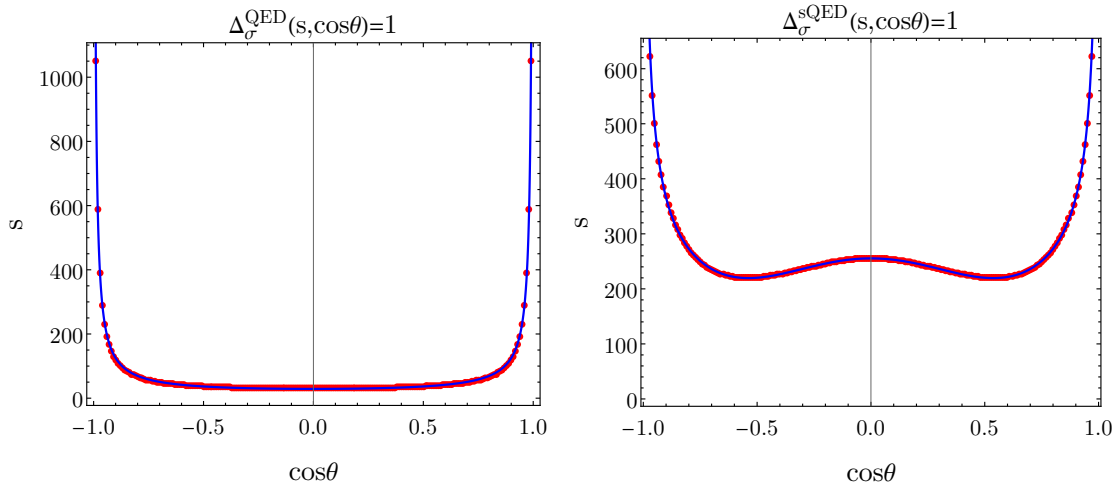

Fig. 4.15 The exact numerical solution of the equation $\Delta_\sigma(s,\theta)=1$ (red points) together with its fit given by Eq. (4.69) (blue solid line) is shown for QED (left) and sQED (right) boxes.

with additional parameters x_0 and w, which define the central transition point and the effective width of the transition between two solutions, respectively.

Finally, we arrive at the following set of helicity amplitudes comprising our full model for real LbL scattering, which is valid at all energies up to electroweak scale:

$$M_{++++}(s,t,u) = M^{\mathrm{model}}_{++++}(s,t,u)f(s;s(\theta),w) + M^{\mathrm{pQCD}}_{++++}(s,t,u)(1-f(s;s(\theta),w)), \tag{4.73a}$$

$$M_{+--+}(s,t,u) = M^{\mathrm{model}}_{+--+}(s,t,u)f(s;s(\theta),w) + M^{\mathrm{pQCD}}_{+--+}(s,t,u)(1-f(s;s(\theta),w)), \tag{4.73b}$$

$$M_{+-+-}(s,t,u) = M^{\mathrm{model}}_{+-+-}(s,t,u)f(s;s(\theta),w) + M^{\mathrm{pQCD}}_{+-+-}(s,t,u)(1-f(s;s(\theta),w)), \tag{4.73c}$$

$$M_{+++-}(s,t,u) = 0, \tag{4.73d}$$

$$M_{++--}(s,t,u) = M^{\mathrm{model}}_{++--}(s,t,u)f(s;s(\theta),w) + M^{\mathrm{pQCD}}_{++--}(s,t,u)(1-f(s;s(\theta),w)). \tag{4.73e}$$

Here the amplitudes M^{model} are given by Eqs. (4.57) and (4.62) (or (4.61)), while M^{pQCD} are the leading-order one-loop pQCD amplitudes, which are listed in Appendix 4.A. The matching function f depends on the variable s and the scattering angle θ via the matching curve $s(\theta)$ discussed above. The parameter w can be conveniently chosen around 1 GeV^2.

In conclusion, the full model provided by Eqs. (4.73) can cover exactly the pQCD region, the non-perturbative forward scattering regime, and can approximate the low-energy scattering up to the two-proton threshold with reasonable accuracy. The intermediate region is covered by smooth transition between the partial wave-expansion and sum rule-based model and pQCD amplitudes. Since all the polarized two-photon fusion cross sections will be measured, it can be applied to simulate the background of the real LbL scattering at low and intermediate energies in a simple fashion. For the present moment, when only the unpolarized two-photon fusion cross section is known experimentally,

the model seems to be applied as well, but just for qualitative estimations (giving the correct order of magnitude for the off-forward LbL cross section).

4.3 LbL scattering and fully-charmed tetraquarks

4.3.1 Observation of fully-charmed tetraquarks in di-J/ψ and $J/\psi\psi(2S)$ spectra

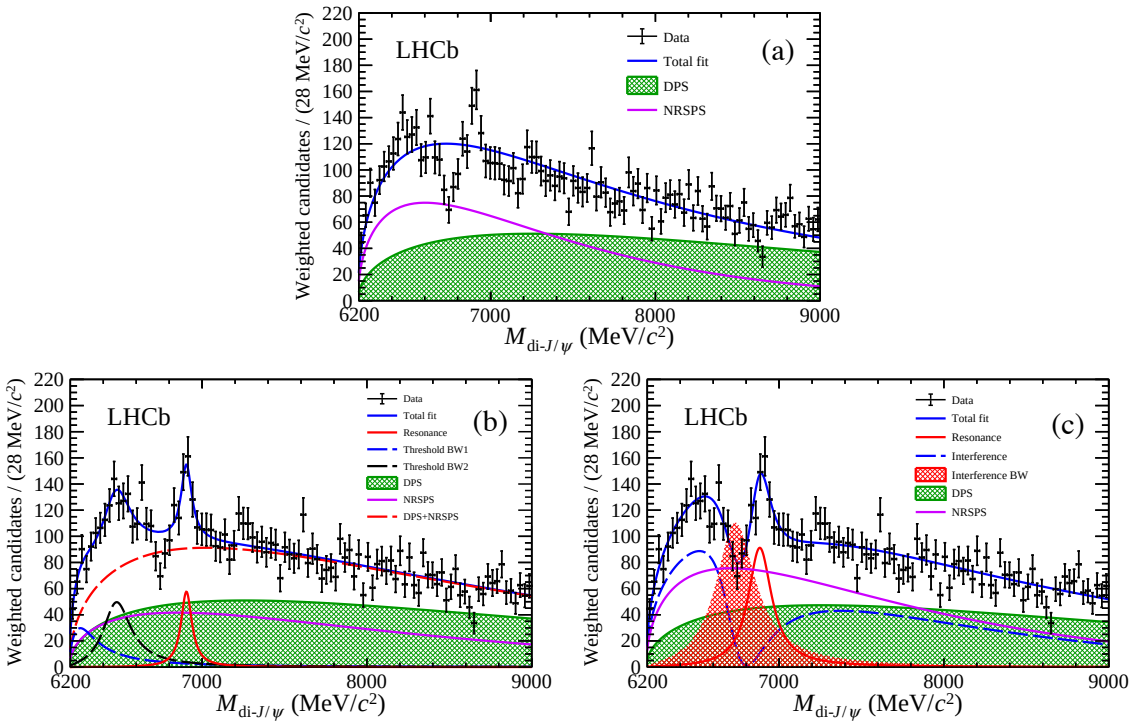

Fig. 4.16 The invariant mass spectrum of weighted di-J/ψ candidates with transverse momentum cut $p_{\text{T}}^{\text{di-}J/\psi} > 5.2$ GeV and overlaid projections of the fit using (a) the NRSPS plus DPS model, (b) model I, and (c) model II. Figures are taken from [40].

In 2020 the LHCb Collaboration reported on the observation of several structures in the di-J/ψ mass spectrum that are inconsistent with the non-resonant single-parton scattering (NRSPS) and double-parton scattering (DPS) production mechanisms of a J/ψ pair [40]. It can be clearly seen from the Fig. 4.16 (a), taken from [40], where the obtained data points are shown together with the NRSPS plus DPS prediction. The most sharp structure was observed at around 6.9 GeV in di-J/ψ mass and treated as a novel narrow resonant state X(6900). The other observed structures, such as a pronounced di-J/ψ threshold enhancement at approximately 6.5 GeV and a small peak at around 7.2 GeV were also reported. In order to describe the data, two different models were developed. The first model (referred as model I, or "No-int. sc.") contained one Breight-Wigner function to describe a peak at 6.9 GeV and two other Breight-Wigner functions were utilized for the threshold enhancement. In this model all Breight-Wigner functions did not interfere with the NRSPS and DPS background. However,

Parameter	model I	model II
m_X [MeV]	$6905 \pm 11 \pm 7$	$6886 \pm 11 \pm 11$
$\Gamma_{X\to J/\psi J/\psi}$ [MeV]	$80 \pm 19 \pm 33$	$168 \pm 33 \pm 69$

Table 4.3 Parameters of X(6900) state according to LHCb analysis [40].

Parameter	X(6600)	X(6900)	X(7200)
m_X [MeV]	$6638^{+43\ +16}_{-38\ -31}$	$6841^{+44\ +48}_{-28\ -20}$	$7134^{+48\ +41}_{-25\ -15}$
$\Gamma_{X\to J/\psi J/\psi}$ [MeV]	$440^{+230\ +110}_{-200\ -240}$	$191^{+66\ +25}_{-49\ -17}$	$97^{+40\ +29}_{-29\ -26}$

Table 4.4 Best-fit Parameters of the states observed by CMS [81].

being fitted to the data, this model was unable to reproduce the dip around 6.8 GeV, which is shown in Fig. 4.16(b). Therefore another fitting model (referred as model II, or "Int. sc.") was applied, where the observed peak at 6.9 GeV was described by the Breight-Wigner function allowing for interference with the NRSPS background. This made it possible to describe both the threshold enhancement and the dip, which is demonstrated in Fig. 4.16(c). Thus, the X(6900) state was established with around a 5σ significance. Depending on the fitting scenario, its mass m_X and di-J/ψ decay width $\Gamma_{X\to J\psi J\psi}$ are given in Tab. 4.3.

The subsequent measurements by CMS [81] and ATLAS [82] Collaborations confirmed the results obtained by LHCb. Measuring the di-J/ψ invariant mass spectrum, the CMS Collaboration observed three structures at around 6.6, 6.9 and 7.1 GeV with the local significance of 7.9, 9.8 and 4.7 σ, correspondingly. Similarly to LHCb analysis, the best fit, which correctly described peaks and dips in between, was achieved allowing the interfrence between components of the fit function. Specifically, the interference between all three Breigt-Wigner structures that describe three peaks was allowed. The resonance parameters obtained from this fit are listed in Tab. 4.4. Thus, the X(6900) resonance and the structure at around 7.2 GeV (say X(7200)), observed by LHCb, were confirmed.In addition, the third resonance was found in a region where only a threshold enhancement was previously observed in LHCb data. This resonance is referred to as X(6600).

The ATLAS Collaboration [82] has provided the analysis of both di-J/ψ and $J/\psi\psi(2S)$ invariant mass spectra. According to their analysis, the X(6900) state was confirmed in di-J/ψ events with more than 5σ significance, and it has also been observed in $J/\psi\psi(2S)$ invariant mass spectrum. In addition, observations of a broad resonance similar to X(6600) in the di-J/ψ spectrum and a resonance around 7.2 GeV in the $J/\psi\psi(2S)$ spectrum were reported. Depending on the different fitting models (see [82] for details), the parameters of the observed resonances are given in Tab. 4.5.

According to various quark-model calculations [258–274], QCD-sum rules [262, 275–279], pole search [280–282] and other theoretical analyses [283–286], the observed series of structures could be

di-J/ψ, model A			
Parameter	X(6400)	X(6600)	X(6900)
m_X [GeV]	$6.41 \pm 0.08^{+0.08}_{-0.03}$	$6.63 \pm 0.05^{+0.08}_{-0.01}$	$6.86 \pm 0.03^{+0.01}_{-0.02}$
$\Gamma_{X\to J/\psi J/\psi}$ [GeV]	$0.59 \pm 0.35^{+0.12}_{-0.20}$	$0.35 \pm 0.11^{+0.11}_{-0.04}$	$0.11 \pm 0.05^{+0.02}_{-0.01}$
di-J/ψ, model B			
Parameter	X(6400)	X(6600)	X(6900)
m_X [GeV]	–	$6.65 \pm 0.02^{+0.03}_{-0.02}$	$6.91 \pm 0.01 \pm 0.01$
$\Gamma_{X\to J/\psi J/\psi}$ [GeV]	–	$0.44 \pm 0.05^{+0.06}_{-0.05}$	$0.15 \pm 0.03 \pm 0.01$

$J/\psi\,\psi(2S)$, model α		
Parameter	X(6900)	X(7200)
m_X [GeV]	fixed from di-J/ψ channel	$7.22 \pm 0.03^{+0.01}_{-0.04}$
$\Gamma_{X\to J/\psi\,\psi(2S)}$ [GeV]		$0.09 \pm 0.06^{+0.06}_{-0.05}$
$J/\psi\,\psi(2S)$, model β		
Parameter	X(6900)	X(7200)
m_X [GeV]	$6.96 \pm 0.05 \pm 0.03$	–
$\Gamma_{X\to J/\psi\,\psi(2S)}$ [GeV]	$0.51 \pm 0.17^{+0.11}_{-0.10}$	–

Table 4.5 Parameters of the states observed by ATLAS [82].

associated with excitations [4] of a (possibly the lightest) fully-charmed tetraquark state (see also [289] for review). Given that the discovered states still have unknown quantum numbers of the total angular momentum and parity, the theoretical models have to consider all possibilities: $J^{PC} = 0^{\pm+}, 1^{-+}, 2^{\pm+}, \ldots$ (see, e.g. [290] for the allowed quantum numbers). Unfortunately, various cited analyses yield quite dense excitation spectra, so one cannot really distinguish between different quantum numbers pertinent to the observed states at the current level of experimental precision. However, the new X-states with even spin, as long as they decay to two vector particles, would also couple to two photons and hence contribute to the LbL scattering [291, 292, 237]. From this point of view, the LbL channel can be used as a filter for the resonances with even spin. Such resonances can in principle be responsible for the aforementioned discrepancy between theory and experiment observed in LbL scattering by the ATLAS Collaboration [72]. Therefore it is interesting to either estimate the width of possible electromagnetic two-photon decay of X-states or extract the resonance parameters fitting the states to existing data on LbL scattering.

In general, the electromagnetic decay width of a hadronic state is highly sensitive to its internal structure. Indeed, usually the compact state has smaller decay width than the molecular state (see, e.g. [293]). At the quark level, the internal structure of X-states allows for two different pictures: charmonium molecule ($q\bar{q} - q\bar{q}$) or diquark-antidiquark state ($qq - \bar{q}\bar{q}$). The former implies the decay mechanism that at leading order corresponds to the VMD model. Below both the decays of charmonium molecule and diquark-antidiquark state are considered.

4.3.2 Two-photon decay width estimation in VMD model

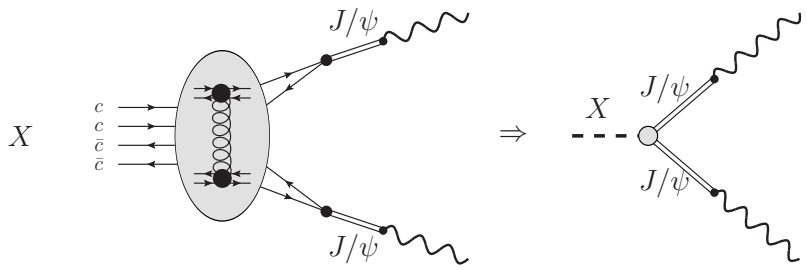

Fig. 4.17 (Left) Electromagnetic decay of fully charmed tetraquark as a charmonium molecule. (Right) The picture of this decay in VMD model.

Firstly we estimate the two-photon decay width of the fully-charmed tetraquark state X by exploiting the VMD hypothesis as shown in Fig. 4.17. The VMD implies that the photon $|\gamma\rangle$ couples via a

[4] It should be mentioned that in [287, 288] the non-resonant mechanism for the observed structures was proposed, explaining them simply by threshold cusp effects. However, the fits were performed with more than ten parameters, which seems to be already quite a substantial number in the considered cases (cf. the pole analysis by Dong et al. [280]). Furthermore, the χ^2 values of approximately 0.7 could indicate a slight overfitting.

vector-meson state $|V\rangle$ as follows [294, 295]:

$$|\gamma\rangle \to \frac{e}{M_V} f_V |V\rangle, \tag{4.74}$$

where e is the electron charge, f_V is the corresponding vector-meson decay constant, which is observed in $V \to e^+e^-$ decay, and M_V is the vector-meson mass. Introduced in this way, the decay constant has a dimension of mass.

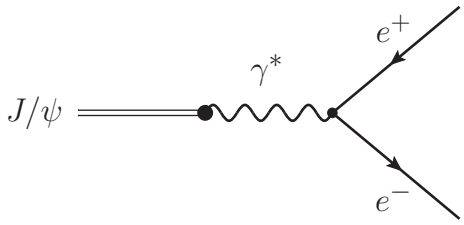

Fig. 4.18 The VMD mechanism of $J/\psi \to e^+e^-$ decay which determines the γ-J/ψ coupling.

The J/ψ decay decay constant f_ψ can be obtained from the $J/\psi \to e^+e^-$ decay width, cf. Fig. 4.18:

$$\Gamma_{J/\psi \to e^+e^-} = \frac{4\pi\alpha^2 f_\psi^2}{3m_\psi}. \tag{4.75}$$

Using recent values [251] for J/ψ mass $m_\psi = 3096.900 \pm 0.006$ MeV and electron-positron decay width $\Gamma_{J/\psi \to e^+e^-} = 5.55 \pm 0.17$ keV, one finds $f_\psi = 278 \pm 9$ MeV.

Assuming the zeroth spin of the X-state, the decay widths $\Gamma_{X\to\gamma\gamma}$ and $\Gamma_{X\to J/\psi J/\psi}$ can be obtained via the imaginary part of the X-resonance self-energy derived from the following effective interactions

$$\mathcal{L}_{X\gamma\gamma} = -g_{X\gamma\gamma}\phi_X F^{\mu\nu}F_{\mu\nu}, \tag{4.76}$$

$$\mathcal{L}_{XJ/\psi\gamma} = -g_{X\gamma\psi}\phi_X G^{\mu\nu}F_{\mu\nu}, \tag{4.77}$$

$$\mathcal{L}_{XJ/\psi J/\psi} = -g_{X\psi\psi}\phi_X G^{\mu\nu}G_{\mu\nu}, \tag{4.78}$$

where $g_{X\gamma\gamma}$, $g_{X\gamma\psi}$ and $g_{X\psi\psi}$ are dimensionful coupling constants, $F_{\mu\nu} = \partial_\mu A_\nu - \partial_\nu A_\mu$ is the photon field tensor, and $G_{\mu\nu} = \partial_\mu B_\nu - \partial_\nu B_\mu$ is the J/ψ field tensor, ϕ_X is the scalar field of the X-meson. Note that we require gauge-invariance with respect to vector fields, including the massive one. For the pseudoscalar case, one of the field tensors is replaced by its dual, i.e.,

$$F^{\mu\nu} \to \widetilde{F}^{\mu\nu} = \frac{1}{2}\epsilon^{\mu\nu\alpha\beta}F_{\alpha\beta}, \tag{4.79}$$

$$G^{\mu\nu} \to \widetilde{G}^{\mu\nu} = \frac{1}{2}\epsilon^{\mu\nu\alpha\beta}G_{\alpha\beta}. \tag{4.80}$$

The X-V-V vertex that correspond to each of the Lagrangians (4.76)-(4.78) is (cf. Eq. (4.10))

$$V^{\mu\nu}(q_1, q_2) = -2ig_{XV_1V_2}(q_1 \cdot q_2\, g^{\mu\nu} - q_1^\nu q_2^\mu). \tag{4.81}$$

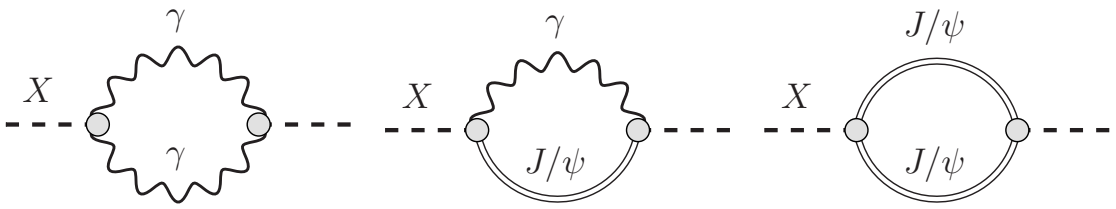

Fig. 4.19 The one-loop graphs of the X-self energy caused by two photons, photon and J/ψ-meson, and two J/ψ-mesons, correspondingly.

For the pseudoscalar, the vertex reads as (cf. Eq. (4.11)):

$$\widetilde{V}^{\mu\nu}(q_1,q_2) = 2i\widetilde{g}_{XV_1V_2}\epsilon^{\mu\nu\alpha\beta}q_{1\alpha}q_{2\beta}. \tag{4.82}$$

Employing the optical theorem, one can write the imaginary part of the self-energy

$$\mathrm{Im}\,\Pi_{V_1V_2}(s) = \frac{\lambda^{1/2}(s,m_1^2,m_2^2)}{16\pi s}\sum_{\lambda_1\lambda_2}\left|\mathcal{M}^{\chi_1\chi_2}_{X\to V_1V_2}\right|^2, \tag{4.83}$$

where χ_i are the helicities,

$$\sum_{\lambda_1\lambda_2}|\mathcal{M}^{\lambda_1\lambda_2}_{X\to V_1V_2}|^2 = \begin{cases} 4g^2_{XV_1V_2}\left[2(q_1\cdot q_2)^2+q_1^2q_2^2\right], \\ 8\widetilde{g}^2_{XV_1V_2}\left[(q_1\cdot q_2)^2-q_1^2q_2^2\right], \end{cases} \tag{4.84}$$

and $\lambda(s,m_1^2,m_2^2) = [s-(m_1+m_2)^2][s-(m_1-m_2)^2]$.

Hence, for the scalar and pseudoscalar cases of the X-state we obtain,

$$\mathrm{Im}\,\Pi_{\gamma\gamma}(s) = \frac{s^2}{16\pi}\theta(s)\times\begin{cases} g^2_{X\gamma\gamma}, \\ \widetilde{g}^2_{X\gamma\gamma}, \end{cases} \tag{4.85}$$

$$\mathrm{Im}\,\Pi_{\gamma J/\psi}(s) = \frac{(s-m_\psi^2)^3}{8\pi s}\theta\left(s-m_\psi^2\right)\times\begin{cases} g^2_{X\gamma\psi}, \\ \widetilde{g}^2_{X\gamma\psi}, \end{cases} \tag{4.86}$$

$$\mathrm{Im}\,\Pi_{J/\psi J/\psi}(s) = \frac{1}{16\pi}\sqrt{1-\frac{4m_\psi^2}{s}}\theta\left(s-4m_\psi^2\right)\times\begin{cases} g^2_{X\psi\psi}\left[\left(s-2m_\psi^2\right)^2+2m_\psi^4\right], \\ \widetilde{g}^2_{X\psi\psi}s\left(s-4m_\psi^2\right). \end{cases} \tag{4.87}$$

The corresponding diagrams for $\Pi_{\gamma\gamma}$, $\Pi_{\gamma J/\psi}$ and $\Pi_{J/\psi J/\psi}$ self energies are show in Fig. 4.19.

Assuming $\Gamma_{\rm tot} = \Gamma_{X\to J/\psi J/\psi}$, one thus obtains the following relations between the decay widths of $X(6900)$ into the two-photon and di-J/ψ channels:

$$\Gamma^S_{X\to\gamma\gamma} = \Gamma_{X\to J/\psi J/\psi}\left(\frac{ef_\psi}{m_\psi}\right)^4\left\{\sqrt{1-\frac{4m_\psi^2}{m_X^2}}\left[\left(1-\frac{2m_\psi^2}{m_X^2}\right)^2+2\left(\frac{m_\psi}{m_X}\right)^4\right]\right\}^{-1} \tag{4.88}$$

for the scalar X-resonance, which is consistent with a result provided by Esposito et al. [291], and

$$\Gamma^{PS}_{X\to\gamma\gamma} = \Gamma_{X\to J/\psi J/\psi}\left(\frac{e f_\psi}{m_\psi}\right)^4\left(1-\frac{4m_\psi^2}{m_X^2}\right)^{-\frac{3}{2}} \tag{4.89}$$

for the pseudoscalar X-state. Applying these relations to the $X(6900)$ state observed by LHCb [40] with parameters given in Tab. 4.3, we obtain the following estimate for branching ratios $\mathcal{B}(X\to\gamma\gamma)\equiv\Gamma_{X\to\gamma\gamma}/\Gamma_{X\to J/\psi J/\psi}$ in the scalar and pseudoscalar case, respectively [237]:

$$\mathcal{B}^{\mathrm{S}}_{\mathrm{VMD}}(X(6900)\to\gamma\gamma) = (2.8\pm0.4)\times10^{-6}, \tag{4.90a}$$

$$\mathcal{B}^{\mathrm{PS}}_{\mathrm{VMD}}(X(6900)\to\gamma\gamma) = (6.4\pm0.8)\times10^{-6}. \tag{4.90b}$$

The uncertainties originate from the parameters entering Eqs. (4.88) and (4.89), i.e. the X and J/ψ masses and J/ψ decay constant. Analogously, for the X-states, observed by CMS [81], we obtain the branching ratios listed in Tab. 4.6. It worth mentioning that in [238] the parameters of X-states,

X-state nature	$\mathcal{B}_{\mathrm{VMD}}(X(6600)\to\gamma\gamma)$	$\mathcal{B}_{\mathrm{VMD}}(X(6900)\to\gamma\gamma)$	$\mathcal{B}_{\mathrm{VMD}}(X(7300)\to\gamma\gamma)$
scalar	$(3.67\pm0.52)\times10^{-6}$	$(2.98\pm0.41)\times10^{-6}$	$(4.47\pm0.65)\times10^{-6}$
pseudoscalar	$(11.7\pm2.2)\times10^{-6}$	$(7.11\pm1.2)\times10^{-6}$	$(2.40\pm0.32)\times10^{-6}$

Table 4.6 The VMD estimate of two-photon branching ratios for resonances detected at CMS [81] with the parameters from Tab. 4.4.

detected by CMS, were taken from CMS preprint [296]. These parameters do not correspond to the best-fit parameters in [81], which causes a slight discrepancy between the results provided in [238] and in Tab. 4.6. The obtained branching ratios of the X-state decay into two photons are quite small.

X-state nature	$\Gamma_{X(6600)\to\gamma\gamma}$ [keV]	$\Gamma_{X(6900)\to\gamma\gamma}$ [keV]	$\Gamma_{X(7300)\to\gamma\gamma}$ [keV]
scalar	1.6 ± 1.1	0.57 ± 0.18	0.23 ± 0.11
pseudoscalar	5.1 ± 3.4	1.4 ± 0.4	0.43 ± 0.21

Table 4.7 The VMD estimate of two-photon branching ratios for resonances detected at CMS [81] with the parameters from Tab. 4.4.

Assuming that the main decay channel of X-state comes is the di-J/ψ decay, we find that the absolute values of the two-photon decay are of order 1 keV. These results are close to the ones obtained in the corresponding quark-model calculations [297, 298], where the electromagnetic decay of the tetraquark X-resonance is considered as the decay of dicharmonium system.

4.3.3 Two-photon decay width estimation in diquark-antidiquark picture

While the Vector Meson Dominance (VMD) mechanism is the most straightforward approach to explain the two-photon decay of a tetraquark that decays into two neutral hadronic vector states, other possibilities exist that do not involve the formation of vector states prior to photon emission. One such possibility involves a specific assumption about the internal structure of the tetraquark ground state, considering it as a diquark-antidiquark molecule. Moreover, various quark-model analyses, which predict the spectrum of X-states very close to those observed by LHCb, CMS, and ATLAS, rely on this assumption (cf., e.g., [263, 266, 274, 285, 290, 299]). Therefore, it is important to estimate the two-photon decay width of such a state and compare it with the VMD prediction, which, again, is based on a completely different assumption about the internal structure of the tetraquark.

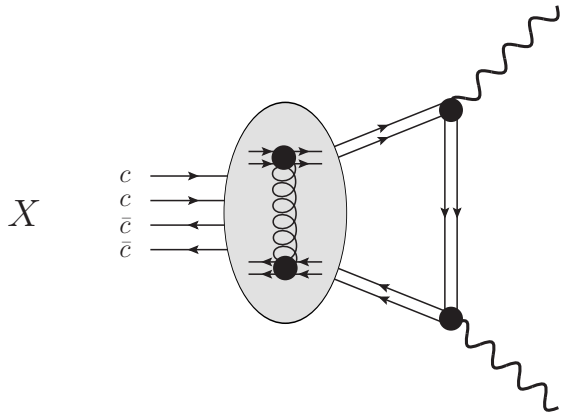

Fig. 4.20 Electromagnetic decay of fully charmed tetraquark in diquark-antidiquark picture.

The way we choose to estimate the two-photon decay of the fully-charmed tetraquark is similar to the well-known analysis of the charmonium decay. As a particular example of such an analysis, we refer to the Appendix of [300]. The idea is to consider the X-state as a bound state of diquark and antidiquark, bounded by the QCD-inspired potential, and calculate its decay into two photons as shown in Fig. 4.20. The potential should be taken similar to the one used for the charmonium, but with properly adjusted color factor. In what follows, we focus on the X(6600) state seen by CMS and ATLAS, assuming that it is a scalar state.

In terms of SU(3) group representations, the tetraquark state can be expressed as the diquark-antidiquark state as follows:

$$[3\otimes 3]\otimes\left[\bar{3}\otimes\bar{3}\right]=\left[\bar{3}\oplus 6+\ldots\right]\otimes\left[3\oplus\bar{6}+\ldots\right]=\left[\bar{3}\right]\otimes[3]+\left[\bar{6}\right]\otimes[6]+\ldots. \tag{4.91}$$

This means that starting from the charm quarks in fundamental representation of SU(3) group, we firstly arrive at diquark and antidiquark configurations belonging to the color triplet and antitriplet, respectively. These representations yield the attractive potential between the quarks inside the (anti)diquark, with a color factor $\kappa=-2/3$. Secondly, the corresponding term $\left[\bar{3}\right]\otimes[3]$ can be

decomposed as $1 \oplus 8$, thus forming a color singlet. This causes the leading attractive component of the diquark-antidiquark binding potential.

To proceed further, one needs to solve the Schrödinger or Dirac equation with the corresponding quark-model potential and find a wave function that correctly reproduces the spectrum. Such an information is given, e.g., in the work by Debastiani & Navarra [263]. According to their analysis, the simplest state that corresponds to X(6600) state detected is a scalar bound state with quantum numbers $N_{\rm T}^{2S_{\rm T}+1}L_{\rm T} = 2^1S$, which is composed of diquark and antdiquark being in a ground state with spin-1 and zeroth angular momentum. The value of the tetraquark wave function Ψ at the origin is given by

$$|R(0)|^2/\mathrm{GeV}^3 \equiv 4\pi|\Psi(0)|^2 = 2.8414 \tag{4.92}$$

whereas the mass of the tetraquark state is $M_T = 6.6633$ GeV.

The relevant $qq + \bar{q}\bar{q} \to \gamma + \gamma$ tree-level helicity amplitudes are

$$\mathcal{M}_{++;++}(s) = \mathcal{M}_{--;--}(s) = 2e_{cc}^2 \frac{(1+\beta)^2}{1-\beta^2\cos^2\theta}, \tag{4.93}$$

$$\mathcal{M}_{++;00}(s) = \mathcal{M}_{--;00}(s) = 2e_{cc}^2 \frac{1-\beta^2}{1-\beta^2\cos^2\theta}, \tag{4.94}$$

$$\mathcal{M}_{++;--}(s) = \mathcal{M}_{--;++}(s) = 2e_{cc}^2 \frac{(1-\beta)^2}{1-\beta^2\cos^2\theta}, \tag{4.95}$$

where $\mathcal{M}_{\lambda_1\lambda_2;\chi_1,\chi_2} \equiv \langle\vec{p}|M_{\chi_1,\chi_2}|\vec{q},\lambda_1,\lambda_2\rangle$ is the helicity amplitude of two photons with helicities λ_1 and λ_2 that go into vector diquark and antidiquark with corresponding helicities χ_1 and χ_2; $\beta(s)$ stands for $2|\vec{p}|/\sqrt{s} = \sqrt{1-4m^2/s}$, where $m = 3.1334$ GeV and $e_{cc} = 4/3e$ are the diquark mass and electric charge correspondingly. The momenta $\vec{q}$ and $\vec{p}$ denote the photon and (anti)diquark momenta in c.o.m. frame, respectively.

Since the mass of the tetraquark bound state is comparable to the sum of the masses of diquark and antidiquark, i.e. $M_T \approx 2m$, a nonrelativistic approximation can be applied. Thus, the decay amplitude reduces to a product of the nonrelativistic tetraquark wave function $\Psi_{N_TL_Tm_L}(\vec{p})$, taken at the origin, $\vec{p} = 0$, and a combination of the tree-level helicity amplitudes of the free diquark-antidiquark pair that scatter into the pair of real photons. For the chosen 2^1S tetraquark state it reads

$$\begin{aligned}
&\langle\vec{q},\pm\pm|M|2^1S,0\rangle = \\
&= \int \frac{d^3\vec{p}}{(2\pi)^3}\frac{\sqrt{2M_T}}{2\sqrt{E_1(\vec{p})E_2(\vec{p})}}\Psi^*_{200}(\vec{p})\langle 00|0000\rangle\sum_{s_1,s_2}\langle 00|1\,s_1\,1\,s_2\rangle\langle\vec{q},\lambda_1,\lambda_2|M_{\chi_1\chi_2}|\vec{p}\rangle \\
&= \frac{C_F}{\sqrt{m}}\Psi^*_{200}(0)\frac{1}{\sqrt{3}}\left(\mathcal{M}_{\pm\pm;++} - \mathcal{M}_{\pm\pm;00} + \mathcal{M}_{\pm\pm;--}\right)\Big|_{\vec{p}\to 0},
\end{aligned} \tag{4.96}$$

where $C_F = 4/3$ is a color factor. A nonrelativistic expansion for the sum of helicity amplitudes reads

$$\left(\mathcal{M}_{\pm\pm;++} - \mathcal{M}_{\pm\pm;00} + \mathcal{M}_{\pm\pm;--}\right) = 2 + 2(3+\cos^2\theta)\beta^2 + 2(3\cos^2\theta + \cos^4\theta)\beta^4 + O(\beta^5), \tag{4.97}$$

with $\beta(s) \approx |\vec{p}|/m$. The $X \to \gamma\gamma$ decay rate can then be calculated as follows:

$$\Gamma_{\gamma\gamma} \approx \frac{1}{2} C_F^2 \frac{\int d\Omega}{32\pi^2} \frac{1}{2M_T} \left[\left| \langle \vec{q}, ++ | M | 2^1S, 0 \rangle \right|^2 + \left| \langle \vec{q}, -- | M | 2^1S, 0 \rangle \right|^2 \right]$$
$$= \frac{C_F^2}{m^2} \frac{2\pi}{3} \left(\frac{4}{3} \right)^4 \alpha^2 |\Psi_{200}(0)|^2 = C_F^2 \times 8.12\text{keV} = 14.4\text{keV}. \tag{4.98}$$

As one can see, the obtained estimate is around one-two orders bigger than the VMD prediction. This is due to the fact that the diquark-antidiquark state is more compact than the charmonium molecule. Thus, measuring the strength of the electromagnetic decay width would provide strong evidence in favor of one scenario or another regarding the internal structure of the X-state.

It is important to note, however, that the non-relativistic approximation, which was used to obtain Eq. (4.98) is known not to work very accurately for charm quarks. Hence, in order to refine the prediction, one should carefully take into account the relativistic effects.

4.3.4 Fitting X-states into LbL scattering

According to the recent comprehensive analysis of the LbL events in ultraperipheral Pb-Pb scattering done by ATLAS Collaboration [73], a mild excess over the Standard Model prediction is centered on the diphoton invariant mass region of 5 to 10 GeV (cf. Fig. 1.2). A similar excess between 5-7 GeV of the diphoton invariant mass was seen by CMS Collaboration [74] as well. Given that the observed states in di-J/ψ spectrum are pertinent to the same mass region, we can explore the possibility of the excess seen in ATLAS experiment is due to the two-photon decay of these states.

Firstly we fitted the data on the LbL scattering with only one X-resonance, namely X(6900), with parameters given by LHCb [40] (cf. Tab. 4.3). We have extended the Monte-Carlo code `SuperChic v3.05` [226, 301, 77][5] used in the original interpretation of the ATLAS data [73], by including the X(6900) resonance along with the well-known bottomonium states [302] pertinent to this energy region, see Table 4.8. Note that `SuperChic v3.05` includes otherwise only the simplest pQCD contributions to LbL scattering, i.e., the quark-loop contribution. However, given the experimental cuts, it is unnecessary to extend the hadronic LbL model to diphoton masses below 5 GeV or to the near-forward scattering regime with small scattering angles. The next-to-leading order pQCD corrections were shown to contribute at the order of few percent [303–305, 79], which is negligible at the current level of experimental precision.

The X-state together with bottomonium resonances were implemented at the level of helicity amplitudes using the model described by Eqs. (4.24). In the narrow resonance approximation, the LbL cross section depends only on the ratio $\Gamma_{X\to\gamma\gamma}/\sqrt{\Gamma_{\text{tot}}}$, and hence we take it as a fitting parameter. The total width is assumed to be dominated by the di-J/ψ decay (i.e., $\Gamma_{\text{tot}} \simeq \Gamma_{X\to J/\psi\, J/\psi}$).

The fit has been performed to the unfolded diphoton invariant mass spectrum of the ATLAS data. The CMS data is not used in the present analysis since the corresponding spectrum is not unfolded.

[5] Although this is not the most recent version, subsequent updates do not relate to LbL scattering.

Meson	J^{PC}	M, [MeV]	$\Gamma_{\rm tot}$, [MeV]	$\Gamma_{\gamma\gamma}/\Gamma_{\rm tot}$ [%]
$\eta_b(1S)$	0^{-+}	9399.0	17.9	5.87×10^{-3}
$\eta_b(2S)$	0^{-+}	9999.0	8.34	5.86×10^{-3}
$\chi_{b0}(1P)$	0^{++}	9859.44	3.39	5.87×10^{-3}
$\chi_{b0}(2P)$	0^{++}	10232.5	3.54	5.41×10^{-3}

Table 4.8 Bottomonium resonances included in this work.

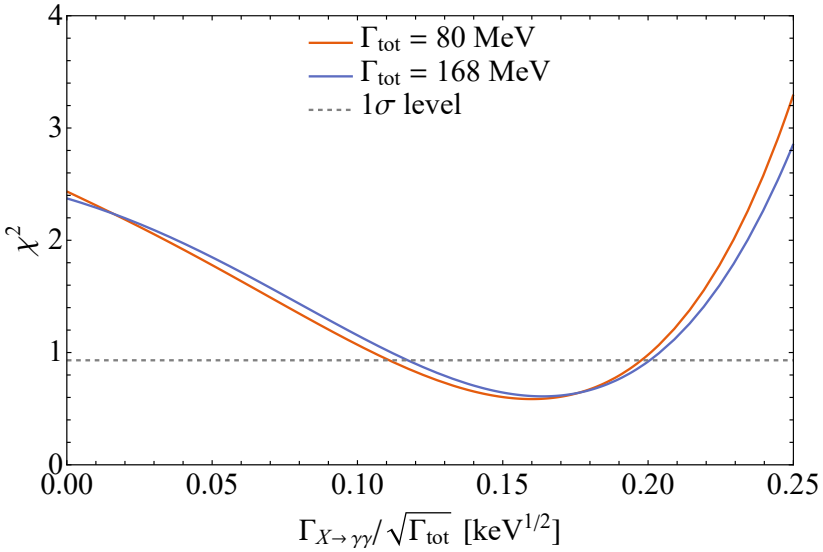

Fig. 4.21 The profile of χ^2 (divided by #d.o.f. = 3) for the values of $\Gamma_{\rm tot}$ used in the two LHCb scenarios. The gray dashed line cuts out the 1σ interval.

We have explored both the scalar and pseudoscalar nature of $X(6900)$, but the corresponding results of the fit turn out to be indistinguishable at the current level of statistical accuracy. We therefore show only the results for the scalar X(6900). Since the main uncertainties in ATLAS data has a statistical origin, then for reasons of simplicity we take the total experimental uncertainties as the uncertainties for χ^2 function. The resulting χ^2 is shown in Fig. 4.21, for the two scenarios provided by the LHCb experiment. The best fit yields the following branching ratio ($\Gamma_{X\to\gamma\gamma}/\Gamma_{\rm tot}$):

$$\mathcal{B}(X\to\gamma\gamma) = \begin{cases} 5.6^{+1.3}_{-1.6}\times10^{-4}, & \text{No-int. sc,} \\ 4.0^{+0.9}_{-1.1}\times10^{-4}, & \text{Int. sc..} \end{cases} \tag{4.99}$$

The corresponding values for the $X\to\gamma\gamma$ decay width are

$$\Gamma_{X\to\gamma\gamma} = \begin{cases} 67^{+15}_{-19}\,[\text{keV}], & \text{No-int. sc,} \\ 45^{+11}_{-14}\,[\text{keV}], & \text{Int. sc..} \end{cases} \tag{4.100}$$

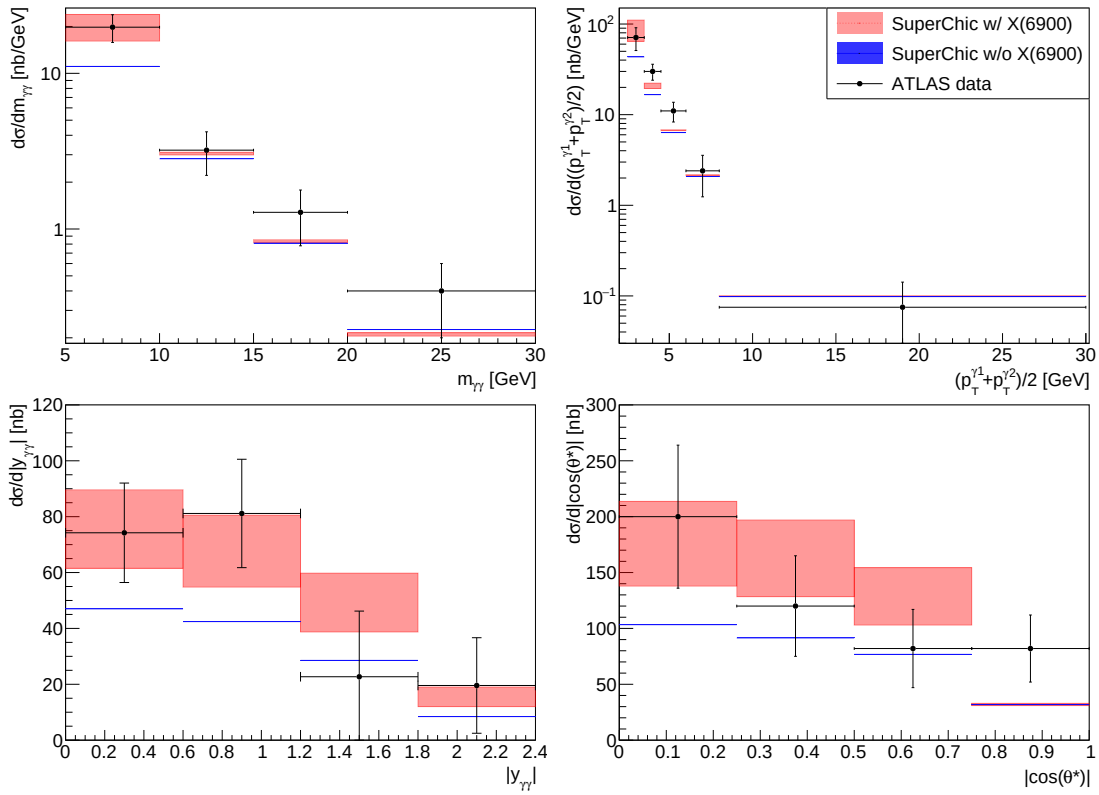

Fig. 4.22 Differential fiducial cross sections of $\gamma\gamma \to \gamma\gamma$ production in Pb+Pb collisions at a centre-of-mass energy of $\sqrt{s_{NN}} = 5.02$ TeV with integrated luminositiy 2.2 nb^{-1} for four observables (from left to right and top to bottom): diphoton invariant mass $m_{\gamma\gamma}$, diphoton absolute rapidity $|y_{\gamma\gamma}|$, average photon transverse momentum $(p_T^{\gamma_1} + p_T^{\gamma_2})/2$ and diphoton $|cos(\theta^*)| \equiv |\tanh(\Delta y_{\gamma_1,\gamma_2}/2)|$. The red band represents an uncertainty (1σ range) of the fit with $X(6900)$. The blue band contains only the statistical uncertainty of the `SuperChic` simulation without X-resonance.

Figure 4.22 shows the exclusive differential cross sections with and without the inclusion of $X(6900)$, versus the the ATLAS data [73]. The statistical uncertainties of the `SuperChic` results were highly reduced by simulating a large enough number of events (10^4), thus they were neglected in analysis and are not visible on the plots of Fig. 4.22. The fit yields the integrated fiducial cross section of $\sigma_{\text{fid}}^X = 121 \pm 20$ nb. It can be compared with the reference `SuperChic` value without X-resonance, $\sigma_{\text{fid}}^0 = 76$ nb and with the experimental value, $\sigma_{\text{fid}}^{\text{exp.}} = 120 \pm 17(\text{stat.}) \pm 13(\text{syst.}) \pm 4(\text{lumi.})$ nb, reported by ATLAS [73]. The description of ATLAS data with $X(6900)$ is better than without it by about 2.3σ.

The ratio $\Gamma_{X\to\gamma\gamma}/\Gamma_{X\to J/\psi J/\psi}$ can be estimated via the VMD mechanism described in Sect. 4.3.2. As one can see from Eqs. (4.90a) and (4.90b) , the central values of this estimate is about two orders of magnitude smaller than we obtained from the fit, Eq. (4.99); although, given the large uncertainties, the difference is fairly insignificant. Moreover, the inclusion the X(6600) and X(7200) states, observed by CMS and ATLAS, with VMD-predicted two-photon decay widths (cf. Tab. 4.7) is still not sufficient to describe the excess in LbL data [238]. However, as was shown in the previous section, the decay

of diquark-antidiquark state has bigger two-photon decay width than the charmonium molecule. Therefore, the obtained results from fitting the X-states into the LbL scattering data may indicate a possible diquark-antidiquark internal structure of these states. Certainly, a more thorough and detailed analysis of the tetraquark spectra, as well as higher statistical precision in LbL scattering measurements, is necessary to validate these assumptions. However, such investigations are beyond the scope of the present work.

4.4 Summary

The LbL scattering of real photons is a complicated, essentially quantum process with a small cross section, which is hard to measure. Nevertheless, it has been measured for the first time in ultraperipheral heavy-ion collisions at LHC during Run-2 by ATLAS and CMS Collaborations. This measurement provided a unique opportunity to test SM prediction, especially the hadronic part, for the LbL scattering. Obtaining a consistent description of the hadronic contribution, which would be valid at all energies, is extremely challenging task due to the non-perturbative nature of QCD. In particular, the low-energy region below 1 GeV in diphoton mass, where QCD possesses a hadronic spectrum, can be described by the chiral perturbation theory and partial-wave dispersive approaches. However, due to the multitude of intermediate states, such as hadronic bound states and resonances, it is practically too complicated to account for them altogether consistently in the mentioned approaches. Moreover, at high energies, the perturbative regime of QCD at short distances coexists with the non-perturbative diffractive phenomena at small scattering angles. While the former can be calculated in systematic fashion in perturbation theory, the latter is an area of Regge phenomenology. Lastly, all listed approaches should be properly matched in a region, where no approach to find a QCD solution has been found so far.

A simple receipt to overcome the aforementioned issues is to use the phenomenological model based on forward LbL sum rules, which treats both low-energy and Regge energy regions on the same footing. This model incorporates only three observables (polarized $\gamma\gamma \to$had. cross sections) that are pertinent to the *forward* real LbL scattering. It is shown on various examples of QED, sQED and scalar meson exchange contributions that this input is enough to describe the low-energy region sufficiently well. The pQCD region, however, requires different approach involving direct calculation of leading pQCD contributions. Therefore the pQCD and low-energy plus Regge regions should be systematically matched in the end. The proposed model could serve as a simple background estimate for the low-energy real LbL scattering at all scattering angles. Moreover, it could be easily incorporated at the level of helicity amplitudes into the existing simulators of LbL events, which is of great practical interest for the future runs at LHC.

Being sensitive to new physics, the LbL scattering could serve a precise filter for exotic resonances. In particular, the contribution to the LbL scattering from the new states in di-J/ψ mass spectrum, observed by LHCb and confirmed by CMS and ATLAS, were analysed in details. Their two-photon decay widths were estimated in various ways: in the VMD model, in the quark-model treating the

resonance as a diquark-antidiquark bound state, and by fitting the resonance parameters to the LbL scattering data measured by ATLAS. It turns out that these states indeed could be responsible for the mild excess in the LbL scattering data over the SM prediction seen by ATLAS between 5 and 10 GeV. The two-photon decay width, extracted from the fit, hints towards the diquark-antidiquark nature of the (at least one) tetraquark state. To make the statistically significant conclusion, however, more LbL scatterin data is needed, which become available from the future LHC runs. Moreover, a prospective measuremet of two-photon hadroproduction in ultraperipheral heavy-ion collisions could be an alternative and very clean channel to study the aforementioned exotic states. Being complemented with possible lattice QCD studies, these experiments could reveal the nature of fully charmed tetraquarks in details, identifying their internal structure and quantum numbers.

Appendices

4.A One-loop contributions to real LbL

The one-loop contributions to LbL that come from QED, perturbative QCD (quarks) and $W^{\pm}$ bosons are given in a compact way in terms of the one-loop scalar integrals in works [169, 168]. Here we quote these results.

The $\{++++\}$ helicity amplitude is described by different functions for each case of the charged particle in the loop, scalar (S), fermion (f) or vector (W), namely

$$\begin{aligned}
M^{S}_{++++}(s,t,u) = 4\alpha^2_{\rm em}Q^4_S\Bigg\{&1-\left(1+\frac{2u}{s}\right)B_0(u)-\left(1+\frac{2t}{s}\right)B_0(t)+\frac{2m_S^2tu}{s}D_0(t,u)\\
&-\frac{2m_S^2}{s}\left(1+\frac{ut}{2m_S^2s}\right)\left[2tC_0(t)+2uC_0(u)-tuD_0(t,u)\right]\\
&+2m_s^4\left[D_0(s,t)+D_0(s,u)+D_0(t,u)\right]\Bigg\},
\end{aligned} \tag{4.101}$$

$$\begin{aligned}
M^{f}_{++++}(s,t,u) = 8\alpha^2_{\rm em}Q^4_f\Bigg\{&-1+\left(1+\frac{2u}{s}\right)B_0(u)+\left(1+\frac{2t}{s}\right)B_0(t)\\
&-\left(\frac{t^2+u^2}{s^2}-\frac{4m_f^2}{s}\right)\left[tC_0(t)+uC_0(u)\right]+m_f^2(s-2m_f^2)\left[D_0(s,t)+D_0(s,u)\right]\\
&-\frac{1}{2}\left[4m_f^2-(2sm_f^2+tu)\frac{t^2+u^2}{s^2}+\frac{4m_f^2tu}{s}\right]D_0(t,u)\Bigg\},
\end{aligned} \tag{4.102}$$

$$\begin{aligned}
M^{W}_{++++}(s,t,u) = 12\alpha^2_{\rm em}Q^4_W\Bigg\{&1-\left(1+\frac{2u}{s}\right)B_0(u)-\left(1+\frac{2t}{s}\right)B_0(t)+\frac{2m_S^2tu}{s}D_0(t,u)\\
&+\left(\frac{4}{3}-\frac{2m_W^2}{s}-\frac{tu}{s^2}\right)\left[2tC_0(t)+2uC_0(u)-tuD_0(t,u)\right]\\
&+\frac{2}{3}(s-m_W^2)(s-3m_W^2)\left[D_0(s,t)+D_0(s,u)+D_0(t,u)\right]\Bigg\}.
\end{aligned} \tag{4.103}$$

Here $Q_{\{S,f,W\}}$ stands for the electromagnetic charge of the corresponding particle. Note that the expressions above show the explicit crossing symmetry with respect to the exchange $t \leftrightarrow u$.

The fully crossing-invariant $\{+++-\}$ helicity amplitude has the same functional dependence for scalars, fermions and vectors in the loop, with the only difference in an overall factor:

$$\begin{aligned}
M^{S}_{+++-}(s,t,u) =&4\alpha^2_{\rm em}Q^4_S\Bigg\{-1+2m_S^4\left[D_0(s,t)+D_0(s,u)+D_0(t,u)\right]\\
&+m_S^2stu\left[\frac{D_0(s,t)}{u^2}+\frac{D_0(s,u)}{t^2}+\frac{D_0(t,u)}{s^2}\right]\\
&-2m_S^2\left(\frac{1}{s}+\frac{1}{t}+\frac{1}{u}\right)\left[tC_0(t)+uC_0(u)+sC_0(s)\right]\Bigg\}
\end{aligned}$$

$$= -\frac{1}{2} M^{f}_{+++-}(s,t,u)\Big|^{m_S\to m_f}_{Q_S\to Q_f} = \frac{1}{3} M^{W}_{+++-}(s,t,u)\Big|^{m_S\to m_W}_{Q_S\to Q_W}. \tag{4.104}$$

The same is true for the fully crossing-invariant $\{++--\}$ helicity amplitude as well:

$$\begin{aligned} M^{S}_{++--}(s,t,u) =& 4\alpha^2_{\rm em} Q^4_S \left\{ -1 + 2m^4_S \left[D_0(s,t) + D_0(s,u) + D_0(t,u) \right] \right\} \\ =& -\frac{1}{2} M^{f}_{++--}(s,t,u)\Big|^{m_S\to m_f}_{Q_S\to Q_f} = \frac{1}{3} M^{W}_{++--}(s,t,u)\Big|^{m_S\to m_W}_{Q_S\to Q_W}. \end{aligned} \tag{4.105}$$

4.B Two-photon fusion cross sections with real photons in QED and sQED

In the real-photon limit, the tree-level two-photon fusion QED cross sections, which enter the forward LbL sum rules, are given by

$$\sigma_{TT}(s) = \frac{4\pi\alpha^2_{\rm em}}{s} \left\{ (\bar{a}-2)\sqrt{\bar{a}} + \left(3-\bar{a}^2\right) \bar{L} \right\}, \tag{4.106a}$$

$$\tau_{TT}(s) \equiv \sigma_{\parallel} - \sigma_{\perp} = -\frac{4\pi\alpha^2_{\rm em}}{s} (1-\bar{a}) \left\{ (1-\bar{a})\bar{L} + \sqrt{\bar{a}} \right\}, \tag{4.106b}$$

$$\tau^{a}_{TT}(s) \equiv \frac{\sigma_0 - \sigma_2}{2} = -\frac{4\pi\alpha^2_{\rm em}}{s} \left\{ 2\,\mathrm{arccosh}(1/\sqrt{1-\bar{a}}) - 3\sqrt{\bar{a}} \right\}, \tag{4.106c}$$

while in case of sQED they read

$$\sigma_{TT} = \frac{4\pi\alpha^2_{\rm em}}{s} \left\{ (2-\bar{a})\sqrt{\bar{a}} - \left(1-\bar{a}^2\right) \bar{L} \right\}, \tag{4.107a}$$

$$\tau_{TT} \equiv \sigma_{\parallel} - \sigma_{\perp} = \frac{2\pi\alpha^2_{\rm em}}{s} (1-\bar{z}a) \left\{ (1-\bar{a})\bar{L} + \sqrt{\bar{a}} \right\}, \tag{4.107b}$$

$$\tau^{a}_{TT} \equiv \frac{\sigma_0 - \sigma_2}{2} = \frac{2\pi\alpha^2_{\rm em}}{s} \left\{ 2(1-\bar{a})\bar{L} - \sqrt{\bar{a}} \right\}. \tag{4.107c}$$

In the Eqs. (4.106) and (4.107) we use the following notations:

$$\bar{a} = 1 - \frac{4m^2}{s}, \quad \bar{L} = \log\left(\frac{1+\sqrt{\bar{a}}}{\sqrt{1-\bar{a}}} \right), \quad s = 2\nu, \quad \nu_{\rm thr.} = 4m^2. \tag{4.108}$$

Chapter 5

Electromagnetic corrections to HVP via the Cottingham-like formula

In this Chapter, a computational strategy that enables much more direct comparisons between lattice QCD and hadron phenomenology in the evaluation of electromagnetic corrections to HVP, is discussed. In its simplest realization, the idea is to add and subtract a Pauli-Villars term [306] to the photon propagator[1],

$$\frac{1}{k^2} = \left(\frac{1}{k^2} - \frac{1}{k^2+\Lambda^2}\right) + \frac{1}{k^2+\Lambda^2}, \tag{5.1}$$

where k is the Euclidean four-momentum and Λ is a typical hadronic scale. The first term leads to a UV-finite effect on the HVP and is sensitive to long-distance contributions such as the $\pi^0\gamma$ and $\eta\gamma$ channels; it can be treated analogously to the HLbL contribution to the muon AMM by using coordinate-space methods [308, 309, 146], whereby power-law effects due to the internal photon propagators are avoided. The second can be treated entirely in lattice regularization by having the photon field defined on the same lattice as the QCD fields [120]. However, since a photon regulator mass is now present, no issue with the photon zero-mode arises, nor do power-law finite-size effects occur. We return to this aspect in section 5.7 but remark here that a number of different methods have been used in the extensive literature on incorporating the coupling of quarks to photons into lattice QCD calculations (see [310–323] for a representative set of publications).

How then can one predict the leading QED correction to the HVP with a UV-regularized photon propagator in place? We shall express it through the forward HLbL amplitude [324–326], as shown in Fig. 5.1. As has been noted [326], the connection between the forward HLbL amplitude and the e.m. correction to the HVP bears a strong resemblance with the Cottingham formula [327–331], which expresses e.m. mass splittings in terms of the forward Compton scattering amplitude. The analogy becomes apparent if one views light-by-light (LbL) scattering as Compton scattering off a photon.

[1] Such a decomposition of the photon propagator has been found to be helpful in other contexts; see in particular Ref. [307].

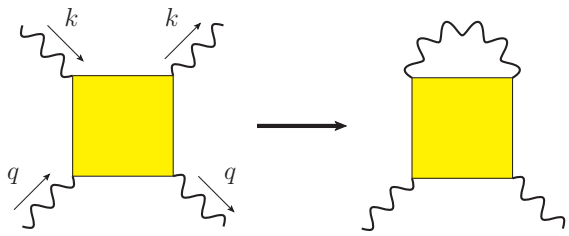

Fig. 5.1 Cottingham-like formula for QCD LbL amplitude.

However, not much practical use has so far emerged from this connection. Perhaps the main reason is that the insertion of two standard $\bar{q}q\gamma$ vertices leads to a divergence, requiring the insertion of $O(e^2)$ counterterms to cancel it. From the standpoint of the HLbL amplitude, the divergence appears due to the forward HLbL falling off too slowly (as $1/k^2$) for one of the incoming photon momenta becoming large. However, the first term on the right-hand side of Eq. (5.1) amounts to a UV-regularization of the photon propagator, and in this case the integral over the forward HLbL amplitude yielding an e.m. correction to the HVP becomes finite. Therefore, with sufficient knowledge of the forward HLbL amplitude, obtained either by using the dispersive sum rules [167] or direct lattice calculations [332], one can make a definite prediction for this correction. The comparison can even be done in a more differential way, at the integrand level, as we shall illustrate. Also, accumulated knowledge on the HLbL amplitudes, for example concerning the relative importance of the different quark Wick-contraction topologies [333, 166], can be usefully applied to the leading QED corrections to the HVP.

The work in this Chapter is based on the publication in Ref. [334].

5.1 A Cottingham-like formula for light-by-light amplitude

The first correction $\Delta\Pi(Q^2)$ to the leading HVP[2] $\Pi_{e^2}(Q^2)$ can be written in the form

$$\Delta\Pi(Q^2) = \lim_{\Lambda\to\infty}\Big(\Pi_{4\text{pt}}(Q^2,\Lambda) + \Pi_{\text{ct}}(Q^2,\Lambda)\Big), \tag{5.2}$$

where Λ is a UV-regularization parameter. We begin by establishing a formula for $\Pi_{4\text{pt}}(Q^2,\Lambda)$, named in this way because it involves the four-point function of the e.m. current, which at the same time provides the quantum field-theoretic definition of the LbL scattering amplitude. The second term, $\Pi_{\text{ct}}(Q^2,\Lambda)$, consists of the required counterterms and the strong-isospin breaking contribution. While its precise form is not needed here, more details will be given in section 5.7.

The LbL scattering amplitude $\mathcal{M}^{\mu_1\mu_2\mu_3\mu_4}$ depends on the four-momenta of the incoming (q_1, q_2) and outgoing (q_3, q_4) photons. The forward kinematics correspond to $q_1 = q_3 \equiv k$ and $q_2 = q_4 \equiv q$,

[2] In our notation throughout this section, the HVP contains an additional factor e^2 relative to the notation widely used in lattice QCD calculations, for instance in Refs. [335, 336].

see Fig. 5.1. Contracting the photon-line 1 with 3, we obtain a contribution to the VP tensor:

$$\Pi_{4\text{pt}}^{\mu_2\mu_4}(q^2,\Lambda) = \frac{1}{2}\int \frac{d^4k}{(2\pi)^4}\left[\frac{-ig_{\mu_1\mu_3}}{k^2+i0^+}\right]_\Lambda \mathcal{M}^{\mu_1\mu_2\mu_3\mu_4}(k,q)\,, \tag{5.3}$$

where the factor of one-half is the symmetry factor; in square brackets is the Feynman-gauge photon propagator, regulated at the scale Λ, for instance à la Pauli-Villars, $[1/k^2]_\Lambda = 1/k^2 - 1/(k^2-\Lambda^2)$. Due to gauge invariance, the VP tensor has the following general form,

$$\Pi^{\mu\nu}(q) = \Pi(q^2)(q^2 g^{\mu\nu} - q^\mu q^\nu), \tag{5.4}$$

and hence its scalar part can be expressed as:

$$\Pi_{4\text{pt}}(q^2,\Lambda) = \frac{1}{6q^2}\int \frac{d^4k}{(2\pi)^4}\left[\frac{-i}{k^2+i0^+}\right]_\Lambda \mathcal{M}(k,q)\,, \tag{5.5}$$

where

$$\mathcal{M} \equiv g_{\mu_1\mu_3}g_{\mu_2\mu_4}\mathcal{M}^{\mu_1\mu_2\mu_3\mu_4}(k,q)\,, \tag{5.6}$$

is the traced LbL amplitude. The latter is a scalar function of three invariants: k^2, q^2, and $\nu \equiv k\cdot q$. It is even in ν and symmetric under the interchange of k and q. We shall write it as $\mathcal{M}(\nu,K^2,Q^2)$, where $K^2=-k^2$ and $Q^2=-q^2$ will further be assumed to be positive, i.e., the photons are spacelike.

Introducing the helicity LbL amplitudes as (cf. (2.54))

$$M_{\lambda_1\lambda_2\lambda_3\lambda_4} = \varepsilon^{\mu_1}_{\lambda_1}(q_1)\,\varepsilon^{\mu_2}_{\lambda_2}(q_2)\,\varepsilon^{*\mu_3}_{\lambda_3}(q_3)\varepsilon^{*\mu_4}_{\lambda_4}(q_4)\,\mathcal{M}_{\mu_1\mu_2\mu_3\mu_4}\,, \tag{5.7}$$

with $\varepsilon^\mu_\lambda(q)$ the photon polarization vectors, the traced amplitude can be written as [164]:

$$\mathcal{M} = \sum_{\lambda,\sigma=\pm,0}(-1)^{\lambda+\sigma}M_{\lambda\sigma\lambda\sigma} = 4\mathcal{M}_{TT} - 2\mathcal{M}_{LT} - 2\mathcal{M}_{TL} + \mathcal{M}_{LL}\,, \tag{5.8}$$

where the following combinations of the helicity amplitudes are used:

$$\begin{aligned}&\mathcal{M}_{TT} = \tfrac{1}{2}\big(M_{++++} + M_{+-+-}\big), \quad \mathcal{M}_{LL} = M_{0000}\,,\\ &\mathcal{M}_{LT} = M_{0+0+}, \quad \mathcal{M}_{TL} = M_{+0+0}\,.\end{aligned} \tag{5.9}$$

For spacelike photon virtualities, the optical theorem relates the imaginary part of these amplitudes to a $\gamma^*\gamma^*$-fusion cross section [167, Eq. (16)], so that

$$\operatorname{Im}\mathcal{M}(\nu,k^2,q^2) = 2\sqrt{X}\,\sigma(\nu,k^2,q^2), \tag{5.10}$$

where $\sigma = 4\sigma_{TT} - 2\sigma_{TL} - 2\sigma_{LT} + \sigma_{LL}$[3] is the total unpolarized $\gamma^*\gamma^*$-fusion cross section, and $X = \nu^2 - q^2 k^2$. Furthermore, the analytic properties of the ν-dependence warrant a dispersive representation. Since all relevant LbL amplitudes are even in ν and require one subtraction [167, Section II. C], the dispersion relation takes the form

$$\begin{aligned}
\mathcal{M}(\nu, K^2, Q^2) &= \mathcal{M}(\bar{\nu}, K^2, Q^2) + \overline{\mathcal{M}}(\nu, K^2, Q^2), \\
\overline{\mathcal{M}}(\nu, K^2, Q^2) &= \frac{2}{\pi}(\nu^2 - \bar{\nu}^2) \int\limits_{\nu_{\text{thr.}}}^{\infty} d\nu' \, \frac{\nu' \, \text{Im}\, \mathcal{M}(\nu', K^2, Q^2)}{(\nu'^2 - \bar{\nu}^2)(\nu'^2 - \nu^2)},
\end{aligned} \tag{5.11}$$

where we are free to choose any subtraction point $\bar{\nu}$, and $\nu_{\text{thr.}}$ is the lowest particle production threshold. For example, in QED, $\nu_{\text{thr.}} = {}^1\!/_2(K^2 + Q^2) + 2m_e^2$ is the threshold for e^+e^- production; see Appendix 5.B for further details.

To proceed further, let us choose the convenient reference frame, where the four momentum q^μ is given by

$$q^\mu = \left\{ iQ, \vec{0} \right\}, \tag{5.12}$$

so that the components of the four vector k^μ can be expressed in terms of ν, K and Q in a simple way:

$$k^0 = -i\frac{\nu}{Q}, \quad |\vec{k}| = \sqrt{K^2 - \frac{\nu^2}{Q^2}}. \tag{5.13}$$

The dispersive representation justifies the Wick rotation in the evaluation of Eq. (5.5). Under this rotation, the loop integral transforms as

$$-i \int d^4k \to 4\pi \int \frac{d(k^0)^2}{2\sqrt{(k^0)^2}} \int \frac{\vec{k}^2 d\vec{k}^2}{2\sqrt{\vec{k}^2}} \to \pi \int d\nu^2 \int dK^2 \sqrt{\frac{K^2Q^2}{\nu^2} - 1}. \tag{5.14}$$

and we obtain the Cottingham formula analogue,

$$\Pi_{4\text{pt}}(Q^2, \Lambda) = \frac{1}{6Q^4(2\pi)^3} \int\limits_0^\infty dK^2 \left[\frac{1}{K^2}\right]_\Lambda \int\limits_0^{K^2Q^2} d\nu^2 \left(\frac{K^2Q^2}{\nu^2} - 1\right)^{1/2} \mathcal{M}(\nu, K^2, Q^2), \tag{5.15}$$

which by a variable change, $\nu = KQx$, is cast into

$$\Pi_{4\text{pt}}(Q^2, \Lambda) = \frac{1}{3(2\pi)^3 Q^2} \int\limits_0^\infty dK^2 \int\limits_0^1 dx \sqrt{1 - x^2} \, \mathcal{M}(KQx, K^2, Q^2), \tag{5.16}$$

where the explicit cutoff dependence has been suppressed for brevity, but is still assumed.

[3]The conventions on the polarization vectors, which lead to this relation among the corss sections, are defined in Eqs. (2.52) and (2.53). In these notations, all of the cross sections entering the relation are positively defined.

Substituting the dispersive representation of the LbL amplitude (5.11) and the optical theorem (5.14), we obtain the dispersive representation of the Cottingham formula in therms of $\gamma^*\gamma^*$-fusion cross sections:

$$\Pi_{4\text{pt}}(Q^2,\Lambda) = \frac{1}{3(2\pi)^3 Q^2}\int_0^\infty dK^2 \left[\frac{\pi}{4}\mathcal{M}(\bar{\nu},K^2,Q^2) + \int_{\nu_{\text{thr.}}}^\infty d\nu \left(\frac{2}{\nu+\sqrt{X}} - \frac{\nu}{\nu^2-\bar{\nu}^2}\right)\sqrt{X}\,\sigma(\nu,K^2,Q^2)\right]. \tag{5.17}$$

As indicated in Eq. (5.2), the contribution $\Pi_{4\text{pt}}$ must be combined with the appropriate counterterm, to which we return in section 5.7, in order to obtain the first correction $\Delta\Pi(Q^2)$ to the HVP.

At this point, let us briefly comment on the flavor structure of the HLbL amplitude $\mathcal{M}$, particularly regarding to isospin, which plays an important role at low energies. The e.m. current carried by the quarks contains both an isovector and an isoscalar component. The LbL amplitude can be written as the sum of the three partial contributions where (i) all four currents are isovector; (ii) all four currents are isoscalar; and (iii) in one pair of currents, both are isovector, while in the complementary pair, both are isoscalar, and one sums over all six possible pairings. Pole contributions of isovector mesons such as the pion only occur in the third contribution, while isoscalar-meson exchanges appear in all three contributions.

5.2 Reproducing the two-loop vacuum polarization in QED and sQED

5.2.1 The two-loop QED vacuum polarization

In order to test our Cottingham analogue, Eq. (5.15), we apply it to the QED VP: we expect the one-loop LbL amplitude to provide the two-loop VP, see Fig. 5.2.

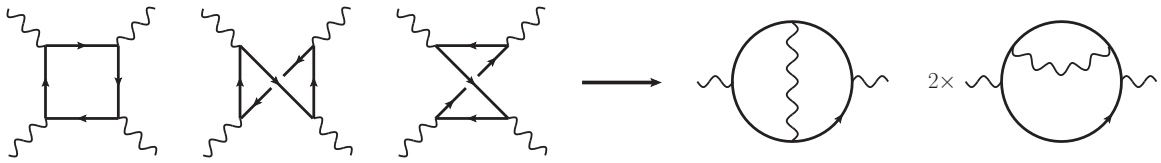

Fig. 5.2 One-loop LbL scattering (left three diagrams) and the resulting two-loop vacuum polarization in QED.

Substituting the one-loop LbL amplitude (cf. 5.A.1) into Eq. (5.15) yields a complicated expression, which we only show here in the expanded form:

$$\Pi_{4\text{pt}}^{\text{QED}}(Q^2,\Lambda) = \frac{\alpha_{\text{em}}^2}{\pi^2}\left[-\frac{1}{2} + \frac{329}{1620}\frac{Q^2}{m_\ell^2} - \frac{2333}{75600}\left(\frac{Q^2}{m_\ell^2}\right)^2 + \frac{43579}{7938000}\left(\frac{Q^2}{m_\ell^2}\right)^3 + O\left(\frac{Q^8}{m_\ell^8}\right)\right]$$

$$-\frac{\alpha_{\rm em}^2}{\pi^2}\log\frac{\Lambda}{m_\ell}\left[-\frac{1}{2}+\frac{1}{5}\frac{Q^2}{m_\ell^2}-\frac{3}{70}\left(\frac{Q^2}{m_\ell^2}\right)^2+\frac{1}{105}\left(\frac{Q^2}{m_\ell^2}\right)^3+O\left(\frac{Q^8}{m_\ell^8}\right)\right], \tag{5.18}$$

up to terms that vanish for $\Lambda\to\infty$. Hereafter m_ℓ stands for the lepton mass appearing in the loops. In this calculation we have in fact adopted a simpler, momentum-cutoff regularization: $[\frac{1}{k^2}]_\Lambda=\frac{\theta(\Lambda^2-k^2)}{k^2}$. In the present context, this form of regularization is equivalent to Pauli-Villars regularization, up to terms suppressed by $1/\Lambda^2$.

The counterterm, $\overline{\Pi}_{\rm ct}(Q^2,\Lambda)$, can be obtained in the following way

$$\overline{\Pi}_{\rm ct}(q^2,\Lambda)=-\left[m_\ell\delta_2-\delta_{m_\ell}\right]\frac{\partial}{\partial m_\ell}\overline{\Pi}_{e^2}(q^2), \tag{5.19}$$

where in the on-shell renormalization scheme[4] and in Minkowski-space notation

$$m_\ell\delta_2^{\rm QED}-\delta_{m_\ell}^{\rm QED}=\Sigma_2^{\rm QED}(\not{p}=m_\ell)=\delta m_\ell=3m_\ell\frac{\alpha_{\rm em}}{2\pi}\left[\frac{1}{4}+\log\frac{\Lambda}{m_\ell}\right], \tag{5.20}$$

$$\overline{\Pi}_{e^2}^{\rm QED}(q^2)=\frac{-2\alpha_{\rm em}}{\pi}\int_0^1 dx(1-x)x\log\frac{m_\ell^2}{m_\ell^2-x(1-x)q^2}, \tag{5.21}$$

leading to

$$\begin{aligned}\overline{\Pi}_{\rm ct}^{\rm QED}(Q^2,\Lambda)&=6\frac{\alpha_{\rm em}^2}{\pi^2}\left(\frac{1}{4}+\log\frac{\Lambda}{m_\ell}\right)\left[\frac{1}{6}-\frac{1}{\kappa^2}+\frac{4}{\kappa^3\sqrt{4+\kappa^2}}\operatorname{arctanh}\left(\frac{\kappa}{\sqrt{4+\kappa^2}}\right)\right]\\&=\frac{\alpha_{\rm em}^2}{\pi^2}\left(\frac{1}{4}+\log\frac{\Lambda}{m_\ell}\right)\left[\frac{1}{5}\kappa^2-\frac{3}{70}\kappa^4+\frac{1}{105}\kappa^6+O(\kappa^8)\right],\end{aligned} \tag{5.22}$$

where $\kappa=Q/m_\ell$. Altogether [cf. Eq. (5.2)], we obtain the following result for the small-Q^2 expansion of the two-loop VP:

$$\Delta\overline{\Pi}^{\rm QED}(Q^2)=\frac{\alpha_{\rm em}^2}{\pi^2}\left[\frac{41}{162}\frac{Q^2}{m_\ell^2}-\frac{449}{10800}\left(\frac{Q^2}{m_\ell^2}\right)^2+\frac{62479}{7938000}\left(\frac{Q^2}{m_\ell^2}\right)^3+O\left(\frac{Q^8}{m_\ell^8}\right)\right]. \tag{5.23}$$

Note that:

$$\overline{\Pi}(Q^2)\equiv\Pi(Q^2)-\Pi(0), \tag{5.24}$$

with $\Pi_{\rm 4pt}(0,\Lambda)$ given, in general, by:

$$\Pi_{\rm 4pt}(0,\Lambda)=\frac{1}{3(2\pi)^3}\int_0^\infty dK^2\int_0^1 dx\sqrt{1-x^2}\,\frac{\mathcal{M}(KQx,K^2,Q^2)}{Q^2}\Big|_{Q^2=0}. \tag{5.25}$$

[4] See Ref. [337], whose notation we borrow, in particular their Eqs. (7.28) and (7.91).

In the case of two-loop QED we obtain:

$$\Pi_{\text{4pt}}^{\text{QED}}(0,\Lambda) = -\frac{\alpha_{\text{em}}^2}{4\pi^2}\int_0^\infty dK^2 \left\{ \frac{12m_\ell^4\left(K^2+2m_\ell^2\right)\log\left[\frac{1}{2}\frac{K^2}{m_\ell^2}\left(\sqrt{1+\frac{4m_\ell^2}{K^2}}+1\right)+1\right]}{K^3\left(K^2+4m_\ell^2\right)^{5/2}} - \frac{\left(K^2+2m_\ell^2\right)^2+8m_\ell^4}{K^2\left(K^2+4m_\ell^2\right)^2}\right\}, \tag{5.26}$$

which is finite upon any regularization set by Λ.

To check this result, we use the well-known dispersion relation:

$$\overline{\Pi}(Q^2) = -\frac{Q^2}{\pi}\int_{4m_\ell^2}^\infty \frac{dt}{t(t+Q^2)}\,\text{Im}\,\Pi(t). \tag{5.27}$$

together with the well-known O(e^4) imaginary part, first computed in 1955 [338] as well as in [339], given for instance in [340] (Eq. (5-4.200) on p. 109) and in [341]. Using this well-known result, we reproduce Eq. (5.23) obtained via the Cottingham formula. We have also checked this numerically for arbitrary Q^2.

5.2.2 The two-loop sQED vacuum polarization

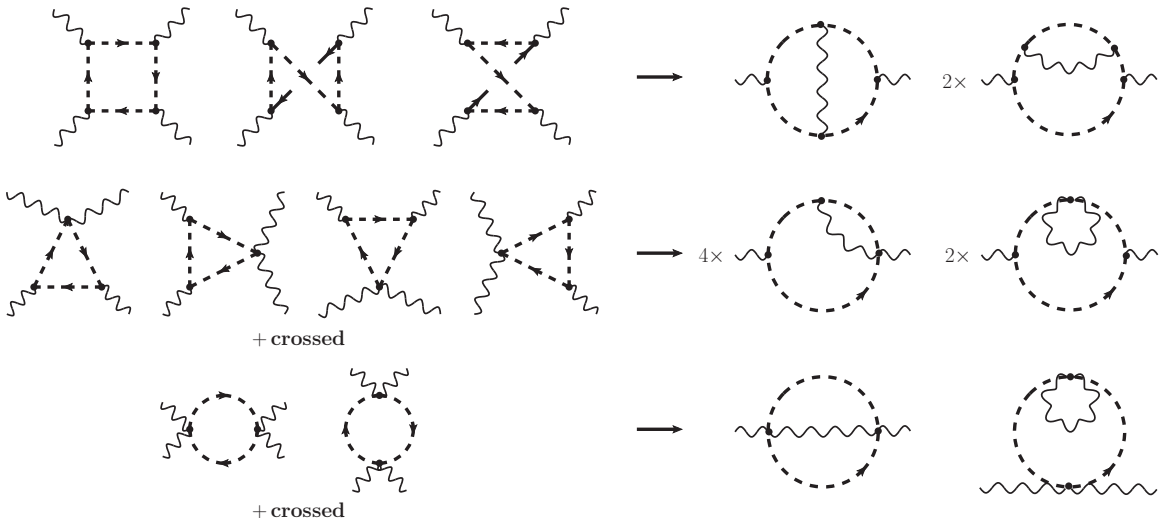

Fig. 5.3 One-loop LbL scattering (left three diagrams) and the resulting two-loop vacuum polarization in sQED.

In the context of phenomenological models for LbL amplitudes, particularly with the inclusion of charged meson loops, it is also crucial to test the Cottingham-like formula (5.15) in sQED. Due to a

presence of seagull photon-scalar vertices, the number of diagrams increases in comparison to QED, as is shown in Fig. 5.3.

Again, substitution of the one-loop LbL amplitude (cf. 5.A.2) into Eq. (5.15) yields a complicated expression, which we can expand into a series in Q:

$$\begin{aligned}\Pi_{\text{4pt}}^{\text{sQED}}(Q^2,\Lambda) = &\frac{\alpha_{\text{em}}^2}{\pi^2}\left[\frac{3}{16}+\frac{707}{25920}\frac{Q^2}{m_\pi^2}-\frac{589}{302400}\left(\frac{Q^2}{m_\pi^2}\right)^2+\frac{26113}{127008000}\left(\frac{Q^2}{m_\pi^2}\right)^3+O\left(\frac{Q^8}{m_\pi^8}\right)\right]\\ &+\frac{\alpha_{\text{em}}^2}{\pi^2}\left(\frac{\Lambda^2}{m_\pi^2}+\log\frac{\Lambda^2}{m_\pi^2}\right)\left[-\frac{3}{16}-\frac{1}{160}\frac{Q^2}{m_\pi^2}+\frac{1}{1120}\left(\frac{Q^2}{m_\pi^2}\right)^2-\frac{1}{6720}\left(\frac{Q^2}{m_\pi^2}\right)^3+O\left(\frac{Q^8}{m_\pi^8}\right)\right]\\ &+\frac{\alpha_{\text{em}}^2}{4\pi^2}\frac{\Lambda^2}{m_\pi^2},\end{aligned} \tag{5.28}$$

where m_π stands for the mass of charged scalar particle in the LbL loop (e.g. pion). The value of the two-loop vacuum polarization at zero photon virtuality reads

$$\Pi_{\text{4pt}}^{\text{sQED}}(0,\Lambda) = \frac{\alpha_{\text{em}}^2}{4\pi^2}\int_0^\infty dK^2\left\{\frac{3m_\pi^4\log\left[\frac{1}{2}\frac{K^2}{m_\pi^2}\left(\sqrt{1+\frac{4m_\pi^2}{K^2}}+1\right)+1\right]}{K^3\left(K^2+4m_\pi^2\right)^{3/2}}+\frac{K^4+m_\pi^2K^2-6m_\pi^4}{4m_\pi^2K^2\left(K^2+4m_\pi^2\right)}\right\}. \tag{5.29}$$

Due to the gauge invariance, the counterterm in sQED is also given by Eq. (5.19). The one-loop vacuum polarization in sQED has the form

$$\overline{\Pi}_{e^2}^{\text{sQED}}(q) = -\frac{\alpha_{\text{em}}}{2\pi}\int_0^1 dx x(2x-1)\log\frac{m_\pi^2}{m_\pi^2-q^2x(1-x)} \tag{5.30}$$

so that the derivative with respect to the mass reads

$$\begin{aligned}\frac{\partial}{\partial m_\pi^2}\overline{\Pi}_{e^2}^{\text{sQED}}(q) =&\frac{\alpha_{\text{em}}}{\pi}\left(\frac{\sqrt{4m_\pi^2-q^2}\tan^{-1}\left(\frac{q}{\sqrt{4m_\pi^2-q^2}}\right)}{q^3}+\frac{1}{12m_\pi^2}-\frac{1}{q^2}\right)\\ =&\frac{\alpha_{\text{em}}}{\pi}\frac{1}{m_\pi^2}\left[-\frac{q^2/m_\pi^2}{120\pi}-\frac{(q^2/m_\pi^2)^2}{840\pi}-\frac{(q^2/m_\pi^2)^3}{5040\pi}+O\left(\frac{q^8}{m_\pi^8}\right)\right]\end{aligned} \tag{5.31}$$

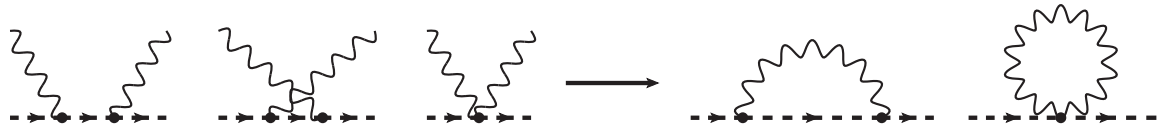

Fig. 5.4 Self energy in sQED via the Cottingham formula.

Due to the worse asymptotic behavior of sQED, even the leading-order results would depend on the regularization. In particular, contrary to QED, the cutoff, Pauli-Villars and dimensional regularizations

will result in a different finite parts for the scalar particle self energy at one loop. In order to follow the same regularization scheme in both Cottingham-like formula and counterterm calculations, we can also apply Cottingham formula for derivation of the one-loop self-energy counterterm $\Sigma(m)$, depicted on Fig. 5.4. For that purpose we need to integrate the tree-level scalar QED forward Compton amplitude over the photon momentum. This amplitude, being contracted with $g_{\mu\nu}$, has the following form

$$\begin{aligned}\mathcal{M}_{e^2}(\nu,k^2) \equiv& g_{\mu\nu}\mathcal{M}^{\mu\nu}_{e^2}(\nu,k^2)\\ =&4\pi\alpha_{\rm em}\left(\frac{4m_\pi^2-K^2+2(s-m_\pi^2+K^2)}{s-m_\pi^2}+\frac{4m_\pi^2-K^2-2(s+K^2-m_\pi^2)}{-2K^2+m_\pi^2-s}-8\right),\end{aligned} \tag{5.32}$$

where $s=(p+k)^2=m_\pi^2-K^2+2\nu$ is the usual Mandelstam variable, $\nu=p\cdot k$, with p and k being the (on-shell) four-momentum of the scalar particle, $p^2=m_\pi^2$, and the four-momentum of the virtual photon, $k^2=-K^2$, respectively. Introducing the variable x as $x=\nu/(im_\pi K)$, one arrives to a very simple expression for the traced Compton amplitude

$$\mathcal{M}_{e^2}(x,K^2)=-8\pi\alpha_{\rm em}\frac{4+8x^2+3K^2/m_\pi^2}{4x^2+K^2/m_\pi^2}. \tag{5.33}$$

Thus the application of the Cottingham formula reduces to the integration of that amplitude over the photon momentum, which yields

$$\begin{aligned}\Sigma_2^{\rm sQED}(p^2=m_\pi^2)=&\delta m_\pi^2=\int\frac{d^4k}{(2\pi)^4}\frac{1}{k^2}\mathcal{M}_{e^2}(\nu,k^2)=\int_0^\Lambda KdK\int_0^1 dx\sqrt{1-x^2}\mathcal{M}_{e^2}(x,K^2)\\ =&-\frac{\alpha_{\rm em}}{\pi}m_\pi^2\left[\frac{9}{8}+\frac{3}{4}\left(\frac{\Lambda^2}{m_\pi^2}+\log\frac{\Lambda^2}{m_\pi^2}\right)\right].\end{aligned} \tag{5.34}$$

Here, similarly to Eq. (5.28), the cutoff regularization was applied. Finally, we obtain the following series expansion for the counterterm

$$\overline{\Pi}_{\rm ct}(Q,\Lambda)=\frac{\alpha_{\rm em}^2}{\pi^2}\left[\frac{3}{2}+\left(\frac{\Lambda^2}{m_\pi^2}+\log\frac{\Lambda^2}{m_\pi^2}\right)\right]\left(\frac{Q^2/m_\pi^2}{160}-\frac{(Q^2/m_\pi^2)^2}{1120}+\frac{(Q^2/m_\pi^2)^3}{6720}+O\left(\frac{Q^8}{m_\pi^8}\right)\right). \tag{5.35}$$

This counterterm, being added to $\overline{\Pi}^{\rm sQED}_{\rm 4pt}$, gives the finite result, which corresponds to the one obtained following either Eq. (5.27) with the correct imaginary part (cf. Appendix 5.C) or exact two-loop calculation [342]. Its series expansion reads:

$$\Delta\overline{\Pi}^{\rm sQED}(Q^2)=\frac{\alpha_{\rm em}^2}{\pi^2}\frac{Q^2}{m_\pi^2}\left(\frac{95}{2592}-\frac{71}{21600}\frac{Q^2}{m_\pi^2}+\frac{54463}{127008000}\left(\frac{Q^2}{m_\pi^2}\right)^2+O\left(\frac{Q^6}{m_\pi^6}\right)\right). \tag{5.36}$$

5.3 Evaluation of the fourth-order vacuum polarization contribution to the muon $(g-2)$

We now test the Cottingham-like formula beyond the small-Q^2 expansion and compute the fourth-order VP contribution to the muon AMM using numerical integration. In order to avoid numerical instabilities emerging in loop integrals, that in the case of the virtual LbL amplitude we found to persist in all familiar packages for one-loop numerical integration, we choose the more elegant way and calculate the LbL amplitude $\mathcal{M}(\nu, K^2, Q^2)$ itself via the dispersive approach, utilizing Eq. (5.17) The imaginary part $\mathrm{Im}\,\mathcal{M}(\nu, K^2, Q^2)$ in terms of the tree level two-photon fusion cross sections in QED and sQED, as well as expressions for the subtraction term $\mathcal{M}(\bar{\nu}, K^2, Q^2)$ for the two choices of subtraction point $\bar{\nu}_1 = 0$ and $\bar{\nu}_2 = KQ$ are provided in Appendix 5.A.

The $O\left(e^6\right)$ contribution of the regulated fourth-order vacuum polarization to the AMM can be computed using the general formula [343–345]:

$$\varkappa_\mu = \frac{\alpha_{\mathrm{em}}}{\pi} \int_0^\infty dQ^2\, \mathcal{K}(Q^2)\, \overline{\Pi}(Q^2), \tag{5.37}$$

where the kernel function is given by

$$\mathcal{K}(Q^2) = \frac{1}{2m_\mu^2} \frac{(v-1)^3}{2v(v+1)}, \qquad v = \sqrt{1+\frac{4m_\mu^2}{Q^2}}, \tag{5.38}$$

with m_μ the muon mass. The integral over the kernel function alone gives the Schwinger term, $\Delta\varkappa_\mu = \alpha_{\mathrm{em}}/2\pi$. Therefore, substituting the renormalized vacuum polarization, we obtain:

$$\varkappa_\mu = -\frac{\alpha_{\mathrm{em}}}{2\pi}\Pi(0) + \frac{\alpha_{\mathrm{em}}}{\pi} \int_0^\infty dQ^2\, \mathcal{K}(Q^2)\, \Pi(Q^2). \tag{5.39}$$

Consequently, the subtraction term in $\overline{\Pi}_{4\mathrm{pt}}(Q^2, \Lambda)$ contributes $-\alpha_{\mathrm{em}}/2\pi\,\Pi_{4\mathrm{pt}}(0, \Lambda)$ to $\varkappa_\mu$. To facilitate the comparison of continuum results with lattice calculations, it is advantageous to define the contribution to the anomalous magnetic moment (AMM) arising solely from the Cottingham formula result subtracted at $Q = 0$:

$$\varkappa_\mu^* \equiv -\frac{\alpha_{\mathrm{em}}}{2\pi}\Pi_{4\mathrm{pt}}(0) + \frac{\alpha_{\mathrm{em}}}{\pi} \int_0^\infty dQ^2 \mathcal{K}(Q^2) \Pi_{4\mathrm{pt}}(Q^2) \tag{5.40}$$

This component can be directly computed on the lattice in its entirety, whereas the evaluation of the counterterm necessitates a distinct computational approach.

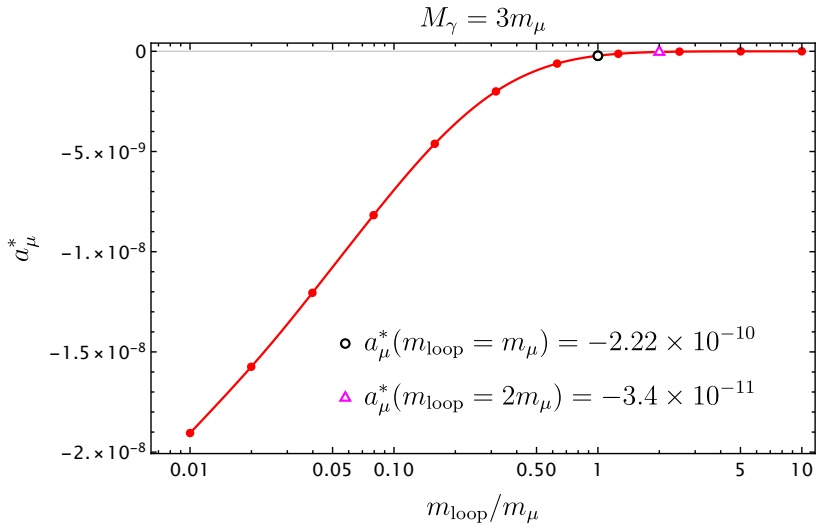

Fig. 5.5 Anomalous magnetic moment $a_\mu^* \equiv \varkappa_\mu^*$ via the Cottingham formula without the counterterm to be compared with lattice QCD: varying the mass inside the VP. The cutoff scale is chosen to be $\Lambda \equiv M_\gamma = 3m_\mu$.

For QED, results obtained with a Pauli-Villars regulator,

$$\left[\frac{1}{k^2}\right]_\Lambda^{\rm PV} \to \frac{\Lambda^2}{k^2(\Lambda^2-k^2)}, \tag{5.41}$$

and $\Lambda = 3m_\mu$[5] are provided as a function of the lepton mass m_ℓ appearing in the vacuum polarization in Fig. 5.5. Furthermore, adding the contribution of the appropriate counterterm and subsequently taking the limit $\Lambda \to \infty$, we obtain the full $\mathrm{O}(e^4)$ QED vacuum polarization to $\varkappa_\mu$. For a muon in the vacuum polarization loop, we obtain:

$$\Delta\varkappa_\mu \simeq 6.6\times10^{-10}. \tag{5.42}$$

The result numerically agrees with Ref. [346].

For sQED, a single Pauli-Villars regulator to the photon propagator is not sufficient to regularize the UV divergences. Instead one can consider a "double Pauli-Villars" regulator of the form:

$$\left[\frac{1}{k^2}\right]_\Lambda^{\rm dPV} \to \left(\frac{1}{k^2} - G_{\rm sub}(k^2,\zeta,\Lambda)\right) + G_{\rm sub}(k^2,\zeta,\Lambda), \tag{5.43}$$

$$G_{\rm sub}(k^2,\zeta,\Lambda) = \frac{1}{1-\zeta}\left(\frac{1}{k^2+\zeta\Lambda^2} - \frac{\zeta}{k^2+\Lambda^2}\right), \qquad 0<\zeta<1. \tag{5.44}$$

[5]This cutoff value serves as one of several reference points used to further validate the lattice QCD setup and benchmark its results against continuum calculations. The selection of this specific value is primarily methodological rather than physical; it serves as a computational tool for comparison and validation purposes.

This regularization with $\zeta \neq 1$ is particularly useful for the lattice application in the position space, where it allows one to improve convergence while removing unnecessary singular terms. The photon propagator in position space is then written as

$$G(x) = G_0(x) + \frac{\zeta^2}{1-\zeta^2} G(m,x) - \frac{1}{1-\zeta^2} G(\zeta m, x), \tag{5.45}$$

where

$$G_0(x) = \int \frac{d^4k}{(2\pi)^4} \frac{e^{ik\cdot x}}{k^2} = \frac{1}{4\pi^2 x^2}, \quad G_m(x) = \int \frac{d^4k}{(2\pi)^4} \frac{e^{ik\cdot x}}{k^2+m^2} = \frac{m}{4\pi^2|x|} K_1(m|x|). \tag{5.46}$$

Another possibility to regularize the vacuum polarization is to supplement each $\gamma\pi^+\pi^-$ vertex with the VMD vector form factor of the monopole form

$$F_{\gamma\pi^+\pi^-}(Q^2) = \frac{M_V^2}{Q^2+M_V^2}. \tag{5.47}$$

The chiral-limit behavior of the contribution to AMM through the Cottingham formula with a charged pion loop is defined just by the subtraction term $-\alpha_{\rm em}/2\pi\,\Pi(0)$. Being regularized by the VMD form factors, it behaves at $m_\pi \to 0$ as

$$a_\mu^* = -\frac{\alpha_{\rm em}}{2\pi} [\Pi(0)]^{\rm VMD}_{M_V} + O(m_\pi^0) = -\frac{\alpha_{\rm em}^3}{32\pi^3} \frac{M_V^2}{m_\pi^2} + O(m_\pi^0). \tag{5.48}$$

Here M_V is the vector-meson mass from VMD form factor. For double Pauli-Villars regulator without VMD form factors, it reads

$$a_\mu^* = -\frac{\alpha_{\rm em}}{2\pi} [\Pi(0)]^{\rm dPV}_{\Lambda} + O(m_\pi^0) = -\frac{\alpha_{\rm em}^3}{32\pi^3} \frac{\Lambda^2}{m_\pi^2} \frac{\log(\zeta^2)}{\zeta^2-1} + O(m_\pi^0) \tag{5.49}$$

We also calculate the pion mass dependence at small muon mass, while keeping $m_\mu \ll m_\pi < M_V$. To get the analytical result, we use the low-Q expansion of the two-loop vacuum polarization. By straightforward calculation we obtain

$$\begin{aligned} a_\mu^* &= -\frac{\alpha_{\rm em}}{2\pi}\Pi(0) + \frac{\alpha_{\rm em}}{\pi} \int_0^\infty {\rm d}Q^2\, \mathcal{K}(Q^2)\, \Pi(Q^2) \\ &\approx \frac{\alpha_{\rm em}}{\pi} \int_0^\infty {\rm d}Q^2\, \mathcal{K}(Q^2) \frac{1}{\left(Q^2/M_V^2+1\right)^2} \left[-\frac{\alpha^2}{160\pi^2} \frac{M_V^2}{m_\pi^4} Q^2 + O(Q^4) \right] \\ &\overset{m_\mu \to 0}{=} -\frac{\alpha_{\rm em}^3}{480\pi^3} \frac{m_\mu^2 M_V^2}{m_\pi^4} \end{aligned} \tag{5.50}$$

Without any approximations and regulators, the exact on-shell renormalized $O(e^4)$ sQED vacuum polarization with the charged pion loop contributes to $\varkappa_\mu$ as follows:

$$\Delta\varkappa_\mu \simeq 7.0\times 10^{-11}. \tag{5.51}$$

5.4 Sum rule for the subtraction function in Cottingham-like formula

Although the dispersive representation (5.17) relates the vacuum polarization with the total unpolarized two-photon fusion cross section in a model-independent way, the unknown subtraction function due to $\mathcal{M}(\bar{\nu}, K^2, Q^2)$ persists. This prevents one from constructing a fully data-driven approach for the Cottingham formula. Fortunately, there exists a way how to relate the subtraction function to the polarized two-photon fusion cross sections under some assumptions.

Let us consider the LbL amplitude $\mathcal{M}_{\mu\alpha\nu\beta}$, summed over polarizations of the incoming an outgoing photons with virtuality $K^2 = -k^2$,

$$g^{\alpha\beta}\mathcal{M}_{\mu\alpha\nu\beta} = -\left(g_{\mu\nu} - \frac{q_\mu q_\nu}{q^2}\right) M_1 + \frac{\hat{k}_\mu \hat{k}_\nu}{k^2} M_2, \tag{5.52}$$

where

$$\hat{k}_\mu = k_\mu - \frac{k\cdot q}{q^2} q_\mu. \tag{5.53}$$

The Eq. (5.52) is basically a spin-independent part of the Compton tensor (cf. Eq. (2.79)). The traced amplitude $\mathcal{M}$, given by Eq. (5.8), then can be written in terms of M_1 and M_2 as

$$\mathcal{M} = -3M_1 - \frac{X}{q^2 k^2} M_2, \tag{5.54}$$

It is convenient to introduce the longitudinal amplitude,

$$\mathcal{M}_L = M_{\mu\nu}\varepsilon_L^\mu \varepsilon_L^{*\nu} = -M_1 - M_2 \frac{X}{q^2 k^2}. \tag{5.55}$$

which corresponds to the scattering of longitudinally-polarized photon with momentum q on the unpolarized one with momentum k. Its imaginary part is related via the optical theorem to the polarized two-photon fusion cross sections σ_{LL} and σ_{LT} as follows:

$$\begin{aligned}\operatorname{Im}\mathcal{M}_L =& \operatorname{Im}\left(M_{0000} - M_{0+0+} - M_{0-0-}\right)\\ =& 2\sqrt{X}\left(\sigma_{LL} - 2\sigma_{LT}\right) \equiv 2\sqrt{X}\sigma_L.\end{aligned} \tag{5.56}$$

Let us assume that the longitudinal amplitude should satisfy the unsubtracted dispersion relation

$$\mathcal{M}_L(\nu, K^2, Q^2) = \frac{4}{\pi} \int\limits_{\nu_{\text{thr.}}}^{\infty} d\nu' \, \frac{\nu' \sqrt{X'} \sigma_L(\nu', K^2, Q^2)}{\nu'^2 - \nu^2 - i0^+}, \tag{5.57}$$

where $X' = \nu'^2 - K^2 Q^2$. Similarly, one can introduce the transverse amplitude,

$$\mathcal{M}_T = M_{\mu\nu}(\varepsilon_+^\mu \varepsilon_+^{*\nu} + \varepsilon_-^\mu \varepsilon_-^{*\nu}) = -2M_1, \tag{5.58}$$

which corresponds to the scattering of longitudinally-polarized photon with momentum q on the unpolarized one with momentum k. Its imaginary part, in its turn, is related to the polarized two-photon fusion cross sections σ_{TL} and σ_{TT}:

$$\begin{aligned} \operatorname{Im} \mathcal{M}_T =& \operatorname{Im}(-2M_{+0+0} + 2M_{++++} + 2M_{+-+-}) \\ =& 2\sqrt{X}(-2\sigma_{TL} + 4\sigma_{TT}). \end{aligned} \tag{5.59}$$

At the "Siegert" point $\nu = QK$ (where three-momenta of both photons are zero) the longitudinal and the transverse (and hence the total) LbL amplitudes are related as follows:

$$\mathcal{M}_L(\nu = QK, K^2, Q^2) = -M_1(\nu = QK, K^2, Q^2) = \mathcal{M}(\nu = QK, K^2, Q^2)/3. \tag{5.60}$$

Combining the dispersion relation for the total LbL amplitude, given by Eq. (5.11) with the dispersion relation for the longitudinal amplitude (5.57) at the Siegert point (5.60), one can write down the dispersive representation for the subtraction function:

$$\mathcal{M}(\bar{\nu}, K^2, Q^2) = \frac{4}{\pi} \int\limits_{\nu_{\text{thr.}}}^{\infty} d\nu' \, \frac{\nu'}{\sqrt{X'}} \left[3\sigma_L(\nu', Q^2) + \frac{\bar{\nu}^2 - (KQ)^2}{\nu'^2 - \bar{\nu}^2} \sigma(\nu', Q^2) \right]. \tag{5.61}$$

This relation, if valid, can be further substituted into Eq. (5.11), providing a unique opportunity to define the total LbL amplitude in a fully data-driven fashion. The resulting expression for the amplitude $\mathcal{M}(\nu, K^2, Q^2)$ then follows from Eq. (5.61) by replacing $\bar{\nu}$ with ν. This leads to the following master formula for the data-driven evaluation of the vacuum polarization correction:

$$\Pi_{4\text{pt}} = \frac{1}{3(2\pi)^3 Q^2} \int_0^\infty dK^2 \int_{\nu_{\text{thr.}}}^\infty d\nu' \, \frac{\nu'}{\sqrt{X'}} \left[3\sigma_L^{\text{sym}} + \left(-1 + \frac{2X'}{K^2 Q^2} \left(1 - \frac{\sqrt{X'}}{\nu'} \right) \right) \sigma \right]. \tag{5.62}$$

However, in QED the sum rule (5.61) works up to a ν-independent function:

$$\mathcal{M}(\bar{\nu}, K^2, Q^2) = \frac{4}{\pi} \int\limits_{\nu_{\text{thr.}}}^{\infty} d\nu' \, \frac{\nu'}{\sqrt{X'}} \left[3\sigma_L(\nu, Q^2) + \frac{\bar{\nu}^2 - (KQ)^2}{\nu'^2 - \bar{\nu}^2} \sigma(\nu, Q^2) \right]$$

$$+96\alpha_{\rm em}^2\left\{1-2\frac{\log\frac{1}{2}\left(Q^2+\sqrt{Q^2(Q^2+4)}+2\right)}{\sqrt{Q^2(Q^2+4)}}\right\}, \tag{5.63}$$

where the lepton mass is taken as unity. This expression can be written in symmetric form,

$$\begin{aligned}\mathcal{M}(\bar{\nu},K^2,Q^2)=&\frac{4}{\pi}\int\limits_{\nu_{\rm thr.}}^{\infty}d\nu'\,\frac{\nu'}{\sqrt{X'}}\left[3\sigma_L^{\rm sym}(\nu,Q^2)+\frac{\bar{\nu}^2-(KQ)^2}{\nu'^2-\bar{\nu}^2}\sigma(\nu,Q^2)\right]\\&+48\alpha_{\rm em}^2\left\{1-2\frac{\log\frac{1}{2}\left(Q^2+\sqrt{Q^2(Q^2+4)}+2\right)}{\sqrt{Q^2(Q^2+4)}}\right\}\\&+48\alpha_{\rm em}^2\left\{1-2\frac{\log\frac{1}{2}\left(K^2+\sqrt{K^2(K^2+4)}+2\right)}{\sqrt{K^2(K^2+4)}}\right\},\end{aligned} \tag{5.64}$$

where the symmetrized longitudinal cross section was introduced:

$$\sigma_L^{\rm sym}(\nu,Q^2)=\sigma_{LL}(\nu,Q^2)-\left[\sigma_{LT}(\nu,Q^2)+\sigma_{TL}(\nu,Q^2)\right]. \tag{5.65}$$

The same is true for the sQED case. These ν-independent functions are caused by the nonvanishing value of the longitudinal amplitude at infinite energy. Thus, according to the Sugawara-Kanazawa theorem [158], the dispersion relation (5.57) should be changed as follows

$$\mathcal{M}_L(\nu,K^2,Q^2)=\mathcal{M}_L(\nu\to\infty,K^2,Q^2)+\frac{4}{\pi}\int\limits_{\nu_{\rm thr.}}^{\infty}d\nu'\,\frac{\nu'\sqrt{X'}\sigma_L(\nu',K^2,Q^2)}{\nu'^2-\nu^2-i0^+}. \tag{5.66}$$

The situation when the real physical amplitude (and any connected physical quantity) at arbitrary low energies "feels" the physics at infinitely large energies looks ridiculous. Indeed, it means that we can probe the physics beyond the Planck scale by the low-energy observables. Therefore, assuming the convergence of the dispersive integral, which is proven in QED and sQED, we tend to treat the nonzero amplitude at infinite energy as an artifact of the (low-energy) theory. Further discussion of this phenomenon in the Compton scattering will continue in Chapter 7.

5.4.1 Formula for $\mathcal{M}_{TT}$

A formula similar to Eq. (5.61) can be derived for the polarized LbL amplitude $\mathcal{M}_{TT}$. Defining $\widetilde{LT}$ as a symmetric combination $LT+TL$,

$$\mathcal{M}_{\widetilde{LT}}(\nu,K^2,Q^2)\equiv\mathcal{M}_{TL}(\nu,K^2,Q^2)+\mathcal{M}_{LT}(\nu,K^2,Q^2), \tag{5.67}$$

the following dispersive representations for polarized LbL amplitudes can be written:

$$\mathcal{M}_{TT}(\nu,K^2,Q^2) = \mathcal{M}_{TT}(\bar{\nu},K^2,Q^2) + \frac{4}{\pi}(\nu^2-\bar{\nu}^2)\int_{\nu_{\text{thr.}}}^{\infty} d\nu' \frac{\nu'\sqrt{X'}\sigma_{TT}(\nu',K^2,Q^2)}{(\nu'^2-\bar{\nu}^2)(\nu'^2-\nu^2)}, \tag{5.68}$$

$$\mathcal{M}_{\widetilde{LT}}(\nu,K^2,Q^2) = \mathcal{M}_{\widetilde{LT}}(\nu\to\infty,K^2,Q^2) + \frac{4}{\pi}\int_{\nu_{\text{thr.}}}^{\infty} d\nu' \frac{\nu'\sqrt{X'}\sigma_{\widetilde{LT}}(\nu',K^2,Q^2)}{\nu'^2-\nu^2}, \tag{5.69}$$

$$\mathcal{M}_{LL}(\nu,K^2,Q^2) = \frac{4}{\pi}\int_{\nu_{\text{thr.}}}^{\infty} d\nu' \frac{\nu'\sqrt{X'}\sigma_{LL}(\nu',K^2,Q^2)}{\nu'^2-\nu^2}, \tag{5.70}$$

In QED, the asymptotic value $\mathcal{M}_{\widetilde{LT}}(\nu\to\infty,K^2,Q^2)$ is given by

$$\mathcal{M}_{\widetilde{LT}}(\nu\to\infty,K^2,Q^2) = -32\alpha_{\text{em}}^2\left\{1 - \frac{\log\frac{1}{2}(2+K^2+\sqrt{K^2(4+K^2)})}{\sqrt{K^2(4+K^2)}} - \frac{\log\frac{1}{2}(2+Q^2+\sqrt{Q^2(4+Q^2)})}{\sqrt{Q^2(4+Q^2)}}\right\} \tag{5.71}$$

From Eq. (5.54) written in the point $\nu = QK$ one can read off the following relation

$$2\mathcal{M}_{TT}(\nu=KQ,K^2,Q^2) = \mathcal{M}_{LL}(\nu=KQ,K^2,Q^2) - \frac{1}{2}\mathcal{M}_{\widetilde{LT}}(\nu=KQ,K^2,Q^2). \tag{5.72}$$

Inserting the dispersive representations for the amplitudes into the latter relation, one can determine the subtraction function $\mathcal{M}_{TT}(\bar{\nu},K^2,Q^2)$

$$\begin{aligned}\mathcal{M}_{TT}(\bar{\nu},K^2,Q^2) = \frac{2}{\pi}\int_{\nu_{\text{thr.}}}^{\infty} d\nu' \frac{\nu'}{\sqrt{X'}}\Bigg[&2\frac{\bar{\nu}^2-K^2Q^2}{\nu'^2-\bar{\nu}^2}\sigma_{TT}(\nu',K^2,Q^2)\\ &+\sigma_{LL}(\nu',K^2,Q^2) - \frac{1}{2}\sigma_{\widetilde{LT}}(\nu',K^2,Q^2)\Bigg] - \frac{1}{4}\mathcal{M}_{\widetilde{LT}}^{\nu\to\infty}(K^2,Q^2).\end{aligned} \tag{5.73}$$

It worth noting that all the dispersion relations above are also valid in sQED, however, with the different asymptotic function

$$\begin{aligned}\mathcal{M}_{\widetilde{LT},\,\text{sQED}}(\nu\to\infty,K^2,Q^2) = 4\alpha_{\text{em}}^2\Bigg\{&4 - \sqrt{1+\frac{4}{K^2}}\log\frac{1}{2}(2+K^2+\sqrt{K^2(4+K^2)})\\ &- \sqrt{1+\frac{4}{Q^2}}\log\frac{1}{2}(2+Q^2+\sqrt{Q^2(4+Q^2)})\Bigg\}.\end{aligned} \tag{5.74}$$

Again, we opt to treat the asymptotic function as a high-energy artifact of the theory, which should vanish in real physical amplitude as long as the dispersive integral is convergent. Thus, the data-driven dispersion formula for $\mathcal{M}_{TT}$ becomes

$$\mathcal{M}_{TT}(\nu,K^2,Q^2) = \frac{1}{\pi}\int_{\nu_{\text{thr.}}}^{\infty} d\nu' \frac{\nu'}{\sqrt{X'}}\Bigg[4\frac{X}{\nu'^2-\nu^2}\sigma_{TT}(\nu',K^2,Q^2)$$

$$+2\sigma_{LL}(\nu', K^2, Q^2) - \sigma_{\widetilde{LT}}(\nu', K^2, Q^2)\Big]. \tag{5.75}$$

5.4.2 Scalar and pseudoscalar exchanges

Along with the lepton and scalar LbL boxes, it is interesting to test the formula (5.73) on a more elementary case of the scalar particle exchange. The amplitude of the two-photon fusion into the scalar particle of mass m_S consists of two pieces, transversal and longitudinal [167]:

$$\mathcal{M}_{\lambda_k,\lambda_q}(\nu, K^2, Q^2) = 4\pi\alpha_{\rm em}\varepsilon_\mu(k,\lambda_k)\varepsilon_\nu(q,\lambda_q)\frac{\nu}{m_S} \times\left\{-R^{\mu\nu}(k,q)F^T_{S\gamma^*\gamma^*}(K^2,Q^2) + \frac{QK\nu}{X}l_k^\mu l_q^\nu F^L_{S\gamma^*\gamma^*}(K^2,Q^2)\right\}. \tag{5.76}$$

Here $\varepsilon(k(q),\lambda_k(\lambda_q))$ are the polarization vectors of the photons with corresponding helicities $\lambda_{k(q)}$ and four-vectors $k(q)$ with virtualities $k^2 = -K^2$ and $q^2 = -Q^2$. The notations for the tensor structures are given by Eq. (2.51). A scalar exchange is described by its mass m_S and the longitudinal (transverse) transition form factors $F^{L(T)}_{S\gamma^*\gamma^*}$.

There are only three non-vanishing amplitudes for this process:

$$\mathcal{M}_{++}(\nu, K^2, Q^2) = \mathcal{M}_{--}(\nu, K^2, Q^2) = 4\pi\alpha_{\rm em}\frac{\nu}{m_S}F^T_{S\gamma^*\gamma^*}(K^2,Q^2) \tag{5.77}$$

$$\mathcal{M}_{00}(\nu, K^2, Q^2) = -4\pi\alpha_{\rm em}\frac{KQ}{m_S}F^L_{S\gamma^*\gamma^*}(K^2,Q^2), \tag{5.78}$$

so the corresponding cross sections are simply given by

$$\sigma_{TT}(\nu, K^2, Q^2) = \delta(\nu-\nu_{\rm S})\frac{\pi}{8}\frac{16\pi^2\alpha_{\rm em}^2}{m_S^2}\frac{\nu^2}{\sqrt{X}}F^T_{S\gamma^*\gamma^*}(K^2,Q^2) \tag{5.79}$$

$$\sigma_{LL}(\nu, K^2, Q^2) = \delta(\nu-\nu_{\rm S})\frac{\pi}{4}\frac{16\pi^2\alpha_{\rm em}^2}{m_S^2}\frac{K^2Q^2}{\sqrt{X}}F^L_{S\gamma^*\gamma^*}(K^2,Q^2), \tag{5.80}$$

where $\nu_{\rm S} = (m_S^2 + K^2 + Q^2)/2$. From Eq. (5.76), the amplitudes $\mathcal{M}_{TT}$ and $\mathcal{M}_{LL}$ of the forward LbL scattering via the scalar exchange can be easily obtained, yielding

$$\mathcal{M}_{TT}(\nu, K^2, Q^2) = \frac{1}{2}\frac{16\pi^2\alpha_{\rm em}^2}{m_S^2}\left[F^T_{S\gamma^*\gamma^*}(K^2,Q^2)\right]^2\frac{\nu^2\nu_{\rm S}}{\nu_{\rm S}^2-\nu^2}, \tag{5.81}$$

$$\mathcal{M}_{LL}(\nu, K^2, Q^2) = \frac{16\pi^2\alpha_{\rm em}^2}{m_S^2}\left[F^L_{S\gamma^*\gamma^*}(K^2,Q^2)\right]^2\frac{K^2Q^2\nu_{\rm S}}{\nu_{\rm S}^2-\nu^2}. \tag{5.82}$$

It is straightforward to see that Eq. (5.70) is satisfied.

Let us then find the subtraction function for $\mathcal{M}_{TT}$ using Eq. (5.73):

$$\begin{aligned}
\mathcal{M}_{TT}(\bar{\nu},K^2,Q^2) &= \frac{2}{\pi}\int_{\nu_0}^{\infty} d\nu' \frac{\nu'}{\sqrt{X'}}\left[2\frac{\bar{\nu}^2-K^2Q^2}{\nu'^2-\bar{\nu}^2}\sigma_{TT}(\nu',K^2,Q^2)+\sigma_{LL}(\nu',K^2,Q^2)\right] \\
&= \frac{8\pi^2\alpha_{\rm em}^2}{m_S^2}\int_{\nu_0}^{\infty} d\nu' \frac{\nu'}{X'}\left[\frac{\bar{\nu}^2-K^2Q^2}{\nu'^2-\bar{\nu}^2}\nu'^2\left(F^T_{S\gamma^*\gamma^*}(K^2,Q^2)\right)^2+K^2Q^2\left(F^L_{S\gamma^*\gamma^*}(K^2,Q^2)\right)^2\right]\delta(\nu'-\nu_{\rm S}) \\
&= \frac{8\pi^2\alpha_{\rm em}^2}{m_S^2}\frac{\nu_{\rm S}^3}{\nu_{\rm S}^2-K^2Q^2}\left[\frac{\bar{\nu}^2-K^2Q^2}{\nu_{\rm S}^2-\bar{\nu}^2}\left(F^T_{S\gamma^*\gamma^*}(K^2,Q^2)\right)^2+\frac{K^2Q^2}{\nu_{\rm S}^2}\left(F^L_{S\gamma^*\gamma^*}(K^2,Q^2)\right)^2\right],
\end{aligned} \tag{5.83}$$

where ν_0 is the first inelastic threshold of $\gamma\gamma$ fusion process, so that $\nu_S > \nu_0$. At this point one can make an assumption that the transversal and longitudinal form factors are the same, i.e. $F^T_{S\gamma^*\gamma^*} = F^L_{S\gamma^*\gamma^*} \equiv F_{S\gamma^*\gamma^*}$. The subtraction function then simplifies to

$$\begin{aligned}
\mathcal{M}_{TT}(\bar{\nu},K^2,Q^2) &= \frac{8\pi^2\alpha_{\rm em}^2}{m_S^2}\left(F_{S\gamma^*\gamma^*}(K^2,Q^2)\right)^2\int_{\nu_0}^{\infty} d\nu' \frac{\nu'}{\nu'^2-\bar{\nu}^2}\frac{\bar{\nu}^2\left(\nu'^2-K^2Q^2\right)}{X'}\delta(\nu'-\nu_{\rm S}) \\
&= \frac{8\pi^2\alpha_{\rm em}^2}{m_S^2}\left(F_{S\gamma^*\gamma^*}(K^2,Q^2)\right)^2\frac{\nu_{\rm S}\bar{\nu}^2}{\nu_{\rm S}^2-\bar{\nu}^2}.
\end{aligned} \tag{5.84}$$

On the other hand, applying the dispersive representation Eq.(5.68), one obtains the following reference expression for the subtraction function:

$$\begin{aligned}
\mathcal{M}_{TT}(\bar{\nu},K^2,Q^2) &= \mathcal{M}_{TT}(\nu,K^2,Q^2)-\frac{4}{\pi}(\nu^2-\bar{\nu}^2)\int_{\nu_0}^{\infty} d\nu' \frac{\nu'\sqrt{X'}\sigma_{TT}(\nu',Q^2,K^2)}{(\nu'^2-\bar{\nu}^2)(\nu'^2-\nu^2)} \\
&= \frac{1}{2}\frac{16\pi^2\alpha_{\rm em}^2}{m_S^2}\left(F^T_{S\gamma^*\gamma^*}(K^2,Q^2)\right)^2\left[\frac{\nu^2\nu_{\rm S}}{\nu_{\rm S}-\nu}-\frac{\nu_{\rm S}^3(\nu^2-\bar{\nu}^2)}{(\nu_{\rm S}^2-\bar{\nu}^2)(\nu_{\rm S}^2-\nu^2)}\right] \\
&= \frac{1}{2}\frac{16\pi^2\alpha_{\rm em}^2}{m_S^2}\left(F^T_{S\gamma^*\gamma^*}(K^2,Q^2)\right)^2\frac{\nu_{\rm S}\bar{\nu}^2}{\nu_{\rm S}^2-\bar{\nu}^2}.
\end{aligned} \tag{5.85}$$

Under an assumption of equivalence of the transversal and longitudinal squared form factors, this subtraction function is identical to the one given by Eq. (5.84), which was obtained using the dispersive formula (5.73). Thus the latter, if it works, can provide useful constraints on the two-photon transition form factors of the scalar particles.

A simple scenario arises in the case of pseudoscalar exchanges, which are characterized by a single transverse two-photon transition form factor [167],

$$\mathcal{M}_{\lambda_k,\lambda_q} = -4i\pi\alpha_{\rm em}\epsilon_{\mu\nu\alpha\beta}\varepsilon^{\mu}(k,\lambda_k)\varepsilon^{\nu}(q,\lambda_q)k^{\alpha}q^{\beta}F_{P\gamma^*\gamma^*}(K^2,Q^2), \tag{5.86}$$

only the amplitudes with transversal photons are non-zero:

$$\mathcal{M}_{++}(\nu,K^2,Q^2) = -\mathcal{M}_{--}(\nu,K^2,Q^2) = -4\pi\alpha_{\rm em}\sqrt{X}. \tag{5.87}$$

Hence the LbL amplitude with the longitudinally-polarized photons does not emerge. Performing the same steps as for the case of the scalar exchange, one obtains similar expression for the subtraction function,

$$\mathcal{M}(\bar{\nu}, K^2, Q^2) = \frac{8\pi^2\alpha_{\rm em}^2}{m_P^2}\left(F_{P\gamma^*\gamma^*}(K^2, Q^2)\right)^2 \frac{\nu_{\rm S}(\bar{\nu}^2 - K^2Q^2)}{\nu_{\rm S}^2 - \bar{\nu}^2}, \tag{5.88}$$

with m_P being the mass of the exchanged particle. However, this subtraction function can be exactly reproduced by the formula (5.73) without any further assumptions.

5.5 Forward LbL amplitude at large virtuality from the Operator Product Expansion

Since the forward HLbL amplitude $\mathcal{M}(k,q)$ is finite, the divergence of Eq. (5.5) as $\Lambda \to \infty$ can only arise from performing the k integral. The question is then, what is the large-k behaviour of $\mathcal{M}(k,q)$ for fixed q. This is a typical application for the Operator Product Expansion (OPE). In this section we work in Euclidean space and our starting point is

$$\left\langle V_\mu^{\rm em}(x) V_\nu^{\rm em}(y) V_\sigma^{\rm em}(z) V_\lambda^{\rm em}(0)\right\rangle = \int_{q_1,q_2,q_3} e^{i(q_1x+q_2y+q_3z)}\,\Pi_{\mu\nu\sigma\lambda}(q_1,q_2,q_3), \tag{5.89}$$

the e.m. current carried by the quarks, in units of the positron charge, being given by $V_\mu^{\rm em} = \frac{2}{3}\bar{u}\gamma_\mu u - \frac{1}{3}\bar{d}\gamma_\mu d - \ldots$ We recall that the HLbL amplitude is directly related to $\Pi_{\mu\nu\sigma\lambda}$ [332]. In particular, for the forward amplitude Eq. (5.6), the connection reads

$$\mathcal{M}(k\cdot q, k^2, q^2) = e^4\delta_{\mu\nu}\delta_{\sigma\lambda}\Pi_{\mu\nu\sigma\lambda}(-k,k,-q), \tag{5.90}$$

where the scalar products on the left-hand side are Euclidean. The large momentum k "forces" the two vertices x and y to come close together. From a power-counting perspective, it is the dimension-four operators that can cause a logarithmically divergent behaviour in Eq. (5.5), since they contribute as $O^{(4)}/k^2$. It is then only necessary to know their Wilson coefficients to order α_s included, since $\alpha_s(k^2)^2 O^{(4)}/k^2$ multiplied by a photon propagator already yields a UV-finite integral.

Note that the two indices of the vector currents are contracted with each other (thus cancelling the axial current contribution in the OPE), and that we may average the result over the direction of k, given that we are interested in subsequently integrating over k in Eq. (5.5). The result of the OPE can then only contain operators with vacuum quantum numbers.

From a different perspective, the divergence resulting from the integral over the photon momentum k must be removable by the available counterterms of the theory. Moreover, since vector currents do not renormalize in QCD, the relevant counterterms are only those associated with the parameters of the theory, which are the gauge coupling and the quark masses. These parameters are respectively associated with the operators $G^a_{\alpha\beta}G^a_{\alpha\beta}$ and $m_f\bar{\psi}_f\psi_f$ for each quark flavor f.

The Wilson coefficients of scalar operators appearing in the OPE of QCD currents have been calculated a long time ago [347]. We report only the result up to the order required for our purposes[6],

$$\begin{aligned}&\left\langle \int d^4x\, e^{ikx}\, \mathrm{T}(\bar\psi_f(x)\gamma_\mu\psi_f(x)\;\bar\psi_f(0)\gamma_\mu\psi_f(0))\right\rangle_{\hat k} \\ &\overset{k^2\to\infty}{=} \frac{3}{k^2}\Big[2\Big(1+\frac{\alpha_s}{3\pi}\Big)m_f\bar\psi_f\psi_f+\frac{\alpha_s}{12\pi}\Big(1+\frac{7}{6}\frac{\alpha_s}{\pi}\Big)G^a_{\alpha\beta}G^a_{\alpha\beta}\Big]\,.\end{aligned} \tag{5.91}$$

Interpreting the gluonic operator in terms of the (renormalization group invariant) trace anomaly $\theta(x)=\frac{2\beta(g)}{g}\mathcal{L}_\mathrm{g}$, where $\mathcal{L}_\mathrm{g}=\frac{1}{4}G^a_{\alpha\beta}G^a_{\alpha\beta}$ is the gluonic Lagrangian density and $\beta(g)=\mu\frac{\partial g}{\partial\mu}=-g^3(b_0+b_1g^2+...)$ the QCD beta function[7], we rewrite

$$\frac{\alpha_s}{12\pi}\Big(1+\frac{7}{6}\frac{\alpha_s}{\pi}\Big)G^a_{\alpha\beta}(x)G^a_{\alpha\beta}(x)=\frac{-1}{24\pi^2b_0}\left(1+g^2\big(\tfrac{7}{24\pi^2}-\tfrac{b_1}{b_0}\big)+\mathrm{O}(g^4)\right)\theta(x)\,. \tag{5.92}$$

Thereby we arrive at the following prediction for the asymptotic large-k^2 behaviour of the four-point amplitude

$$\begin{aligned}&\int\frac{d\Omega_k}{2\pi^2}\left\langle\int d^4x\int d^4y\, e^{ik(x-y)}\,V^\mathrm{em}_\mu(x)V^\mathrm{em}_\mu(y)V^{(1)}_\sigma(z)V^{(2)}_\lambda(0)\right\rangle \\ &\overset{k^2\to\infty}{=}\frac{3}{k^2}\sum_f Q_f^2\Big[2\Big(1+\frac{\alpha_s}{3\pi}\Big)m_f\left\langle\int d^4x\,\bar\psi_f\psi_f V^{(1)}_\sigma(z)V^{(2)}_\lambda(0)\right\rangle \\ &\qquad-\frac{1}{24\pi^2b_0}\left(1+g^2\big(\tfrac{7}{24\pi^2}-\tfrac{b_1}{b_0}\big)\right)\left\langle\int d^4x\,\theta(x)V^{(1)}_\sigma(z)V^{(2)}_\lambda(0)\right\rangle\Big]\,,\end{aligned} \tag{5.93}$$

where $Q_f=\{2/3,-1/3,\dots\}$ are the quark electric charges. At this point, we keep the currents $V^{(1)}_\sigma(z)$ and $V^{(2)}_\lambda(0)$ unspecified, in particular in their flavour structure.

The effect of inserting the mass operator into a correlation function is to differentiate the latter with respect to the quark mass,

$$\left\langle A\int d^4x\, m\bar\psi_x\psi_x\right\rangle=-m\frac{\partial}{\partial m}\langle A\rangle\,, \tag{5.94}$$

while the effect of the trace anomaly on a renormalization-group invariant correlation function of mass-dimension n is to differentiate with respect to all scales on which the correlation function depends,

$$\left\langle A(y,z,...,m_1,m_2,...)\int d^4x\,\theta(x)\right\rangle=\Big(-n-y_\nu\frac{\partial}{\partial y_\nu}-z_\nu\frac{\partial}{\partial z_\nu}-\dots+\sum_j m_j\frac{\partial}{\partial m_j}\Big)\langle A(y,z,...)\rangle\,, \tag{5.95}$$

[6] As we shall see explicitly in the following subsection, the leading term $(6/k^2)m_f\bar\psi_f\psi_f$ also applies to the QED case. The other displayed terms are for the gauge group SU(3) and do not depend on the number of quark flavors n_f. The leading coefficient of $m_f\bar\psi_f\psi_f$ and the leading coefficient of $G^a_{\alpha\beta}G^a_{\alpha\beta}$ are consistent with the calculation of [348].

[7] In these conventions, $b_0=\frac{1}{(4\pi)^2}(11-\frac{2}{3}n_f)$ and $b_1=\frac{1}{(4\pi)^4}(102-\frac{38}{3}n_f)$.

where y and z are space-time coordinates. We now set $V_\sigma^{(1)}(z) = V_\sigma^{\rm em}(z)$ and $V_\lambda^{(2)}(0) = V_\lambda^{\rm em}(0)$. Let $H_{\lambda\sigma}(z)$ be the kernel yielding the leading-order subtracted VP when integrated over with the correlator $e^2\left\langle V_\sigma^{\rm em}(z)V_\lambda^{\rm em}(0)\right\rangle$ (see Eqs. 5.135 and 5.136 below). Acting with the linear operator

$$-\frac{e^4}{2}\int\frac{d^4k}{(2\pi)^4}\left[\frac{1}{k^2}\right]_\Lambda\int d^4z\,H_{\lambda\sigma}(z)\,, \tag{5.96}$$

on both sides of Eq. (5.93), we conclude that the asymptotic large-Λ behaviour of the four-point amplitude contribution to the fourth-order VP is given by

$$\begin{aligned}\overline{\Pi}_{\rm 4pt}(Q^2,\Lambda)\overset{\Lambda\to\infty}{=}\frac{3e^2}{8\pi^2}\sum_f Q_f^2\Bigg[&\left(\log\left(\frac{\Lambda}{\mu_{\rm IR}}\right)+\frac{1}{24\pi^2 b_0}\log\left(\frac{\alpha_s(\mu_{\rm IR})}{\alpha_s(\Lambda)}\right)\right)m_f\frac{\partial}{\partial m_f}\\ &+\frac{1}{48\pi^2 b_0}\left(\log\left(\frac{\Lambda}{\mu_{\rm IR}}\right)+\frac{1}{2b_0}\left(\tfrac{7}{24\pi^2}-\tfrac{b_1}{b_0}\right)\log\left(\tfrac{\alpha_s(\mu_{\rm IR})}{\alpha_s(\Lambda)}\right)\right)\left(2q^2\tfrac{\partial}{\partial q^2}+\textstyle\sum_{f'}m_{f'}\tfrac{\partial}{\partial m_{f'}}\right)\Bigg]\overline{\Pi}_{e^2}(Q^2).\end{aligned} \tag{5.97}$$

5.5.1 Explicit OPE calculation at leading order

Consider then the OPE of two vector currents at leading order,

$$\bar\psi_x\gamma_\mu\psi_x\,\bar\psi_y\gamma_\nu\psi_y=\bar\psi_x\gamma_\mu S(x-y)\gamma_\nu\psi_y+\bar\psi_y\gamma_\nu S(y-x)\gamma_\mu\psi_x, \tag{5.98}$$

with $S(x)$ the position-space fermion propagator, which is given by

$$S(x)=\frac{m^2}{4\pi^2|x|}\left[\not{x}\frac{K_2(m|x|)}{|x|}+K_1(m|x|)\right], \tag{5.99}$$

$$S(x\to 0)=\frac{1}{2\pi^2x^4}\left[\not{x}+\frac{1}{2}mx^2+O\left(|x|^3\log m|x|\right)\right]. \tag{5.100}$$

If points x and y are far from the origin and z, then the expansion of the fields at y around the point x yields the following expression for the symmetric part of two currents:

$$\begin{aligned}\bar\psi_x\gamma_{\{\mu}\psi_x\,\bar\psi_y\gamma_{\nu\}}\psi_y=&\frac{1}{2\pi^2|x-y|^4}\Bigg\{m(x-y)^2\delta_{\mu\nu}\bar\psi_x\psi_x\\ &-(x-y)^\beta\left[(x-y)_\mu O_{\nu\beta}(x)+(x-y)_\nu O_{\mu\beta}(x)-\delta_{\mu\nu}(x-y)^\alpha O_{\alpha\beta}(x)\right]\Bigg\},\end{aligned} \tag{5.101}$$

where the operator $O_{\mu\nu}(x)$ was introduced as

$$O_{\mu\nu}(x)=\bar\psi_x\gamma_\mu(\overrightarrow{\partial}_\nu-\overleftarrow{\partial_\nu})\psi_x. \tag{5.102}$$

The Fourier-transformed expression (5.101), being subsequently contracted with $\delta_{\mu\nu}$, reads

$$\delta_{\mu\nu}\int d^4y e^{i(x-y)}\bar\psi_x\gamma_{\{\mu}\psi_x\,\bar\psi_y\gamma_{\nu\}}\psi_y=\frac{8m}{k^2}\bar\psi_x\psi_x+\frac{2}{k^2}O_{\alpha\beta}(\delta_{\alpha\beta}-2k_\alpha k_\beta). \tag{5.103}$$

Eventually, after averaging over direction of k and rearranging the terms, one finds

$$\int \frac{d\Omega_k}{2\pi^2} \int d^4y\, e^{ik(x-y)}\, \bar{\psi}_x \gamma_\mu \psi_x\, \bar{\psi}_y \gamma_\mu \psi_y = \frac{6m}{k^2} \bar{\psi}_x \psi_x + \frac{2}{k^2} \left(\tfrac{1}{2} \bar{\psi}_x \gamma_\alpha (\overrightarrow{\partial}_\alpha - \overleftarrow{\partial}_\alpha) \psi_x + m \bar{\psi}_x \psi_x \right). \tag{5.104}$$

We have already noted the effect of the mass-operator insertion in terms of differentiating the correlation function with respect to the quark mass. To understand the effect of inserting the 'equation of motion' (EOM) operator appearing in brackets in Eq. (5.104), imagine multiplying the Euclidean quark action by λ, $S_E(\lambda) = \lambda \bar{\psi}(\not{D} + m)\psi$. In the Euclidean path integral, we can take expectation values $\langle A \rangle_\lambda$ using $\exp(-S_E(\lambda))$ as weight: it simply means that each quark propagator contains an additional $1/\lambda$ factor. Thus, if computing $\langle A \rangle_\lambda$ involves n_p propagators,

$$-\frac{\partial}{\partial \lambda} \langle A \rangle_\lambda \Big|_{\lambda=1} = n_p\ \langle A \rangle_{\lambda=1}\,. \tag{5.105}$$

On the other hand, the same derivative can be expressed as

$$-\frac{\partial}{\partial \lambda} \langle A \rangle_\lambda \Big|_{\lambda=1} = \left\langle A \int d^4x\, (\tfrac{1}{2} \bar{\psi}_x \gamma_\alpha (\overrightarrow{\partial}_\alpha - \overleftarrow{\partial}_\alpha) \psi_x + m \bar{\psi}_x \psi_x) \right\rangle. \tag{5.106}$$

Thus the insertion of the EOM operator simply multiplies the observable with the number of propagators n_p needed to compute it. Thus the leading contribution of x and y being close together in the vector four-point function ($V_\mu \equiv \bar{\psi} \gamma_\mu \psi$) is

$$\int \frac{d\Omega_k}{2\pi^2} \left\langle \int d^4x \int d^4y\, e^{ik(x-y)}\, V_\mu(x) V_\mu(y) V_\sigma(z) V_\lambda(0) \right\rangle \overset{k^2 \to \infty}{=} \left(-\frac{6}{k^2} m \frac{\partial}{\partial m} + \frac{4}{k^2} \right) \langle V_\sigma(z) V_\lambda(0) \rangle\,. \tag{5.107}$$

We now move to the case of x and y simultaneously being in close vicinity of a third current at position z. In terms of Wick contractions, the relevant case is where the connecting point is z, i.e. there are propagators $(y \to z \to x)$ or $(x \to z \to y)$. The cases where the connecting point is x or y do not contribute to the $\mathrm{O}(1/k^2)$ behaviour, given that the corresponding integrals of the type

$$\int d^4x \int d^4y e^{ik(x-y)} \frac{(x-y)_\alpha}{|x-y|^4} \frac{(y-z)_\alpha}{|y-z|^4} \tag{5.108}$$

vanish due to the symmetry arguments. A straightforward if somewhat tedious calculation then gives the following expression for the Fourier-transformed $\delta_{\mu\nu}$-contracted expansion of three currents

$$\int d^4x \int d^4y e^{ik(x-y)} \bar{\psi}_x \gamma_\mu \psi_x \bar{\psi}_z \gamma_\sigma \psi_z \bar{\psi}_y \gamma_\mu \psi_y = \frac{4k_\sigma}{|k|^4} \bar{\psi}_z \not{k} \psi_z + \frac{4}{|k|^4} \left(k_\sigma k_\lambda - \delta_{\sigma\lambda} k^2 \right) \bar{\psi}_z \gamma_\lambda \psi_z \tag{5.109}$$

Finally, averaging over k yields

$$\int \frac{d\Omega_k}{2\pi^2} \int d^4x \int d^4y \, e^{ik(x-y)} \, \bar{\psi}_x \gamma_\mu \psi_x \, \bar{\psi}_z \gamma_\sigma \psi_z \, \bar{\psi}_y \gamma_\mu \psi_y \overset{k^2\to\infty}{=} -\frac{2}{k^2} \bar{\psi}_z \gamma_\sigma \psi_z . \tag{5.110}$$

The same contribution appears when (x, y) are close to the origin, thus doubling this contribution in the four-point function of the vector current.

Altogether, from Eqs. (5.107) and (5.110), we then find in leading order of the OPE

$$\int \frac{d\Omega_k}{2\pi^2} \left\langle \int d^4x \int d^4y \, e^{ik(x-y)} \, V_\mu(x) V_\mu(y) V_\sigma(z) V_\lambda(0) \right\rangle \overset{k^2\to\infty}{=} -\frac{6}{k^2} m \frac{\partial}{\partial m} \langle V_\sigma(z) V_\lambda(0) \rangle . \tag{5.111}$$

The terms not leading to mass-derivatives cancel, and only the mass-derivative of the vector two-point function determines the large-k^2 asymptotics of the forward LbL amplitude. Thus we have reproduced the very first term in Eq. (5.93). Acting on both sides of Eq. (5.111) with Eq. (5.96) leads to the first term in Eq. (5.97) (with $n_f = 1$ and $Q_f = 1$).

The leading-order calculation above is equally valid for the QED as for the QCD four-point function. In the pure QED context, one easily verifies with the help of Eqs. (5.19) and (5.20) that the textbook O(e^2) mass counterterm removes the $\log(\Lambda)$ term in $\overline{\Pi}_{\text{4pt}}$ predicted by the OPE. We have thus verified Eq. (5.97) in the pure QED case: given that $\overline{\Pi}_{e^2}(Q^2)$ given in Eq. (5.21) only depends on Q^2/m^2, the effect of inserting the trace anomaly, proportional to $(2Q^2 \frac{\partial}{\partial Q^2} + m \frac{\partial}{\partial m})$, would cancel.

5.5.2 Cottingham-like formula for the isovector contribution to HVP

Starting from Eq. (5.93) with

$$V_\rho^{(1)} = V_\rho^{(2)} := \frac{1}{2} (\bar{u} \gamma_\rho u - \bar{d} \gamma_\rho d) \tag{5.112}$$

the isovector component of the e.m. current, the same steps lead to the analogue of Eq. (5.97), with $\overline{\Pi}_{e^2}$ now replaced by the isovector contribution $\overline{\Pi}^{33}_{e^2}(Q^2)$ to the leading HVP, and $\overline{\Pi}^{\gamma\gamma 33}_{\text{4pt}}(Q^2, \Lambda)$ the corresponding QED correction to that contribution. The same steps once again could be taken with the charged isovector currents

$$V_\rho^{(1)} := \frac{1}{\sqrt{2}} \, \bar{u} \gamma_\rho d, \qquad V_\rho^{(2)} := \frac{1}{\sqrt{2}} \, \bar{d} \gamma_\rho u, \tag{5.113}$$

which leads to the quantities $\overline{\Pi}^{-+}_{e^2}(Q^2)$ and its QED correction $\overline{\Pi}^{\gamma\gamma -+}_{\text{4pt}}(Q^2, \Lambda)$. Taking the difference of Eq. (5.93) obtained once with the choice of currents from Eq. (5.112) and once with the choice of Eq. (5.113), one finds that all terms on the right-hand side cancel. This is clear for the contribution from the insertion of isoscalar operators, whose correlation function is identical with two members of the same isospin multiplet. For the isovector mass insertion $(\bar{u}u - \bar{d}d)$, G-parity ensures that this insertion vanishes separately in the neutral and in the charged isovector channel. In other words, all

counterterms from the action cancel in this difference[8], as has been noted in Ref. [349], which contains an exploratory lattice-QCD calculation of this quantity. However, care must be taken of the fact that, unlike the cases considered so far, the currents of Eq. (5.113) are not gauge invariant with respect to QED. Therefore this case requires further study. We note that, in the radiative corrections to the leptonic decay of a charged pion [350], the e.m. correction to a charged-current correlator represents one of several contributions.

Other flavor cases may be of interest, in particular the correlator between the isovector and the isoscalar components of the photon, which vanishes in isospin-symmetric QCD in the absence of quark electric charges. In this case, the action counterterms do not vanish altogether, though only the isovector mass insertion $(\bar{u}u - \bar{d}d)$ contributes in the analogue of Eq. (5.97).

5.5.3 Moving UV divergences into subtraction function

In the context of the dispersive representation of the Cottingham formula (5.17), it is interesting to determine whether the leading UV divergence, predicted by the OPE, is contained in the dispersive term, the subtraction function, or both. To answer this question, it worth considering the subtraction point

$$\bar{\nu} = \frac{1}{2}KQ. \tag{5.114}$$

If the euclidean four-vectors q_μ and k_μ have the following hyperspherical components

$$q_\mu = Q\begin{pmatrix}1\\0\\0\\0\end{pmatrix} \quad k_\mu = K\begin{pmatrix}\cos\phi\\ \sin\phi\cos\theta\\ \sin\phi\sin\theta\cos\varphi\\ \sin\phi\sin\theta\sin\varphi\end{pmatrix}, \quad \phi,\theta\in[0,\pi], \quad \varphi\in[0,2\pi], \tag{5.115}$$

then the aforementioned subtraction point corresponds to fixing the value of the angle ϕ between the temporal components of q_μ and k_μ to 60°. At this point, the dispersive term is suppressed due to the coefficient $(\nu^2 - 1/4K^2Q^2)$ (cf. Eq. (5.11)), which itself vanishes after the integration over x,

$$\int_0^1 dx\sqrt{1-x^2}\left(x^2 - \frac{1}{4}\right) = 0. \tag{5.116}$$

This effect was also discussed in the work by Gasser et al. [329] in context of the usual Cottingham formula.

Turning to the leading-order OPE contribution, one can point out that the Eqs. (5.103) and (5.109) contain terms either scalar in k_μ or of combination of two vectors $k_\alpha k_\beta$. For both these structures the averaging over all three angles ϕ, θ and φ is equivalent to averaging over two angles θ and φ while

[8] A very similar observation was already made in the case of the pion e.m. mass splitting in Ref. [120].

keeping the angle ϕ fixed to 60°. Indeed, in the coordinate system defined by Eq. (5.115) one obtains

$$\frac{\int_0^{2\pi} d\varphi \int_0^{\pi} d\theta \sin\theta \int_0^{\pi} d\phi \sin^2\phi k_\mu k_\nu}{\int_0^{2\pi} d\varphi \int_0^{\pi} d\theta \sin\theta \int_0^{\pi} d\phi \sin^2\phi} = \frac{\int_0^{2\pi} d\varphi \int_0^{\pi} d\theta \sin\theta k_\mu k_\nu}{\int_0^{2\pi} d\varphi \int_0^{\pi} d\theta \sin\theta}\bigg|_{\cos\phi=1/2} = K^2 \mathrm{diag}\left(\frac{1}{4}\right). \quad (5.117)$$

Therefore, the forward LbL amplitude taken at the energy given by Eq. (5.114), fully determines the UV behavior of the total result. For QED, this can be seen exactly from the series expansion at low Q^2 of the vacuum polarization, calculated from the LbL subtraction function at the point(5.114) via the Cottingham formula. Imposing the hard cut-off $\Lambda \to \infty$, one obtains

$$\begin{aligned}\Pi_{\mathrm{subtr}}(Q^2,\Lambda) =& \frac{\alpha_{\mathrm{em}}^2}{\pi^2}\left[-\frac{1}{2} + \frac{53}{270}\frac{Q^2}{m_\ell^2} - \frac{2167}{75600}\left(\frac{Q^2}{m_\ell^2}\right)^2 + \frac{2167}{441000}\left(\frac{Q^2}{m_\ell^2}\right)^3 + O\left(\frac{Q^8}{m_\ell^8}\right)\right] \\ & - \frac{\alpha_{\mathrm{em}}^2}{\pi^2}\log\frac{\Lambda}{m_\ell}\left[-\frac{1}{2} + \frac{1}{5}\frac{Q^2}{m_\ell^2} - \frac{3}{70}\left(\frac{Q^2}{m_\ell^2}\right)^2 + \frac{1}{105}\left(\frac{Q^2}{m_\ell^2}\right)^3 + O\left(\frac{Q^8}{m_\ell^8}\right)\right]. \quad (5.118)\end{aligned}$$

This result can be compared with Eq. (5.18) concluding that both expressions have the same divergent part.

It is also instructive to look at the vacuum polarization contributions stemming from the particular LbL helicity amplitudes via the Cottingham formula. The finite piece $\bar{\Delta}\Pi_{4\mathrm{pt}}$, which remains after removing the part $\Pi_{4\mathrm{pt}}^{x=1/2}$ that correspond to the LbL subtraction function at the considered subtraction point (5.114) from the full result of Cottingham formula, namely

$$\overline{\Delta}\Pi_{4\mathrm{pt}}(Q^2,\Lambda) = \Pi_{4\mathrm{pt}}(Q^2,\Lambda) - \Pi_{4\mathrm{pt}}^{x=1/2}(Q^2,\Lambda), \quad (5.119)$$

is of particular interest. It corresponds to applying the Cottingham formula for the dispersive part of the LbL amplitude. For QED, we obtain the following series terms at low Q^2:

$$\overline{\Delta}\Pi_{4\mathrm{pt}}^{TT}(Q^2,\Lambda) = \frac{1}{2}\frac{\alpha_{\mathrm{em}}^2}{\pi^2}\left[\frac{5}{1296}\frac{Q^2}{m_\ell^2} - \frac{19}{18144}\left(\frac{Q^2}{m_\ell^2}\right)^2 + \frac{12529}{47628000}\left(\frac{Q^2}{m_\ell^2}\right)^3 + O\left(\frac{Q^8}{m_\ell^8}\right)\right], \quad (5.120a)$$

$$\overline{\Delta}\Pi_{4\mathrm{pt}}^{LT}(Q^2,\Lambda) = \frac{\alpha_{\mathrm{em}}^2}{\pi^2}\left[\frac{31}{226800}\left(\frac{Q^2}{m_\ell^2}\right)^2 - \frac{41}{793800}\left(\frac{Q^2}{m_\ell^2}\right)^3 + O\left(\frac{Q^8}{m_\ell^8}\right)\right], \quad (5.120b)$$

$$\overline{\Delta}\Pi_{4\mathrm{pt}}^{TL}(Q^2,\Lambda) = \frac{\alpha_{\mathrm{em}}^2}{\pi^2}\left[\frac{1}{2160}\frac{Q^2}{m_\ell^2} - \frac{1}{15120}\left(\frac{Q^2}{m_\ell^2}\right)^2 + \frac{13}{793800}\left(\frac{Q^2}{m_\ell^2}\right)^3 + O\left(\frac{Q^8}{m_\ell^8}\right)\right], \quad (5.120c)$$

$$\overline{\Delta}\Pi_{4\mathrm{pt}}^{LL}(Q^2,\Lambda) = \frac{\alpha_{\mathrm{em}}^2}{\pi^2}\left[\frac{1}{25200}\left(\frac{Q^2}{m_\ell^2}\right)^2 - \frac{1}{48600}\left(\frac{Q^2}{m_\ell^2}\right)^3 + O\left(\frac{Q^8}{m_\ell^8}\right)\right]. \quad (5.120d)$$

Here the subscripts TT, LT, TL and LL refer to the particular LbL helicity amplitude, which the vacuum polarization was obtained from. From Eqs. (5.120) one can see that $\Pi_{4\text{pt}}^{x=1/2}$ fully cancels the $\Pi_{4\text{pt}}(0)$-part in all cases of photon polarizations. Moreover, for $\Pi_{4\text{pt}}^{LT}$ and $\Pi_{4\text{pt}}^{LL}$, the cancellation of the finite parts occurs for the terms of order Q^2. The same results can be obtained in sQED.

In conclusion, we would like to outline two attractive features of using the subtraction point (5.114):

1. The subtraction of $\Pi_{4\text{pt}}^{x=1/2}$ from the full Cottingham formula result renders it finite without invoking any additional counterterms, which is proven by the leading-order OPE calculation. Thus, this procedure should be associated with a form of physical renormalization, albeit distinct from the on-shell scheme.

2. It makes possible to completely isolate the full UV-divergence within the LbL subtraction function. This separation can be particularly important for improving the stability of numerical calculations.

5.6 The π^0-exchange contribution

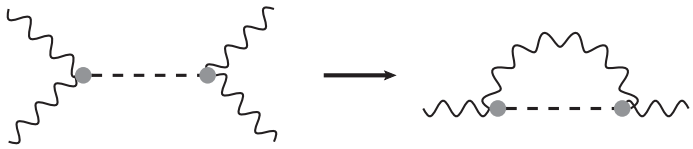

Fig. 5.6 π^0-exchange contribution to the VP via Cottingham-like formula.

In this section, the form of the π^0-exchange contribution to the forward HLbL amplitude $\mathcal{M}$, cf. Fig. 5.6, is presented, since it is the longest-range contribution. Working in Euclidean space, we define the Fourier transform of the four-point function of this current as in Eq. (5.89) and the forward amplitude is obtained as in Eq. (5.90). The O(e^4) contribution to the polarization tensor with a regularized internal photon propagator then reads

$$\Pi_{4\text{pt};\mu\lambda}(q,\Lambda) = -\frac{e^4}{2}\int \frac{d^4k}{(2\pi)^4}\left[\frac{1}{k^2}\right]_\Lambda \Pi_{\mu\sigma\sigma\lambda}(q,k,-k) = (q_\mu q_\lambda - \delta_{\mu\lambda}q^2)\,\Pi_{4\text{pt}}(q^2,\Lambda). \tag{5.121}$$

For the π^0-exchange contribution, proportional to the square of its transition form factor $\mathcal{F}$, we have

$$\begin{aligned}\Pi_{\mu\sigma\sigma\lambda}(q,k,-k) = -\epsilon_{\mu\sigma\alpha\beta}\,\epsilon_{\sigma\lambda\gamma\delta}\,q_\alpha\,k_\beta\,k_\gamma\,q_\delta\,\mathcal{F}(-q^2,-k^2)^2 \\ \times\left[\frac{1}{(q+k)^2+m_\pi^2}+\frac{1}{(q-k)^2+m_\pi^2}\right].\end{aligned} \tag{5.122}$$

We perform the angular integration by using the Gegenbauer polynomial expansion of propagators (see for instance [124]), and the final expression is

$$\Pi_{4\mathrm{pt}}(q^2,\Lambda) = \frac{-e^4}{16\pi^2|q|}\int_0^\infty d|k|\,|k|^4\Big[\frac{1}{k^2}\Big]_\Lambda \mathcal{F}(-q^2,-k^2)^2\, Z^{m_\pi}_{|q|,|k|}\Big(1-\frac{1}{3}(Z^{m_\pi}_{|q|,|k|})^2\Big), \tag{5.123}$$

$$Z^m_{|q|,|k|} = \frac{1}{2|q||k|}\Big(q^2+k^2+m^2-\sqrt{(q^2+k^2+m^2)^2-4q^2k^2}\Big). \tag{5.124}$$

This expression, once inserted into Eq. (5.37), can be viewed as the VP analogue of the Jegerlehner-Nyffeler relation for the π^0 contribution to HLbL scattering in the muon $(g-2)$ [351, 352]. In the present case, the kinematics are simpler, and correspondingly $\Delta a_\mu^{\pi^0}$ takes the form of a two- rather than three-dimensional integral for a yet to be specified transition form factor $\mathcal{F}$. The unsubtracted VP is UV-finite for fixed Λ, while the subtracted VP $\overline{\Pi}_{4\mathrm{pt}}(q^2,\Lambda)$ remains UV-finite for $\Lambda\to\infty$, unlike in the full QCD case, as we have seen in section 5.5, when short-distance contributions from quarks are taken into account.

As an example, for the VMD parameterization of the transition form factor,

$$\mathcal{F}(-q_1^2,-q_2^2) = \frac{\mathcal{F}(0,0)}{(1+q_1^2/m_V^2)(1+q_2^2/m_V^2)}, \tag{5.125}$$

one obtains, near the chiral limit, the singular behaviour

$$\lim_{\Lambda\to\infty}\frac{\partial\Pi_{4\mathrm{pt}}}{\partial Q^2}(Q^2=0,\Lambda) = \frac{\alpha_{\mathrm{em}}^2}{6}\,\mathcal{F}(0,0)^2\,\Big[5+\log\Big(\frac{m_V^2}{m_\pi^2}\Big)+\mathrm{O}(m_\pi^2/m_V^2)\Big]. \tag{5.126}$$

For a pion mass which is still heavy relative to the muon mass, the contribution reads $\Delta a_\mu \simeq \frac{\alpha_{\mathrm{em}} m_\mu^2}{3\pi}\,\Pi'_{4\mathrm{pt}}(0)$. Parametrically, this contribution behaves similarly to the π^0 contribution to the HLbL contribution to a_μ [353, 325], except that in the latter case the chiral logarithm enters quadratically.

Numerically, with $\mathcal{F}(0,0) = (4\pi^2 f_\pi)^{-1}$ and $f_\pi = 92.4\,\mathrm{MeV}$, $m_V = 0.77549\,\mathrm{GeV}$, and the physical π^0 mass one obtains from Eq. (5.123) with the QED kernel (5.37) the following contribution to a_μ,

$$\Delta a_\mu^{\pi^0} = 0.370\times 10^{-10}. \tag{5.127}$$

This result agrees with the value given in [325]. We note that the result is more than an order of magnitude smaller than the contribution of the $e^+e^-\to\pi^0\gamma$ channel in the dispersive representation of a_μ^{VP} [9], however the quantity $\Delta a_\mu^{\pi^0}$ computed here is not precisely the same. We finally remark that the master relation Eq. (5.123) applies equally well to the other pseudoscalar mesons, notably the η and η'.

[9]The vastly different size of the result of Ref. [325] as compared to the $e^+e^-\to\pi^0\gamma$ channel contribution was pointed out to one of us in 2016 by Andreas Nyffeler. See also the recent Ref. [354], appendix D.

5.7 Electromagnetic correction to the HVP in lattice QCD: a computational strategy

The general structure of Eq. (5.2) also applies to the calculation of the isospin-breaking contribution to the leading HVP $\Pi_{e^2}(Q^2)$ (from QED and strong isospin breaking) in lattice regularization, in which case the inverse lattice spacing $1/a$ plays the role of the UV cutoff. To be more specific, we note that lattice QCD admits $(N_\mathrm{f}+1)$ bare parameters, i.e., the SU(3) gauge coupling and the N_f quark masses, which we assemble into a vector $\vec{\mathrm{b}}^{\,\mathrm{lat}}$. When correcting the isosymmetric theory for isospin breaking, the bare parameters must be readjusted. The shifts $\delta\mathrm{b}_i^{\mathrm{lat}}$ in the bare parameters are determined by requiring that the theory with isospin breaking reproduces $(N_\mathrm{f}+1)$ suitable experimental observables [120]; typically, the masses of hadrons which are stable in the absence of weak interactions,

$$M_h^{\mathrm{phys}} = M_h^{\mathrm{iso}} + M_{4\mathrm{pt},h}^{\mathrm{lat}}(a;0) + \sum_{i=1}^{N_\mathrm{f}+1} J_h^{\mathrm{lat}\,(i)}\ \delta\mathrm{b}_i^{\mathrm{lat}} \qquad (h=1,\ldots,N_\mathrm{f}+1), \tag{5.128}$$

where M_h^{phys} is the experimental hadron mass, M_h^{iso} is its value at the chosen expansion point in isosymmetric QCD, $M_{4\mathrm{pt},h}^{\mathrm{lat}}(a;M_\gamma)$ is the $\mathrm{O}(e^2)$ e.m. contribution computed with (in general) a photon mass M_γ and $J_h^{\mathrm{lat}\,(i)} \equiv \partial M_h/\partial \mathrm{b}_i^{\mathrm{lat}} = \left\langle h|O_{\mathrm{lat}}^{(i)}|h\right\rangle$ is given by the forward matrix element of the operator conjugate to parameter $\mathrm{b}_i^{\mathrm{lat}}$. Thus, given a lattice calculation of $\vec{M}^{\mathrm{iso}}$, $\vec{M}_{4\mathrm{pt}}^{\mathrm{lat}}(a;0)$ and the matrix J^{lat}, the vector $\delta\vec{\mathrm{b}}^{\,\mathrm{lat}}$ is obtained by solving a linear system.

We are now in a position to write the lattice-regularization analogue of Eq. (5.2) for the subtracted HVP as

$$\Delta\overline{\Pi}(Q^2) = \lim_{a\to 0}\left(\overline{\Pi}_{4\mathrm{pt}}^{\mathrm{lat}}(Q^2,a;0) + \overline{\Pi}_{\mathrm{ct}}^{\mathrm{lat}}(Q^2,a)\right), \tag{5.129}$$

where the counterterm has the form

$$\overline{\Pi}_{\mathrm{ct}}^{\mathrm{lat}}(Q^2,a) = \sum_{i=1}^{N_\mathrm{f}+1} \delta\mathrm{b}_i^{\mathrm{lat}}\frac{\partial}{\partial \mathrm{b}_i^{\mathrm{lat}}}\overline{\Pi}_{e^2}(Q^2), \tag{5.130}$$

and $\overline{\Pi}_{4\mathrm{pt}}^{\mathrm{lat}}(Q^2,a;M_\gamma)$ denotes the e.m. four-point function contribution to the HVP, computed (in general) with an internal photon of mass M_γ. Massive QED has previously been used to control photon zero modes in finite volume, with the physical limit $M_\gamma \to 0$ taken after extrapolating to infinite volume [314, 322, 355, 356]; our approach, by contrast, is to keep $\Lambda = M_\gamma$ fixed and use it for separating long-range contributions from UV-divergent ones. Based on the identity of Eq. (5.1) for the photon propagator with a fixed $\Lambda \sim 400$ MeV, we propose to perform the following decompositions[10],

$$\overline{\Pi}_{4\mathrm{pt}}^{\mathrm{lat}}(Q^2,a;0) = \overline{\Pi}_{4\mathrm{pt}}(Q^2,\Lambda=M_\gamma) + \overline{\Pi}_{4\mathrm{pt}}^{\mathrm{lat}}(Q^2,a;M_\gamma), \tag{5.131}$$

$$\vec{M}_{4\mathrm{pt}}^{\mathrm{lat}}(a;0) = \vec{M}_{4\mathrm{pt}}(\Lambda=M_\gamma) + \vec{M}_{4\mathrm{pt}}^{\mathrm{lat}}(a;M_\gamma). \tag{5.132}$$

[10] Eq. (5.131) and Eq. (5.132) hold up to corrections suppressed by one or two powers of the lattice spacing.

Up to the subtraction at $Q^2 = 0$, the function $\overline{\Pi}_{4\text{pt}}(Q^2, \Lambda)$ is the same as in Eq. (5.2). Since Λ plays the role of the Pauli-Villars UV regularization scale, the continuum limit $a \to 0$ can be taken for this quantity. Similarly, $\vec{M}_{4\text{pt}}(\Lambda)$ represents the e.m. hadron-mass corrections computed with the Pauli-Villars regulated photon propagator. The continuum limit can also be taken in this case, since the same OPE, as reviewed in section 5.5, determines the asymptotic behaviour of the forward Compton amplitude on hadron h [348].

Given a choice of M_γ, each term on the right-hand side of Eq. (5.131) is affected by rather different systematics on the lattice and is meant to be evaluated separately. The same observation applies to the two terms on the right-hand side of Eq. (5.132). The UV-finite part $\overline{\Pi}_{4\text{pt}}(Q^2, \Lambda)$ of Eq. (5.131) receives long-distance contributions due to the long-range photon propagator. A coordinate-space representation free of power-law finite-volume effects is presented below in subsection 5.7.1. The result can be compared to an evaluation based on our Cottingham-like formula, Eq. (5.11) and Eq. (5.15). For the second term of Eq. (5.131), one possible expression in the time-momentum representation [336] is

$$\overline{\Pi}^{\text{lat}}_{4\text{pt}}(Q^2, a; M_\gamma) = -\frac{e^4}{2}\frac{a^{12}}{L^3 L_0}\sum_{z_0>0}\left(z_0^2 - \frac{4}{Q^2}\sin^2\frac{|Q|z_0}{2}\right)\sum_k G^{\text{lat}}_{\mu\nu}(k) \tag{5.133}$$
$$\left\langle \sum_{x,y} e^{ik(x-y)} \sum_{\vec{z}} V^{\text{em}}_\sigma(z) V^{\text{em}}_\nu(y) V^{\text{em}}_\mu(x) V^{\text{em}}_\lambda(0) + \text{ tadpoles} \right\rangle,$$

where $V^{\text{em}}_\nu(y)$ and $V^{\text{em}}_\mu(x)$ are discretized as conserved currents and the simplest form of the photon propagator (in Feynman gauge) is

$$G^{\text{lat}}_{\mu\nu}(k) = \frac{\delta_{\mu\nu}}{\hat{k}^2 + M_\gamma^2}, \qquad \hat{k}^2 \equiv \tfrac{4}{a^2}\sum_{\mu=0}^{3}\sin^2\tfrac{ak_\mu}{2}, \tag{5.134}$$

and the tadpole terms ensure the transversality of the four-point function with respect to contracting it with $\hat{k}_\mu$ or $\hat{k}_\nu$. Similarly, $\vec{M}^{\text{lat}}_{4\text{pt}}(a; M_\gamma)$ can be determined by well-established methods where the (now massive) photon is treated as part of the finite-volume lattice field theory.

We now briefly discuss how to compute the hadronic mass shifts $\vec{M}_{4\text{pt}}(\Lambda)$ with a long-range, but Pauli-Villars regulated photon propagator. As for $\overline{\Pi}_{4\text{pt}}(Q^2, \Lambda)$, it is possible to avoid power-law effects in the volume [357] by using coordinate-space methods and, additionally, by explicitly correcting the elastic contribution of the forward Compton amplitude for finite-volume effects. As a slight variation to the concrete proposal in [357], this correction could be done with the help of a separate calculation of the e.m. form factor(s) of the hadron whose mass correction is being computed. These methods could also be applied to the difference of $M_{4\text{pt},h}(\Lambda)$ between proton and neutron, a quantity that could be compared to predictions based on the original Cottingham formula.

We remark that the currently most frequently used formulation of lattice QCD coupled to photons consists in removing the photon zero-mode in every time-slice [358]. The corresponding finite-size effects on the HVP have recently been investigated and found to be parametrically of order $1/L^3$,

and numerically small in the framework of scalar QED [342]. Another recent investigation provides a systematic analysis of various finite-size effects beyond the pointlike approximation of hadrons, in particular of pseudoscalar mesons masses [359] (see also references therein). As an alternative method, first results (primarily on hadron masses) based on simulating QCD+QED with C^* boundary conditions have recently been presented [360].

In conclusion, while the numerical practicability of the presented method remains to be demonstrated, we have established that it is possible to avoid power-law finite-volume effects altogether in computing $\Delta\Pi(Q^2)$ on the lattice. How large the discretization errors on this quantity are at finite lattice spacing with the method proposed above will need to be explored in practice. Here we remark that the Pauli-Villars regularization of the photon propagator is only one of many posssible choices. For instance, with the double Pauli-Villars regularization (5.43) of the photon propagator, the same strategy as described above can be carried out, now with the expression in brackets in (5.43) falling off as fast as $1/k^6$ at large k^2.

5.7.1 Coordinate-space representation of $\overline{\Pi}_{4\text{pt}}(Q^2,\Lambda)$ free of power-law finite-size effects

A Euclidean coordinate-space expression for the subtracted HVP is

$$\overline{\Pi}(Q^2) = \int_z H_{\lambda\sigma}(z)\,\tilde{\Pi}_{\sigma\lambda}(z)\,, \tag{5.135}$$

where the leading contribution is $\tilde{\Pi}_{e^2;\sigma\lambda}(z) = e^2\left\langle V^{\text{em}}_\sigma(z)\,V^{\text{em}}_\lambda(0)\right\rangle$, the relevant ($Q$-dependent) coordinate-space kernel $H_{\lambda\sigma}(z)$ was derived in [361] (Sect. II.B.2) and we have abridged $\int_z \equiv \int d^4z$. Expanding a QCD correlation function to second order in the e.m. coupling leads to the insertion of the product of two e.m. currents, whose relative positions are weighted by the internal photon propagator. Thus, using Feynman gauge for the latter, we arrive at the expression

$$\overline{\Pi}_{4\text{pt}}(Q^2,\Lambda) = -\frac{e^4}{2}\delta_{\mu\nu}\int_{x,y,z} H_{\lambda\sigma}(z)\Big[G_0(y-x)\Big]_\Lambda\left\langle V^{\text{em}}_\sigma(z)V^{\text{em}}_\nu(y)V^{\text{em}}_\mu(x)V^{\text{em}}_\lambda(0)\right\rangle, \tag{5.136}$$

for the regulated contribution to the subtracted HVP. The Pauli-Villars regulated photon propagator in position space reads

$$\Big[G_0(x)\Big]_\Lambda = \frac{1}{4\pi^2x^2} - \frac{\Lambda K_1(\Lambda|x|)}{4\pi^2|x|}, \tag{5.137}$$

which is only logarithmically divergent for $x^2 \to 0$. Here K_1 is the modified Bessel function of the second kind. We note a close analogy of expression (5.136) with the master relation used for the HLbL contribution to the AMM in Refs. [362, 146, 147]. Similarly, $\varkappa_\mu^{\text{VP}}$ can be obtained from Eq. (5.136) by replacing the kernel $H_{\lambda\sigma}$ by the appropriate one given in Sect. II.B.3 of Ref. [361]. The main feature of our proposal is that no IR-regularization of the photon propagator is needed. Thus finite-size effects are expected to be on the order of $\exp(-m_\pi L/2)$, as in the case of the HLbL contribution [362].

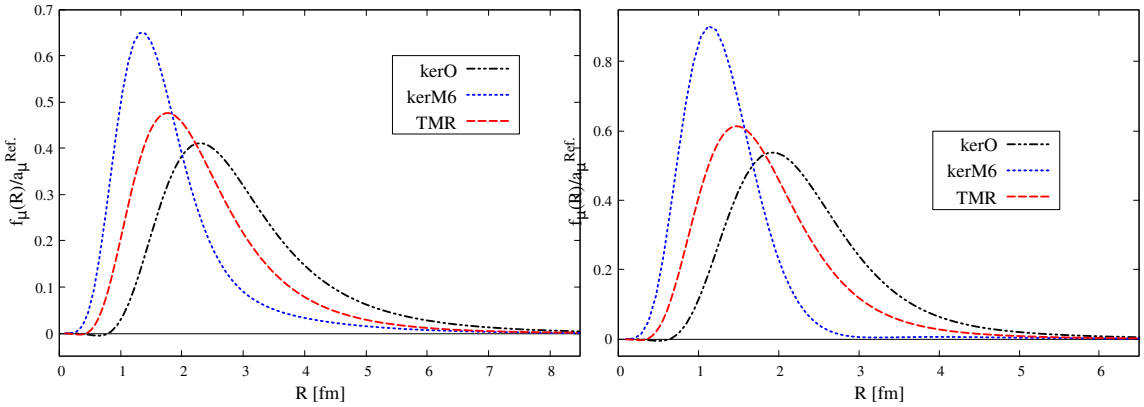

Fig. 5.7 Comparison between the normalized integrands from different representations of the π^0-exchange contribution to $\varkappa_\mu$ for $\Lambda = 3m_\mu$ (left panel) and $\Lambda = 200m_\mu$ (right panel), where 'kerO' is obtained with the original coordinate-space kernel, 'kerM6' with improved kernel (see [334] for details). The integrands are normalized such that the area under the curves equals unity. Figure is taken from [334].

5.7.2 Computing $\varkappa_\mu^{\mathrm{HVP}}$: π^0-exchange contribution to the coordinate-space integrand

By Fourier-transforming the polarization tensor associated with Eq. (5.123) (see Eq. (5.121)), one obtains the $\mathrm{O}(e^4)$ contribution $\tilde{\Pi}_{4\mathrm{pt};\sigma\lambda}(z,\Lambda)$. After insertion into Eq. (5.135) and contraction of the indices, the integrand is a scalar function of $|z|$. We illustrate the integrand of this last scalar integral in the following. Alternatively to the proposed position-space approach, one can reach the widely used time-momentum representation (TMR) [336] by Fourier-transforming the polarization tensor at vanishing spatial momentum only with respect to q_0.

Choosing the same parameters as in section 5.6 for the VMD parameterisation of the transition form factor, we obtain the integrands as functions of $R \equiv |z|$ (and $R \equiv z_0$ for the TMR case) as shown in Fig. 5.7, where the results with the original [361] position-space kernel (kerO) and the TMR are compared, calculated in the continuum and infinite volume at two different Pauli-Villars masses $\Lambda = 3\,m_\mu$ and $200\,m_\mu$; recall that the π^0-exchange contribution by itself remains finite as $\Lambda \to \infty$. Both integrands are rather long-range, an observation which implies a certain difficulty for lattice calculations if the $\mathrm{O}(e^4)$ contribution is to be computed with good relative precision. We remark that the integrand displayed in Fig. 5.7 corresponds to the sum of all Wick contractions contributing to the four-point function of the e.m. current, but, using the results in appendix A of Ref. [146], it would be fairly straightforward to adapt the prediction to individual Wick contractions of the quark fields.

As a consequence of the Ward-Identity of the vector current, a term $\partial_\lambda\,[z_\sigma F(|z|)]$ can be added to the position-space kernel $H_{\lambda\sigma}(z)$ without changing the integrated result of Eq. (5.135) in infinite volume [363]. With a judiciously chosen subtraction, one can make the z-integrand in Eq. (5.136) more peaked in the small-$|z|$ region. As in practice, a calculation on the lattice is limited by the degrading signal-to-noise ratio when the arguments of the correlator are far apart in position-space,

the possibility of reshaping the integrand makes the position-space representation appealing. Such a technique has also been used for lattice determinations of the HLbL scattering contribution to a_μ [364, 362]. Figure 5.7 thus also shows the result of improving the kernel (kerM6) to make the integrand shorter-range; details of its construction are given in [334]. For the $\Lambda = 3\,m_\mu$ case, the partially-integrated $a_\mu(R)$ obtained with kerM6 already reaches about 70% of its final value $a_\mu(\infty)$ at $R = 2$ fm, but only about 50% with the TMR. For $\Lambda = 200\,m_\mu$, the benefit becomes even more apparent: 95% with kerM6 and merely about 65% with the TMR. We thus expect that the position-space method with an improved kernel should offer a good opportunity to compute the e.m. correction to a_μ^{HVP} on the lattice, with better controlled finite-volume effects.

5.8 Conclusions and outlook

We have derived a Cottingham-like formula for the leading QED correction to the HVP, $\Pi_{4\mathrm{pt}}$, expressed primarily in terms of the traced forward HLbL scattering amplitude, $\mathcal{M}$, (see Eqs. (5.16) and (5.17) with corresponding explanations):

$$\begin{aligned}\Pi_{4\mathrm{pt}}(Q^2,\Lambda) &= \frac{1}{3(2\pi)^3 Q^2}\int_0^\infty dK^2 \int_0^1 dx\,\sqrt{1-x^2}\,\mathcal{M}(KQx, K^2, Q^2) \\ &= \frac{1}{3(2\pi)^3 Q^2}\int_0^\infty dK^2 \left[\frac{\pi}{4}\mathcal{M}(\bar{\nu}, K^2, Q^2) + \int_{\nu_{\mathrm{thr.}}}^\infty d\nu \left(\frac{2}{\nu+\sqrt{X}} - \frac{\nu}{\nu^2-\bar{\nu}^2}\right)\sqrt{X}\,\sigma(\nu, K^2, Q^2)\right].\end{aligned} \tag{5.138}$$

Although $\mathcal{M}$ a physical amplitude, contracting the incoming and outgoing photon lines leads to a logarithmically divergent momentum integral in the UV. The necessary counterterms to cancel this divergence have been outlined in Section 5.5, using the OPE. These counterterms involve derivatives with respect to the quark masses and the virtuality of the leading HVP. However, the finite part of these counterterms is sensitive to the specific point in the parameter space of isospin-symmetric QCD chosen as the basis for calculating isospin-breaking effects.

Currently, the most promising application of the Cottingham-like formula seems to involve implementing it with a finite regulator on the order of a few hundred MeV. This regularization approach entails replacing the internal photon line with a Pauli-Villars regulated propagator, or any other convenient form of propagator regularization. The leading QED correction to the HVP, with such a regularized photon propagator, can be computed in lattice QCD using coordinate-space techniques similar to those used for calculating the HLbL contribution to the muon AMM, while avoiding power-law finite-size effects.

When working on very large lattices, as seen in master-field simulations [365, 366], these techniques are particularly natural [367]. Whether using this new approach or the established method involving the removal of the spatial zero-mode of the photon, a direct comparison becomes possible

between the lattice QCD calculation and the Cottingham-like formula prediction. For the latter, it is important to note that the traced forward HLbL amplitude can be represented dispersively in terms of the $\gamma^*\gamma^* \to$ hadrons fusion cross-section, with one subtraction term. The complementary part, i.e., the second term in Eq. (5.1), features a massive photon propagator in the case of Pauli-Villars regularization. Here, the lattice naturally provides UV regularization, eliminating the need for handling the photon zero mode on a finite lattice due to the photon mass.

Lastly, in the context of the original Cottingham formula, it would be intriguing to compute the electromagnetic contribution to the proton-neutron mass difference using a regularized photon propagator. This could then be directly compared, without scheme uncertainties, to predictions from the well-established dispersive treatment of the forward Compton amplitude (see [330] and references therein).

Appendices

5.A One-loop forward doubly-virtual LbL amplitudes

Here the exact expressions for the forward doubly-virtual LbL amplitudes are provided in terms of the Passarino-Veltman scalar integral $C_0(p_1^2, p_2^2, (p_1+p_2)^2; m_1, m_2, m_3)$. The latter is given in the `Package-X` [5, 6] notation. The directions of the space-like photon momenta k and q correspond to the left part of Fig. 5.1. Other conventions are explained in Sect. 5.1. The forward one-loop LbL amplitudes has been derived with the help of `Package-X`. For the sake of brevity, in this section the lepton and charged scalar masses are taken to be unity.

5.A.1 QED

The helicity-averaged forward LbL amplitude is given by:

$$
\begin{aligned}
\mathcal{M}^{\mathrm{QED}}(\nu, K^2, Q^2) = 16\alpha_{\mathrm{em}}^2 \Bigg(& 6 - \Bigg\{ \frac{2\log\left[\frac{1}{2}Q\left(\sqrt{Q^2+4}+Q\right)+1\right]}{\sqrt{Q^2+4}} \\
& \times \Bigg(-4\nu^2 Q^2 \left[\left(K^2-2\right)\left(K^2+1\right)Q^4 + \left(K^2+2\right)\left(7K^2-2\right)Q^2 + 6K^4 + 52K^2 + 16\right] \\
& + K^2 Q^4 \left(K^2+Q^2+4\right)^2 \left[K^2\left(Q^2+4\right) - 2Q^2 + 4\right] + 96\nu^4 \Bigg) \Bigg/ \Bigg(K^4 Q^5 \left(K^2+Q^2+4\right)^2 \\
& + 16\nu^4 Q - 4K^2\nu^2 Q^3 \left[K^2\left(Q^2+2\right) + 2\left(Q^2+4\right)\right] \Bigg) + \{K \leftrightarrow Q\} \Bigg\} \\
& + \Bigg\{ \frac{2\sqrt{1+\frac{4}{K^2+2\nu+Q^2}}\log\left[\frac{1}{2}\left(\sqrt{\left(K^2+2\nu+Q^2\right)\left(K^2+2\nu+Q^2+4\right)} + K^2+2\nu+Q^2+2\right)\right]}{K^2Q^2\left(K^2+Q^2+2\nu+4\right) - 4\nu^2} \\
& \times \Big(K^2Q^2(K^2+Q^2+2\nu) - 2(K^2+Q^2)(\nu-1) - (K^4+Q^4) - 2\nu(\nu+2) \Big) \\
& + \frac{(K^2+Q^2)^2 + 2\nu(K^2+Q^2) + 2\nu(\nu-2) - 4}{\nu} C_0\left(-K^2, -Q^2, -K^2-2\nu-Q^2; 1, 1, 1\right) \\
& + \{\nu \to -\nu\} \Bigg\} \Bigg)
\end{aligned}
\tag{5.139}
$$

The expressions for the subtraction function for the cases of $\bar{\nu} = 0$ and $\bar{\nu} = KQ$ are, respectively:

$$
\begin{aligned}
\mathcal{M}^{\mathrm{QED}}(0, K^2, Q^2) = -32\alpha_{\mathrm{em}}^2 \Bigg\{ & \frac{Q^6 + Q^4\left(3K^2+2\right) + 2Q^2\left(K^4+7K^2-4\right) + 4K^2(2K^2+5)}{K^2Q\sqrt{Q^2+4}\left(K^2+Q^2+4\right)} \\
& \times \log\left[\frac{1}{2}Q\left(\sqrt{Q^2+4}+Q\right)+1\right]
\end{aligned}
$$

$$
\begin{aligned}
&+\frac{K^6+K^4\left(3Q^2+2\right)+2K^2\left(Q^4+7Q^2-4\right)+4Q^2\left(2Q^2+5\right)}{Q^2K\sqrt{K^2+4}\left(K^2+Q^2+4\right)}\\
&\times\log\left[\frac{1}{2}K\left(\sqrt{K^2+4}+K\right)+1\right]\\
&-\frac{Q^6+K^6-2(Q^4+K^4)+5Q^2K^2(Q^2+K^2)}{K^2Q^2\sqrt{\left(K^2+Q^2\right)\left(K^2+Q^2+4\right)}}\\
&\times\log\left[\frac{1}{2}\left(K^2+\sqrt{\left(K^2+Q^2\right)\left(K^2+Q^2+4\right)}+Q^2+2\right)\right]\\
&-2\left(K^2+Q^2-2\right)C_0\left(-Q^2,-K^2,-K^2-Q^2;1,1,1\right)-3\Bigg\},
\end{aligned}
\tag{5.140}
$$

$$
\begin{aligned}
\mathcal{M}^{\rm QED}(KQ,K^2,Q^2)=&-16\alpha_{\rm em}^2\Bigg\{-6+\frac{\left(K^2+Q^2-2\right)\left[(K+Q)^2+4\right]^{3/2}}{K^2Q^2(K+Q)}\\
&\times\log\left[\frac{1}{2}(K+Q)\left(\sqrt{(K+Q)^2+4}+K+Q\right)+1\right]\\
&+\frac{\left(K^2+Q^2-2\right)\left[(K-Q)^2+4\right]^{3/2}}{K^2Q^2|K-Q|}\\
&\times\log\left[\frac{1}{2}|K-Q|\left(|K-Q|+\sqrt{(K-Q)^2+4}\right)+1\right]\\
&-\frac{2\left[\left(K^4+2K^2+28\right)Q^2+K^6+6K^4-32\right]}{KQ^2\sqrt{K^2+4}\left(K^2-Q^2\right)}\\
&\times\log\left[\frac{1}{2}K\left(\sqrt{K^2+4}+K\right)+1\right]\\
&-\frac{2\left[\left(Q^4+2Q^2+28\right)K^2+Q^6+6Q^4-32\right]}{K^2Q\sqrt{Q^2+4}\left(Q^2-K^2\right)}\\
&\times\log\left[\frac{1}{2}Q\left(\sqrt{Q^2+4}+Q\right)+1\right]\Bigg\}.
\end{aligned}
\tag{5.141}
$$

5.A.2 sQED

The helicity-averaged forward LbL amplitude is given by:

$$
\begin{aligned}
&\mathcal{M}^{\rm sQED}(\nu,K^2,Q^2)=2\alpha^2\Bigg(-24+\Bigg\{2\sqrt{Q^2+4}\log\left[\frac{1}{2}Q(Q+\sqrt{Q^2-4})\right]\\
&\times\Bigg(K^2Q^4(4+7K^2)(4+K^2+Q^2)^2\\
&-4\nu^2Q^2\left[(4+K^2)(4+15K^2)+Q^2(4+17K^2+7K^4)\right]+96\nu^4\Bigg)\Bigg/\Bigg(Q\left[(KQ)^4(4+K^2+Q^2)^2\right.
\end{aligned}
$$

$$
\begin{aligned}
&-4(KQ)^2\left(K^2(Q^2+2)+2(Q^2+4)\right)\nu^2+16\nu^4]\Big)+\{K\leftrightarrow Q\}\Big\}\\
&-\Bigg\{\frac{2\sqrt{1+\frac{4}{K^2+Q^2+2\nu}}\log\left[\frac{1}{2}\left(\sqrt{(K^2+2\nu+Q^2)(K^2+2\nu+Q^2+4)}+K^2+2\nu+Q^2+2\right)\right]}{K^2Q^2(K^2+Q^2+2\nu+4)-4\nu^2}\\
&\times\left((16+4(K^2+Q^2)+5K^2Q^2)(\nu+2(K^2+Q^2))+8((K^2+Q^2)K^2Q^2-\nu^2)\right)\\
&+\frac{\left(K^2+Q^2+2\nu+6\right)(K^2+Q^2)+\frac{1}{2}K^2Q^2+8(\nu+1)}{\nu}C_0(-K^2,-Q^2,-K^2-2\nu-Q^2;1,1,1)\\
&+\{\nu\to-\nu\}\Bigg\}\Bigg)
\end{aligned}
\tag{5.142}
$$

The expressions for the subtraction function for the cases of $\bar{\nu}=0$ and $\bar{\nu}=KQ$ are, respectively:

$$
\begin{aligned}
&\mathcal{M}^{\text{sQED}}(0,K^2,Q^2)=4\alpha_{\text{em}}^2\Bigg\{-12+4(K^2+Q^2+4)C_0(-K^2,-Q^2,-K^2-Q^2;1,1,1)\\
&+\frac{\sqrt{K^2+4}\left[-2K^4+2K^2(Q^2-2)+5Q^2(Q^2+4)\right]}{KQ^2(K^2+Q^2+4)}\log\left[\frac{1}{2}K\left(K+\sqrt{K^2+4}\right)+1\right]\\
&+\frac{\sqrt{Q^2+4}\left[-2Q^4+2Q^2(K^2-2)+5K^2(K^2+4)\right]}{QK^2(K^2+Q^2+4)}\log\left[\frac{1}{2}Q\left(Q+\sqrt{Q^2+4}\right)+1\right]\\
&+2\sqrt{\frac{K^2+Q^2+4}{K^2+Q^2}}\frac{(K^4+Q^4)}{K^2Q^2}\log\left[\frac{1}{2}\left(K^2+Q^2\sqrt{(K^2+Q^2)(K^2+Q^2+4)}\right)+1\right]\Bigg\}
\end{aligned}
\tag{5.143}
$$

$$
\begin{aligned}
&\mathcal{M}^{\text{sQED}}(KQ,K^2,Q^2)=4\alpha_{\text{em}}^2\Bigg\{-12+\frac{\left(K^2+Q^2-2\right)\sqrt{(K+Q)^2+4}}{K^2Q^2(K+Q)}\\
&\times\left[(K^2+Q^2)\left((K+Q)^2+4\right)+3\left(8+2(K+Q)^2+K^2Q^2\right)\right]\\
&\times\log\left[\frac{1}{2}(K+Q)\left(\sqrt{(K+Q)^2+4}+K+Q\right)+1\right]\\
&+\frac{\left(K^2+Q^2-2\right)\sqrt{(K-Q)^2+4}}{K^2Q^2|K-Q|}\\
&\times\left[(K^2+Q^2)\left((K-Q)^2+4\right)+3\left(8+2(K-Q)^2+K^2Q^2\right)\right]\\
&\times\log\left[\frac{1}{2}|K-Q|\left(|K-Q|+\sqrt{(K-Q)^2+4}\right)+1\right]\\
&+\frac{\sqrt{K^2+4}\left[2(K^2+4)^2+4(2K^2-1)Q^2-9Q^4\right]}{KQ^2\left(K^2-Q^2\right)}\\
&\times\log\left[\frac{1}{2}K\left(\sqrt{K^2+4}+K\right)+1\right]\\
&+\frac{\sqrt{Q^2+4}\left[2(Q^2+4)^2+4(2Q^2-1)K^2-9K^4\right]}{K^2Q\left(Q^2-K^2\right)}
\end{aligned}
$$

$$\times \log\left[\frac{1}{2}Q\left(\sqrt{Q^2+4}+Q\right)+1\right]\Bigg\}. \tag{5.144}$$

5.B Polarized two-photon fusion cross sections in QED and sQED

Here the tree-level cross sections for the $\gamma^*\gamma^*$-fusion process in QED and sQED with polarized virtual photons. The conventions are the same as in Refs. [167] and [165]:

$$L \equiv \log\left(\frac{1+\sqrt{a}}{\sqrt{1-a}}\right), \quad a \equiv \frac{X}{\nu^2}\left(1-\frac{4m^2}{s}\right), \quad X = \nu^2 - Q^2K^2, \tag{5.145}$$

where $s = (k+q)^2 = 2\nu - K^2 - Q^2$, $\nu = k\cdot q$; $Q^2 = -q^2$ and $K^2 = -k^2$ are the spacelike photon virtualities. The threshold energy in this case is given by $\nu_{\text{thr.}} = 2m^2 + {}^1\!/_2(K^2+Q^2)$.

5.B.1 QED

The cross sections corresponding to the fusion of two polarized photons, either transverse (T) or longitudinal (L), to two spinor QED fermions, read:

$$\begin{aligned}\sigma_{TT}(\nu,Q^2,K^2) =& \frac{1}{2}\left(\sigma_{\parallel}+\sigma_{\perp}\right)\\ =& \frac{\pi\alpha_{\text{em}}^2}{2}\frac{s^2\nu^3}{X^3}\Bigg\{\sqrt{a}\Bigg[-4\left(1-\frac{X}{s\nu}\right)^2-(1-a)+\frac{K^2Q^2}{\nu^2}\left(2-\frac{1}{(1-a)}\frac{4X^2}{s^2\nu^2}\right)\Bigg]\\ &+\left[3-a^2+2\left(1-\frac{2X}{s\nu}\right)^2-\frac{2K^2Q^2}{\nu^2}(1+a)\right]L\Bigg\}.\end{aligned} \tag{5.146}$$

$$\begin{aligned}\sigma_{LT}(\nu,Q^2,K^2) =& \sigma_{TL}(\nu,K^2,Q^2)\\ =& \pi\alpha_{\text{em}}^2Q^2\frac{s}{\nu X^2}\Bigg\{\Bigg[\left(\nu-K^2\right)^2\left(-2(1-a)-(3-a)\frac{Q^2K^2}{X}\right)+2\nu K^2(1+a)\\ &-K^4(3+a)\Bigg]L+\sqrt{a}\Bigg[\left(\nu-K^2\right)^2\left(2+\frac{3Q^2K^2}{X}\right)-2\nu K^2+K^4\frac{3-a}{1-a}\Bigg]\Bigg\}.\end{aligned} \tag{5.147}$$

$$\sigma_{LL}(\nu,Q^2,K^2) = 2\pi\alpha_{\text{em}}^2Q^2K^2\frac{s^2}{\nu X^2}\left\{\sqrt{a}\left[-2-\frac{3-2a}{1-a}\frac{Q^2K^2}{X}\right]+\left(2+\frac{3Q^2K^2}{X}\right)L\right\}. \tag{5.148}$$

The total cross section requied for the Cottingham formula is given by

$$\begin{aligned}\sigma =& 4\sigma_{TT}-2\sigma_{LT}-2\sigma_{TL}+\sigma_{LL} = \frac{8\pi\alpha_{\text{em}}^2}{X\nu}\Bigg\{2\nu\sqrt{X\frac{4+K^2+Q^2-2\nu}{K^2+Q^2-2\nu}}\\ &\times\frac{2\nu[K^2Q^2+2+\nu]-K^2[K^2(Q^2-1)+2(1+\nu)]-Q^2[Q^2(K^2-1)+2(1+\nu)]}{K^2Q^2(4-2\nu+K^2+Q^2)-4\nu^2}\end{aligned}$$

$$+\left[(K^2+Q^2-\nu)^2+\nu^2+4(\nu-1)\right]\log\frac{1+\sqrt{\frac{X}{\nu^2}\frac{4+K^2+Q^2-2\nu}{K^2+Q^2-2\nu}}}{\sqrt{1-\frac{X}{\nu^2}\frac{4+K^2+Q^2-2\nu}{K^2+Q^2-2\nu}}}\Bigg\}, \tag{5.149}$$

where the fermion mass m is set to be equal to unity.

5.B.2 sQED

The cross sections corresponding to the fusion of two polarized photons, either transverse (T) or longitudinal (L), to two charged spin-0 particles, read:

$$\begin{aligned}
\sigma_{TT}(\nu,Q^2,K^2) =&\frac{1}{2}\left(\sigma_{\parallel}+\sigma_{\perp}\right)\\
=&\frac{\alpha_{\rm em}^2\pi}{4}\frac{s^2\nu^3}{X^3}\Bigg\{\sqrt{a}\left[2-a+\left(1-\frac{2X}{s\nu}\right)^2\right]\\
&-(1-a)\left[3+a-\frac{4X}{s\nu}\right]L\Bigg\},
\end{aligned} \tag{5.150}$$

$$\begin{aligned}
\sigma_{LT}(\nu,Q^2,K^2) =&\sigma_{TL}(\nu,K^2,Q^2)\\
=&\frac{\pi\alpha_{\rm em}^2}{2}Q^2\frac{s\nu}{X^3}(\nu-K^2)^2\Bigg\{-3\sqrt{a}+(3-a)L\Bigg\},
\end{aligned} \tag{5.151}$$

$$\begin{aligned}
\sigma_{LL}(\nu,Q^2,K^2) =&\pi\alpha_{\rm em}^2Q^2K^2\frac{s^2\nu}{X^3}\Bigg\{\sqrt{a}\left[2+\frac{\left(1-\frac{X}{s\nu}\right)^2}{1-a}\right]\\
&-\left[3+\frac{X}{s\nu}\right]\left[1-\frac{X}{s\nu}\right]L\Bigg\}
\end{aligned} \tag{5.152}$$

The total cross section requied for the Cottingham formula is given by

$$\begin{aligned}
\sigma =&4\sigma_{TT}-2\sigma_{LT}-2\sigma_{TL}+\sigma_{LL}=\frac{\pi\alpha_{\rm em}^2}{X\nu}\Bigg\{\nu\sqrt{X\frac{4+K^2+Q^2-2\nu}{K^2+Q^2-2\nu}}\\
&\times\frac{K^2[K^2(5Q^2+4)+8(2-\nu)]+Q^2[Q^2(5K^2+4)+8(2-\nu)]-2\nu[8(2+\nu)+5K^2Q^2])}{K^2Q^2(4-2\nu+K^2+Q^2)-4\nu^2}\\
&+\left[2(K^2+Q^2)(K^2+Q^2+2(3-\nu))+K^2Q^2+16(1-\nu)\right]\log\frac{1+\sqrt{\frac{X}{\nu^2}\frac{4+K^2+Q^2-2\nu}{K^2+Q^2-2\nu}}}{\sqrt{1-\frac{X}{\nu^2}\frac{4+K^2+Q^2-2\nu}{K^2+Q^2-2\nu}}}\Bigg\}
\end{aligned} \tag{5.153}$$

5.C Imaginary parts of two-loop vacuum polarization in QED and sQED

The two-loop vacuum polarization can be found via its imaginary part according to the dispersion relation (5.27). The imaginary part of the two-loop vacuum polarization for QED reads

$$\begin{aligned}\mathrm{Im}\,\overline{\Pi}^{\mathrm{QED}}_{\text{2-loop}}(t) = &-\frac{\alpha_{\mathrm{em}}^2}{3\pi}\left\{\frac{3}{8}v(5-3v^2)-v(3-v^2)\left[2\log(v)-3\log\left(\frac{1+v}{2}\right)\right]\right.\\ &-\frac{1}{16}\left(-33+72v-22v^2-24v^3+7v^4\right)\log\left(\frac{1+v}{1-v}\right)\\ &+\frac{1}{2}(3-v^2)(1+v^2)\left[\frac{\pi^2}{6}+\log\left(\frac{1+v}{2}\right)\log\left(\frac{1+v}{1-v}\right)\right.\\ &\left.\left.+\mathrm{Li}_2(v^2)+2\left(\mathrm{Li}_2\left(\frac{1-v}{1+v}\right)+\mathrm{Li}_2\left(\frac{1+v}{2}\right)-\mathrm{Li}_2\left(\frac{1-v}{2}\right)\right)-4\mathrm{Li}_2(v)\right]\right\},\end{aligned} \tag{5.154}$$

The imaginary part of the two-loop vacuum polarization for sQED is provided in the same book [340] (Vol.III, p.99, Eq.(5-4.132))

$$\begin{aligned}\mathrm{Im}\,\overline{\Pi}^{\mathrm{sQED}}_{\text{2-loop}}(t) = &-\frac{\alpha_{\mathrm{em}}^2}{12\pi}\left\{v^2(1+v^2)\left[\frac{\pi^2}{6}+\log\frac{1+v}{2}\log\frac{1+v}{1-v}\right.\right.\\ &\left.+2\mathrm{Li}_2\left(\frac{1-v}{1+v}\right)+2\mathrm{Li}_2\left(\frac{1+v}{2}\right)-2\mathrm{Li}_2\left(\frac{1-v}{2}\right)-4\mathrm{Li}_2(v)+\mathrm{Li}_2(v^2)\right]\\ &+\left[5\left(\frac{1+v^2}{2}\right)^2-2-3v^2\right]\log\frac{1+v}{1-v}+6v^3\log\frac{1+v}{2}\\ &\left.-4v^3\log v+\frac{3}{2}v(1+v^2)\right\},\end{aligned} \tag{5.155}$$

where $v=\sqrt{1-4m_\pi^2/t}$. This answer satisfies the low- and high-energy limits, which are also provided in the book - see Eqs.(5-4.133) and (5-4.134) in [340]. They read

$$\frac{-1}{\pi}\lim_{t\gg(2m_\pi)^2}\mathrm{Im}\,\overline{\Pi}^{\mathrm{sQED}}_{\text{2-loop}}(t)=\frac{\alpha_{\mathrm{em}}^2}{4\pi^2} \tag{5.156}$$

$$\frac{-1}{\pi}\lim_{t\to(2m_\pi)^2}\mathrm{Im}\,\overline{\Pi}^{\mathrm{sQED}}_{\text{2-loop}}(t)=\frac{\alpha_{\mathrm{em}}^2}{24}v^2. \tag{5.157}$$

However, the imaginary part 5.155 results in a strange series of $\overline{\Pi}^{\rm sQED}_{2-\rm loop}(Q^2)$ in Q^2, which contains irrational numbers ($\log(2)$)

$$\overline{\Pi}^{\rm sQED}_{2-\rm loop}(Q^2) = \frac{\alpha_{\rm em}^2}{\pi^2}\frac{Q^2}{m_\pi^2}\left(\frac{119-648\log(2)}{12960} - \frac{29-270\log(2)}{75600}\frac{Q^2}{m_\pi^2} + O(Q^4)\right) \tag{5.158}$$

Moreover, it does not satisfy the result given on p.95 in Eq.(5-4.104) [11]

$$\frac{1}{\pi}\int dv^2 t\,\mathrm{Im}\,\overline{\Pi}_{2-\rm loop}(t) = \frac{4m_\pi^2}{\pi}\int dt\frac{\mathrm{Im}\,\overline{\Pi}_{2-\rm loop}(t)}{t^2} = \frac{\alpha_{\rm em}^2}{12\pi^2}\frac{95}{54}. \tag{5.159}$$

The direct evaluation of the integrals in Eqs.(5-4.71), (5-4.80) and (5-4.87), which are assumed to give the answer (5.155), gives the expression, different to (5.155). The missing piece, which should be added to the answer (5.155), reads

$$\begin{aligned}\Delta\,\mathrm{Im}\,\overline{\Pi}^{\rm sQED}_{2-\rm loop}(t) = -\frac{\alpha_{\rm em}^2}{12\pi}\frac{1}{4}v^2\Bigg\{&12(1-v)\log\frac{1+v}{1-v}\\ &+(1+v^2)\Bigg[\pi^2+\log\frac{1+v}{1-v}\left(8\log(v)-6\log\frac{1+v}{2}\right)\\ &+2\left(\mathrm{Li}_2\left(\frac{1-v}{2}\right)-\mathrm{Li}_2\left(\frac{1+v}{2}\right)\right)\\ &+4\left(\mathrm{Li}_2\left(\frac{2v}{v-1}\right)-\mathrm{Li}_2\left(\frac{2v}{v+1}\right)-\mathrm{Li}_2\left(\frac{v+1}{v-1}\right)\right)\\ &-8\mathrm{Li}_2\left(\frac{1-v}{1+v}\right)\Bigg]\Bigg\}\end{aligned} \tag{5.160}$$

The corrected answer satisfies both energy limits and the integral result of Eq.(5-4.104). Furthermore, it gives the series of $\overline{\Pi}_{2-\rm loop}(Q^2)$ with rational numbers only. Thus, we conclude that now we indeed have the correct answer. It yields the series coefficients given by Eq. (5.36).

As an ultimate check, the same series can be obtained by direct calculation of the two-loop integrals in dimensional regularization, as was done in [342, 368].

5.D Contribution of different helicity amplitudes to the Cottingham-like formula

The contribution to vacuum polarization via the Cottingham-like formula can be divided based on the different LbL helicity amplitudes involved in the calculation:

$$\Pi = 4\Pi^{\rm TT} - 2\Pi^{\rm LT} - 2\Pi^{\rm TL} + \Pi^{\rm LL}. \tag{5.161}$$

[11] It is proportional to the first term of the series in Q^2 of the dispersion relation integral 5.27

The first letter in the superscript refers to the polarization of the photon with momentum q. For instance, LT means that we integrate the amplitude with longitudinal photons with momentum q and transversal photons with integration momentum k. In QED, the first terms of the series expansion in Q^2 of these parts of the vacuum polarization are

$$\begin{aligned}\Pi^{\mathrm{TT}}(Q^2,\Lambda) =&\frac{1}{2}\frac{\alpha_{\mathrm{em}}^2}{\pi^2}\left[-\frac{13}{72}-\frac{1}{1296}\frac{Q^2}{m_\ell^2}-\frac{433}{226800}\frac{Q^4}{m_\ell^4}+\frac{88553}{190512000}\frac{Q^6}{m_\ell^6}+O\left(\frac{Q^8}{m_\ell^8}\right)\right]\\&+\frac{1}{2}\frac{\alpha_{\mathrm{em}}^2}{\pi^2}\log\frac{\Lambda}{m_\ell}\left[-\frac{4\log\frac{\Lambda}{m_\ell}-9}{36}+0\times\frac{Q^2}{m_\ell^2}+\frac{1}{420}\frac{Q^4}{m_\ell^4}-\frac{2}{2835}\frac{Q^6}{m_\ell^6}+O\left(\frac{Q^8}{m_\ell^8}\right)\right],\end{aligned}\tag{5.162}$$

$$\begin{aligned}\Pi^{\mathrm{LT}}(Q^2,\Lambda) =&\frac{\alpha_{\mathrm{em}}^2}{\pi^2}\left[-\frac{1}{18}-\frac{17}{2160}\frac{Q^2}{m_\ell^2}+\frac{23}{21600}\frac{Q^4}{m_\ell^4}-\frac{2453}{12700800}\frac{Q^6}{m_\ell^6}+O\left(\frac{Q^8}{m_\ell^8}\right)\right]\\&+\frac{\alpha_{\mathrm{em}}^2}{\pi^2}\log\frac{\Lambda}{m_\ell}\left[0+\frac{1}{90}\frac{Q^2}{m_\ell^2}-\frac{1}{420}\frac{Q^4}{m_\ell^4}+\frac{1}{1890}\frac{Q^6}{m_\ell^6}+O\left(\frac{Q^8}{m_\ell^8}\right)\right],\end{aligned}\tag{5.163}$$

$$\begin{aligned}\Pi^{\mathrm{TL}}(Q^2,\Lambda) =&\frac{\alpha_{\mathrm{em}}^2}{\pi^2}\left[\frac{17}{72}-\frac{5}{108}\frac{Q^2}{m_\ell^2}+\frac{659}{90720}\frac{Q^4}{m_\ell^4}-\frac{73}{56700}\frac{Q^6}{m_\ell^6}+O\left(\frac{Q^8}{m_\ell^8}\right)\right]\\&+\frac{\alpha_{\mathrm{em}}^2}{\pi^2}\log\frac{\Lambda}{m_\ell}\left[-\frac{1}{6}+\frac{2}{45}\frac{Q^2}{m_\ell^2}-\frac{1}{105}\frac{Q^4}{m_\ell^4}+\frac{2}{945}\frac{Q^6}{m_\ell^6}+O\left(\frac{Q^6}{m_\ell^6}\right)\right],\end{aligned}\tag{5.164}$$

$$\begin{aligned}\Pi^{\mathrm{LL}}(Q^2,\Lambda) =&\frac{\alpha_{\mathrm{em}}^2}{\pi^2}\left[\frac{2}{9}+\frac{13}{135}\frac{Q^2}{m_\ell^2}-\frac{157}{15120}\frac{Q^4}{m_\ell^4}+\frac{68}{42525}\frac{Q^6}{m_\ell^6}+O\left(\frac{Q^8}{m_\ell^8}\right)\right]\\&+\frac{\alpha_{\mathrm{em}}^2}{\pi^2}\log\frac{\Lambda}{m_\ell}\left[\frac{2\log\frac{\Lambda}{m_\ell}-3}{9}-\frac{4}{45}\frac{Q^2}{m_\ell^2}+\frac{1}{70}\frac{Q^4}{m_\ell^4}-\frac{8}{2835}\frac{Q^6}{m_\ell^6}+O\left(\frac{Q^8}{m_\ell^8}\right)\right],\end{aligned}\tag{5.165}$$

where $\Lambda\to\infty$ is the hard cut-off adopted in the same way as in Eq. (5.18). One can also introduce the combinations that correspond to longitudinal or transversal polarization of the photon with momentum q being averaged over helicity of the photon with momentum k as

$$\Pi^{\mathrm{T}} = 2\Pi^{\mathrm{TT}} - \Pi^{\mathrm{TL}},\tag{5.166}$$

$$\Pi^{\mathrm{L}} = \Pi^{\mathrm{LL}} - 2\Pi^{\mathrm{LT}},\tag{5.167}$$

such that $\Pi = 2\Pi^{\mathrm{T}} + \Pi^{\mathrm{L}}$. These terms have the following series expansion in Q^2:

$$\begin{aligned}\Pi^{\mathrm{L}}(Q^2,\Lambda) =&\frac{\alpha_{\mathrm{em}}^2}{\pi^2}\left[\frac{1}{3}+\frac{121}{1080}\frac{Q^2}{m_\ell^2}-\frac{473}{37800}\frac{Q^4}{m_\ell^4}+\frac{37823}{19051200}\frac{Q^6}{m_\ell^6}+O\left(\frac{Q^8}{m_\ell^8}\right)\right]\\&+\frac{\alpha_{\mathrm{em}}^2}{\pi^2}\log\frac{\Lambda}{m_\ell}\left[\frac{2\log\frac{\Lambda}{m_\ell}-3}{9}-\frac{1}{9}\frac{Q^2}{m_\ell^2}+\frac{2}{105}\frac{Q^4}{m_\ell^4}-\frac{11}{2835}\frac{Q^6}{m_\ell^6}+O\left(\frac{Q^8}{m_\ell^8}\right)\right],\end{aligned}\tag{5.168}$$

$$\Pi^{\mathrm{T}}(Q^2,\Lambda) =\frac{\alpha_{\mathrm{em}}^2}{\pi^2}\left[-\frac{5}{12}+\frac{59}{1296}\frac{Q^2}{m_\ell^2}-\frac{1387}{151200}\frac{Q^4}{m_\ell^4}+O\left(\frac{Q^8}{m_\ell^8}\right)\right]$$

$$+\frac{\alpha_{\rm em}^2}{\pi^2}\log\frac{\Lambda}{m_\ell}\left[-\frac{4\log\frac{\Lambda}{m_\ell}-15}{36}-\frac{2}{45}\frac{Q^2}{m_\ell^2}+\frac{1}{84}\frac{Q^4}{m_\ell^4}-\frac{8}{2835}\frac{Q^6}{m_\ell^6}+O\left(\frac{Q^8}{m_\ell^8}\right)\right]. \tag{5.169}$$

Series terms for the integrated subtraction function at the subtraction point $\bar{\nu} = {}^1\!/_2 KQ$ read

$$\Pi^{\rm TT}_{\rm subtr}(Q^2,\Lambda) = \frac{1}{2}\frac{\alpha_{\rm em}^2}{\pi^2}\left[-\frac{13}{72}-\frac{1}{216}\frac{Q^2}{m_\ell^2}-\frac{391}{453600}\frac{Q^4}{m_\ell^4}+\frac{5491}{27216000}\frac{Q^6}{m_\ell^6}+O\left(\frac{Q^8}{m_\ell^8}\right)\right]$$
$$+\frac{1}{2}\frac{\alpha_{\rm em}^2}{\pi^2}\log\frac{\Lambda}{m_\ell}\left[-\frac{4\log\frac{\Lambda}{m_\ell}-9}{36}+0\times\frac{Q^2}{m_\ell^2}+\frac{1}{420}\frac{Q^4}{m_\ell^4}-\frac{2}{2835}\frac{Q^6}{m_\ell^6}+O\left(\frac{Q^8}{m_\ell^8}\right)\right], \tag{5.170}$$

$$\Pi^{\rm LT}_{\rm subtr}(Q^2,\Lambda) = \frac{\alpha_{\rm em}^2}{\pi^2}\left[-\frac{1}{18}-\frac{17}{2160}\frac{Q^2}{m_\ell^2}+\frac{421}{453600}\frac{Q^4}{m_\ell^4}-\frac{599}{4233600}\frac{Q^6}{m_\ell^6}+O\left(\frac{Q^8}{m_\ell^8}\right)\right]$$
$$+\frac{\alpha_{\rm em}^2}{\pi^2}\log\frac{\Lambda}{m_\ell}\left[0+\frac{1}{90}\frac{Q^2}{m_\ell^2}-\frac{1}{420}\frac{Q^4}{m_\ell^4}+\frac{1}{1890}\frac{Q^6}{m_\ell^6}+O\left(\frac{Q^8}{m_\ell^8}\right)\right], \tag{5.171}$$

$$\Pi^{\rm TL}_{\rm subtr}(Q^2,\Lambda) = \frac{\alpha_{\rm em}^2}{\pi^2}\left[\frac{17}{72}-\frac{101}{2160}\frac{Q^2}{m_\ell^2}+\frac{19}{2592}\frac{Q^4}{m_\ell^4}-\frac{23}{17640}\frac{Q^6}{m_\ell^6}+O\left(\frac{Q^8}{m_\ell^8}\right)\right]$$
$$+\frac{\alpha_{\rm em}^2}{\pi^2}\log\frac{\Lambda}{m_\ell}\left[-\frac{1}{6}+\frac{2}{45}\frac{Q^2}{m_\ell^2}-\frac{1}{105}\frac{Q^4}{m_\ell^4}+\frac{2}{945}\frac{Q^6}{m_\ell^6}+O\left(\frac{Q^8}{m_\ell^8}\right)\right], \tag{5.172}$$

$$\Pi^{\rm LL}_{\rm subtr}(Q^2,\Lambda) = \frac{\alpha_{\rm em}^2}{\pi^2}\left[\frac{2}{9}+\frac{13}{135}\frac{Q^2}{m_\ell^2}-\frac{197}{18900}\frac{Q^4}{m_\ell^4}+\frac{551}{340200}\frac{Q^6}{m_\ell^6}+O\left(\frac{Q^8}{m_\ell^8}\right)\right]$$
$$+\frac{\alpha_{\rm em}^2}{\pi^2}\log\frac{\Lambda}{m_\ell}\left[\frac{2\log\frac{\Lambda}{m_\ell}-3}{9}-\frac{4}{45}\frac{Q^2}{m_\ell^2}+\frac{1}{70}\frac{Q^4}{m_\ell^4}-\frac{8}{2835}\frac{Q^6}{m_\ell^6}+O\left(\frac{Q^8}{m_\ell^8}\right)\right] \tag{5.173}$$

Chapter 6

Anomalous magnetic moment of the muon via the Schwinger sum rule

Schwinger sum rule approach, proposed in [149], provides the way to obtain all the leading hadronic contributions to AMM in a unified data-driven fashion. The authors have shown that the Schwinger sum rule already encodes the well-known dispersive data-driven relation for HVP, and they have proposed a scheme to evaluate the leading-order meson contributions to HLbL in a data-driven fashion as well. However, in the theoretical estimation of the HLbL contribution following this scheme, additional difficulties may occur: the divergence of the dispersive integral and the emergence of nonzero subtraction constants for some particular contributions. While the former is usually associated with oversimplified effective couplings that violate unitarity, the latter points to an extra physics input.

In this chapter, we investigate the origins of the violation of the Schwinger sum rule in perturbative examples such as LO BχPT, the linear σ-model, and the electroweak sector of the SM. We demonstrate that with appropriate UV completions – such as introducing the σ-meson for the π^0 in χPT or the Higgs field for the Z^0 boson in the SM – the Schwinger sum rule remains entirely valid. Additionally, we discuss subtleties in the treatment of contributions from $W^\pm$ bosons. We conclude the chapter by reviewing the π^0 exchange contribution to HLbL correction to AMM, obtained through the Schwinger sum rule approach.

The results described in this Chapter are based upon the work, which is currently in preparation for publication.

6.1 Longitudinal-transverse photoabsorption cross section

For $\hat{P}$- and $\hat{T}$-symmetric theories, such as QED, the longitudinal-transverse photoabsorption cross section can be defined in the following way (see Fig. 6.1):

$$\sigma_{LT}(\nu, Q^2) = \frac{1}{\sqrt{2}} \frac{(2\pi)^4}{4m\sqrt{\nu^2+Q^2}} \int \prod_{i=1}^{n} \frac{d^3k_i}{(2\pi)^3 2E_i} \delta^4\left(p+q-\sum_{i=1}^{n} k_i\right) |\mathcal{M}(\nu, Q^2, k_i)|^2_{LT}. \tag{6.1}$$

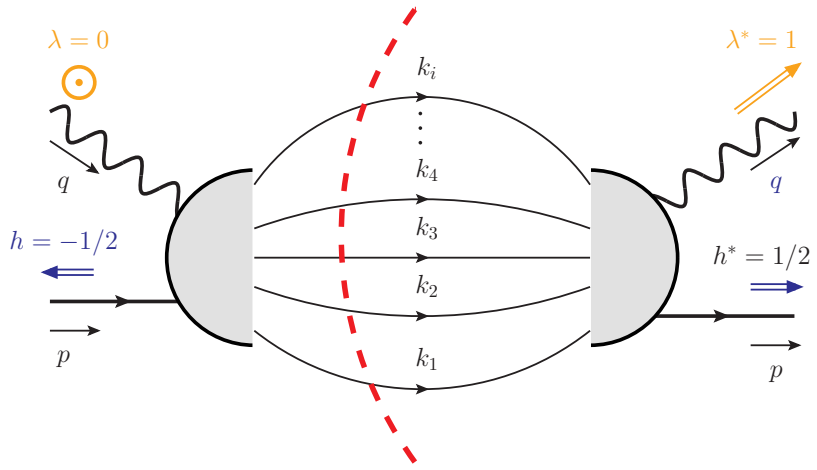

Fig. 6.1 Schematic definition of the polarized observable $\sigma_{\rm LT}$ in terms of the unitarity cut (red dashed line) of the forward LT-polarized Compton amplitude. Spin alignment of each external particle is shown by colored double arrows.

Here the "squared modulus" of the scattering amplitude is defined as

$$|\mathcal{M}(\nu, Q^2, k_i)|^2_{LT} = \mathrm{Re} \sum_{\chi_1,\ldots,\chi_n} \mathcal{M}^{\dagger}_{1,\frac{1}{2}\to\chi_1,\ldots,\chi_n} \mathcal{M}_{0,-\frac{1}{2}\to\chi_1,\ldots,\chi_n}, \tag{6.2}$$

where the sum runs over all possible polarization states $\chi_1, \ldots, \chi_n$ of the intermediate particle states with momenta $k_1, \ldots, k_n$.

However, in theories that do not respect the aforementioned symmetries, the definition (6.1) should be improved. In order to exclude the terms in σ_{LT} that violate $\hat{P}$ and $\hat{T}$ symmetries and are related to the nonzero anapole and electric dipole moments, Eq. (6.1) should be symmetrized with respect to $\hat{P}$ and $\hat{T}$ symmetries. Let us define:

$$\frac{d\sigma^{+}_{LT}}{dk_1 \ldots dk_n} \sim \sum_{\chi_1,\ldots,\chi_n} \mathcal{M}^{\dagger}_{-1,-\frac{1}{2}\to\chi_1,\ldots,\chi_n} \mathcal{M}_{0,\frac{1}{2}\to\chi_1,\ldots,\chi_n}, \tag{6.3a}$$

$$\frac{d\sigma^{-}_{LT}}{dk_1 \ldots dk_n} \sim \sum_{\chi_1,\ldots,\chi_n} \mathcal{M}^{\dagger}_{1,\frac{1}{2}\to\chi_1,\ldots,\chi_n} \mathcal{M}_{0,-\frac{1}{2}\to\chi_1,\ldots,\chi_n}, \tag{6.3b}$$

$$\frac{d\bar{\sigma}^{+}_{LT}}{dk_1 \ldots dk_n} \sim \sum_{\chi_1,\ldots,\chi_n} \mathcal{M}^{\dagger}_{0,\frac{1}{2}\to\chi_1,\ldots,\chi_n} \mathcal{M}_{-1,-\frac{1}{2}\to\chi_1,\ldots,\chi_n}, \tag{6.3c}$$

$$\frac{d\bar{\sigma}^{-}_{LT}}{dk_1 \ldots dk_n} \sim \sum_{\chi_1,\ldots,\chi_n} \mathcal{M}^{\dagger}_{0,-\frac{1}{2}\to\chi_1,\ldots,\chi_n} \mathcal{M}_{1,\frac{1}{2}\to\chi_1,\ldots,\chi_n}. \tag{6.3d}$$

Then $\sigma_{\rm LT}$ in Eq. (2.123) must be replaced by the $\hat{P}$- and $\hat{T}$-symmetrized photoabsorption cross section

$$\sigma^{\rm sym.}_{LT} = \frac{1}{4}\left[\sigma^{+}_{LT} + \sigma^{-}_{LT} + \bar{\sigma}^{+}_{LT} + \bar{\sigma}^{-}_{LT}\right], \tag{6.4}$$

where $\sigma^{+}_{\rm LT}$, $\sigma^{-}_{\rm LT}$, $\bar{\sigma}^{+}_{\rm LT}$ and $\bar{\sigma}^{-}_{\rm LT}$ are the quantities given by Eqs. (6.3), integrated over phase-space. Particularly, it is important to symmetrize the cross section when dealing with contributions of the parity-violating currents of the SM (e.g. Z^0-boson contribution). In that cases the non-symmetrized definition (6.2) may contain contributions to the anapole moment along with the AMM. Thus, the symmetrization (6.4) isolates only the contribution to the AMM.

6.2 Flavour-conserved neutral-current contributions to anomalous magnetic moment

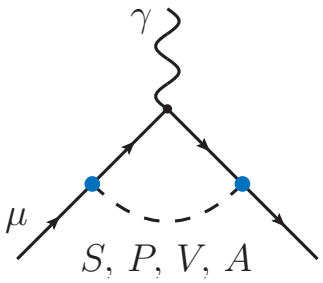

Fig. 6.2 One-loop diagram contributing to $\varkappa$. Here S, P, V, A denote several types of neutral particle exchanges.

Let us consider the one-loop contributions to $\varkappa$ that originate from the neutral scalar (S), pseudoscalar (P), vector (V) and axial-vector (A) particle exchanges, depicted diagrammatically in Fig. 6.2. We assume that these particles interact with the muon via the following simple Lagrangian interaction terms

$$\mathcal{L}^{S}_{\rm int} = C_{\rm S}\overline{\psi}(x)\psi(x)\phi(x) \tag{6.5a}$$
$$\mathcal{L}^{P}_{\rm int} = C_{\rm P}\overline{\psi}(x)i\gamma_5\psi(x)\phi(x) \tag{6.5b}$$
$$\mathcal{L}^{V}_{\rm int} = C_{\rm V}\overline{\psi}(x)\gamma^{\rho}\psi(x)\mathcal{V}_{\rho}(x) \tag{6.5c}$$
$$\mathcal{L}^{A}_{\rm int} = C_{\rm A}\overline{\psi}(x)\gamma^{\rho}\gamma_5\psi(x)\mathcal{A}_{\rho}(x). \tag{6.5d}$$

In these terms $\psi(x)$ stands for the muon spinor, $\phi(x)$ is the real (pseudo)scalar field, $\mathcal{V}_{\rho}(x)$ $\mathcal{A}_{\rho}(x)$ are the real vector and axial vector fields, respectively, and $C_{\{\rm S,P,V,A\}}$ are corresponding coupling constants. The corresponding LT-polarized tree-level cross sections, shown in Fig. 6.3, are

$$\left.\frac{\sigma^{\gamma\mu\to S\mu}_{LT}(\nu,Q^2)}{Q}\right|_{Q^2\to 0} = \frac{C_S^2\alpha_{\rm em}}{16\nu^3}\left\{\left[(3-\eta_S^2)-\tilde{s}(2\eta_S^2+7)\right]\lambda_S+\left(\eta_S^2-4-\tilde{s}\right)\log\frac{\beta_S+\lambda_S}{\beta_S-\lambda_S}\right\}, \tag{6.6a}$$

$$\left.\frac{\sigma^{\gamma\mu\to P\mu}_{LT}(\nu,Q^2)}{Q}\right|_{Q^2\to 0} = -\frac{C_P^2\alpha_{\rm em}}{16\nu^3}\left\{\left[(1+\eta_P^2)-\tilde{s}(2\eta_P^2-5)\right]\lambda_P+\left(\eta_P^2-2-\tilde{s}\right)\log\frac{\beta_P+\lambda_P}{\beta_P-\lambda_P}\right\}, \tag{6.6b}$$

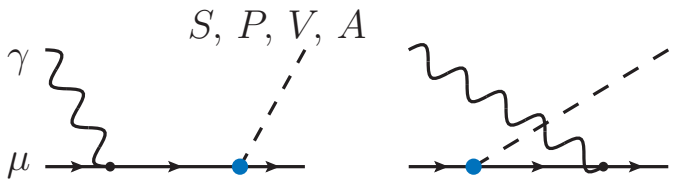

Fig. 6.3 Tree-level muon photoabsorption amplitudes, which contribute to the LT-polarized tree-level cross section in order to reproduce $\varkappa$ via the Schwinger sum rule at the same order as the one-loop diagram depicted in Fig. 6.2.

$$\left.\frac{\sigma_{LT}^{\gamma\mu\to V\mu}(\nu,Q^2)}{Q}\right|_{Q^2\to 0} = \frac{C_V^2\alpha_{\rm em}}{8\nu^3}\left\{-\left(1+\eta_V^2+5\tilde{s}\right)\lambda_V+\left(2+2\eta_V^2+\tilde{s}\right)\log\frac{\beta_V+\lambda_V}{\beta_V-\lambda_V}\right\}, \tag{6.6c}$$

$$\left.\frac{\sigma_{LT}^{\gamma\mu\to A\mu}(\nu,Q^2)}{Q}\right|_{Q^2\to 0} = \frac{C_A^2\alpha_{\rm em}}{8\eta_A^2\nu^3}\left\{-\left[\tilde{s}\left(10-7\eta_A^2\right)-5\eta_A^2+2+\eta_A^4\right]\lambda_A + \left(2-\eta_A^2\right)\left(2-2\eta_A^2+\tilde{s}\right)\log\frac{\beta_A+\lambda_A}{\beta_A-\lambda_A}\right\}. \tag{6.6d}$$

where the following conventions are used

$$\tilde{s}=\frac{s}{m_\mu^2}, \qquad \eta_X=\frac{M_X}{m_\mu},$$

$$\beta_X=\frac{s+m_\mu^2-M_X^2}{2s}, \qquad \lambda_X=\frac{\sqrt{[s-(m_\mu+M_X)^2][s-(m_\mu-M_X)^2]}}{2s},$$

for each type of particles $X=\{S,P,V,A\}$. Integration of the Eqs. (6.6) within the Schwinger sum rule should yield the corresponding contributions to the AMM of the muon, i.e. reproduce results of computation of the corresponding one-loop vertex diagram. However, the sum rule integral results in the following:

$$\varkappa_\mu^S[\text{sum rule}]=\frac{C_S^2}{8\pi^2}\left[\frac{1}{2}-\eta_S^2+\eta_S^2(\eta_S^2-3)\log\eta_S+\eta_S(\eta_S^2-1)\sqrt{\eta_S^2-4}\log\frac{\eta_S-\sqrt{\eta_S^2-4}}{2}\right], \tag{6.7}$$

$$\varkappa_\mu^P[\text{sum rule}]=\frac{C_P^2}{8\pi^2}\left[\frac{1}{2}-\eta_P^2+\eta_P^2(\eta_P^2-1)\log\eta_P+\frac{\eta_P^3(\eta_P^2-3)}{\sqrt{\eta_P^2-4}}\log\frac{\eta_P-\sqrt{\eta_P^2-4}}{2}\right], \tag{6.8}$$

$$\varkappa_\mu^V[\text{sum rule}]=\frac{C_V^2}{4\pi^2}\left[\frac{1}{2}-\eta_V^2+\eta_V^2(\eta_V^2-2)\log\eta_V+\eta_V\frac{\eta_V^4-4\eta_V^2+2}{\sqrt{\eta_V^2-4}}\log\frac{\eta_V-\sqrt{\eta_V^2-4}}{2}\right], \tag{6.9}$$

$$\varkappa_{\mu}^{A}[\text{sum rule}] = \frac{C_A^2}{4\pi^2}\left[\frac{5}{2} - \frac{\eta_A^4 - 1}{\eta_A^2} + (\eta_A^4 - 4\eta_A^2 + 2)\log\eta_A + \eta_A \frac{\eta_A^4 - 6\eta_A^2 + 8}{\sqrt{\eta_A^2 - 4}} \log\frac{\eta_A - \sqrt{\eta_A^2 - 4}}{2}\right]. \tag{6.10}$$

Comparing these results to the well-known direct loop calculation [369], we obtain the following tension for scalar, pseudoscalar and axial-vector exchanges:

$$\varkappa_{\mu}^{S}[\text{sum rule}] = \varkappa_{\mu}^{S}[\text{loop}] - \frac{C_S^2}{8\pi^2} \tag{6.11}$$

$$\varkappa_{\mu}^{P}[\text{sum rule}] = \varkappa_{\mu}^{P}[\text{loop}] + \frac{C_S^2}{8\pi^2} \tag{6.12}$$

$$\varkappa_{\mu}^{A}[\text{sum rule}] = \varkappa_{\mu}^{A}[\text{loop}] + \frac{C_S^2}{8\pi^2}\left(\frac{2m_{\mu}}{M_X}\right)^2. \tag{6.13}$$

The issue with the sum rule-based evaluation stems from the high-energy behavior of the Compton amplitude. If the latter approaches a nonzero constant value at infinite energy, then, following the Sugawara-Kanazawa theorem [158], this value should be added to the sum rule dispersive integral in order to obtain the correct result. Hence the Schwinger sum rule should be modified as follows

$$\varkappa = \frac{1}{2\pi\alpha_{\text{em}}} \lim_{\nu\to\infty} S_{LT}(\nu, Q^2 = 0) + \frac{m_{\mu}^2}{\pi^2\alpha_{\text{em}}} \int_{\nu_0}^{\infty} \mathrm{d}\nu \left[\frac{\sigma_{LT}(\nu, Q^2)}{Q}\right]_{Q^2\to 0}, \tag{6.14}$$

where the value of the Compton amplitude at infinite energy (asymptotic value) for each kind of interactions from Eq. (6.5) is given by

$$\frac{1}{2\pi\alpha_{\text{em}}} \lim_{\nu\to\infty} S_{LT}^{S}(\nu, Q^2 = 0) = \frac{C_S^2}{8\pi^2}, \tag{6.15a}$$

$$\frac{1}{2\pi\alpha_{\text{em}}} \lim_{\nu\to\infty} S_{LT}^{P}(\nu, Q^2 = 0) = -\frac{C_P^2}{8\pi^2}, \tag{6.15b}$$

$$\frac{1}{2\pi\alpha_{\text{em}}} \lim_{\nu\to\infty} S_{LT}^{V}(\nu, Q^2 = 0) = 0, \tag{6.15c}$$

$$\frac{1}{2\pi\alpha_{\text{em}}} \lim_{\nu\to\infty} S_{LT}^{A}(\nu, Q^2 = 0) = -\frac{C_A^2}{8\pi^2}\left(\frac{2m_{\mu}}{M_X}\right)^2. \tag{6.15d}$$

Note that the Compton amplitude for the vector contribution tends to zero at infinite energy regardless of the mass of the vector field. The asymptotic values for the scalar and pseudoscalar contributions are also mass-independent and have the opposite signs and the same absolute values as long as their coupling constants are identical.

However, the constant for axial-vector contribution depends on both lepton and axial-vector masses. This dependence, though, is expectable due to the equivalence of the pseudoscalar and axial-vector couplings at this level (similar to the pseudoscalar and pseudovector coupling equivalence in χPT). It

stems from the "longitudinal" part $\propto k^\mu k^\nu / M_X^2$ of the axial-vector propagator. In order to show it explicitly, let us choose the loop momentum k^μ along the axial-vector exchange going in clockwise direction in Fig. 6.2, and fix the initial (p^μ) and final ($p'^\mu = (p+q)^\mu$) four-momenta of the muon. Then we need to consider the following loop integral:

$$I_A^\mu = -\frac{1}{M_X^2}\int d^4k \frac{\bar{\mu}(p'+k)\not{k}\gamma_5\Delta^\mu(p')\gamma^\mu\Delta^\mu(p+k)\not{k}\gamma_5\mu(p)}{k^2-M_X^2}, \tag{6.16}$$

where Δ^μ is the muon propagator defined in Appendix 6.C and $\mu(p)$ and $\bar{\mu}$ are the on-shell muon spinors. By expressing the loop momentum as $\not{k} = \not{p}' + \not{k} - \not{p}' = \not{p} + \not{k} - \not{p}$ and using the Dirac equation for the on-shell muons, the integral can be simplified to the following form

$$I_A^\mu = \frac{4m_\mu^2}{M_X^2} I_P^\mu + \bar{\mu}(p')\gamma^\mu\mu(p)(...), \tag{6.17a}$$

$$I_P^\mu = \int d^4k \frac{\bar{\mu}(p'+k)\gamma_5\Delta^\mu(p')\gamma^\mu\Delta^\mu(p+k)\gamma_5\mu(p)}{k^2-M_X^2}, \tag{6.17b}$$

where the integral I_P^μ essentially corresponds to the the exchange with the pseudoscalar coupling inside the loop, while the second term in Eq. (6.17a) does not contribute to the AMM.

The situation when the physical Compton amplitude at infinite energy approaches some particular model-dependent constant value, which is not driven by any of the fundamental physical principles, looks very unnatural. Although the unitarity is not violated in this case, it can be treated as an artifact due to incompleteness of the theory (e.g. incorrect behaviour at high energies). By contrast, in the complete physical theory we expect that the Schwinger sum rule holds without any additional constant.

Since the contributions written in Eqs. (6.15a)-(6.15d) have different signs, the key observation lies in the following: if the theory contains different types of particles, the cancellation between the asymptotic values of the corresponding Compton amplitudes may occur. Indeed, the simplest case of such a cancellation may occur between the scalar and pseudoscalar contributions, i.e. between Eqs. (6.15a) and (6.15b). It happens, e.g., in the linear σ-model for the neutral-current contribution to the AMM of the proton, arising from the π^0 and σ mesons. The more complicated scenario, when the cancellation occurs between the scalar and axial-vector asymptotic values, say between Eqs. (6.15a) and (6.15d), is realized in the SM for Z^0-boson and Higgs particle contributions. These two mentioned cases will be considered in more details in the following sections.

6.3 Schwinger sum rule in low-energy effective field theories

The Schwinger sum rule was verified in heavy-baryon chiral perturbation theory two decades ago (see, e.g., [370]). Here, we focus on its verification at the leading-order contributions in relativistic low-energy theories, such as the linear σ-model and BχPT. In what follows, we argue that the Schwinger sum rule remains valid and that the high-energy artifacts of low-energy effective field

theories can always be removed through proper UV-completion. This argument is particularly relevant to the evaluation of the pseudoscalar meson exchange contribution to the HLbL of the muon AMM, which will be discussed in Section 6.5.

6.3.1 AMM of the proton

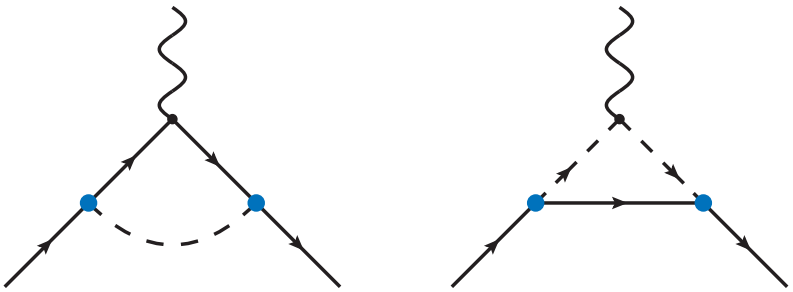

Fig. 6.4 The one-loop contributions to the nucleon anomalous magnetic moment.

The leading-order hadronic correction to the anomalous magnetic moment of the proton can be estimated by considering the one-loop pion contributions to the nucleon-photon vertex, as shown in Fig. 6.4. One of the simplest models to account for the pion-nucleon interactions is the linear σ-model. Its meson-nucleon part, which contributes to the AMM of the proton, reads

$$\begin{aligned}\mathcal{L}_{\text{int}}^{\pi N} &= g_{\pi N}\left(\bar{\psi}_p\psi_p\right)\sigma + g_{\pi N}\left(\bar{\psi}_p i\gamma_5\psi_p\right)\pi^0 \\ &\quad +\sqrt{2}g_{\pi N}\bar{\psi}_p i\gamma_5\psi_n\pi^+ + \sqrt{2}g_{\pi N}\bar{\psi}_n i\gamma_5\psi_p\pi^-,\end{aligned} \tag{6.18}$$

where ψ_p and ψ_n are the proton and neutron spinors whereas the part responsible for the electromagnetic interactions, consists of the QED term for proton and the scalar QED for charged pions,

$$\begin{aligned}\mathcal{L}_{\text{int}}^{\text{EM}} &= -\bar{\psi}_p\gamma^\mu\psi_p A_\mu + iA_\mu(\pi^+\partial^\mu\pi^- - \pi^-\partial^\mu\pi^+) \\ &\quad +A_\mu A^\mu\pi^+\pi^-.\end{aligned} \tag{6.19}$$

In this model, the LT-polarized cross section in the Schwinger sum rule contains contributions from three different channels,depicted in the three lines of Fig. 6.5, which differ by the particles in the final states. The contribution to the Schwinger sum rule from the amplitudes in the first line of Fig. 6.5 corresponds to the left vertex diagram in Fig. 6.4. We checked that the loop answer for this contribution (see, e.g. [371]) is exactly reproduced via the Schwinger sum rule without any additional constants.

Being taken separately, the π^0 contribution, however, cannot be reproduced via Eq. (2.123) because of the nonvanishing constant behavior of the corresponding Compton amplitude at infinite energy, given by Eq. (6.15b) with $C_S = g_{\pi N}$. The Schwinger sum rule result for the σ-meson contribution is also shifted with respect to the loop result by the value given in Eq. (6.15a) with $C_P = g_{\pi N}$. Fortunately, the constants for π^0 and σ-meson have the same moduli, but the opposite signs. Therefore

the Schwinger sum rule holds exactly when these contributions are both taken into account,

$$\varkappa_p^{\sigma\text{-model}}[\text{loop}] = \varkappa_p^{\sigma\text{-model}}[\text{sum rule}], \tag{6.20}$$

where the loop result $\varkappa^{\sigma\text{-model}}[\text{loop}]$ is provided in Eq. 6.112 of Appendix 6.A.

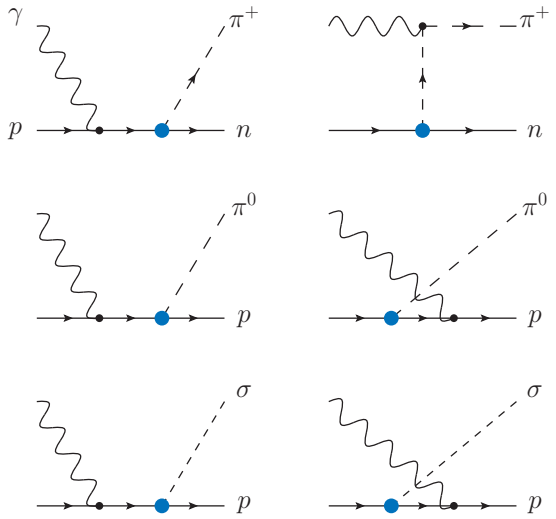

Fig. 6.5 Amplitudes that contribute to the proton photoabsorption cross section. The inclusion of the σ along with the π^0 with the same coupling fixes the Schwinger sum rule.

In BχPT, however, the situation is different. In contrast to the linear σ-model, this theory does not contain scalar degrees of freedom. Therefore, at the order $O(p^3)$ the Schwinger sum rule fails to reproduce the correct result of the proton AMM since the asymptotoic constant is not compensated:

$$\varkappa_p^{\text{B}\chi\text{PT}}[\text{loop}] = \varkappa_p^{\text{B}\chi\text{PT}}[\text{sum rule}] - \frac{g_{\pi N}^2}{8\pi^2}, \tag{6.21}$$

where the loop result $\varkappa^{\text{B}\chi\text{PT}}[\text{loop}]$ is given in Eq. (6.111) of Appendix 6.A. Analyzing the behavior of the corresponding one-loop diagrams, which constitute the Compton scattering amplitude, one can find out that the nonzero asymptotic constant stems from the box diagram with the neutral pion (Fig. 6.6). Moreover, the part of the box diagram, which is responsible for the constant at infinite energy, has a "triangular" topology (i.e. the box with cancelled pion propagator) that is shown in the right-hand side

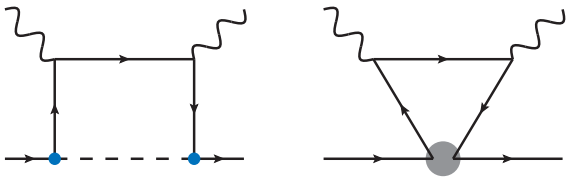

Fig. 6.6 Box diagram of Compton scattering at LO in BχPT, which is responsible for an asymptotic constant (left) and its effective UV completion (right).

of Fig. 6.6. In fact, this triangular diagram corresponds to the nucleon-antinucleon interaction, which cannot be described by just the LO BχPT. In this case one can introduce the effective UV completion of BχPT, which implies the subtraction of such contributions from the Compton amplitude. In this way, the Schwinger sum rule remains valid.

6.3.2 Comment on Schwinger sum rule for neutron

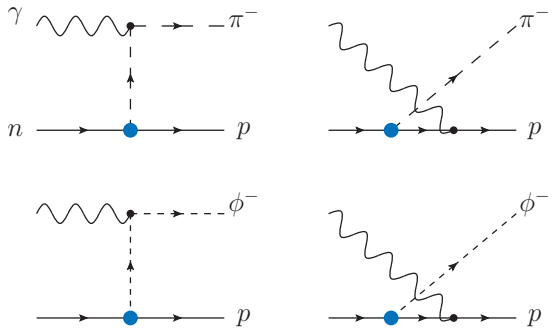

Fig. 6.7 Amplitudes that contribute to the neutron photoabsorption cross section.

The magnetic moment of the neutron, as a pointlike neutral particle, equals zero, while the anomalous part of the magnetic moment can appear in higher-order quantum corrections. For example, taking into account the $O(p^3)$ χPT correction, depicted diagrammatically in Fig. 6.4, already results in the nonzero contribution to the neutron AMM (see, e.g. [371]).

Though the quantum corrections produce the nonzero AMM of the neutron, the Schwinger sum rule must always give zero on the l.h.s. due to the zero charge of the neutron, i.e.,

$$0 \times \varkappa_n = \frac{m_n^2}{\pi^2 \alpha} \int_{\nu_0}^{\infty} \mathrm{d}\nu \left[\frac{\sigma_{LT}^n(\nu, Q^2)}{Q} \right]_{Q^2 \to 0} = 0, \tag{6.22}$$

serving as a superconvergent relation. However, the sum rule integral over the corresponding polarized cross section (the amplitudes are schematically shown in the top line of Fig. 6.7) yields the nonzero answer,

$$\frac{m_n^2}{\pi^2 \alpha} \int_{\nu_0}^{\infty} \mathrm{d}\nu \left[\frac{\sigma_{LT}^{n,(p^3)}(\nu, Q^2)}{Q} \right]_{Q^2 \to 0} = \frac{g_{\pi N}^2}{4\pi^2}. \tag{6.23}$$

This mass-independent constant is also due to the nonzero asymptotic value of the corresponding Compton amplitude. It comes from the same box diagram as in the case of the proton (see Fig. 6.6), but with the charged pion inside the loop. This constant can be cancelled by adding a contribution from a charged scalar field $\phi^{\pm}$, as shown in the bottom line of Fig. 6.7. Moreover, it was checked explicitly, that at this order of χPT, the presence or absence of the charged scalar particle in the theory does not have any influence on the result for the proton AMM. However, there is no experimental evidence for the existence of the charged scalar particle that consists of u and d quarks: the lowest-lying charge

scalar is $D^*_{s0}(2317)^\pm$, which has the quark content $c\bar{s}$ or $s\bar{c}$. Nevertheless, the arguments on the effective UV completion of BχPT could be repeated here as well: in order to make the sum rule valid in this theory, one needs to effectively fix the nucleon-antinucleon interaction by subtracting the ill-behaved contributions from the Compton amplitude.

6.4 Electroweak contributions to muon AMM

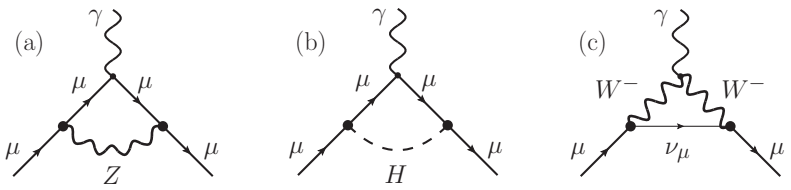

Fig. 6.8 Electroweak contributions to the AMM of the muon at one loop: (a) Z^0-boson, (b) Higgs and (c) $W^\pm$-boson.

The leading-order correction to the AMM of the muon due to the electroweak sector of the SM is shown in Fig. 6.8. These diagrams have been calculated long time ago by Brodsky and Sullivan [372], Bars and Yoshimura [373], Jackiw and Weinberg [374], Fujikawa et al. [375], Aydin et al. [376] and others. There has been an intensive discussion on the correct evaluation of the Z^0-boson contribution due to the apparent arbitrariness of the result. This puzzle was fundamentally explained in the work by Fujikawa et al. [375]. It was shown that the specific divergence structure (linearly-divergent loop integral), which is similar to the case of celebrated axial anomaly, was responsible for this issue, but, in contrast to the axial anomaly, can be easily overcome. The work of Fujikawa et al. is also remarkable for the clear formulation of the spontaneously broken gauge theories using generalized renormalizable (linear) R_ξ gauge. In particular, it was demonstrated that in the Weinberg-Salam model the one-loop contributions to the AMM of the lepton, depicted in Fig. 6.8, are gauge-independent as long as the AMM of the $W^\pm$-boson vanishes, i.e. $g_W = 2$ at tree-level. The latter guarantees the tree-level unitarity for Compton cross sections. However, it was pointed out that the electromagnetic form factors with the nonzero photon virtuality are, in general, gauge-dependent quantities, since they are not the observable S-matrix elements. This fact brings the ambiguity into the definition of, e.g., the neutrino charge radius. Subsequently, numerous efforts have been performed in order to find an unambiguous definitions for the electromagnetic form factors. The calculations using background-field method and current algebra formalism have been led to the formal prescription called “pinch technique” (see the comprehensive review [377] and references therein).

Regarding the Compton scattering sum rules, to the best of our knowledge, so far only the GDH sum rule was tested against the electroweak theory [378, 379]. The test was performed at leading order, when only the tree-level diagrams were included in the polarized cross section. The sum rule then yielded zero, as it should be at the considered order. What is also important, the corresponding Compton amplitude as well as its imaginary part are gauge-independent in the limit of real photons.

In view of this history of direct calculations, the verification of the Schwinger sum rule in the electroweak theory becomes a highly intriguing task. On the one hand, similar to the GDH sum rule, it involves an observable of lepton-muon scattering – the LT-polarized cross section. On the other hand, since this observable involves a virtual photon, thus it can suffer from the same gauge-dependence issues as the electromagnetic form factors in gauge theories. In following, an attempt to solve the mentioned task is provided. It is convenient to separate the Z^0-boson and Higgs scalar contributions from $W^\pm$ one, since they are independent in a sense of the gauge parameters and also different in technical complexity.

6.4.1 Neutral-current contribution from Z^0 and Higgs

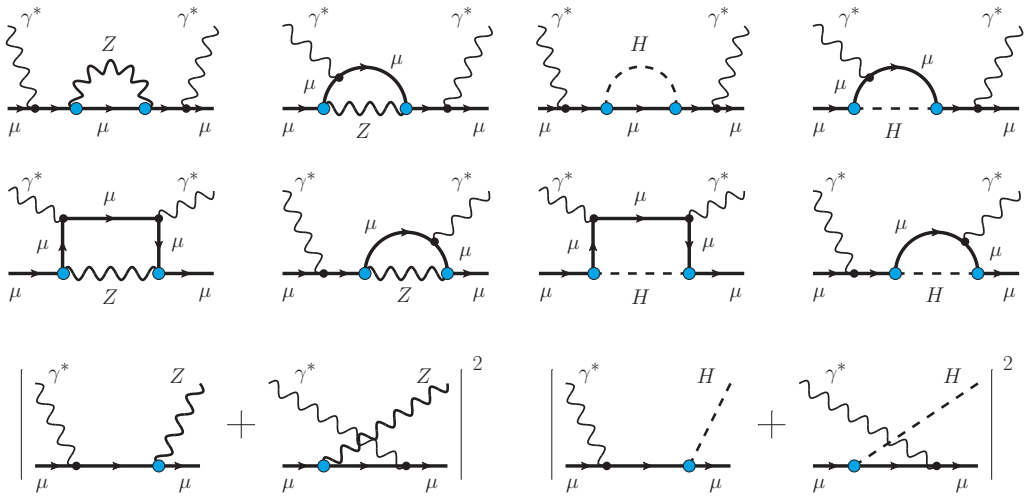

Fig. 6.9 Z^0-boson and Higgs contributions to the forward doubly-virtual Compton amplitude at one-loop level (first and second rows) and the corresponding cross sections (third row), that reproduces its imaginary part.

According to the SM Lagrangian, the interactions of Z^0 and Higgs bosons with the charged lepton $l = e, \mu, \tau$, which has a mass m_l, have the following form

$$\mathcal{L}_{\text{int}}^{Z^0+H} = \frac{g}{4\cos\theta_W}\bar{l}\not{Z}^0\left[\mathbb{1}(1-4\sin^2\theta_W)-\gamma_5\right]l - \frac{gm_l}{2M_Z\cos\theta_W}H\bar{l}l. \tag{6.24}$$

Here $g = \sqrt{4\pi\alpha}/\sin\theta_W$ is the electroweak coupling constant and θ_W is the Weinberg angle.

The corresponding one-loop Compton amplitudes that are important for the Schwinger sum rule, are shown in Fig. 6.9 along with the tree-level amplitudes, relevant for the LT-polarized cross sections[1]. These diagrams immediately bring us to the conclusion: at this order, the Schwinger sum rule result cannot depend on the gauge of Z^0-boson. It simply follows from the absence of the virtual intermediate Z^0-bosons in the tree-level diagrams, which enter the LT-polarized cross section.

[1]Given that in R_ξ gauges fixing the gauge of the Z^0-boson is independent of the gauge of the photon and $W^\pm$-bosons, it is enough to consider neutral bosons just in unitary gauge.

Given that the Z^0-boson contribution includes the vector and axial-vector part, the latter causes the following nonzero constant behavior of the Compton amplitude at infinite energy

$$\frac{1}{2\pi\alpha_{\rm em}}\lim_{\nu\to\infty} S_{LT}^{Z^0}(\nu, Q^2=0) = -\frac{[g/(4\cos\theta_W)]^2}{8\pi^2}\left(\frac{2m_\mu}{M_Z}\right)^2. \tag{6.25}$$

However, the Compton amplitude with the contribution from the Higgs particle also produces the constant at infinite energy,

$$\frac{1}{2\pi\alpha_{\rm em}}\lim_{\nu\to\infty} S_{LT}^{H}(\nu, Q^2=0) = \frac{1}{8\pi^2}\left[\frac{g m_\mu}{2M_Z\cos\theta_W}\right]^2. \tag{6.26}$$

Finally, we observe that

$$\lim_{\nu\to\infty}\left[S_{LT}^{Z^0}(\nu, Q^2=0) + S_{LT}^{H}(\nu, Q^2=0)\right] = 0. \tag{6.27}$$

Consequently, the dispersive integral in the Schwinger sum rule exactly reproduces the direct loop calculation (cf. [369, 372–375]) only for the entire contribution of Z^0-boson and Higgs, but fails for the individual contributions when taken separately. This example clearly illustrates the point that the sum rule should hold in the UV-complete theories without any additional constants.

6.4.2 The charged-current contribution from $W^\pm$-boson

Besides the Z^0-boson and the Higgs scalar, the charged $W^\pm$-boson also contributes to the lepton AMM at the same order of the electroweak coupling, as shown in Fig: 6.8(c). The calculation of this diagram in unitary gauge gives the following result for the AMM contribution (see, e.g. [369], eq. (4))

$$\begin{aligned} \varkappa_\mu(W) &= \frac{g^2 m_\mu^2}{16\pi^2}\int_0^1 dx\, x\,\frac{1+x-\frac{m_\mu^2}{2M_W^2}(1-x)}{m_\mu^2 x + (M_W^2 - m_\mu^2)} && (6.28)\\ &= \frac{g^2}{64\pi^2}\frac{\mu^2\left(\mu^4+8\mu^2-4\right) - 2\left(3\mu^4-5\mu^2+2\right)\log\left(1-\mu^2\right)}{\mu^4} \\ &= \frac{5g^2}{96\pi^2}\mu^2 + O(\mu^4) \approx \frac{5\sqrt{2}}{24\pi^2}G_F m_\mu^2 && (6.29)\end{aligned}$$

with the mass ratio $\mu = m_\mu/M_W$ and the Fermi constant $G_F = \sqrt{2}(g^2/8M_W^2)$. It was shown in several works, e.g. [373–375], that this result is independent on the gauge of the $W^\pm$-boson as long as the AMM of this boson vanishes (see Appendix 6.B). One might expect that this contribution can be reproduced using the Schwinger sum rule as well. We will discuss this in the following subsections.

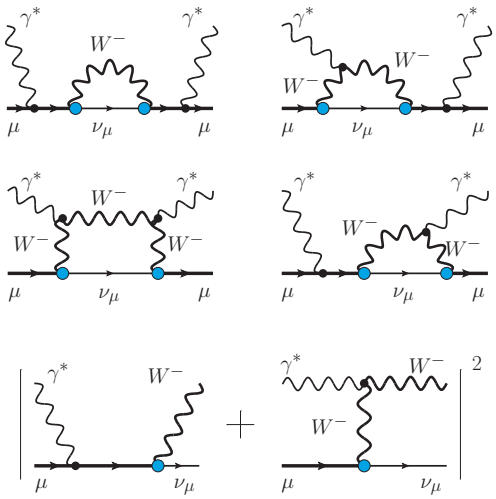

Fig. 6.10 $W^{\pm}$-boson contribution to the forward doubly-virtual Compton amplitude at one-loop level (first and second rows) and the corresponding cross sections (third row), that reproduces its imaginary part.

6.4.2.1 Unitary gauge

Let us start with the calculation of the doubly-virtual one-loop Compton LT-polarized amplitude S_{LT} with $W^{\pm}$-bosons in unitary gauge. The diagrams for this amplitude are shown in Fig. 6.10 and are explicitly written in Appendix 6.D. The total amplitude divided by Q, in the limit $Q \to 0$ reads

$$\begin{aligned}
\lim_{Q\to 0}\frac{1}{Q}S_{LT}(\nu,Q) = \frac{g^2e^2}{512\pi^2 m_\mu \mu^2}\Bigg\{&\frac{8\mu^4\left(4\mu^2-15w^2\right)}{\mu^2-4w^2}\\
&+\frac{2\left(1-\mu^2\right)\left(\mu^4\left(w^2-11\right)+\mu^2\left(3w^2-13\right)+2\right)}{w^2}\log\left[1-\mu^2\right]\\
&+\Bigg[\frac{\mu\left(\mu^2-2\mu w-1\right)}{w^2(\mu-2w)^2}\Big(-4w\\
&\quad+\mu\left(2-13\mu^2-11\mu^4+42\mu(1+\mu^2)v+(-32-37\mu^2+\mu^4)v^2-2\mu(4+\mu^2)v^3\right)\Big)\\
&\qquad\times\log\left[1-\mu(\mu-2w)\right]\\
&+\frac{4\mu^4(\mu(-((\mu-2w)(\mu+w))-10)+6w)C_0\left(0,\mu^2,\mu(\mu-2w);1,1,0\right)}{w}+\{w\to -w\}\Bigg]\Bigg\},
\end{aligned}\tag{6.30}$$

where the rescaled energy $w \equiv \nu/M_W$ was introduced.

The low-energy limit of this amplitude,

$$\lim_{\substack{Q\to 0\\ \nu\to 0}}\frac{1}{Q}S_{LT}(\nu,Q) = \frac{g^2e^2}{2m_\mu}\left[\frac{\mu^2(\mu^4+8\mu^2-4)-2\left(3\mu^4-5\mu^2+2\right)\log\left(1-\mu^2\right)}{64\pi^2\mu^4}\right],\tag{6.31}$$

in full agreement with the low-energy theorem, exactly reproduces the result for the AMM given by Eq. (6.29).

According to the optical theorem, the imaginary part of the aforementioned amplitude,

$$\begin{aligned}
&\mathrm{Im}\lim_{Q\to 0}\frac{1}{Q}S_{LT}(\nu,Q)=\frac{g^2e^2}{512\pi m_\mu\mu^2w^2(\mu+2w)^2}\theta\left[w-\frac{\mu^2-1}{2\mu}\right]\\
&\times\Big\{(-1+\mu(\mu-2w))\left[\mu^4w^2(\mu+2w)-\mu^2\left(42w\mu^2+11\mu^3-8w^3+37w^2\mu\right)\right.\\
&\quad\left.+2(\mu+2w)-\mu(\mu+2w)(13\mu+16w)\right]\\
&\quad-2\mu^2(\mu+2w)^2\left[w\mu^2+\mu^3-2w^2\mu+2(5\mu+3w)\right]\log\left[\mu(\mu+2w)\right]\Big\},
\end{aligned}\tag{6.32}$$

should be directly related to the corresponding LT cross section, namely

$$\mathrm{Im}\lim_{Q\to 0}\frac{1}{Q}S_{LT}(\nu,Q)=m_\mu\lim_{Q\to 0}\frac{\sqrt{\nu^2+Q^2}\sigma_{LT}(\nu,Q^2)}{Q}.\tag{6.33}$$

The tree-level amplitude for this cross section reads

$$\begin{aligned}
\mathcal{M}_{\lambda,h\to\lambda',h'}=&\frac{ge}{2\sqrt{2}}\overline{\nu}_{h'}(l')\Big\{\frac{\gamma_\sigma(\mathbb{1}-\gamma_5)(\not{l}+\not{q}+m_\mu)\gamma_\mu}{s-m_\mu^2}\\
&+\frac{1}{t-M_W^2}\left[-g^{\rho\alpha}+\frac{(q'-q)^\rho(q'-q)^\alpha}{M_W^2}\right]\Gamma^{\mathrm{U}}_{\alpha\mu\sigma}(q,q')\gamma_\rho(\mathbb{1}-\gamma_5)\Big\}\mu_h(l)\varepsilon^\mu_\lambda(q)\chi^{\sigma\,*}_{\lambda'}(q'),
\end{aligned}\tag{6.34}$$

where q and q' (ε and χ) are the four-momenta (polarization vectors) of the incoming photon and outgoing W^--boson, respectively, while μ_h and $\overline{\nu}_{h'}$ are, correspondingly, the Dirac spinors for initial muon and final neutrino states. The three-boson vertex in unitary gauge has the form (cf. Appendix 6.C)

$$\Gamma^{\mathrm{U}}_{\alpha\mu\sigma}(q,q')=g_{\mu\sigma}(q+q')_\alpha+g_{\alpha\mu}(q'-2q)_\sigma+g_{\alpha\sigma}(q-2q')_\mu,\tag{6.35}$$

In order to obtain the matrix element responsible for the LT-polarized cross section, the following completeness relation for the $W^\pm$-boson polarization vectors is applied

$$\sum_{\lambda=-1,0,1}\chi^\alpha_\lambda(q')\chi^{*\beta}_\lambda(q')=-g^{\alpha\beta}+\frac{q'^{\,\alpha}q'^{\,\beta}}{M_W^2}.\tag{6.36}$$

Then, for the LT cross section one finds the result, which is in full agreement with the optical theorem (6.33). At the asymptotically high energies, the cross section behaves as

$$\lim_{\substack{Q\to 0\\ \nu\to\infty}}\frac{\sigma_{LT}(\nu,Q)}{Q}=\frac{g^2e^2}{512\pi m_\mu^2M_W}\left[1+4\frac{M_W^2}{m_\mu^2}\left(1-\log\frac{2m_\mu\nu}{M_W^2}\right)\right]\frac{1}{\nu}+O\left(\frac{\log\nu}{\nu^2}\right).\tag{6.37}$$

Thus, the integral over this cross section in the Schwinger sum rule (2.123) will be logarithmically divergent at the upper limit. At this point, we can conclude, that in unitary gauge

- the optical theorem (unitarity) holds,
- the sum rule integral is logarithmically divergent.

It is well known, however, that in unitary gauge the gauge theory with vector bosons has several caveats connected to the tree-level unitarity. The simplest way to overcome these issues is to carry out the calculations in a different gauge, e.g., in the Feynman-t'Hooft gauge.

6.4.2.2 Feynman-t'Hooft gauge in the linear gauge condition

As soon as the linear gauge condition on the $W^{\pm}$-bosons is imposed [375, 380], the propagators of the bosons become gauge-dependent. Furthermore, now one needs to take care of the charged scalar modes with gauge-dependent propagators, which will be present in the diagrams along with $W^{\pm}$-bosons. The three-boson interaction vertex, however, stays gauge-independent in this case (cf. Appendix 6.C). In the Feynman-t'Hooft gauge, the gauge parameter ξ is set to be equal to unity. In this way, the longitudinal degrees of freedom of the exchanged $W^{\pm}$-bosons are absorbed into the charged scalar exchanges with the same mass, and no unphysical thresholds will be introduced. The total Compton amplitude is then given by

$$\begin{aligned}
\lim_{Q\to 0}\frac{1}{Q}S_{LT}(\nu,Q) = \frac{g^2e^2}{512\pi^2 m_\mu \mu^2}\Bigg\{ & 48\mu^4 \\
& + \frac{2\left(\mu^2-1\right)\left(11\mu^4+\mu^2\left(8\nu^2+13\right)-2\right)}{w^2}\log\left(1-\mu^2\right) \\
& + \Bigg[\frac{\mu\left(1-\mu(\mu-2w)\right)}{w^2(\mu-2w)}\Big(\mu\left(11\mu^3+13\mu+8\mu w^2-8\left(3\mu^2+2\right)w\right)-2\Big) \\
& \quad \times\log\left(1-\mu(\mu-2w)\right) \\
& \quad - \frac{4\mu^4\left(\mu^3+10\mu-\left(\mu^2+8\right)w\right)C_0\left(0,\mu^2,\mu(\mu-2w);1,1,0\right)}{w} + \{w\to -w\}\Bigg]\Bigg\},
\end{aligned} \tag{6.38}$$

and has the same low-energy limit (6.31). The tree-level amplitude for the Schwinger sum rule reads

$$\begin{aligned}
\mathcal{M}_{\lambda,h\to\lambda',h'} = \frac{ge}{2\sqrt{2}}\bar{v}_{h'}(l')\Big\{ & \frac{\gamma_\sigma(\mathbb{1}-\gamma_5)(\not{l}+\not{q}+m_\mu)\gamma_\mu}{s-m_\mu^2} \\
& + \frac{1}{t-M_W^2}\left[-g^{\rho\alpha}\Gamma_{\alpha\mu\sigma}(q,q')\gamma_\rho(\mathbb{1}-\gamma_5)+m_\mu g_{\mu\sigma}(\mathbb{1}+\gamma_5)\right]\Big\}\mu_h(l)\varepsilon_\lambda^\mu(q)\chi_{\lambda'}^{\sigma\,*}(q').
\end{aligned} \tag{6.39}$$

Now it includes the extra exchange of the scalar mode (second term in the rectangular brackets). Calculation of the LT cross section is carried out similarly to the case of unitary gauge, and gives the

following result

$$\lim_{Q\to 0}\frac{\sigma_{LT}(\nu,Q^2)}{Q}=\frac{g^2e^2}{512\pi m_\mu^3 w^3(\mu+2w)}$$
$$\times\Big\{(-1+\mu(\mu+2w))\left(-2+\mu(16w+\mu(13+(\mu+2w)(11\mu+2w)))\right)$$
$$-2\mu^2(\mu+2w)\left(2w\mu^2+\mu^3+10\mu+7w\right)\log\left[\mu(\mu+2w)\right]\Big\}$$
$$=\frac{g^2e^2}{128\pi\nu M_W^2}+O\left(\frac{1}{\nu^2}\right). \tag{6.40}$$

This cross section also has $O(\nu^{-1})$ asymptotic behavior, hence the sum rule integral is again divergent as for the calculation in unitary gauge. Moreover, Eq. (6.40) does not coincide with the imaginary part of the corresponding Compton amplitude - the unitarity is violated!

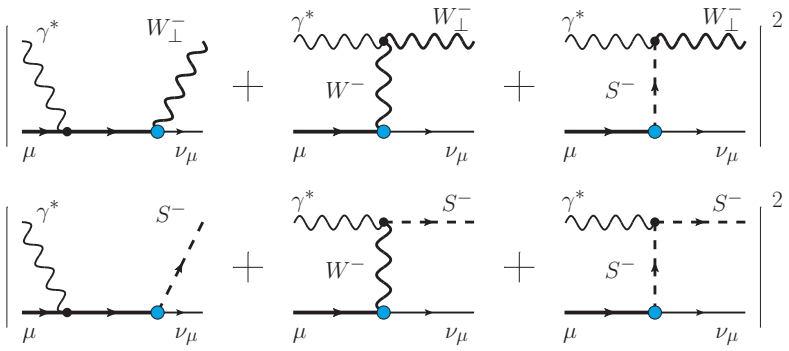

Fig. 6.11 The alternative way to obtain the cross section in Feynman-t'Hooft gauge, invoking the unphysical scalar modes in the final state.

In order to check the result (6.40), the alternative way of calculating this cross section is performed. It resides in dropping out the longitudinal polarizations of $W^\pm$ from the sum (6.36), taking

$$\sum_{\lambda=-1,1}\chi_\lambda^\alpha(q')\chi_\lambda^{*\beta}(q')=-g^{\alpha\beta}. \tag{6.41}$$

while adding the cross section of the similar process, but with the scalar modes in final states, to the final answer (see Fig. 6.11). This way should result in the same answer due to the Goldstone boson equivalence theorem. Evaluation of the corresponding cross sections gives

$$\lim_{Q\to 0}\frac{\sigma_{LT}^{W_\perp}(\nu,Q^2)}{Q}=-\frac{g^2e^2}{256\pi M_W w^2Q^2(\mu+2w)}\left\{\mu(\mu+2w)\left[1-\log\left(\mu(\mu+2w)\right)\right]-1\right\}$$
$$+\frac{g^2e^2}{1024\pi m_\mu^3 w^4(\mu+2w)^2}\Big\{(\mu(\mu+2w)-1)\left[16w\mu^5-3\mu^4\left(1-24w^2\right)\right.$$

$$+6w\mu^3\left(16w^2+1\right)+\mu^2\left(32w^4+44w^2-1\right)-8w\mu\left(1-6w^2\right)-12w^2 1\big]$$
$$-2\mu(\mu+2w)^2\big[17w\mu^2-2\mu\left(1-8w^2\right)-3wM^2\big]\log\left(\mu(\mu+2w)\right)\Big\}, \tag{6.42}$$

$$\lim_{Q\to 0}\frac{\sigma_{LT}^{S}(\nu,Q^2)}{Q}=\frac{g^2e^2}{256\pi M_W w^2Q^2(\mu+2w)}\left\{\mu(\mu+2w)\left[1-\log\left(\mu(\mu+2w)\right)\right]-1\right\}$$
$$+\frac{g^2e^2}{1024\pi m_\mu^3 w^4(\mu+2w)^2}\Big\{\left(\mu(\mu+2w)-1\right)\left[6w\mu^5+16w^3\mu\left(\mu^2+1\right)\right.$$
$$+4w^2\left(10\mu^2+5\mu^4+1\right)+4w\mu\left(5\mu^2+1\right)+\mu^2\left(3\mu^2+1\right)\big]$$
$$-2\mu(\mu+2w)^2\big[2\mu^3w(\mu+w)+3\mu^2w+(2\mu+3w)\big]\log\left(\mu(\mu+2w)\right)\Big\}. \tag{6.43}$$

The terms that are inversely proportional to Q^2 indicate the violation of the gauge invariance with respect to the incoming virtual photon. However, the sum of these cross sections results in the gauge-invariant expression,

$$\lim_{Q\to 0}\frac{\sigma_{LT}^{W_\perp}(\nu,Q^2)+\sigma_{LT}^{S}(\nu,Q^2)}{Q}=\frac{g^2e^2}{512\pi m_\mu^3 w^3(\mu+2w)}$$
$$\times\Big\{\left(-1+\mu(\mu+2w)\right)\left(-2+\mu(16w+\mu(13+(\mu+2w)(11\mu+2w)+4w^2))\right)$$
$$-2\mu^2(\mu+2w)\left(w\mu^2+\mu^3+10\mu+8w\right)\log\left[\mu(\mu+2w)\right]\Big\}. \tag{6.44}$$

While not agreeing with Eq. (6.40), this expression exactly reproduces the corresponding imaginary part of the doubly-virtual Compton amplitude via the optical theorem, thus the unitarity relation is restored. Unfortunately, the cross section given by Eq. (6.44) also behaves as $O(1/\nu)$ at high energies,

$$\lim_{Q\to 0}\frac{\sigma_{LT}^{W_\perp}(\nu,Q^2)+\sigma_{LT}^{S}(\nu,Q^2)}{Q}=\frac{g^2e^2}{64\pi M_W^2\nu}+O\left(\frac{1}{\nu^2}\right), \tag{6.45}$$

thus making the integral over this cross section logarithmically divergent in the upper limit.

6.4.2.3 Feynman-t'Hooft gauge in the nonlinear gauge condition

First introduced by Lee and Yang [381] and then used by Fujikawa for electroweak gauge theories [380], the non-linear gauge condition implies the gauge-dependent three-boson vertex (cf. Appendix 6.C). The technical advantage of this gauge lies in the absence of the three-boson vertices with one scalar mode, say the γWS-vertices. This fact crucially reduces the number of Feynman diagrams compared to the case when the linear gauge is applied, leaving us with just sixteen diagrams (see Fig. 6.12) instead of thirty six. Moreover, in Feynman-t'Hooft gauge, the γWW vertex has an especially simple

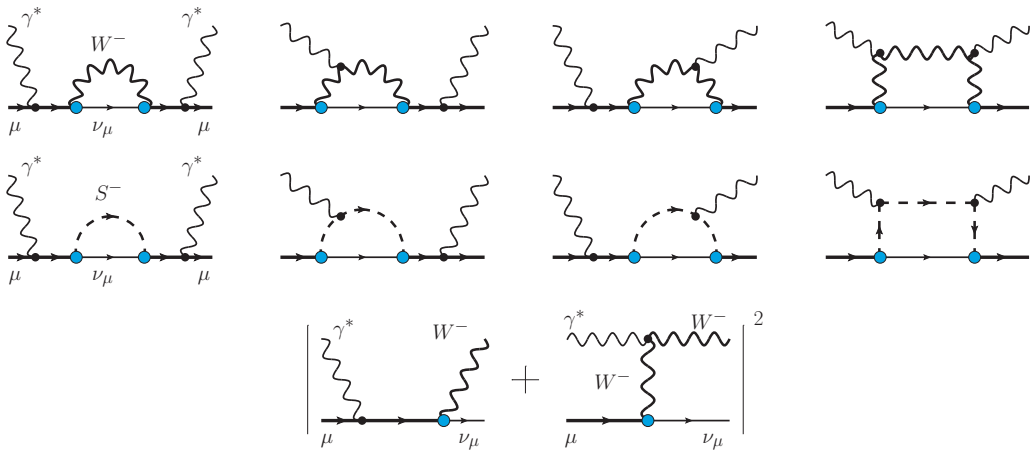

Fig. 6.12 $W^{\pm}$-boson contribution in arbitrary gauge (nonlinear gauge condition is imposed) to the one-loop doubly-virtual Compton scattering amplitude (first and second rows, crossed diagrams are not shown) and the corresponding cross section (third row), that reproduces its imaginary part.

form

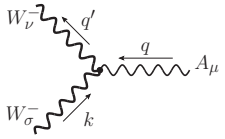

$$\Gamma^{\text{nonlin;FtH}}_{\mu\sigma\nu} = ie\left(g_{\nu\sigma}(2q'-q)_\mu - 2g_{\mu\nu}q_\sigma + 2g_{\sigma\mu}q'_\nu\right). \tag{6.46}$$

Calculation of the one-loop Compton amplitude in Feynman-t'Hooft gives

$$\begin{aligned}\lim_{Q\to 0}\frac{1}{Q}S_{LT}(\nu,Q^2) = \frac{g^2e^2}{512\pi^2 m_\mu \mu^2}\Bigg\{&32\mu^4 + \frac{2}{w^2}\left(11\mu^6+2\mu^4-15\mu^2+2\right)\log\left[1-\mu^2\right]\\ &+\Bigg[-\frac{\mu(\mu(\mu-2w)-1)}{(\mu-2w)w^2}\left(11\mu^4+13\mu^2-4\mu(2\mu^2+4)w-2\right)\\ &\log\left[1-\mu(\mu-2w)\right]\\ &-\frac{4\mu^4\left(\mu^3+10\mu-(\mu^2+6)w\right)}{w}C_0\left(0,\mu^2,\mu(\mu-2w);1,1,0\right)+\{w\to -w\}\Bigg]\Bigg\}\end{aligned} \tag{6.47}$$

The low-energy limit of this amplitude again reproduces the loop result for the AMM, thus is in full agreement with the low-energy theorem for the LT-polarized Compton amplitude. The high-energy behavior of this amplitude acquires a constant value at infinite energy,

$$\lim_{\substack{Q\to 0\\ \nu\to\infty}}\frac{1}{Q}S_{LT}(\nu,Q^2) = \frac{g^2e^2}{16\pi^2}\frac{m_\mu}{M_W^2} + O\left(\frac{1}{\nu}\right). \tag{6.48}$$

This fact already gives a hint that, as soon as the optical theorem works, the integral in the Schwinger sum rule should converge in this case, but, possibly, to a wrong value. In order to check this guess, the corresponding LT cross section should be obtained independently. As in the previous case with linear

gauge condition, we decide to obtain the physical degrees of freedom of the $W^{\pm}$-boson in the final state by considering the scalar mode instead of the longitudinal polarization of $W^{\pm}$. The tree-level diagrams are similar to those in linear gauge (see Fig. 6.11, excluding those with γWS-vertices).

The tree-level amplitudes for LT cross section read

$$\mathcal{M}^{W}_{\lambda,h\to\lambda',h'} = -\frac{ge}{2\sqrt{2}}\overline{\nu}_{h'}(l')\Big\{\frac{\gamma_\sigma(\mathbb{1}-\gamma_5)(\not{l}+\not{q}+m_\mu)\not{\varepsilon}_\lambda}{s-m_\mu^2} + \frac{1}{t-M_W^2}\left[2\not{\varepsilon}_\lambda q_\sigma + \gamma_\sigma(2q'-q)\cdot\varepsilon_\lambda - 2\varepsilon_{\lambda\sigma}\not{q}\right](\mathbb{1}-\gamma_5)\Big\}\mu_h(l)\chi^{\sigma\,*}_{\lambda'}(q'), \tag{6.49}$$

$$\mathcal{M}^{S}_{\lambda,h\to h'} = \frac{ge}{2\sqrt{2}}\frac{m_\mu}{M_W}\overline{\nu}_{h'}(l')\Big\{\frac{(\mathbb{1}+\gamma_5)(\not{l}+\not{q}+m_\mu)\not{\varepsilon}_\lambda}{s-m_\mu^2} + \frac{1}{t-M_W^2}\left[(2q'-q)\cdot\varepsilon_\lambda\right](\mathbb{1}+\gamma_5)\Big\}\mu_h(l) \tag{6.50}$$

and the LT cross sections are

$$\lim_{Q\to 0}\frac{\sigma^{W_\perp}_{LT}(\nu,Q^2)}{Q} = \frac{g^2e^2}{256\pi m_\mu^3\nu^3M_W^2(m_\mu+2\nu)} \times\Big\{(-1+\mu(\mu+2w))\left[-1+\mu(8w+\mu(7+4\mu(\mu+2w)))\right] - 2\mu^2(\mu+2w)(5\mu+3w)\log\left[\mu(\mu+2w)\right]\Big\}, \tag{6.51}$$

$$\lim_{Q\to 0}\frac{\sigma^{S}_{LT}(\nu,Q^2)}{Q} = \frac{g^2e^2}{512\pi m_\mu w^3\mu(\mu+2w)} \times\Big\{(-1+\mu(\mu+2w))\left(3\mu^2+4w\mu-1\right) - 2\mu^2(\mu+w)(\mu+2w)\log\left(\mu(\mu+2w)\right)\Big\}. \tag{6.52}$$

It is remarkable to mention that, in contrast to linear gauge, in nonlinear gauge these cross sections do not elucidate the violation of the gauge invariance – the terms, inversely proportional to the photon virtuality, are absent. The total cross section reads

$$\lim_{Q\to 0}\frac{\sigma_{LT}(\nu,Q^2)}{Q} = \lim_{Q\to 0}\frac{\sigma^{W_\perp}_{LT}(\nu,Q^2)+\sigma^{S}_{LT}(\nu,Q^2)}{Q} = \frac{g^2e^2}{512\pi m_\mu^3w^3(\mu+2w)}\Big\{(-1+\mu(\mu+2w))\left[-2+13\mu^2+11\mu^4+4\mu w(4+5\mu^2)\right] - 2\mu^2(\mu+2w)\left(6w+\mu(10+\mu(\mu+w))\right)\log\left[\mu(\mu+2w)\right]\Big\}. \tag{6.53}$$

This cross section satisfies the optical theorem, and the Schwinger sum rule holds as follows

$$\frac{m_\mu^2}{\pi^2\alpha}\int_{\nu_{\text{th.}}}^{\infty} d\nu \lim_{Q\to 0}\frac{\sigma_{LT}(\nu,Q^2)}{Q} = \lim_{\substack{Q\to 0\\ \nu\to 0}}\frac{1}{Q}S_{LT}(\nu,Q^2) - \lim_{\substack{Q\to 0\\ \nu\to\infty}}\frac{1}{Q}S_{LT}(\nu,Q^2) \tag{6.54}$$

6.4.2.4 Arbitrary gauge in the nonlinear gauge condition

The aforementioned results show that, despite of the correct low-energy behavior of the Compton amplitude in all considered cases, the unitarity relation (optical theorem) works only in a particular calculation scheme, which is obviously nonsense. This might point to the fact that something is missing in the calculation, so the cross section defined by Eq. (6.1) is in general gauge-dependent. In order to check this, a calculation of the polarized Compton amplitude in arbitrary gauge is performed. The nonlinear gauge condition was chosen for the sake of simplicity: as was already mentioned, it reduces the number of relevant diagrams to just sixteen. The result for the Compton amplitude reads

$$\begin{aligned}
&\lim_{Q\to 0}\frac{1}{Q}S_{LT}(\nu,Q^2) = \frac{g^2e^2}{512\pi^2 m_\mu \mu^2}\\
&\times\Bigg\{32\mu^4+\frac{2}{w^2}\left(2-15\mu^2+2\mu^4+11\mu^6\right)\log(1-\mu^2)\\
&\Bigg[-\frac{\mu^4(1+\xi)\left(-1+\mu\xi(\mu-2w)\right)\log(-\xi\mu(\mu-2w)+1)}{w(\mu-2w)\xi^2}\\
&-\frac{\mu(-1+\mu(\mu-2w))\left(\mu^3 w-2\xi+\mu(-16w+\mu(13+11\mu^2-21\mu w))\xi\right)}{w^2(\mu-2w)\xi}\\
&\quad\times\log(1-\mu(\mu-2w))\\
&-\frac{4\mu^4\left(\mu^3(\xi-1)-6w(\xi-1)+2\mu(5(\xi-1)+w^2)+\mu^2 w(1-\xi)\right)}{w(\xi-1)}\\
&\quad\times C_0(0,\mu^2,\mu(\mu-2w);1,1,0)\\
&+\frac{\mu^4\left(4w\xi(\xi-1)+2\mu^2 w\xi(\xi^2-1)+\mu(1-\xi+(-1+8w^2)\xi^2+\xi^3)\right)}{w\xi^2(\xi-1)}\\
&\quad\times C_0(0,\mu^2,\mu(\mu-2w);1,\xi^{-1/2},0)\\
&-\frac{\mu^4\left(4w\xi(\xi-1)+2\mu^2 w\xi(\xi^2-1)-\mu(1-\xi+(-1+8w^2)\xi^2+\xi^3)\right)}{w\xi^2(\xi-1)}\\
&\quad\times C_0(0,\mu^2,\mu(\mu-2w),\xi^{-1/2},1,0)\\
&-\frac{8\mu^5 w}{\xi-1}C_0(0,\mu^2,\mu(\mu-2w);\xi^{-1/2},\xi^{-1/2},0)+\{w\to -w\}\Bigg]\Bigg\},
\end{aligned}\tag{6.55}$$

where ξ is an arbitrary gauge-fixing parameter. The low-energy limit of this amplitude is gauge-independent and coincides with the common result given by Eq. (6.31). The high-energy behavior,

however, turns to be gauge-dependent

$$\lim_{\substack{Q\to 0\\ \nu\to\infty+i0}} \frac{1}{Q} S_{LT}^{\text{tot}}(\nu,Q,\xi) = \frac{g^2e^2}{32}\frac{m_\mu}{2\pi^2 M_W^2}\left\{1+\frac{\log^2\xi}{8\,(\xi-1)}\right\} \tag{6.56}$$

$$\xrightarrow[\textbf{Feynman gauge}]{\xi\to 1} \frac{g^2e^2}{32}\frac{m_\mu}{2\pi^2 M_W^2} \tag{6.57}$$

$$\xrightarrow[\textbf{unitary gauge}]{\xi\to 0} \frac{g^2e^2}{32}\frac{m_\mu}{4M_W^2\pi^2}\left[1-\frac{1}{2}\log^2\xi\right]. \tag{6.58}$$

The latter expression demonstrates that the amplitude is divergent at high energies in unitary gauge, so the limits $\nu\to\infty$ and $\xi\to 0$ cannot be interchanged.

As expected, the imaginary part of the Compton amplitude is gauge-dependent and reads

$$\begin{aligned}
&\operatorname{Im}\lim_{Q\to 0}\frac{S_{LT}(\nu,Q^2,\xi)}{Q} = \theta\left[-1+\mu(\mu+2w)\right]\lim_{Q\to 0}\frac{m_\mu\nu\sigma_{LT}(\nu,Q,\xi)}{Q}\\
&+\theta\left[\mu(\mu+2w)-\xi^{-1}\right]\frac{\mu^2}{1024\pi m_\mu\mu w^2(\mu+2w)(\xi-1)\xi^2}\\
&\quad\times\Bigg\{2\mu w\left(-1+\mu(\mu+2w)\xi\right)\left(\xi^2-1\right)\\
&\quad+(\mu+2w)\Bigg[\left(-1+\xi+2\mu w\xi\right)\Big(4w\xi+\mu(\xi^2-1)\Big)\log\frac{\mu(\xi-1)+2w\xi}{(\mu+2w)(-1+\xi+2\mu w\xi)}\\
&\quad+8\mu w^2\xi^2\log\left(\xi\mu(\mu+2w)\right)\Bigg]\Bigg\},
\end{aligned} \tag{6.59}$$

where σ_{LT} is the corresponding (gauge-dependent) LT-polarized cross section, calculated for the physical W-boson in the final state (with all three physical polarization states encountered). The explicit expression for this cross section reads

$$\begin{aligned}
&\lim_{Q\to 0}\frac{\sigma_{LT}(\nu,Q,\xi)}{Q} = \frac{e^2g^2}{1024\pi(\xi-1)m_\mu^3\xi^2w^3(\mu+2w)}\\
&\times\Bigg\{2(\xi-1)\xi\left(\mu^2+2\mu w-1\right)\Big(\left(11\mu^4+13\mu^2-2\right)\xi+\mu^3(21\xi+1)w+16\mu\xi w\Big)\\
&+\mu^2(1-\xi)(\mu+2w)\left(\mu+2\left(\mu^2+2\right)\xi w+\xi^2\left(4\mu^3+39\mu+6\left(\mu^2+4\right)w\right)\right)\log(\mu(\mu+2w))\\
&+\mu^2(\mu+2w)(\xi(2\mu w-1)+1)\left(-\mu\xi^2+\mu+4\xi w\right)\log\frac{(1-\xi)+2\mu w\xi}{\mu\left(\mu(1-\xi)+2w\right)}\Bigg\}\\
&=\frac{g^2e^2}{128\pi M_W^2\nu(\xi-1)}\log\xi+O\left(\frac{1}{\nu^2}\right).
\end{aligned} \tag{6.60}$$

Substituting the Eqs. (6.59) and (6.60) into the optical theorem (6.33), one can see that for an arbitrary value of the gauge parameter ξ the optical theorem is violated. It is worth mentioning here, that despite the two different θ-functions, the imaginary part is smooth in ν. Another important

feature of the imaginary part is its behavior at $\nu \to \infty$ as $O(1/\nu)$, thus the dispersive integral will be convergent. However, the LT cross section has a different behavior

$$\lim_{\substack{Q\to 0 \\ \nu\to\infty+i0}} \frac{\sigma_{LT}^{W}(\nu,Q,\xi)}{Q} = \frac{\alpha_{\rm em} g^2}{4M_W^2}\frac{\log(\xi)}{(\xi-1)}\frac{1}{\nu} + O\left(\frac{1}{\nu^2}\right), \tag{6.61}$$

which makes the corresponding dispersive integral divergent at the upper bound.

These results are an unavoidable indication of the missing contribution, which should enter at the same order in couplings, but cannot be described in terms of the forward doubly-virtual Compton scattering process. Before finding the source of this missing contribution, let us first consider the dispersion relation for the one-loop vertex diagram with one off-shell muon leg, the so-called sideways dispersion relation. It is simpler than the doubly-virtual Compton scattering, but should have similar features regarding the gauge-dependence.

6.4.2.5 Sideways dispersion relation

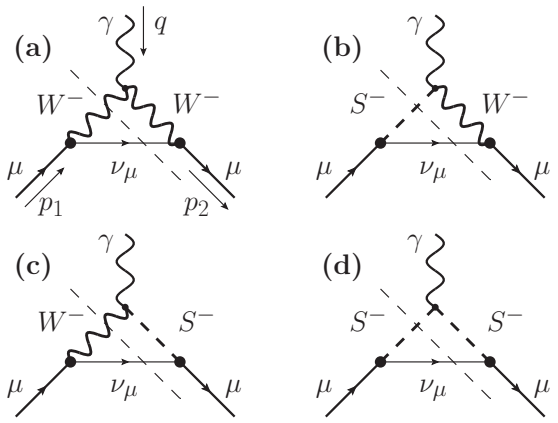

Fig. 6.13 The cuts for sideways dispersion relations of the muon form factor.

According to [382] we can write the dispersion relation for the Pauli form factor,

$$\mathcal{F}_2(s) = \frac{1}{\pi}\int_{M_W^2}^{\infty} ds' \frac{\mathrm{Im}\,\mathcal{F}_2(s')}{s'-s}, \tag{6.62}$$

which corresponds to the cuts shown in Fig. 6.13. The form factor can be defined with the help of the corresponding projector

$$\mathcal{F}_2(s) = \mathrm{tr}\left[(\not{p}_2 + m_\mu)\Gamma^\lambda(p_1,p_2)\mathcal{P}_\lambda^{\mathcal{F}_2}(p_1,p_2)\right], \tag{6.63}$$

where Γ^λ is the $\gamma\mu\mu$ vertex with the off-shell photon with momentum $q = p_2 - p_1$, $q^2 = -Q^2$, the off-shell muon with momentum p_1, $p_1^2 = s$ and the on-shell muon with momentum p_2, $p_2 = m_\mu^2$. The

projector is given by [383, 384]

$$\mathcal{P}_{\lambda}^{\mathcal{F}_2}(p_1,p_2) = -\frac{m_\mu}{2(s-m_\mu^2)^2}\left[(\not{p}_1+m_\mu)i\sigma_{\lambda\tau}(p_1-p_2)^\tau + 3(p_1-p_2)_\lambda(\not{p}_1-m_\mu)\right]. \tag{6.64}$$

In the unitary gauge one has only one loop diagram (a) out of four shown in Fig. 6.13, and for $\mathcal{F}_2$ one obtains [2]

$$\begin{aligned}\mathcal{F}_2(\zeta) = \frac{g^2}{32\pi^2(\zeta-\mu^2)}\Bigg\{&\frac{1}{\zeta} - 3\mu\left(\zeta-\mu^2\right)C_0(0,\mu^2,\zeta;1,1,0)\\ &+\frac{\mu^2}{\zeta^2}\left(1-5\zeta+4\zeta^2\right)\log(1-\zeta) - \frac{1-5\mu^2+4\mu^4}{\mu^2}\log(1-\mu^2)\Bigg\},\end{aligned} \tag{6.65}$$

where $\zeta = s/M_W^2$, with the imaginary part

$$\mathrm{Im}\,\mathcal{F}_2(\zeta) = \frac{\theta(\zeta-1)}{32\pi}\mu^2\frac{1-5\zeta+4\zeta^2-3\zeta^2\log\zeta}{\zeta^2\left(\mu^2-\zeta\right)} \tag{6.66}$$

The corresponding dispersive integral in Eq. (6.62) converges, and the sideways dispersion relation works without any subtraction, but the limit $s \to m^2$ (or $\zeta \to \mu^2$) differs from the correct result (6.29) by the term $g^2m^2/(64\pi^2M^2)$:

$$\mathcal{F}_2\left(\zeta\to\mu^2\right) = \frac{g^2}{64\pi^2\mu^4}\left[\mu^2(8\mu^2-4) - 2\left(3\mu^4-5\mu^2+2\right)\log\left(1-\mu^2\right)\right]. \tag{6.67}$$

For the case of Feynman-t'Hooft gauge with the full set of diagrams shown in Fig. 6.13 one obtains

$$\begin{aligned}\mathcal{F}_2(\zeta) = \frac{g^2}{64\pi^2\zeta^2\mu^2\left(\zeta-\mu^2\right)}\Bigg\{&8\zeta^2\mu^4\left(\mu^2-\zeta\right)C_0\left(0,\zeta,\mu^2;1,1,0\right)\\ &+(\zeta-1)\mu^4\left((\zeta-1)\mu^2+10\zeta-2\right)\log(1-\zeta)\\ &+\zeta\left(\left(\mu^2+2\right)\mu^2\left(\mu^2-\zeta\right) - \zeta\left(\mu^6+8\mu^4-11\mu^2+2\right)\log\left(1-\mu^2\right)\right)\Bigg\}\end{aligned} \tag{6.68}$$

with corresponding imaginary part

$$\mathrm{Im}\,\mathcal{F}_2(\zeta) = \theta(\zeta-1)\frac{\mu^2(1-\zeta)\left[\mu^2(1-\zeta)+2-5\zeta\right]-8\zeta^2\log\zeta}{64\pi\zeta^2\left(\mu^2-\zeta\right)}. \tag{6.69}$$

[2] Here $C_0\left(0,m^2,s;M,M,0\right) = \left[2\mathrm{Li}_2\left(\frac{M^2}{m^2}\right)+\log^2\left(-\frac{M^2}{m^2}\right)-2\mathrm{Li}_2\left(\frac{M^2}{s}\right)-\log^2\left(-\frac{M^2}{s}\right)\right]/(2m^2-2s)$ and the imaginary part is given by $\mathrm{Im}\,C_0\left(0,m^2,s;M,M,0\right) = -\pi\theta\left(s-M^2\right)\log\left(\frac{M^2}{s}\right)/(m^2-s)$

The corresponding sideways relation works without any additional subtractions just as in the previous case, however, now the limit $\mathcal{F}_2(s \to m^2)$ reproduces the correct answer for the AMM correction

$$\mathcal{F}_2(\zeta \to \mu^2) = \frac{g^2}{64\pi^2\mu^4}\left[\mu^2(\mu^4+8\mu^2-4) - 2\left(3\mu^4-5\mu^2+2\right)\log\left(1-\mu^2\right)\right]. \tag{6.70}$$

The general expression for $\mathcal{F}_2(s)$ in arbitrary gauge (the nonlinear gauge is used, given that only (a) and (d) graphs from Fig. 6.13 contribute) reads

$$\begin{aligned}\mathcal{F}_2(\zeta,\xi) = \frac{g^2}{64\pi^2\zeta^2\mu^2\xi^2\left(\mu^2-\zeta\right)}\Big\{&2\xi^2\zeta^2\left(4\mu^4-5\mu^2+1\right)\log\left(1-\mu^2\right)\\ &+\mu^2\left[\zeta\xi\left(\zeta-\mu^2\right)\left(\mu^2+2\xi\right)+\zeta^2\left(\mu^4\xi^2-1\right)\log\left(1-\mu^2\xi\right)\right.\\ &+\mu^2\Big\{-(\zeta\xi-1)\left(\zeta\left(\mu^2\xi+2\right)-\mu^2\right)\log(1-\zeta\xi)\\ &\quad\left.-2(\zeta-1)(4\zeta-1)\xi^2\log(1-\zeta)\Big\}\right]\\ &+2\xi\zeta^2\mu^4\left(\zeta-\mu^2\right)\left(3\xi C_0\left(0,\zeta,\mu^2;1,1,0\right)+C_0\left(0,\zeta,\mu^2;\frac{1}{\sqrt{\xi}},\frac{1}{\sqrt{\xi}},0\right)\right)\Big\}\end{aligned} \tag{6.71}$$

where ξ is the gauge-fixing parameter. It can be shown by explicit calculation, that the result given by Eq. (6.71) obey the following dispersion relations

$$\mathcal{F}_2(\zeta,\xi) = \begin{cases}\dfrac{1}{\pi}\displaystyle\int_1^\infty ds' \frac{\operatorname{Im}\mathcal{F}_2(s',\xi)}{s'-\zeta}, & \xi^{-\frac{1}{2}} > 1 > \mu;\\ \dfrac{1}{\pi}\displaystyle\int_{\xi^{-1}}^\infty ds' \frac{\operatorname{Im}\mathcal{F}_2(s',\xi)}{s'-\zeta}, & 1 > \xi^{-\frac{1}{2}} > \mu;\\ \dfrac{1}{\pi}\displaystyle\int_{-\infty}^\infty ds' \frac{\operatorname{Im}\mathcal{F}_2(s',\xi)}{s'-\zeta}, & 1 > \mu > \xi^{-\frac{1}{2}}.\end{cases} \tag{6.72}$$

Taken at the limit $s \to m^2$ ($\zeta \to \mu^2$), the obtained form factor yields the correct gauge-independent result for the AMM

$$\mathcal{F}_2(\zeta \to \mu^2,\xi) = \frac{g^2}{64\pi^2\mu^4}\left[\mu^2(\mu^4+8\mu^2-4) - 2\left(3\mu^4-5\mu^2+2\right)\log\left(1-\mu^2\right)\right]. \tag{6.73}$$

The same result can be obtained imposing the linear gauge condition as well.

As a result, the off-shell Pauli form factor obtained via the sideways dispersion relation is gauge-dependent akin to the LT-polarized doubly-virtual forward Compton amplitude with $W^\pm$-bosons in arbitrary gauge. The low-energy behavior of the off-shell vertex and the Compton amplitude is similar as well: both give the correct gauge-independent result for the AMM. However, the sideways dispersion relation does not require the subtraction, while the Schwinger sum rule has a gauge-dependent subtraction constant, given by Eq. (6.56), in the considered gauge.

6.4.3 $W^{\pm}$-boson contribution inside physical process

Now we want to understand the origin of the gauge dependence in the doubly-virtual forward Compton amplitude with $W^{\pm}$-bosons. The fact that this amplitude depend on the gauge parameter does not contradict with the physical principles, given that the doubly-virtual Compton process is not an observable process with external physical particles (two photons are off-shell). Thus one needs to wrap the Compton amplitude in a physical process and analyse its observables. Here we limit ourselves by considering only the imaginary part of such a process, since the corresponding real part can be anyway reconstructed via a dispersion relation.

Let us consider the simplest physical process, which incorporates the discussed Compton amplitude with $W^{\pm}$ bosons: the inelastic electron-muon scattering with the electron e, the W-boson and the muonic neutrino ν_μ in the final state, say $\mu(p)+e(\ell)\to\nu_\mu(p')+e(\ell')+W^-(q')$ (the letters in the brackets mean the corresponding particle momenta). At tree level there are only two topologies that contain the internal off-shell W-boson, that causes the gauge dependence. They are shown in Fig. 6.14. Here the linear gauge condition is imposed, hence the three-boson vertex with one charged scalar mode is possible. Moreover, since the gauge-fixing conditions of the photon, Z^0- and $W^{\pm}$-bosons are independent, it is convenient to consider photon and Z^0-boson just in unitary gauge. The diagram on the left-hand side of Fig. 6.14 with a photon is related to the virtual Compton scattering, while all the other diagrams cannot be related to that process. However, these Compton-unrelated diagrams appear at the same order of the electroweak coupling and should guarantee the gauge invariance of the final result.

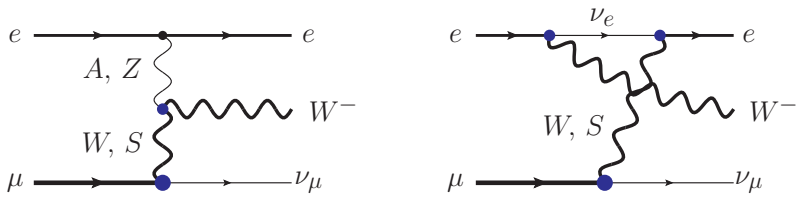

Fig. 6.14 The physical process of $\mu e\to\nu_\mu eW^-$ scattering, which contains the gauge-dependence in W propagators (and vertices if the gauge-dependent vertex is used, cf. [380]).

Let us write the W propagator $\Delta^W_{\mu\nu}$ in arbitrary gauge, separating out the part that corresponds to the unitary gauge:

$$\Delta^W_{\mu\nu}(k)=U_{\mu\nu}(k)-\frac{k_\mu k_\nu}{M_W^2}\Delta^S(k), \tag{6.74}$$

where $U_{\mu\nu}$ is the W-boson propagator in unitary gauge,

$$U_{\mu\nu}(k)\equiv -i\frac{g_{\mu\nu}-k_\mu k_\nu/M_W^2}{k^2-M_W^2+i0}. \tag{6.75}$$

Splitting the W-boson propagator in such a way allows one to hide all gauge dependence into the second term of (6.74), which is proportional to the propagator of the unphysical Goldstone boson Δ^S,

$$\Delta^S(k) = \frac{i}{k^2 - M_W^2/\xi}. \tag{6.76}$$

Starting with the right diagram on Fig. 6.14, one can write down the gauge-dependent part of the amplitude

$$\begin{aligned}
\mathcal{M}_W &= -i\left(\frac{g}{\sqrt{2}}\right)^3 \frac{1}{M_W^2}\Delta^S(q)\bar{e}(\vec{\ell}\,')\not{q}\mathbf{P}_\mathrm{L}\Delta^{\nu_e}(\ell-q')\not{\chi}^*(q')P_L e(\vec{\ell})\bar{\nu}_\mu(\vec{p}\,')\not{q}\mathbf{P}_\mathrm{L}\mu(\vec{p}) \\
&= -i\left(\frac{g}{\sqrt{2}}\right)^3 \frac{1}{M_W^2}\Delta^S(q)\bar{e}(\vec{\ell}\,')\left[\not{\ell}' - (\Delta^{\nu_e}(\ell-q'))^{-1}\right]\Delta^{\nu_e}(\ell-q')\not{\chi}^*(q')\mathbf{P}_\mathrm{L}e(\vec{\ell}) \\
&\quad \times \bar{\nu}_\mu(\vec{p}\,')\left[\not{p}' - \not{p}\right]\mathbf{P}_\mathrm{L}\mu(\vec{p}) \\
&= -i\left(\frac{g}{\sqrt{2}}\right)^3 \frac{m_\mu}{M_W^2}\Delta^S(q)\bar{e}(\vec{\ell}\,')\not{\chi}^*(q')\mathbf{P}_\mathrm{L}e(\vec{\ell})\bar{\nu}_\mu(\vec{p}\,')\mathbf{P}_\mathrm{R}\mu(\vec{p}) \\
&\quad + i\left(\frac{g}{\sqrt{2}}\right)^3 \frac{m_\mu m_e}{M_W^2}\Delta^S(q)\bar{e}(\vec{\ell}\,')\Delta^{\nu_e}(\ell-q')\not{\chi}^*(q')\mathbf{P}_\mathrm{L}e(\vec{\ell})\bar{\nu}_\mu(\vec{p}\,')\mathbf{P}_\mathrm{R}\mu(\vec{p})
\end{aligned} \tag{6.77}$$

where the chiral projectors $\mathbf{P}_\mathrm{L} = \frac{\mathbb{1}-\gamma_5}{2}$ and $\mathbf{P}_\mathrm{R} = \frac{\mathbb{1}+\gamma_5}{2}$ were introduced; $\chi^*(q')$ is the polarization vector of the outgoing W^--boson.

The contribution from the unphysical charged Goldstone mode gives

$$\mathcal{M}_S = -i\left(\frac{g}{\sqrt{2}}\right)^3 \frac{m_\mu m_e}{M_W^2}\Delta^S(q)\bar{e}(\vec{\ell}\,')\Delta^{\nu_e}(\ell-q')\not{\chi}^*(q')\mathbf{P}_\mathrm{L}e(\vec{\ell})\bar{\nu}_\mu(\vec{p}\,')\mathbf{P}_\mathrm{R}\mu(\vec{p}), \tag{6.78}$$

which cancel the second term in (6.77). Thus the total gauge-dependent contribution from the right diagram in Fig. 6.14 is

$$\mathcal{M}_W + \mathcal{M}_S = -i\left(\frac{g}{\sqrt{2}}\right)^3 \frac{m_\mu}{M_W^2}\Delta^S(q)\bar{e}(\vec{\ell}\,')\not{\chi}^*(q')\mathbf{P}_\mathrm{L}e(\vec{\ell})\bar{\nu}_\mu(\vec{p}\,')\mathbf{P}_\mathrm{R}\mu(\vec{p}). \tag{6.79}$$

It should be cancelled by the contribution from the left diagram in Fig. 6.14. In order to evaluate these diagrams, let us consider the gauge-independent γWW vertex,

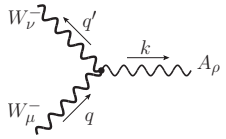

$$\begin{aligned}
\Gamma_{\mu\nu\rho} &= ie\left[g_{\mu\nu}(q+q')_\rho + g_{\nu\rho}(q-2q')_\mu + g_{\mu\rho}(q'-2q)_\nu\right] \\
&= ie\left[g_{\mu\nu}(q+q')_\rho + g_{\nu\rho}(k-q')_\mu + g_{\mu\rho}(-k-q)_\nu\right],
\end{aligned} \tag{6.80}$$

where $k = q - q'$. The contraction of this vertex with the on-shell W-boson polarization vector $\chi^{*\nu}(q')$ is given by

$$\chi^{*\nu}_W \Gamma_{\mu\nu\rho} = ie\left[\chi^*_\mu(q+q')_\rho + \chi^*_\rho(q-2q')_\mu - 2g_{\mu\rho}(q\cdot\chi^*)\right], \tag{6.81}$$

and subsequent contraction with the off-shell photon momentum q^μ gives

$$q^\mu \chi^{*\nu}_W \Gamma_{\mu\nu\rho} = ie\left[\chi^*_\rho(k^2 - M_W^2) - k_\rho(q\cdot\chi^*)\right]. \tag{6.82}$$

For the WWZ vertex the similar expressions can be obtained, but with the different overall factor, which corresponds to the Z^0 coupling to $W^\pm$-bosons. Consequently, the amplitudes with W-W-vector vertices can be written as

$$\mathcal{M}_{\triangle WWA} = i\frac{g}{\sqrt{2}}e^2\frac{m_\mu}{M_W^2}\Delta^S(q)\frac{k^2 - M_W^2}{k^2}\bar{e}(\vec{\ell}')\not{\chi}^*(q')e(\vec{\ell})\bar{\nu}_\mu(\vec{p}')\mathbf{P}_\mathrm{R}\mu(\vec{p}) \tag{6.83}$$

$$\begin{aligned}\mathcal{M}_{\triangle WWZ_V} =& i\frac{g}{\sqrt{2}}e^2\frac{\cos\theta_W}{\sin\theta_W}\frac{1-4\sin^2\theta_W}{4\cos\theta_W\sin\theta_W}\\ &\times\frac{m_\mu}{M_W^2}\Delta^S(q)\frac{k^2 - M_W^2}{k^2 - M_Z^2}\bar{e}(\vec{\ell}')\not{\chi}^*(q')e(\vec{\ell})\bar{\nu}_\mu(\vec{p}')\mathbf{P}_\mathrm{R}\mu(\vec{p}).\end{aligned} \tag{6.84}$$

Substitution $e = g\sin\theta_W$ yields

$$\mathcal{M}_{\triangle WWA} = i\frac{g^3}{\sqrt{2}}\sin^2\theta_W\frac{m_\mu}{M_W^2}\Delta^S(q)\frac{k^2 - M_W^2}{k^2}\bar{e}(\vec{\ell}')\not{\chi}^*(q')e(\vec{\ell})\bar{\nu}_\mu(\vec{p}')\mathbf{P}_\mathrm{R}\mu(\vec{p}) \tag{6.85}$$

$$\mathcal{M}_{\triangle WWZ_V} = i\frac{g^3}{\sqrt{2}}\left(\frac{1}{4} - \sin^2\theta_W\right)\frac{m_\mu}{M_W^2}\Delta^S(q)\frac{k^2 - M_W^2}{k^2 - M_Z^2}\bar{e}(\vec{\ell}')\not{\chi}^*(q')e(\vec{\ell})\bar{\nu}_\mu(\vec{p}')\mathbf{P}_\mathrm{R}\mu(\vec{p}). \tag{6.86}$$

The axial part of Z^0-boson gives

$$\begin{aligned}\mathcal{M}_{\triangle WWZ_A} =& -i\frac{g^3}{4\sqrt{2}}\frac{m_\mu}{M_W^2}\Delta^S(q)\frac{1}{k^2 - M_Z^2}\Big[\bar{e}(\vec{\ell}')\not{\chi}^*(q')\gamma_5 e(\vec{\ell})(k^2 - M_W^2)\\ &+ 2m_e\bar{e}(\vec{\ell}')\gamma_5 e(\vec{\ell})q\cdot\chi^*(q')\sin^2\theta_W\Big]\bar{\nu}_\mu(\vec{p}')\mathbf{P}_\mathrm{R}\mu(\vec{p}).\end{aligned} \tag{6.87}$$

The corresponding contribution of the internal charged scalar Goldstone mode propagation instead of the internal W^--boson reads

$$\mathcal{M}_{\triangle SWA} = i\frac{g^3}{\sqrt{2}}\sin^2\theta_W\frac{m_\mu}{M_W^2}\Delta^S(q)\frac{M_W^2}{k^2}\bar{e}(\vec{\ell}')\not{\chi}^*(q')e(\vec{\ell})\bar{\nu}_\mu(\vec{p}')\mathbf{P}_\mathrm{R}\mu(\vec{p}) \tag{6.88}$$

$$\mathcal{M}_{\triangle SWZ_V} = -i\frac{g^3}{\sqrt{2}}\left(\frac{1}{4} - \sin^2\theta_W\right)\frac{m_\mu}{M_W^2}\Delta^S(q)\frac{M_Z^2 - M_W^2}{k^2 - M_Z^2}\bar{e}(\vec{\ell}')\not{\chi}^*(q')e(\vec{\ell})\bar{\nu}_\mu(\vec{p}')\mathbf{P}_\mathrm{R}\mu(\vec{p}). \tag{6.89}$$

$$\mathcal{M}_{\triangle SWZ_A} = -(-i)\frac{g^3}{4\sqrt{2}}\frac{m_\mu}{M_W^2}\Delta^S(q)\frac{1}{k^2-M_Z^2}\Bigg[\bar{e}(\vec{\ell}')\not{\chi}^*(q')\gamma_5 e(\vec{\ell})(M_Z^2-M_W^2) + 2m_e\bar{e}(\vec{\ell}')\gamma_5 e(\vec{\ell})q\cdot\chi^*(q')\sin^2\theta_W\Bigg]\bar{\nu}_\mu(\vec{p}')\mathbf{P}_\mathrm{R}\mu(\vec{p}). \tag{6.90}$$

Finally we observe the following cancellation

$$\begin{aligned}
&\mathcal{M}_{\triangle WWA}+\mathcal{M}_{\triangle SWA}+\mathcal{M}_{\triangle WWZ}+\mathcal{M}_{\triangle SWZ}\\
&= i\left(\frac{g}{\sqrt{2}}\right)^3\frac{m_\mu}{M_W^2}\Delta^S(q)\bar{e}(\vec{\ell}')\not{\chi}^*(q')\mathbf{P}_\mathrm{L}e(\vec{\ell})\bar{\nu}_\mu(\vec{p}')\mathbf{P}_\mathrm{R}\mu(\vec{p})\\
&= -(\mathcal{M}_W+\mathcal{M}_S).
\end{aligned} \tag{6.91}$$

This simple calculation shows, that in the real physical process, the non-Compton contributions with the off-shell Z^0 and $W^\pm$-bosons should be taken into account in order to obtain the gauge-invariant result. This mechanism is well-known and very important for the correct definition of the off-shell form factors. For example, even in the earliest work on this topic by Fujikawa et al. [375] it was mentioned that in order to obtain the gauge-invariant Pauli form factor at nonzero photon virtuality, one needs to consider the vertex correction inside the real physical process along with the WW-box (see Fig. 6.15).

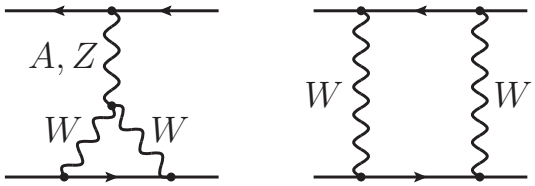

Fig. 6.15 A set of contributions that produces the gauge-invariant result for $W^\pm$-boson contribution to the off-shell Pauli form factor.

6.4.3.1 Real photons and Gerasimov-Drell-Hearn sum rule

The above discussion revealed several caveats with electroweak corrections to the AMM, which are evaluated via the sum rules that involve off-shell photons. It is then interesting to consider the sum rules with real photons and see whether we will run into the same issue with gauge dependence of the observables. The natural candidate to compare with the Schwinger sum rule is the GDH sum rule. It defines the AMM $\varkappa_\mu$ via the helicity difference cross section σ_{TT} for real photons ($Q^2=0$)

$$\varkappa_\mu^2 = -\frac{m_\mu^2}{\pi^2\alpha_{\mathrm{em}}}\int_{\nu_{\mathrm{th}}}^{\infty}d\nu\frac{\sigma_{TT}(\nu)}{\nu}. \tag{6.92}$$

Since the l.h.s. of the GDH sum rule is given by the squared AMM, the leading-order (tree-level) electroweak contribution to $\sigma_{\rm TT}$ should not contribute to AMM, resulting in a vanishing the sum rule integral. This fact has been already verified long time ago, although without much details, in the work by Altarelli et al. [378]. In this note, the $W^{\pm}$-boson contribution to the TT-polarized Compton amplitude and, subsequently, the GDH sum rule is revisited.

Let us consider the one-loop correction to the Compton amplitude in a general gauge, with a nonlinear gauge condition imposed for simplicity (depicted in Fig. 6.12). In the real photon limit, the spin-dependent amplitude S_1 reads ($M_W > m_\mu$ is assumed)

$$\begin{aligned}
S_1(w) =& \frac{g^2e^2}{256\pi^2}\Bigg\{-\frac{4\left(\mu^2+2\right)}{\mu(\mu^2-4w^2)} \\
&+\frac{2\left(\mu^6+18\mu^4-17\mu^2-2\right)\log\left(1-\mu^2\right)}{\mu^3w^2} \\
&+\Bigg[\Bigg(-\mu\left(\mu^6+18\mu^4-17\mu^2-2\right)+4\mu^2\left(\mu^2+26\right)w^3-4\mu\left(2\mu^4+45\mu^2-10\right)w^2 \\
&\quad+\left(5\mu^6+100\mu^4-55\mu^2-6\right)w\Bigg)\frac{\log\left(-\mu^2+2\mu w+1\right)}{\mu^2w^2(\mu-2w)^2} \\
&-4\frac{\left(5\mu^2-4\mu w+6\right)}{w}C_0\left(0,\mu^2,\mu(\mu-2w);1,1,0\right)+\{w\to -w\}\Bigg]\Bigg\} \qquad (6.93) \\
=& \frac{e^2g^2}{96\pi^2\mu^7(\mu^2-1)}\Big\{\mu^2\left(24-36\mu^2+10\mu^4+\mu^6\right) \\
&-2\left(-12+24\mu^2-13\mu^4+\mu^6\right)\log(1-\mu^2)\Big\}w^2+O(w^4), \qquad (6.94)
\end{aligned}$$

where $w=\nu/m_\mu$, $\mu=m_\mu/M_W$ and $M_W=1$. This amplitude is entirely gauge invariant and has correct low-energy behavior, $O(\nu^2)$, respecting the low-energy theorem at the given order.

The corresponding TT-polarized photoabsorption cross section is given by

$$\begin{aligned}
\sigma_{\rm TT}(w) =& \frac{g^2e^2}{256\pi w^2\mu^3M_W^2(\mu+2w)^2} \\
&\times\Bigg\{2\mu(\mu+2w)^2(5\mu^2+4\mu w+6)\log\left[\mu(\mu+2w)\right] \\
&-(\mu^2+\mu w-1)\left[2\mu w^2\left(\mu^2+26\right)+w\left(3\mu^4+65\mu^2+6\right)\right. \\
&\left.+\mu^5+19\mu^3+2\mu\right]\Bigg\}, \qquad (6.95)
\end{aligned}$$

which is in agreement with [379] (see Appendix of the *arXiv* version). It is gauge-invariant as well and respects the optical theorem

$$\mathrm{Im}\, S_1(w) = M_W m_\mu w\sigma_{\rm TT}(w). \qquad (6.96)$$

Finally, the direct evaluation of the dispersive integral in (2.88c) for $Q^2 = 0$ exactly reproduces the amplitude S_1 given by Eq. (6.93).

The considered example shows that in the real-photon limit there is a decoupling of the (in general gauge-dependent) photoabsorption process from the other electroweak interactions (see Fig. 6.14) in such a way, that it does not depend on the gauge of the $W^{\pm}$-bosons. Thus, all of the sum rules that originate from the Compton scattering with real photons, can be applied to evaluate perturbative electroweak corrections without any caveats.

6.5 π^0-exchange contribution to HLbL via Schwinger sum rule

An important test of the Schwinger sum rule approach [149] is to evaluate the leading HLbL contribution, which comes from the lightest meson exchange: the π^0-exchange. For this purpose, the various contributions to the LT-polarized photoabsorption cross section, shown in Fig. 6.16, should be calculated. In general, these contributions are divided into hadron photoproduction channels with hadrons in the final state (Fig. 6.16, I. and II.), and electromagnetic channels with only a muon and photons in the final state (Fig. 6.16, III. and IV.). Although all the depicted contributions contribute at

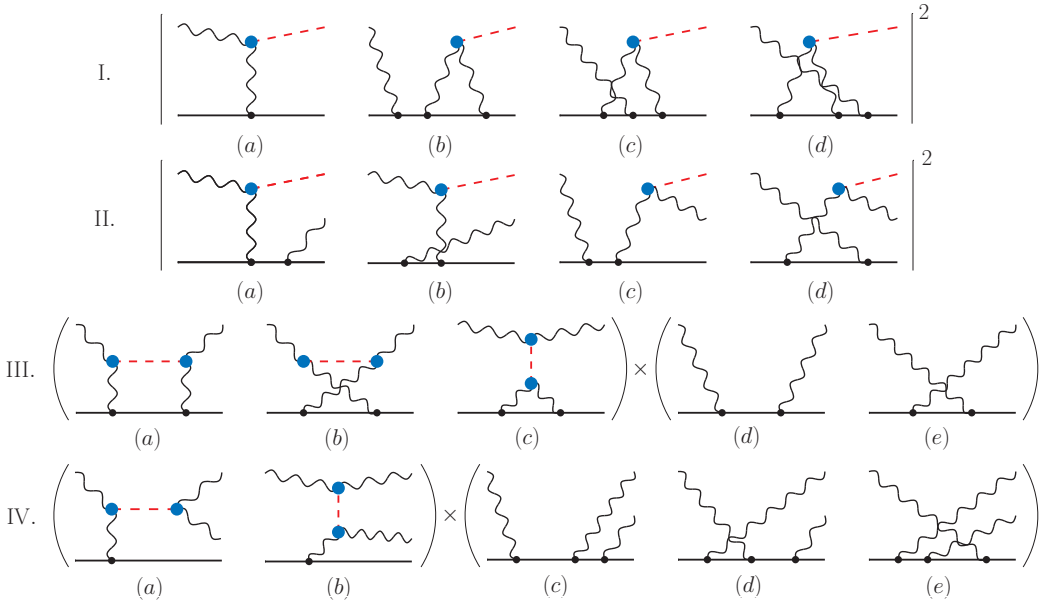

Fig. 6.16 Hadron photoproduction channels (I. and II.) and electromagnetic channels (III. and IV.) that contain a neutral pion and contribute to HLbL via the Schwinger sum rule.

the same $O(\alpha_{\text{em}}^3)$, it is natural to expect the hadron photoproduction channels to dominate. If this hypothesis is true, then the HLbL contibution to the AMM could be determined predominantly with hadron photoproduction data, which could potentially be measured at muon beam facilities, e.g. as background to the MUonE experiment. This will make the Schwinger sum rule approach a very powerful and essentially data-driven method for both HVP and HLbL.

In order to confirm the dominance of the hadron photoproduction channels, a calculation of all contributions shown in Fig. 6.16 is needed. This calculation should be carried out with models for the $\pi^0\gamma\gamma$ vertex, which are presently accepted by the Muon $g-2$ Theory Initiative [87]. The obtained full result then could be compared to the one, obtained in an alternative framework (e.g. [123]), which will verify the approach in general. After that a comparison of particular contributions of the hadron and electromagnetic channels could be performed. In this way, the aforementioned hypothesis will be confirmed or disproved. Only the contributions from channels I. and III. were evaluated so far, and the obtained results support the mentioned hypothesis. Although the channels II. and IV. contain three-particle cuts and thought to be smaller then I. and III., their evaluation is also required for the complete picture.

Let us consider the evaluation of the π^0-exchange contribution starting with channel I, which among other channels should contribute the most. It was found [385] that the squared diagram I.(a), which is usually called Primakoff scattering diagram, does not contribute at all. On one hand, from naïve counting, it should contribute at $O(\alpha_{\text{em}}^2)$, while on the other hand its contribution is identiacally zero, which can be also proven by looking at the asymptotic behavior of the corresponding Compton amplitude:

$$
\begin{aligned}
\mathcal{M}_{LT}^{\text{Primakoff}} &\sim \int \frac{d^4k}{(2\pi)^4} \frac{\bar{\mu}(\vec{p})\gamma^\rho(\not{p}+\not{k}+m_\mu)\gamma^\alpha\mu(\vec{p})\epsilon_{\alpha\beta\alpha'\beta'}\varepsilon^\beta(q)k^{\alpha'}q^{\beta'}\epsilon_{\rho\sigma\rho'\sigma'}\varepsilon^{*\sigma}(q)k^{\rho'}q^{\sigma'}}{k^4\left[(k+p)^2-m_\mu^2\right]\left[(q-k)^2-m_{\pi^0}^2\right]} \\
&= \frac{Q}{64\pi^2\nu^2}\Bigg[\frac{(-3m_\mu m_{\pi^0}^2+5m_{\pi^0}^2\nu+2m_\mu\nu^2)\sqrt{(m_{\pi^0}^2+2m_\mu\nu)^2-(2m_\mu m_{\pi^0})^2}}{m_\mu(m_\mu-2\nu)} \\
&\quad\times\log\frac{m_{\pi^0}^2+2m_\mu\nu+\sqrt{(m_{\pi^0}^2+2m_\mu\nu)^2-(2m_\mu m_{\pi^0})^2}}{2m_\mu m_{\pi^0}} \\
&\quad - m_{\pi^0}^2(-3m_\mu m_{\pi^0}^2+2m_{\pi^0}^2\nu+4m_\mu\nu^2)\,C_0\left[0,m_\mu^2,m_\mu^2-2m_\mu\nu,m_{\pi^0},0,m_\mu\right] \\
&\quad + \{\nu\to-\nu\}\Bigg] + O(Q^3) \\
&= Q\frac{\nu^2}{240\pi^2 m_\mu^5 m_{\pi^0}}\Bigg[53m_\mu^4 m_{\pi^0}-18m_\mu^2 m_{\pi^0}^3-2\left(30m_\mu^4 m_{\pi^0}-40m_\mu^2 m_{\pi^0}^3+9m_{\pi^0}^5\right)\log\frac{m_\mu}{m_{\pi^0}} \\
&\quad - 2\sqrt{m_{\pi^0}^2-4m_\mu^2}\left(4m_\mu^4-22m_\mu^2 m_{\pi^0}^2+9m_{\pi^0}^4\right)\log\frac{m_{\pi^0}+\sqrt{m_{\pi^0}^2-4m_\mu^2}}{2m_\mu}\Bigg] + O(Q\nu^4) + O(Q^3) \\
&= O(Q\nu^2) + O(Q^3).
\end{aligned}
\tag{6.97}
$$

Hence only the interference between I.(a) and I.(b)-(d) survives, contributing at $O(\alpha_{\text{em}}^3)$. The contribution of the squared diagrams I.(b)-(d) is of higher-order in α_{em}, $O(\alpha_{\text{em}}^4)$, and therefore can be neglected. The proper computation of the contribution from channel I requires knowledge of the $\pi^0\to\gamma\gamma$ pion transition form factor, $F_{\pi^0\gamma\gamma}(Q_1^2,Q_2^2)$, shown in Fig. 6.17, where Q_1 and Q_2 are the virtualities of incoming photons.

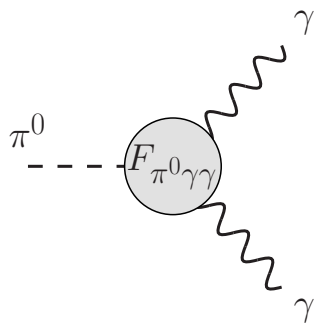

Fig. 6.17 Pion transition form factor.

This form factor is rather challenging observable either for experimental measurement or for the lattice QCD evaluation. It is especially hard to obtain the behavior in doubly-virtual case, which will be valid at all energies. Unfortunately, in contrast to the rest II.-IV. contributions in Fig. 6.16, which involve just a single-virtual pion transition form factor, the leading contribution I. requires the knowledge of this form factor in doubly-virtual region. Therefore the first estimation of the leading contribution was performed using the constant effective $\pi^0\mu\mu$ coupling, the value of which can be precisely fixed from the pion-muon decay width combined with the dispersion relation [386, 387] for such a vertex. This means that the effects of the off-shell internal muon, as well as the contribution from the box diagram I.(c) have been neglected. This simple estimation yielded the following result for the neutral pion exchange contribution:

$$\Delta a_\mu(\text{I.}) = 166^{+41}_{-37} \times 10^{-11}. \tag{6.98}$$

The obtained value is more than two times larger than the most recent value of the pion-pole contribution, which has entered the White Paper in 2020 [87], is $\Delta a_\mu(\pi^0\text{-pole}) = (63.6 \pm 2.7) \times 10^{-11}$. This could point to the fact that the dispersive pion-pole approach [123] cannot be trivially mapped to the Schwinger sum rule approach, since discontinuities of different quantities are considered: $\pi^0\mu$ cut of the pion photoproduction amplitude in case of the Schwinger sum rule versus π^0 cut of the two-loop $\gamma\mu$-vertex correction in case of the pion-pole approach. Nevertheless, the significant difference between the results could mean that either the neglected off-shell effects play an important role in channel I. Hence, in order to refine the estimation, we decided to take into account the off-shell effects in that channel by evaluating all the diagrams I.(b)-(d). These diagrams do not contain UV divergences, but being taken without the form factors attached to the $\pi^0\gamma\gamma$ vertex, they lead to a divergent sum rule integral over the cross section. One of the simplest form factors that makes the integral finite is the VMD transition form factor of the form

$$F_{\pi^0\gamma\gamma}(q_1^2, q_2^2) \propto \frac{\Lambda^4}{(q_1^2 - \Lambda^2)(q_2^2 - \Lambda^2)}, \tag{6.99}$$

where q_1 and q_2 are the photon momenta, Λ is a typical hadronic scale (e.g. ρ-meson mass) that plays the role of a soft cut-off. Such a simple form of the pion transition form factor does not respect the correct high-energy behavior that follows from the short-distance constraints, but has been used among other parametrizations to evaluate the pion-pole contribution in the classical work by Knecht and Nyffeler [124]. For the improved forms of this form factor one can consider, e.g. LMD-V, which was also used in [124] and in calculation of Melnikov and Vainshtein [138], or the pQCD-inspired parametrization proposed in [388, Eq. 83]. Alternatively, one can incorporate the dispersive treatmet of this form factor combined with the asymptotic constraints from QCD, provided in [389, 390]. However, in order to simplify the calculations while aiming for the comparison of the results to the ones obtained by Knecht and Nyffeler, we decided to use the the VMD pion transition form factor of the form given by Eq. (6.99), with the parameters quoted in [124].

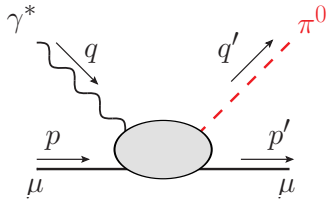

Fig. 6.18 Neutral pion photoproduction on the muon.

In order to obtain the one-loop pion photoproduction amplitude $\mathcal{M}^\mu(s,t)$, we expand it in the following tensor basis

$$\mathcal{M}^\mu(s,t) = \sum_{i=1}^{6} M_i(s,t) O_i^\mu(q,p,p'), \tag{6.100a}$$

$$O_1^\mu(q,p,p') = \langle i\sigma^{\mu\rho}(p'-p)_\rho \gamma_5 \rangle, \tag{6.100b}$$

$$O_2^\mu(q,p,p') = \langle i\sigma^{\mu\rho} q_\rho \gamma_5 \rangle, \tag{6.100c}$$

$$O_3^\mu(q,p,p') = \langle \gamma_5 \rangle (p'-p)^\mu, \tag{6.100d}$$

$$O_4^\mu(q,p,p') = \langle \gamma^\mu \gamma_5 \rangle, \tag{6.100e}$$

$$O_5^\mu(q,p,p') = \langle \not{q} \gamma_5 \rangle p^\mu, \tag{6.100f}$$

$$O_6^\mu(q,p,p') = \langle \not{q} \gamma_5 \rangle p'^\mu. \tag{6.100g}$$

All the momenta are shown in Fig. 6.18 and related to the Mandelstam invariants as $s = (p+q)^2 = (p'+q')^2$, $t = (q-q')^2 = (p-p')^2$. The Ward-Takahashi identity implies

$$q_\mu \mathcal{M}^\mu(s,t) = \sum_{i=1}^{6} M_i(s,t) q_\mu O_i^\mu(q,p,p') = 0, \tag{6.101}$$

which was checked by explicit calculation. Since we are interested in the real-photon limit $Q^2 \to 0$ it is enough to consider the scalar amplitudes M_i up to $O(Q^2)$ in the photon virtuality, namely

$$M_i(s,t) = a_i(s,t) + b_i(s,t)Q^2 + O(Q^4). \tag{6.102}$$

According to the gauge invariance, the amplitude with longitudinally polarized photon should be proportional to its virtuality,

$$\varepsilon_{L\mu}\mathcal{M}^{\mu}(s,t) \sim Q. \tag{6.103}$$

Meanwhile the tensor structures in Eqs. (6.100), being contracted with the longitudinal photon polarization vector, are proportional to Q^{-1}. Thus, the first expansion terms a_i of the amplitudes M_i should satisfy the following relation

$$\begin{aligned}\left[(t-m_\pi^2)^2+4t\nu^2\right]&\left[a_1(s,t)\left(t-m_\pi^2+4\nu\right)+a_3(s,t)(t-m_\pi^2)\right]\\ &-2\nu(t-m_\pi^2)\left[2a_4(s,t)(t-m_\pi^2)+2a_5(s,t)\nu+a_6(s,t)(t-m_\pi^2+2\nu)\right]=0,\end{aligned} \tag{6.104}$$

which can be obtained requiring the absence of terms proportional to Q^{-1} in the LT-polarized cross section. This relation has also been proven by explicit calculation. The numerical integration of the obtained LT-polarized cross section reads

$$\Delta\varkappa_\mu(\text{I.}) = (49 \pm 5) \times 10^{-11}. \tag{6.105}$$

This value is already very close to the one obtained by Knecht and Nyffeler [124] in the pion-pole approach with the same pion transition form factor,

$$\Delta\varkappa_\mu(\text{Knecht\&Nyffeler}) = (56 \pm 10) \times 10^{-11}, \tag{6.106}$$

and almost coincides with the pion-pole dispersive calculation (6.98). So far we can conclude that the off-shell effects in the pion photoproduction channel I. are indeed of high importance.

Now let us turn to the hadron photoproduction channels. Given that the contributions III and IV contain $\pi^0\gamma\gamma$ vertices with off-shell photons, a knowledge of the pion transition form factor is inevitably needed. Moreover, in both mentioned contributions the neutral pion can go off-shell. This means that the π^0-exchange contribution to these channels cannot be directly fixed from experimental data on, e.g. transition form factors, and requires a considerable part of modelling. A simple estimation for this channel was performed in V.B.'s master thesis (2019). It results in

$$\Delta\varkappa_\mu(\text{III.}) = (5 \pm 3) \times 10^{-11}, \tag{6.107}$$

where the uncertainty has only systematical origin and comes from different ways of regularizing the integral over the LT-polarized cross section. The major contribution to the number (6.107) comes from the diagrams (a) and (b). With a constant $\pi^0\gamma\gamma$ coupling, these diagrams yield a cross section, which

at the energies $\nu \gtrsim 1$ GeV grows faster than $O(1)$. As a result, this contribution strongly depends on the model for $\pi^0\gamma\gamma$ vertex. In particular, the implementation of a VMD-inspired monopole form factor for each virtual photon propagator does not yield satisfactory results. This modification, represented by the transformation of the propagator as

$$\frac{1}{k^2} \to \frac{1}{k^2} - \frac{1}{k^2 - \Lambda^2} = \frac{1}{k^2}\frac{\Lambda^2}{\Lambda^2 - k^2}, \tag{6.108}$$

where k denotes the virtual photon momentum and Λ represents a characteristic hadronic scale, dramatically overestimates the result. Similarly, employing a dipole form factor for each photon also proves inadequate in achieving the reasonable outcome. Only the tripole form factor, i.e.

$$\frac{1}{k^2} \to \frac{1}{k^2}\prod_{i=1}^{3}\frac{\Lambda_i^2}{\Lambda_i^2 - k^2}, \tag{6.109}$$

with three regulator masses $\Lambda_1..\Lambda_3$, can effectively regularize the integral and bring us to the physically reasonable answer mentioned above. It worth mentioning that a similar number was obtained in two alternative approaches, either imposing a hard cut-off or evaluation of the leading convergent part of the integral via its expansion into a series of the suitably-constructed "velocity-like" variable $v = \sqrt{1 - m_\mu^2/s}$. The diagram III.(c) was estimated using the dispersive model for the $\pi^0\mu\mu$ coupling from [386, 387], and the effective $\pi^0\gamma\gamma$ vertex with a triangular nucleon loop inserted. Its contribution turned out to be negligible.

6.6 Summary and outlook

In this Chapter, we examined the Schwinger sum rule approach to the hadronic contributions to the anomalous magnetic moment (AMM) of the muon. Starting with basic examples of neutral scalar, pseudoscalar, vector, and axial-vector contributions at one-loop level, described by the interaction terms (6.5), we identified the contributions influenced by asymptotic constants. These constants, which, according to the Sugawara-Kanasawa theorem [158], correspond to the values of the amplitude at infinite energy, were shown to vanish in a complete calculation within a properly UV-completed theory, thereby validating the Schwinger sum rule. Specifically, this cancellation was explicitly demonstrated in baryon chiral perturbation theory (BχPT) for the proton's AMM, where the theory was completed by the inclusion of the σ-meson. A similar result was found for the one-loop Standard Model (SM) contribution to the muon's AMM, which arises from Z^0 and Higgs boson exchanges. However, regarding the contribution from the $W^\pm$ bosons, certain caveats were identified, particularly related to virtual photons involved in the Schwinger sum rule observable. Thus, fully incorporating this contribution into the Schwinger sum rule framework requires further modifications. Nonetheless, these challenges do not hinder the application of the Schwinger sum rule to the hadronic contributions

to the muon AMM, as the electroweak corrections influence the hadronic photoabsorption cross section only at higher orders.

To demonstrate the applicability of the Schwinger sum rule to the hadronic light-by-light (HLbL) correction to the muon AMM, we considered the leading contribution, which arises from π^0 exchange. In terms of the photoabsorption cross section, the dominant contribution related to this exchange likely originates from the pion photoproduction channel (cf. Fig.6.16, I.). Employing a simple vector meson dominance (VMD) parametrization, commonly used in the literature [124] for the pion transition form factor, we obtained a reasonable estimate (6.105) for the muon's AMM from this channel. Other contributions depicted in Fig.6.16 were discussed to be small, a conclusion further supported by an estimation of the contribution from the electromagnetic channel III.

As a prospective direction for future research, we consider the extension of the Schwinger sum rule methodology to non-abelian gauge theories, a crucial step for accurately incorporating the electroweak sector of the Standard Model, viz. $W^{\pm}$-bosons. With regard to the dominant hadronic light-by-light (HLbL) contributions, a comprehensive evaluation of the approach necessitates the estimation of all channels illustrated in Fig.6.16. Ideally, this assessment should be conducted using a self-consistent theoretical framework.

Appendices

6.A Nucleon AMM

The one-loop computation of the nucleon anomalous magnetic moment (AMM) in BχPT and the linear σ-model involves evaluating the diagrams shown in Fig. 6.4. The general contributions arising from these diagrams can be expressed as

$$\begin{aligned}\varkappa^{(\pi)}(\mu) &= \frac{g_{\pi N}^2}{16\pi^2}\int_0^1 dx \frac{2x(1-x)^2}{x\mu^2+(1-x)^2} \\ &= \frac{g_{\pi N}^2}{16\pi^2}\left\{1-2\mu^2-\frac{\mu}{\sqrt{1-\mu^2/4}}\left(2-4\mu^2+\mu^4\right)\arccos\frac{\mu}{2}+\mu^2(-2+\mu^2)\log\mu^2\right\}, \qquad (6.110a)\\ \varkappa^{(N)}(\mu) &= \frac{g_{\pi N}^2}{16\pi^2}\int_0^1 dx \frac{2x^3}{(1-x)\mu^2+x^2} \\ &= \frac{g_{\pi N}^2}{16\pi^2}\left\{1+2\mu^2+\frac{\mu^3}{\sqrt{1-\mu^2/4}}\left(-3+\mu^2\right)\arccos\frac{\mu}{2}+\mu^2(1-\mu^2)\log\mu^2\right\}, \qquad (6.110b)\end{aligned}$$

where $\varkappa^{(\pi)}$ refers to the diagram on the right-hand side of Fig. 6.4, while $\varkappa^{(N)}$ comes from the diagram shown on the left-hand side of this Figure. Here $\mu \equiv m/M$ is the ratio of the (pseudo)scalar meson mass m and the nucleon mass M, appearing in the loop.

The one-loop calculation of the proton anomalous magnetic moment at $O(p^3)$ in BχPT then reads

$$\begin{aligned}\varkappa_p^{\mathrm{B}\chi\mathrm{PT}}[\mathrm{loop}] &= \left[2\varkappa^{(\pi)}-\varkappa^{(N)}\right](\mu_\pi) \\ &= \frac{g_{\pi N}^2}{16\pi^2}\left\{-\mu_\pi\frac{4-11\mu_\pi^2+3\mu_\pi^4}{\sqrt{1-\mu_\pi^2/4}}\arccos\frac{\mu_\pi}{2}+1-6\mu_\pi^2+\mu_\pi^2(-5+3\mu_\pi^2)\log\mu_\pi^2\right\} \\ &\overset{\mu_\pi\to 0}{=} \frac{g_{\pi N}^2}{16\pi^2}\left\{1-2\pi\mu_\pi-2(2+5\log\mu_\pi)\mu_\pi^2+\frac{21\pi}{4}\mu_\pi^3+O(\mu_\pi^4)\right\}, \qquad (6.111)\end{aligned}$$

where $\mu_\pi = m_\pi/M_N$. The proton AMM in the linear σ-model is then given by

$$\begin{aligned}\varkappa_p^{\sigma\text{-model}}[\mathrm{loop}] &= 2\varkappa^{(\pi)}(\mu_\pi)-\varkappa^{(N)}(\mu_\pi)+\varkappa^{(N)}(\mu_\sigma) \\ &= \frac{g_{\pi N}^2}{16\pi^2}\left\{2-6\mu^2+2\mu_\sigma^2+\mu^2(-5+3\mu^2)\log\mu^2+\mu_\sigma^2(1-\mu_\sigma^2)\log\mu_\sigma^2\right. \\ &\quad \left.-\mu_\pi\frac{4-11\mu_\pi^2+3\mu_\pi^4}{\sqrt{1-\mu_\pi^2/4}}\arccos\frac{\mu_\pi}{2}+\mu_\sigma^3\frac{-3+\mu_\sigma^2}{\sqrt{1-\mu_\sigma^2/4}}\arccos\frac{\mu_\sigma}{2}\right\}, \qquad (6.112)\end{aligned}$$

with $\mu_\sigma = m_\sigma/M_N$.

6.B Nonlinear R_ξ gauges

The Lagrangian of the bosonic sector of $SU(2)\times U(1)$ SM consists of four parts

$$\mathcal{L} = \mathcal{L}_{\rm YM} + \mathcal{L}_H + \mathcal{L}_{\rm gauge} + \mathcal{L}_{\rm FP}, \tag{6.113}$$

where $\mathcal{L}_{\rm YM}$ is the Yang-Mills Lagrangian of the $W^\pm$- and Z^0-bosons and electromagnetic gauge fields A, $\mathcal{L}_H$ is the Lagrangian of Higgs field and two last terms, $\mathcal{L}_{\rm gauge}$ and $\mathcal{L}_{\rm FP}$ are the gauge-fixing term and the Lagrangian of the Faddeev-Popov ghosts. The latter are usually given by

$$\mathcal{L}_{\rm gauge} + \mathcal{L}_{\rm FP} = -\frac{1}{2}G(\omega)^2 - \bar{c}\frac{\delta G(\omega)}{\delta\omega}c. \tag{6.114}$$

Here, $\bar{c}$ and c are the Faddeev-Popov ghosts (anticommuting scalar fields), $G(\omega)$ is the gauge-fixing function that depends on the parameter ω of the infinitesimal gauge transformation.

The crucial step towards the quantization of the non-Abelian theory was performed by t'Hooft, who considered the theory in R_ξ gauge introducing the (linear) gauge function as

$$\mathcal{L}^{\rm linear}_{\rm gauge} = -\frac{1}{2\xi_A}\left(\partial_\mu A^\mu\right)^2 - \frac{1}{2\xi_Z}\left(\partial_\mu Z^\mu + \xi_Z M_Z \chi\right)^2 - \frac{1}{\xi_W}\left|\partial_\mu W^{+\mu} + i\xi_W M_W \phi^+\right|^2. \tag{6.115}$$

Here ξ_A, ξ_Z and ξ_W are the gauge-fixing parameters, χ and $\phi^\pm$ are the unphysical components of the Higgs doublet ϕ,

$$\phi = \frac{1}{\sqrt{2}}\begin{pmatrix}\phi^1 + i\phi^2\\ H + i\chi\end{pmatrix} + \frac{1}{\sqrt{2}}\begin{pmatrix}0\\ v\end{pmatrix}. \tag{6.116}$$

This choice of the gauge function results in cancellation of the terms that are non-diagonal in gauge bosons and derivatives of Higgs field,

$$iM_W W^{-\mu}\partial_\mu\phi^+ - iM_W W^{+\mu}\partial_\mu\phi^- - M_Z Z^\mu\partial_\mu\chi, \tag{6.117}$$

and allows for the proper renormalization of the theory. However, this choice of this type of gauge function is not unique, and in general it could be done as [391]

$$\begin{aligned}\mathcal{L}^{\rm non\text{-}linear}_{\rm gauge} = &-\frac{1}{2\xi_A}\left(\partial_\mu A^\mu\right)^2\\ &-\frac{1}{2\xi_Z}\left(\partial_\mu Z^\mu + \xi_Z\frac{g}{2\cos\theta_W}(v+\tilde{e}H)\chi\right)^2\\ &-\frac{1}{\xi_W}\left|\left(\partial_\mu + ie\tilde{a}A_\mu + ig\cos\theta_W\tilde{b}Z_\mu\right)W^{+\mu} + i\xi_W\frac{g}{2}(v+\tilde{d}H - i\tilde{k}\chi)\phi^+\right|^2,\end{aligned} \tag{6.118}$$

with the real parameters $\tilde{a}$, $\tilde{b}$, $\tilde{d}$, $\tilde{e}$ and $\tilde{k}$. The certain values of these parameters can yield a gauge function that respects a symmetry of some subgroup of $SU(2)\times U(1)$ and remove some types of

interaction vertices from the initial Lagrangian. For instance, one can choose [380, 392, 393]

$$\tilde{a} = \tilde{b} = 1, \quad \tilde{d} = \tilde{k} = \tilde{e} = 0, \tag{6.119}$$

which corresponds to the replacement of the partial derivative in the linear gauge function by the covariant one that is associated with the $U(1)\times U(1)$ subgroup of $SU(2)\times U(1)$

$$\partial_\mu W^{+\mu} \to \hat{D}_\mu W^{+\mu} = \left(\partial_\mu + ieA_\mu + ig\cos\theta_W Z_\mu\right) W^{+\mu}. \tag{6.120}$$

Thus, the gauge-fixing function explicitly invariant with respect to the electromagnetic $U(1)$ group.

The main advantage of the chosen gauge-fixing function is that it gets rid of the vertex $\gamma W^\pm \phi^\mp$ and keeps the same Lorentz structure for the $WW\gamma$ and WWZ vertices. Therefore the number of the Feynman diagrams can be essentially reduced, while the structure of remaining ones is simplified. The Feynman rules, which are relevant to this study, are listed in (see (6.121i) in Appendix 6.C).

6.C Feynman rules for electroweak sector of SM

A list of the Feynman rules in nonlinear gauges can be found in, e.g., [392] (contains incorrect rule for $WW\gamma\gamma$ contact vertex!), [393] or [391]. The classical works on the subject in general gauge are [375] and [380]. In what follows, only those Feynman rules are provided, which are needed for our calculations.

Propagators:

$$\begin{aligned}
\text{lepton:} \quad \Delta^l(k) &= \frac{i}{\not{k} - m + i0^+} \\
\text{photon:} \quad \Delta_{\mu\nu}(k) &= -i\frac{g_{\mu\nu}}{k^2 + i0^+} \\
W^\pm\text{-boson:} \quad \Delta^W_{\mu\nu}(k) &= -i\left[g_{\mu\nu} - \left(1 - \frac{1}{\xi}\right)\frac{k_\mu k_\nu}{k^2 - M_W^2/\xi}\right]\frac{1}{k^2 - M_W^2 + i0^+} \\
\text{scalar:} \quad \Delta^S(k) &= \frac{i}{k^2 - M_W^2/\xi + i0^+}
\end{aligned}$$

Vertices:

$$= -ie\overline{\mu}\gamma_\alpha\mu, \tag{6.121a}$$

$$= -i\frac{g}{\cos\Theta_W}\,\overline{\mu}\gamma_\alpha\left[\sin^2\theta_W\left(\frac{1+\gamma_5}{2}\right) - \frac{\cos 2\theta_W}{2}\left(\frac{1-\gamma_5}{2}\right)\right]\mu, \tag{6.121b}$$

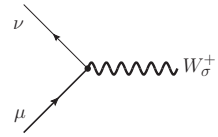

$$= -i\frac{g}{\sqrt{2}}\overline{\nu}\gamma_\sigma\left(\frac{1-\gamma_5}{2}\right)\mu, \tag{6.121c}$$

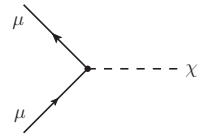

$$= -i\frac{g\,m_\mu}{2M_W}\overline{\mu}i\gamma_5\mu, \tag{6.121d}$$

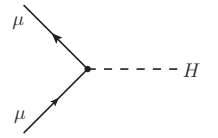

$$= -i\frac{g\,m_\mu}{2M_W}\overline{\mu}\mu, \tag{6.121e}$$

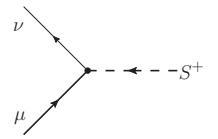

$$= -i\frac{g\,m_\mu}{\sqrt{2}M_W}\overline{\nu}\left(\frac{1+\gamma_5}{2}\right)\mu, \tag{6.121f}$$

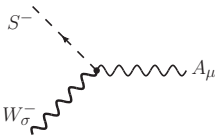

$$= -ie\,M_W g_{\mu\sigma}, \qquad \mathrm{R}_\xi \text{ linear gauge} \tag{6.121g}$$

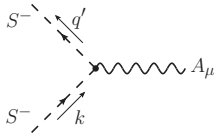

$$= -ie\,(k+q')_\mu, \tag{6.121h}$$

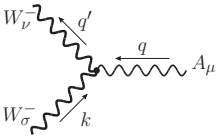

$$= \begin{cases} ie\left[g_{\nu\sigma}(k+q')_\mu - g_{\mu\nu}(q+q')_\sigma - g_{\sigma\mu}(k-q)_\nu\right] & \mathrm{R}_\xi \text{ linear gauge} \\ ie\left[g_{\nu\sigma}(k+q')_\mu - g_{\mu\nu}(q'+q-\xi k)_\sigma - g_{\sigma\mu}(k-q-\xi q')_\nu\right] & \mathrm{R}_\xi \text{ nonlinear gauge} \end{cases} \tag{6.121i}$$

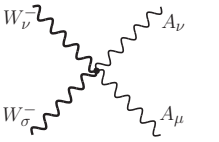

$$= \begin{cases} -ie^2\left[2g_{\mu\nu}g_{\alpha\beta} - g_{\mu\alpha}g_{\nu\beta} - g_{\nu\alpha}g_{\mu\beta}\right] & \mathrm{R}_\xi \text{ linear gauge} \\ -ie^2\left[\,2g_{\mu\nu}g_{\alpha\beta} - (1-\xi)(g_{\mu\alpha}g_{\nu\beta} + g_{\nu\alpha}g_{\mu\beta})\right] & \mathrm{R}_\xi \text{ nonlinear gauge} \end{cases} \tag{6.121j}$$

6.D One-loop VVCS amplitude with $W^\pm$-bosons in unitary gauge

The diagrams for this amplitude are shown in Fig. 6.10. The s-channel graph with the muon self-energy correction is given by the following loop integral

$$[S_{LT}]_s^{\mathrm{SE}}(\nu, Q^2) = \frac{e^2 g^2}{2(2m_\mu\nu - Q^2)^2}\left(-g_{\alpha\beta} + \frac{k_\alpha k_\beta}{M_W^2}\right)$$

$$\times \int \frac{d^4k}{(2\pi)^4} \frac{\bar{u}(\vec{p}) \not{\varepsilon}^*(q) (\not{p} + \not{q} + m_\mu) \gamma^\beta P_L (\not{p} + \not{q} + \not{k}) \gamma^\alpha P_L (\not{p} + \not{q} + m_\mu) \not{\varepsilon}(q) u(\vec{p})}{(k^2 - M_W^2)(p+q+k)^2}. \tag{6.122}$$

The s-channel amplitudes with vertex correction are

$$\begin{aligned}
[S_{LT}]_s^{\mathrm{V}_1}(\nu, Q^2) = &- \frac{e^2 g^2}{2(2m_\mu \nu - Q^2)} \left[-g_{\beta_1\beta_2} + \frac{(k+q)_{\beta_1}(k+q)_{\beta_2}}{M_W^2} \right] \left[-g_{\alpha_1\alpha_2} + \frac{k_{\alpha_1} k_{\alpha_2}}{M_W^2} \right] \\
&\times \int \frac{d^4k}{(2\pi)^4} \frac{\bar{u}(\vec{p}) \not{\varepsilon}^*(q) (\not{p} + \not{q} + m_\mu) \gamma_{\beta_1} P_L (\not{p} - \not{k}) \gamma_{\alpha_1} P_L u(\vec{p})}{(k^2 - M_W^2) \left[(k+q)^2 - M_W^2 \right] (p-k)^2} \\
&\times \left[g^{\alpha_1\alpha_2} (2k+q)^\mu - g^{\mu\alpha_2} (k-q)^{\beta_2} - g^{\mu\beta_2} (k+2q)^{\alpha_2} \right] \varepsilon_\mu(q), \qquad (6.123) \\
[S_{LT}]_s^{\mathrm{V}_2}(\nu, Q^2) = &- \frac{e^2 g^2}{2(2m_\mu \nu - Q^2)} \left[-g_{\beta_1\beta_2} + \frac{k_{\beta_1} k_{\beta_2}}{M_W^2} \right] \left[-g_{\alpha_1\alpha_2} + \frac{(k+q)_{\alpha_1}(k+q)_{\alpha_2}}{M_W^2} \right] \\
&\times \int \frac{d^4k}{(2\pi)^4} \frac{\bar{u}(\vec{p}) \gamma_{\beta_1} P_L (\not{p} - \not{k}) \gamma_{\alpha_1} P_L (\not{p} + \not{q} + m_\mu) \not{\varepsilon}(q) u(\vec{p})}{(k^2 - M_W^2) \left[(k+q)^2 - M_W^2 \right] (p-k)^2} \\
&\times \left[g^{\alpha_1\alpha_2} (2k+q)^\nu - g^{\nu\alpha_2} (k+2q)^{\beta_2} - g^{\nu\beta_2} (k-q)^{\alpha_2} \right] \varepsilon^*_\nu(q). \qquad (6.124)
\end{aligned}$$

The s-channel box amplitude is

$$\begin{aligned}
[S_{LT}]_s^{\mathrm{B}}(\nu, Q^2) = &\int \frac{d^4k}{(2\pi)^4} \frac{\bar{u}(\vec{p}) \gamma^{\rho_1} P_L (\not{p} - \not{k} + \not{q}) \gamma^{\alpha_1} P_L \not{\varepsilon}(q) u(\vec{p})}{(k^2 - M_W^2) \left[(k-q)^2 - M_W^2 \right]^2 (p-k+q)^2} \\
&\times \left[-g_{\rho_1\rho_2} + \frac{(k-q)_{\rho_1}(k-q)_{\rho_2}}{M_W^2} \right] \left[g^{\rho_2\beta_2} (2k-q)^\nu - g^{\beta_2\nu} (k+q)^{\rho_2} - g^{\rho_2\nu} (k-2q)^{\beta_2} \right] \\
&\times \left[-g_{\beta_1\beta_2} + \frac{k_{\beta_1} k_{\beta_2}}{M_W^2} \right] \left[g^{\alpha_2\beta_1} (2k-q)^\mu - g^{\alpha_2\mu} (k-2q)^{\beta_1} - g^{\beta_1\mu} (k+q)^{\alpha_2} \right] \\
&\times \left[-g_{\alpha_1\alpha_2} + \frac{(k-q)_{\alpha_1}(k-q)_{\alpha_2}}{M_W^2} \right] \varepsilon^*_\nu(q) \varepsilon_\mu(q). \qquad (6.125)
\end{aligned}$$

Chapter 7

A sum rule for electric polarizability

This chapter is devoted to the Bernabéu-Tarrach (BT) sum rule for electric polarizability, given by Eq. (2.133). Being complemented with Baldin sum rule [186], this sum rule, if convergent, provides a separate data-driven evaluation of proton electric and magnetic polarizabilities, which would be extremely interesting in comparing these polarizabilities with Compton scattering experiments at HIGS [156] and MAMI [157] as well as with BχPT predictions [39, 394–396], as shown in Tab. 7.1. Another important implication of such BT sum rule estimate would be the possibility of a data-driven

Polarizability	HIGS [156]	A2 [157]	BχPT
α^p_{E1} [$\times 10^{-4}$fm^3]	13.8(1.2)	10.99(0.63)	10.65(0.47) [394, 395] 10.8(0.7) [39, 396]
β^p_{M1} [$\times 10^{-4}$fm^3]	0.2(1.2)	3.14(0.51)	3.25(0.47) [394, 395] 3.9(0.7) [39, 396]

Table 7.1 Electric and magnetic dipole polarizabilities of the proton measured by HIGS and A2 Collaborations in comparison to BχPT predictions.

evaluation of the "subtraction-function contribution" to the proton-structure effects in the Lamb shift of muonic hydrogen. This contribution brings one of the significant uncertainties in the extraction of the proton charge radius from muonic hydrogen spectroscopy [397–400, 153], see also [151, 401] for the most recent reviews.

The first attempt to verify the BT sum rule was performed by Llanta and Tarrach [402], who computed the l.h.s and r.h.s of Eq. (2.133) in QED to leading order in $\alpha_{\rm em}$. They showed that the dispersive integral over the photoabsorption cross section, while convergent, does not reproduce the correct value of the electric polarizability. Moreover, they demonstrated that the difference arises due to the real constant value of the corresponding Compton amplitude at infinite energy. This finding is not surprising if one recalls the Sugawara-Kanazava theorem [158], which was briefly explained in Sec. 2.1.

Another argument casting doubt on the validity of the BT sum rule was provided by calculating the electric polarizability of the neutral pion[1]: various pre-χPT models (see [403] and references therein) together with the linear σ-model [404] predicted the negative value of this quantity. Moreover, the calculations in meson χPT at NLO [405, 406] and even NNLO [407, 408] also provided the negative result within the theoretical uncertainty. Although the charged pion polarizabilities has been extracted in the Primakoff process using charged pion beam by the COMPASS Collaboration [409], the experimental extraction of the polarizabilities of the neutral pion still remains a serious experimental challenge. Existing indirect extractions, based on dispersive analysis of $\gamma\gamma \to \pi\pi$ scattering data, cannot fix the sign of this polarizability within the uncertainty just from the data without imposing additional constraints, such as the Adler zero [410, 411], or relating the polarizabilities with chiral couplings [412].

Finally, there exist the argument against the convergence of the integral of BT sum rule due to the Regge asymptotics of the amplitude T_L [331, 413]. It relies on the expectation from the Regge theory that T_L may also have a soft-Pomeron behavior at high energies,

$$T_L(\nu, Q^2) \sim \nu^{\alpha_{P_s}}, \quad \alpha_{P_s} \approx 1.0667, \tag{7.1}$$

thus making the integral in Eq. (2.133) approximately linearly divergent.

In view of the provided arguments, the BT sum rule was discarded [413] (more recently, in [331]); its use for nuclei was discussed in [414]. However, in what follows, we revisit the aforementioned arguments, making an effort to rehabilitate the (BT) sum rule.

In Section 7.1, the application of the BT sum rule to nucleons, specifically protons, is considered. This section identifies specific cases where the sum rule holds exactly and derives the sum rule for the subtraction-function contribution to proton-structure effects in the Lamb shift of muonic hydrogen, with perturbative verification. Furthermore, the saturation of both sum rule integrals is investigated using available low-energy data. The section concludes with a discussion on the BT sum rule convergence at high energies, contextualized within available high-energy data on the longitudinal structure function. Section 7.2 revisits the status of electromagnetic polarizabilities of the neutral pion. It begins by examining the meson χPT calculations that yield a negative electric polarizability for π^0. Subsequently, an alternative estimation of this quantity is provided, conducted within the non-perturbative framework using the light-front valence quark wave function. The Chapter concludes with remarks addressing the question: "To subtract or not to subtract?" in relation to the BT sum rule.

The work presented in this chapter on nucleon polarizabilities is based on the publication [415]. The section addressing pion polarizabilities is currently being prepared for publication.

[1]Written initially for the Compton scattering on a spin-1/2 particle, it can be easily generalized for the spinless particles by dropping out the term with the anomalous magnetic moment.

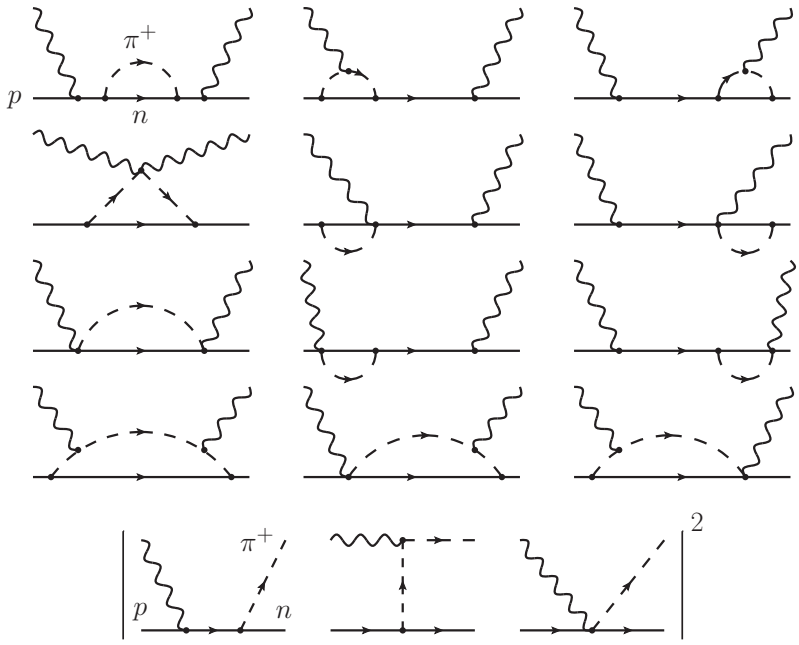

Fig. 7.1 The $\pi^+ n$ contributions to the sum rule, where the loops contribute to the left-hand side and the tree-level cross sections to the right-hand side.

7.1 Nucleons

For nucleons, notably protons, there is quite a lot of experimental information on scattering and low-energy observables. Extensive experimental study of pion photoproduction gave rise to the comprehensive models for the corresponding amplitudes and cross sections, such as SAID [416] and MAID [417]. These models provide a precise behavior of the scattering observables at low photon energies up to first nucleon resonances, i.e. $\Delta(1232)$-resonance. On the other hand, a manifestly covariant BχPT was proven to have large predictive power on low-energy observables, such as spin-independent and spin-dependent polarizabilities. Despite the direct measurements, the χPT predictions on the polarizability effects were precisely tested by spectroscopy experiments in light hydrogen-like atoms. These facts prove BχPT to be particularly successful in describing strong interaction effects in Compton scattering at low-energies. Therefore we begin by testing the BT sum rule at the leading order in this theory.

7.1.1 Validation in Baryon χPT

Consider the manifestly covariant baryon χPT calculation of the proton polarizabilities to leading order [418, 419], and check whether it can be reproduced by the Baldin and BT sum rules. For the Baldin sum rule, this exercise was done in [420, 421] by calculating the tree-level pion photoproduction, see Figs. 7.1 and 7.2. Here, we have verified the BT sum rule, by using the longitudinal cross section σ_L of charged-pion photoproduction [422, 423] (note that at this order the $\varkappa^2$ contribution to the sum

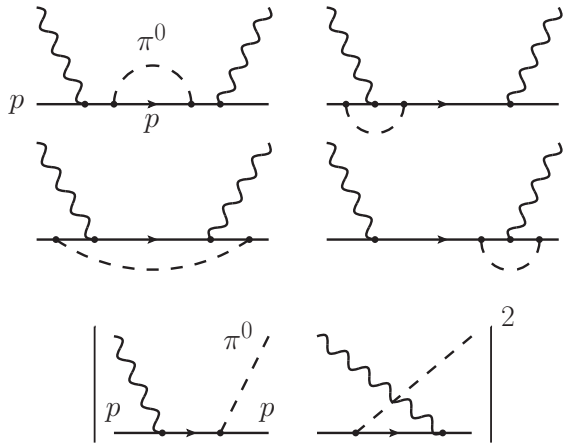

Fig. 7.2 The $\pi^0 p$ contributions to the sum rule, where the loops contribute to the left-hand side and the tree-level cross sections to the right-hand side.

rule is 0). We have also verified explicitly that in this case the VVCS amplitude at infinite energy is vanishing,

$$T_L^{\pi^+ n\text{-loops}}(\infty, Q^2) = 0. \tag{7.2}$$

Hence the sum rule works exactly, and not just up to a constant.

For the loops involving the neutral pion, corresponding to the $\pi^0 p$-channel on the cross-section side, the amplitude at infinity is not vanishing. As in QED, the constant in the asymptotic value of T_L [2],

$$T_L^{\pi^0 p\text{-loops}}(\infty, Q^2) = -\frac{\alpha_{\text{em}}}{12\pi}\frac{g_{\pi N}^2}{M^3}Q^2 + O(Q^4) \tag{7.3}$$

(here $g_{\pi N}$ is the pion-nucleon coupling constant) comes from the one-particle-irreducible graph, where both photons couple to the Dirac fermion in the loop. It suggests that this artefact may be handled by a simple ultraviolet completion involving a short-range fermion-fermion interaction.

We therefore conclude that the sum rule works, albeit only for the $\pi^+ n$ channel without the caveat. For an empirical evaluation of the sum rule, one can safely neglect the value of the amplitude at infinity. As the next step, we check the empirical sum rule estimate for the proton polarizability. Unfortunately, we have found only one viable empirical model for $\left[\sigma_L/Q^2\right]_{Q^2=0}$ of the proton – the MAID [417]. Other parametrizations [424, 425] do not have a good behavior in the small Q^2 limit and consequently do not allow for a stable extrapolation to $Q^2 = 0$. The MAID, however, provides only one of the contributions to the inclusive cross sections – the single-pion production (πN) channel. At least it is the dominant channel at low energies.

We have studied the sum rule integrals as functions of the upper limit of integration,

$$I_{\text{BT}}(\Lambda) = \frac{1}{2\pi^2}\int_{\nu_0}^{\Lambda} d\nu \left[\frac{\sigma_L(\nu, Q^2)}{Q^2}\right]_{Q^2\to 0}, \tag{7.4a}$$

[2]The asymptotic values of the Compton amplitudes were conveniently calculated using Package-X [5, 6].

$$I_{\rm Baldin}(\Lambda) = \frac{1}{2\pi^2}\int_{\nu_0}^{\Lambda} d\nu \frac{\sigma_T(\nu)}{\nu^2}. \tag{7.4b}$$

The MAID results are shown in Fig. 7.3 by dashed curves. They can be compared to the solid curves representing the χPT calculation of the πN channel, as explained above. Note that for the Baldin sum rule the discrepancy between MAID and χPT is very large because of the $\Delta(1232)$ and other N^* resonances. For the BT sum rule, the leading-order χPT describes the empirial MAID cross section rather well, and hence their BT integrals agree at such low cutoffs.

Furthermore, from the χPT calculation we know that the full BT integral gives, $I_{\rm BT}(\Lambda\to\infty) \simeq 7\times10^{-4}$ fm^3. Taking into account the anomalous magnetic moment term,

$$\frac{\alpha_{\rm em}\varkappa_p^2}{4M_p^3} \simeq 0.54\times10^{-4}\,{\rm fm}^3, \tag{7.5}$$

we obtain the proton electric polarizability of about 7.5 (in the usual units). This can be compared to the PDG value [426]: $\alpha_{E1}^p = 11.2\pm0.4$. It is quite plausible that this difference will be diminished by inclusion of other channels, predominately the $\pi\pi N$ channel. One can see that for the Baldin sum rule the single-πN-channel value of about 11.6 is also different from the inclusive result of 14 ± 0.2. The relative difference here is smaller than in the BT sum rule, because apparently the Baldin sum rule converges faster.

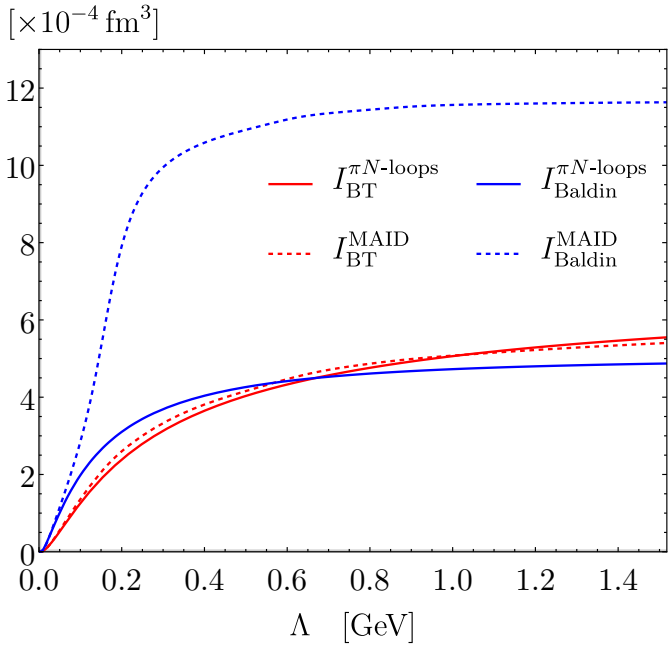

Fig. 7.3 Saturation of the Bernabéu-Tarrach and Baldin integrals [Eqs. (7.4a), (7.4b)] for the proton, using the leading-order χPT and the empirical MAID model.

7.1.2 Sum rule for the subtraction function

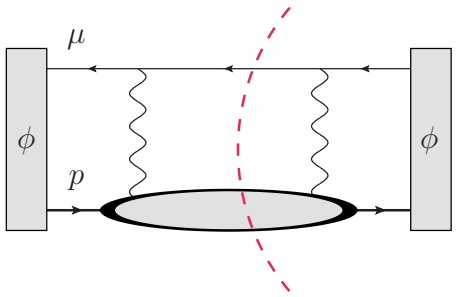

Fig. 7.4 Leading-order $O((Z\alpha_{\rm em})^5)$ two-photon exchange contribution to the Lamb shift of muonic hydrogen.

It remains to be seen whether the BT sum rule converges, but if it does, there would be a few important implications. First of all, it will provide an independent determination of the nucleon electric polarizability and can be compared with the two most recent Compton experiments: HIγS [156] versus MAMI [157]. Secondly, it will allow to evaluate the VVCS amplitude T_L via the dispersion relation (2.131). This is particularly important for the data-driven evaluation of the leading-order proton polarizability effect on the Lamb shift in muonic hydrogen. This effect is described by the (forward) two-photon exchange diagram (cf. Fig. 7.4), which incorporates the spin-independent Compton scattering, yielding

$$\Delta E_{\rm LS}^{2\gamma}(nS) = 8\pi\alpha_{\rm em} m_\mu \phi_n^2 \frac{1}{i}\int_{-\infty}^{\infty}\frac{d\nu}{2\pi}\int\frac{d\mathbf{q}}{(2\pi)^3}\frac{(Q^2-2\nu^2)T_1(\nu,Q^2)-(Q^2+\nu^2)T_2(\nu,Q^2)}{Q^4(Q^4-4m_\mu^2\nu^2)}. \tag{7.6}$$

Here $\phi_n = 1/(\pi n^3 a_B^2)$ is the wave function of the nS-level at the origin, and $a_B = [\alpha_{\rm em} m_\mu M/(m_\mu + M)]^{-1}$ is the Bohr radius; M and m_μ are the proton and the muon masses, respectively, and $Q^2 = \mathbf{q}^2 - \nu^2$. While the invariant Compton amplitude T_2 obeys unsubtracted dispersion relation, thus can be fully determined by the corresponding proton structure function or the photoabsorption cross section, see Eq. (2.88b), the invariant amplitude T_1 requires a subtraction (2.88a). However, provided that the unsubtracted relation for T_L holds (2.131), this subtraction function can be calculated via T_L using Siegert's theorem [427], which equates (up to a phase factor) the transverse and longitudinal amplitudes in the limit of $\nu \to iQ$:

$$T_1(iQ, Q^2) = -T_L(iQ, Q^2). \tag{7.7}$$

Now, this is all that is needed for the subtraction point of $\nu = iQ$ [428]. More usual is the subtraction at $\nu = 0$, which implies the following dispersion relation for T_1, given by Eq. (2.88a). Combining it with the dispersion relation for $T_L(iQ, Q^2)$ and the Siegert theorem, the conventional subtraction

function has the following expression:

$$T_1(0,Q^2) = \frac{2}{\pi}Q^2 \int_{\nu_0}^{\infty} \frac{d\nu \sqrt{1+\frac{Q^2}{\nu^2}}}{\nu^2+Q^2} \left[\sigma_T - \frac{\nu^2}{Q^2}\sigma_L\right](\nu,Q^2). \tag{7.8}$$

We have verified this sum rule exactly in the χPT example above, including the charged-pion channel. Note that at this order we only verify the polarizability contribution and not any of the possible non-pole VVCS contributions coming from the Born term (expressed by the elastic form factors).

In Fig. 7.5, we show the non-Born part of the VVCS amplitudes as functions of Q^2 evaluated through the integrals on the right-hand side of Eq. (7.8) (left panel) and Eq. (2.131) (right panel) using MAID [417]. In order to obtain the non-Born part, from the above dispersion relations, one has to subtract the non-pole Born parts. For T_L, it is given by (cf. Eq. (2.130))

$$T_L(\text{nonpole Born}) = -\frac{\pi\alpha_{\text{em}}Q^2}{M^3}\mathcal{F}_2(Q^2). \tag{7.9}$$

In the case of $T_1(0,Q^2)$ evaluated through Eq. (7.8), one has to add Eq. (7.9). At first glance, this might look counterintuitive, since the non-pole Born part of $T_1(\nu,Q^2)$ is given by $T_1(\text{non-pole Born}) = -4\pi\alpha_{\text{em}}\mathcal{F}_1^2(Q^2)/M$. The difference comes from the mismatch of the non-pole parts in Eq. (7.7): this equality is valid for the full Born amplitudes, but not separately for the pole and non-pole contributions. As the result, we have the following expressions for the non-Born parts of the subtraction functions, plotted in Fig. 7.5:

$$\begin{aligned}
\overline{T}_1(0,Q^2) &= -\frac{\pi\alpha_{\text{em}}Q^2}{M^3}\mathcal{F}_2^2(Q^2) + \frac{2}{\pi}Q^2\int_{\nu_0}^{\infty}\frac{d\nu}{\nu^2\sqrt{1+\frac{Q^2}{\nu^2}}}\left[\sigma_T - \frac{\nu^2}{Q^2}\sigma_L\right](\nu,Q^2),\\
\overline{T}_L(iQ,Q^2) &= \frac{\pi\alpha_{\text{em}}Q^2}{M^3}\mathcal{F}_2^2(Q^2) + \frac{2}{\pi}\int_{\nu_0}^{\infty} d\nu\,\frac{\sigma_L(\nu,Q^2)}{\sqrt{1+\frac{Q^2}{\nu^2}}} = -\overline{T}_1(iQ,Q^2),
\end{aligned}$$

where ν_0 is again the inelastic threshold. In calculating the Pauli form factor ($\mathcal{F}_2$) contribution, we are using the empirical parametrization of nucleon form factors from Ref. [429].

In the limit of $Q^2 = 0$, the $\overline{T}_L(iQ,Q^2)/4\pi Q^2$ amplitude yields α_{E1}, cf. (2.129), whereas $\overline{T}_1(0,Q^2)/4\pi Q^2$ yields β_{M1}. Their sum is consistent with the MAID evaluation of the Baldin sum rule shown in Fig. 7.3.

Besides the data-driven evaluations of the subtractions functions based on the MAID pion-production cross sections, we show in Fig. 7.5 the leading and next-to-leading χPT predictions of the amplitudes, and the PDG values of the proton polarizabilities. The Figure (right panel) shows that the agreement of BχPT prediction with the empirical value of α_{E1}^p is only achieved at the next-to-leading order, where the $\pi\Delta$-loops are included. This would correspond to the inclusion of $\pi\Delta$-production channel in L, which goes beyond MAID. Hence one would need to include at least the two-pion

production channel (second diagram in r.h.s of Fig 7.6) to saturate the BT sum rule in a data-driven evaluation.

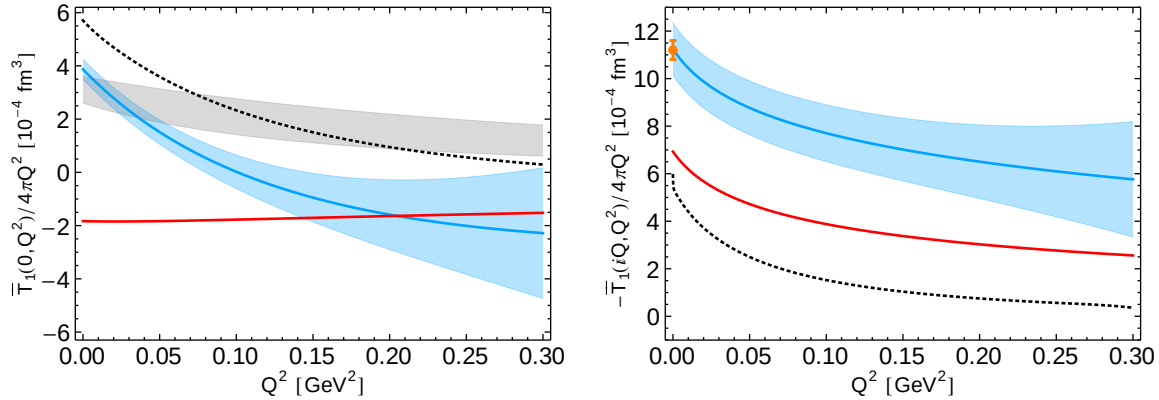

Fig. 7.5 Non-Born part of the subtraction functions, $\overline{T}_1(0,Q^2)$ (left panel) and $\overline{T}_L(iQ,Q^2)$ (right panel), evaluated with MAID [417] through Eqs. (7.8) and (2.131) (black dotted). For comparison we show: the heavy-baryon χPT calculation [153] (gray band); the next-to-leading-order χPT calculation [422, 430] (blue solid with a band); the leading χPT πN-loop contribution (red solid); At the real photon point, the PDG value for $\alpha_{E1} = (11.2 \pm 0.4) \times 10^{-4}$ fm^3 [426] is shown. Figure is taken form [415].

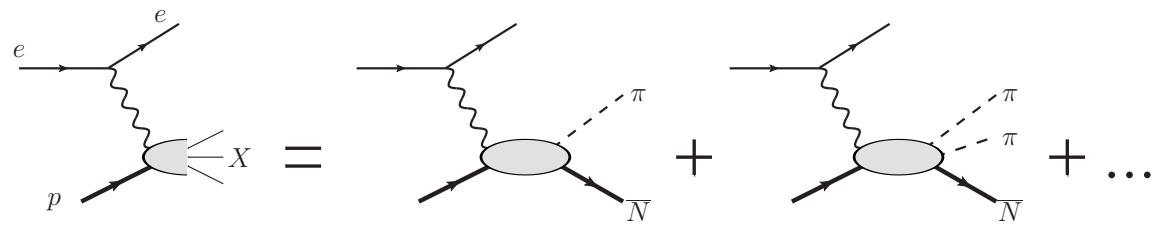

Fig. 7.6 One- and two-pion photoproduction channels that contribute to σ_L saturating the BT sum rule.

7.1.3 Validation in the parton model

Another interesting regime where the relations (2.131) and (7.8) could be checked theoretically is the domain of Bjorken scaling. In this limit the virtuality Q^2 and the energy ν of the incoming photon are taken to be very large, while preserving the finiteness of the Bjorken variable $x = Q^2/2M\nu$. The Bjorken scaling implies the validity of the perturbative expansion of QCD, with the leading-order contribution given by the naïve parton model.

In this model the deep inelastic scattering off the proton is described by the scattering off the individual partons (quarks) with electric charges e_q and parton distribution functions $f_q(x)$. The structure functions f_1 and f_2 are then given by (see, e.g., Sec. 18.5 in [337])

$$f_1(x,Q^2) = \frac{1}{e^2}\sum_q e_q^2 f_q(x), \tag{7.11a}$$

$$f_2(x,Q^2) = 2x f_1(x,Q^2), \tag{7.11b}$$

while the corresponding forward Compton amplitudes are:

$$T_1(x,Q^2) = \frac{2}{M}\int_0^1 \frac{d\xi}{\xi}\frac{\sum_q e_q^2 f_q(\xi)}{(\frac{x}{\xi})^2 - 1 - i\epsilon}, \tag{7.12a}$$

$$T_2(x,Q^2) = 8\frac{Mx^2}{Q^2}\int_0^1 \frac{d\xi}{\xi}\frac{\sum_q e_q^2 f_q(\xi)}{(\frac{x}{\xi})^2 - 1 - i\epsilon}. \tag{7.12b}$$

The longitudinal structure function f_L is given in this model by

$$\begin{aligned} f_L(x,Q^2) &= \left(1 + \frac{4M^2x^2}{Q^2}\right) f_2(x,Q^2) - 2x f_1(x,Q^2) \\ &= \frac{4M^2x^2}{Q^2} f_2(x,Q^2) \\ &= \frac{M^2}{e^2}\sum_q e_q^2 f_q(x)\frac{8x^3}{Q^2}, \end{aligned} \tag{7.13}$$

and the corresponding Compton amplitude is

$$\begin{aligned} T_L(x,Q^2) &= \left(1 + \frac{\nu^2}{Q^2}\right) T_2(x,Q^2) - T_1(x,Q^2) \\ &= T_2(x,Q^2) \end{aligned} \tag{7.14}$$

This relation immediately implies the convergence of the unsubtracted dispersion relation for T_L, as long as the unsubtracted relation is valid for T_2.

A remarkable feature of the parton model is the Callan-Gross relation [431] in Eq. (7.11b) or, equivalently, in terms of the cross sections,

$$\sigma_L = \frac{Q^2}{\nu^2}\sigma_T = \frac{4M^2x^2}{Q^2}\sigma_T, \tag{7.15}$$

which implies that σ_L falls with energy considerably faster than σ_T at twist-2 accuracy. Writing the unsubtracted dispersion relations for the Compton amplitudes in the parton model,

$$T_1(x,Q^2) = \frac{2e^2}{M}\int_0^1 \frac{d\zeta}{\zeta^3}\frac{x^2 f_1(\zeta,Q^2)}{(\frac{x}{\zeta})^2 - 1 - i\epsilon}, \tag{7.16a}$$

$$T_2(x,Q^2) = \frac{4Me^2}{Q^2}\int_0^1 \frac{d\zeta}{\zeta^2}\frac{x^2 f_2(\zeta,Q^2)}{(\frac{x}{\zeta})^2 - 1 - i\epsilon}, \tag{7.16b}$$

one can deduce that the amplitude T_2 (and, consequently, T_L) satisfies the unsubtracted dispersion relation, but T_1 does not. The latter, however, satisfies the once-subtracted dispersion relation with vanishing subtraction function. Using the Callan-Gross relation one trivially verifies the sum rule for

the subtraction function $T_1(0, Q^2)$, given by (7.8). Hence, we conclude that the dispersion relation for T_L (2.131) as well as the sum rule for the subtraction function (7.8) hold exactly in the naïve parton model.

7.1.4 Longitudinal cross section at high energies and BT sum rule convergence

Coming back to the BT sum rule integral convergence, we need to consider also the high-energy behavior of the longitudinal cross section. In the limit of interest, $\nu \to \infty$ and $Q^2 \to 0$, this behavior corresponds to the soft diffractive scattering, where QCD becomes essentially non-perturbative. Therefore one cannot make *ab initio* theoretical predictions on a certain behavior of the amplitudes. Practically, this region is described by Regge phenomenology, fitting the data by a simplest Regge ansatz, which gives the best χ^2 with the smallest number of parameters. Of course, having no systematic theory behind, this way should be treated as an *ad hoc* approach, which should not necessarily be extended on any other amplitudes. In this sense, one should not expect that the amplitude T_L must have the same asymptotic energy behavior as T_1 or T_2 even so it is a linear combination of both. In other words, no one knows *a priori* whether T_L has a hard or soft-Pomeron behavior at high energies until the precise independent measurement of this amplitude will be performed.

Another important remark concerns the experimental extraction of the corresponding proton structure functions f_2 and f_L from the data on inclusive electron-proton scattering. The analyses of the SLAC data [432–434] at relatively low photon energy $\nu \sim 10...20$ GeV as well as the results of New Muon Collaboration (NMC) [435] at the photon energies $\nu \sim 100$ GeV and various photon virtualities, do not provide the directly measured f_L. In fact, the longitudinal structure function is extracted from f_2 using certain model assumptions stemming from perturbative QCD (see, e.g., [378]). In the soft scattering regime, however, these assumptions can potentially lead to inadequate values for f_L. Therefore the sufficiently large values of f_L at low Q^2, which were obtained in the listed experiments, look somewhat questionable.

A model-independent extraction of f_L was performed by ZEUS [436] and H1 [437] Collaborations at HERA. The total data points were collected for the photon energies $\nu \sim 14...30$ TeV and virtualities $Q^2 \sim 1.5...800$ GeV^2. These results has been already used in a global Regge fit [438], where f_1, f_2 and f_L structure functions are treated within the same unified Regge framework. Concerning the f_L structure function, this fit suggests the presence of the soft-Pomeron component at high energies. However, despite the high statistics, the data on f_L are quite uncertain, especially in comparison to the f_2 structure function, for making concrete statements on the precise behavior of f_L. Moreover, as was mentioned above, if f_L is measured directly, then it is natural to fit it without relying on any additional constraints from f_2 or f_1. To the best of our knowledge, this was not done so far.

Thus, we can conclude that currently it is still not possible to make a rigorous statement on the high-energy behavior of the longitudinal structure function (and hence on the σ_L), and hence make a conclusion on the convergence of the BT sum rule at least for protons. Further investigations of the

inclusive electron-proton scattering, with increased sensitivity on f_L, are highly required. This input can be given in future by Electron-Ion Collider (EIC) project [439].

7.2 Neutral pion

The study of pion static electric (α_{E1}) and magnetic (β_{M1}) dipole polarizabilities provides crucial insights into the underlying dynamics of QCD at low energies. In contrast to nucleons, currently it is impossible to measure pion polarizabilities directly via the Compton scattering reaction. This is because of extreme experimental difficulties in creation and maintaining a target of pions due to their highly unstable nature. Therefore the reaction of two-photon fusion into two pions is usually studied. While the charged pion polarizabilities are known sufficiently well from direct measurement performed by COMPASS [409],

$$\alpha_{E1}^{\pi^\pm} = -\beta_{M1}^{\pi^\pm} = [2.0 \pm 0.6(\text{stat.}) \pm 0.7(\text{syst.})] \times 10^{-4}\text{fm}^3, \tag{7.17}$$

no direct measurement was performed for the neutral pion polarizabilities so far. The indirect extractions of the polarizabilities from the $\gamma\gamma \to \pi^0\pi^0$ scattering data via dispersive techniques have relatively weak sensitivity to the dipole polarizabilities [440], thus resulting in rather uncertain results [441, 442]. Even with the high-statistics data from Belle [443, 444], there is still lack of the precise data near two-pion threshold, which makes impossible to even constrain the sign of polarizability. Therefore one needs to impose additional constraints, such as the Adler zero [410, 411] or relate the polarizabilities with chiral couplings [412], stemming from the meson χPT. Recent lattice QCD simulations [445, 446] also have rather uncertain results for the electric polarizability of π^0. These facts make the subject of the π^0 electromagnetic polarizabilities of a great theoretical interest.

In this section, we consider the polarizabilities of the π^0 by analyzing forward doubly-virtual Compton scattering on the pion at low energies, in conjunction with the Baldin and BT sum rules. Compton scattering on a spinless particle is described by the spin-independent part of the Compton tensor (2.79)

$$T^{\mu\nu}(p,q) = \left(-g^{\mu\nu} + \frac{q^\mu q^\nu}{q^2}\right) T_1(\nu, Q^2) + \frac{1}{m_\pi^2}\left(p^\mu - \frac{p\cdot q}{q^2} q^\mu\right)\left(p^\nu - \frac{p\cdot q}{q^2} q^\nu\right) T_2(\nu, Q^2). \tag{7.18}$$

The low-energy theorems for the invariant Compton amplitudes T_1, T_2, and T_L, expressed for their non-Born components, take the form

$$\overline{T}_1(\nu, Q^2) = 4\pi(\alpha_{E1}^{\pi^0} + \beta_{M1}^{\pi^0})\nu^2 + 4\pi m_\pi \beta_{M1}^{\pi^0} Q^2 + O(E^4), \tag{7.19a}$$

$$\overline{T}_2(\nu, Q^2) = 4\pi(\alpha_{E1}^{\pi^0} + \beta_{M1}^{\pi^0})Q^2 + O(E^4), \tag{7.19b}$$

$$\overline{T}_L(\nu, Q^2) = 4\pi\alpha_{E1}^{\pi^0} Q^2 + O(E^4). \tag{7.19c}$$

where $\mathcal{E}$ refers to either Q or ν. The imaginary parts of these amplitudes are connected to the corresponding photoabsorption cross sections via the optical theorem according to Eqs. (2.83a), (2.83b) and (2.132).

Let us start by revisiting the meson χPT results for pion polarizabilities, which are state-of-the-art theoretical predictions of these quantities.

7.2.1 Pion polarizabilities in meson χPT

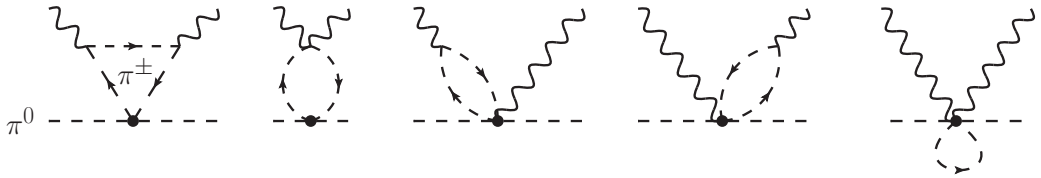

Fig. 7.7 One-loop contribution to the electromagnetic polarizabilities of the neutral pion in meson χPT at $O(p^4)$.

Before meson (χPT) was concretely established, several "pre-χPT" calculations of the neutral pion polarizabilities were conducted, as partly summarized in [403]. Perhaps the most notable calculation was carried out by L'vov using the linear σ-model. His results for π^0 are equivalent to those of meson χPT in the limit of infinitely large σ-meson mass. The first calculation in pure meson χPT was performed in the works by Bijnens and Cornett [406] and Donoghue, Holstein and Lin [405], which focused on the $\gamma\gamma \to \pi\pi$ scattering process. It was found that the leading non-vanishing contribution to $\gamma\gamma \to \pi^0\pi^0$ appears only at one loop with charged pions, i.e. at $O(p^4)$ in meson χPT power counting. Similar finding was previously seen in pre-χPT calculations by [447], who demonstrated that the contribution from the nucleon box is suppressed by the pion-nucleon mass ratio $(m_\pi/M_N)^4$, thus only the charged pion loops contribute. Moreover, in contrast to the charged pions, the amplitudes for neutral pions at this order are convergent hence do not require any low-energy constants for renormalization from the χPT Lagrangian. Thus, evaluating the set of diagrams shown in Fig. 7.7 results in the following answer for the polarizabilities:

$$\alpha_{E1}^{\pi^0,\,O(p^4)} = -\beta_{M1}^{\pi^0,\,O(p^4)} = -\frac{\alpha_{\rm em}}{96\pi^2 f_\pi^2 m_\pi} \approx -0.5\times 10^{-4}\text{fm}^3. \tag{7.20}$$

As one can see, Eq. (7.20) contains just the fundamental constants of the theory: pion mass m_π, pion decay constant f_π and fine structure constant $\alpha_{\rm em}$. It is worth mentioning that the calculation in [406, 405] was carried out assuming the equal masses of charged and neutral pion. If one wants to account for the difference between these masses, one arrives at Eq. (7.83). In contrast to Eq. (7.20), the latter result has the correct behavior in chiral limit.

The obtained negative result for static electric dipole polarizability is highly nontrivial and counter-intuitive, because it violates not only classical electrodynamics and thermodynamics (cf. Section 14 in [448]), but also the quantum mechanics. Indeed, using second-order perturbation theory,

one defines the electric polarizability in quantum mechanics in terms of the dipole operator $\hat{d}$ as

$$\alpha_{E1} = 2\sum_n \frac{\left|\langle n|\hat{d}|0\rangle\right|^2}{E_n - E_0} \geq 0, \tag{7.21}$$

which is obviously positive-definite. A possible negative sign was qualitatively explained in [449, 450] by a large negative QFT vacuum contribution, which is absent in quantum mechanics. From the experimental side, however, no stable systems with negative static electric dipole polarizability were evidently detected so far.

As shown in Appendix 7.A, the result (7.20) is robust. It does not depend on a representation of pion matrix and has a definite sign independent of the energy range of running internal loop momentum. Moreover, in the given low-energy limit, the negative sign of the electric polarizability corresponds to a stable vacuum of the theory. Indeed, the forward Compton tensor (7.82), obtained in meson χPT, is equivalent to the one calculated in ϕ^4 theory with the interaction Lagrangian

$$\mathcal{L}^{\phi^4}_{\text{int}} = -\lambda\pi^+\pi^-\pi^0\pi^0, \tag{7.22}$$

with the positive coupling $\lambda = \frac{m_\pi^2}{f_\pi^2} > 0$.

Regarding the polarizability sum rules, the result (7.20), obviously, satisfies the Baldin sum rule and violates the BT sum rule, since the diagrams in Fig. 7.7 have no dispersive parts. In principle, this fail of the BT sum rule could be illusive if the contributions of the higher orders of χPT will come with the opposite signs making the polarizability positive at the end. However, the next-to-leading order calculation in χPT at $O(p^6)$ also suggests the negative contribution within the uncernainty [407, 408]:

$$\alpha_{E1}^{\pi^0,O(p^6)} = [-0.4 \pm 0.2]\times 10^{-4}\,\text{fm}^3, \quad \beta_{M1}^{\pi^0,O(p^6)} = [1.5 \pm 0.2]\times 10^{-4}\,\text{fm}^3. \tag{7.23}$$

This contribution already has non-vanishing dispersive part, which stems from the diagrams depicted in Fig. 7.8. However, due to momentum-dependent couplings, the corresponding L-polarized cross section of $\gamma\pi^0 \to \pi^0\pi^+\pi^-$ process grows linearly with energy, which makes impossible to check the BT sum rule.

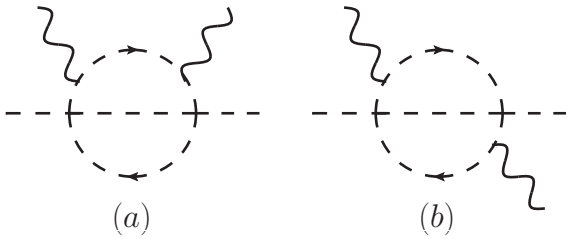

Fig. 7.8 The diagrams for Compton scattering on a pion at NNLO ChPT that have nonzero s-channel cut. The box (a) and acnode (b) topoligies are shown.

In context of possibly missed contributions, it could be interesting to look at the χPT extention with ρ-mesons included. Given that incorporating vector particles in a gauge-invariant renormalizable framework is a nontrivial task, we can do a simple estimation using a toy model with "scalar" ρ-mesons. According to calculations provided in Appendix. 7.B, both Baldin and BT sum rules hold exactly in this theory, while the electric dipole polarizability is positive. This result leaves an intriguing avenue for further investigations.

7.2.2 Neutral pion polarizabilities in light-front quark model

An interesting alternative way to obtain the pion polarizabilities is to invoke the light-front quark model. This model particularly succeed in description of the charged-pion electromagnetic form factor and the pion transition form factor. Thus, we can apply similar formalism here for calculating the low-energy Compton scattering. The essence of the model is comprised in the so-called light-front wave function (LFWF), which corresponds to the valence quark component and carries out the non-perturbative nature of QCD ineraction of quarks forming a pion.

We consider the valence quark-antiquark state in the pion in which the quark has light-front momentum fraction x of the pion light-front momentum p^+, i.e. $k^+ = xp^+$, and has a relative transverse momentum $\boldsymbol{\kappa}_\perp$, whereas the antiquark having momentum fraction $\bar{x}$ and relative transverse momentum $-\boldsymbol{\kappa}_\perp$. The LFWF for the valence quark component in the pion $\Psi_{q\bar{q}/\pi}(x, \boldsymbol{\kappa}_\perp)$, denoted for simplicity as $\Psi_\pi(x, \boldsymbol{\kappa}_\perp)$, is defined through the bilocal matrix element at equal light-front time $y^+ = 0$:

$$\Psi_\pi(x, \boldsymbol{\kappa}_\perp) \equiv \frac{1}{\sqrt{6}} \int d^2\boldsymbol{y}_\perp e^{-i\boldsymbol{\kappa}_\perp \cdot \boldsymbol{y}_\perp} \int dy^- e^{ixp^+y^-} \langle 0|\bar{d}(0)\gamma^+\gamma_5 u(y)|\pi^+(p)\rangle\big|_{y^+=0}. \tag{7.24}$$

In Eq. (7.24), the LFWF definition is shown for the π^+ flavor state, with $d(0)$ and $u(y)$ the quark spinor fields in position space, and where $\sqrt{2N_c} = \sqrt{6}$ is a conventional normalization factor related to the number of colors N_c. Due to the approximate isospin symmetry, the same LFWF also applicable for π^0.

The normalization of the valence quark LFWF in the pion is obtained from the local matrix element:

$$\langle 0|\bar{d}(0)\gamma^\mu\gamma_5 u(0)|\pi^+(p)\rangle = \sqrt{2} f_\pi p^\mu, \tag{7.25}$$

through the pion decay constant $f_\pi = 92.4$ MeV. This yields the integral

$$\int_0^1 dx \phi_\pi(x) = \int_0^1 dx \int \frac{d^2\boldsymbol{\kappa}_\perp}{16\pi^3} \Psi_\pi(x, \boldsymbol{\kappa}_\perp) = \frac{f_\pi}{2\sqrt{3}}. \tag{7.26}$$

On the other hand, the probability for the valence quark Fock component in the pion state is given by the integral of the squared modulus of the valence quark wave function:

$$P_{q\bar{q}} = \int_0^1 dx \int \frac{d^2\boldsymbol{\kappa}_\perp}{16\pi^3} |\Psi_\pi(x, \boldsymbol{\kappa}_\perp)|^2. \tag{7.27}$$

In QCD hard processes, the non-perturbative object which enters factorization theorems is obtained by integrating the LFWF over the quark transverse momentum up to a scale μ, yielding the distribution amplitude (DA):

$$\phi_\pi(x,\mu) \equiv \int^{\mu^2} \frac{d^2\boldsymbol{\kappa}_\perp}{16\pi^3}\Psi_\pi(x,\boldsymbol{\kappa}_\perp). \tag{7.28}$$

For $\mu \to \infty$, the expression of the distribution amplitude is given by its asymptotic form, denoted by $\phi_\pi^{as}(x)$:

$$\phi_\pi(x,\mu\to\infty) = \phi_\pi^{as}(x) = \frac{f_\pi}{2\sqrt{3}}6x\bar{x}. \tag{7.29}$$

In the following, we don't write the explicit μ dependence of the DA, which can be expressed as the one-dimensional Fourier integral along the light-cone direction y^-, at equal light-front time $y^+ = 0$ and equal transverse distance $\boldsymbol{y}_\perp = 0$:

$$\phi_\pi(x) \equiv \frac{1}{\sqrt{6}}\frac{1}{4\pi}\int dy^- e^{ixp^+y^-}\langle 0|\bar{d}(0)\gamma^+\gamma_5 u(y)|\pi^+(p)\rangle\Big|_{y^+=\boldsymbol{y}_\perp=0}. \tag{7.30}$$

Perturbative QCD allows to express observables at large momentum transfers in terms of the LFWF of the leading (valence quark) Fock component. A well-studied example is the $\gamma^*(q_1)\gamma^*(q_2)\to\pi^0$ transition form factor (TFF), defined as:

$$\int d^4y e^{-iq_1y}\langle\pi^0(p)|T\left[J_\mu(y)J_\nu(0)\right]|0\rangle = i\,\varepsilon_{\mu\nu\alpha\beta}q_1^\alpha q_2^\beta F_{\pi^0\gamma^*\gamma^*}(q_1^2,q_2^2), \tag{7.31}$$

with $J_\mu(y)$ the electromagnetic current operator, and $F_{\pi^0\gamma^*\gamma^*}(q_1^2,q_2^2)$ the TFF. As example, the asymptotic expression for the TFF when one photon has a large spacelike virtuality $-q^2 = Q^2 \to \infty$, while the second photon is real, is given by:

$$F_{\pi^0\gamma^*\gamma^*}(q^2,0) \longrightarrow \frac{1}{Q^2}\frac{2}{\sqrt{3}}\int_0^1 \phi_\pi(x)\left[\frac{1}{x}+\frac{1}{\bar{x}}\right]. \tag{7.32}$$

Using the asymptotic pion DA of Eq. (7.29), this yields the leading-order prediction at large Q^2: $F_{\pi^0\gamma^*\gamma^*}(q^2,0)\to 2f_\pi/Q^2$. Thus, the Eqs. (7.26) and (7.32) put the constraints on the possible form of LFWF.

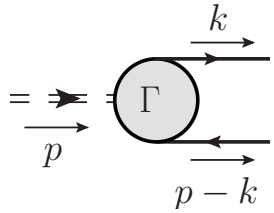

Fig. 7.9 Pion-quark-antiquark vertex function $\Gamma(k, p-k)$.

Now let us discuss the connection of LFWF with the covariant formalism. In time-ordered QFT, the pion-quark-antiquark vertex function $\Gamma(k, p-k)$, which is shown in Fig. 7.9, is related to the covariant Bethe-Salpeter wavefunction of a pion [451–453], denoted by $\Psi^{\rm BS}(k, p-k)$, as:

$$\Psi^{\rm BS}(k,p-k) = \frac{\Gamma(k,p-k)}{(k^2-m^2+i\epsilon)\left[(p-k)^2-m^2+i\epsilon\right]}. \tag{7.33}$$

The valence quark light-front wave function (LFWF), in its turn, is obtained as a light-front projection of the Bethe-Salpeter wave function, integrating the latter over the "−" component of the active quark momentum:

$$\Psi_\pi(x,\boldsymbol{\kappa}_\perp) = i2p^+\sqrt{x\bar{x}}\int\frac{dk^-}{2\pi}\Psi^{\rm BS}(k,p-k). \tag{7.34}$$

To establish the connection between covariant and light-front descriptions in actual calculation of the Compton amplitudes, we will consider the simple model for the vertex function corresponding to the local (contact) interaction between the pion and its constituents derived from the Lagrangian term:

$$\mathcal{L}_{\rm int} = -g\varphi^\dagger(x)\varphi(x)\pi(x) + \text{h.c.} \tag{7.35}$$

Here $\varphi(x)$ is a complex scalar quark field with a charge e_q and mass m, and $\pi(x)$ is the pion field. Note that the coupling g in this theory has a dimension of mass. For this model, the Bethe-Salpeter wave function is given by:

$$\Psi^{\rm BS}(k,p-k) = \frac{g}{(k^2-m^2+i\epsilon)\left[(p-k)^2-m^2+i\epsilon\right]}. \tag{7.36}$$

The valence quark LFWF, in its turn, is obtained from Eq. (7.34), yielding the following form in the covariant model:

$$\Psi_\pi(x,\boldsymbol{\kappa}_\perp) = i2p^+\sqrt{x\bar{x}}\int\frac{dk^-}{2\pi}\Psi^{\rm BS}(k,p-k) = \frac{g}{\sqrt{x\bar{x}}}\frac{1}{\left(m_\pi^2-\frac{\boldsymbol{\kappa}_\perp^2+m^2}{x\bar{x}}\right)} = -\frac{g\sqrt{x\bar{x}}}{\boldsymbol{\kappa}_\perp^2+\mu^2(x)}. \tag{7.37}$$

Here the relative transverse quark momentum $\boldsymbol{\kappa}_\perp = \boldsymbol{k}_\perp - x\boldsymbol{p}_\perp$ was introduced, and $\mu^2(x) \equiv m^2 - x\bar{x}m_\pi^2$. Note that for a bound state ($m_\pi < 2m$) one has $\mu^2(x) > 0$.

In what follows, we will focus on the Compton scattering on the neutral pion, whose valence quark flavor structure is given by:

$$|\pi^0\rangle = \frac{1}{\sqrt{2}}\left(|u\bar{u}\rangle - |d\bar{d}\rangle\right). \tag{7.38}$$

Furthermore, in the following calculation, the u and d quarks, with corresponding charges $e_u = 2/3$ and $e_d = -1/3$, will be taken as scalar particles for simplicity. The structure of the neutral pion state will be reflected in the overall charge factor $C_q^{\pi^0}$ in the Compton amplitudes, which is given by the

combination of the quark charges:

$$C_q^{\pi^0} = \frac{1}{2}\left(e_u^2 + e_d^2\right) = \frac{5}{18}. \tag{7.39}$$

7.2.2.1 Covariant calculation

We start by calculating the forward Compton scattering amplitudes in the covariant model, which was defined by Eqs. (7.35) and (7.36). In such model, where the pion-quark-antiquark vertex is given by a contact term, the Compton scattering process is described by the Feynman diagrams shown in Fig. 7.10. There are two types of contributions: the seagull, direct, and crossed diagrams involve one active quark, whereas the cat-ear diagrams, which are required to satisfy the low-energy theorem involve two active quarks.

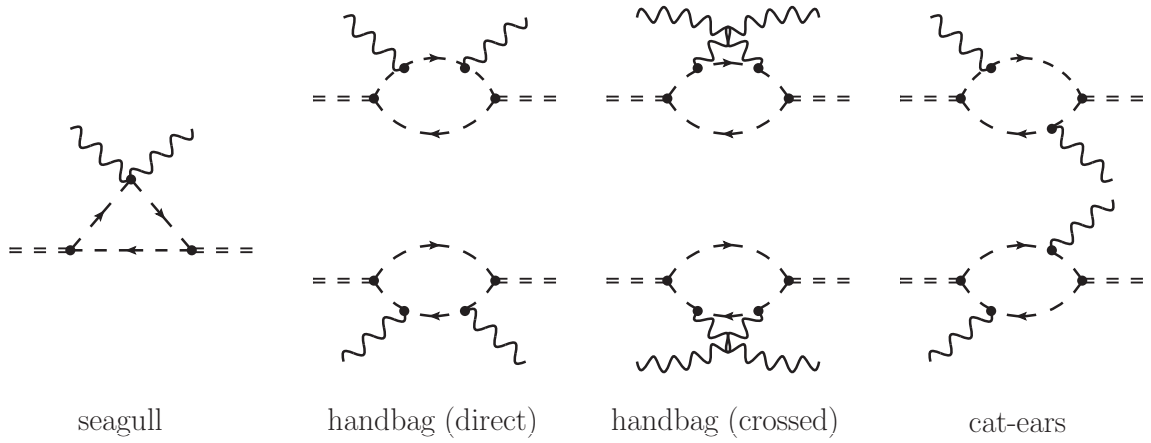

Fig. 7.10 Valence scalar quark contribution to the Compton scattering on the neutral pion: the seagull, direct, and crossed handbag diagrams involve one active quark, whereas the cat-ears diagram involves two active quarks.

In order to evaluate the pion polarizabilities through the valence quark light-front wave function, we choose a reference frame with purely transversal momentum transfer (Drell-Yan-West frame),

$$p = (p^+, p^-, \boldsymbol{p}_\perp), \qquad \boldsymbol{p}_\perp \equiv (p^x, p^y) = \left(-\frac{m_\pi \nu}{Q}, 0\right), \qquad p^- = \frac{m_\pi^2}{2p^+}\left(1 + \frac{\nu^2}{Q^2}\right) \tag{7.40a}$$

$$q = (0, 0, \boldsymbol{q}_\perp), \qquad \boldsymbol{q}_\perp \equiv (q^x, q^y) = (Q, 0), \tag{7.40b}$$

By considering different light-front components of the Compton tensor (7.18), one can extract the invariant Compton amplitudes:

$$T^{++} = \frac{(p^+)^2}{m_\pi^2} T_2, \tag{7.41a}$$

$$T^{+-} = -T_1 + \frac{1}{2}\left(1 + \frac{\nu^2}{Q^2}\right) T_2, \tag{7.41b}$$

$$T^{--} = \frac{m_\pi^2}{4(p^+)^2}\left(1+\frac{\nu^2}{Q^2}\right)^2 T_2, \tag{7.41c}$$

$$T^{xx} = T^{+x} = T^{+y} = 0, \tag{7.41d}$$

$$T^{yy} = T_1. \tag{7.41e}$$

The tensor structures which do not contain the "−" component are free of endpoint singularities [454, 455], and are therefore of particular interest.

In the Drell-Yan-West frame, the analogous procedure as was applied in Ref. [456] to obtain the valence quark contribution to the pion vector form factor via the residue analysis in the k^--complex plane yields the following individual contributions to the forward Compton tensor $T^{\mu\nu}$, where μ and ν stand for either "+" or "⊥" components:

$$T^{\mu\nu}_{\text{seagull}} = 2g^{\mu\nu} C_q^{\pi^0} \frac{\alpha_{\text{em}} g^2}{4\pi m_\pi} \int_0^1 dx \frac{\bar{x}}{\mu^2(x)}, \tag{7.42a}$$

$$T^{\mu\nu}_{\text{direct}} = C_q^{\pi^0} \frac{\alpha_{\text{em}} g^2}{4\pi^2 m_\pi} \int_0^1 dx \int d^2\boldsymbol{k}_\perp \frac{\bar{x}^2 (2k+q)^\mu (2k+q)^\nu}{\left[(\boldsymbol{k}_\perp - x\boldsymbol{p}_\perp)^2 + \mu^2(x)\right]^2} \times \left[(\boldsymbol{k}_\perp - x\boldsymbol{p}_\perp)^2 + \bar{x}(\boldsymbol{q}_\perp^2 + 2\boldsymbol{k}_\perp\cdot\boldsymbol{q}_\perp) + \mu^2(x) - i\epsilon\right]^{-1}, \tag{7.42b}$$

$$T^{\mu\nu}_{\text{crossed}} = C_q^{\pi^0} \frac{\alpha_{\text{em}} g^2}{4\pi^2 m_\pi} \int_0^1 dx \int d^2\boldsymbol{k}_\perp \frac{\bar{x}^2 (2k-q)^\mu (2k-q)^\nu}{\left[(\boldsymbol{k}_\perp - x\boldsymbol{p}_\perp)^2 + \mu^2(x)\right]^2} \times \left[(\boldsymbol{k}_\perp - x\boldsymbol{p}_\perp)^2 + \bar{x}(\boldsymbol{q}_\perp^2 - 2\boldsymbol{k}_\perp\cdot\boldsymbol{q}_\perp) + \mu^2(x)\right]^{-1}, \tag{7.42c}$$

$$T^{\mu\nu}_{\text{cat-ears}} = C_q^{\pi^0} \frac{\alpha_{\text{em}} g^2}{4\pi^2 m_\pi} \int_0^1 dx \int d^2\boldsymbol{k}_\perp \frac{x\bar{x}(2k+q)^\mu (2(k-p)+q)^\nu}{\left[(\boldsymbol{k}_\perp - x\boldsymbol{p}_\perp)^2 + \mu^2(x)\right]\left[(\boldsymbol{k}_\perp - x\boldsymbol{p}_\perp + \boldsymbol{q}_\perp)^2 + \mu^2(x)\right]} \times \left\{ \frac{2\pi i}{\bar{x}} \delta(\boldsymbol{q}_\perp^2 + 2\boldsymbol{k}_\perp\cdot\boldsymbol{q}_\perp) + \frac{1}{(\boldsymbol{k}_\perp - x\boldsymbol{p}_\perp + x\boldsymbol{q}_\perp)^2 + x\bar{x}(\boldsymbol{q}_\perp^2 + 2m_\pi\nu) + \mu^2(x)} + \frac{1}{(\boldsymbol{k}_\perp - x\boldsymbol{p}_\perp + \bar{x}\boldsymbol{q}_\perp)^2 + x\bar{x}(\boldsymbol{q}_\perp^2 - 2m_\pi\nu) + \mu^2(x) - i\epsilon} \right\}. \tag{7.42d}$$

Here $\mu^2(x) \equiv m^2 - x\bar{x}m_\pi^2$. Note that the Eqs. (7.42) are valid only for the "+" and "⊥" components which are free of endpoint singularities. For the Compton tensor involving "−" components, the result of the contour integration over the infinitely large semicircle should be added [455]. It is worth mentioning that the symmetry properties of the amplitudes were used in the derivation of Eqs. (7.42), i.e. the top and bottom rows of the diagrams shown in Fig. 7.10 yield the same contribution for the Compton amplitude on a neutral pion target.

By calculating the ++ and yy Compton tensor components of Eqs. (7.42) allows to extract the invariant amplitudes T_1 and T_2 according to Eqs. (7.41a) and (7.41e) respectively. An explicit

calculation of the low-energy series terms of T_1 and T_2 is in full agreement with the low-energy theorems (7.19a) and (7.19b) respectively, yielding the polarizability results:

$$\alpha_{E1} = C_q^{\pi^0} \frac{\alpha_{\rm em} g^2}{48\pi^2 m_\pi^5} \frac{\zeta^2}{(1-\zeta^2)^2} \left(-\left(3 - 10\zeta^2 + 4\zeta^4\right) + \left(3 - 4\zeta^2 + 4\zeta^4\right) \frac{\arcsin\zeta}{\zeta\sqrt{1-\zeta^2}} \right), \tag{7.43a}$$

$$\beta_{M1} = -C_q^{\pi^0} \frac{\alpha_{\rm em} g^2}{12\pi^2 m_\pi^5} \frac{\zeta^4}{(1-\zeta^2)} \left(1 + \frac{\arcsin\zeta}{\zeta\sqrt{1-\zeta^2}} \right), \tag{7.43b}$$

with dimensionless ratio $\zeta = m_\pi/(2m)$. These results agree to the Feynman diagram calculation obtained in time-ordered perturbation theory. It can be shown as well that in the considered model these polarizabilities can be obtained from the Baldin and Bernabéu-Tarrach sum rules. The corresponding cross sections for $\gamma\pi^0 \to q\bar{q}$ scattering at tree-level, which is shown in Fig. 7.11, are calculated in Appendix 7.C.

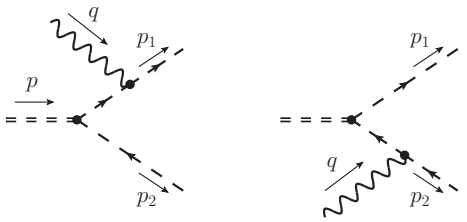

Fig. 7.11 The (scalar) quark-antiquark photoproduction on a neutral pion.

We show the results for the neutral pion polarizabilities in the covariant model with scalar quarks in Fig. 7.12 as function of the mass ratio $m_\pi/2m$ under the assumption that we fix the normalization constant g in Eq. (7.43) considering the probability of valence quark state in the pion to be $P_{q\bar{q}} = 1$,

$$P_{q\bar{q}} = \int_0^1 dx \int \frac{d^2\boldsymbol{\kappa}_\perp}{16\pi^3} |\Psi_\pi(x, \boldsymbol{\kappa}_\perp)|^2 = 1. \tag{7.44}$$

Hence, the coupling constant will be given by

$$g = \frac{4\pi m}{\sqrt{N(\zeta)}}, \quad N(\zeta) = \frac{1}{4\zeta^2} \left[\frac{\arcsin\zeta}{\zeta\sqrt{1-\zeta^2}} - 1 \right], \quad \zeta = \frac{m_\pi}{2m} < 1. \tag{7.45}$$

We notice from Fig. 7.12 that for all values of $m_\pi/2m$ the electric polarizability of the valence quark contribution is positive, while the magnetic polarizability is negative. The small positive value of $\alpha_{E1} + \beta_{M1}$ results from a strong cancellation between both individual components.

7.2.2.2 Calculation using non-perturbative valence quark light-front wave functions

We are now in a position to generalize the result for the forward Compton amplitudes obtained in the covariant model and express it in terms of a general non-perturbative LFWF. Using the identification of Eq. (7.37) for the LFWF, the forward Compton tensor, corresponding to the diagrams of Fig. 7.13,

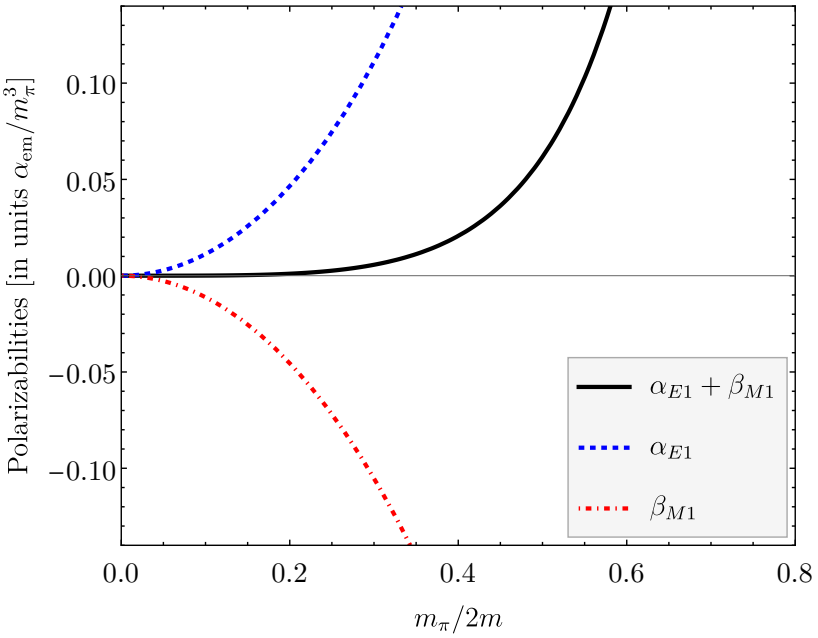

Fig. 7.12 The behavior of electromagnetic polarizabilities calculated using the covariant model depending on the pion over constituent quark mass ratio is shown. The electric α_{E1} (blue dashed line) and magnetic polarizabilities β_{M1} (red dash-dotted line) as well as their sum (black solid line) are displayed.

is given by:

$$T^{\mu\nu}_{\rm seagull} = 2g^{\mu\nu}C_q^{\pi^0}\frac{\alpha_{\rm em}}{4\pi^2 m_\pi}\int_0^1\frac{dx}{x}\int d^2\boldsymbol{\kappa}_\perp|\Psi_\pi(x,\boldsymbol{\kappa}_\perp)|^2, \tag{7.46a}$$

$$T^{\mu\nu}_{\rm direct} = C_q^{\pi^0}\frac{\alpha_{\rm em}}{8\pi^2 m_\pi}\int_0^1 dx\int d^2\boldsymbol{\kappa}_\perp|\Psi_\pi(x,\boldsymbol{\kappa}_\perp)|^2 \times\left\{\frac{\bar{x}\,(2k+q)^\mu(2k+q)^\nu\big|_{\boldsymbol{k}_\perp=\boldsymbol{\kappa}_\perp+x\boldsymbol{p}_\perp}}{x\left[\boldsymbol{\kappa}_\perp^2+2\bar{x}\boldsymbol{\kappa}_\perp\cdot\boldsymbol{q}_\perp+\bar{x}Q^2-2x\bar{x}m_\pi\nu+\mu^2(x)-i\epsilon\right]}+\Big[k\to p-k\Big]\right\}, \tag{7.46b}$$

$$T^{\mu\nu}_{\rm crossed} = C_q^{\pi^0}\frac{\alpha_{\rm em}}{8\pi^2 m_\pi}\int_0^1 dx\int d^2\boldsymbol{\kappa}_\perp|\Psi_\pi(x,\boldsymbol{\kappa}_\perp)|^2 \times\left\{\frac{\bar{x}\,(2k-q)^\mu(2k-q)^\nu\big|_{\boldsymbol{k}_\perp=\boldsymbol{\kappa}_\perp+x\boldsymbol{p}_\perp}}{x\left[\boldsymbol{\kappa}_\perp^2-2\bar{x}\boldsymbol{\kappa}_\perp\cdot\boldsymbol{q}_\perp+\bar{x}Q^2+2x\bar{x}m_\pi\nu+\mu^2(x)\right]}+\Big[k\to p-k\Big]\right\}, \tag{7.46c}$$

$$T^{\mu\nu}_{\rm cat\text{-}ears} = C_q^{\pi^0}\frac{\alpha_{\rm em}}{8\pi^2 m_\pi}\int_0^1 dx\int d^2\boldsymbol{\kappa}_\perp\Psi_\pi^*\left(x,\boldsymbol{\kappa}_\perp+\frac{\boldsymbol{q}_\perp}{2}\right)\Psi_\pi\left(x,\boldsymbol{\kappa}_\perp-\frac{\boldsymbol{q}_\perp}{2}\right) \times(2k+q)^\mu(2(k-p)+q)^\nu\big|_{\boldsymbol{k}_\perp=\boldsymbol{\kappa}_\perp+x\boldsymbol{p}_\perp-\boldsymbol{q}_\perp/2} \times\left\{\frac{2\pi i}{\bar{x}}\delta\left(2\boldsymbol{q}_\perp\cdot(\boldsymbol{\kappa}_\perp+x\boldsymbol{p}_\perp)\right)\right.$$

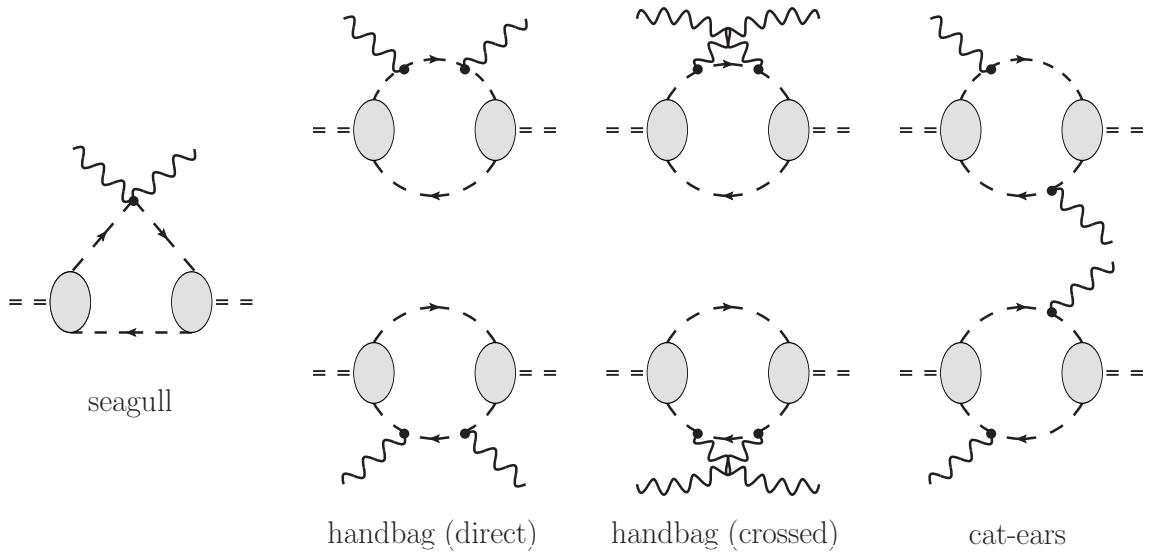

Fig. 7.13 Valence scalar quark contribution to the Compton scattering on the neutral pion with the non-perturbative pion LFWF shown as a gray blob: seagull, direct and crossed handbag, and cat-ears diagrams.

$$+\frac{1}{\boldsymbol{\kappa}_\perp^2-(\bar{x}-x)\boldsymbol{\kappa}_\perp\cdot\boldsymbol{q}_\perp+Q^2/4+2x\bar{x}m_\pi\nu+\mu^2(x)} \\ +\frac{1}{\boldsymbol{\kappa}_\perp^2+(\bar{x}-x)\boldsymbol{\kappa}_\perp\cdot\boldsymbol{q}_\perp+Q^2/4-2x\bar{x}m_\pi\nu+\mu^2(x)-i\epsilon}\Bigg\}+\Big[q\to-q\Big], \quad (7.46d)$$

where we introduced the quark relative transverse momentum $\boldsymbol{\kappa}_\perp \equiv \boldsymbol{k}_\perp - x\boldsymbol{p}_\perp$ in the handbag diagram, and $\boldsymbol{\kappa}_\perp \mp \boldsymbol{q}_\perp/2 \equiv \boldsymbol{k}_\perp - x\boldsymbol{p}_\perp$ in the direct ($-$ sign) and crossed ($+$ sign) cat ears diagrams respectively.

The essential subtlety, which immediately arises as soon as one moves from the covariant Feynman diagram calculation to the nonperturbative calculation using the LFWF identification of Eq. (7.37), is the violation of gauge invariance. It is clearly manifested in the amplitude T_1, calculated from the yy component of the Compton tensor, as a violation of the low-energy theorem. The reason of such a violation is not surprising as for a general momentum dependence of the vertex function Γ entering Eq. (7.33), which is the case for a general non-perturbative LFWF, one also needs terms where the photon couples to the vertex in order to preserve gauge invariance. In the covariant calculation above, which approximates the vertex function by a constant contact term, such vertex correction terms are absent. A straightforward way to obtain a gauge invariant result also in the case of a general non-perturbative LFWF is to exclude the gauge invariance-violating pieces from the Compton amplitudes, through the procedure discussed next.

In general, a Lorentz-invariant forward Compton tensor $\widetilde{T}^{\mu\nu}$ can be written as

$$\widetilde{T}^{\mu\nu}(p,q) = T^{\mu\nu}(p,q) + \mathcal{T}^{\mu\nu}(p,q), \quad (7.47)$$

where $T^{\mu\nu}$ is the gauge-invariant part given by Eq. (2.79), and $\mathcal{T}^{\mu\nu}$ is the gauge invariance-violating part, which for a spin-0 target can be parametrized introducing two extra scalar amplitudes T_3 and T_4:

$$\mathcal{T}^{\mu\nu}(p,q) = g^{\mu\nu}T_3(\nu,Q^2) + \frac{p^\mu p^\nu}{m_\pi^2}T_4(\nu,Q^2). \tag{7.48}$$

For the "+" or "$\perp$" components of $\widetilde{T}^{\mu\nu}$, which are free of endpoint singularities, the expressions read

$$\widetilde{T}^{++} = \frac{(p^+)^2}{m_\pi^2}(T_2+T_4), \tag{7.49a}$$

$$\widetilde{T}^{+x} = -\frac{p^+\nu}{m_\pi Q}T_4, \tag{7.49b}$$

$$\widetilde{T}^{xx} = -T_3 + \frac{\nu^2}{Q^2}T_4, \tag{7.49c}$$

$$\widetilde{T}^{yy} = T_1 - T_3. \tag{7.49d}$$

Therefore the gauge-invariant amplitudes T_1 and T_2 are given by

$$T_1 = \widetilde{T}^{yy} - \widetilde{T}^{xx} - \widetilde{T}^{+x}\frac{m_\pi\nu}{p^+Q}, \quad T_2 = \frac{m_\pi^2}{(p^+)^2}\left(\widetilde{T}^{++} + \frac{p^+Q}{m_\pi\nu}\widetilde{T}^{+x}\right). \tag{7.50}$$

Using these definitions, one can also construct the gauge-invariant longitudinal amplitude T_L of Eq. (2.128) as:

$$T_L = \left(1+\frac{\nu^2}{Q^2}\right)T_2 - T_1 = \frac{m_\pi^2}{(p^+)^2}\left(1+\frac{\nu^2}{Q^2}\right)\widetilde{T}^{++} + \frac{m_\pi}{p^+}\left(\frac{Q}{\nu}+2\frac{\nu}{Q}\right)\widetilde{T}^{+x} + \widetilde{T}^{xx} - \widetilde{T}^{yy}. \tag{7.51}$$

We note from Eqs. (7.46) that the quadratic LFWF combination entering the forward Compton amplitudes is given by

$$\Psi_\pi^*(x,\boldsymbol{\kappa}_\perp+\boldsymbol{\Delta}_\perp)\Psi_\pi(x,\boldsymbol{\kappa}_\perp-\boldsymbol{\Delta}_\perp), \tag{7.52}$$

with $\boldsymbol{\Delta}_\perp = 0$ for the seagull and handbag diagrams, and $\boldsymbol{\Delta}_\perp = \boldsymbol{q}_\perp/2$ for the cat-ears diagrams. Furthermore, for a spin-0 system as the pion, the LFWF $\Psi(x,\boldsymbol{\kappa}_\perp)$ can only have a dependence on $\boldsymbol{\kappa}_\perp^2$. We therefore denote the LFWF in the following explicitly as $\Psi_\pi(x,\boldsymbol{\kappa}_\perp^2)$. As we are interested in a low-energy expansion of the forward Compton amplitudes, we need the Q^2 expansion of the quadratic wave function combination entering the amplitude for the cat-ears diagrams in Eqs. (7.46). It can be expressed as:

$$\begin{aligned}&\Psi_\pi\left(x,(\boldsymbol{\kappa}_\perp-\boldsymbol{q}_\perp/2)^2\right)\Psi_\pi^*\left(x,(\boldsymbol{\kappa}_\perp+\boldsymbol{q}_\perp/2)^2\right) = |\Psi_\pi(x,\boldsymbol{\kappa}_\perp^2)|^2\\ &+\frac{Q^2}{2}\left[\frac{1}{2}\partial_{\boldsymbol{\kappa}_\perp^2}|\Psi(x,\boldsymbol{\kappa}_\perp^2)|^2 + \boldsymbol{\kappa}_\perp^2\cos^2\phi\,\mathcal{D}_{Q^2}|\Psi_\pi(x,\boldsymbol{\kappa}_\perp^2)|^2\right] + O(Q^4),\end{aligned} \tag{7.53}$$

with $\cos\phi = \hat{\boldsymbol{k}}_\perp \cdot \hat{\boldsymbol{q}}_\perp$, where $\partial_{\boldsymbol{\kappa}_\perp^2}$ is a partial derivative with respect to $\boldsymbol{\kappa}_\perp^2$, and where the derivative $\mathcal{D}_{Q^2}$ is defined as:

$$\mathcal{D}_{Q^2}|\Psi_\pi(x,\boldsymbol{\kappa}_\perp^2)|^2 \equiv 2\,\mathrm{Re}\left[\Psi_\pi^*(x,\boldsymbol{\kappa}_\perp^2)\partial^2_{\boldsymbol{\kappa}_\perp^2}\Psi_\pi(x,\boldsymbol{\kappa}_\perp^2)\right] - 2\left|\partial_{\boldsymbol{\kappa}_\perp^2}\Psi_\pi(x,\boldsymbol{\kappa}_\perp^2)\right|^2. \tag{7.54}$$

We note that for a class of LFWF models, which the gaussian models belong to, the wave function product of Eq. (7.52) exhibits an azimuthal symmetry, and only depends upon $\boldsymbol{\kappa}_\perp^2$ and $\boldsymbol{\Delta}_\perp^2$. For such models, the $\cos^2\phi$ dependent term in Eq. (7.53), proportional to $\mathcal{D}_{Q^2}|\Psi_\pi(x,\boldsymbol{\kappa}_\perp^2)|^2$, is absent.

We next perform the low-energy expansion of the Compton tensor expressions of Eqs. (7.46) corresponding with the seagull, handbag, and cat-ears diagrams. Keeping the terms proportional to Q^2 and ν^2 in the expansion, we can perform the angular integration in Eqs. (7.46) analytically. The explicit expressions for the forward Compton tensor components of Eqs. (7.49), as well as for the non-Born invariant amplitudes $\overline{T}_1$, $\overline{T}_2$, and $\overline{T}_L$ are given in Appendix 7.D. The low-energy expansion of $\overline{T}_1$, $\overline{T}_2$, and $\overline{T}_L$ allows to extract the dipole polarizabilities, using Eqs. (7.19a), (7.19b), and (7.19c). For the gauge-invariance corrected amplitudes, we verified explicitly that the ν^2-dependent term in $\overline{T}_1$ and the Q^2-dependent term in $\overline{T}_2$ yield the same polarizability combination $\alpha_{E1}+\beta_{M1}$, as required by the low-energy expansion, see Eqs. (7.123). Furthermore, the Q^2-dependent term in $\overline{T}_1$ yields β_{M1}. In this way, we extract the polarizability expressions for the neutral pion as:

$$\alpha_{E1}+\beta_{M1} = C_q^{\pi^0}\alpha_{\mathrm{em}} m_\pi \int_0^1 dx\, 4x\bar{x}\int_0^\infty \frac{d\boldsymbol{\kappa}_\perp^2}{(4\pi)^2}\,\frac{|\Psi_\pi(x,\boldsymbol{\kappa}_\perp^2)|^2}{\left[\mu^2(x)+\boldsymbol{\kappa}_\perp^2\right]^3}\left[\mu^2(x)-\boldsymbol{\kappa}_\perp^2\right], \tag{7.55a}$$

$$\begin{aligned}\beta_{M1} = -C_q^{\pi^0}\frac{\alpha_{\mathrm{em}}}{m_\pi}\int_0^1 dx\int_0^\infty \frac{d\boldsymbol{\kappa}_\perp^2}{(4\pi)^2}\Bigg\{&\frac{|\Psi_\pi(x,\boldsymbol{\kappa}_\perp^2)|^2}{\left[\mu^2(x)+\boldsymbol{\kappa}_\perp^2\right]^3}\left(\frac{(1-4x\bar{x})}{x\bar{x}}\left[\mu^2(x)-\boldsymbol{\kappa}_\perp^2\right]^2+2\mu^4(x)\right)\\ &+\frac{\mathcal{D}_{Q^2}|\Psi_\pi(x,\boldsymbol{\kappa}_\perp^2)|^2}{\left[\mu^2(x)+\boldsymbol{\kappa}_\perp^2\right]}\boldsymbol{\kappa}_\perp^4\Bigg\}.\end{aligned} \tag{7.55b}$$

Note that the last term in Eq. (7.55b), which contains $\mathcal{D}_{Q^2}$, is due to the cat-ears diagrams for the case of a LFWF product in Eq. (7.53) which has an explicit dependence on $\cos^2\phi$.

As in the covariant model, the Eqs. (7.55) can be exactly reproduced via Baldin (2.124) and BT (2.133) sum rules. The corresponding cross sections can be obtained by following the steps of calculation in the covariant model (cf. Appendix 7.C). The nonperturbative pion wave functions can be associated to the the perturbative ones, which appear from the denominators of the tree-level amplitude (7.113) as follows:

$$\frac{g}{(p_1-q)^2-m^2+i\epsilon} = -\frac{g\bar{x}}{\left[\boldsymbol{\kappa}_\perp^2+\mu^2(x)\right]} \to \sqrt{\frac{\bar{x}}{x}}\Psi_\pi(x,\boldsymbol{\kappa}_\perp), \tag{7.56a}$$

$$\frac{g}{(p_2-q)^2-m^2+i\epsilon} = -\frac{gx}{\left[(\boldsymbol{\kappa}_\perp+\boldsymbol{q}_\perp)^2+\mu^2(x)\right]} \to \sqrt{\frac{x}{\bar{x}}}\Psi_\pi(x,\boldsymbol{\kappa}_\perp+\boldsymbol{q}_\perp), \tag{7.56b}$$

where the relative momentum is introduced as

$$\boldsymbol{\kappa}_\perp = (\boldsymbol{p}_{1\perp} - \boldsymbol{q}_\perp) - x\boldsymbol{p}_\perp = (\boldsymbol{p}_\perp - \boldsymbol{p}_{2\perp}) - x\boldsymbol{p}_\perp. \tag{7.57}$$

7.2.2.3 Results and discussion

In order to estimate pion polarizabilities through the Eqs. (7.55), we applied the LFWF model taken from Refs. [457, 458]. This LFWF belongs to a class of gaussian models, in which the LFWF can be parameterized as

$$\Psi_\pi(x, \boldsymbol{\kappa}_\perp) = \frac{4\pi}{\sqrt{\sigma}} f(x) e^{-\frac{\boldsymbol{\kappa}_\perp^2}{2\sigma x\bar{x}}}. \tag{7.58}$$

Here σ is a parameter, proportional to the average squared transverse momentum of the valence quarks in the pion, and $f(x)$ is a shape function, which for the considered model is given by the constant

$$f(x) = \sqrt{\frac{3}{2}}. \tag{7.59}$$

Using Eq. (7.28), this leads to the pion distribution amplitude,

$$\phi_\pi(x) = \frac{\sqrt{2\sigma}}{4\pi} \frac{6x\bar{x}}{2\sqrt{3}}. \tag{7.60}$$

The LFWF normalization of Eq. (7.26) is ensured by the choice $\sigma = 8\pi^2 f_\pi^2 \simeq 0.674$ GeV^2, which leads to the identification with the asymptotic pion DA of Eq. (7.29). In this model, the valence quark probability is given by

$$P_{q\bar{q}} = \frac{1}{4}. \tag{7.61}$$

Substituting this model into Eqs. (7.55), we obtain the results for polarizabilities shown in Fig. 7.14. The obtained result for electric polarizability is positive in the full range of the model parameters. In particular, at $m_\pi/2m = 0.2$, which is close to the value typically chosen in light-front quark model calculaitons of the pion vector form factor [459], the polarizabilities amount

$$\alpha_{E1}^{\pi^0} = 3.24 \times 10^{-4}\,\mathrm{fm}^3, \quad \beta_{M1}^{\pi^0} = -3.18 \times 10^{-4}\,\mathrm{fm}^3, \quad \alpha_{E1}^{\pi^0} + \beta_{M1}^{\pi^0} = 0.05 \times 10^{-4}\,\mathrm{fm}^3. \tag{7.62}$$

Since the calculations were carried out in the model with scalar quarks, the obtained results could serve as a qualitative estimate. Moreover, the valence quark probability (7.61), pertinent to the considered model, suggests that the non-valence contribution might be significant. The latter requires much more involved modeling, being less constrained from the measurable quantities. Thus, the solid conclusions, which can be made at this stage, are

- In the light-front quark model with scalar quarks, both Baldin and BT sum rules work exactly for the valence quark contribution. We expect this to be also true in the model with spin-1/2 quarks.

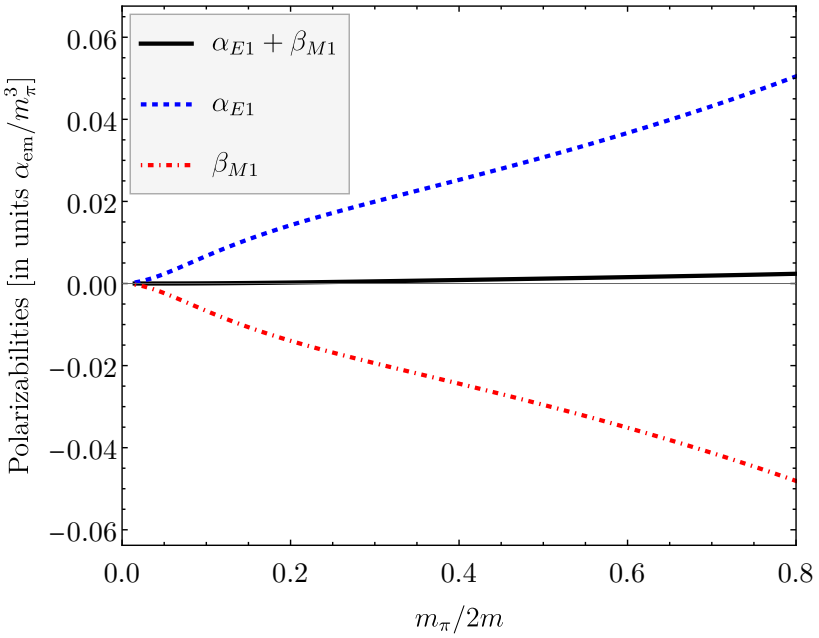

Fig. 7.14 Neutral pion electric and magnetic polarizability as well as their sum, calculated using gaussian model from Refs. [457, 458] for the valence quark LFWF.

- The obtained positive contribution into $\alpha_{E1}^{\pi^0}$, which contradicts with χPT results (7.20) and (7.23), could potentially be explained by large negative counterpart stemming from disconnected quark contributions shown on Fig. 7.15. In lattice QCD studies, such a part arises naturally, and always should be taken into account to obtain the full result.

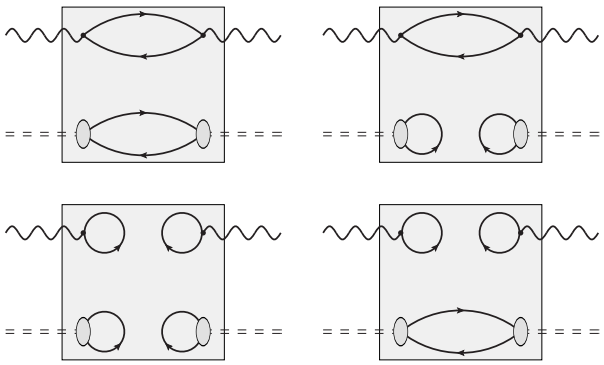

Fig. 7.15 Disconnected quark contributions from QCD to the Compton scattering on the neutral pion. The quark lines interact nonperturbatively via the gluon field.

7.3 Conclusion

We conclude that the BT sum rule for the nucleon electric polarizability is at the same level of validity as the commonly used Baldin sum rule, despite an appreciably worse convergence. Previously, the arguments leading to the dismissal of this sum rule were based on the failure of the perturbative QED [402] and χPT [413] tests, as well as the heuristic arguments of Regge phenomenology [413, 331].

We have established at least one simple example where the BT sum rule passes the perturbative test – the $\pi^+ n$ channel at leading-order χPT. In other cases, most notably the leading-order QED, the sum rule holds up to a constant yielded by an unphysical behavior of the VVCS amplitude at infinite energy. Thus the aspect of perturbative verifications is well understood.

The projected Regge behavior of the longitudinal photoabsorption cross section σ_L would invalidate the entire hypothesis of the unsubtracted dispersion relation for the longitudinal VVCS amplitude T_L. However, at the present there are no reliable experimental data corroborating the equivalent Regge behavior for transverse and longitudinal photons, $\sigma_L \sim \sigma_T$. In fact, the naïve parton model yields quite a different behavior, encompassed in the Callan-Gross relation which shows a significant suppression of σ_L/σ_T with energy. The parton model thus verifies the unsubtracted dispersion relation for the longitudinal amplitude, while confirming the need for a subtraction in the transverse amplitude T_1.

Another implication of the unsubtracted dispersion relation for T_L is a sum rule for the subtraction function (7.8), which may allow for a fully data-driven evaluation of the proton polarizability contribution to the Lamb shift of (muonic-)hydrogen. To carry out such an evaluation, we need high-quality and precision parametrization of $\sigma_L(\nu, Q^2)$ for the proton [equivalently, the longitudinal structure function $f_L(x, Q^2)$]. High-quality parametrizations of σ_L are needed as well to determine the proton electric polarizability from the BT sum rule itself. We expect that the inclusion of the two-pion production channel, in addition to the single-pion production parametrized by MAID, will be sufficient to saturate the sum rule to a large extent.

While the negative sign of electric polarizability of the neutral pion, as robustly predicted by χPT, immediately invalidates the BT sum rule, this result looks rather aberrant. Conversely, the light-front calculation of valence (scalar) quark contribution suggest the positive sign of this observable, thereby preserving the validity of the BT sum rule. Consequently, a definitive resolution to this discrepancy might be drawn only after a precise lattice QCD calculation of this quantitiy is executed.

Appendices

7.A Neutral pion polarizabilities at $O(p^4)$ in meson χPT

Let us consider the chiral Lagrangian at $O(p^4)$. Follwing [406, 405], it is written as

$$\mathcal{L} = \frac{f_\pi^2}{4}\mathrm{tr}\left(D_\mu \Sigma D^\mu \Sigma^\dagger\right) + \frac{f_\pi^2}{4} m^2 \mathrm{tr}\left(\Sigma + \Sigma^\dagger\right), \tag{7.63}$$

where Σ is the meson matrix, which is the function of $\hat{\pi} \equiv \vec{\pi}\cdot\vec{\tau}$. The covariand derivative of the meson matrix Σ is defined as follows

$$D_\mu \Sigma = \partial_\mu \Sigma + ieA_\mu \left[Q, \Sigma\right], \tag{7.64}$$

$$D_\mu \Sigma^\dagger = \partial_\mu \Sigma^\dagger + ieA_\mu \left[Q, \Sigma^\dagger\right]. \tag{7.65}$$

with the charge matrix Q, defined as

$$Q = \begin{pmatrix} \frac{2}{3} & 0 \\ 0 & -\frac{1}{3} \end{pmatrix}. \tag{7.66}$$

The commutator of the charge matrix Q and the pion fields $\hat{\pi}$ reads

$$[Q, \hat{\pi}] = \begin{pmatrix} 0 & \sqrt{2}\pi^+ \\ -\sqrt{2}\pi^- & 0 \end{pmatrix}. \tag{7.67}$$

Writing the covariant derivatives explicitly in Eq. (7.63), we arrive at the following expression for the χPT Lagrangian:

$$\begin{aligned} \mathcal{L} = \frac{f_\pi^2}{4}\Big\{ & \partial_\mu \Sigma \partial^\mu \Sigma^\dagger + ieA_\mu \left(\partial^\mu \Sigma \left[Q, \Sigma^\dagger\right] + \left[Q, \Sigma\right]\partial^\mu \Sigma^\dagger\right) \\ & - e^2 A_\mu A^\mu \left[Q, \Sigma\right]\left[Q, \Sigma^\dagger\right] + m^2 \mathrm{tr}\left(\Sigma + \Sigma^\dagger\right)\Big\}. \end{aligned} \tag{7.68}$$

Let us now consider the meson matrix in general representation up to $O(1/f_\pi^4)$

$$\Sigma = 1 + ia_1 \frac{\hat{\pi}}{f_\pi} - a_2 \frac{\pi^2}{2! f_\pi^2} - ia_3 \frac{\pi^2 \hat{\pi}}{3! f_\pi^3} + a_4 \frac{\pi^4}{4! f_\pi^4} + O\left(\frac{1}{f_\pi^5}\right). \tag{7.69}$$

Particularly, in the exponential representation, $\Sigma^{\mathrm{exp}} = \exp i\frac{\hat{\pi}}{f_\pi}$, all the a_i equal to one. Requiring the meson matrix to be unitary, i.e. $\Sigma\Sigma^\dagger = 1$, we can set up the following constraints on the coefficients a_i:

$$a_1^2 - a_2 = 0, \quad 3a_2^2 - 4a_1 a_3 + a_4 = 0. \tag{7.70}$$

Now we can expand the Lagrangian (7.68) up to $O(1/f_\pi^4)$ and derive the Feynman rules. For the first term in Eq. (7.68) we have

$$\begin{aligned}
&\frac{f_\pi^2}{4}\mathrm{tr}\partial_\mu\Sigma\partial^\mu\Sigma^\dagger \\
&= \frac{f_\pi^2}{4}\mathrm{tr}\left(ia_1\frac{\partial_\mu\hat{\pi}}{f_\pi} - a_2\frac{\partial_\mu(\pi^2)}{2!f_\pi^2} - ia_3\frac{\partial_\mu(\pi^2\hat{\pi})}{3!f_\pi^3}\right)\left(-ia_1\frac{\partial^\mu\hat{\pi}}{f_\pi} - a_2\frac{\partial^\mu(\pi^2)}{2!f_\pi^2} + ia_3\frac{\partial^\mu(\pi^2\hat{\pi})}{3!f_\pi^3}\right) \\
&= \frac{a_1^2}{2}\partial_\mu\hat{\pi}\partial^\mu\hat{\pi} + \frac{f_\pi^2}{2}\left(\frac{a_2^2}{4f_\pi^4}\partial_\mu(\pi^2)\partial^\mu(\pi^2) - \frac{a_1a_3}{3f_\pi^4}\partial_\mu\hat{\pi}\partial^\mu(\pi^2\hat{\pi})\right) \\
&= \frac{a_1^2}{2}\partial_\mu\hat{\pi}\partial^\mu\hat{\pi} + \frac{1}{2f_\pi^2}\left(a_2^2(\hat{\pi}\cdot\partial_\mu\hat{\pi})(\hat{\pi}\cdot\partial^\mu\hat{\pi}) - \frac{a_1a_3}{3}\left(2(\hat{\pi}\cdot\partial_\mu\hat{\pi})(\hat{\pi}\cdot\partial^\mu\hat{\pi}) + \pi^2\partial_\mu\hat{\pi}\partial^\mu\hat{\pi}\right)\right). \qquad (7.71)
\end{aligned}$$

Requiring the coefficient near the kinetic term $\partial_\mu\hat{\pi}\partial^\mu\hat{\pi}$ to be equal to $1/2$, we immediately obtain an additional constraint on a_1. Together with Eq. (7.70), this constraint fixes the possible values of the coefficients $a_1 ... a_4$ to be

$$a_1 = a_2 = 1, \quad a_4 - 4a_3 + 3 = 0. \qquad (7.72)$$

Substituting these relations in Eq. (7.71) gives the following result for the first term of the Lagrangian (7.68),

$$\frac{f_\pi^2}{4}\mathrm{tr}\partial_\mu\Sigma\partial^\mu\Sigma^\dagger = \frac{1}{2}\partial_\mu\hat{\pi}\partial^\mu\hat{\pi} + \frac{1}{6f_\pi^2}\left((3-2a_3)(\hat{\pi}\cdot\partial_\mu\hat{\pi})(\hat{\pi}\cdot\partial^\mu\hat{\pi}) - a_3\hat{\pi}^2\partial_\mu\hat{\pi}\partial^\mu\hat{\pi}\right), \qquad (7.73)$$

where the second term in r.h.s is responsible for the four-pion interaction. For the $\pi^+\pi^-\pi^0\pi^0$ vertex, this term becomes

$$\begin{aligned}
&\frac{1}{6f_\pi^2}\left((3-2a_3)(\hat{\pi}\cdot\partial_\mu\hat{\pi})(\hat{\pi}\cdot\partial^\mu\hat{\pi}) - a_3\pi^2\partial_\mu\hat{\pi}\partial^\mu\hat{\pi}\right) \\
&\to \frac{1}{3f_\pi^2}\left[(3-2a_3)(\pi^-\partial_\mu\pi^+ + \pi^+\partial_\mu\pi^-)\pi^0\partial^\mu\pi^0 - a_3\left(\pi^+\pi^-\partial_\mu\pi^0\partial^\mu\pi^0 + (\pi^0)^2\partial_\mu\pi^+\partial^\mu\pi^-\right)\right]. \qquad (7.74)
\end{aligned}$$

Taking into account the mass term in Eq. (7.68), it results in the following Feynman rule:

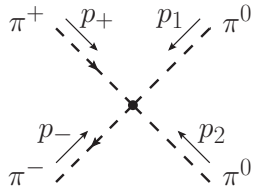

$$= \frac{i}{3f_\pi^2}\left[2a_3(p_1\cdot p_2 + p_+\cdot p_-) - (3-2a_3)(p_+ + p_-)\cdot(p_1+p_2) + a_4m^2\right]. \qquad (7.75)$$

From the second and third terms of the Lagrangian (7.68), one can read out the four-pion interaction vertices with an electromagnetic field insertions. Particularly, the second term in (7.68) yields a

four-pion vertex with one electromagnetic field insertion,

$$\frac{f_\pi^2}{4} ieA_\mu \mathrm{tr}\left(\partial^\mu \Sigma \left[Q, \Sigma^\dagger\right] + [Q, \Sigma]\, \partial^\mu \Sigma^\dagger\right)$$
$$\to -a_3 \frac{f_\pi^2}{4} \frac{ieA_\mu}{6 f_\pi^4} 2(\pi^0)^2 \mathrm{tr}\left\{\partial^\mu \hat{\pi}, [Q, \hat{\pi}]\right\} = a_3 \frac{ieA_\mu}{3 f_\pi^2} (\pi^0)^2 \left(\pi^- \partial^\mu \pi^+ - \pi^+ \partial^\mu \pi^-\right), \tag{7.76}$$

with the corresponding Feynman rule

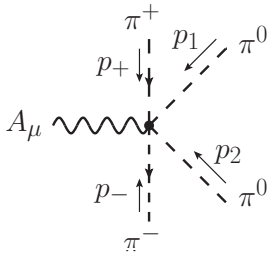

$$= a_3 \frac{2ie}{3 f_\pi^2} (p_+ - p_-)_\mu. \tag{7.77}$$

The third term in (7.68) results in a four-pion interaction with two electromagnetic field insertions,

$$-\frac{f_\pi^2}{4} e^2 A_\mu A^\mu \mathrm{tr}\left[Q, \Sigma\right]\left[Q, \Sigma^\dagger\right] \to -a_1 a_3 \frac{e^2}{3 f_\pi^2} A_\mu A^\mu (\pi^0)^2 \pi^+ \pi^-, \tag{7.78}$$

which yields the following Feynman rule:

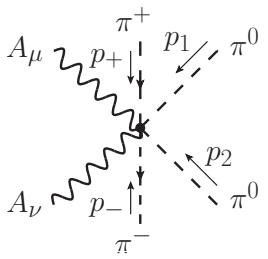

$$= -i \frac{4 a_3 e^2}{3 f_\pi^2} g_{\mu\nu}. \tag{7.79}$$

Now we want to consider the case of different charged and neutral pion masses caused by electromagnetic interactions. This can be taken into account by adding to the Lagrangian (7.63) the following isospin-breaking term:

$$\Delta\mathcal{L} = \Delta m_{\pi^\pm}^2 \frac{f_\pi^2}{2} \mathrm{tr}\left(Q \Sigma Q \Sigma^\dagger\right)$$
$$= \Delta m_{\pi^\pm}^2 \frac{f_\pi^2}{2} \left\{ \mathrm{tr} Q^2 + \frac{1}{f_\pi^2}\left(\mathrm{tr} Q \hat{\pi} Q \hat{\pi} - \pi^2 \mathrm{tr} Q^2\right) + \frac{1}{f_\pi^4}\left(\frac{a_4}{12}\pi^4 \mathrm{tr} Q^2 - \frac{a_3}{3}\pi^2 \mathrm{tr} Q \hat{\pi} Q \hat{\pi} + \frac{1}{4}\pi^4 \mathrm{tr} Q^2\right)\right\}. \tag{7.80}$$

where $\Delta m^2_{\pi^\pm} = m^2_{\pi^\pm} - m^2_{\pi^0} > 0$ is the differece of the squared masses of the charged and neutral pions. Calculating the traces and omitting the constant term, we obtain

$$\Delta\mathcal{L} = -\Delta m^2_{\pi^\pm}\pi^+\pi^- + a_3\frac{\Delta m^2_{\pi^\pm}}{3f_\pi^2}(\pi^0)^2\pi^+\pi^-. \tag{7.81}$$

Here the first term in r.h.s belongs to the mass term of the charged pion, while the second term modifies the four-pion interaction. Hence, the Feynman rule (7.75) should be modified by adding a term $2a_3\Delta m^2_{\pi^\pm}$ in the square brackets and treating mass m as a mass of the neutral pion.

Calculation of the diagrams shown in Fig. 7.7 using Feynman rules (7.77), (7.79) and modified (7.75) yields the representation-independent result for the Compton tensor:

$$\begin{aligned} T_{\mu\nu} &= \frac{e^2 m_{\pi^0}}{16\pi^2 f_\pi^2}\left(g_{\mu\nu} + \frac{q_\mu q_\nu}{Q^2}\right)\left\{4 - 2\sqrt{1+\frac{4m^2_{\pi^\pm}}{Q^2}}\log\left[1+\frac{Q^2}{2m^2_{\pi^\pm}}\left(1+\sqrt{1+\frac{4m^2_{\pi^\pm}}{Q^2}}\right)\right]\right\} \\ &= \frac{e^2 m_{\pi^0}}{16\pi^2 f_\pi^2}\left(g_{\mu\nu} + \frac{q_\mu q_\nu}{Q^2}\right)\left\{-\frac{1}{3}\frac{Q^2}{m^2_{\pi^\pm}} + \frac{1}{30}\left(\frac{Q^2}{m^2_{\pi^\pm}}\right)^2\right\} + O\left(\left(\frac{Q^2}{m^2_{\pi^\pm}}\right)^3\right). \end{aligned} \tag{7.82}$$

Hence, the electric and magnetic dipole polarizabilities are given by

$$\alpha^{\pi^0}_{E1} = -\beta^{\pi^0}_{M1} = -\frac{\alpha_{\rm em} m_{\pi^0}}{96\pi^2 f_\pi^2 m^2_{\pi^\pm}}. \tag{7.83}$$

The obtained result exhibits the correct physical behavior as pion masses approach zero: it vanishes when the neutral pion mass becomes zero, while demonstrating a singular behavior as the charged pion mass approaches small values. In the SU(2)-symmetric point, when there is no mass splitting between charged and neutral pions, Eq. (7.83) exactly reproduces the well-known literature result [406, 405].

Since the χPT is valid at low energies, it is also instructive to ensure ourselves that the result (7.83) is primarily saturated by the low values of the loop momentum. For this purpose, let us impose a hard cut-off regularization on the Euclidean loop momentum while evaluating (7.83). The part of the one-loop Compton amplitude, which is sensitive to polarizabilities, is given by the following loop integral [3]:

$$I^{\mu\nu}(q,\Lambda) = 2\frac{e^2}{f_\pi^2}\int_\Lambda \frac{d^4l}{i(2\pi)^4}\frac{g^{\mu\nu}(l^2-m^2) - (2l+q)^\mu(2l+q)^\nu}{\left[(l+q)^2-m^2\right]^2(l^2-m^2)} = \left(g^{\mu\nu} - \frac{q^\mu q^\nu}{q^2}\right)f(q^2,\Lambda). \tag{7.84}$$

To avoid the discussion of the correct determination of the integral

$$\int_\Lambda \frac{d^4l}{(2\pi)^4}\frac{l^\mu l^\nu}{(l^2-m^2)^3} \tag{7.85}$$

[3] In this calculation we take the same mass m for all pions without loss of generality.

in the cut-off regularization scheme (see, e.g. [460]), we will focus on the second term that is proportional to $q^\mu q^\nu$. Employing the Feynman parameterization, we obtain

$$f(q^2,\Lambda) = \frac{e^2}{4\pi^2 f_\pi^2}\int_0^1 dx x\int_0^\Lambda l_E^3 dl_E \frac{2q^2(2x-1)^2}{\left[l_E^2+(m^2-q^2x(x-1))\right]^3}$$
$$= -\frac{\alpha_{\rm em}}{4\pi^2 f_\pi^2}\frac{Q^2}{3m^2}\frac{\Lambda^4}{(m^2+\Lambda^2)^2}+O(Q^4), \tag{7.86}$$

so that the polarizabilities are given by

$$\alpha_{E1}^{\pi^0}(\Lambda) = -\beta_{M1}^{\pi^0}(\Lambda) = -\frac{\alpha_{\rm em}}{96\pi^2 f_\pi^2 m}\frac{1}{\left(1+\frac{m^2}{\Lambda^2}\right)^2}. \tag{7.87}$$

We can conclude that the obtained result has a definite sign for all values of the hard cut-off Λ.

The alternative way is to impose a soft cut-off imposing the Pauli-Villars regularization with large mass M for each pion propagator,

$$\frac{1}{k^2-m^2} \to \frac{1}{k^2-m^2}-\frac{1}{k^2-M^2}. \tag{7.88}$$

This yields the following dependence of the polarizabilities on the cut-off parameter M:

$$\alpha_{\rm em} = -\lambda\frac{\alpha_{\rm em}}{96\pi^2 m^3}\left(1-\frac{m^2}{M^2}\right), \tag{7.89}$$

which also has a definite sign as long as $M > m$.

The obtained results with hard and soft cut-off demonstrate that the loop integral mainly saturates by low loop momenta, i.e. of order of the pion mass. Moreover, the cut-off dependence is monotonic and sign-definite at all values of the cut-off parameter.

7.B Neutral pion polarizabilities in ϕ^3-theory with massive charged scalar

Let us consider a theory with pions which couple to a charged scalar field $\phi^\pm$ with mass $M \gg m_\pi$:

$$\mathcal{L}_{\rm int} = g\pi^0\pi^+\phi^- + \text{h.c.}. \tag{7.90}$$

The scalar field in this theory can be thought as a "scalar version" of ρ-meson.

The forward Compton scattering on a neutral pion is then given by the one-loop diagram shown in Fig. 7.16 with all possible photon insertions. These diagrams have nonzero dispersive contribution, thus we can easily test the Baldin and BT sum rule in this model. The low-energy expansion of the

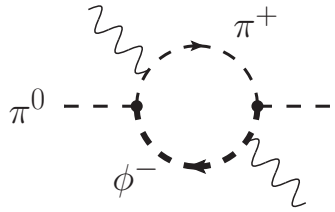

Fig. 7.16 Compton scattering on the neutral pion in ϕ^3-theory described by the interaction (7.90)

corresponding Compton amplitude yields the following result for $\alpha_{\mathrm{E1}}^{\pi^0}$:

$$\alpha_{\mathrm{E1}}^{\pi^0} = \frac{\alpha g^2}{48\pi^2 M^3 (M^2-4)^3}\left\{28M^3 - 11M^5 + M^7 + 4\sqrt{M^2-4}(M^2+8)\log\left[\frac{1}{2}\left(M+\sqrt{M^2-4}\right)\right]\right\} \tag{7.91}$$

$$= \frac{\alpha g^2}{48\pi^2 M^2} + O(M^{-4}), \tag{7.92}$$

where the pion mass is set to unity. The BT sum rule exactly reproduces this result, which can be shown by explicit integration of the corresponding L-polarized cross section

$$\sigma_L = \frac{\alpha_{\mathrm{em}} g^2}{16\nu^5 M^2}\left\{\sqrt{M^4+4\nu^2-4M^2(1+\nu)}\left(M^6+\nu^2-M^4(3+2\nu)+M^2(4+\nu(6+\nu))\right)\right.$$
$$\left. + 4M^2(M^2-\nu-2)(M^2+\nu)\operatorname{arccoth}\left[\frac{2\nu-M^2}{\sqrt{M^4+4\nu^2-4M^2(1+\nu)}}\right]\right\}. \tag{7.93}$$

Moreover, the obtained polarizability is positive-definite for all values of M. The sum of electric and magnetic polarizabilities can be found from unpolarized forward Compton amplitude with real photons. It reads

$$\alpha_{\mathrm{E1}} + \beta_{M1} = \frac{\alpha_{\mathrm{em}} g^2}{12\pi^2 M^3}\left\{-\frac{3M}{(M^2-4)^2} + 2\frac{(2+M^2)\log\left[\frac{1}{2}(M+\sqrt{M^2-4})\right]}{\left(M^2-4\right)^{\frac{5}{2}}}\right\}. \tag{7.94}$$

This result can be exactly reproduced via the Baldin sum rule, integrating the unpolarized cross section σ_T

$$\sigma_T(\nu) = \frac{\alpha g^2}{4\nu^3}\left\{-\sqrt{M^4+4\nu^2-4M^2(1+\nu)} + (M^2-2\nu)\operatorname{arccoth}\left[\frac{M^2-2\nu}{\sqrt{M^4+4\nu^2-4M^2(1+\nu)}}\right].\right\} \tag{7.95}$$

Thus, both Baldin and BT sum rules work exactly in the considered theory, providing the positive electric polarizability.

7.C Photoabsorption cross section with non-perturbative light-front wave function

In order to derive the formula for the photoabsorption cross section with the $q\bar{q}$-pair in the final state (see Fig. 7.11) in light-front formalism, let us firstly rewrite the two-particle phase space integral Π in light-cone coordinates,

$$\begin{aligned}
\Pi(p,q;p_1,p_2) &\equiv \int \frac{d^3\boldsymbol{p}_1}{(2\pi)^3 2E_{p_1}} \int \frac{d^3\boldsymbol{p}_2}{(2\pi)^3 2E_{p_2}} \delta^{(4)}\left(p+q-p_1-p_2\right) \\
&= \int \frac{dp_1^+ dp_1^- d\boldsymbol{p}_{1\perp}}{(2\pi)^3} \int \frac{dp_2^+ dp_2^- d\boldsymbol{p}_{2\perp}}{(2\pi)^3} \delta(p_1^2-m^2)\delta(p_2^2-m^2)(2\pi)^4\delta^{(4)}\left(p+q-p_1-p_2\right) \\
&= \frac{1}{(2\pi)^2} \int \frac{dp_1^+ d\boldsymbol{p}_{1\perp}}{2p_1^+} \int \frac{dp_2^+ d\boldsymbol{p}_{2\perp}}{2p_2^+} \delta^{(4)}\left(p+q-p_1-p_2\right) \\
&= \frac{1}{4\pi^2} \int \frac{dp_1^+ d\boldsymbol{p}_{1\perp}}{4p_1^+ p_2^+} \delta(p^- + q^- - p_1^- - p_2^-).
\end{aligned} \tag{7.96}$$

Given that the quarks in the final state are on-shell, we have

$$p_{1,2}^- = \frac{\boldsymbol{p}_{1,2\perp}^2 + m^2}{2p_{1,2}^+}, \tag{7.97}$$

so that the phase-space integral becomes

$$\Pi(p,q;p_1,p_2) = \frac{1}{4\pi^2} \int \frac{dp_1^+ d\boldsymbol{p}_{1\perp}}{4p_1^+ p_2^+} \delta\left(p^- + q^- - \frac{\boldsymbol{p}_{1\perp}^2 + m^2}{2p_1^+} - \frac{\boldsymbol{p}_{2\perp}^2 + m^2}{2p_2^+}\right). \tag{7.98}$$

Now let us choose the frame given by Eqs. (7.40). In this frame, the perpendicular momenta of the quarks are related via

$$\boldsymbol{p}_{2\perp} + \boldsymbol{p}_{1\perp} = \boldsymbol{q}_\perp \left(1 - \frac{m_\pi \nu}{Q^2}\right). \tag{7.99}$$

In order to easily reveal the light-front wave function of π^0 in the end, it is convenient to change variables introducing the four-momentum k as

$$p_1 - q = k, \quad p_2 = p - k, \tag{7.100}$$

and introduce the momentum fraction x so that

$$k^+ = x p^+. \tag{7.101}$$

Then the phase-space integral becomes

$$\Pi(p,q;p_1,p_2) = \frac{1}{16\pi^2 p^+} \int \frac{dx}{x\bar{x}} \int d\boldsymbol{k}_\perp \delta\left(p^- - \frac{(\boldsymbol{k}_\perp + \boldsymbol{q}_\perp)^2 + m^2}{2xp^+} - \frac{(\boldsymbol{p}_\perp - \boldsymbol{k}_\perp)^2 + m^2}{2\bar{x}p^+}\right). \tag{7.102}$$

Introducing the relative quark momentum $\boldsymbol{\kappa}_\perp$ inside the pion,

$$\boldsymbol{\kappa}_\perp = \boldsymbol{k}_\perp - x\boldsymbol{p}_\perp, \tag{7.103}$$

we obtain

$$\Pi(p,q;p_1,p_2) = -\frac{1}{8\pi^2}\int dx \int d\boldsymbol{\kappa}_\perp \delta\left[\boldsymbol{\kappa}_\perp^2 + 2\bar{x}\boldsymbol{\kappa}_\perp\cdot\boldsymbol{q}_\perp + \bar{x}Q^2 - 2x\bar{x}m_\pi\nu + \mu^2(x)\right]. \tag{7.104}$$

The argument of the delta-function reads

$$\begin{aligned}&\boldsymbol{\kappa}_\perp^2 + 2\bar{x}\boldsymbol{\kappa}_\perp\cdot\boldsymbol{q}_\perp + \bar{x}Q^2 - 2x\bar{x}m_\pi\nu + \mu^2(x)\\ &= (\kappa + \bar{x}q\cos\phi)^2 + m^2 - x\bar{x}s + \bar{x}^2Q^2\sin^2\phi,\end{aligned} \tag{7.105}$$

where $\kappa = |\boldsymbol{\kappa}_\perp|$, $s = m_\pi^2 + 2m_\pi\nu - Q^2$, and implies two roots with respect to κ:

$$\kappa_\pm = -\bar{x}q\cos\phi \pm \sqrt{x\bar{x}s - m^2 - \bar{x}^2Q^2\sin^2\phi}. \tag{7.106}$$

The positiveness of the modulus of κ dictates to take the positive root (with "+"), while keeping the square root real. The latter constraints the integration domain of the variable x as follows:

$$x \in \{x_-, x_+\}, \quad x_\pm = \frac{s + 2Q^2\sin^2\phi \pm \sqrt{s(s-4m^2) - 4m^2Q^2\sin^2\phi}}{2(s + Q^2\sin^2\phi)}. \tag{7.107}$$

Note that the integration boundaries in x-variable are now Q^2-dependent. To remove this dependence, one can choose the new variable ξ such that:

$$x = \frac{s + 2Q^2\sin^2\phi + \xi\sqrt{s(s-4m^2) - 4m^2Q^2\sin^2\phi}}{2(s + Q^2\sin^2\phi)}, \quad \xi \in \{-1, 1\}, \tag{7.108}$$

with the Q^2- and ϕ-dependent Jakobian

$$J_{x\to\xi}(Q^2,\phi) = \frac{\partial x}{\partial\xi} = \frac{\sqrt{s(s-4m^2) - 4m^2Q^2\sin^2\phi}}{2(s + Q^2\sin^2\phi)}. \tag{7.109}$$

Thus the integrated photoabsorption cross section could be represented by the following formula:

$$\sigma(\nu,Q^2) = \frac{1}{64\pi^2 m_\pi\sqrt{\nu^2+Q^2}}\int_{-1}^{1} d\xi \int_0^{2\pi} d\phi \frac{J_{x\to\xi}(Q^2,\phi)}{1 + \frac{\bar{x}Q}{\kappa}\cos\phi}|\mathcal{M}(x,\phi,\kappa)|^2\Big|_{\kappa=\kappa_+}, \tag{7.110}$$

where $\mathcal{M}(x,\phi,\kappa)$ is the scattering amplitude of the photoabsorption process shown in Fig. 7.11.

For the Baldin and BT sum rule calculations, where the cross section is integrated over ν with some weight, it is technically more convenient to rearrange the integration order over x and ν,

$$\int_{\nu_{\rm th}}^{\infty} d\nu \int_{x_-}^{x_+} dx \to \int_0^1 dx \int_{\nu_{\rm th}(x)}^{\infty} d\nu = \int_0^1 dx \int_1^{\infty} \nu_{\rm th}(x) d\tilde{\nu}, \tag{7.111}$$

whith

$$\nu_{\rm th}(x) = \frac{\mu^2(x) + Q^2 \bar{x}(1 - \bar{x}\cos^2\phi)}{2x\bar{x}}. \tag{7.112}$$

In a considered theory with scalar quarks the photoabsorption amplitude is given by

$$\mathcal{M}_\lambda = M_\mu \varepsilon_\lambda^\mu(q) = g e_q \left[\frac{(2p_1 - q)_\mu}{(p_1 - q)^2 - m^2} - \frac{(2p_2 - q)_\mu}{(p_2 - q)^2 - m^2} \right] \varepsilon_\lambda^\mu(q), \tag{7.113}$$

where ε_λ^μ is polarization vector of the photon carrying the momentum q and helicity λ, while the neutral pion was treated for simplicity as a neutral system consisting of a quark and an antiquark of one flavour having the electric charge e_q. In terms of the four-momentum k, the denominator of the first propagator in the amplitude is given by

$$(p_1 - q)^2 - m^2 = k^2 - m^2 = 2k^+k^- - \boldsymbol{k}_\perp^2 - m^2. \tag{7.114}$$

Given that this propagator corresponds to the diagram for wich $p_2^2 = m^2$, we have

$$(p - k)^2 = m^2 \to k^- = p^- - \frac{(\bar{x}\boldsymbol{p}_\perp - \boldsymbol{\kappa}_\perp)^2 + m^2}{2\bar{x}p^+}. \tag{7.115}$$

Then, with $\boldsymbol{\kappa}_\perp$ introduced via Eq. (7.103), the denominator reads

$$\begin{aligned} 2k^+k^- - \boldsymbol{k}_\perp^2 - m^2 &= 2xp^+ \left[p^- - \frac{(\bar{x}\boldsymbol{p}_\perp - \boldsymbol{\kappa}_\perp)^2 + m^2}{2\bar{x}p^+} \right] - (x\boldsymbol{p}_\perp + \boldsymbol{\kappa}_\perp)^2 - m^2 \\ &= \frac{1}{\bar{x}} \left[2x\bar{x}p^+p^- - m^2 - \boldsymbol{\kappa}_\perp^2 - x\bar{x}\boldsymbol{p}_\perp^2 \right] = -\frac{1}{\bar{x}} \left[\boldsymbol{\kappa}_\perp^2 + \mu^2(x) \right]. \end{aligned} \tag{7.116}$$

Analogously, the denominator of the second propagator reads

$$(p_2 - q)^2 - m^2 = -\frac{1}{x} \left[(\boldsymbol{\kappa}_\perp + \boldsymbol{q}_\perp)^2 + \mu^2(x) \right]. \tag{7.117}$$

In order to obtain polarized photoabsorption cross sections, it is convenient to consider the photoabsorption amplitudes for different light-front components, not the photon helicities. Making use of the optical theorem and (7.41), we can write

$$\begin{aligned} &\sigma_T(\nu, Q^2) \equiv \sigma^{yy}(\nu, Q^2) \\ &= \frac{1}{64\pi^2 m_\pi \sqrt{\nu^2 + Q^2}} \int_{-1}^{1} d\xi \int_0^{2\pi} d\phi \frac{J_{x\to\xi}(Q^2, \phi)}{1 + \frac{\bar{x}Q}{\kappa}\cos\phi} |M^y(x, \phi, \kappa)|^2 \Big|_{\kappa=\kappa_+} \end{aligned}$$

$$\frac{Q^2}{\nu^2+Q^2}\left[\sigma_T(\nu,Q^2)+\sigma_L(\nu,Q^2)\right] \equiv \frac{m_\pi^2}{(p^+)^2}\sigma^{++}(\nu,Q^2)$$
$$= \frac{m_\pi}{64\pi^2\sqrt{\nu^2+Q^2}(p^+)^2}\int_{-1}^{1}d\xi\int_0^{2\pi}d\phi\frac{J_{x\to\xi}(Q^2,\phi)}{1+\frac{\bar{x}Q}{\kappa}\cos\phi}|M^+(x,\phi,\kappa)|^2\Big|_{\kappa=\kappa_+}, \tag{7.118a}$$

from which one can find both σ_T and σ_L. However, in case of the model that does not preserve gauge invariance, these definitions should be modified according to Eqs. (7.50) and (7.51), yielding

$$\sigma_T(\nu,Q^2) = \sigma^{yy}(\nu,Q^2)-\sigma^{xx}(\nu,Q^2)-\frac{m_\pi\nu}{p^+Q}\sigma^{+x}(\nu,Q^2), \tag{7.119a}$$
$$\sigma_L(\nu,Q^2) = \left(1+\frac{\nu^2}{Q^2}\right)\frac{m_\pi^2}{(p^+)^2}\sigma^{++}(\nu,Q^2)+\left(\frac{Q}{\nu}+2\frac{\nu}{Q}\right)\frac{m_\pi}{p^+}\sigma^{+x}(\nu,Q^2)$$
$$+\sigma^{xx}(\nu,Q^2)-\sigma^{yy}(\nu,Q^2). \tag{7.119b}$$

with the gauge-invariance-violating cross sections σ^{xx} and σ^{+x} included. These cross sections are defined in a way similar to Eqs. (7.118), namely with the substitutions $|\mathcal{M}|^2\to|M^x|^2$ and $|\mathcal{M}|^2\to(M^+)^*M^x/p^+$, respectively.

In the covariant model, the leading terms in Q^2 of the polarized cross sections σ_T and σ_L are given by

$$\sigma_T(\nu,Q) = \frac{g^2e_q^2}{32\pi m_\pi^3\nu^3}\left\{-s\sqrt{1-\frac{4m^2}{s}}+2(s-2m^2)\operatorname{arctanh}\sqrt{1-\frac{4m^2}{s}}\right\}+O(Q^2), \tag{7.120a}$$
$$\sigma_L(\nu,Q) = Q^2\frac{g^2e_q^2}{256\pi m_\pi^5m^2\nu^5}(s+m_\pi^2)^2\left\{s\sqrt{1-\frac{4m^2}{s}}-4m^2\operatorname{arctanh}\sqrt{1-\frac{4m^2}{s}}\right\}+O(Q^4). \tag{7.120b}$$

Substituting these cross sections into the Baldin (2.124) and BT (2.133) sum rules and correcting the charge factor in accordance with the realistic pion,

$$e_q^2\to C_q^{\pi^0}, \tag{7.121}$$

we immediately obtain the exact expressions (7.43) for the electromagnetic polarizabilities in the covariant model.

7.D Light-front components of the Compton tensor

In this Appendix we provide the general expressions for the relevant light-front components of the Compton tensor. The explicit calculation of the diagrams shown in Fig. 7.13, assuming that the quarks with momentum fractions x ($\bar{x}$) have charges $e_1(e_2)$ respectively, results in the following expressions for the $++$, xx, yy and $+x$ light-front components:

$$\frac{m_\pi^2}{(p^+)^2}\widetilde{T}^{++} = 2m_\pi \int_0^1 dx\, x\bar{x} \int_0^\infty \frac{d\boldsymbol{\kappa}_\perp^2}{(4\pi)^2} \frac{\left|\Psi_\pi\left(x,\boldsymbol{\kappa}_\perp^2\right)\right|^2}{\left[\boldsymbol{\kappa}_\perp^2+\mu^2(x)\right]^3} \Bigg\{ 2(e_1+e_2)^2$$
$$\times \left([\boldsymbol{\kappa}_\perp^2+\mu^2(x)]^2 + 4m_\pi^2 \nu^2 (x\bar{x})^2 \right)$$
$$- Q^2 \Bigg(2e_1^2 \bar{x} \left[\boldsymbol{\kappa}_\perp^2 (x-\bar{x}) + \mu^2(x)\right] + 2e_2^2 x \left[\boldsymbol{\kappa}_\perp^2 (\bar{x}-x) + \mu^2(x)\right]$$
$$+ e_1 e_2 \Bigg[\boldsymbol{\kappa}_\perp^2 (8x\bar{x}-1) + \mu^2(x)$$
$$- [\boldsymbol{\kappa}_\perp^2+\mu^2(x)]^2 \frac{\partial_{\boldsymbol{\kappa}_\perp^2} |\Psi_\pi(x,\boldsymbol{\kappa}_\perp^2)|^2 + \boldsymbol{\kappa}_\perp^2 \mathcal{D}_{Q^2} |\Psi_\pi(x,\boldsymbol{\kappa}_\perp^2)|^2}{|\Psi_\pi(x,\boldsymbol{\kappa}_\perp^2)|^2} \Bigg] \Bigg) \Bigg\} + \ldots, \tag{7.122a}$$

$$\widetilde{T}^{xx} = \frac{1}{2m_\pi} \int_0^1 dx \frac{1}{x\bar{x}} \int_0^\infty \frac{d\boldsymbol{\kappa}_\perp^2}{(4\pi)^2} \frac{\left|\Psi_\pi(x,\boldsymbol{\kappa}_\perp^2)\right|^2}{\left[\boldsymbol{\kappa}_\perp^2+\mu^2(x)\right]^3}$$
$$\times \Bigg\{ [\boldsymbol{\kappa}_\perp^2+\mu^2(x)]^2$$
$$\times \Big[-2e_1^2\bar{x}\left[\boldsymbol{\kappa}_\perp^2(x-\bar{x})+\mu^2(x)\right] - 2e_2^2 x\left[\boldsymbol{\kappa}_\perp^2(\bar{x}-x)+\mu^2(x)\right] - 8e_1e_2x\bar{x}\boldsymbol{\kappa}_\perp^2 \Big]$$
$$+ \frac{8m_\pi^2\nu^2}{Q^2}(e_1+e_2)^2(x\bar{x})^2[\boldsymbol{\kappa}_\perp^2+\mu^2(x)]^2$$
$$+ Q^2 \Bigg(2e_1^2\bar{x}^2 \left[\Big((1-3\bar{x})\boldsymbol{\kappa}_\perp^2+\mu^2(x)\Big)^2 - 3\bar{x}^2\boldsymbol{\kappa}_\perp^4 \right]$$
$$+ 2e_2^2x^2 \left[\Big((1-3x)\boldsymbol{\kappa}_\perp^2+\mu^2(x)\Big)^2 - 3x^2\boldsymbol{\kappa}_\perp^4 \right]$$
$$+ e_1e_2x\bar{x}\boldsymbol{\kappa}_\perp^2 \Bigg[-4(1-6x\bar{x})\boldsymbol{\kappa}_\perp^2 + 2\mu^2(x)$$
$$- [\boldsymbol{\kappa}_\perp^2+\mu^2(x)]^2 \frac{2\partial_{\boldsymbol{\kappa}_\perp^2}\left|\Psi_\pi(x,\boldsymbol{\kappa}_\perp^2)\right|^2 + 3\boldsymbol{\kappa}_\perp^2\mathcal{D}_{Q^2}\left|\Psi_\pi(x,\boldsymbol{\kappa}_\perp^2)\right|^2}{\left|\Psi_\pi(x,\boldsymbol{\kappa}_\perp^2)\right|^2} \Bigg] \Bigg)$$
$$- 4m_\pi^2\nu^2(x\bar{x})^2 \Bigg(6e_1^2\bar{x}\left[(1-4\bar{x})\boldsymbol{\kappa}_\perp^2+\mu^2(x)\right] + 6e_2^2x\left[(1-4x)\boldsymbol{\kappa}_\perp^2+\mu^2(x)\right]$$
$$+ e_1e_2 \Bigg[3(1-4\bar{x})(1-4x)\boldsymbol{\kappa}_\perp^2 + \mu^2(x)$$
$$- [\boldsymbol{\kappa}_\perp^2+\mu^2(x)]^2 \frac{\partial_{\boldsymbol{\kappa}_\perp^2}\left|\Psi_\pi(x,\boldsymbol{\kappa}_\perp^2)\right|^2 + \boldsymbol{\kappa}_\perp^2\mathcal{D}_{Q^2}\left|\Psi_\pi(x,\boldsymbol{\kappa}_\perp^2)\right|^2}{\left|\Psi_\pi(x,\boldsymbol{\kappa}_\perp^2)\right|^2} \Bigg] \Bigg) \Bigg\}$$
$$+ \ldots, \tag{7.122b}$$

$$\widetilde{T}^{yy} = \frac{1}{2m_\pi} \int_0^1 dx \frac{1}{x\bar{x}} \int_0^\infty \frac{d\boldsymbol{\kappa}_\perp^2}{(4\pi)^2} \frac{\left|\Psi_\pi(x,\boldsymbol{\kappa}_\perp^2)\right|^2}{\left[\boldsymbol{\kappa}_\perp^2+\mu^2(x)\right]^3}$$

$$
\begin{aligned}
&\times\Bigg\{\Big[\boldsymbol{\kappa}_\perp^2+\mu^2(x)\Big]^2\\
&\quad\times\Big[-2e_1^2\bar{x}\left[\boldsymbol{\kappa}_\perp^2(x-\bar{x})+\mu^2(x)\right]-2e_2^2x\left[\boldsymbol{\kappa}_\perp^2(\bar{x}-x)+\mu^2(x)\right]-8e_1e_2x\bar{x}\boldsymbol{\kappa}_\perp^2\Big]\\
&-Q^2\boldsymbol{\kappa}_\perp^2\Bigg(4e_1^2\bar{x}^3[x\boldsymbol{\kappa}_\perp^2+\mu^2(x)]+4e_2^2x^3[\bar{x}\boldsymbol{\kappa}_\perp^2+\mu^2(x)]\\
&-e_1e_2x\bar{x}\Bigg[2[4x\bar{x}\boldsymbol{\kappa}_\perp^2+\mu^2(x)]\\
&\quad-[\boldsymbol{\kappa}_\perp^2+\mu^2(x)]^2\frac{2\partial_{\boldsymbol{\kappa}_\perp^2}\left|\Psi_\pi(x,\boldsymbol{\kappa}_\perp^2)\right|^2+\boldsymbol{\kappa}_\perp^2\mathcal{D}_{Q^2}\left|\Psi_\pi(x,\boldsymbol{\kappa}_\perp^2)\right|^2}{\left|\Psi_\pi(x,\boldsymbol{\kappa}_\perp^2)\right|^2}\Bigg]\Bigg)\\
&+16m_\pi^2\nu^2(x\bar{x})^2(xe_2-\bar{x}e_1)^2\boldsymbol{\kappa}_\perp^2\Bigg\}+\ldots,
\end{aligned}
\tag{7.122c}
$$

$$
\begin{aligned}
\frac{m_\pi}{p^+}\widetilde{T}^{+x}&=2m_\pi\int_0^1dx\,x\bar{x}\int_0^\infty\frac{d\boldsymbol{\kappa}_\perp^2}{(4\pi)^2}\frac{\left|\Psi_\pi\left(x,\boldsymbol{\kappa}_\perp^2\right)\right|^2}{\left[\boldsymbol{\kappa}_\perp^2+\mu^2(x)\right]^3}\\
&\times\Bigg\{-\frac{\nu}{Q}2(e_1+e_2)^2\Big(\left[\boldsymbol{\kappa}_\perp^2+\mu^2(x)\right]^2+4m_\pi^2\nu^2(x\bar{x})^2\Big)\\
&+Q\nu\Bigg(4e_1^2\bar{x}\left[(1-3\bar{x})\boldsymbol{\kappa}_\perp^2+\mu^2(x)\right]+4e_2^2x\left[(1-3x)\boldsymbol{\kappa}_\perp^2+\mu^2(x)\right]\\
&+e_1e_2\Bigg[(24x\bar{x}-5)\boldsymbol{\kappa}_\perp^2+\mu^2(x)\\
&\quad-[\boldsymbol{\kappa}_\perp^2+\mu^2(x)]^2\frac{\partial_{\boldsymbol{\kappa}_\perp^2}\left|\Psi_\pi(x,\boldsymbol{\kappa}_\perp^2)\right|^2+\boldsymbol{\kappa}_\perp^2\mathcal{D}_{Q^2}\left|\Psi_\pi(x,\boldsymbol{\kappa}_\perp^2)\right|^2}{\left|\Psi_\pi(x,\boldsymbol{\kappa}_\perp^2)\right|^2}\Bigg]\Bigg)\Bigg\}\\
&+\ldots,
\end{aligned}
\tag{7.122d}
$$

where the ellipsis stands for higher order terms in either Q or ν. Note that in the above expressions, the terms proportional to $e_1^2(e_2^2)$ originate from the handbag diagrams resulting from the Compton scattering off a quark (anti-quark) with momentum fraction $x(\bar{x})$ respectively. The terms proportional to e_1e_2 result from the cat-ears diagrams.

Using Eqs. (7.50), one can then extract the non-Born parts of the gauge-invariance corrected amplitudes T_1 and T_2 as:

$$
\begin{aligned}
\overline{T}_1&=\frac{1}{2m_\pi}\int_0^1dx\,\frac{1}{x\bar{x}}\int_0^\infty\frac{d\boldsymbol{\kappa}_\perp^2}{(4\pi)^2}\frac{\left|\Psi_\pi\left(x,\boldsymbol{\kappa}_\perp^2\right)\right|^2}{\left[\boldsymbol{\kappa}_\perp^2+\mu^2(x)\right]^3}\\
&\times\Bigg\{-2Q^2\Big(e_1^2\bar{x}^2[\boldsymbol{\kappa}_\perp^2(x-\bar{x})+\mu^2(x)]^2+e_2^2x^2[\boldsymbol{\kappa}_\perp^2(\bar{x}-x)+\mu^2(x)]^2
\end{aligned}
$$

$$
\begin{aligned}
&\quad - e_1 e_2 x\bar{x}\boldsymbol{\kappa}_\perp^4 \left[2(1-4x\bar{x}) + [\boldsymbol{\kappa}_\perp^2 + \mu^2(x)]^2 \frac{\mathcal{D}_{Q^2}|\Psi_\pi(x,\boldsymbol{\kappa}_\perp^2|^2}{|\Psi_\pi(x,\boldsymbol{\kappa}_\perp^2|^2} \right] \Bigg) \\
&+ 8m_\pi^2 \nu^2 (x\bar{x})^2 \Bigg(e_1^2 \bar{x}[\boldsymbol{\kappa}_\perp^2(1-4\bar{x}) + \mu^2(x)] \\
&\qquad + e_2^2 x[\boldsymbol{\kappa}_\perp^2(1-4x) + \mu^2(x)] \\
&\qquad - 2e_1 e_2 \boldsymbol{\kappa}_\perp^2 (1-4x\bar{x}) \Bigg) \Bigg\} + O(\mathcal{E}^4), \qquad (7.123a)
\end{aligned}
$$

$$
\begin{aligned}
\overline{T}_2 &= 4m_\pi \int_0^1 dx\, x\bar{x} \int_0^\infty \frac{d\boldsymbol{\kappa}_\perp^2}{(4\pi)^2} \frac{\left|\Psi_\pi\left(x,\boldsymbol{\kappa}_\perp^2\right)\right|^2}{\left[\boldsymbol{\kappa}_\perp^2 + \mu^2(x)\right]^3} \\
&\times Q^2 \Bigg\{ e_1^2 \bar{x}[\boldsymbol{\kappa}_\perp^2(1-4\bar{x}) + \mu^2(x)] + e_2^2 x[\boldsymbol{\kappa}_\perp^2(1-4x) + \mu^2(x)] - 2e_1 e_2 \boldsymbol{\kappa}_\perp^2 (1-4x\bar{x}) \Bigg\} + O(\mathcal{E}^4), \qquad (7.123b)
\end{aligned}
$$

up to terms of fourth-order proportional to Q^4, ν^4, or $Q^2\nu^2$.

Chapter 8

Sum rules for parity- and time-reversal-violating Compton scattering

In this chapter, we consider an elementary extension of the forward doubly-virtual Compton scattering on a spin-1/2 particle to the cases of parity (P) and time-reversal (T) invariance violation. We obtain new sum rules, which relate P-violating anapole moment $\mathfrak{a}$ [461] and PT-violating electric dipole moment $\mathfrak{d}$ with certain polarized photoabsorption cross sections, and verify them in simple extensions of χPT. The obtained results, while being rather academic, may provide additional checks towards self-consistency of various models of new physics.

The results presented in this Chapter have not been published yet.

8.1 Compton tensor structure and dispersion relations

Let us consider the electromagnetic current of the spin-1/2 particle N with mass M, which violates P and T symmetries. The most common parametrization of the parity-violating Compton tensor is provided by Particle Data Group [462] in Eq. (18.6). In order to violate the time-reversal invariance, it should be supplemented with the T-violating tensor structures $(\hat{p}^\mu \hat{\jmath}^\nu - \hat{p}^\nu \hat{\jmath}^\mu)$ and $(\hat{p}^\mu \jmath_\perp^\nu + \hat{p}^\nu \jmath_\perp^\mu)$ with corresponding spin-dependent invariant amplitudes S_6 and S_7 (see, e.g., [463]):

$$
\begin{aligned}
T^{\mu\nu}_{\text{PVTV}}(p,q) = {} & \left(-g^{\mu\nu} + \frac{q^\mu q^\nu}{q^2}\right) T_1 + \frac{\hat{p}^\mu \hat{p}^\nu}{M^2} T_2 + \frac{i\epsilon^{\mu\nu\alpha\beta} q_\alpha}{M} \left[\jmath^\beta S_1 + \left(\jmath^\beta (p\cdot q) - (\jmath\cdot q) p^\beta\right) \frac{1}{M^2} S_2\right] \\
& + \frac{i\epsilon^{\mu\nu\alpha\beta} p_\alpha q_\beta}{2M^2} T_3 + \left[\left(\hat{p}^\mu \hat{\jmath}^\nu + \hat{p}^\nu \hat{\jmath}^\mu\right) \frac{(p\cdot q)}{2} - (\jmath\cdot q)\hat{p}^\mu \hat{p}^\nu\right] \frac{1}{M^3} S_3 + \frac{\hat{p}^\mu \hat{p}^\nu (\jmath\cdot q)}{M^3} S_4 \\
& + \left(-g^{\mu\nu} + \frac{q^\mu q^\nu}{q^2}\right) \frac{(\jmath\cdot q)}{M} S_5 + \frac{\hat{p}^\mu \hat{\jmath}^\nu - \hat{p}^\nu \hat{\jmath}^\mu}{2M} S_6 + \frac{\hat{p}^\mu \jmath_\perp^\nu + \hat{p}^\nu \jmath_\perp^\mu}{2M} S_7,
\end{aligned}
\tag{8.1}
$$

with the conventions

$$\hat{p}_\mu = p_\mu - \frac{p\cdot q}{q^2}q_\mu, \quad \hat{\mathfrak{z}}_\mu = \mathfrak{z}_\mu - \frac{\mathfrak{z}\cdot q}{q^2}q_\mu, \quad \mathfrak{z}_\perp^\mu = \frac{i\epsilon^{\mu\alpha\beta\gamma}p_\alpha q_\beta \mathfrak{z}_\gamma}{M^2}. \tag{8.2}$$

Similar to Eq. (2.79), p and $\mathfrak{z}$ are the momentum and spin four-vectors of the spin-1/2 target, and q is the four-momentum of the incident virtual photon. Given that the invariant amplitudes T_i and S_i are analytic functions of ν having definite parity under crossing $\nu \to -\nu$,

$$\{T_1,T_2,T_3,S_1\}(\nu,Q^2) = \{T_1,T_2,T_3,S_1\}(-\nu,Q^2), \tag{8.3}$$

$$\{S_2,S_3,S_4,S_5,S_6,S_7\}(\nu,Q^2) = -\{S_2,S_3,S_4,S_5,S_6,S_7\}(-\nu,Q^2), \tag{8.4}$$

they should satisfy the following dispersion relations

$$\left\{ \begin{array}{c} T_1,T_2,T_3,S_1, \\ \nu(S_2,S_3,S_4,S_5,S_6,S_7) \end{array} \right\}(\nu,Q^2) = \\ = \frac{2}{\pi}\int_{\nu_{\rm el}}^{\infty}\frac{d\nu'\nu'}{\nu'^2-\nu^2-i0^+}\,{\rm Im}\left\{ \begin{array}{c} T_1,T_2,T_3,S_1, \\ \nu'(S_2,S_3,S_4,S_5,S_6,S_7) \end{array} \right\}(\nu',Q^2). \tag{8.5}$$

We define the helicity amplitudes of the forward Compton scattering as

$$T(\lambda,h\to\lambda',h') = \varepsilon_\mu^*(\lambda')T^{\mu\nu}_{\rm PVTV}(h',h)\varepsilon_\nu(\lambda), \tag{8.6}$$

where $\lambda(\lambda')$ and $h(h')$ are the helicities of an initial (final) virtual photon and a spin-$1/2$ target, respectively. Then the ten nonvanishing helicity amplitudes could be written in terms of the invariant amplitudes as follows [1]

$$T(\pm1,\pm\{\mp\}\tfrac{1}{2}\to\pm1,\pm\{\mp\}\tfrac{1}{2}) = T_1 \pm \frac{\sqrt{\nu^2+Q^2}}{2M}T_3 - \{+\}\left(S_1\frac{\nu}{M} - \frac{Q^2}{M^2}S_2\right) \mp \{\pm\}\frac{\sqrt{\nu^2+Q^2}}{M}S_5, \tag{8.7a}$$

$$T(0,\pm\tfrac{1}{2}\to0,\pm\tfrac{1}{2}) = T_2\left(1+\frac{\nu^2}{Q^2}\right) - T_1 \pm \frac{\sqrt{\nu^2+Q^2}}{M}\left[S_3 - S_4\left(1+\frac{\nu^2}{Q^2}\right)+S_5\right], \tag{8.7b}$$

$$T(0,\pm\tfrac{1}{2}\to\mp1,\mp\tfrac{1}{2}) = -\frac{\sqrt{2}Q}{M}\left(S_1+\frac{\nu}{M}S_2\right) \mp \frac{\sqrt{Q^2+\nu^2}}{\sqrt{2}Q}\left(\frac{\nu}{M}S_3+S_6\right) - \frac{(Q^2+\nu^2)}{\sqrt{2}QM}S_7, \tag{8.7c}$$

$$T(\mp1,\mp\tfrac{1}{2}\to0,\pm\tfrac{1}{2}) = -\frac{\sqrt{2}Q}{M}\left(S_1+\frac{\nu}{M}S_2\right) \mp \frac{\sqrt{Q^2+\nu^2}}{\sqrt{2}Q}\left(\frac{\nu}{M}S_3-S_6\right) + \frac{(Q^2+\nu^2)}{\sqrt{2}QM}S_7. \tag{8.7d}$$

These helicity amplitudes correspond to the amount of the invariant amplitudes T_i and S_i thus forming a complete basis in helicity space. It is convenient to introduce the T, TT and LT helicity amplitudes as

$$T_{\rm T}^{\pm} \equiv \frac{1}{2}\left[T(\pm1,\pm\tfrac{1}{2}\to\pm1,\pm\tfrac{1}{2}) + T(\pm1,\mp\tfrac{1}{2}\to\pm1,\mp\tfrac{1}{2})\right], \tag{8.8}$$

[1] Similar expressions can be found in [463, 464]. They can be reduced to ours via a linear transformation.

$$T^{\pm}_{\rm TT} \equiv \frac{1}{2}\left[T(\pm1,\pm\tfrac{1}{2}\to\pm1,\pm\tfrac{1}{2}) - T(\pm1,\mp\tfrac{1}{2}\to\pm1,\mp\tfrac{1}{2})\right], \tag{8.9}$$

$$T^{\pm}_{\rm L} \equiv T(0,\pm\tfrac{1}{2}\to0,\pm\tfrac{1}{2}), \tag{8.10}$$

$$T^{\pm}_{\rm LT} \equiv T(0,\pm\tfrac{1}{2}\to\mp1,\mp\tfrac{1}{2}), \tag{8.11}$$

$$T^{\pm}_{\rm TL} \equiv T(\mp1,\mp\tfrac{1}{2}\to0,\pm\tfrac{1}{2}). \tag{8.12}$$

The imaginary parts of these helicity ammplitudes are related to the corresponding polarized photoabsorption cross sections σ via the optical theorem,

$$\mathrm{Im}T(\nu,Q^2) = \frac{\sqrt{\nu^2+Q^2}}{4\pi}\sigma(\nu,Q^2). \tag{8.13}$$

8.1.1 Low-energy theorems and sum rules

The leading low-energy behavior of the invariant amplitudes T_i and S_i is given by the Born contributions. Given in Appendix 8.A, these contributions can be substituted in Eqs. (8.12), yielding the low-energy behavior of the helicity amplitudes. The corresponding Born non-pole terms of Compton helicity amplitudes in terms of the vertex form factors[2], which are useful for deriving sum rules, are given below:

$$4\pi M\, T^{\rm Born,\,n/pole}(\pm1,\pm\{\mp\}\tfrac{1}{2}\to\pm1,\pm\{\mp\}\tfrac{1}{2}) = -\mathcal{F}_1^2 - \mathcal{G}_1^2\frac{Q^4}{M^4} - \{+\}(\mathcal{F}_2^2-\mathcal{G}_2^2)\frac{\nu}{2M}$$
$$\mp\{\pm\}\sqrt{1+\frac{Q^2}{\nu^2}}\frac{2Q^2}{M^2}(\mathcal{F}_1+\mathcal{F}_2)\mathcal{G}_1, \tag{8.14a}$$

$$4\pi M\, T^{\rm Born,\,n/pole}(0,\pm\tfrac{1}{2}\to0,\pm\tfrac{1}{2}) = -\frac{Q^2}{4M^2}\left(\mathcal{F}_2^2-\mathcal{G}_2^2\right), \tag{8.14b}$$

$$4\pi M\, T^{\rm Born,\,n/pole}(0,\pm\tfrac{1}{2}\to\mp1,\mp\tfrac{1}{2}) = \frac{Q}{\sqrt{2}M}\left(\mathcal{F}_1\mathcal{F}_2+\mathcal{G}_2^2+\frac{4Q^2}{M^2}\mathcal{G}_1^2\right)+\frac{\sqrt{2}Q(Q^2+\nu^2)}{M^2\nu}\mathcal{G}_1\mathcal{G}_2$$
$$\pm\frac{Q\sqrt{Q^2+\nu^2}}{\sqrt{2}M\nu}\left[2\frac{\nu}{M}\mathcal{F}_2\mathcal{G}_1-(\mathcal{F}_1+\mathcal{F}_2)\,\mathcal{G}_2\right] \tag{8.14c}$$

$$4\pi M\, T^{\rm Born,\,n/pole}(\mp1,\mp\tfrac{1}{2}\to0,\pm\tfrac{1}{2}) = \frac{Q}{\sqrt{2}M}\left(\mathcal{F}_1\mathcal{F}_2-\mathcal{G}_2^2+\frac{4Q^2}{M^2}\mathcal{G}_1^2\right)-\frac{\sqrt{2}Q(Q^2+\nu^2)}{M^2\nu}\mathcal{G}_1\mathcal{G}_2$$
$$\pm\frac{Q\sqrt{Q^2+\nu^2}}{\sqrt{2}M\nu}\left[2\frac{\nu}{M}\mathcal{F}_2\mathcal{G}_1+(\mathcal{F}_1+\mathcal{F}_2)\,\mathcal{G}_2\right] \tag{8.14d}$$

Finally, combining the dispersion relations (8.5) with the optical theorem (8.13) and the low-energy theorems (8.14), we obtain the sum rules for the anapole moment,

$$(Z+\varkappa)\,\mathfrak{a} = \frac{M^3}{8\pi^2\alpha_{\rm em}}\lim_{Q^2\to0}\int d\nu\frac{\left[\sigma^-_{TT}-\sigma^+_{TT}\right](\nu,Q^2)}{Q^2} \tag{8.15}$$

[2]Here the limit $Q\to0$ is taken before $\nu\to0$

$$\varkappa\mathfrak{a} = \frac{M^3}{8\sqrt{2}\pi^2\alpha_{\rm em}} \lim_{Q^2\to 0}\int d\nu \frac{\left[\sigma^+_{LT} - \sigma^-_{LT} + \sigma^+_{TL} - \sigma^-_{TL}\right](\nu, Q^2)}{\nu Q}. \tag{8.16}$$

and, similarly, for EDM

$$(Z+\varkappa)\mathfrak{d} = \frac{M^2}{4\sqrt{2}\pi^2\alpha_{\rm em}} \lim_{Q\to 0}\int \frac{d\nu}{Q}\left[\sigma^-_{LT} - \sigma^+_{LT} + \sigma^+_{TL} - \sigma^-_{TL}\right](\nu, Q^2). \tag{8.17}$$

Here $\varkappa$ is the AMM of particle N, and Z is its charge number. Regarding Eq. (8.15), it is worth mentioning that the following relation is assumed

$$\int d\nu \left[\sigma^-_{TT} - \sigma^+_{TT}\right](\nu, Q^2) = 0, \tag{8.18}$$

which reflects the anapole moment renormalization. Thus, for the renormalized anapole moment, the sum rule (8.15) should be written as

$$(Z+\varkappa)\,\mathfrak{a} = \frac{M^3}{8\pi^2\alpha_{\rm em}} \lim_{Q^2\to 0}\int d\nu \frac{\partial}{\partial Q^2}\left[\sigma^-_{TT} - \sigma^+_{TT}\right](\nu, Q^2). \tag{8.19}$$

Moreover, if one takes the limit $\nu \to 0$ before $Q^2 \to 0$ for the invariant amplitude νS_3, then its Born non-pole contribution will be

$$\nu S_3^{\rm Born,\,n/pole} = -\frac{2}{\pi} M \mathcal{F}_1 \mathcal{G}_1, \tag{8.20}$$

which allows for another sum rule for the anapole moment

$$Z\mathfrak{a} = \frac{M^2}{16\sqrt{2}\pi^2\alpha_{\rm em}} \lim_{Q^2\to 0}\int d\nu \frac{\left[(\sigma^-_{LT} + \sigma^-_{TL}) - (\sigma^+_{LT} + \sigma^+_{TL})\right](\nu, Q^2)}{Q}. \tag{8.21}$$

It also possible to find the generalization of the GDH and Schwinger sum rules to the considered case of parity- and time-reversal-violation. Owing that at $Q \to 0$ for the parity-conserving combination of TT helicity amplitudes we have

$$\left(T^+_{TT} + T^-_{TT}\right)^{\rm Born,\,n/pole} = -\frac{\nu}{2M^2\pi}(\mathcal{F}_2^2 - \mathcal{G}_2^2), \tag{8.22}$$

one can identify the extended GDH sum rule:

$$\varkappa^2 - \mathfrak{d}^2 = -\frac{M^2}{4\pi^2\alpha_{\rm em}}\int \frac{d\nu}{\nu}\left[\sigma^+_{TT} + \sigma^-_{TT}\right](\nu), \tag{8.23}$$

which is in agreement with [465]. Given that the parity-conserving combination of LT helicity amplitudes reads

$$T^{B+}_{LT} + T^{B-}_{LT} + T^{B+}_{TL} + T^{B-}_{TL} = Q\frac{\mathcal{F}_1\mathcal{F}_2 + 4\mathcal{G}_1^2 Q^2/M^2 - \mathcal{G}_2^2}{\sqrt{2}\pi M^2}, \tag{8.24}$$

we can write down the extended Schwinger sum rule

$$Z\varkappa + \mathfrak{d}^2 = \frac{M^2}{\sqrt{2}\pi} \lim_{Q\to 0} \int \frac{d\nu}{Q} \left[\sigma_{LT}^{+} + \sigma_{LT}^{-} + \sigma_{TL}^{+} + \sigma_{TL}^{-}\right](\nu, Q^2). \tag{8.25}$$

8.2 Perturbative verification of the sum rules

8.2.1 Parity-violating pion-nucleon Yukawa coupling

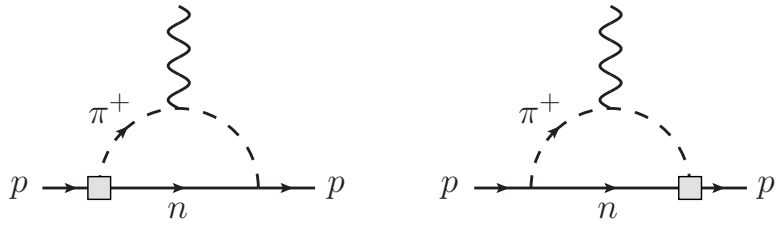

Fig. 8.1 One-loop electromagnetic vertex with PV Yukawa coupling

At low energies, the P-violating πN interaction can be introduced in χPT Lagrangian via the following term [466, 467]:

$$\mathcal{L}_{\pi NN}^{\rm PV} = \frac{h_\pi^1}{\sqrt{2}} \varepsilon_{ab3} \pi^a \bar{N} \tau^b N = i h_\pi^1 (\pi^+ \bar{p} n - \pi^- \bar{n} p), \tag{8.26}$$

with the parity-violating coupling h_π^1 of pions to nucleons. The leading parity-violating contribution to the electromagnetic current arises from the one-loop diagram shown in Fig. 8.1, where the P-violating coupling (8.26) interferes with the parity-conserving coupling given by

$$\mathcal{L}_{\pi NN} = g_{\pi N} \bar{N} i\gamma_5 \vec{\pi} \cdot \vec{\tau} N = \sqrt{2} i g_{\pi N} \left(\pi^+ \bar{n} \gamma_5 p + \pi^- \bar{p} \gamma_5 n\right) + \ldots, \tag{8.27}$$

where $g_{\pi N} = g_A M_N / f_\pi$. The corresponding renormalized contribution to the proton anapole moment is calculated in [468]. In our notations, it reads

$$\begin{aligned} \mathfrak{a}^p = \frac{g_A M_N h_\pi^1}{8\sqrt{2}\pi^2 f_\pi} \frac{1}{6} \Bigg\{ & (-5 + 2\zeta_{\pi N}^2) - (3 - 4\zeta_{\pi N}^2 + \zeta_{\pi N}^4) \log[x^2] \\ & + \frac{2\zeta_{\pi N} \sqrt{\zeta_{\pi N}^2 - 4} (-2 + 9\zeta_{\pi N}^2 - 6\zeta_{\pi N}^4 + \zeta_{\pi N}^6)}{\zeta_{\pi N}^2 (-4 + \zeta_{\pi N}^2)} \log \left[\frac{\zeta_{\pi N} + \sqrt{-4 + \zeta_{\pi N}^2}}{2} \right] \Bigg\}, \end{aligned} \tag{8.28}$$

where $\zeta_{\pi N} = m_\pi / M_N$.

The sum rule (8.21) has been tested for both proton and neutron in the model with parity-violating pion-nucleon Yukawa coupling, which is described above, at leading order. Note that at this order, one has no contribution to the Pauli form factor. Therefore, the l.h.s. of the sum rule should give just

the one-loop result for the anapole moment multiplied by the charge of the nucleon. However, the tests showed that the sum rule holds up to (asymptotic) constants for both the proton and the neutron cases. In accordance with the Sugawara-Kanazawa theorem [158], these constants originate from the (constant) values of the corresponding Compton amplitudes at the infinite energies. The results can be summarized as follows

$$1\times\mathfrak{a}^{\mathrm{p}}=\frac{\partial}{\partial Q^2}\left[2\pi M^2\sqrt{Q^2+\nu^2}S_5^{\mathrm{p}}(\nu,Q^2)\right]\Big|_{\substack{Q^2\to 0\\ \nu\to\infty}}+\frac{M^3}{8\pi^2\alpha_{\mathrm{em}}}\int d\nu'\frac{\partial}{\partial Q^2}\left[\sigma_{TT}^{-,\mathrm{p}}-\sigma_{TT}^{+,\mathrm{p}}\right](\nu,Q^2)\Big|_{Q^2\to 0}, \tag{8.29}$$

$$0\times\mathfrak{a}^{\mathrm{n}}=\frac{\partial}{\partial Q^2}\left[2\pi M^2\sqrt{Q^2+\nu^2}S_5^{\mathrm{n}}(\nu,Q^2)\right]\Big|_{\substack{Q^2\to 0\\ \nu\to\infty}}+\frac{M^3}{8\pi^2\alpha_{\mathrm{em}}}\int d\nu'\frac{\partial}{\partial Q^2}\left[\sigma_{TT}^{-,\mathrm{n}}-\sigma_{TT}^{+,\mathrm{n}}\right](\nu,Q^2)\Big|_{Q^2\to 0}. \tag{8.30}$$

The asymptotic constants for the proton and neutron are related as

$$\begin{aligned}\frac{\partial}{\partial Q^2}\left[2\pi M^2\sqrt{Q^2+\nu^2}S_5^{\mathrm{n}}(\nu,Q^2)\right]\Big|_{\substack{Q^2\to 0\\ \nu\to\infty}}=&\frac{\partial}{\partial Q^2}\left[2\pi M^2\sqrt{Q^2+\nu^2}S_5^{\mathrm{p}}(\nu,Q^2)\right]\Big|_{\substack{Q^2\to 0\\ \nu\to\infty}}\\ &+\frac{5}{48\sqrt{2}\pi^2}\frac{g_A M_N h_\pi^1}{f_\pi}\\ =&\frac{1+5\zeta_{\pi N}^2}{48\sqrt{2}\zeta_{\pi N}^2\pi^2}\frac{g_A M_N h_\pi^1}{f_\pi}.\end{aligned} \tag{8.31}$$

The reason of such a relation becomes clear after looking at the diagrams which could contribute to the asymptotic values of the Compton amplitudes in both cases. These diagrams are shown in Fig. 8.2. In case of the proton, only the diagram (a) contributes, whereas for the neutron all three diagrams

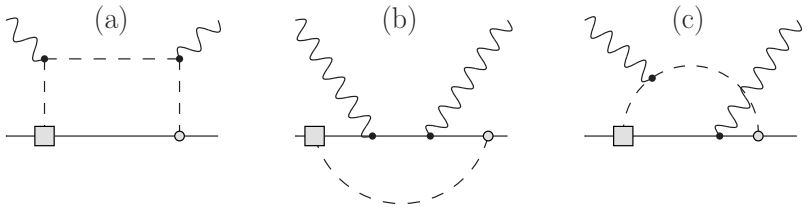

Fig. 8.2 Box diagrams that may contribute to the asymptotic values of the Compton amplitudes. Crossed diagrams are omitted as well as the diagrms with interchanged parity-conserving and parity-violating couplings.

(a)-(c) could contribute. It turns out, however, that the last diagram (c) vanishes at infinitely large energy. Given that the mathematical expression for diagram (a) is similar for proton and neutron, we have the relation (8.31).

8.2.2 Parity- and time-reversal-violating Yukawa coupling

The simplest way to introduce the parity and time-reversal violation simultaneously in χPT is to consider the following Yukawa-type non-derivative interactions [469]:

$$\mathcal{L} = \overline{g}_0 \overline{N}\vec{\pi}\cdot\vec{\tau}N + \overline{g}_1 \overline{N}\pi_3 N + \overline{g}_2 \overline{N}\pi_3\tau_3 N. \tag{8.32}$$

These terms correspond to the isospin singlet, vector and tensor interactions, respectively. Let us focus on the singlet interaction and test sum rule (8.17) by obtaining the nucleon EDM.

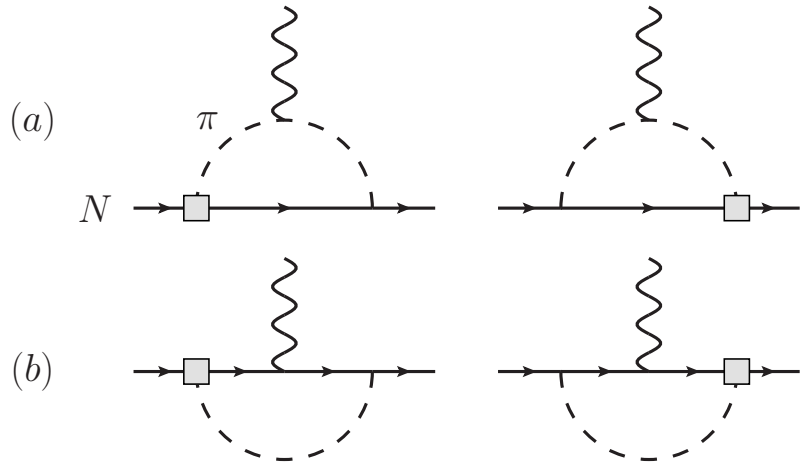

Fig. 8.3 The diagrams that are responsible for the nucleon EDM contribution. The parity- and time-reversal-violating coupling is pointed by gray square.

The nucleon EDM, produced by the coupling $\overline{g}_0$, receives the contributions from the diagrams shown in Fig. 8.3. In particular, the proton EDM comes form the diagrams (a) with the charged pion, and the diagrams (b) with the neutral pion, while the neutron EDM involves the diagrams (a) and (b) with only charged pion in the loop. Thus, the loop calculation yields the following results:

$$\mathfrak{d}^{\mathrm{p}} = \overline{g}_0 g_A \frac{M}{f_\pi}\left[d^N + 2d^\pi\right], \tag{8.33}$$

$$\mathfrak{d}^{\mathrm{p}} = 2\overline{g}_0 g_A \frac{M}{f_\pi}\left[d^N - d^\pi\right], \tag{8.34}$$

where the loop integrals d^N and d^π are given by

$$d^N = \frac{1}{8\pi^2}\left\{-2+\zeta_{\pi N}^2\log[\zeta_{\pi N}^2] - \frac{2\zeta_{\pi N}(\zeta_{\pi N}^2-2)\sqrt{\zeta_{\pi N}^2-4}}{\zeta_{\pi N}^2-4}\log\left[\frac{\zeta_{\pi N}+\sqrt{\zeta_{\pi N}^2-4}}{2}\right]\right\}, \tag{8.35}$$

$$d^\pi = \frac{1}{8\pi^2}\left\{-2+(\zeta_{\pi N}^2-1)\log[\zeta_{\pi N}^2] - \frac{2\zeta_{\pi N}(\zeta_{\pi N}^2-3)\sqrt{\zeta_{\pi N}^2-4}}{\zeta_{\pi N}^2-4}\log\left[\frac{\zeta_{\pi N}+\sqrt{\zeta_{\pi N}^2-4}}{2}\right]\right\}. \tag{8.36}$$

Now let us obtain the polarized photoproduction cross sections relevant for the sum rules (8.17) and (8.17). They can be divided by the charged and neutral pion photoproduction channel, $\gamma N \to \pi^{\pm} N$ and $\gamma N \to \pi^0 N$ correspondingly:

$$\sigma_{\text{EDM}}^{\gamma p \to \pi^+ n} = -Q \frac{4\alpha_{\text{em}} \overline{g}_0 g_A}{\sqrt{2} f_\pi M w^3 (1+2w)} \left\{ (1+w)\sqrt{\lambda} - (\zeta_{\pi N}^2 + w)(1+2w) \text{arccoth} \left[\frac{\zeta_{\pi N}^2 + 2w}{\sqrt{\lambda}} \right] \right\}, \quad (8.37)$$

$$\begin{aligned} \sigma_{\text{EDM}}^{\gamma p \to \pi^0 p} =& Q \frac{\alpha_{\text{em}} \overline{g}_0 g_A}{\sqrt{2} f_\pi M w^3 (1+2w)} \left\{ (-4 + \zeta_{\pi N}^2 + 2w(\zeta_{\pi N}^2 - 3))\sqrt{\lambda} \right. \\ & \left. - 2(1+2w)(\zeta_{\pi N}^2 - 2(2+w)) \text{arccoth} \left[\frac{2(1+w) - \zeta_{\pi N}^2}{\sqrt{\lambda}} \right] \right\}, \end{aligned} \quad (8.38)$$

$$\begin{aligned} \sigma_{\text{EDM}}^{\gamma n \to \pi^- p} =& Q \frac{2\alpha_{\text{em}} \overline{g}_0 g_A}{\sqrt{2} f_\pi M w^3 (1+2w)} \left\{ (\zeta_{\pi N}^2 - 2)\sqrt{\lambda} \right. \\ & \left. + 2(\zeta_{\pi N}^2 + w) \text{arccoth} \left[\frac{4w(1+w) + \lambda + 2\zeta_{\pi N}^2 - \zeta_{\pi N}^4}{2\sqrt{\lambda}(2w+1)} \right] \right\}. \end{aligned} \quad (8.39)$$

where $w = \nu/M$ is the dimensionless energy, and $\lambda \equiv \lambda(\sqrt{1+2w}, \zeta_{\pi N}, 1)$ is the Källen function. Integration of these cross sections according to the sum rule (8.17) yields:

$$\frac{M^3}{8\pi^2 \alpha_{\text{em}}} \lim_{Q^2 \to 0} \int d\nu \frac{1}{Q} \left[\sigma_{\text{EDM}}^{\gamma p \to \pi^+ n} + \sigma_{\text{EDM}}^{\gamma p \to \pi^0 p} \right] (\nu, Q^2) = \mathfrak{d}^p + \frac{\overline{g}_0 g_A}{f_\pi} \frac{1}{4\pi^2}, \quad (8.40)$$

$$\frac{M^3}{8\pi^2 \alpha_{\text{em}}} \lim_{Q^2 \to 0} \int d\nu \frac{1}{Q} \left[\sigma_{\text{EDM}}^{\gamma n \to \pi^- p} \right] (\nu, Q^2) = \frac{\overline{g}_0 g_A}{f_\pi} \frac{1}{2\pi^2}. \quad (8.41)$$

8.3 Summary and conclusions

We have extended the framework of forward doubly-virtual Compton scattering to include cases of parity and time-reversal invariance violations, thereby establishing new sum rules for the anapole moment (8.19) and electric dipole moment (8.17). These sum rules have been perturbatively tested in BχPT, which was extended to account for parity and time-reversal violations. In all cases, the sum rule integrals were convergent but affected by asymptotic constants. Similar to the Schwinger sum rule in χPT (cf. Sect. 6.3), we propose treating these constants as artifacts of low-energy theories, which should be absent in properly UV-completed theories. Furthermore, neither of the sum rules (8.19) and (8.17) is likely to be affected by problematic high-energy behavior due to the absence of Pomeron contributions in these channels. The only possibility might be a parity-violating Odderon, whose existence is questionable and, to the best of our knowledge, has not been evidently observed in available data. Consequently, we consider the derived sum rules to be valid.

The direct practical application of these derived relations is somewhat nuanced. In the case of parity violation, alongside the electromagnetic interaction described by the anapole moment contribution, one must consider weak contributions primarily stemming from Z^0 boson exchange, which is beyond the scope of the considered Compton scattering formalism. Moreover, the experimental measurement

of polarized cross sections with virtual photons, necessary for these sum rules, presents a significant experimental challenge. For instance, determining the EDM of the neutron requires knowledge of the corresponding cross sections to an extremely high precision. Therefore, the primary application of these derived sum rules may lie in providing additional constraints on new physics models and testing their self-consistency.

Appendices

8.A Born contributions

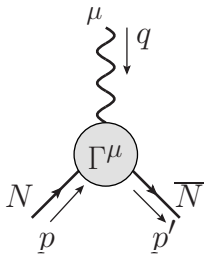

Fig. 8.4 Electromagnetic vertex of spin-1/2 particle N.

Let us consider the electromagnetic current of the spin-1/2 particle N with mass M, which violates P and T symmetries. The gauge-invariant γNN vertex, shown in Fig. 8.4 can be then parameterized in the following way:

$$\bar{u}(\vec{p}\,')\Gamma^{\mu}(q^2)u(\vec{p}) = \bar{u}(\vec{p}\,')\left[\gamma^{\mu}\mathcal{F}_1(q^2) + \frac{i\sigma^{\mu\nu}q_{\nu}}{2M}\mathcal{F}_2(q^2) + \frac{q^2\gamma^{\mu} - \not{q}q^{\mu}}{M^2}\gamma_5\mathcal{G}_1(q^2) + \frac{i\sigma^{\mu\nu}q_{\nu}}{2M}\gamma_5\mathcal{G}_2(q^2)\right]u(\vec{p}), \tag{8.42}$$

$$q_{\mu}\bar{u}(\vec{p}\,')\Gamma^{\mu}(q^2)u(\vec{p}) = 0. \tag{8.43}$$

Along with Dirac and Pauli form factors, $\mathcal{F}_1$ and $\mathcal{F}_2$, it contains the anapole form factor $\mathcal{G}_1$ and the electric dipole form factor $\mathcal{G}_2$. At the limit of zero photon virtuality, the anapole form factor corresponds to the anapole moment, $\mathcal{G}_1(Q^2 \to 0) = \mathfrak{a}$, while the electric dipole form factor yields the EDM, $\mathcal{G}_2(Q^2 \to 0) = \mathfrak{d}$ of the target particle. These observables correspond to the following non-relativistic electromagnetic interactions

$$\mathcal{H}_{\text{int}}^{\text{anapole}} = -\mathfrak{a}\,\vec{\sigma}\cdot\left[\vec{\nabla}\times\vec{B} - \frac{\partial\vec{E}}{\partial t}\right], \quad \mathcal{H}_{\text{int}}^{\text{EDM}} = -\frac{\mathfrak{d}}{2M}\vec{\sigma}\cdot\vec{E}, \tag{8.44}$$

where $\vec{E}$ and $\vec{B}$ are electric and magnetic fields, respectively, and $\vec{\sigma}$ is the spin vector of Pauli matrices. Substituting this vertex into the Born graph of Compton scattering, we obtain the following Born contributions to the invariant amplitudes T_i and S_i:

$$T_1^{\text{Born}} = -\frac{\mathcal{F}_1^2 + \frac{Q^4}{M^4}\mathcal{G}_1^2}{4\pi M} + \frac{Q^4}{4\pi M}\frac{(\mathcal{F}_1+\mathcal{F}_2)^2 + \frac{4Q^2}{M^2}\left(1+\frac{Q^2}{4M^2}\right)\mathcal{G}_1^2}{Q^4 - 4M^2\nu^2}, \tag{8.45a}$$

$$T_2^{\text{Born}} = \frac{MQ^2}{\pi(Q^4 - 4M^2\nu^2)}\left[\mathcal{F}_1^2 + \frac{Q^2}{4M^2}(\mathcal{F}_2^2 - \mathcal{G}_2^2) + \frac{Q^4}{M^4}\mathcal{G}_1^2\right], \tag{8.45b}$$

$$T_3^{\text{Born}} = -\frac{2Q^4(\mathcal{F}_1+\mathcal{F}_2)\mathcal{G}_1}{\pi M(Q^4-4M^2\nu^2)} \tag{8.45c}$$

$$S_1^{\text{Born}} = \frac{1}{8\pi M}(\mathcal{F}_2^2-\mathcal{G}_2^2) - \frac{Q^2M}{2\pi}\frac{\mathcal{F}_1(\mathcal{F}_1+\mathcal{F}_2)+\mathcal{G}_1^2\frac{Q^4}{M^4}}{Q^4-4M^2\nu^2} \tag{8.45d}$$

$$\begin{aligned} S_2^{\text{Born}} &= \frac{M^2\nu\left[\mathcal{F}_2(\mathcal{F}_1+\mathcal{F}_2)+4\mathcal{G}_1^2\frac{Q^2}{M^2}\right]}{2\pi(Q^4-4M^2\nu^2)} \\ &= -\frac{1}{8\pi\nu}\left[\mathcal{F}_2(\mathcal{F}_1+\mathcal{F}_2)+4\mathcal{G}_1^2\frac{Q^2}{M^2}\right] + \frac{Q^4}{8\pi\nu}\frac{\mathcal{F}_2(\mathcal{F}_1+\mathcal{F}_2)+4\mathcal{G}_1^2\frac{Q^2}{M}}{Q^4-4M^2\nu^2}, \end{aligned} \tag{8.45e}$$

$$S_3^{\text{Born}} = -\frac{Q^2}{2\pi M^2\nu}\mathcal{F}_2\mathcal{G}_1 - \frac{2Q^4}{\pi\nu(Q^4-4M^2\nu^2)}\left[\mathcal{F}_1-\frac{Q^2}{4M^2}\mathcal{F}_2\right]\mathcal{G}_1, \tag{8.45f}$$

$$S_4^{\text{Born}} = -\frac{2Q^4\mathcal{F}_1\mathcal{G}_1}{\pi\nu(Q^4-4M^2\nu^2)}, \tag{8.45g}$$

$$S_5^{\text{Born}} = \frac{Q^2(\mathcal{F}_1+\mathcal{F}_2)\mathcal{G}_1}{2\pi M^2\nu} - \frac{Q^6(\mathcal{F}_1+\mathcal{F}_2)\mathcal{G}_1}{2\pi M^2\nu(Q^4-4M^2\nu^2)}, \tag{8.45h}$$

$$S_6^{\text{Born}} = \frac{Q^2}{4\pi M^2\nu}(\mathcal{F}_1+\mathcal{F}_2)\mathcal{G}_2 - \frac{Q^6}{4\pi M^2\nu}\frac{(\mathcal{F}_1+\mathcal{F}_2)\mathcal{G}_2}{Q^4-4M^2\nu^2}, \tag{8.45i}$$

$$S_7^{\text{Born}} = -\frac{Q^2}{2\pi M^2\nu}\mathcal{G}_1\mathcal{G}_2 + \frac{Q^6}{2\pi M^2\nu}\frac{\mathcal{G}_1\mathcal{G}_2}{Q^4-4M^2\nu^2}. \tag{8.45j}$$

Chapter 9

Summary and outlook

In this thesis, several outstanding problems in contemporary hadronic physics, with a particular focus on exotic hadrons, LbL scattering, the muon AMM, Compton scattering and electromagnetic polarizabilities, have been addressed. The key findings are summarized below, accompanied by a brief outlook on potential directions for future research.

1. **Summary:** An improved parametrization for elastic partial-wave amplitudes based on the dispersive representations for the inverse amplitudes was proposed. This so-called dispersive inverse amplitude approach (DIA) rigorously incorporates unitarity and analyticity constraints. The left-hand cut contributions were accounted for in a model-independent manner using an expansion in a conformal variable that maps the left-hand cut plane onto the unit circle. Special attention was given to the S-wave scattering, considering the possible Adler zero contribution, while higher partial waves were treated with carefully implemented angular momentum barrier factors. Our method generalizes existing approaches like the inverse amplitude method and its modified versions, without relying on specific Lagrangian-based forms for the left-hand cuts and subtraction constants. This generality is particularly advantageous for analyzing lattice calculations with relatively large pion masses or for scattering processes involving particles like $\pi\pi$, πK, πD, and KD. Additionally, these parametrizations are beneficial for fitting experimental data constrained by Roy-like equations or forward dispersion relations. The framework's generality makes it a robust tool for analyzing any lattice or experimental data within the elastic scattering region.

   Outlook: Although the DIA method may be employed in future lattice analyses, it can compete with the mIAM method in the context of chiral extrapolation. By incorporating the essence of χPT through Adler zero or threshold parameters while fitting highly precise lattice QCD data, the DIA could impose additional constraints on the low-energy constants.

2. **Summary:** In exploring the real LbL scattering in ultraperipheral heavy-ion collisions, we developed a phenomenological model based on forward LbL sum rules that treat both low-energy and Regge high-energy regions uniformly. This model relies on only three observables (polarized

$\gamma\gamma \to$ hadrons cross sections) pertinent to forward real LbL scattering. We demonstrated, through various examples like QED, sQED, and scalar meson exchange contributions, that this minimal input suffices for a satisfactory low-energy description. For the pQCD region at high energies, direct calculations of leading pQCD contributions are necessary, and we proposed a systematic matching between the low-energy plus Regge regions and the pQCD regime. This model serves as a practical background estimate for LbL scattering at all scattering angles and can be readily incorporated into existing LbL event simulators, which is highly beneficial for future LHC runs.

We also investigated the sensitivity of LbL scattering to new physics by analyzing the contributions from newly observed states in the di-J/ψ mass spectrum, which have been identified by the LHCb Collaboration and confirmed by CMS and ATLAS. We estimated their two-photon decay widths using various methods, including the VMD model, quark models treating the resonances as diquark-antidiquark bound states, and by fitting the resonance parameters to LbL scattering data measured by ATLAS. Our findings suggest that these states could account for the mild excess observed in the LbL scattering data over the SM predictions between 5 and 10 GeV. The extracted two-photon decay widths hint at a diquark–antidiquark nature of at least one of the tetraquark states.

Outlook: In order to draw statistically significant conclusions, more LbL scattering data from future LHC runs are necessary. Additionally, prospective measurements of two-photon hadroproduction in ultraperipheral heavy-ion collisions offer an alternative and clean channel to study these exotic states. Complemented by lattice QCD studies, these experiments could elucidate the nature of fully charmed tetraquarks in detail, identifying their internal structures and quantum numbers.

3. **Summary:** Further, we derived a Cottingham-like formula for the leading electromagnetic correction to the HVP, expressed primarily in terms of the traced forward hadronic LbL scattering amplitude. Despite being a physical amplitude, contracting the incoming and outgoing photon lines leads to a logarithmically divergent momentum integral in the UV region. We outlined the necessary counterterms to cancel this divergence using the OPE and verified all the results in QED and sQED at two loops. Importantly, the finite parts of these counterterms are sensitive to the specific point in the parameter space of isospin-symmetric QCD chosen as the basis for calculating isospin-breaking effects.

   Implementing the Cottingham-like formula with a finite regulator on the order of a few hundred MeV appears to be the most promising approach. This regularization involves replacing the internal photon line with a Pauli-Villars regulated propagator or any convenient form of propagator regularization. The leading QED correction to the HVP, with such a regularized photon propagator, can be computed in lattice QCD using coordinate-space techniques similar to those used for calculating the HLbL contribution to the muon AMM, while avoiding power-law finite-size effects. This approach is particularly natural when working on very large lattices, as

demonstrated in master-field simulations. Within this new method, a direct comparison becomes possible between the lattice QCD calculation and the Cottingham-like formula prediction. For the latter, it is crucial that the traced forward HLbL amplitude can be represented dispersively in terms of the $\gamma^*\gamma^* \to$ hadrons fusion cross section, with one subtraction term. The lattice provides UV regularization, eliminating the need to handle the photon zero mode on a finite lattice due to the photon mass introduced in the regularization.

Outlook: The proposed approach to electromagnetic corrections to the HVP should be fully implemented on the lattice, an effort that is already underway. Future measurements of polarized two-photon fusion cross sections, involving photons with space-like virtualities, will enable data-driven results based on the dispersive formulation of a Cottingham-like formula. Within the framework of the original Cottingham formula, there is potential to compute the electromagnetic contribution to the proton-neutron mass difference using a regularized photon propagator on the lattice. Such a computation could then be directly compared, without scheme-dependent uncertainties, to predictions from the well-established dispersive treatment of the forward Compton amplitude.

4. **Summary:** We examined the Schwinger sum rule approach to the hadronic contributions to the AMM of the muon. Starting with basic examples of neutral scalar, pseudoscalar, vector, and axial-vector contributions at the one-loop level, we identified contributions influenced by asymptotic constants. According to the Sugawara–Kanazawa theorem, these constants, corresponding to the values of the amplitude at infinite energy, vanish in a complete calculation within a properly UV-completed theory, thereby validating the Schwinger sum rule. This cancellation was explicitly demonstrated in BχPT for the proton's AMM, where the theory was completed by the inclusion of the σ-meson. A similar result was found for the one-loop SM contributions to the muon's AMM arising from Z^0 and Higgs boson exchanges. However, for contributions from the $W^\pm$ bosons, certain caveats were identified, particularly related to virtual photons involved in the Schwinger sum rule observable, indicating that fully incorporating this contribution may require further modifications. Nonetheless, these challenges do not hinder the application of the Schwinger sum rule to the hadronic contributions to the muon's AMM, as the electroweak corrections influence the hadronic photoabsorption cross section only at higher orders.

   To demonstrate the applicability of the Schwinger sum rule to the HLbL correction to the muon AMM, we considered the leading contribution from the π^0 exchange. In terms of the photoabsorption cross section, the dominant contribution related to this exchange likely originates from the pion photoproduction channel. Using a simple VMD parametrization for the pion transition form factor, we obtained a reasonable estimate for the muon AMM from this channel. Other contributions were discussed and determined to be small, further supported by an estimation of contribution from one of the electromagnetic channels.

Outlook: A proper generalization of the Schwinger sum rule approach to the entire electroweak sector of the SM is of significant interest. Moreover, to provide stronger support for the Schwinger sum rule approach to the HLbL contribution to the muon AMM, quantitative estimates for the remaining channels, specifically II and IV, depicted in Fig. 6.16, should be provided. As soon as the LT-polarized cross section is measured in electron-muon scattering [1], the Schwinger sum rule will offer an alternative and fully data-driven check of the hadronic contributions to the AMM of the muon.

5. **Summary:** We also revisited the Bernabéu-Tarrach (BT) sum rule for the nucleon electric polarizability, concluding that it is valid in perturbative QFT, despite exhibiting slower convergence compared to the commonly used Baldin sum rule. Previous dismissals of this sum rule were based on its failure in perturbative QED tests, and heuristic arguments from Regge phenomenology. We established at least one simple example where the BT sum rule passes the perturbative test – the $\pi^+ n$ channel at LO BχPT. In other considered cases the sum rule holds up to a constant resulting from unphysical behavior of the virtual Compton scattering amplitude at infinite energy, an artifact understood within low-energy theories. The Regge behavior of the longitudinal photoabsorption cross section, σ_L, when naïvely inferred from the transversal photoabsorption cross section, σ_T, would invalidate the applicability of the unsubtracted dispersion relation for the longitudinal amplitude, T_L. An implication of the unsubtracted dispersion relation for T_L is a sum rule for the T_1 subtraction function, potentially allowing for a fully data-driven evaluation of the proton polarizability contribution to the Lamb shift in (muonic) hydrogen.

   In context of the BT sum rule, we also revisited the meson χPT result for the static electric polarizability of the neutral pion. By the alternative calculation in the light-front quark model with scalar quarks, we obtained a positive result for this polarizability, thus qualitatively contradicting the leading-order χPT result. However, the obtained contradiction can be interpreted as a quark-connected contribution, which, in terms of the lattice QCD, should be supplemented with a (possibly negative and large) disconnected one. This disconnected contribution may then correspond with a charged-pion loop between the photons and the neutral pion in the LO χPT result, as shown in Fig. 9.1.

   Outlook: Although the naïve parton model suggests a significant suppression of σ_L/σ_T with increasing energy, the Regge behavior of the longitudinal cross section remains insufficiently understood to draw definitive conclusions. Future data from the Electron-Ion Collider (EIC) may provide deeper insights into this behavior. The data-driven evaluation of the subtraction function T_1 via the proposed sum rule requires high-quality parametrizations of $\sigma_L(\nu, Q^2)$

[1] For MuOnE kinematics, provided in [470], with a muon beam line energy E_μ = 150GeV, the coverage of the hadroproduction region starting from the pion photoproduction up to 400 MeV requires detection of the scattered electrons at the energy $E'_e \approx 1$ GeV spanning the scattering angle $\theta_e = 0..3$ mrad.

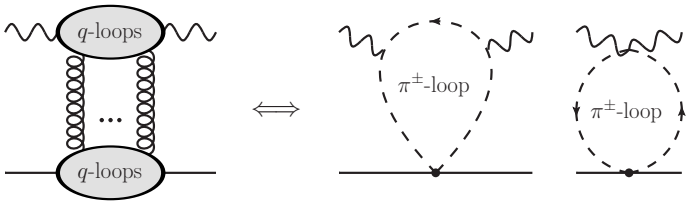

Fig. 9.1 Disconnected contributions to the forward Compton scattering on a nucleon or pion in lattice QCD (left) and the associated terms in χPT (left).

for the proton. We expect that including the two-pion production channel, in addition to the single-pion production parametrized by MAID, will sufficiently saturate the sum rule.

Concerning the neutral pion electric polarizability, the lattice QCD calculation of these separate contributions is highly desirable. The obtained results, in turn, should be compared to the upcoming calculation in the light-front quark model with spin-1/2 quarks.

6. **Summary:** Finally, we extended the framework of forward doubly-virtual Compton scattering to include cases of parity and time-reversal invariance violations, establishing new sum rules for the anapole moment and EDM. These sum rules were perturbatively tested in BχPT, which was extended to account for parity and time-reversal violations. In all cases, the sum rule integrals were convergent but affected by asymptotic constants. Similar to the Schwinger sum rule in χPT, we propose treating these constants as artifacts of low-energy theories, which should be absent in properly UV-completed theories. The derived sum rules are likely valid due to the absence of Pomeron contributions in these channels. Practical applications of these relations are nuanced; for instance, measuring the EDM of the neutron requires knowledge of corresponding cross sections to extremely high precision, presenting significant experimental challenges. Therefore, the primary application of these sum rules may lie in providing additional constraints on new physics models and testing their self-consistency.

   Outlook: Further testing of these sum rules in the SM and its extensions is an intriguing avenue for exploration, which already requires a generalization of the framework to properly account for all electroweak contributions. On the experimental side, precise measurements of doubly-polarized electron-proton scattering are essential.

Nomenclature

Greek Symbols

α_{em}	electromagnetic fine structure constant
$\varkappa$	anomalous magnetic moment

Acronyms / Abbreviations

AMM	anomalous magnetic moment
BχPT	(covariant) baryon chiral perturbation theory
c.o.m	center-of-momentum frame
c.o.m.	center-of-momentum frame
d.o.f.	degree(s) of freedom
EDM	electric dipole moment
HLbL	hadronic light-by-light
HVP	hadronic vacuum polarization
LbL	light-by-light
LO	leading order
NLO	next-to-leading order
NNLO	next-to-next-to-leading order
ppm	parts per million
pQCD	perturbative quantum chromodynamics
QCD	quantum chromodynamics
QED	quantum electrodynamics

QFT	quantum field theory
SM	Standard Model
sQED	scalar quantum electrodynamics (with scalar electrons)
UV	ultraviolet
VMD	vector meson dominance
VP	vacuum polarization

References

[1] D. Binosi, J. Collins, C. Kaufhold, and L. Theussl, "JaxoDraw: A Graphical user interface for drawing Feynman diagrams. Version 2.0 release notes," *Comput. Phys. Commun.* **180** (2009) 1709–1715, arXiv:0811.4113 [hep-ph].

[2] "Wolfram Mathematica v. 13.3" https://www.wolfram.com/mathematica/.

[3] https://superchic.hepforge.org.

[4] https://www.adobe.com/products/illustrator.html.

[5] H. H. Patel, "Package-X: A Mathematica package for the analytic calculation of one-loop integrals," *Comput. Phys. Commun.* **197** (2015) 276–290, arXiv:1503.01469 [hep-ph].

[6] H. H. Patel, "Package-X 2.0: A Mathematica package for the analytic calculation of one-loop integrals," *Comput. Phys. Commun.* **218** (2017) 66–70, arXiv:1612.00009 [hep-ph].

[7] T. Hahn and M. Perez-Victoria, "Automatized one loop calculations in four-dimensions and D-dimensions," *Comput. Phys. Commun.* **118** (1999) 153–165, arXiv:hep-ph/9807565.

[8] J. A. M. Vermaseren, "New features of FORM," arXiv:math-ph/0010025.

[9] https://chatgpt.com.

[10] H. Yukawa, "On the Interaction of Elementary Particles I," *Proc. Phys. Math. Soc. Jap.* **17** (1935) 48–57.

[11] M. Gell-Mann, "Isotopic Spin and New Unstable Particles," *Phys. Rev.* **92** (1953) 833–834.

[12] K. Nishijima, "Charge Independence Theory of V Particles," *Prog. Theor. Phys.* **13** no. 3, (1955) 285–304.

[13] M. Gell-Mann, "The interpretation of the new particles as displaced charge multiplets," *Nuovo Cim.* **4** no. S2, (1956) 848–866.

[14] M. Gell-Mann, "The Eightfold Way: A Theory of strong interaction symmetry,".

[15] Y. Ne'eman, "Derivation of strong interactions from a gauge invariance," *Nucl. Phys.* **26** (1961) 222–229.

[16] M. Gell-Mann, "A Schematic Model of Baryons and Mesons," *Phys. Lett.* **8** (1964) 214–215.

[17] G. Zweig, *An SU(3) model for strong interaction symmetry and its breaking. Version 2*, pp. 22–101. 2, 1964.

[18] O. W. Greenberg, "Spin and Unitary Spin Independence in a Paraquark Model of Baryons and Mesons," *Phys. Rev. Lett.* **13** (1964) 598–602.

[19] M. Y. Han and Y. Nambu, "Three Triplet Model with Double SU(3) Symmetry," *Phys. Rev. B* **139** (1965) 1006–1010.

[20] L. D. Landau, A. A. Abrikosov, and I. M. Khalatnikov, "The Removal of Infinities in Quantum Electrodynamics," *Dokl. Akad. Nauk SSSR* **95** (1954) .

[21] L. D. Landau and I. Y. Pomeranchuk, "On point interactions in quantum electrodynamics," *Dokl. Akad. Nauk SSSR* **102** no. 3, (1955) 489–492.

[22] L. D. Landau, A. Abrikosov, and L. Halatnikov, "On the Quantum theory of fields," *Nuovo Cim. Suppl.* **3** (1956) 80–104.

[23] M. Breidenbach, J. I. Friedman, H. W. Kendall, E. D. Bloom, D. H. Coward, H. C. DeStaebler, J. Drees, L. W. Mo, and R. E. Taylor, "Observed behavior of highly inelastic electron-proton scattering," *Phys. Rev. Lett.* **23** (1969) 935–939.

[24] R. P. Feynman, "Very high-energy collisions of hadrons," *Phys. Rev. Lett.* **23** (1969) 1415–1417.

[25] H. Fritzsch, M. Gell-Mann, and H. Leutwyler, "Advantages of the Color Octet Gluon Picture," *Phys. Lett. B* **47** (1973) 365–368.

[26] G. 't Hooft, "Renormalizable Lagrangians for Massive Yang-Mills Fields," *Nucl. Phys. B* **35** (1971) 167–188.

[27] G. 't Hooft and M. J. G. Veltman, "Regularization and Renormalization of Gauge Fields," *Nucl. Phys. B* **44** (1972) 189–213.

[28] L. D. Faddeev and V. N. Popov, "Feynman Diagrams for the Yang-Mills Field," *Phys. Lett. B* **25** (1967) 29–30.

[29] D. J. Gross and F. Wilczek, "Ultraviolet Behavior of Nonabelian Gauge Theories," *Phys. Rev. Lett.* **30** (1973) 1343–1346.

[30] H. D. Politzer, "Reliable Perturbative Results for Strong Interactions?," *Phys. Rev. Lett.* **30** (1973) 1346–1349.

[31] K. G. Wilson, "Confinement of Quarks," *Phys. Rev. D* **10** (1974) 2445–2459.

[32] **BMW** Collaboration, S. Durr *et al.*, "Ab-Initio Determination of Light Hadron Masses," *Science* **322** (2008) 1224–1227, `arXiv:0906.3599 [hep-lat]`.

[33] S. Weinberg, "Phenomenological Lagrangians," *Physica A* **96** no. 1-2, (1979) 327–340.

[34] J. Gasser and H. Leutwyler, "Chiral Perturbation Theory to One Loop," *Ann. Phys.* **158** (1984) 142.

[35] J. Gasser and H. Leutwyler, "Chiral Perturbation Theory: Expansions in the Mass of the Strange Quark," *Nucl. Phys. B* **250** (1985) 465–516.

[36] J. Gasser, M. E. Sainio, and A. Svarc, "Nucleons with chiral loops," *Nucl. Phys. B* **307** (1988) 779–853.

[37] G. Colangelo, J. Gasser, and H. Leutwyler, "$\pi\pi$ scattering," *Nucl. Phys. B* **603** (2001) 125–179, `arXiv:hep-ph/0103088`.

[38] V. Bernard, N. Kaiser, and U.-G. Meissner, "Chiral dynamics in nucleons and nuclei," *Int. J. Mod. Phys. E* **4** (1995) 193–346, arXiv:hep-ph/9501384.

[39] V. Lensky and V. Pascalutsa, "Predictive powers of chiral perturbation theory in Compton scattering off protons," *Eur. Phys. J. C* **65** (2010) 195–209, arXiv:0907.0451 [hep-ph].

[40] **LHCb** Collaboration, R. Aaij *et al.*, "Observation of structure in the J/ψ -pair mass spectrum," *Sci. Bull.* **65** no. 23, (2020) 1983–1993, arXiv:2006.16957 [hep-ex].

[41] **LHCb** Collaboration, R. Aaij *et al.*, "Observation of a narrow pentaquark state, $P_c(4312)^+$, and of two-peak structure of the $P_c(4450)^+$," *Phys. Rev. Lett.* **122** no. 22, (2019) 222001, arXiv:1904.03947 [hep-ex].

[42] **LHCb** Collaboration, R. Aaij *et al.*, "Observation of $J/\psi p$ Resonances Consistent with Pentaquark States in $\Lambda_b^0 \to J/\psi K^- p$ Decays," *Phys. Rev. Lett.* **115** (2015) 072001, arXiv:1507.03414 [hep-ex].

[43] **COMPASS** Collaboration, C. Adolph *et al.*, "Odd and even partial waves of $\eta\pi^-$ and $\eta'\pi^-$ in $\pi^- p \to \eta^{(\prime)}\pi^- p$ at 191 GeV/c," *Phys. Lett. B* **740** (2015) 303–311, arXiv:1408.4286.

[44] R. Garcia-Martin, R. Kaminski, J. Pelaez, J. Ruiz de Elvira, and F. Yndurain, "The Pion-pion scattering amplitude. IV: Improved analysis with once subtracted Roy-like equations up to 1100 MeV," *Phys. Rev. D* **83** (2011) 074004, arXiv:1102.2183.

[45] R. Garcia-Martin, R. Kaminski, J. R. Pelaez, and J. Ruiz de Elvira, "Precise determination of the f0(600) and f0(980) pole parameters from a dispersive data analysis," *Phys. Rev. Lett.* **107** (2011) 072001, arXiv:1107.1635 [hep-ph].

[46] J. R. Pelaez, A. Rodas, and J. Ruiz De Elvira, "Global parameterization of $\pi\pi$ scattering up to 2 GeV," *Eur. Phys. J. C* **79** no. 12, (2019) 1008, arXiv:1907.13162 [hep-ph].

[47] B. Ananthanarayan, G. Colangelo, J. Gasser, and H. Leutwyler, "Roy equation analysis of pi pi scattering," *Phys. Rept.* **353** (2001) 207–279, arXiv:hep-ph/0005297.

[48] I. Caprini, G. Colangelo, and H. Leutwyler, "Mass and width of the lowest resonance in QCD," *Phys. Rev. Lett.* **96** (2006) 132001, arXiv:hep-ph/0512364.

[49] H. Leutwyler, "Model independent determination of the sigma pole," *AIP Conf. Proc.* **1030** no. 1, (2008) 46–55, arXiv:0804.3182 [hep-ph].

[50] P. Buettiker, S. Descotes-Genon, and B. Moussallam, "A new analysis of pi K scattering from Roy and Steiner type equations," *Eur. Phys. J. C* **33** (2004) 409–432, arXiv:hep-ph/0310283.

[51] S. Descotes-Genon and B. Moussallam, "The $K_0^*(800)$ scalar resonance from Roy-Steiner representations of πK scattering," *Eur. Phys. J. C* **48** (2006) 553, arXiv:hep-ph/0607133.

[52] J. R. Peláez and A. Rodas, "Determination of the lightest strange resonance $K_0^*(700)$ or κ, from a dispersive data analysis," *Phys. Rev. Lett.* **124** no. 17, (2020) 172001, arXiv:2001.08153 [hep-ph].

[53] J. Peláez and A. Rodas, "Dispersive $\pi K \to \pi K$ and $\pi\pi \to K\bar{K}$ amplitudes from scattering data, threshold parameters and the lightest strange resonance κ or $K_0^*(700)$," *Phys. Rept.* **969** (2022) 1–126, arXiv:2010.11222.

[54] S. M. Roy, "Exact integral equation for pion pion scattering involving only physical region partial waves," *Phys. Lett. B* **36** (1971) 353–356.

[55] S. Prelovsek, T. Draper, C. B. Lang, M. Limmer, K.-F. Liu, N. Mathur, and D. Mohler, "Lattice study of light scalar tetraquarks with $I = 0, 2, 1/2, 3/2$: Are σ and κ tetraquarks?," *Phys. Rev. D* **82** (2010) 094507, arXiv:1005.0948 [hep-lat].

[56] R. A. Briceno, J. J. Dudek, and R. D. Young, "Scattering processes and resonances from lattice QCD," *Rev. Mod. Phys.* **90** no. 2, (2018) 025001, arXiv:1706.06223 [hep-lat].

[57] M. R. Shepherd, J. J. Dudek, and R. E. Mitchell, "Searching for the rules that govern hadron construction," *Nature* **534** no. 7608, (2016) 487–493, arXiv:1802.08131 [hep-ph].

[58] R. A. Briceno, J. J. Dudek, R. G. Edwards, and D. J. Wilson, "Isoscalar $\pi\pi$ scattering and the σ meson resonance from QCD," *Phys. Rev. Lett.* **118** no. 2, (2017) 022002, arXiv:1607.05900 [hep-ph].

[59] D. Guo, A. Alexandru, R. Molina, M. Mai, and M. Döring, "Extraction of isoscalar $\pi\pi$ phase-shifts from lattice QCD," *Phys. Rev.* **D98** no. 1, (2018) 014507, arXiv:1803.02897.

[60] D. J. Wilson, R. A. Briceno, J. J. Dudek, R. G. Edwards, and C. E. Thomas, "The quark-mass dependence of elastic πK scattering from QCD," *Phys. Rev. Lett.* **123** no. 4, (2019) 042002, arXiv:1904.03188 [hep-lat].

[61] G. Rendon, L. Leskovec, S. Meinel, J. Negele, S. Paul, M. Petschlies, A. Pochinsky, G. Silvi, and S. Syritsyn, "$I = 1/2$ S-wave and P-wave $K\pi$ scattering and the κ and K^* resonances from lattice QCD," *Phys. Rev. D* **102** no. 11, (2020) 114520, arXiv:2006.14035 [hep-lat].

[62] **Hadron Spectrum** Collaboration, L. Gayer, N. Lang, S. M. Ryan, D. Tims, C. E. Thomas, and D. J. Wilson, "Isospin-1/2 Dπ scattering and the lightest D_0^* resonance from lattice QCD," *JHEP* **07** (2021) 123, arXiv:2102.04973 [hep-lat].

[63] **Hadron Spectrum** Collaboration, G. K. C. Cheung, C. E. Thomas, D. J. Wilson, G. Moir, M. Peardon, and S. M. Ryan, "DK I = 0, $D\overline{K}$ I = 0, 1 scattering and the $D_{s0}^*(2317)$ from lattice QCD," *JHEP* **02** (2021) 100, arXiv:2008.06432 [hep-lat].

[64] S. Prelovsek, S. Collins, D. Mohler, M. Padmanath, and S. Piemonte, "Charmonium-like resonances with $J^{PC} = 0^{++}, 2^{++}$ in coupled $D\overline{D}$, $D_s\overline{D}_s$ scattering on the lattice," *JHEP* **06** (2021) 035, arXiv:2011.02542 [hep-lat].

[65] C. B. Lang, L. Leskovec, D. Mohler, S. Prelovsek, and R. M. Woloshyn, "Ds mesons with DK and D*K scattering near threshold," *Phys. Rev. D* **90** no. 3, (2014) 034510, arXiv:1403.8103 [hep-lat].

[66] G. F. Chew and S. Mandelstam, "Theory of low-energy pion pion interactions," *Phys. Rev.* **119** (1960) 467–477.

[67] C. F. von Weizsacker, "Radiation emitted in collisions of very fast electrons," *Z. Phys.* **88** (1934) 612–625.

[68] E. J. Williams, "Nature of the high-energy particles of penetrating radiation and status of ionization and radiation formulae," *Phys. Rev.* **45** (1934) 729–730.

[69] V. Budnev, I. Ginzburg, G. Meledin, and V. Serbo, "The Two photon particle production mechanism. Physical problems. Applications. Equivalent photon approximation," *Phys.Rept.* **15** (1975) 181–281.

[70] D. d'Enterria and G. G. da Silveira, "Observing light-by-light scattering at the Large Hadron Collider," *Phys. Rev. Lett.* **111** (2013) 080405, arXiv:1305.7142 [hep-ph]. [Erratum: Phys.Rev.Lett. 116, 129901 (2016)].

[71] **ATLAS** Collaboration, M. Aaboud *et al.*, "Evidence for light-by-light scattering in heavy-ion collisions with the ATLAS detector at the LHC," *Nature Phys.* **13** no. 9, (2017) 852–858, arXiv:1702.01625 [hep-ex].

[72] **ATLAS** Collaboration, G. Aad *et al.*, "Observation of light-by-light scattering in ultraperipheral Pb+Pb collisions with the ATLAS detector," *Phys. Rev. Lett.* **123** no. 5, (2019) 052001, arXiv:1904.03536 [hep-ex].

[73] **ATLAS** Collaboration, G. Aad *et al.*, "Measurement of light-by-light scattering and search for axion-like particles with 2.2 nb^{-1} of Pb+Pb data with the ATLAS detector," *JHEP* **03** (2021) 243, arXiv:2008.05355 [hep-ex].

[74] **CMS** Collaboration, A. M. Sirunyan *et al.*, "Evidence for light-by-light scattering and searches for axion-like particles in ultraperipheral PbPb collisions at $\sqrt{s_{\text{NN}}} = 5.02$ TeV," *Phys. Lett. B* **797** (2019) 134826, arXiv:1810.04602 [hep-ex].

[75] M. Kłusek-Gawenda, P. Lebiedowicz, and A. Szczurek, "Light-by-light scattering in ultraperipheral Pb-Pb collisions at energies available at the CERN Large Hadron Collider," *Phys. Rev. C* **93** no. 4, (2016) 044907, arXiv:1601.07001 [nucl-th].

[76] L. A. Harland-Lang, V. A. Khoze, and M. G. Ryskin, "Exclusive LHC physics with heavy ions: SuperChic 3," *Eur. Phys. J. C* **79** no. 1, (2019) 39, arXiv:1810.06567 [hep-ph].

[77] https://superchic.hepforge.org.

[78] https://www.hepdata.net/record/ins1811464.

[79] A. A H, E. Chaubey, M. Fraaije, V. Hirschi, and H.-S. Shao, "Light-by-light scattering at next-to-leading order in QCD and QED," *Phys. Lett. B* **851** (2024) 138555, arXiv:2312.16956 [hep-ph].

[80] LHCb collaboration, "Observation of structure in the j/ψ-pair mass spectrum," *Science Bulletin* **65** no. 23, (Dec., 2020) 1983–1993. https://doi.org/10.1016/j.scib.2020.08.032.

[81] **CMS** Collaboration, A. Hayrapetyan *et al.*, "New Structures in the J/ψJ/ψ Mass Spectrum in Proton-Proton Collisions at s=13 TeV," *Phys. Rev. Lett.* **132** no. 11, (2024) 111901, arXiv:2306.07164 [hep-ex].

[82] **ATLAS** Collaboration, G. Aad *et al.*, "Observation of an Excess of Dicharmonium Events in the Four-Muon Final State with the ATLAS Detector," *Phys. Rev. Lett.* **131** no. 15, (2023) 151902, arXiv:2304.08962 [hep-ex].

[83] M. Lindner, M. Platscher, and F. S. Queiroz, "A Call for New Physics : The Muon Anomalous Magnetic Moment and Lepton Flavor Violation," *Phys. Rept.* **731** (2018) 1–82, arXiv:1610.06587 [hep-ph].

[84] F. Jegerlehner, "The Anomalous Magnetic Moment of the Muon," *Springer Tracts Mod. Phys.* **274** (2017) pp. 1–693.

[85] **Muon g-2** Collaboration, G. W. Bennett *et al.*, "Final Report of the Muon E821 Anomalous Magnetic Moment Measurement at BNL," *Phys. Rev. D* **73** (2006) 072003, arXiv:hep-ex/0602035.

[86] **Muon g-2** Collaboration, D. P. Aguillard *et al.*, "Detailed report on the measurement of the positive muon anomalous magnetic moment to 0.20 ppm," *Phys. Rev. D* **110** no. 3, (2024) 032009, arXiv:2402.15410 [hep-ex].

[87] T. Aoyama *et al.*, "The anomalous magnetic moment of the muon in the Standard Model," *Phys. Rept.* **887** (2020) 1–166, arXiv:2006.04822 [hep-ph].

[88] T. Aoyama, M. Hayakawa, T. Kinoshita, and M. Nio, "Complete Tenth-Order QED Contribution to the Muon $g-2$," *Phys. Rev. Lett.* **109** (2012) 111808, arXiv:1205.5370 [hep-ph].

[89] S. Volkov, "Calculating the five-loop QED contribution to the electron anomalous magnetic moment: Graphs without lepton loops," *Phys. Rev. D* **100** no. 9, (2019) 096004, arXiv:1909.08015 [hep-ph].

[90] S. Volkov, "Calculation of the total 10th order QED contribution to the electron magnetic moment," *Phys. Rev. D* **110** no. 3, (2024) 036001, arXiv:2404.00649 [hep-ph].

[91] A. Czarnecki, W. J. Marciano, and A. Vainshtein, "Refinements in electroweak contributions to the muon anomalous magnetic moment," *Phys. Rev. D* **67** (2003) 073006, arXiv:hep-ph/0212229. [Erratum: Phys.Rev.D 73, 119901 (2006)].

[92] C. Gnendiger, D. Stöckinger, and H. Stöckinger-Kim, "The electroweak contributions to $(g-2)_\mu$ after the Higgs boson mass measurement," *Phys. Rev. D* **88** (2013) 053005, arXiv:1306.5546 [hep-ph].

[93] T. Ishikawa, N. Nakazawa, and Y. Yasui, "Numerical calculation of the full two-loop electroweak corrections to muon (g-2)," *Phys. Rev. D* **99** no. 7, (2019) 073004, arXiv:1810.13445 [hep-ph].

[94] A. Kurz, T. Liu, P. Marquard, and M. Steinhauser, "Hadronic contribution to the muon anomalous magnetic moment to next-to-next-to-leading order," *Phys. Lett. B* **734** (2014) 144–147, arXiv:1403.6400 [hep-ph].

[95] M. Davier, A. Hoecker, B. Malaescu, and Z. Zhang, "Reevaluation of the hadronic vacuum polarisation contributions to the Standard Model predictions of the muon $g-2$ and $\alpha(m_Z^2)$ using newest hadronic cross-section data," *Eur. Phys. J. C* **77** no. 12, (2017) 827, arXiv:1706.09436 [hep-ph].

[96] A. Keshavarzi, D. Nomura, and T. Teubner, "Muon $g-2$ and $\alpha(M_Z^2)$: a new data-based analysis," *Phys. Rev. D* **97** no. 11, (2018) 114025, arXiv:1802.02995 [hep-ph].

[97] A. Keshavarzi, D. Nomura, and T. Teubner, "$g-2$ of charged leptons, $\alpha(M_Z^2)$, and the hyperfine splitting of muonium," *Phys. Rev. D* **101** no. 1, (2020) 014029, arXiv:1911.00367 [hep-ph].

[98] G. Colangelo, M. Hoferichter, and P. Stoffer, "Two-pion contribution to hadronic vacuum polarization," *JHEP* **02** (2019) 006, arXiv:1810.00007 [hep-ph].

[99] M. Hoferichter, B.-L. Hoid, and B. Kubis, "Three-pion contribution to hadronic vacuum polarization," *JHEP* **08** (2019) 137, arXiv:1907.01556 [hep-ph].

[100] M. Davier, A. Hoecker, B. Malaescu, and Z. Zhang, "A new evaluation of the hadronic vacuum polarisation contributions to the muon anomalous magnetic moment and to $\alpha(\mathbf{m_Z^2})$," *Eur. Phys. J. C* **80** no. 3, (2020) 241, arXiv:1908.00921 [hep-ph]. [Erratum: Eur.Phys.J.C 80, 410 (2020)].

[101] G. Colangelo, A. X. El-Khadra, M. Hoferichter, A. Keshavarzi, C. Lehner, P. Stoffer, and T. Teubner, "Data-driven evaluations of Euclidean windows to scrutinize hadronic vacuum polarization," *Phys. Lett. B* **833** (2022) 137313, arXiv:2205.12963 [hep-ph].

[102] C. Bouchiat and L. Michel, "La résonance dans la diffusion méson π— méson π et le moment magnétique anormal du méson μ," *J. Phys. Radium* **22** no. 2, (1961) 121–121.

[103] **CMD-2** Collaboration, R. R. Akhmetshin *et al.*, "Reanalysis of hadronic cross-section measurements at CMD-2," *Phys. Lett. B* **578** (2004) 285–289, arXiv:hep-ex/0308008.

[104] **CMD-2** Collaboration, V. M. Aul'chenko *et al.*, "Measurement of the pion form-factor in the range 1.04 – 1.38 GeV with the CMD-2 detector," *JETP Lett.* **82** (2005) 743–747, arXiv:hep-ex/0603021.

[105] **CMD-2** Collaboration, R. R. Akhmetshin *et al.*, "High-statistics measurement of the pion form factor in the rho-meson energy range with the CMD-2 detector," *Phys. Lett. B* **648** (2007) 28–38, arXiv:hep-ex/0610021.

[106] M. N. Achasov *et al.*, "Update of the $e^+e^- \to \pi^+\pi^-$ cross-section measured by spherical neutral detector in the energy region $400 < \sqrt{s} < 1000$ MeV," *J. Exp. Theor. Phys.* **103** (2006) 380–384, arXiv:hep-ex/0605013.

[107] **KLOE** Collaboration, F. Ambrosino *et al.*, "Measurement of $\sigma(e^+e^- \to \pi^+\pi^-)$ from threshold to 0.85 GeV^2 using Initial State Radiation with the KLOE detector," *Phys. Lett. B* **700** (2011) 102–110, arXiv:1006.5313 [hep-ex].

[108] **KLOE** Collaboration, D. Babusci *et al.*, "Precision measurement of $\sigma(e^+e^- \to \pi^+\pi^-\gamma)/\sigma(e^+e^- \to \mu^+\mu^-\gamma)$ and determination of the $\pi^+\pi^-$ contribution to the muon anomaly with the KLOE detector," *Phys. Lett. B* **720** (2013) 336–343, arXiv:1212.4524 [hep-ex].

[109] **BaBar** Collaboration, J. P. Lees *et al.*, "Precise Measurement of the $e^+e^- \to \pi^+\pi^-(\gamma)$ Cross Section with the Initial-State Radiation Method at BABAR," *Phys. Rev. D* **86** (2012) 032013, arXiv:1205.2228 [hep-ex].

[110] **BESIII** Collaboration, M. Ablikim *et al.*, "Measurement of the $e^+e^- \to \pi^+\pi^-$ cross section between 600 and 900 MeV using initial state radiation," *Phys. Lett. B* **753** (2016) 629–638, arXiv:1507.08188 [hep-ex]. [Erratum: Phys.Lett.B 812, 135982 (2021)].

[111] T. Xiao, S. Dobbs, A. Tomaradze, K. K. Seth, and G. Bonvicini, "Precision Measurement of the Hadronic Contribution to the Muon Anomalous Magnetic Moment," *Phys. Rev. D* **97** no. 3, (2018) 032012, arXiv:1712.04530 [hep-ex].

[112] **CMD-3** Collaboration, F. V. Ignatov *et al.*, "Measurement of the Pion Form Factor with CMD-3 Detector and its Implication to the Hadronic Contribution to Muon (g-2)," *Phys. Rev. Lett.* **132** no. 23, (2024) 231903, arXiv:2309.12910 [hep-ex].

[113] **CMD-3** Collaboration, F. V. Ignatov *et al.*, "Measurement of the e+e-$\to\pi$+π- cross section from threshold to 1.2 GeV with the CMD-3 detector," *Phys. Rev. D* **109** no. 11, (2024) 112002, arXiv:2302.08834 [hep-ex].

[114] **RBC, UKQCD** Collaboration, T. Blum, P. A. Boyle, V. Gülpers, T. Izubuchi, L. Jin, C. Jung, A. Jüttner, C. Lehner, A. Portelli, and J. T. Tsang, "Calculation of the hadronic vacuum polarization contribution to the muon anomalous magnetic moment," *Phys. Rev. Lett.* **121** no. 2, (2018) 022003, arXiv:1801.07224 [hep-lat].

[115] S. Borsanyi *et al.*, "Leading hadronic contribution to the muon magnetic moment from lattice QCD," *Nature* **593** no. 7857, (2021) 51–55, arXiv:2002.12347 [hep-lat].

[116] M. Cè *et al.*, "Window observable for the hadronic vacuum polarization contribution to the muon g-2 from lattice QCD," *Phys. Rev. D* **106** no. 11, (2022) 114502, arXiv:2206.06582 [hep-lat].

[117] **Extended Twisted Mass** Collaboration, C. Alexandrou *et al.*, "Lattice calculation of the short and intermediate time-distance hadronic vacuum polarization contributions to the muon magnetic moment using twisted-mass fermions," *Phys. Rev. D* **107** no. 7, (2023) 074506, arXiv:2206.15084 [hep-lat].

[118] **Fermilab Lattice, MILC, HPQCD** Collaboration, C. T. H. Davies *et al.*, "Windows on the hadronic vacuum polarization contribution to the muon anomalous magnetic moment," *Phys. Rev. D* **106** no. 7, (2022) 074509, arXiv:2207.04765 [hep-lat].

[119] A. Risch and H. Wittig, "Leading isospin breaking effects in the HVP contribution to a_μ and to the running of α," *PoS* **LATTICE2021** (2022) 106, arXiv:2112.00878 [hep-lat].

[120] **RM123** Collaboration, G. M. de Divitiis, R. Frezzotti, V. Lubicz, G. Martinelli, R. Petronzio, G. C. Rossi, F. Sanfilippo, S. Simula, and N. Tantalo, "Leading isospin breaking effects on the lattice," *Phys. Rev. D* **87** no. 11, (2013) 114505, arXiv:1303.4896 [hep-lat].

[121] G. Colangelo, M. Hoferichter, M. Procura, and P. Stoffer, "Dispersive approach to hadronic light-by-light scattering," *JHEP* **09** (2014) 091, arXiv:1402.7081.

[122] G. Colangelo, M. Hoferichter, B. Kubis, M. Procura, and P. Stoffer, "Towards a data-driven analysis of hadronic light-by-light scattering," *Phys. Lett. B* **738** (2014) 6–12, arXiv:1408.2517 [hep-ph].

[123] G. Colangelo, M. Hoferichter, M. Procura, and P. Stoffer, "Dispersion relation for hadronic light-by-light scattering: theoretical foundations," *JHEP* **09** (2015) 074, arXiv:1506.01386 [hep-ph].

[124] M. Knecht and A. Nyffeler, "Hadronic light by light corrections to the muon g-2: The Pion pole contribution," *Phys. Rev. D* **65** (2002) 073034, arXiv:hep-ph/0111058.

[125] T. Lenz, A. Denig, and C. F. Redmer, "Measurement of the Time-like Pion Transition Form Factor at BESIII," *EPJ Web Conf.* **212** (2019) 04013.

[126] A. Gérardin, H. B. Meyer, and A. Nyffeler, "Lattice calculation of the pion transition form factor with $N_f = 2+1$ Wilson quarks," *Phys. Rev. D* **100** no. 3, (2019) 034520, arXiv:1903.09471 [hep-lat].

[127] P. Masjuan and P. Sanchez-Puertas, "Pseudoscalar-pole contribution to the $(g_\mu - 2)$: a rational approach," *Phys. Rev. D* **95** no. 5, (2017) 054026, arXiv:1701.05829 [hep-ph].

[128] G. Colangelo, M. Hoferichter, M. Procura, and P. Stoffer, "Dispersion relation for hadronic light-by-light scattering: two-pion contributions," *JHEP* **04** (2017) 161, arXiv:1702.07347 [hep-ph].

[129] I. Danilkin, O. Deineka, and M. Vanderhaeghen, "Dispersive analysis of the $\gamma^*\gamma^* \to \pi\pi$ process," *Phys. Rev. D* **101** no. 5, (2020) 054008, arXiv:1909.04158 [hep-ph].

[130] M. Hoferichter and P. Stoffer, "Dispersion relations for $\gamma^*\gamma^* \to \pi\pi$: helicity amplitudes, subtractions, and anomalous thresholds," *JHEP* **07** (2019) 073, arXiv:1905.13198 [hep-ph].

[131] M. Hoferichter and P. Stoffer, "Asymptotic behavior of meson transition form factors," *JHEP* **05** (2020) 159, arXiv:2004.06127 [hep-ph].

[132] I. Danilkin, M. Hoferichter, and P. Stoffer, "A dispersive estimate of scalar contributions to hadronic light-by-light scattering," *Phys. Lett. B* **820** (2021) 136502, arXiv:2105.01666 [hep-ph].

[133] S. Holz, J. Plenter, C. W. Xiao, T. Dato, C. Hanhart, B. Kubis, U. G. Meißner, and A. Wirzba, "Towards an improved understanding of $\eta \to \gamma^*\gamma^*$," *Eur. Phys. J. C* **81** no. 11, (2021) 1002, arXiv:1509.02194 [hep-ph].

[134] S. Holz, C. Hanhart, M. Hoferichter, and B. Kubis, "A dispersive analysis of $\eta' \to \pi^+\pi^-\gamma$ and $\eta' \to \ell^+\ell^-\gamma$," *Eur. Phys. J. C* **82** no. 5, (2022) 434, arXiv:2202.05846 [hep-ph]. [Addendum: Eur.Phys.J.C 82, 1159 (2022)].

[135] M. Zanke, M. Hoferichter, and B. Kubis, "On the transition form factors of the axial-vector resonance $f_1(1285)$ and its decay into e^+e^-," *JHEP* **07** (2021) 106, arXiv:2103.09829 [hep-ph].

[136] M. Hoferichter, B. Kubis, and M. Zanke, "Axial-vector transition form factors and $e^+e^- \to f_1\pi^+\pi^-$," *JHEP* **08** (2023) 209, arXiv:2307.14413 [hep-ph].

[137] O. Deineka, I. Danilkin, and M. Vanderhaeghen, "A dispersive estimate of the $a_0(980)$ contribution to $(g-2)_\mu$," arXiv:2410.12894 [hep-ph].

[138] K. Melnikov and A. Vainshtein, "Hadronic light-by-light scattering contribution to the muon anomalous magnetic moment revisited," *Phys. Rev. D* **70** (2004) 113006, arXiv:hep-ph/0312226.

[139] G. Colangelo, F. Hagelstein, M. Hoferichter, L. Laub, and P. Stoffer, "Longitudinal short-distance constraints for the hadronic light-by-light contribution to $(g-2)_\mu$ with large-N_c Regge models," *JHEP* **03** (2020) 101, arXiv:1910.13432 [hep-ph].

[140] G. Colangelo, F. Hagelstein, M. Hoferichter, L. Laub, and P. Stoffer, "Short-distance constraints on hadronic light-by-light scattering in the anomalous magnetic moment of the muon," *Phys. Rev. D* **101** no. 5, (2020) 051501, arXiv:1910.11881 [hep-ph].

[141] J. Bijnens, N. Hermansson-Truedsson, L. Laub, and A. Rodríguez-Sánchez, "Short-distance HLbL contributions to the muon anomalous magnetic moment beyond perturbation theory," *JHEP* **10** (2020) 203, arXiv:2008.13487 [hep-ph].

[142] G. Colangelo, F. Hagelstein, M. Hoferichter, L. Laub, and P. Stoffer, "Short-distance constraints for the longitudinal component of the hadronic light-by-light amplitude: an update," *Eur. Phys. J. C* **81** no. 8, (2021) 702, arXiv:2106.13222 [hep-ph].

[143] J. Bijnens, N. Hermansson-Truedsson, L. Laub, and A. Rodríguez-Sánchez, "The two-loop perturbative correction to the $(g-2)_\mu$ HLbL at short distances," *JHEP* **04** (2021) 240, arXiv:2101.09169 [hep-ph].

[144] J. Bijnens, N. Hermansson-Truedsson, and A. Rodríguez-Sánchez, "Constraints on the hadronic light-by-light in the Melnikov-Vainshtein regime," *JHEP* **02** (2023) 167, arXiv:2211.17183 [hep-ph].

[145] T. Blum, N. Christ, M. Hayakawa, T. Izubuchi, L. Jin, C. Jung, and C. Lehner, "The hadronic light-by-light scattering contribution to the muon anomalous magnetic moment from lattice QCD," *Phys. Rev. Lett.* **124** no. 13, (2020) 132002, arXiv:1911.08123 [hep-lat].

[146] E.-H. Chao, R. J. Hudspith, A. Gérardin, J. R. Green, H. B. Meyer, and K. Ottnad, "Hadronic light-by-light contribution to $(g-2)_\mu$ from lattice QCD: a complete calculation," *Eur. Phys. J. C* **81** no. 7, (2021) 651, arXiv:2104.02632 [hep-lat].

[147] E.-H. Chao, R. J. Hudspith, A. Gérardin, J. R. Green, and H. B. Meyer, "The charm-quark contribution to light-by-light scattering in the muon $(g-2)$ from lattice QCD," *Eur. Phys. J. C* **82** no. 8, (2022) 664, arXiv:2204.08844 [hep-lat].

[148] C. M. Carloni Calame, M. Passera, L. Trentadue, and G. Venanzoni, "A new approach to evaluate the leading hadronic corrections to the muon g-2," *Phys. Lett. B* **746** (2015) 325–329, arXiv:1504.02228 [hep-ph].

[149] F. Hagelstein and V. Pascalutsa, "Dissecting the Hadronic Contributions to $(g-2)_\mu$ by Schwingers Sum Rule," *Phys. Rev. Lett.* **120** no. 7, (2018) 072002 [hep–ph/1710.04571], arXiv:1710.04571 [hep-ph].

[150] A. Antognini *et al.*, "Proton Structure from the Measurement of $2S-2P$ Transition Frequencies of Muonic Hydrogen," *Science* **339** (2013) 417–420.

[151] A. Antognini, F. Hagelstein, and V. Pascalutsa, "The proton structure in and out of muonic hydrogen," *Ann. Rev. Nucl. Part. Sci.* **72** (2022) 389, arXiv:2205.10076 [nucl-th].

[152] V. Lensky, F. Hagelstein, V. Pascalutsa, and M. Vanderhaeghen, "Sum rules across the unpolarized Compton processes involving generalized polarizabilities and moments of nucleon structure functions," *Phys. Rev. D* **97** no. 7, (2018) 074012, arXiv:1712.03886 [hep-ph].

[153] M. C. Birse and J. A. McGovern, "Proton polarisability contribution to the Lamb shift in muonic hydrogen at fourth order in chiral perturbation theory," *Eur. Phys. J. A* **48** (2012) 120, arXiv:1206.3030 [hep-ph].

[154] J. Sucher, "Sign of the Static Electric Polarizability in Relativistic Quantum Theory," *Phys. Rev. D* **6** (1972) 1798–1800.

[155] J. Bernabeu and R. Tarrach, "Unsubtracted Dispersion Relation for the Longitudinal Compton Amplitude," *Phys. Lett. B* **55** (1975) 183–186.

[156] X. Li *et al.*, "Proton Compton Scattering from Linearly Polarized Gamma Rays," *Phys. Rev. Lett.* **128** (2022) 132502, arXiv:2205.10533 [nucl-ex].

[157] **A2 Collaboration at MAMI** Collaboration, E. Mornacchi *et al.*, "Measurement of Compton Scattering at MAMI for the Extraction of the Electric and Magnetic Polarizabilities of the Proton," *Phys. Rev. Lett.* **128** no. 13, (2022) 132503, arXiv:2110.15691 [nucl-ex].

[158] M. Sugawara and A. Kanazawa, "Subtractions in Dispersion Relations," *Phys. Rev.* **123** (1961) 1895–1902.

[159] S. Mandelstam, "Determination of the pion - nucleon scattering amplitude from dispersion relations and unitarity. General theory," *Phys. Rev.* **112** (1958) 1344–1360.

[160] S. Mandelstam, "Analytic properties of transition amplitudes in perturbation theory," *Phys. Rev.* **115** (1959) 1741–1751.

[161] L. Castillejo, R. H. Dalitz, and F. J. Dyson, "Low's scattering equation for the charged and neutral scalar theories," *Phys. Rev.* **101** (1956) 453–458.

[162] M. Luming, "Application of N/D and Determinantal Methods to Yukawa Potential Scattering," *Phys. Rev.* **136** (1964) B1120–B1133.

[163] P. W. Johnson and R. L. Warnock, "Solution of the unitarity equation with overlapping left and right cuts: a tool for study of the S^* and similar systems," *J. Math. Phys.* **22** (1981) 385.

[164] V. M. Budnev, V. L. Chernyak, and I. F. Ginzburg, "Kinematics of $\gamma\gamma$ scattering," *Nucl. Phys. B* **34** (1971) 470–476.

[165] V. M. Budnev, I. F. Ginzburg, G. V. Meledin, and V. G. Serbo, "The Two photon particle production mechanism. Physical problems. Applications. Equivalent photon approximation," *Phys. Rept.* **15** (1975) 181–281.

[166] A. Gérardin, J. Green, O. Gryniuk, G. von Hippel, H. B. Meyer, V. Pascalutsa, and H. Wittig, "Hadronic light-by-light scattering amplitudes from lattice QCD versus dispersive sum rules," *Phys. Rev. D* **98** no. 7, (2018) 074501, arXiv:1712.00421 [hep-lat].

[167] V. Pascalutsa, V. Pauk, and M. Vanderhaeghen, "Light-by-light scattering sum rules constraining meson transition form factors," *Phys. Rev. D* **85** (2012) 116001, arXiv:1204.0740 [hep-ph].

[168] G. Jikia and A. Tkabladze, "Photon-photon scattering at the photon linear collider," *Phys. Lett. B* **323** (1994) 453–458, arXiv:hep-ph/9312228.

[169] G. J. Gounaris, P. I. Porfyriadis, and F. M. Renard, "The $\gamma\gamma \to \gamma\gamma$ process in the standard and susy models at high-energies," *Eur. Phys. J. C* **9** (1999) 673–686, arXiv:hep-ph/9902230.

[170] D. Drechsel, B. Pasquini, and M. Vanderhaeghen, "Dispersion relations in real and virtual Compton scattering," *Phys. Rept.* **378** (2003) 99–205, arXiv:hep-ph/0212124.

[171] F. Hagelstein, R. Miskimen, and V. Pascalutsa, "Nucleon Polarizabilities: from Compton Scattering to Hydrogen Atom," *Prog. Part. Nucl. Phys.* **88** (2016) 29–97, arXiv:1512.03765 [nucl-th].

[172] V. Pascalutsa, *Causality Rules*. IOP Concise Physics. Morgan & Claypool Publishers, 2018.

[173] V. Pascalutsa, *Causality Rules (Second Edition): Dispersion theory in non-elementary particle physics*. IOP Publishing, Apr., 2024. http://dx.doi.org/10.1088/978-0-7503-3431-0.

[174] F. J. Gilman, "Kinematics and saturation of the sum rules and inequalities for inelastic electron-nucleon scattering," *Phys. Rev.* **167** (1968) 1365–1371.

[175] B. R. Holstein, D. Drechsel, B. Pasquini, and M. Vanderhaeghen, "Higher order polarizabilities of the proton," *Phys. Rev. C* **61** (2000) 034316, arXiv:hep-ph/9910427.

[176] S. Ragusa, "Third order spin polarizabilities of the nucleon," *Phys. Rev. D* **47** (1993) 3757–3767.

[177] D. Babusci, G. Giordano, A. I. L'vov, G. Matone, and A. M. Nathan, "Low-energy Compton scattering of polarized photons on polarized nucleons," *Phys. Rev. C* **58** (1998) 1013–1041, arXiv:hep-ph/9803347.

[178] S. Gerasimov, "A Sum rule for magnetic moments and the damping of the nucleon magnetic moment in nuclei," *Sov. J. Nucl. Phys.* **2** (1966) 430–433.

[179] S. Drell and A. C. Hearn, "Exact Sum Rule for Nucleon Magnetic Moments," *Phys. Rev. Lett.* **16** (1966) 908–911.

[180] M. Hosoda and K. Yamamoto, "Sum rule for the magnetic moment of the dirac particle," *Prog. Theoret. Phys.* **36** no. 2, (1966) 425–426.

[181] O. Gryniuk, F. Hagelstein, and V. Pascalutsa, "Evaluation of the forward compton scattering off protons: Spin-independent amplitude," *Phys. Rev. D* **92** (2015) 074031, arXiv:1508.07952 [nucl-th].

[182] H. Burkhardt and W. N. Cottingham, "Sum rules for forward virtual Compton scattering," *Ann. Phys.* **56** (1970) 453–463.

[183] J. S. Schwinger, "Source Theory Viewpoints in Deep Inelastic Scattering," *Proc. Nat. Acad. Sci.* **72** (1975) 1–5.

[184] J. Schwinger, "Source theory discussion of deep inelastic scattering with polarized particles," *Proceedings of the National Academy of Sciences of the United States of America* **72** no. 4, (04, 1975) 1559–1563. http://www.ncbi.nlm.nih.gov/pmc/articles/PMC432577/.

[185] W.-y. Tsai, L. L. DeRaad, Jr., and K. A. Milton, "Verification of virtual Compton-scattering sum rules in quantum electrodynamics," *Phys. Rev. D* **11** (1975) 3537. [Erratum: Phys.Rev.D 13, 1144 (1976)].

[186] A. M. Baldin, "Polarizability of nucleons," *Nucl. Phys.* **18** (1960) 310–317.

[187] M. Damashek and F. J. Gilman, "Forward Compton Scattering," *Phys. Rev. D* **1** (1970) 1319–1332.

[188] A. Donnachie and P. V. Landshoff, "Does the hard pomeron obey Regge factorization?," *Phys. Lett. B* **595** (2004) 393–399, arXiv:hep-ph/0402081.

[189] G. Passarino and M. J. G. Veltman, "One Loop Corrections for e^+e^- Annihilation Into mu^+mu^- in the Weinberg Model," *Nucl. Phys. B* **160** (1979) 151–207.

[190] I. Danilkin, V. Biloshytskyi, X.-L. Ren, and M. Vanderhaeghen, "Analytical dispersive parametrization for elastic scattering of spinless particles," *Phys. Rev. D* **107** no. 7, (2023) 074021, arXiv:2206.15223 [hep-ph].

[191] I. Danilkin, O. Deineka, and M. Vanderhaeghen, "Data-driven dispersive analysis of the $\pi\pi$ and πK scattering," *Phys. Rev. D* **103** no. 11, (2021) 114023, arXiv:2012.11636 [hep-ph].

[192] O. Deineka, I. Danilkin, and M. Vanderhaeghen, "Dispersive analysis of the $\pi\pi$ and πK scattering data," *PoS* **CD2021** (2024) 046, arXiv:2203.02215 [hep-ph].

[193] J. R. Pelaez and F. J. Yndurain, "The Pion-pion scattering amplitude," *Phys. Rev. D* **71** (2005) 074016, arXiv:hep-ph/0411334.

[194] I. Caprini, "Finding the sigma pole by analytic extrapolation of $\pi\pi$ scattering data," *Phys. Rev. D* **77** (2008) 114019, arXiv:0804.3504 [hep-ph].

[195] J. R. Pelaez and A. Rodas, "Pion-kaon scattering amplitude constrained with forward dispersion relations up to 1.6 GeV," *Phys. Rev. D* **93** no. 7, (2016) 074025, arXiv:1602.08404 [hep-ph].

[196] V. Biloshytskyi, I. Danilkin, X.-L. Ren, and M. Vanderhaeghen, "Analytical dispersive parameterization for S-wave $\pi\pi$ and πK scattering," arXiv:2302.08443 [hep-ph].

[197] A. Gasparyan and M. F. M. Lutz, "Photon- and pion-nucleon interactions in a unitary and causal effective field theory based on the chiral Lagrangian," *Nucl. Phys. A* **848** (2010) 126–182, arXiv:1003.3426 [hep-ph].

[198] I. V. Danilkin, A. M. Gasparyan, and M. F. M. Lutz, "On causality, unitarity and perturbative expansions," *Phys. Lett. B* **697** (2011) 147–152, arXiv:1009.5928 [hep-ph].

[199] I. V. Danilkin, L. I. R. Gil, and M. F. M. Lutz, "Dynamical light vector mesons in low-energy scattering of Goldstone bosons," *Phys. Lett. B* **703** (2011) 504–509, arXiv:1106.2230 [hep-ph].

[200] A. M. Gasparyan, M. F. M. Lutz, and E. Epelbaum, "Two-nucleon scattering: Merging chiral effective field theory with dispersion relations," *Eur. Phys. J. A* **49** (2013) 115, arXiv:1212.3057 [nucl-th].

[201] W. R. Frazer, "Applications of Conformal Mapping to the Phenomenological Representation of Scattering Amplitudes," *Phys. Rev.* **123** (1961) 2180–2182.

[202] A. M. Badalian, L. P. Kok, M. I. Polikarpov, and Y. A. Simonov, "Resonances in Coupled Channels in Nuclear and Particle Physics," *Phys. Rept.* **82** (1982) 31–177.

[203] A. Gomez Nicola and J. R. Pelaez, "Meson meson scattering within one loop chiral perturbation theory and its unitarization," *Phys. Rev. D* **65** (2002) 054009, arXiv:hep-ph/0109056.

[204] D. Iagolnitzer, J. Zinn-Justin, and J. B. Zuber, "Yang-mills fields and pseudoscalar meson scattering," *Nucl. Phys. B* **60** (1973) 233–266.

[205] "Particle Data Group (2023)," https://pdg.lbl.gov/2023/reviews/rpp2023-rev-resonances.pdf.

[206] F. J. Yndurain, R. Garcia-Martin, and J. R. Pelaez, "Experimental status of the $\pi\pi$ isoscalar S wave at low energy: $f_0(600)$ pole and scattering length," *Phys. Rev. D* **76** (2007) 074034, arXiv:hep-ph/0701025.

[207] T. N. Truong, "Chiral Perturbation Theory and Final State Theorem," *Phys. Rev. Lett.* **61** (1988) 2526.

[208] A. Dobado, M. J. Herrero, and T. N. Truong, "Unitarized Chiral Perturbation Theory for Elastic Pion-Pion Scattering," *Phys. Lett. B* **235** (1990) 134–140.

[209] T. N. Truong, "Remarks on the unitarization methods," *Phys. Rev. Lett.* **67** (1991) 2260–2263.

[210] A. Dobado and J. R. Pelaez, "A Global fit of pi pi and pi K elastic scattering in ChPT with dispersion relations," *Phys. Rev. D* **47** (1993) 4883–4888, arXiv:hep-ph/9301276.

[211] A. Gomez Nicola, J. Pelaez, and G. Rios, "The Inverse Amplitude Method and Adler Zeros," *Phys. Rev. D* **77** (2008) 056006, arXiv:0712.2763.

[212] C. Hanhart, J. R. Pelaez, and G. Rios, "Quark mass dependence of the rho and sigma from dispersion relations and Chiral Perturbation Theory," *Phys. Rev. Lett.* **100** (2008) 152001, arXiv:0801.2871.

[213] J. Pelaez and G. Rios, "Chiral extrapolation of light resonances from one and two-loop unitarized Chiral Perturbation Theory versus lattice results," *Phys. Rev. D* **82** (2010) 114002, arXiv:1010.6008.

[214] J. Nebreda and J. Pelaez., "Strange and non-strange quark mass dependence of elastic light resonances from SU(3) Unitarized Chiral Perturbation Theory to one loop," *Phys. Rev. D* **81** (2010) 054035, arXiv:1001.5237 [hep-ph].

[215] L. Y. Dai, X. G. Wang, and H. Q. Zheng, "Pole Analysis on Unitarized $SU(3) \times SU(3)$ One Loop χPT Amplitudes," *Commun. Theor. Phys.* **57** (2012) 841–848, arXiv:1108.1451 [hep-ph].

[216] M. Niehus, M. Hoferichter, B. Kubis, and J. Ruiz de Elvira, "Two-Loop Analysis of the Pion Mass Dependence of the ρ Meson," *Phys. Rev. Lett.* **126** no. 10, (2021) 102002, arXiv:2009.04479 [hep-ph].

[217] J. Bijnens and G. Ecker, "Mesonic low-energy constants," *Ann. Rev. Nucl. Part. Sci.* **64** (2014) 149–174, arXiv:1405.6488.

[218] J. R. Pelaez, "From controversy to precision on the sigma meson: a review on the status of the non-ordinary $f_0(500)$ resonance," *Phys. Rept.* **658** (2016) 1, arXiv:1510.00653.

[219] J. R. Peláez, A. Rodas, and J. R. de Elvira, "Precision dispersive approaches versus unitarized chiral perturbation theory for the lightest scalar resonances $\sigma/f_0(500)$ and $\kappa/K_0^*(700)$," *Eur. Phys. J. ST* **230** no. 6, (2021) 1539–1574, arXiv:2101.06506 [hep-ph].

[220] **Hadron Spectrum** Collaboration, J. J. Dudek, R. G. Edwards, and C. E. Thomas, "Energy dependence of the ρ resonance in $\pi\pi$ elastic scattering from lattice QCD," *Phys. Rev. D* **87** no. 3, (2013) 034505, arXiv:1212.0830 [hep-ph]. [Erratum: Phys.Rev.D 90, 099902 (2014)].

[221] D. J. Wilson, R. A. Briceno, J. J. Dudek, R. G. Edwards, and C. E. Thomas, "Coupled $\pi\pi, K\bar{K}$ scattering in P-wave and the ρ resonance from lattice QCD," *Phys. Rev. D* **92** no. 9, (2015) 094502.

[222] M. Bruno, T. Korzec, and S. Schaefer, "Setting the scale for the CLS $2+1$ flavor ensembles," *Phys. Rev. D* **95** no. 7, (2017) 074504, arXiv:1608.08900 [hep-lat].

[223] **Extended Twisted Mass, ETM** Collaboration, M. Fischer, B. Kostrzewa, M. Mai, M. Petschlies, F. Pittler, M. Ueding, C. Urbach, and M. Werner, "The ρ-resonance from $N_f = 2$ lattice QCD including the physical pion mass," *Phys. Lett. B* **819** (2021) 136449, arXiv:2006.13805 [hep-lat].

[224] S. Paul, A. D. Hanlon, B. Hörz, D. Mohler, C. Morningstar, and H. Wittig, "I=1 π-π scattering at the physical point," *PoS* **LATTICE2021** (2022) 551, arXiv:2112.07385 [hep-lat].

[225] J. Pelaez and A. Rodas, "$\pi\pi \to K\bar{K}$ scattering up to 1.47 GeV with hyperbolic dispersion relations," *Eur. Phys. J. C* **78** no. 11, (2018) 897, arXiv:1807.04543 [hep-ph].

[226] L. A. Harland-Lang, V. A. Khoze, and M. G. Ryskin, "Exclusive physics at the LHC with SuperChic 2," *The European Physical Journal C* **76** no. 1, (Jan., 2016) .

[227] **JADE** Collaboration, W. Bartel *et al.*, "A measurement of the η radiative width $\Gamma_{\eta\to\gamma\gamma}$," *Phys. Lett. B* **158** (1985) 511.

[228] **TPC/Two Gamma** Collaboration, H. Aihara *et al.*, "A study of η formation in photon-photon collisions at PEP," *Phys. Rev. D* **33** (1986) 844.

[229] **Crystal Ball** Collaboration, D. Williams *et al.*, "Formation of the Pseudoscalars π^0, η and η' in the Reaction $\gamma\gamma \to \gamma\gamma$," *Phys. Rev. D* **38** (1988) 1365.

[230] **PLUTO** Collaboration, C. Berger *et al.*, "Measurement of the Total Photon-photon Cross-section for the Production of Hadrons at Small Q^2," *Phys. Lett. B* **149** (1984) 421–426.

[231] **TPC/Two Gamma** Collaboration, D. Bintinger *et al.*, "Measurement of the Total Hadronic Cross-section in Photon-photon Interactions," *Phys. Rev. Lett.* **54** (1985) 763.

[232] **TPC/Two Gamma** Collaboration, H. Aihara *et al.*, "A measurement of the total hadronic cross-section in tagged $\gamma\gamma$ reactions," *Phys. Rev. D* **41** (1990) 2667.

[233] S. E. Baru *et al.*, "Total cross-section of two photon production of hadrons," *Z. Phys. C* **53** (1992) 219–224.

[234] **L3** Collaboration, M. Acciarri *et al.*, "Cross-section of hadron production in gamma gamma collisions at LEP," *Phys. Lett. B* **408** (1997) 450–464.

[235] **L3** Collaboration, M. Acciarri *et al.*, "Total cross-section in $\gamma\gamma$ collisions at LEP," *Phys. Lett. B* **519** (2001) 33–45, arXiv:hep-ex/0102025.

[236] **OPAL** Collaboration, G. Abbiendi *et al.*, "Total hadronic cross-section of photon-photon interactions at LEP," *Eur. Phys. J. C* **14** (2000) 199–212, arXiv:hep-ex/9906039.

[237] V. Biloshytskyi, V. Pascalutsa, L. Harland-Lang, B. Malaescu, K. Schmieden, and M. Schott, "Two-photon decay of X(6900) from light-by-light scattering at the LHC," *Phys. Rev. D* **106** no. 11, (2022) L111902, arXiv:2207.13623 [hep-ph].

[238] V. Biloshytskyi, L. Harland-Lang, B. Malaescu, V. Pascalutsa, K. Schmieden, and M. Schott, "Two-photon decay of fully-charmed tetraquarks from light-by-light scattering at the LHC," *EPJ Web Conf.* **274** (2022) 06007, arXiv:2211.10266 [hep-ph].

[239] R. Karplus and M. Neuman, "The scattering of light by light," *Phys. Rev.* **83** (1951) 776–784.

[240] B. De Tollis, "Dispersive approach to photon-photon scattering," *Nuovo Cim.* **32** no. 3, (1964) 757–768.

[241] B. De Tollis, "The scattering of photons by photons," *Nuovo Cim.* **35** no. 4, (1965) 1182–1193.

[242] D. Bardin, L. Kalinovskaya, and E. Uglov, "Standard Model light-by-light scattering in SANC: analytic and numeric evaluation," *Phys. Atom. Nucl.* **73** (2010) 1878–1888, arXiv:0911.5634 [hep-ph].

[243] W. Heisenberg and H. Euler, "Consequences of Dirac's theory of positrons," *Z. Phys.* **98** no. 11-12, (1936) 714–732, arXiv:physics/0605038.

[244] D. A. Dicus, C. Kao, and W. W. Repko, "Effective Lagrangians and low-energy photon-photon scattering," *Phys. Rev. D* **57** (1998) 2443–2447, arXiv:hep-ph/9709415.

[245] V. Pascalutsa and M. Vanderhaeghen, "Sum rules for light-by-light scattering," *Phys.Rev.Lett.* **105** (2010) 201603, arXiv:1008.1088 [hep-ph].

[246] L. D. Landau, "On the angular momentum of a system of two photons," *Dokl. Akad. Nauk SSSR* **60** no. 2, (1948) 207–209.

[247] C.-N. Yang, "Selection Rules for the Dematerialization of a Particle Into Two Photons," *Phys. Rev.* **77** (1950) 242–245.

[248] P. Lebiedowicz and A. Szczurek, "The role of meson exchanges in light-by-light scattering," *Phys. Lett. B* **772** (2017) 330–335, 1705.06535 [hep-ph].

[249] G. A. Schuler and T. Sjostrand, "A Scenario for high-energy gamma gamma interactions," *Z. Phys. C* **73** (1997) 677–688, arXiv:hep-ph/9605240.

[250] A. Donnachie and P. V. Landshoff, "Total cross-sections," *Phys. Lett. B* **296** (1992) 227–232, arXiv:hep-ph/9209205.

[251] P. D. Group, R. L. Workman, *et al.*, "Review of Particle Physics," *Progress of Theoretical and Experimental Physics* **2022** no. 8, (08, 2022) 083C01, https://academic.oup.com/ptep/article-pdf/2022/8/083C01/49175539/ptac097.pdf. https://doi.org/10.1093/ptep/ptac097.

[252] **Particle Data Group** Collaboration, C. Patrignani *et al.*, "Review of Particle Physics," *Chin. Phys. C* **40** no. 10, (2016) 100001.

[253] W. Heisenberg, "Mesonenerzeugung als Stosswellenproblem," *Z. Phys.* **133** (1952) 65.

[254] G. Baur, K. Hencken, D. Trautmann, S. Sadovsky, and Y. Kharlov, "Coherent $\gamma\gamma$ and γA interactions in very peripheral collisions at relativistic ion colliders," *Phys. Rept.* **364** (2002) 359–450, arXiv:hep-ph/0112211.

[255] E. Gotsman, E. Levin, U. Maor, and E. Naftali, "The components of the $\gamma^*\gamma^*$ cross-section," *Eur. Phys. J. C* **14** (2000) 511–523, arXiv:hep-ph/0001080.

[256] B. Badełek, M. Krawczyk, J. Kwieciński, and A. M. Staśto, "Parametrization of F_2^γ at low Q^2 and of $\sigma_{\gamma\gamma}$ and $\sigma_{\gamma^*\gamma}$ at high energies," *Phys. Rev. D* **62** (2000) 074021, arXiv:hep-ph/0001161.

[257] https://gg-lat.readthedocs.io.

[258] N. Barnea, J. Vijande, and A. Valcarce, "Four-quark spectroscopy within the hyperspherical formalism," *Phys. Rev. D* **73** (2006) 054004, arXiv:hep-ph/0604010.

[259] A. V. Berezhnoy, A. V. Luchinsky, and A. A. Novoselov, "Tetraquarks Composed of 4 Heavy Quarks," *Phys. Rev. D* **86** (2012) 034004, arXiv:1111.1867 [hep-ph].

[260] M. Karliner, S. Nussinov, and J. L. Rosner, "$QQ\bar{Q}\bar{Q}$ states: masses, production, and decays," *Phys. Rev. D* **95** no. 3, (2017) 034011, arXiv:1611.00348 [hep-ph].

[261] J. Wu, Y.-R. Liu, K. Chen, X. Liu, and S.-L. Zhu, "Heavy-flavored tetraquark states with the $QQ\bar{Q}\bar{Q}$ configuration," *Phys. Rev. D* **97** no. 9, (2018) 094015, arXiv:1605.01134 [hep-ph].

[262] Z.-G. Wang, "Analysis of the $QQ\bar{Q}\bar{Q}$ tetraquark states with QCD sum rules," *Eur. Phys. J. C* **77** no. 7, (2017) 432, arXiv:1701.04285 [hep-ph].

[263] V. R. Debastiani and F. S. Navarra, "A non-relativistic model for the $[cc][\bar{c}\bar{c}]$ tetraquark," *Chin. Phys. C* **43** no. 1, (2019) 013105, arXiv:1706.07553 [hep-ph].

[264] M.-S. Liu, Q.-F. Lü, X.-H. Zhong, and Q. Zhao, "All-heavy tetraquarks," *Phys. Rev. D* **100** no. 1, (2019) 016006, arXiv:1901.02564 [hep-ph].

[265] G.-J. Wang, L. Meng, and S.-L. Zhu, "Spectrum of the fully-heavy tetraquark state $QQ\bar{Q}'\bar{Q}'$," *Phys. Rev. D* **100** no. 9, (2019) 096013, arXiv:1907.05177 [hep-ph].

[266] M. A. Bedolla, J. Ferretti, C. D. Roberts, and E. Santopinto, "Spectrum of fully-heavy tetraquarks from a diquark+antidiquark perspective," *Eur. Phys. J. C* **80** no. 11, (2020) 1004, arXiv:1911.00960 [hep-ph].

[267] M.-S. liu, F.-X. Liu, X.-H. Zhong, and Q. Zhao, "Fully heavy tetraquark states and their evidences in LHC observations," *Phys. Rev. D* **109** no. 7, (2024) 076017, arXiv:2006.11952 [hep-ph].

[268] Q.-F. Lü, D.-Y. Chen, and Y.-B. Dong, "Masses of fully heavy tetraquarks $QQ\bar{Q}\bar{Q}$ in an extended relativized quark model," *Eur. Phys. J. C* **80** no. 9, (2020) 871, arXiv:2006.14445 [hep-ph].

[269] J.-M. Richard, "About the J/ψ J/ψ peak of LHCb: fully-charmed tetraquark?," *Sci. Bull.* **65** (2020) 1954–1955, arXiv:2008.01962 [hep-ph].

[270] X.-Z. Weng, X.-L. Chen, W.-Z. Deng, and S.-L. Zhu, "Systematics of fully heavy tetraquarks," *Phys. Rev. D* **103** no. 3, (2021) 034001, arXiv:2010.05163 [hep-ph].

[271] C. Deng, H. Chen, and J. Ping, "Towards the understanding of fully-heavy tetraquark states from various models," *Phys. Rev. D* **103** no. 1, (2021) 014001, arXiv:2003.05154 [hep-ph].

[272] P. Lundhammar and T. Ohlsson, "Nonrelativistic model of tetraquarks and predictions for their masses from fits to charmed and bottom meson data," *Phys. Rev. D* **102** no. 5, (2020) 054018, arXiv:2006.09393 [hep-ph].

[273] R. N. Faustov, V. O. Galkin, and E. M. Savchenko, "Heavy tetraquarks in the relativistic quark model," *Universe* **7** no. 4, (2021) 94, arXiv:2103.01763 [hep-ph].

[274] H. Mutuk, "Nonrelativistic treatment of fully-heavy tetraquarks as diquark-antidiquark states," *Eur. Phys. J. C* **81** no. 4, (2021) 367, arXiv:2104.11823 [hep-ph].

[275] W. Chen, H.-X. Chen, X. Liu, T. G. Steele, and S.-L. Zhu, "Hunting for exotic doubly hidden-charm/bottom tetraquark states," *Phys. Lett. B* **773** (2017) 247–251, 1605.01647 [hep-ph].

[276] B.-D. Wan and C.-F. Qiao, "Gluonic tetracharm configuration of $X(6900)$," *Phys. Lett. B* **817** (2021) 136339, arXiv:2012.00454 [hep-ph].

[277] R. M. Albuquerque, S. Narison, A. Rabemananjara, D. Rabetiarivony, and G. Randriamanatrika, "Doubly-hidden scalar heavy molecules and tetraquarks states from QCD at NLO," *Phys. Rev. D* **102** no. 9, (2020) 094001, arXiv:2008.01569 [hep-ph].

[278] S. S. Agaev, K. Azizi, B. Barsbay, and H. Sundu, "Exploring fully heavy scalar tetraquarks $QQ\overline{QQ}$," *Phys. Lett. B* **844** (2023) 138089, arXiv:2304.03244 [hep-ph].

[279] C.-M. Tang, C.-G. Duan, and L. Tang, "Fully charmed tetraquark states in $8_{[c\bar{c}]} \otimes 8_{[c\bar{c}]}$ color structure via QCD sum rules," *Eur. Phys. J. C* **84** no. 7, (2024) 743, arXiv:2405.05042 [hep-ph].

[280] X.-K. Dong, V. Baru, F.-K. Guo, C. Hanhart, and A. Nefediev, "Coupled-Channel Interpretation of the LHCb Double- J/ψ Spectrum and Hints of a New State Near the $J/\psi J/\psi$ Threshold," *Phys. Rev. Lett.* **126** no. 13, (2021) 132001, 2009.07795 [hep-ph]. [Erratum: Phys.Rev.Lett. 127, 119901 (2021)].

[281] Z.-H. Guo and J. A. Oller, "Insights into the inner structures of the fully charmed tetraquark state $X(6900)$," *Phys. Rev. D* **103** no. 3, (2021) 034024, arXiv:2011.00978 [hep-ph].

[282] Z.-R. Liang, X.-Y. Wu, and D.-L. Yao, "Hunting for states in the recent LHCb di-J/ψ invariant mass spectrum," *Phys. Rev. D* **104** no. 3, (2021) 034034, arXiv:2104.08589 [hep-ph].

[283] J. Sonnenschein and D. Weissman, "Deciphering the recently discovered tetraquark candidates around 6.9 GeV," *Eur. Phys. J. C* **81** no. 1, (2021) 25, arXiv:2008.01095 [hep-ph].

[284] R. Zhu, "Fully-heavy tetraquark spectra and production at hadron colliders," *Nucl. Phys. B* **966** (2021) 115393, arXiv:2010.09082 [hep-ph].

[285] Q. Li, C.-H. Chang, G.-L. Wang, and T. Wang, "Mass spectra and wave functions of $T_{QQ\bar{Q}\bar{Q}}$ tetraquarks," *Phys. Rev. D* **104** no. 1, (2021) 014018, arXiv:2104.12372 [hep-ph].

[286] H.-W. Ke, X. Han, X.-H. Liu, and Y.-L. Shi, "Tetraquark state $X(6900)$ and the interaction between diquark and antidiquark," *Eur. Phys. J. C* **81** no. 5, (2021) 427, arXiv:2103.13140 [hep-ph].

[287] J.-Z. Wang, D.-Y. Chen, X. Liu, and T. Matsuki, "Producing fully charm structures in the J/ψ -pair invariant mass spectrum," *Phys. Rev. D* **103** no. 7, (2021) 071503, 2008.07430 [hep-ph].

[288] J.-Z. Wang and X. Liu, "Improved understanding of the peaking phenomenon existing in the new di-J/ψ invariant mass spectrum from the CMS Collaboration," *Phys. Rev. D* **106** no. 5, (2022) 054015, 2207.04893 [hep-ph].

[289] H.-X. Chen, W. Chen, X. Liu, Y.-R. Liu, and S.-L. Zhu, "An updated review of the new hadron states," arXiv:2204.02649 [hep-ph].

[290] W.-C. Dong and Z.-G. Wang, "Going in quest of potential tetraquark interpretations for the newly observed $T_{\psi\psi}$ states in light of the diquark-antidiquark scenarios," *Phys. Rev. D* **107** no. 7, (2023) 074010, arXiv:2211.11989 [hep-ph].

[291] A. Esposito, C. A. Manzari, A. Pilloni, and A. D. Polosa, "Hunting for tetraquarks in ultraperipheral heavy ion collisions," *Phys. Rev. D* **104** no. 11, (2021) 114029, arXiv:2109.10359 [hep-ph].

[292] V. P. Gonçalves and B. D. Moreira, "Fully - heavy tetraquark production by $\gamma\gamma$ interactions in hadronic collisions at the LHC," *Phys. Lett. B* **816** (2021) 136249, arXiv:2101.03798 [hep-ph].

[293] V. P. Goncalves, B. D. Moreira, R. Molina, and F. S. Navarra, "Exotic charmonium and light-by-light scattering in heavy ion collisions," *PoS* **Hadron2017** (2018) 126.

[294] V. Barger and R. Phillips, "Properties of ψn scattering," *Physics Letters B* **58** no. 4, (Sept., 1975) 433–436. https://doi.org/10.1016/0370-2693(75)90582-1.

[295] K. Redlich, H. Satz, and G. M. Zinovjev, "Photoproduction constraints on J / psi nucleon interactions," *Eur. Phys. J. C* **17** (2000) 461–465, arXiv:hep-ph/0003079.

[296] **CMS** Collaboration, "Observation of new structures in the J/ψJ/ψ mass spectrum in pp collisions at $\sqrt{s}$ = 13 TeV." 2022. https://cds.cern.ch/record/2815336. CMS-PAS-BPH-21-003.

[297] A. M. Badalian, B. L. Ioffe, and A. V. Smilga, "Four-quark states in heavy quark systems," *Nucl. Phys. B* **281** (1987) 85.

[298] W.-L. Sang, T. Wang, Y.-D. Zhang, and F. Feng, "Electromagnetic and hadronic decay of fully heavy tetraquarks," *Phys. Rev. D* **109** no. 5, (2024) 056016, arXiv:2307.16150 [hep-ph].

[299] A. M. Badalian, "The $X(6550)$, $X(6900)$, $X(7280)$ Resonances as the nS, $cc\bar{c}\bar{c}$ States," *Phys. Atom. Nucl.* **86** no. 5, (2023) 701–708.

[300] I. Danilkin and M. Vanderhaeghen, "Light-by-light forward scattering sum rules for charmonium states," *Phys. Rev. D* **96** no. 5, (2017) 056003, arXiv:1705.01179 [hep-ph].

[301] L. A. Harland-Lang, V. A. Khoze, and M. G. Ryskin, "Exclusive LHC physics with heavy ions: SuperChic 3," *The European Physical Journal C* **79** no. 1, (Jan., 2019) .

[302] J. Z. Wang, Z. F. Sun, X. Liu, and T. Matsuki, "Higher bottomonium zoo," *European Physical Journal C* **78** no. 11, (2018) 1–43, arXiv:1802.04938.

[303] Z. Bern, A. De Freitas, L. J. Dixon, A. Ghinculov, and H. L. Wong, "QCD and QED corrections to light by light scattering," *JHEP* **11** (2001) 031, arXiv:hep-ph/0109079.

[304] M. Kłusek-Gawenda, W. Schäfer, and A. Szczurek, "Two-gluon exchange contribution to elastic $\gamma\gamma \to \gamma\gamma$ scattering and production of two-photons in ultraperipheral ultrarelativistic heavy ion and proton-proton collisions," *Phys. Lett. B* **761** (2016) 399–407, arXiv:1606.01058 [hep-ph].

[305] G. K. Krintiras, I. Grabowska-Bold, M. Kłusek-Gawenda, E. Chapon, R. Chudasama, and R. Granier de Cassagnac, "Light-by-light scattering cross-section measurements at LHC," arXiv:2204.02845 [hep-ph].

[306] W. Pauli and F. Villars, "On the Invariant regularization in relativistic quantum theory," *Rev. Mod. Phys.* **21** (1949) 434–444.

[307] A. Sirlin, "Radiative Corrections in the SU(2)-L x U(1) Theory: A Simple Renormalization Framework," *Phys. Rev. D* **22** (1980) 971–981.

[308] N. Asmussen, J. Green, H. B. Meyer, and A. Nyffeler, "Position-space approach to hadronic light-by-light scattering in the muon $g-2$ on the lattice," *PoS* **LATTICE2016** (2016) 164, arXiv:1609.08454 [hep-lat].

[309] T. Blum, N. Christ, M. Hayakawa, T. Izubuchi, L. Jin, C. Jung, and C. Lehner, "Using infinite volume, continuum QED and lattice QCD for the hadronic light-by-light contribution to the muon anomalous magnetic moment," *Phys. Rev. D* **96** no. 3, (2017) 034515, arXiv:1705.01067 [hep-lat].

[310] T. Blum, R. Zhou, T. Doi, M. Hayakawa, T. Izubuchi, S. Uno, and N. Yamada, "Electromagnetic mass splittings of the low lying hadrons and quark masses from 2+1 flavor lattice QCD+QED," *Phys. Rev. D* **82** (2010) 094508, arXiv:1006.1311 [hep-lat].

[311] T. Ishikawa, T. Blum, M. Hayakawa, T. Izubuchi, C. Jung, and R. Zhou, "Full QED+QCD low-energy constants through reweighting," *Phys. Rev. Lett.* **109** (2012) 072002, arXiv:1202.6018 [hep-lat].

[312] S. Aoki *et al.*, "1+1+1 flavor QCD + QED simulation at the physical point," *Phys. Rev. D* **86** (2012) 034507, arXiv:1205.2961 [hep-lat].

[313] **BMW** Collaboration, S. Borsanyi *et al.*, "Ab initio calculation of the neutron-proton mass difference," *Science* **347** (2015) 1452–1455, arXiv:1406.4088 [hep-lat].

[314] M. G. Endres, A. Shindler, B. C. Tiburzi, and A. Walker-Loud, "Massive photons: an infrared regularization scheme for lattice QCD+QED," *Phys. Rev. Lett.* **117** no. 7, (2016) 072002, arXiv:1507.08916 [hep-lat].

[315] R. Horsley *et al.*, "Isospin splittings of meson and baryon masses from three-flavor lattice QCD + QED," *J. Phys. G* **43** no. 10, (2016) 10LT02, arXiv:1508.06401 [hep-lat].

[316] Z. Fodor, C. Hoelbling, S. Krieg, L. Lellouch, T. Lippert, A. Portelli, A. Sastre, K. K. Szabo, and L. Varnhorst, "Up and down quark masses and corrections to Dashen's theorem from lattice QCD and quenched QED," *Phys. Rev. Lett.* **117** no. 8, (2016) 082001, arXiv:1604.07112 [hep-lat].

[317] D. Giusti, V. Lubicz, C. Tarantino, G. Martinelli, F. Sanfilippo, S. Simula, and N. Tantalo, "Leading isospin-breaking corrections to pion, kaon and charmed-meson masses with Twisted-Mass fermions," *Phys. Rev. D* **95** no. 11, (2017) 114504, arXiv:1704.06561 [hep-lat].

[318] P. Boyle, V. Gülpers, J. Harrison, A. Jüttner, C. Lehner, A. Portelli, and C. T. Sachrajda, "Isospin breaking corrections to meson masses and the hadronic vacuum polarization: a comparative study," *JHEP* **09** (2017) 153, arXiv:1706.05293 [hep-lat].

[319] X. Feng, L. Jin, and M. J. Riberdy, "Lattice QCD Calculation of the Pion Mass Splitting," *Phys. Rev. Lett.* **128** no. 5, (2022) 052003, arXiv:2108.05311 [hep-lat].

[320] R. Frezzotti, G. Gagliardi, V. Lubicz, G. Martinelli, F. Sanfilippo, and S. Simula, "Lattice calculation of the pion mass difference Mπ+-Mπ0 at order O(αem)," *Phys. Rev. D* **106** no. 1, (2022) 014502, arXiv:2202.11970 [hep-lat].

[321] A. Portelli, "Inclusion of isospin breaking effects in lattice simulations," *PoS* **LATTICE2014** (2015) 013, arXiv:1505.07057 [hep-lat].

[322] A. Patella, "QED Corrections to Hadronic Observables," *PoS* **LATTICE2016** (2017) 020, arXiv:1702.03857 [hep-lat].

[323] **Flavour Lattice Averaging Group (FLAG)** Collaboration, Y. Aoki *et al.*, "FLAG Review 2021," *Eur. Phys. J. C* **82** no. 10, (2022) 869, arXiv:2111.09849 [hep-lat].

[324] M. Knecht, "The Anomalous magnetic moment of the muon: A Theoretical introduction," *Lect. Notes Phys.* **629** (2004) 37–84, arXiv:hep-ph/0307239 [hep-ph].

[325] I. R. Blokland, A. Czarnecki, and K. Melnikov, "Pion pole contribution to hadronic light by light scattering and muon anomalous magnetic moment," *Phys. Rev. Lett.* **88** (2002) 071803, arXiv:hep-ph/0112117.

[326] V. Pascalutsa, "Cottingham-type formula for the LbL contribution to HVP," https://indico.fnal.gov/event/13795/contributions/21818/. Contribution to the First workshop on Muon g-2 Theory Initiative, Fermilab, June 3–6, 2017.

[327] W. N. Cottingham, "The neutron proton mass difference and electron scattering experiments," *Annals Phys.* **25** (1963) 424–432.

[328] A. Walker-Loud, C. E. Carlson, and G. A. Miller, "The Electromagnetic Self-Energy Contribution to $M_p - M_n$ and the Isovector Nucleon MagneticPolarizability," *Phys. Rev. Lett.* **108** (2012) 232301, arXiv:1203.0254 [nucl-th].

[329] J. Gasser, H. Leutwyler, and A. Rusetsky, "On the mass difference between proton and neutron," *Phys. Lett. B* **814** (2021) 136087, arXiv:2003.13612 [hep-ph].

[330] J. Gasser, H. Leutwyler, and A. Rusetsky, "Sum rule for the Compton amplitude and implications for the proton–neutron mass difference," *Eur. Phys. J. C* **80** no. 12, (2020) 1121, arXiv:2008.05806 [hep-ph].

[331] J. Gasser, M. Hoferichter, H. Leutwyler, and A. Rusetsky, "Cottingham formula and nucleon polarisabilities," *Eur. Phys. J. C* **75** no. 8, (2015) 375, arXiv:1506.06747 [hep-ph]. [Erratum: Eur. Phys. J. C 80, 353 (2020)].

[332] J. Green, O. Gryniuk, G. von Hippel, H. B. Meyer, and V. Pascalutsa, "Lattice QCD calculation of hadronic light-by-light scattering," *Phys. Rev. Lett.* **115** no. 22, (2015) 222003, arXiv:1507.01577 [hep-lat].

[333] J. Bijnens and J. Relefors, "Pion light-by-light contributions to the muon $g-2$," *JHEP* **09** (2016) 113, arXiv:1608.01454 [hep-ph].

[334] V. Biloshytskyi, E.-H. Chao, A. Gérardin, J. R. Green, F. Hagelstein, H. B. Meyer, J. Parrino, and V. Pascalutsa, "Forward light-by-light scattering and electromagnetic correction to hadronic vacuum polarization," *JHEP* **03** (2023) 194, arXiv:2209.02149 [hep-lat].

[335] T. Blum, "Lattice calculation of the lowest order hadronic contribution to the muon anomalous magnetic moment," *Phys.Rev.Lett.* **91** (2003) 052001, arXiv:hep-lat/0212018 [hep-lat].

[336] D. Bernecker and H. B. Meyer, "Vector Correlators in Lattice QCD: Methods and applications," *Eur. Phys. J. A* **47** (2011) 148, arXiv:1107.4388 [hep-lat].

[337] M. E. Peskin and D. V. Schroeder, *An Introduction to quantum field theory*. Addison-Wesley, 1995.

[338] G. Källén and A. Sabry, "Fourth order vacuum polarization," *Dan. Mat. Fys. Medd.* **29** no. 17, (1955) . http://publ.royalacademy.dk/books/75/442.

[339] B. E. Lautrup and E. De Rafael, "Calculation of the sixth-order contribution from the fourth-order vacuum polarization to the difference of the anomalous magnetic moments of muon and electron," *Phys. Rev.* **174** (1968) 1835–1842.

[340] J. Schwinger, *Particles, Sources, And Fields, Volume 3*. Advanced Books Classics. Avalon Publishing, 1998. https://books.google.de/books?id=ltHvAAAAMAAJ.

[341] J. Charles, E. de Rafael, and D. Greynat, "Mellin-Barnes approach to hadronic vacuum polarization and $g_\mu - 2$," *Phys. Rev. D* **97** no. 7, (2018) 076014, arXiv:1712.02202 [hep-ph].

[342] J. Bijnens, J. Harrison, N. Hermansson-Truedsson, T. Janowski, A. Jüttner, and A. Portelli, "Electromagnetic finite-size effects to the hadronic vacuum polarization," *Phys. Rev. D* **100** no. 1, (2019) 014508, arXiv:1903.10591 [hep-lat].

[343] B. Lautrup and E. de Rafael, "On sixth-order radiative corrections to the muon g-factor," *Nuovo Cim.* **64A** (1969) 322–324.

[344] B. Lautrup, A. Peterman, and E. de Rafael, "Recent developments in the comparison between theory and experiments in quantum electrodynamics," *Phys. Rept.* **3** (1972) 193–260.

[345] E. de Rafael, "Hadronic contributions to the muon g-2 and low-energy QCD," *Phys. Lett. B* **322** (1994) 239–246, arXiv:hep-ph/9311316.

[346] J. A. Mignaco and E. Remiddi, "Fourth-order vacuum polarization contribution to the sixth-order electron magnetic moment," *Il Nuovo Cimento A (1965-1970)* **60** no. 4, (1969) 519–529. https://doi.org/10.1007/BF02757285.

[347] K. Chetyrkin, V. Spiridonov, and S. Gorishnii, "Wilson expansion for correlators of vector currents at the two loop level: dimension four operators," *Phys. Lett. B* **160** (1985) 149–153.

[348] R. J. Hill and G. Paz, "Nucleon spin-averaged forward virtual Compton tensor at large Q^2," *Phys. Rev. D* **95** no. 9, (2017) 094017, arXiv:1611.09917 [hep-ph].

[349] M. Bruno, T. Izubuchi, C. Lehner, and A. Meyer, "On isospin breaking in τ decays for $(g-2)_\mu$ from Lattice QCD," *PoS* **LATTICE2018** (2018) 135, arXiv:1811.00508 [hep-lat].

[350] N. Carrasco, V. Lubicz, G. Martinelli, C. T. Sachrajda, N. Tantalo, C. Tarantino, and M. Testa, "QED Corrections to Hadronic Processes in Lattice QCD," *Phys. Rev. D* **91** no. 7, (2015) 074506, arXiv:1502.00257 [hep-lat].

[351] F. Jegerlehner and A. Nyffeler, "The Muon g-2," *Phys.Rept.* **477** (2009) 1–110, arXiv:0902.3360 [hep-ph].

[352] A. Nyffeler, "Precision of a data-driven estimate of hadronic light-by-light scattering in the muon $g-2$: Pseudoscalar-pole contribution," *Phys. Rev. D* **94** no. 5, (2016) 053006, arXiv:1602.03398 [hep-ph].

[353] M. Knecht, A. Nyffeler, M. Perrottet, and E. de Rafael, "Hadronic light by light scattering contribution to the muon g-2: An Effective field theory approach," *Phys. Rev. Lett.* **88** (2002) 071802, arXiv:hep-ph/0111059 [hep-ph].

[354] A. Crivellin and M. Hoferichter, "Width effects of broad new resonances in loop observables and application to (g-2)μ," *Phys. Rev. D* **108** no. 1, (2023) 013005, arXiv:2211.12516 [hep-ph].

[355] A. Bussone, M. Della Morte, and T. Janowski, "Electromagnetic corrections to the hadronic vacuum polarization of the photon within $\mathrm{QED_L}$ and $\mathrm{QED_M}$," *EPJ Web Conf.* **175** (2018) 06005, arXiv:1710.06024 [hep-lat].

[356] M. A. Clark, M. Della Morte, Z. Hall, B. Hörz, A. Nicholson, A. Shindler, J. T. Tsang, A. Walker-Loud, and H. Yan, "QED with massive photons for precision physics: zero modes and first result for the hadron spectrum," *PoS* **LATTICE2021** (2022) 281, arXiv:2201.03251 [hep-lat].

[357] X. Feng and L. Jin, "QED self energies from lattice QCD without power-law finite-volume errors," *Phys. Rev. D* **100** no. 9, (2019) 094509, arXiv:1812.09817 [hep-lat].

[358] M. Hayakawa and S. Uno, "QED in finite volume and finite size scaling effect on electromagnetic properties of hadrons," *Prog. Theor. Phys.* **120** (2008) 413–441, arXiv:0804.2044 [hep-ph].

[359] M. Di Carlo, M. T. Hansen, A. Portelli, and N. Hermansson-Truedsson, "Relativistic, model-independent determination of electromagnetic finite-size effects beyond the pointlike approximation," *Phys. Rev. D* **105** no. 7, (2022) 074509, arXiv:2109.05002 [hep-lat].

[360] **RCstar** Collaboration, L. Bushnaq, I. Campos, M. Catillo, A. Cotellucci, M. Dale, P. Fritzsch, J. Lücke, M. Krstić Marinković, A. Patella, and N. Tantalo, "First results on QCD+QED with C^* boundary conditions," *JHEP* **03** (2023) 012, arXiv:2209.13183 [hep-lat].

[361] H. B. Meyer, "Lorentz-covariant coordinate-space representation of the leading hadronic contribution to the anomalous magnetic moment of the muon," *Eur. Phys. J. C* **77** no. 9, (2017) 616, arXiv:1706.01139 [hep-lat].

[362] E.-H. Chao, A. Gérardin, J. R. Green, R. J. Hudspith, and H. B. Meyer, "Hadronic light-by-light contribution to $(g-2)_\mu$ from lattice QCD with SU(3) flavor symmetry," *Eur. Phys. J. C* **80** no. 9, (2020) 869, arXiv:2006.16224 [hep-lat].

[363] M. Cè, A. Gérardin, K. Ottnad, and H. B. Meyer, "The leading hadronic contribution to the running of the Weinberg angle using covariant coordinate-space methods," *PoS* **LATTICE2018** (2018) 137, arXiv:1811.08669 [hep-lat].

[364] T. Blum, N. Christ, M. Hayakawa, T. Izubuchi, L. Jin, C. Jung, and C. Lehner, "Connected and Leading Disconnected Hadronic Light-by-Light Contribution to the Muon Anomalous Magnetic Moment with a Physical Pion Mass," *Phys. Rev. Lett.* **118** no. 2, (2017) 022005, arXiv:1610.04603 [hep-lat].

[365] M. Lüscher, "Stochastic locality and master-field simulations of very large lattices," *EPJ Web Conf.* **175** (2018) 01002, arXiv:1707.09758 [hep-lat].

[366] A. Francis, P. Fritzsch, M. Lüscher, and A. Rago, "Master-field simulations of O(a)-improved lattice QCD: Algorithms, stability and exactness," *Comput. Phys. Commun.* **255** (2020) 107355, arXiv:1911.04533 [hep-lat].

[367] M. Cè, M. Bruno, J. Bulava, A. Francis, P. Fritzsch, J. R. Green, M. T. Hansen, and A. Rago, "Approaching the master-field: Hadronic observables in large volumes," *PoS* **LATTICE2021** (2022) 383, arXiv:2110.15375 [hep-lat].

[368] N. Hermansson-Truedsson, private communication.

[369] J. P. Leveille, "The Second Order Weak Correction to (G-2) of the Muon in Arbitrary Gauge Models," *Nucl. Phys. B* **137** (1978) 63–76.

[370] C. W. Kao, T. Spitzenberg, and M. Vanderhaeghen, "Burkhardt-Cottingham sum rule and forward spin polarizabilities in heavy baryon chiral perturbation theory," *Phys. Rev. D* **67** (2003) 016001, arXiv:hep-ph/0209241.

[371] V. Pascalutsa, "GDH sum rule in QED and ChPT," *Nucl. Phys. A* **755** (2005) 657–660.

[372] S. J. Brodsky and J. D. Sullivan, "W-Boson Contribution to the Anomalous Magnetic Moment of the Muon," *Phys. Rev.* **156** (1967) 1644–1647.

[373] I. Bars and M. Yoshimura, "Muon magnetic moment in a finite theory of weak and electromagnetic interaction," *Phys. Rev. D* **6** (1972) 374–376.

[374] R. Jackiw and S. Weinberg, "Weak interaction corrections to the muon magnetic moment and to muonic atom energy levels," *Phys. Rev. D* **5** (1972) 2396–2398.

[375] K. Fujikawa, B. W. Lee, and A. I. Sanda, "Generalized Renormalizable Gauge Formulation of Spontaneously Broken Gauge Theories," *Phys. Rev. D* **6** (1972) 2923–2943.

[376] Z. Z. Aydin, S. A. Baran, and A. O. Barut, "Dispersion-theoretic calculation of the lepton magnetic moment and form-factors in the gauge theory of weak interactions," *Nucl. Phys. B* **55** (1973) 601–611.

[377] D. Binosi and J. Papavassiliou, "Pinch Technique: Theory and Applications," *Phys. Rept.* **479** (2009) 1–152, arXiv:0909.2536 [hep-ph].

[378] G. Altarelli, N. Cabibbo, and L. Maiani, "The Drell-Hearn sum rule and the lepton magnetic moment in the Weinberg model of weak and electromagnetic interactions," *Phys. Lett. B* **40** (1972) 415.

[379] K. Kurek and L. Lukaszuk, "Superconvergence relations and parity violating analog of GDH sum rule," *Phys. Rev. C* **70** (2004) 065204, arXiv:hep-ph/0402297.

[380] K. Fujikawa, "Xi-limiting process in spontaneously broken gauge theories," *Phys. Rev. D* **7** (1973) 393–398.

[381] T. D. Lee and C.-N. Yang, "Theory of Charged Vector Mesons Interacting with the Electromagnetic Field," *Phys. Rev.* **128** (1962) 885–898.

[382] B. R. Holstein, V. Pascalutsa, and M. Vanderhaeghen, "Sum rules for magnetic moments and polarizabilities in QED and chiral effective-field theory," *Phys. Rev. D* **72** (2005) 094014, arXiv:hep-ph/0507016.

[383] A. M. Bincer, "Electromagnetic structure of the nucleon," *Phys. Rev.* **118** (1960) 855–863.

[384] S. D. Drell and H. R. Pagels, "Anomalous Magnetic Moment of the Electron, Muon, and Nucleon," *Phys. Rev.* **140** (1965) B397–B407.

[385] F. Hagelstein and V. Pascalutsa, "Pseudoscalar-Meson Contributions to $g-2$ via Schwinger's Sum Rule," in *PoS CD2018 (2019) 066 [hep-ph/1907.06927]*. 2019. arXiv:1907.06927 [hep-ph].

[386] S. D. Drell, "Direct decay $\pi^0 \to e^+ + e^-$," *Il Nuovo Cimento (1955-1965)* **11** no. 5, (Mar, 1959) 693–697.

[387] L. Ametller, A. Bramon, and E. Masso, "Pseudoscalar-meson decays into lepton pairs," *Phys. Rev. D* **30** (1984) 251.

[388] I. Danilkin, C. F. Redmer, and M. Vanderhaeghen, "The hadronic light-by-light contribution to the muon's anomalous magnetic moment," *Prog. Part. Nucl. Phys.* **107** (2019) 20–68, arXiv:1901.10346 [hep-ph].

[389] M. Hoferichter, B.-L. Hoid, B. Kubis, S. Leupold, and S. P. Schneider, "Pion-pole contribution to hadronic light-by-light scattering in the anomalous magnetic moment of the muon," *Phys. Rev. Lett.* **121** no. 11, (2018) 112002, arXiv:1805.01471 [hep-ph].

[390] M. Hoferichter, B.-L. Hoid, B. Kubis, S. Leupold, and S. P. Schneider, "Dispersion relation for hadronic light-by-light scattering: pion pole," *JHEP* **10** (2018) 141, arXiv:1808.04823 [hep-ph].

[391] F. Boudjema and E. Chopin, "Double Higgs production at the linear colliders and the probing of the Higgs selfcoupling," *Z. Phys. C* **73** (1996) 85–110, arXiv:hep-ph/9507396.

[392] M. Bace and N. D. Hari Dass, "Parity Violating Compton Amplitude in Unified Theories," *Annals Phys.* **94** (1975) 349.

[393] M. B. Gavela, G. Girardi, C. Malleville, and P. Sorba, "A Nonlinear R_ξ Gauge Condition for the Electroweak SU(2)×U(1) Model," *Nucl. Phys. B* **193** (1981) 257–268.

[394] J. A. McGovern, D. R. Phillips, and H. W. Griesshammer, "Compton scattering from the proton in an effective field theory with explicit Delta degrees of freedom," *Eur. Phys. J. A* **49** (2013) 12, arXiv:1210.4104 [nucl-th].

[395] H. W. Griesshammer, J. A. McGovern, and D. R. Phillips, "Nucleon Polarisabilities at and Beyond Physical Pion Masses," *Eur. Phys. J. A* **52** no. 5, (2016) 139, arXiv:1511.01952 [nucl-th].

[396] V. Lensky, J. McGovern, and V. Pascalutsa, "Predictions of covariant chiral perturbation theory for nucleon polarisabilities and polarised Compton scattering," *Eur. Phys. J. C* **75** no. 12, (2015) 604, arXiv:1510.02794 [hep-ph].

[397] R. Pohl *et al.*, "The size of the proton," *Nature* **466** (2010) 213–216.

[398] A. Antognini, F. Kottmann, F. Biraben, P. Indelicato, F. Nez, and R. Pohl, "Theory of the 2S-2P Lamb shift and 2S hyperfine splitting in muonic hydrogen," *Ann. Phys.* **331** (2013) 127–145, arXiv:1208.2637 [physics.atom-ph].

[399] A. Antognini *et al.*, "Proton Structure from the Measurement of $2S-2P$ Transition Frequencies of Muonic Hydrogen," *Science* **339** (2013) 417–420, arXiv:1208.2637 [physics.atom-ph].

[400] C. E. Carlson and M. Vanderhaeghen, "Higher-order proton structure corrections to the Lamb shift in muonic hydrogen," *Phys. Rev. A* **84** (2011) 020102, arXiv:1101.5965 [hep-ph].

[401] K. Pachucki, V. Lensky, F. Hagelstein, S. S. Li Muli, S. Bacca, and R. Pohl, "Comprehensive theory of the Lamb shift in light muonic atoms," *Rev. Mod. Phys.* **96** no. 1, (2024) 015001, arXiv:2212.13782 [physics.atom-ph].

[402] E. Llanta and R. Tarrach, "Polarizability Sum Rules in QED," *Phys. Lett. B* **78** (1978) 586–588.

[403] E. Llanta and R. Tarrach, "Pion Electromagnetic Polarizabilities and Quarks," *Phys. Lett. B* **91** (1980) 132–136.

[404] A. I. L'vov, "Pion Polarizabilities in the Sigma Model With Quarks," *Sov. J. Nucl. Phys.* **34** (1981) 289.

[405] J. F. Donoghue, B. R. Holstein, and Y. C. Lin, "The reaction $\gamma\gamma \to \pi^0\pi^0$ and chiral loops," *Phys. Rev. D* **37** (1988) 2423.

[406] J. Bijnens and F. Cornet, "Two Pion Production in Photon-Photon Collisions," *Nucl. Phys. B* **296** (1988) 557–568.

[407] S. Bellucci, J. Gasser, and M. E. Sainio, "Low-energy photon-photon collisions to two loop order," *Nucl. Phys. B* **423** (1994) 80–122, arXiv:hep-ph/9401206. [Erratum: Nucl.Phys.B 431, 413–414 (1994)].

[408] J. Gasser, M. A. Ivanov, and M. E. Sainio, "Low-energy photon-photon collisions to two loops revisited," *Nucl. Phys. B* **728** (2005) 31–54, arXiv:hep-ph/0506265.

[409] **COMPASS** Collaboration, C. Adolph *et al.*, "Measurement of the charged-pion polarizability," *Phys. Rev. Lett.* **114** (2015) 062002, arXiv:1405.6377 [hep-ex].

[410] L.-Y. Dai and M. R. Pennington, "Pion polarizabilities from $\gamma\gamma \to \pi\pi$ analysis," *Phys. Rev. D* **94** no. 11, (2016) 116021, arXiv:1611.04441 [hep-ph].

[411] V. Ermolina, I. Danilkin, and M. Vanderhaeghen, "Pion polarizabilities from a dispersive analysis of $\gamma\gamma \to \pi\pi$," in *16th International Conference on Meson-Nucleon Physics and the Structure of the Nucleon*. 7, 2024. arXiv:2407.21471 [hep-ph].

[412] R. Garcia-Martin and B. Moussallam, "MO analysis of the high statistics Belle results on $\gamma\gamma \to \pi^+\pi^-, \pi^0\pi^0$ with chiral constraints," *Eur. Phys. J. C* **70** (2010) 155–175, arXiv:1006.5373 [hep-ph].

[413] A. I. L'vov, "Electric polarizability of nuclei and a longitudinal sum rule," *Nucl. Phys. A* **638** (1998) 756–764, arXiv:nucl-th/9804033.

[414] J. Bernabeu, D. Gomez Dumm, and G. Orlandini, "Electric polarizability of nuclei from a longitudinal sum rule," *Nucl. Phys. A* **634** (1998) 463–471, arXiv:nucl-th/9802011.

[415] V. Biloshytskyi, I. Ciobotaru-Hriscu, F. Hagelstein, V. Lensky, and V. Pascalutsa, "QED of Bernabéu-Tarrach sum rule for electric polarizability and its implication for the Lamb shift," *Phys. Rev. D* **109** no. 1, (2024) 016026, arXiv:2305.08814 [hep-ph].

[416] R. L. Workman, M. W. Paris, W. J. Briscoe, and I. I. Strakovsky, "Unified Chew-Mandelstam SAID analysis of pion photoproduction data," *Phys. Rev. C* **86** (2012) 015202, arXiv:1202.0845 [hep-ph]. http://gwdac.phys.gwu.edu.

[417] D. Drechsel, S. S. Kamalov, and L. Tiator, "Unitary Isobar Model - MAID2007," *Eur. Phys. J. A* **34** (2007) 69–97, arXiv:0710.0306 [nucl-th]. https://maid.kph.uni-mainz.de/.

[418] V. Bernard, N. Kaiser, and U. G. Meissner, "Chiral expansion of the nucleon's electromagnetic polarizabilities," *Phys. Rev. Lett.* **67** (1991) 1515–1518.

[419] V. Bernard, N. Kaiser, J. Kambor, and U.-G. Meißner, "Chiral structure of the nucleon," *Nucl. Phys. B* **388** (1992) 315–345.

[420] A. I. Lvov, "A dispersion look at the chiral perturbation theory. Nucleon electromagnetic polarizabilities," *Phys. Lett. B* **304** (1993) 29–34.

[421] V. Pascalutsa, "Some electromagnetic properties of the nucleon from relativistic chiral effective field theory," *Prog. Part. Nucl. Phys.* **55** (2005) 23–34, arXiv:nucl-th/0412008.

[422] V. Lensky, J. M. Alarcón, and V. Pascalutsa, "Moments of nucleon structure functions at next-to-leading order in baryon chiral perturbation theory," *Phys. Rev. C* **90** no. 5, (2014) 055202, arXiv:1407.2574 [hep-ph].

[423] J. M. Alarcón, V. Lensky, and V. Pascalutsa, "Chiral perturbation theory of muonic hydrogen Lamb shift: polarizability contribution," *Eur. Phys. J. C* **74** no. 4, (2014) 2852, arXiv:1312.1219 [hep-ph].

[424] M. E. Christy and P. E. Bosted, "Empirical fit to precision inclusive electron-proton cross-sections in the resonance region," *Phys. Rev. C* **81** (2010) 055213, arXiv:0712.3731 [hep-ph].

[425] A. N. Hiller Blin *et al.*, "Nucleon resonance contributions to unpolarised inclusive electron scattering," *Phys. Rev. C* **100** no. 3, (2019) 035201, arXiv:1904.08016 [hep-ph].

[426] **Particle Data Group** Collaboration, R. L. Workman *et al.*, "Review of Particle Physics," *PTEP* **2022** (2022) 083C01.

[427] A. J. F. Siegert, "Note on the interaction between nuclei and electromagnetic radiation," *Phys. Rev.* **52** (1937) 787–789.

[428] F. Hagelstein and V. Pascalutsa, "The subtraction contribution to the muonic-hydrogen Lamb shift: A point for lattice QCD calculations of the polarizability effect," *Nucl. Phys. A* **1016** (2021) 122323, arXiv:2010.11898 [hep-ph].

[429] R. Bradford, A. Bodek, H. S. Budd, and J. Arrington, "A New parameterization of the nucleon elastic form-factors," *Nucl. Phys. Proc. Suppl.* **159** (2006) 127–132, arXiv:hep-ex/0602017 [hep-ex].

[430] J. M. Alarcón, F. Hagelstein, V. Lensky, and V. Pascalutsa, "Forward doubly-virtual Compton scattering off the nucleon in chiral perturbation theory: the subtraction function and moments of unpolarized structure functions," *Phys. Rev. D* **102** no. 1, (2020) 014006, arXiv:2005.09518 [hep-ph].

[431] C. G. Callan, Jr. and D. J. Gross, "High-energy electroproduction and the constitution of the electric current," *Phys. Rev. Lett.* **22** (1969) 156–159.

[432] L. W. Whitlow, S. Rock, A. Bodek, E. M. Riordan, and S. Dasu, "A Precise extraction of $R = \sigma_L/\sigma_T$ from a global analysis of the SLAC deep inelastic e-p and e-d scattering cross-sections," *Phys. Lett. B* **250** (1990) 193–198.

[433] **E140X** Collaboration, L. H. Tao *et al.*, "Precision measurement of $R = \sigma_L/\sigma_T$ on hydrogen, deuterium and beryllium targets in deep inelastic electron scattering," *Z. Phys. C* **70** (1996) 387–390.

[434] **E143** Collaboration, K. Abe *et al.*, "Measurements of $R = \sigma_L/\sigma_T$ for $0.03 < x < 0.1$ and fit to world data," *Phys. Lett. B* **452** (1999) 194–200, arXiv:hep-ex/9808028.

[435] **New Muon** Collaboration, M. Arneodo *et al.*, "Measurement of the proton and deuteron structure functions, F_2^p and F_2^d, and of the ratio σ_L/σ_T," *Nucl. Phys. B* **483** (1997) 3–43, arXiv:hep-ph/9610231.

[436] **ZEUS** Collaboration, H. Abramowicz *et al.*, "Deep inelastic cross-section measurements at large y with the ZEUS detector at HERA," *Phys. Rev. D* **90** no. 7, (2014) 072002, arXiv:1404.6376 [hep-ex].

[437] **H1** Collaboration, V. Andreev *et al.*, "Measurement of inclusive ep cross sections at high Q^2 at $\sqrt{s} = 225$ and 252 GeV and of the longitudinal proton structure function F_L at HERA," *Eur. Phys. J. C* **74** no. 4, (2014) 2814, arXiv:1312.4821 [hep-ex].

[438] D. Britzger, C. Ewerz, S. Glazov, O. Nachtmann, and S. Schmitt, "The Tensor Pomeron and Low-x Deep Inelastic Scattering," *Phys. Rev. D* **100** no. 11, (2019) 114007, arXiv:1901.08524 [hep-ph].

[439] A. Accardi *et al.*, "Electron Ion Collider: The Next QCD Frontier: Understanding the glue that binds us all," *Eur. Phys. J. A* **52** no. 9, (2016) 268, arXiv:1212.1701 [nucl-ex].

[440] J. F. Donoghue and B. R. Holstein, "Photon-photon scattering, pion polarizability and chiral symmetry," *Phys. Rev. D* **48** (1993) 137–146, arXiv:hep-ph/9302203.

[441] A. E. Kaloshin and V. V. Serebryakov, "π^+ and π^0 polarizabilities from $\gamma\gamma \to \pi\pi$ data," *Z. Phys. C* **64** (1994) 689–694, arXiv:hep-ph/9306224.

[442] L. V. Fil'kov and V. L. Kashevarov, "Compton scattering on the charged pion and the process $\gamma\gamma \to \pi^0\pi^0$," *Eur. Phys. J. A* **5** (1999) 285–292, arXiv:nucl-th/9810074.

[443] **Belle** Collaboration, S. Uehara *et al.*, "High-statistics measurement of neutral pion-pair production in two-photon collisions," *Phys. Rev. D* **78** (2008) 052004, arXiv:0805.3387 [hep-ex].

[444] **Belle** Collaboration, S. Uehara *et al.*, "High-statistics study of neutral-pion pair production in two-photon collisions," *Phys. Rev. D* **79** (2009) 052009, arXiv:0903.3697 [hep-ex].

[445] X. Feng, T. Izubuchi, L. Jin, and M. Golterman, "Pion electric polarizabilities from lattice QCD," *PoS* **LATTICE2021** (2022) 362, arXiv:2201.01396 [hep-lat].

[446] F. X. Lee, W. Wilcox, A. Alexandru, C. Culver, and S. Nadeem, "Neutral pion polarizabilities from four-point functions in lattice QCD," arXiv:2408.13388 [hep-lat].

[447] V. N. Pervushin and M. K. Volkov, "Pion Polarizability in Chiral Quantum Field Theory," *Phys. Lett. B* **55** (1975) 405–408.

[448] L. D. Landau, E. M. Lifshitz, and L. P. Pitaevskii, *Course of Theoretical Physics, Vol. 8. Electrodynamics of Continuous Media, 2nd ed.* Pergamon Press, 1984.

[449] M. V. Terentev, "Electromagnetic properties of pions at low energy," *Usp. Fiz. Nauk* **112** (1974) 37–82.

[450] B. R. Holstein, "Pion polarizability and chiral symmetry," *Comments Nucl. Part. Phys.* **19** no. 5, (1990) 221–238.

[451] E. E. Salpeter and H. A. Bethe, "A relativistic equation for bound state problems," *Phys. Rev.* **84** (1951) 1232–1242.

[452] N. Nakanishi, "A general survey of the theory of the bethe-salpeter equation," *Prog. Theor. Phys. Suppl.* **43** (1969) 1–81.

[453] J. Carbonell, V. A. Karmanov, and M. Mangin-Brinet, "Electromagnetic form factor via bethe-salpeter amplitude in minkowski space," *Eur. Phys. J. A* **39** (2009) 53–60, arXiv:0809.3678 [hep-ph].

[454] J. P. B. C. de Melo, J. H. O. Sales, T. Frederico, and P. U. Sauer, "Pairs in the light front and covariance," *Nucl. Phys. A* **631** (1998) 574C–579C, arXiv:hep-ph/9802325.

[455] D. Melikhov and S. Simula, "End point singularities of Feynman graphs on the light cone," *Phys. Lett. B* **556** (2003) 135–141, arXiv:hep-ph/0211277.

[456] M. Sawicki, "Soft charge form-factor of the pion," *Phys. Rev. D* **46** (1992) 474–477.

[457] R. Jakob, P. Kroll, and M. Raulfs, "Meson - photon transition form-factors," *J. Phys. G* **22** (1996) 45–58, arXiv:hep-ph/9410304.

[458] P. Kroll and M. Raulfs, "The Pi gamma transition form-factor and the pion wave function," *Phys. Lett. B* **387** (1996) 848–854, arXiv:hep-ph/9605264.

[459] H.-M. Choi and C.-R. Ji, "Consistency of pion form factor and unpolarized transverse momentum dependent parton distributions beyond leading twist in the light-front quark model," 2403.16703. https://arxiv.org/pdf/2403.16703v1.pdf.

[460] G. Cynolter and E. Lendvai, "Symmetry Preserving Regularization with A Cutoff," *Central Eur. J. Phys.* **9** (2011) 1237–1247, arXiv:1002.4490 [hep-ph].

[461] Y. Zeldovich, "Electromagnetic Interaction with Parity Violation," *Sov. Phys. JETP* **6** (1958) 1184–1186. [Zh. Eksp. Teor. Fiz. 33, 1531-1533 (1957)].

[462] "Particle Data Group (2023)," https://pdg.lbl.gov/2023/reviews/rpp2023-rev-structure-functions.pdf.

[463] J. A. Bartelski, "Deep Inelastic Structure Functions and the Quark Parton Model," *Acta Phys. Polon. B* **10** (1979) 923.

[464] J. Kaur, "Spin Dependent Distributions in the Quark Parton Model," *Nucl. Phys. B* **128** (1977) 219–251.

[465] D. J. Almond, "Low-energy theorem for Compton scattering by a spin 1/2 particle, without c, p, and t-invariance," *Nucl. Phys. B* **11** (1969) 277–285.

[466] D. B. Kaplan and M. J. Savage, "An Analysis of parity violating pion - nucleon couplings," *Nucl. Phys. A* **556** (1993) 653–671. [Erratum: Nucl.Phys.A 570, 833–833 (1994), Erratum: Nucl.Phys.A 580, 679–679 (1994)].

[467] P. F. Bedaque and M. J. Savage, "Parity violation in gamma polarized-p Compton scattering," *Phys. Rev. C* **62** (2000) 018501, arXiv:nucl-th/9909055.

[468] M. J. Musolf and B. R. Holstein, "Observability of the anapole moment and neutrino charge radius," *Phys. Rev. D* **43** (1991) 2956–2970.

[469] J. de Vries, E. Epelbaum, L. Girlanda, A. Gnech, E. Mereghetti, and M. Viviani, "Parity- and Time-Reversal-Violating Nuclear Forces," *Front. in Phys.* **8** (2020) 218, arXiv:2001.09050 [nucl-th].

[470] **MUonE** Collaboration, G. Abbiendi *et al.*, "Measuring the leading hadronic contribution to the muon g-2 via μe scattering," *Eur. Phys. J. C* **77** no. 3, (2017) 139, arXiv:1609.08987 [hep-ex].